

Realizable Markovian Statistical Closures:  
General Theory  
and  
Application to  
Drift-Wave Turbulence

John Clement Bowman

A Dissertation  
presented to the  
faculty of Princeton University  
in candidacy for the degree  
of Doctor of Philosophy

Recommended for acceptance by the  
Department of  
Astrophysical Sciences

January 1992  
2nd edition, June 1998

©1992, 1998  
John Clement Bowman  
ALL RIGHTS RESERVED

# Notes to 2nd edition

1. Figures III.2-5 and III.10-11 are quantitatively incorrect; see Bowman, Krommes, and Ottaviani, *Phys. Fluids B*, **5**, 3558 (1993).
2. In Figs III.7, III.8, and III.12, the vertical labels should read  $\frac{1}{2}\{E_0, E_1, E, U, I\}$ . Also, the  $I$  curve is multiplied by an arbitrary constant factor.
3. On pg. 115, note that the nonrealizability of the closure resulting from the application of Eq(III.50) follows from setting  $C(t) = |2 - t|^{1/2}$  in the example given on pg. 98.
4. For a clearer presentation of Sec. III.F.1 see Bowman, Krommes, and Ottaviani, *Phys. Fluids B*, **5**, 3558 (1993).
5. The RTFM equations on pg. 123 are derived in Bowman and Krommes, *Phys. Plasmas*, **4**, 3895 (1997).
6. On pg. 157, note that a much faster algorithm based on a variable exponential integrating factor has since been devised (see Bowman, "Exponential Algorithms for Stiff Initial Value Problems", submitted to *J. Comp. Phys.*, 1998).
7. Ignore the spurious negative spikes in Figs. VI.6, VI.9, and VI.19 to the left of the energy injection wavenumber  $k_f$ ; only the data to the right of the spikes is relevant. (Actually, Kraichnan's logarithmic correction to the Kolmogorov scaling is probably not relevant to DIA-based closures, which violate RGI; see Bowman, *J. Fluid Mech.*, **306**, 167 (1996).)
8. The calculation of the dissipation wavenumbers on pg. 225 is incorrect (see Bowman, *J. Sci. Comput.*, **11**, 1997).
9. The vertical labels on the right-hand side of Figs. VI.42 and VI.43 should read  $2E(k)$  and  $3E(k)$ , respectively.

# Abstract

A well known Markovian statistical closure for turbulence computations, derivable from the direct-interaction approximation (DIA), is shown to be potentially *nonrealizable* in the presence of the linear wave phenomena encountered in plasma physics and geophysics. This statistical closure is a type of eddy-damped quasinormal Markovian (EDQNM) approximation in which the triad interaction time is obtained not from a phenomenological model but from the use of a Fluctuation-Dissipation (FD) relation in the DIA equations. This choice accounts for the nonlinear renormalization of both the frequency and the damping rate. For the EDQNM, a violation of realizability can have serious physical consequences, including the prediction of negative or even divergent energies. None of these difficulties arise when this closure is applied to the fluid problems for which it was originally designed. A new statistical approximation for wave turbulence, the realizable Markovian closure (RMC), is proposed as a remedy. The RMC is based on a form for the Fluctuation-Dissipation (FD) ansatz more suitable than the one conventionally used to derive the EDQNM. This form is appropriate for nonstationary systems and it reduces to the classical FD Theorem in equilibrium. An underlying Langevin equation is exhibited for the RMC. No assumption of white-noise statistics is made in the construction of this Langevin equation; thus, even in the wave-free case the RMC appears to provide a better representation of the true dynamics than does the EDQNM closure. The RMC is tested numerically for a system of three interacting waves. Although the steady-state forms of both closures agree, the RMC exhibits improved transient behaviour. An anisotropic generalization of the isotropic wavenumber partitioning scheme pioneered by Leith and Kraichnan [1972] is developed; this is used to obtain steady-state solutions of the RMC and DIA closures for two-dimensional models of drift-wave turbulence based on the Hasegawa-Mima and Terry-Horton equations. The closure predictions compare well to spectra obtained by conventional pseudo-spectral methods. The numerical value for the particle diffusion coefficient is found to be more than an order of magnitude higher than a simple mixing-length estimate.

# Contents

|   |       |      |
|---|-------|------|
| <b>Abstract</b>                                   | ----- | ii   |
| <b>List of Figures</b>                            | ----- | viii |
| <b>List of Tables</b>                             | ----- | xiv  |
| <b>Preface</b>                                    | ----- | xv   |
| <b>I Introduction</b>                             | ----- |      |
| I.A Fluid turbulence                              | ----- | 3    |
| I.A.1 Three-dimensional fluid turbulence          | ----- | 6    |
| I.A.2 Two-dimensional fluid turbulence            | ----- | 7    |
| I.B Plasma turbulence                             | ----- | 8    |
| I.B.1 Drift-wave turbulence                       | ----- | 10   |
| I.B.2 Eta-i mode turbulence                       | ----- | 13   |
| I.B.3 Alternative mechanisms                      | ----- | 15   |
| I.C Stochastic processes                          | ----- | 16   |
| I.C.1 Ensemble averages                           | ----- | 16   |
| I.C.2 Linear stochastic processes                 | ----- | 17   |
| I.C.3 Nonlinear stochastic processes              | ----- | 18   |
| I.C.4 Concept of realizability                    | ----- | 24   |
| I.C.5 Concept of Markovian                        | ----- | 26   |
| I.C.6 Passive <i>vs.</i> self-consistent problems | ----- | 28   |
| I.D Analytical transport estimates                | ----- | 28   |
| I.D.1 Linear theory                               | ----- | 29   |
| I.D.2 Dimensional analysis                        | ----- | 30   |
| I.D.3 Mixing-length estimates                     | ----- | 30   |

|            |   |           |
|------------|---|-----------|
| I.D.4      | Survey of statistical approaches                              | 32        |
| I.E        | Statistical closure <i>vs.</i> direct simulation              | 43        |
| I.E.1      | Ensemble average <i>vs.</i> time average                      | 44        |
| I.E.2      | Identification of nonlinear interactions                      | 44        |
| I.F        | Overview of this work   | 45        |
| <b>II</b>  | <b>General Theory of Systematically Renormalized Closures</b> | <b>49</b> |
| II.A       | Overview of closure techniques                                | 49        |
| II.A.1     | Renormalized perturbation theory and MSR                      | 49        |
| II.A.2     | Eulerian <i>vs.</i> Lagrangian formulations                   | 53        |
| II.A.3     | Markovian closures  | 55        |
| II.A.4     | Other schemes   | 55        |
| II.B       | Direct-interaction approximation                              | 58        |
| II.B.1     | Derivations   | 58        |
| II.B.2     | Illustration of the DIA                                       | 65        |
| II.B.3     | Properties  | 71        |
| II.B.4     | Covariant representation                                      | 72        |
| II.B.5     | Failures  | 73        |
| II.B.6     | Numerical considerations                                      | 76        |
| II.C       | DIA-based Markovian closures                                  | 78        |
| <b>III</b> | <b>Theory of Markovian Closures</b>                           | <b>80</b> |
| III.A      | Overview of Markovian closures                                | 81        |
| III.B      | DIA-based one-field EDQNM closure                             | 84        |
| III.B.1    | Derivation of the EDQNM from the DIA                          | 85        |
| III.B.2    | Properties of the EDQNM                                       | 89        |
| III.B.3    | Realizability issues of the EDQNM                             | 90        |
| III.C      | Realizable one-field EDQNM closure                            | 100       |
| III.C.1    | Motivation  | 101       |
| III.C.2    | Derivation of the realizable EDQNM                            | 102       |
| III.C.3    | Properties of the realizable EDQNM                            | 103       |
| III.D      | Realizable multiple-field EDQNM closure                       | 105       |
| III.D.1    | Motivation: inhomogeneous test-field model                    | 105       |
| III.D.2    | Covariant formulation   | 105       |
| III.D.3    | Properties of the realizable multiple-field EDQNM             | 110       |

|  |            |
|--|------------|
| III.D.4 Failure to conserve quadratic invariants           | 112        |
| III.E Realizable Markovian closure (RMC)                   | 114        |
| III.E.1 Modified Fluctuation-Dissipation ansatz            | 115        |
| III.E.2 Properties of the RMC                              | 119        |
| III.E.3 RGI modification                                   | 122        |
| III.E.4 Comparison of the RMC with the realizable EDQNM    | 123        |
| III.F Multiple-field RMC                                   | 125        |
| III.F.1 Modified Fluctuation-Dissipation ansatz            | 125        |
| III.F.2 Properties   | 128        |
| III.F.3 RGI modification                                   | 129        |
| III.G Summary  | 129        |
| <b>IV Numerical Implementation of Statistical Closures</b> | <b>132</b> |
| IV.A Bin-averaging technique                               | 133        |
| IV.A.1 Continuum representation                            | 134        |
| IV.A.2 Wavenumber coordinate system                        | 137        |
| IV.A.3 Fourier harmonic expansion                          | 138        |
| IV.B Geometric weight factors                              | 138        |
| IV.B.1 Isotropic case                                      | 139        |
| IV.B.2 Anisotropic case                                    | 141        |
| IV.C Bin-coupling coefficients                             | 145        |
| IV.C.1 Self-coupling effects                               | 148        |
| IV.C.2 Multiple fields                                     | 151        |
| IV.D Numerical code  | 151        |
| IV.D.1 Predictor-corrector algorithm                       | 151        |
| IV.D.2 Dynamic time stepping                               | 159        |
| IV.D.3 Optimization of the DIA                             | 162        |
| IV.D.4 Reality condition                                   | 162        |
| IV.D.5 Design features                                     | 163        |
| IV.E Summary   | 167        |
| <b>V Application to Three Interacting Waves</b>            | <b>168</b> |
| V.A Real mode coupling and zero growth                     | 170        |
| V.A.1 Resonant case  | 171        |
| V.A.2 Nonresonant case                                     | 183        |

|            |   |            |
|------------|---|------------|
| V.B        | Real mode-coupling and finite growth                      | 191        |
| V.B.1      | Classification of Wersinger <i>et al.</i> [1980]          | 198        |
| V.C        | Complex mode-coupling and finite growth                   | 206        |
| V.D        | Multiple-field formulation                                | 212        |
| V.E        | Summary   | 215        |
| <b>VI</b>  | <b>Application to Drift-Wave Turbulence</b>               | <b>217</b> |
| VI.A       | Continuum <i>vs.</i> discrete representations             | 218        |
| VI.B       | Inviscid Hasegawa-Mima problem                            | 219        |
| VI.B.1     | Inviscid equilibrium                                      | 219        |
| VI.B.2     | Driven two-dimensional fluid turbulence                   | 221        |
| VI.C       | Short-wavelength Hasegawa-Mima equation                   | 231        |
| VI.C.1     | Comparison of closure <i>vs.</i> numerical simulation     | 232        |
| VI.C.2     | Two-time statistics                                       | 238        |
| VI.D       | Hasegawa-Mima equation                                    | 238        |
| VI.D.1     | Two-time statistics                                       | 243        |
| VI.E       | Terry-Horton problem                                      | 245        |
| VI.E.1     | Inviscid equilibrium                                      | 248        |
| VI.E.2     | Saturated turbulent state                                 | 249        |
| VI.E.3     | Two-time statistics                                       | 259        |
| VI.E.4     | Wavenumber scaling of the nonlinear damping               | 259        |
| VI.E.5     | Diffusion coefficient                                     | 262        |
| VI.F       | Summary   | 266        |
| <b>VII</b> | <b>Conclusions</b>  | <b>268</b> |
| VII.A      | Summary; suggestions for further research                 | 269        |
| VII.B      | Error estimates and the optimum theory                    | 276        |
| VII.C      | Final remarks   | 277        |
|            | <b>Appendices:</b>  | <b>278</b> |
| <b>A</b>   | <b>Elementary Derivation of the Terry-Horton Equation</b> | <b>278</b> |
| <b>B</b>   | <b>Fourier Transformation of Fundamental Equation</b>     | <b>280</b> |
| <b>C</b>   | <b>Conservation Properties of the Multiple-Field DIA</b>  | <b>281</b> |

|          |  |     |
|----------|--|-----|
| <b>D</b> | <b>Positive Definiteness in the Realizable EDQNM</b> | 283 |
| <b>E</b> | <b>Energy Conservation of the Realizable EDQNM</b>   | 284 |
| <b>F</b> | <b>Proofs of Theorems</b>                            | 286 |
| <b>G</b> | <b>Isotropic Weight Factors</b>                      | 292 |
| <b>H</b> | <b>Inviscid Equilibria</b>                           | 296 |
| <b>I</b> | <b>Three-Wave Quasistationary EDQNM Formulae</b>     | 303 |
|          | <b>Bibliography</b>                                  | 305 |

# List of Figures

|        |   |     |
|--------|---|-----|
| I.1    | Physical origin of drift waves . . . . .  | 14  |
| I.2    | Concept of realizability. . . . .   | 25  |
| I.3    | Concept of Markovian. . . . .   | 27  |
|        |   |     |
| II.1   | Comparison of exact, DIA, and quasilinear (QL) results for the stochastic oscillator with $K = \infty$ . The numerical prediction of the DIA code coincides with the analytical solution of the DIA, Eq. (II.17). . . . . | 66  |
| II.2   | Comparison of exact and DIA solutions of the oscillatory passive advection problem, Eq. (II.23), with $\lambda = 1$ and $\omega_0 \equiv \beta$ . . . . .   | 69  |
|        |   |     |
| III.1  | Violently unstable behaviour that can arise in the application of the EDQNM closure to drift-wave turbulence. We observe that near $t = 500$ the sample mode energies $E_k$ diverge to $\pm\infty$ . . . . .              | 92  |
| III.2  | Example of the nonrealizability of the EDQNM for wave phenomena. . . . .  | 96  |
| III.3  | Illustration of the negative interaction time underlying the nonrealizability encountered in Fig. III.2. . . . .  | 96  |
| III.4  | Evolution of the eddy damping $\hat{\eta}_k$ in the nonrealizable case of Fig. III.2. . . . .   | 97  |
| III.5  | DIA solution for the case considered in Fig. III.2. The ensemble and DIA solutions coincide (to within the numerical accuracy of the graph). . . . .  | 97  |
| III.6  | Comparison of the realizable EDQNM and the original EDQNM. . . . .  | 104 |
| III.7  | Realizable EDQNM evolution of the quadratic invariants for the two-field $\eta_i$ problem. . . . .  | 113 |
| III.8  | DIA evolution of the quadratic invariants for the two-field $\eta_i$ problem. . . . .   | 113 |
| III.9  | RMC evolution of the mean covariances in the degenerate three-wave case of Fig. III.2. The ensemble and RMC solutions coincide (to within the numerical accuracy of the graph). . . . .                                   | 118 |
| III.10 | Evolution of the quantity $\Theta_{kpq}$ of the RMC closure for the degenerate three-wave case of Fig. III.2. . . . .   | 118 |

---

|        |   |     |
|--------|---|-----|
| III.11 | Evolution of the quantity $\Theta_{pqk}$ of the RMC closure for the degenerate three-wave case of Fig. III.2. . . . .   | 119 |
| III.12 | RMC evolution of the quadratic invariants for the two-field $\eta_i$ problem. . . . .   | 130 |
| IV.1   | Coarse-graining of wavenumber space in a two-dimensional Cartesian bin geometry. The black dots represent individual modes. . . . .   | 134 |
| IV.2   | Logarithmic/linear polar bin geometry for $3 \times 6$ bins. In the code DIA each bin is indexed by the coordinates indicated on the radial and azimuthal axes. . . . .     | 137 |
| IV.3   | Relation between the angles associated with the convolution triangle. . . . .   | 139 |
| IV.4   | Approximation of the integral of $f(t)$ using the nonuniform trapezoidal rule. . . . .  | 161 |
| V.1    | Procedure used to determine the thermal equilibrium energies from the initial conditions for the inviscid case with exactly two quadratic invariants, $E$ and $U$ . . . . . | 172 |
| V.2    | DIA <i>vs.</i> exact evolution of the covariances of three waves with the asymmetric initial condition Eq. (V.6). . . . .   | 173 |
| V.3    | Statistical fluctuation levels in an ensemble of 5000 realizations. . . . .   | 174 |
| V.4    | EDQNM <i>vs.</i> exact evolution of the covariances of three waves with the asymmetric initial condition, Eq. (V.6). . . . .  | 175 |
| V.5    | Quasistationary EDQNM <i>vs.</i> exact evolution of the covariances of three waves with the asymmetric initial condition, Eq. (V.6). . . . .                                | 175 |
| V.6    | Determination of the initial quasistationary EDQNM triad interaction time for the asymmetric initial condition, Eq. (V.6). . . . .  | 176 |
| V.7    | Quasistationary EDQNM evolution of the triad interaction time, starting from the final value obtained in Fig. V.6. . . . .  | 177 |
| V.8    | RMC <i>vs.</i> exact evolution of the covariances of three waves with the asymmetric initial condition, Eq. (V.6). . . . .  | 177 |
| V.9    | Normalized two-time covariances $\mathcal{C}_k(\tau)/\mathcal{C}_k(0)$ <i>vs.</i> $\tau$ evaluated at $t = 3$ for the equipartition case, Eq. (V.8). . . . .                | 178 |
| V.10   | Normalized two-time covariances $\mathcal{C}_q(\tau)/\mathcal{C}_q(0)$ <i>vs.</i> $\tau$ evaluated at $t = 3$ for the equipartition case, Eq. (V.8). . . . .                | 178 |
| V.11   | Normalized two-time covariances $\mathcal{C}_k(\tau)/\mathcal{C}_k(0)$ <i>vs.</i> $\tau$ evaluated at $t = 20$ for the equipartition case, Eq. (V.8). . . . .               | 179 |
| V.12   | DIA response function $R_q(\tau)$ <i>vs.</i> $\tau$ evaluated at $t = 3$ for the equipartition case, Eq. (V.8). . . . .   | 180 |

---

|      |  |     |
|------|--|-----|
| V.13 | Evolution of the EDQNM <i>vs.</i> exact covariances for the degenerate case, Eq. (V.9). . . . .  | 182 |
| V.14 | Evolution of the quasistationary EDQNM <i>vs.</i> exact covariances for the degenerate case, Eq. (V.9) . . . . .   | 182 |
| V.15 | Evolution of the RMC <i>vs.</i> exact covariances for the degenerate case, Eq. (V.9). . . . .  | 184 |
| V.16 | Evolution of the DIA <i>vs.</i> exact covariances for the degenerate case, Eq. (V.9). . . . .  | 184 |
| V.17 | DIA <i>vs.</i> exact evolution of the covariances of three waves with the mode coupling of Eq. (V.5) and the frequencies $\omega_k = \omega_p = \omega_q = 1$ . . . . .          | 189 |
| V.18 | Realizable EDQNM <i>vs.</i> exact evolution for the case in Fig. V.17. . . . .   | 189 |
| V.19 | RMC <i>vs.</i> exact evolution for the case considered in Fig. V.17. . . . .   | 190 |
| V.20 | Extension of Fig. V.19 to the time $t = 30$ . . . . .  | 190 |
| V.21 | Evolution of the DIA <i>vs.</i> exact covariances for the case considered in Fig. V.17 but with the assignments $\gamma_k = -1$ , $\gamma_p = -3$ , and $\gamma_q = 1$ . . . . . | 193 |
| V.22 | Realizable EDQNM <i>vs.</i> exact evolution for the case in Fig. V.21. . . . .   | 194 |
| V.23 | RMC <i>vs.</i> exact evolution for the case considered in Fig. V.21. . . . .   | 194 |
| V.24 | DIA evolution from the Markovian steady state given by Eq. (V.20) to the correct state given by Eq. (V.19). . . . .  | 195 |
| V.25 | Normalized two-time covariances $\mathcal{C}_k(\tau)/\mathcal{C}_k(0)$ <i>vs.</i> $\tau$ for the case considered in Fig. V.21. . . . .   | 195 |
| V.26 | DIA response function $R_k(\tau)$ <i>vs.</i> $\tau$ for the case considered in Fig. V.21. . . . .  | 198 |
| V.27 | DIA <i>vs.</i> ensemble evolution for the case of Wersinger <i>et al.</i> with $\Delta = 2$ and $\Gamma = 2$ . . . . .   | 200 |
| V.28 | DIA <i>vs.</i> ensemble evolution for the case of Wersinger <i>et al.</i> with $\Delta = 2$ and $\Gamma = 3$ . . . . .   | 200 |
| V.29 | DIA <i>vs.</i> ensemble evolution for the case of Wersinger <i>et al.</i> with $\Delta = 2$ and $\Gamma = 9$ . . . . .   | 201 |
| V.30 | DIA <i>vs.</i> ensemble evolution for the case of Wersinger <i>et al.</i> with $\Delta = 2$ and $\Gamma = 12$ . . . . .  | 201 |
| V.31 | DIA <i>vs.</i> ensemble evolution for the case of Wersinger <i>et al.</i> with $\Delta = 2$ and $\Gamma = 13.18$ . . . . .   | 202 |
| V.32 | Realizable EDQNM <i>vs.</i> ensemble evolution for the case of Wersinger <i>et al.</i> with $\Delta = 2$ and $\Gamma = 13.18$ . . . . .  | 202 |
| V.33 | RMC <i>vs.</i> ensemble evolution for the case of Wersinger <i>et al.</i> with $\Delta = 2$ and $\Gamma = 13.18$ . . . . .   | 203 |

---

|      |  |     |
|------|--|-----|
| V.34 | Realizable EDQNM evolution of $\theta_{kpq}$ for the case of Wersinger <i>et al.</i> with $\Delta = 2$ and $\Gamma = 13.18$ . . . . .  | 204 |
| V.35 | Realizable EDQNM evolution of $\eta_k$ for the case of Wersinger <i>et al.</i> with $\Delta = 2$ and $\Gamma = 13.18$ . . . . .  | 204 |
| V.36 | Realizable EDQNM <i>vs.</i> ensemble evolution for the case of Wersinger <i>et al.</i> with $\Delta = 2$ and $\Gamma = 6$ . . . . .  | 205 |
| V.37 | Realizable EDQNM evolution of $\theta_{kpq}$ for the case of Wersinger <i>et al.</i> with $\Delta = 2$ and $\Gamma = 6$ . . . . .  | 205 |
| V.38 | RMC evolution of $\Theta_{kpq}$ for the case of Wersinger <i>et al.</i> with $\Delta = 2$ and $\Gamma = 13.18$ . . . . .   | 206 |
| V.39 | DIA <i>vs.</i> exact evolution of the covariances of three turbulent drift waves. . . . .  | 208 |
| V.40 | Normalized two-time covariances $\mathcal{C}_q(\tau)/\mathcal{C}_q(0)$ <i>vs.</i> $\tau$ evaluated at $t = 120$ for the turbulent drift-wave case. . . . .   | 208 |
| V.41 | RMC <i>vs.</i> exact evolution of the covariances of three turbulent drift waves. . . . .  | 209 |
| V.42 | Correctly scaled results, obtained using Eq. (V.25), that correspond to Fig. 8 of Koniges and Leith [1987]. . . . .  | 210 |
| V.43 | Quasistationary EDQNM <i>vs.</i> exact solution obtained using Eq. (III.19) and corresponding to the case of Fig. V.42. . . . .  | 211 |
| V.44 | Realizable EDQNM <i>vs.</i> exact solution corresponding to the case of Fig. V.42. . . . .   | 211 |
| V.45 | RMC <i>vs.</i> exact solution corresponding to the case of Fig. V.42. . . . .  | 212 |
| V.46 | DIA <i>vs.</i> exact solution corresponding to the case of Fig. V.42. . . . .  | 213 |
| V.47 | Normalized two-time covariances $\mathcal{C}_k(\tau)/\mathcal{C}_k(0)$ <i>vs.</i> $\tau$ evaluated at $t = 15$ for the turbulent drift-wave case. . . . .  | 214 |
| V.48 | DIA response function $R_k(\tau)$ <i>vs.</i> $\tau$ evaluated at $t = 15$ for the turbulent drift-wave case. . . . .   | 214 |
|      |  |     |
| VI.1 | Initial relaxation of the inviscid Hasegawa-Mima problem to the equilibrium solution Eq. (VI.2). Since this problem is isotropic, the equilibrium curves for the three wavenumber angles coincide. . . . . | 220 |
| VI.2 | Final relaxation of the inviscid Hasegawa-Mima problem to the equilibrium solution Eq. (VI.2). . . . .   | 220 |
| VI.3 | Evolution of the quadratic quantities $E$ , $U$ , and $P$ [Eqs. (VI.5)] for two-dimensional fluid turbulence. . . . .  | 223 |
| VI.4 | Saturated energy spectrum of two-dimensional fluid turbulence. . . . .   | 224 |
| VI.5 | Logarithmic slope of the energy spectrum in Fig. VI.4. . . . .   | 224 |

---

|       |   |     |
|-------|---|-----|
| VI.6  | Corrected logarithmic slope of the energy spectrum in Fig. VI.4. . . . .  | 225 |
| VI.7  | Saturated energy spectrum for two-dimensional fluid turbulence with hyperviscosity. . . . .                                       | 227 |
| VI.8  | Logarithmic slope of the energy spectrum in Fig. VI.7. . . . .  | 227 |
| VI.9  | Corrected logarithmic slope of the energy spectrum in Fig. VI.7. . . . .  | 228 |
| VI.10 | Energy transfer for the spectrum given in Fig. VI.4. . . . .  | 230 |
| VI.11 | Enstrophy transfer for the spectrum given in Fig. VI.4. . . . .   | 230 |
| VI.12 | Linear growth rate defined in Eq. (VI.9). . . . .   | 233 |
| VI.13 | Frequency $k_y V_d/k^2$ used in the short-wavelength Hasegawa-Mima problem. . . . .   | 233 |
| VI.14 | Comparison of the time evolution of quadratic quantities predicted by the RMC and conventional numerical simulation. . . . .      | 234 |
| VI.15 | Comparison of the time evolution of quadratic quantities predicted by the RMC and a second realization of the simulation. . . . . | 235 |
| VI.16 | Comparison of the steady-state energy spectra predicted by the RMC and conventional numerical simulation. . . . .                 | 235 |
| VI.17 | Energy spectra predicted by the RMC and second realization of the simulation. . . . .   | 236 |
| VI.18 | Logarithmic slope of the RMC energy spectrum in Fig. VI.16. . . . .   | 237 |
| VI.19 | Corrected logarithmic slope of the RMC energy spectrum in Fig. VI.16. . . . .   | 237 |
| VI.20 | Anisotropy of the energy spectrum of Fig. VI.16. . . . .  | 238 |
| VI.21 | Three-dimensional view of the energy spectrum of Fig. VI.16. . . . .  | 239 |
| VI.22 | Energy transfer for the RMC prediction in Fig. VI.16. . . . .   | 240 |
| VI.23 | Enstrophy transfer for the RMC prediction in Fig. VI.16. . . . .  | 240 |
| VI.24 | Typical correlation function data obtained by initializing the DIA with the spectrum of Fig. VI.16. . . . .                       | 241 |
| VI.25 | Typical response function data obtained by initializing the DIA with the spectrum of Fig. VI.16. . . . .                          | 242 |
| VI.26 | Three-dimensional view of the growth rate used by Waltz. . . . .  | 243 |
| VI.27 | Three-dimensional view of the frequency function $ik_y V_d/(1+k^2)$ . . . . .   | 244 |
| VI.28 | RMC evolution of the quadratic invariants for Waltz's problem. . . . .  | 245 |
| VI.29 | Root-mean-square DIA amplitude level averaged over $k_x$ for Waltz's problem. . . . .   | 246 |
| VI.30 | Typical correlation function data obtained by applying the DIA to Waltz's case. . . . .   | 247 |

---

|       |  |     |
|-------|--|-----|
| VI.31 | Typical response function data obtained by applying the DIA to Waltz's case. . . . .   | 248 |
| VI.32 | Relaxation of the inviscid Terry-Horton problem to the equilibrium solution Eq. (VI.11). The anisotropic mode-coupling leads to different equilibrium curves for each angle. . . . . | 249 |
| VI.33 | Wavenumber bin geometry used for Horton's problem. . . . .   | 252 |
| VI.34 | Three-dimensional view of the growth rate used by Horton. . . . .  | 253 |
| VI.35 | Three-dimensional view of the frequency used by Horton. . . . .  | 254 |
| VI.36 | Two-dimensional cross sections of the growth rate used by Horton. . . . .  | 255 |
| VI.37 | Two-dimensional cross sections of the frequency used by Horton. . . . .  | 255 |
| VI.38 | Evolution of the quadratic quantities for Horton's problem. . . . .  | 256 |
| VI.39 | Saturated RMC energy spectrum for Horton's problem. . . . .  | 256 |
| VI.40 | Logarithmic slope of the energy spectrum in Fig. VI.39. . . . .  | 257 |
| VI.41 | Energy transfer underlying the spectrum given in Fig. VI.39. . . . .   | 257 |
| VI.42 | Enstrophy transfer underlying the spectrum given in Fig. VI.39. . . . .  | 258 |
| VI.43 | Transfer of the nonlinear invariant $W$ for the spectrum of Fig. VI.39. . . . .  | 258 |
| VI.44 | Anisotropy of the energy spectrum of Fig. VI.39. . . . .   | 259 |
| VI.45 | Three-dimensional view of the energy spectrum of Fig. VI.39. . . . .   | 260 |
| VI.46 | DIA energy spectrum for Horton's problem. . . . .  | 261 |
| VI.47 | Typical correlation function data obtained by applying the DIA to Horton's case. . . . .   | 262 |
| VI.48 | Typical response function data obtained by applying the DIA to Horton's case. . . . .  | 263 |
| VI.49 | Scaling of $\hat{\eta}_k$ vs. $k$ for Horton's problem. Logarithmic axes are used whenever $\text{Re } \hat{\eta}_k$ is strictly positive. . . . .                                   | 264 |
| VI.50 | Diffusion coefficient and square of the $\mathbf{E} \times \mathbf{B}$ velocity per unit wavenumber. . . . .   | 266 |
|       |  |     |
| H.1   | DIA vs. exact evolution of the entropy of the three-wave system considered in Fig. V.2. . . . .  | 297 |
| H.2   | EDQNM vs. exact evolution of the entropy of the three-wave system considered in Fig. V.2. . . . .  | 301 |
| H.3   | RMC vs. exact evolution of the entropy of the three-wave system considered in Fig. V.2. . . . .  | 302 |

# List of Tables

|      |   |     |
|------|---|-----|
| I.1  | Hierarchy of several important theories of turbulence. . . . .  | 46  |
| IV.1 | Triangle volume fractions $\bar{v}(i, j)$ for the isotropic problem of Leith and Kraichnan. . . . .   | 146 |
| IV.2 | Exact values $\bar{s}_{\text{exact}}(i, j)$ of the subsidiary correction factors used by Leith and Kraichnan. . . . .   | 147 |
| IV.3 | True corrections $\bar{s}_{\text{actual}}(i, j)$ obtained by properly averaging both $(\mathbf{z} \cdot \mathbf{p} \times \mathbf{q})^2$ factors over each bin. . . . . | 147 |
| VI.1 | Variation of the steady-state spectrum of forced anisotropic turbulence as the number of radial bins is increased. . . . .  | 251 |
| VI.2 | Computation statistics for the three geometries in Table VI.1. . . . .  | 251 |

# Preface

## Guide to this thesis

This thesis contains seven chapters. The first two chapters review background information for the reader who is not acquainted with plasma turbulence theory or the topic of statistical closures. The original material begins in Chapter III; the reader who is already familiar with statistical closures might wish to turn there now to learn about the difficulties that arise when the eddy-damped quasinormal Markovian closure (EDQNM) closure is applied to the turbulence of interacting waves. There, the reader will encounter the most important contribution of this work: the development of the realizable Markovian closure (RMC).

The reader who is primarily interested in numerical techniques for implementing statistical closures for *anisotropic* turbulence will wish to focus on Chapter IV. Here, an important technique of anisotropic wavenumber partitioning is developed to reduce the number of required statistical modes. The code DIA, which was used to perform the numerical computations in this work, is also described.

Chapters V and VI discuss the application of these tools to the problem of three interacting waves and to anisotropic drift-wave turbulence, respectively. A comprehensive outline of the contributions of this work is presented in Chapter VII.

## Acknowledgements

First of all I would like to express my sincere thanks to John Krommes, my thesis advisor, without whom this work would have not been possible. The constant guidance and wisdom he lent to this project is gratefully acknowledged, in addition to the kindness and encouragement he has given me during my entire graduate career. I am indebted to him for educating me in the theory of turbulence, particularly in the topic of statistical closures. His extensive theoretical contributions and careful reading of many early drafts of this thesis no doubt have left a very positive mark on it. I particularly admire his devotion to the educational process, which manifests itself in many ways, including countless hours of time spent in discussion of

mathematical and physical insights, in classroom instruction, and in his personal interest in the well-being of his students.

I would also like to acknowledge the contributions of Maurizio Ottaviani, who was a central figure in this project. His insights into the physics issues and his thoughtful analysis were extremely helpful throughout our attempts at developing a realizable Markovian closure. I am especially indebted to him for pointing out the importance of covariance for multiple-field closures and for the instructive advice he provided after carefully reading a draft of this work.

I must also express my gratitude to the Principal Readers of this dissertation. These were Neil Pomphrey, whose experience with the three-wave problem and stochasticity was very useful, and Steven Orszag, whose expertise in analytic theories of turbulence and the EDQNM was most relevant. They both offered important suggestions that resulted in significant improvements in the quality and focus of this thesis. It is clear that they devoted considerable effort to reading the lengthy manuscript.

Also, I would like to acknowledge the contributions made to the analysis of the three-wave problem by Shayne Johnston and Harry Mynick. I thank Robert Kraichnan for his comments on multiple-field conservation laws and Carl Oberman for his participation in a number of enlightening discussions. Thanks is also due to Charles Karney, David Coster, and many others involved in the support of the local computer resources used to write this dissertation. The faculty and graduate students at the Princeton University Plasma Physics Laboratory deserve a collective thanks for many enjoyable educational interactions.

The encouragement and generous support of my parents and my sister Ann is gratefully acknowledged, along with the kindness and devotion of my friends. Finally, my greatest thanks goes to Eva Garrouette, especially for her love, patience, and emotional support during this long endeavour. Eva wishes that I had named something after her; therefore, for her sake, think of the realizable Markovian closure (RMC) as the eddy viscosity approximation (EVA).

# Chapter I

## Introduction

Turbulence is a ubiquitous phenomenon. We encounter it in the weather systems circulating around planets, in fluid emitted from a nozzle, in a rising smoke plume, on a rough airplane ride, and in the chaotic flow of white-water rapids. The problem of turbulence, particularly the problem of predicting the drag on a body moving through a fluid, has occupied the attention of scientists for centuries. Even today, this problem remains one of the most elusive yet fascinating unsolved puzzles of science. There are vital interests, both scientific and engineering, in understanding and reducing the detrimental effects of enhanced turbulent drag or diffusion in a wide range of applications. Our modern interests in energy-efficient transportation, in accurate weather forecasting, in the prediction of large-scale ocean movements, in global climate modeling, and in magnetic fusion attach an even greater importance to the problem of turbulence.

Despite the intense effort that, over the years, has been devoted to an understanding of turbulence, only limited progress has been made toward the development of a satisfactory mathematical theory. The principal difficulty is not a lack of understanding of the equations of motion for the individual particles comprising the fluid. Indeed, for most applications the particles may be treated classically and their trajectories described by Newton's laws of motion. However, it is an impossible task, practically speaking, to solve these equations simultaneously for the large collection of interacting particles one finds in a macroscopic fluid. Fortunately, we would be content with a description of the evolution of a fluid much less detailed than at the level of particle trajectories. By averaging over all particles in a fluid element, one can often manage with a simpler *fluid description* such as the Navier-Stokes equations.

For a flow with sufficiently small velocities, the motion is *laminar* and can be readily analyzed by perturbation analysis of the Navier-Stokes equations. However, if the flow involves high velocities, the motion becomes *turbulent*, or highly chaotic.

While the Navier-Stokes equations provide, in principle, an adequate model for the behaviour of such a fluid, a new difficulty enters. One finds that the solution of these equations for this case requires so many Fourier harmonics (or other orthogonal functions) that the problem again becomes intractable, both analytically and numerically. For example, Orszag [1970] estimates that solution of highly developed turbulence can require on the order of  $10^{20}$  numerical operations!

Thus, to this day much of our quantitative knowledge of turbulence is empirical. Unfortunately, the experimental database is limited since it is difficult to make the necessary measurements even in controlled laboratory systems, let alone in the turbulent systems of the real world. Turbulence experiments are particularly hard to repeat with the same initial conditions. Until we have a better understanding, it is also not clear which parameters are important and which measurements should be made. Numerical simulation of turbulent systems has become a popular alternative to costly experiments since the advent of the supercomputer, but for the foreseeable future the resolution of even these advanced machines will be insufficient to discern the fine-scale features of fully developed turbulence.

Moreover, both experiments and simulations can at best characterize a series of isolated examples of turbulence that are very difficult to describe within a unified framework. What we lack is the predictive power of an analytic theory. Such a theory would be of great importance not only as a basic scientific achievement but also as a means toward economic optimization of many man-made systems that are subject to turbulent effects. The development of such a theory is the central challenge of turbulence research.

Because the full solution to the exact equations for the particle trajectories or even to the approximate Navier-Stokes equations for the fluid elements is intractable, it is clear that we must be content with further approximations. Putting it differently, perhaps we are asking for too much information. In a highly chaotic fluid the motions are so random that it may not be meaningful or useful to solve for the instantaneous velocity of each fluid element. After all, since one cannot set the initial conditions of an experiment with infinite precision, the extreme sensitivity to initial conditions exhibited by turbulent systems [Lichtenberg and Lieberman 1983] makes it virtually impossible to repeat individual realizations. Perhaps only low-order moments, such as the *average* or *mean square* of the fluid velocity over all possible realizations (subject to statistical constraints on the initial conditions, e.g. specified mean energy) are relevant.

In this work, we take the approach just suggested. We study evolution equations for statistical moments of the fundamental variables rather than for their instantaneous, realization-dependent values. However, the averaging of a nonlinear equation introduces another difficulty, known as the closure problem: the evolution equation for the statistical moments at each order involves higher-order moments.

The impossibility of solving the resulting unclosed, infinite hierarchy of moment equations is circumvented in various ways with closure approximations. The resulting set of approximate but closed equations is known as a *statistical closure*. While for most problems statistical closures still require numerical computation, in some circumstances they have clear computational advantages over conventional numerical simulation of the primitive equations. In addition, statistical closures give more insight into the details of the nonlinear interaction mechanisms than do straightforward numerical simulations and in this sense they are closer to the desired goal of an analytical theory. We investigate several examples of closures, particularly a new closure appropriate for problems involving linear wave phenomena. These approximations are well-suited for two problems of interest to the plasma physics community. The first application is the Hasegawa-Mima equation for drift waves; the second is a simple two-field fluid model of the  $\eta_i$  mode. Both of these waves are present in tokamak fusion reactors and are possible candidates for the observed enhanced particle and energy transport in these machines. To test the validity of statistical closures and to demonstrate the numerical technique, we compare the closure approximations against numerical simulations for the drift-wave problem, obtaining remarkable agreement. Many further applications of the methods described in this work will be possible and, we hope, forthcoming.

This chapter begins with an introduction to some elementary concepts of fluid turbulence. We then motivate our study of plasma turbulence in the larger context of a research program aimed at developing controlled thermonuclear fusion. Building upon the important concept of local transfer in wavenumber space, we relate a simple model for drift waves to the classical problem of two-dimensional turbulence. Next, so that we may eventually compute the transport coefficients associated with the drift instability, we introduce the tools necessary for a statistical treatment of turbulence. Finally, we review the history of several important analytical theories of plasma turbulence.

## I.A Fluid turbulence

Much of the work in turbulence, both experimental and theoretical, has been performed in the context of neutral fluids. Our own work has been heavily influenced by both the successes and failures of the theory of neutral fluid turbulence. Therefore, let us now review the fundamentals of the turbulence associated with the incompressible Navier-Stokes equation:

$$\frac{\partial}{\partial t} \mathbf{u} + \mathbf{u} \cdot \nabla \mathbf{u} = -\frac{1}{\rho} \nabla P + \mu \nabla^2 \mathbf{u}. \quad (\text{I.1})$$

Here  $\rho$  is the fluid mass density,  $P$  is the pressure, and  $\mu$  is the kinematic viscosity. The velocity  $\mathbf{u}(\mathbf{x}, t)$  is the velocity of the fluid element located, at time  $t$ , at a point  $\mathbf{x}$  fixed in the laboratory frame. This function is known as the *Eulerian* velocity. There is another representation,  $\mathbf{u}(\mathbf{x}(t), t)$ , which is known as the *Lagrangian* velocity. This is the velocity of a fluid element that is located, at time  $t$ , at a point  $\mathbf{x}(t)$  moving with the fluid. The relation between the Lagrangian  $d/dt$  and Eulerian  $\partial/\partial t$  time derivatives of the velocity (or any other quantity) is a consequence of the Chain Rule:

$$\frac{d\mathbf{u}}{dt} \doteq \frac{d\mathbf{u}(\mathbf{x}(t), t)}{dt} = \frac{\partial}{\partial t}\mathbf{u}(\mathbf{x}, t) + \mathbf{u}(\mathbf{x}, t) \cdot \nabla \mathbf{u}(\mathbf{x}, t),$$

where we note that  $\partial\mathbf{x}(t)/\partial t$  is just the Eulerian velocity  $\mathbf{u}(\mathbf{x}, t)$ . We see that the operator on the left-hand side of Eq. (I.1) is just the (total) derivative of the velocity in the frame of the moving fluid.

Implicit in Eq. (I.1) is the assumption of incompressibility:

$$\frac{d\rho}{dt} \doteq \frac{\partial\rho}{\partial t} + \mathbf{u} \cdot \nabla \rho = 0,$$

which, from the continuity equation

$$\frac{d\rho}{dt} + \rho \nabla \cdot \mathbf{u} = 0,$$

is equivalent to the assumption  $\nabla \cdot \mathbf{u} = 0$ . This is a good assumption for fluid velocities well below the sound speed.

The last term in Eq. (I.1) is dissipative, but because of the derivative operators appearing in it this term plays a role only at the smallest spatial scales. In the absence of dissipation and under the assumption of an initially uniform mass density, the incompressible Navier-Stokes equation reduces to the Euler equation, which conserves the *energy*, or mean-squared velocity (we adopt units for which the total mass is unity):

$$E \doteq \frac{1}{2} \int d\mathbf{x} |\mathbf{u}(\mathbf{x}, t)|^2. \quad (\text{I.2})$$

By defining the vorticity,

$$\boldsymbol{\omega} \doteq \nabla \times \mathbf{u},$$

we can write Eq. (I.1) in an alternate form in which the pressure does not appear explicitly:

$$\frac{\partial}{\partial t}\boldsymbol{\omega} + \mathbf{u} \cdot \nabla \boldsymbol{\omega} = \boldsymbol{\omega} \cdot \nabla \mathbf{u} + \mu \nabla^2 \boldsymbol{\omega}. \quad (\text{I.3})$$

In the absence of dissipation, this equation states that in the frame of the moving fluid the vorticity is driven only by the term  $\boldsymbol{\omega} \cdot \nabla \mathbf{u}$ . For two-dimensional flows this term vanishes since  $\boldsymbol{\omega}$  must then be perpendicular to the plane of motion. For

these flows the vorticity is conserved in the moving frame, imposing an additional constraint on the motion. The characters of two- and three-dimensional turbulence are therefore quite different and will be discussed separately.

There is much numerical and empirical evidence demonstrating the existence of long-lived *vortex structures* in turbulent flows. Vortex structures are often termed *coherent* because they appear to persist much longer than expected in a completely chaotic flow. Their lifetimes are much longer than the time it takes for a typical eddy to be distorted by interaction with the background turbulence. This latter time is known as the *eddy turnover time* and can be estimated as  $\tau_{\text{eddy}} \doteq \ell/u$ , where  $\ell$  is a measure of the eddy size and  $u$  is its velocity relative to the surrounding fluid. The qualifier “turnover” reminds us that this is the typical rotation time of an eddy.

The existence of coherent structures has caught the attention of modern turbulence researchers since these *may* play an important role in transport processes (e.g., see Scott *et al.* [1991]). Unfortunately, the statistical methods to be considered in this work are generally not well suited for describing the details of higher-order correlations like these; this is one of the principal limitations of statistical closures. However, the extent to which these structures play a role is still not known; while investigation of them is essential, there is also great utility in considering statistical methods, which can provide analytical insight into the turbulent interactions. These methods should be thought of as tools for describing turbulence, bearing in mind that the use of low-order statistics alone may not necessarily tell the whole story.

In studying turbulence, it is useful to consider scalings with dimensionless parameters. The obvious dimensionless parameter here is the Reynolds number, a measure of the typical ratio of the nonlinear terms in Eq. (I.3) to the linear term:

$$R = \frac{UL}{\mu},$$

where  $U$  and  $L$  represent the characteristic velocity and length scales, respectively, of the flow. The utility of the Reynolds number is that a whole family of flows having the same numerical value of  $R$  will exhibit the same turbulent behaviour. One can map the solution of one member exactly onto another by rescaling the velocity, length, and viscosity.

Experimentally, it is found that as  $R$  is gradually increased from zero there is a critical value at which the behaviour of the flow changes markedly from a laminar state, well described by linear theory or weak perturbation theory, to a highly chaotic turbulent state. Theoretical turbulence research is concerned with the development of a mathematical description for the statistical properties of the latter state. A useful review of the statistical theory of fully developed turbulence is found in Rose and Sulem [1978]. The extensive treatise of Monin and Yaglom [1965] is also recommended.

### I.A.1 Three-dimensional fluid turbulence

In three-dimensional turbulence, the term  $\boldsymbol{\omega} \cdot \nabla \mathbf{u}$  is responsible for *vortex stretching*, a phenomenon that cannot occur in two-dimensional models. The vorticity is drawn out into thin filaments that are observed both experimentally and numerically. The vortex-stretching mechanism has been used to formulate heuristic models [Saffman 1970] of *intermittency*, the observation that turbulence is not completely space-filling at all scales. These theories postulate that repeated and stochastically distributed stretching is responsible for the observed intermittency in the vorticity. The possibility of vortex stretching has also raised the question as to whether Eq. (I.3) can lead to singularities in a finite time when the viscosity  $\mu$  vanishes; it is therefore of interest to assess the dynamic alignment of  $\boldsymbol{\omega}$  with the principal axis of the mean rate of strain tensor,  $\frac{1}{2}[\nabla \mathbf{u} + (\nabla \mathbf{u})^T]$ . Furthermore, it is believed that eddies with such an alignment are the most effective in extracting energy from the mean flow [Tennekes and Lumley 1972, pg. 41].

One of the great successes of turbulence theory has been in the modeling of the energy spectrum. Typically, energy is forced into the large spatial scales of Eq. (I.1) by a stirring apparatus<sup>1</sup> or through the boundary conditions. The energy spectrum is observed to exhibit a power-law decay with respect to increasing Fourier wavenumber  $k$  (decreasing spatial scales) until linear viscous damping becomes dominant and the turbulence is dissipated into heat. The intermediate spatial scales where neither energy production nor dissipation occur constitute the *inertial range*.

Kolmogorov [1941] presented a simple argument to describe the energy spectrum in the inertial range. He imagined that the *rate* of energy transfer from large to smaller scales is a constant  $\epsilon$  independent of scale size. If we define  $E(k)$  to be the energy contained in scales with wavenumber  $k$  such that  $E = \int_0^\infty dk E(k)$ , we can use dimensional analysis to find possible power-law behaviours of  $E(k) \sim \ell E$  with respect to  $\epsilon$  and  $k$ , using  $\ell$  and  $t$  to represent the dimensions of length and time:

$$\ell E \sim \epsilon^\alpha k^\beta,$$

$$\ell \left( \frac{\ell^2}{t^2} \right) \sim \left( \frac{\ell^2}{t^3} \right)^\alpha \ell^{-\beta}.$$

Immediately we conclude that  $\alpha = 2/3$  and  $\beta = -5/3$ , so that

$$E(k) = C_K \epsilon^{2/3} k^{-5/3}, \quad (\text{I.4})$$

where  $C_K$  is called the Kolmogorov constant. The Kolmogorov law turns out to be a remarkably good fit to experimental data. Empirically  $C_K$  is found to be about 1.5. Intermittency effects have been thought for some time to result in corrections to

---

<sup>1</sup>This stirring motion is often modeled by the addition of a random force to the right-hand side of Eq. (I.1).

Eq. (I.4) [Kolmogorov 1962, Kraichnan 1974] that become increasingly significant for inertial-range exponents corresponding to higher-order moments [She and Orszag 1991]. However, She *et al.* [1991] believe that these intermittency corrections do not enter the energy spectrum; the  $-5/3$  exponent in Eq. (I.4) is now considered to be exact [Orszag 1991]. The Kolmogorov assumption that the inertial-range energy transfer is local to the inertial range and occurs at a rate independent of wavenumber implies that there is an energy *cascade* from large scales to small scales.

## I.A.2 Two-dimensional fluid turbulence

Turbulence in two dimensions is complicated by the fact that in the absence of dissipation there is an additional conserved quantity. This is the *enstrophy*, or mean-squared vorticity:

$$U \doteq \frac{1}{2} \int d\mathbf{x} |\boldsymbol{\omega}(\mathbf{x}, t)|^2. \quad (\text{I.5})$$

The effect of this second invariant is nontrivial. For example, the energy cascade of three-dimensional turbulence to the very shortest wavelengths cannot occur without violating Eq. (I.5) since relative to Eq. (I.2) the enstrophy is *dominated* by contributions from smaller scales. An energy cascade would eventually cause these enstrophy contributions to exceed the total enstrophy in the system! The only possibility is that there is a direct *enstrophy* cascade from the wavenumbers of energy input to the dissipation range and an *inverse* energy cascade from the input range to the longer wavelengths [Kraichnan 1967]. This scenario is known as the *dual cascade*. Unless there is some dissipation mechanism at the long wavelengths, energy will simply pile up there.

One can apply the Kolmogorov argument separately to each inertial range to discover that, as in the three-dimensional case, the energy inertial range has the form

$$E(k) = C_K \epsilon^{2/3} k^{-5/3}, \quad (\text{I.6})$$

while for wavenumbers higher than those in the injection range there is an enstrophy inertial range of the form

$$E(k) = C'_K \zeta^{2/3} k^{-3}, \quad (\text{I.7})$$

where  $\zeta$  is the rate of enstrophy injection. However, Eq. (I.7) implies a logarithmically divergent total enstrophy. This led Kraichnan [1967, 1971a] to propose the corrected form

$$E(k) = C'_K \zeta^{2/3} k^{-3} \left[ \log \left( \frac{k}{k_1} \right) \right]^{-1/3}, \quad (\text{I.8})$$

where  $k_1$  is the (highest) wavenumber of enstrophy injection.

There is much controversy in the literature in regard to the enstrophy inertial range. In numerical simulations it is found that initial conditions have a great influence on the locality argument on which the Kolmogorov law is based [Benzi *et al.* 1990].

Another feature unique to two-dimensional turbulence is that the incompressibility condition  $\nabla \cdot \mathbf{u} = 0$  implies (assuming the interchangeability of second-order derivatives) the existence of a *stream function*  $\psi$  such that

$$\mathbf{u} = \mathbf{z} \times \nabla \psi,$$

where  $\mathbf{z}$  is perpendicular to the plane of motion. The vorticity then becomes  $\boldsymbol{\omega} = \mathbf{z} \nabla_{\perp}^2 \psi$ , allowing Eq. (I.3) to be written as a vorticity evolution equation:

$$\left( \frac{\partial}{\partial t} + \mathbf{u} \cdot \nabla \right) \nabla_{\perp}^2 \psi = \mu \nabla_{\perp}^2 \nabla_{\perp}^2 \psi. \quad (\text{I.9})$$

In our study of hydromagnetic turbulence, we will assume that the magnetic field is sufficiently strong so that a reduced description of the motion in the two-dimensional surface perpendicular to the magnetic field is adequate. The motion along the field line is essentially that of free streaming particles and it does not directly contribute to radial diffusion. In fact, we will consider a simple model of plasma turbulence that is remarkably similar to the above equation for two-dimensional Navier-Stokes turbulence. It differs from the above equation only by the addition of a linear term that models both oscillatory (wave-like) behaviour (not present in the incompressible Navier-Stokes linearity) and growth phenomena. This provides a mechanism for the addition of energy into the system without the need for an external stirring force.

Two-dimensional turbulence is also a good approximation for problems encountered in meteorology and oceanography since the thickness of the atmosphere and ocean is far smaller than that of the other two dimensions.<sup>2</sup> In these problems, one also has wave-like effects entering the linear term; thus, we will eventually wish to make contact with the substantial geophysical literature that has been written on this subject.

## I.B Plasma turbulence

The quest for a virtually unlimited, safe, and relatively clean source of energy has been the driving force behind fusion research ever since 1951–2, when classified

<sup>2</sup>More precisely, it is the gravitational stratification of the atmosphere that makes it a two-dimensional problem.

projects to develop a controlled thermonuclear fusion reactor were begun at four national laboratories in the United States and at other laboratories around the world. It was known then that fusion of a deuteron and a triton required overcoming the immense repulsive Coulomb force between them, and the only energy-efficient way of doing this appeared to require the creation of an extremely high-temperature plasma, thus mimicking solar fusion in the laboratory. Unfortunately, the gravitational fields available in the sun for confinement cannot be created in the laboratory; it was hoped instead that magnetic confinement of the charged nuclei would be possible.

Initially it was thought that a hot plasma could be confined by a straight magnetic field for a time sufficiently long that more than enough fusion reactions would occur to justify the energy spent to heat the plasma to the reaction temperature. However, it was soon found that particle losses at the ends of these straight pinch machines were disastrous for confinement. It became clear that these end losses had to be eliminated; in the most successful schemes, this was achieved by bending the magnetic field and the surrounding vessel into a torus. But the resulting centrifugal forces and the nonuniformity of the toroidal magnetic field caused the particles to drift upward from the circular magnetic flux surfaces unless a poloidal twist was added to the magnetic field. Two schemes were proposed for doing this: the *stellarator*, with an externally induced twist; and the *tokamak*, with an internally induced twist. Soviet success with the tokamak in 1968 at achieving record high temperatures emphasized its distinct advantage: the same current used to generate the poloidal magnetic field served to heat the plasma. Unfortunately, this current also provides a free energy source for large-scale magnetohydrodynamic (MHD) instabilities that can lead to total disruption of the plasma.

Meanwhile, the theoretical community had been developing the ideal (non-resistive) MHD equations, which provided an excellent theoretical understanding of the large-scale and low-frequency behaviour of tokamak plasmas. According to the MHD theory, tokamaks can be operated in regimes of stable equilibrium. Unfortunately, although the tokamak can successfully suppress the large-scale instabilities, it is found that small-scale instabilities still remain. It is widely held that these instabilities are responsible for the observed enhancement of particle and energy transport relative to the levels expected based on simple classical calculations of diffusion due to infrequent particle collisions.

The goal of modern plasma turbulence theory is to understand this *anomalous transport*, with the ultimate objective of possibly controlling it. At present, the world's largest tokamaks may be nearing breakeven conditions (assuming that extrapolation to deuterium-tritium fusion holds), and even a relatively modest reduction of enhanced transport could make the difference between an economically viable reactor and an unsuccessful one. Thus, there is currently great interest in examining the historical progress made in fluid turbulence with an eye to possible

implications for plasma turbulence. This work closely follows certain methods developed for fluid turbulence and resolves serious difficulties that occur when they are applied to plasma problems.

Let us first describe one of the more popular candidates for the underlying small-scale instability thought to be responsible for anomalous transport.

### I.B.1 Drift-wave turbulence

Drift waves are low-frequency disturbances driven by gradients in the density profile of a plasma. Since a density gradient is inherent in any scheme that confines the plasma away from the walls, the free-energy source for the drift wave is universally present. Hence this instability is sometimes known as the *universal instability* [Krall 1968].

#### Fluid equations:

In their purest form, drift waves are simple electrostatic oscillations with no growth rate. We now give a derivation of a fluid description using the gyrokinetic formalism [Dubin *et al.* 1983], in which all quantities are evaluated at the gyrocenters (the orbit-averaged particle positions) rather than at the instantaneous particle positions. We will denote the *perturbed* density of ion gyrocenters by  $n_i$ . A more elementary derivation in the laboratory frame is given in Appendix A.

The phase velocity of drift waves is intermediate between the ion and electron thermal velocities ( $v_{ti} \ll \omega/k_{\parallel} \ll v_{te}$ ). We therefore treat the ions as a fluid and the electrons as nearly adiabatic.<sup>3</sup> Also, because of their low frequency, we may consider drift waves to be quasineutral, which means that the perturbed densities of ions and electrons are equal at each position in the *laboratory* frame.

We normalize the variables as follows:

$$\begin{aligned}\bar{x} &\doteq \rho_s x, \\ \bar{t} &\doteq \left(\frac{L_n}{c_s}\right)t, \\ \bar{v} &\doteq \left(\frac{\rho_s c_s}{L_n}\right)v, \\ \frac{e\varphi}{T_e} &\doteq \left(\frac{\rho_s}{L_n}\right)\Phi,\end{aligned}$$

---

<sup>3</sup>Here, adiabatic means that the electrons experience equilibrating (in the sense of Maxwell-Boltzmann) motion at a frequency *much greater* than the frequency  $\omega$  of the electrostatic disturbance.

where the barred variables and  $\varphi$  represent physical quantities. Here  $c_s \doteq \sqrt{T_e/m_i}$  is the sound speed and  $\rho_s \doteq c_s/\Omega_i$  (the “sound radius”) is the gyroradius the ions would exhibit if they were at the electron temperature  $T_e$ . The perturbed electrostatic potential is denoted by  $\varphi$ . In these dimensionless units, the diamagnetic velocity  $V_d$  is unity (although for emphasis we sometimes retain it explicitly). In the limit where the ion gyroradius  $\rho_i$  is much less than the density scale length  $L_n$ , the perturbed ion continuity equation can be written

$$\frac{\partial}{\partial t}n_i + V_d \frac{\partial \Phi}{\partial y} + \mathbf{V}_E \cdot \nabla n_i = 0. \quad (\text{I.10})$$

Quasineutrality is expressed by the gyrokinetic Poisson equation

$$\nabla_{\perp}^2 \Phi = -(n_i - n_e),$$

where the ion polarization effects<sup>4</sup> appear on the left-hand side. The  $\perp$  subscript on the Laplacian reminds us that only the projection of the gradients onto the plane perpendicular to the magnetic field contributes.

Because the electrons stream rapidly along the magnetic field lines, they nearly satisfy a Boltzmann distribution; thus, for small perturbations

$$n_e = (1 + i\chi'')\Phi,$$

where  $\chi''$  is an operator representing a nonadiabatic correction. If we define  $\chi \doteq -\nabla_{\perp}^2 + i\chi''$ , then

$$n_i = (1 + \chi)\Phi.$$

Also, the  $\mathbf{E} \times \mathbf{B}$  velocity is  $\mathbf{v}_E = -\nabla \Phi \times \mathbf{z}$ . Fourier transformation and use of the reality condition  $\Phi_{-\mathbf{k}} = \Phi_{\mathbf{k}}^*$  yields

$$(1 + \chi_{\mathbf{k}}) \frac{\partial}{\partial t} \Phi_{\mathbf{k}} = -ik_y V_d \Phi_{\mathbf{k}} + \sum_{\mathbf{k}+\mathbf{p}+\mathbf{q}=\mathbf{0}} \mathbf{z} \cdot (\mathbf{p} \times \mathbf{q}) (1 + \chi_{\mathbf{q}})^* \Phi_{\mathbf{p}}^* \Phi_{\mathbf{q}}^*.$$

Upon symmetrizing, we arrive at the Terry-Horton equation [Terry and Horton 1982, 1983]:

$$\boxed{\left( \frac{\partial}{\partial t} + \nu_{\mathbf{k}} \right) \Phi_{\mathbf{k}} = \frac{1}{2} \sum_{\mathbf{k}+\mathbf{p}+\mathbf{q}=\mathbf{0}} \mathbf{z} \cdot (\mathbf{p} \times \mathbf{q}) \frac{(\chi_{\mathbf{q}} - \chi_{\mathbf{p}})^*}{(1 + \chi_{\mathbf{k}})} \Phi_{\mathbf{p}}^* \Phi_{\mathbf{q}}^*} \quad (\text{I.11})$$

where  $\nu_{\mathbf{k}} = ik_y V_d / (1 + \chi_{\mathbf{k}})$ . The adiabatic limit ( $\chi_{\mathbf{k}} = k_{\perp}^2$ ) is the Hasegawa-Mima equation [Hasegawa and Mima 1977, 1978]. Since only the perpendicular component of the wavenumbers enters Eq. (I.11), we will often drop the  $\perp$  subscript on  $k_{\perp}$ .

<sup>4</sup>These effects arise from the variation of the electric field sensed by the ion as it moves along its gyro-orbit [Chandrasekhar 1960].

An important feature of this equation is that it has terms both linear and quadratically nonlinear in  $\Phi$ . When the linear term vanishes, the Terry-Horton equation conserves the invariant

$$W \doteq \frac{1}{2} \sum_{\mathbf{k}} |1 + \chi_{\mathbf{k}}|^2 |\Phi_{\mathbf{k}}|^2.$$

In the case of the Hasegawa-Mima equation, there are two invariants:

$$E \doteq \frac{1}{2} \sum_{\mathbf{k}} (1 + k^2) |\Phi_{\mathbf{k}}|^2;$$

$$U \doteq \frac{1}{2} \sum_{\mathbf{k}} k^2 (1 + k^2) |\Phi_{\mathbf{k}}|^2.$$

The quantity  $E$  is just the total electrostatic energy;  $U$  is the enstrophy, or mean-squared vorticity.

In the adiabatic limit Eq. (I.11) has no growth rate. However, kinetic effects such as ion-ion or ion-neutral collisions, ion Landau damping, the presence of magnetically trapped particles, and coupling to other modes (such as ion-acoustic waves) [Horton 1986] will typically result in both long- and short-wavelength damping and destabilization at intermediate wavelengths. In a fluid description, these effects may be phenomenologically modeled by the addition of a growth rate  $\hat{\gamma}_{\mathbf{k}}$  to the linear term of Eq. (I.11), so that  $\nu_{\mathbf{k}} = -\hat{\gamma}_{\mathbf{k}} + ik_y V_d / (1 + \chi_{\mathbf{k}})$ . When a nonadiabatic (imaginary) term is included in  $\chi_{\mathbf{k}}$ , growth (or damping) effects<sup>5</sup> also enter *via* the nonlinear term, as Terry and Horton [1982] have stressed.<sup>6</sup>

It is interesting to note that the Hasegawa-Mima equation has a striking similarity to an equation that appears in the oceanic and atmospheric physics literature. If one changes the  $1 + k^2$  factors to just  $k^2$ , (e.g., by considering the short-wavelength limit), the result is the conventional equation for Rossby waves [Holloway and Hendershott 1977], written here in  $x$  space:

$$\left[ \frac{\partial}{\partial t} + (\mathbf{z} \times \nabla \psi) \cdot \nabla \right] \nabla_{\perp}^2 \psi + \beta \frac{\partial \psi}{\partial x} = 0.$$

Here,  $\beta$  is  $L^2/U$  times the gradient of the Coriolis parameter  $2\Omega \sin \theta$ , where  $\theta$  is the latitude and  $\Omega$  is the rotation rate of the earth [Pedlosky 1979, pp. 81–84]. (The inclusion of other physical effects not considered here will add some sort of dissipation term.)

Rossby waves are large-scale disturbances in the atmosphere and ocean that are driven by the gradient in the mean-square potential vorticity. The gradient arises

<sup>5</sup>In our nomenclature, the growth rate may be of either sign: negative growth is equivalent to positive damping.

<sup>6</sup>This is often known as the  $i\delta$  model, where  $\delta \doteq \chi''$ .

from the variation of the Coriolis force with latitude, as opposed to the variation of the density with radial distance in a tokamak. Mathematically, the equations describing these very different phenomena are identical in the short-wavelength limit. In fact, if one accounts for the physical effect of changes in the free-surface elevation of a shallow fluid, which introduces a compressive component to the horizontal velocity, the correspondence becomes even closer. One obtains a factor  $c + k^2$  in place of the factor  $1 + k^2$  in the Hasegawa-Mima equation. This term arises in a derivation of the barotropic vorticity equation from the shallow-water equations in the quasigeostrophic limit [Pedlosky 1979, pp. 99–104].

### **Physical picture:**

In Fig. I.1, a simple scenario is indicated that illustrates the origin of the restoring force in a drift wave [Horton 1984]. In any confinement device, there must exist a density gradient. Let us assume that the temperature is uniform and choose a local Cartesian coordinate system with the pressure gradient in the  $x$  direction. In an equilibrium configuration, the  $\nabla P$  and  $\mathbf{E} \times \mathbf{B}$  forces must balance. Imagine that this equilibrium is disturbed, so that a high density region arises at small  $x$ , as depicted in Fig. I.1. The additional  $\nabla P$  force thereby leads to a diamagnetic drift of the ions in the negative  $y$  direction and of the electrons in the positive  $y$  direction. This charge separation establishes an electric field in the positive  $y$  direction. In turn, the resulting  $\mathbf{E} \times \mathbf{B}$  drift convects both ions and electrons from the high density region to the low density region. The  $\mathbf{E} \times \mathbf{B}$  drift therefore provides for a restoring force that allows the medium to sustain electrostatic waves.

If the electrons are adiabatic, they will quickly move to overcome the electric field perturbation and one finds that the resulting disturbance is strictly oscillatory: in its purest form, the drift wave cannot grow or decay. However, the introduction of a small nonadiabatic component to the electrons (a kinetic effect) is sufficient to generate a linear instability.

## **I.B.2 Eta-i mode turbulence**

The linear restoring term in drift waves arises fundamentally as a result of a pressure gradient. In the derivation of the drift-wave oscillation, we assumed that the temperature was uniform. However, in tokamaks the temperature gradients are as important as density gradients. When both effects are present, the resulting instability is known as the  $\eta_i$  mode, named after the parameter  $\eta_i \doteq d \log T_i / d \log n$ . Because we now allow for both temperature and density fluctuations, we will need to incorporate a second equation into our model.



### I.B.3 Alternative mechanisms

Many other mechanisms have been proposed to explain anomalous transport in a tokamak. It is widely held that some form of turbulence is responsible, but there are many candidates for the basic instability. For example, in addition to drift waves and  $\eta_i$  modes destabilized by kinetic effects there are versions of these basic modes destabilized by magnetic trapping of electrons and ions.

Enhanced diffusion can also result from the breakdown of Kolmogorov-Arnold-Moser (KAM) surfaces in the presence of strong magnetic field perturbations. The stochasticity [Stix 1973, Krommes *et al.* 1983] could be due to microtearing modes [Drake *et al.* 1980] that are related to the large-scale resistive-MHD tearing instability. Another resistive-MHD candidate is the nonlinear rippling mode [Garcia *et al.* 1985]. However, this mode is usually discounted since it is linearly stable for the temperatures of modern tokamaks unless the effects of large impurity gradients are included, even though linear stability does not necessarily preclude nonlinear instability.

There are also mechanisms involving particle-wave resonances such as the fishbone instability [Chen *et al.* 1984]. In addition, there are explanations of anomalous transport that do not involve turbulence. An example is the effect of (stationary) field-line ripple resulting from the nonaxisymmetry inherent in real experimental devices [Mynick and Duvall 1989].

In this work we will focus our attention on turbulence as the fundamental cause of anomalous transport. In support of this explanation are the measurements of highly fluctuating density that have been obtained in the edge region of the TEXT tokamak [Ritz *et al.* 1987]. These measurements have been correlated with both measured and estimated levels of particle and energy transport; they indicate that tokamak transport may be the result of highly chaotic phenomena. Moreover, the observed electrostatic energy spectrum is broadband in frequency. Since this result is in marked contrast to linear theory, which predicts a line-like ( $\delta$  function) spectrum of normal modes, it seems clear that tokamaks operate in a strongly nonlinear regime. These observed disturbances are low frequency (typically 10 – 50 kHz), near the drift-wave frequency  $\omega_* \doteq k_y V_d$ , so it is reasonable to consider drift waves or  $\eta_i$  modes as the fundamental instability.

The importance of doing fully nonlinear calculations of plasma transport coefficients is gradually being recognized by the plasma physics community in view of mounting evidence that simpler quasilinear (perturbative) formulae can grossly overestimate transport phenomena [Tibone *et al.* 1990, Zarnstorff *et al.* 1990, Lee and Tang 1988, Ottaviani *et al.* 1990]. Currently, there is great interest in determining transport coefficients arising from nonlinear fluid equations. The present work serves as a paradigm for the approximate computation, via anisotropic statistical closures, of such coefficients. Regardless of which fundamental instability is actually

responsible for the turbulence, the emphasis of this work is on the development of the *tools* necessary for analyzing the resulting transport. We will also assess the ability of these tools to describe the statistics of a generic nonlinear model equation.

## I.C Stochastic processes

A stochastic process is a mathematical model of a random phenomenon that is controlled by probabilistic laws [Doob 1953]. Turbulence, the name we give to highly chaotic fluid behaviour involving the excitation of many orthogonal modes, would appear extremely well suited to being modeled by stochastic processes. This is true even though the underlying motion is in principle deterministic and time-reversible. We assume that the molecular motion can be treated classically by Newton's laws since the randomness to which we are referring has nothing to do with quantum uncertainty. It is a well-known result of many-body theory that, in the presence of many degrees of freedom and given imprecise initial conditions, systems can exhibit irreversibility and *apparent* indeterminism. More recently, nonlinear equations such as the coupled set of three interacting modes studied by Lorenz [1963] have established that even systems with few degrees of freedom can exhibit exponential sensitivity to initial conditions. Only if we know the initial conditions exactly can we predict the future evolution of such systems precisely. Of course, even then the computations required for turbulence problems would be virtually impossible to carry out and almost certainly will always remain so. For these reasons, we must be content with a statistical description of turbulence.

### I.C.1 Ensemble averages

It has already been emphasized that in the field of turbulence statistical averages are more relevant and useful than the individual values obtained in each realization. Experimental data always has an intrinsic minimum spatial and temporal extent associated with it; hence, it must represent a spatial and temporal average of the instantaneous values. It might be argued on this basis that a spatial or temporal average is the appropriate average upon which to formulate a theory of turbulence, but this requires the specification of a spatial or temporal interval over which to perform the integration. Moreover, upon repetition of the experiment the average obtained in this way could differ due to the fact that the macroscopic initial conditions do not uniquely determine the underlying microscopic configuration. What one is really interested in, it would seem, is a statistical average taken over all possible realizations of the experiment. This is known as the ensemble average. We

compute the ensemble average  $\langle f \rangle$  of any quantity  $f$  by

$$\begin{aligned}\langle f \rangle &= \int f d\mathcal{P} \\ &= \int f(\Gamma)P(\Gamma) d\Gamma,\end{aligned}$$

where  $\mathcal{P}$  is the probability *distribution* of each particular realization,  $\Gamma$  is a parameter uniquely labeling all distinct realizations, and

$$P(\Gamma) \doteq \frac{d\mathcal{P}}{d\Gamma}$$

is the probability *density* function (PDF) for each realization. In initial value problems, there is a one-to-one mapping between  $\Gamma$  and the set of all initial conditions, so that  $P$  is also the probability density function for initial conditions. The ensemble average is then an average over all possible initial conditions weighted by their relative probabilities.

Unfortunately, one does not often know the PDF for the initial conditions in a real experiment. A convenient assumption that facilitates mathematical analysis is that the initial conditions are Gaussianly distributed. That this is a natural choice for the initial conditions is sometimes motivated by the central limit theorem, which states (subject to some restrictions) that the sum of a large number of independent random variables (described by any PDF) is nearly normally distributed [Doob 1953]. However, the assumption of Gaussian statistics in the steady state is well known to be inconsistent with experimental measurements of the two-point velocity distribution in turbulent flows [Batchelor 1953]. Indeed, the Navier-Stokes equation will significantly modify the initial statistics as time evolves. Nevertheless, turbulence generally loses memory of the initial conditions so that the steady state should be independent of the exact prescription for the initial conditions. Generally, it is this steady-state situation that is physically interesting. Therefore, instead of relying on the central limit theorem, it is better to argue that the prescription of Gaussian initial statistics merely helps us pose a well-defined mathematical problem.

Note that we will refer to a variable as *random* if its value varies from realization to realization, and *nonrandom* (or statistically sharp) if it has the same value in all realizations.

## I.C.2 Linear stochastic processes

An elementary example of a stochastic process is the following linear system, known as a Langevin equation:

$$\boxed{\frac{\partial}{\partial t}\psi(t) + \eta(t)\psi(t) = f(t).} \quad (\text{I.13})$$

Here,  $\psi$  is a stochastic quantity whose time evolution we are interested in modeling. The linear damping factor  $\eta$  is a specified *nonrandom* function of time, while the forcing function  $f$  is a *random* function that drives the system. Langevin equations provide a mathematical description of the phenomenon of Brownian motion [Uhlenbeck and Ornstein 1930]. In this case  $\psi$  represents the velocity of a dust particle traveling through a background of air molecules. The dust particle experiences both a random bombardment by air molecules (represented by  $f$ ) and an average drag exerted on it by those same air molecules (represented by  $\eta$ ) as it travels through the medium.<sup>7</sup>

Since Langevin equations are linear in the stochastic variables one can readily solve for the evolution of the mean field:

$$\frac{\partial}{\partial t} \langle \psi(t) \rangle + \eta(t) \langle \psi(t) \rangle = \langle f(t) \rangle. \quad (\text{I.13})$$

Thus, given only the mean quantities  $\langle \psi(0) \rangle$  and  $\langle f(t) \rangle$  along with  $\eta(t)$ , one can solve for the future evolution of  $\langle \psi(t) \rangle$ . Higher moments of  $\psi$ , such as  $\langle \psi(t)\psi(t') \rangle$  can be obtained<sup>8</sup> by expressing quantities like  $\langle f(t)\psi(t') \rangle$  in terms of the Green's function of Eq. (I.13) and the (assumed known) statistical moments of  $f$ . This scenario would then provide as complete a picture as necessary for comparison with experiment. For equations like this that are linear in the random variables, stochasticity clearly presents no difficulty [Van Kampen 1976].

### I.C.3 Nonlinear stochastic processes

Let us now consider a stochastic process described by a nonlinear equation. In general the nonlinearity could be polynomial or even transcendental; however, in this work we will restrict our attention to equations with quadratic nonlinearities. The methods described here can, in principle, be generalized to handle higher-order nonlinearities [Hansen and Nicholson 1981, Sun *et al.* 1985a, 1985b, 1986], but we will find that quadratic nonlinearities lead to equations sufficiently complicated that we will focus on this case alone. Besides, this is the case that seems to appear most frequently in nonlinear problems.

To keep our discussion relatively general, we will study the following generic equation for the evolution of the stochastic variable  $\psi(\mathbf{x}_1, t)$  in a space with dimen-

---

<sup>7</sup>Because the physical origins of both  $f$  and  $\eta$  are ultimately the same, they are connected by an Einstein relation involving the Avogadro number.

<sup>8</sup>Alternatively, elementary techniques may be used to solve the first-order linear differential equation Eq. (I.13) directly in terms of  $f$  and  $\eta$ ; the moments could then be computed directly from this solution.

sion  $d$ :

$$\begin{aligned} \frac{\partial}{\partial t} \mathcal{L}\psi(\mathbf{x}_1, t) + \int_{-\infty}^{\infty} d\mathbf{x}_2 \nu(\mathbf{x}_1, \mathbf{x}_2) \mathcal{L}\psi(\mathbf{x}_2, t) \\ = \int_{-\infty}^{\infty} \int_{-\infty}^{\infty} d\mathbf{x}_2 d\mathbf{x}_3 U(\mathbf{x}_1, \mathbf{x}_2, \mathbf{x}_3) \psi(\mathbf{x}_2, t) \psi(\mathbf{x}_3, t). \end{aligned} \quad (\text{I.14})$$

Here,  $\mathcal{L}$ ,  $\nu$ , and  $U$  are specified time-independent nonrandom operators. All of the stochasticity in this equation is *intrinsic*, in that it arises only from sensitivity to initial conditions and not from an external random source or random coefficient.

In this work we will restrict our attention to *statistically homogeneous* (but not necessarily isotropic) turbulence. This means that all ensemble-averaged quantities are invariant under spatial translations. This is a good approximation in ordinary fluid turbulence in regions far way from walls and where any externally imposed stirring forces are uniform. Unfortunately, homogeneity does not hold in a tokamak with a sheared magnetic field. Magnetic shear tends to stabilize drift waves, so a complete study of drift-wave turbulence should really account for this inhomogeneity. In principle, inhomogeneities can be handled by the statistical methods that this work considers [Similon 1981]; however, they add enormous computational complexity. This will be discussed in greater detail later, when we compare the relative computational feasibility of statistical methods *versus* straightforward numerical simulation of the primitive dynamical equations.

The philosophy adopted in this work is that an understanding of physical systems composed of many competing effects can most easily be understood by first considering the role of each effect in isolation. Only after this has been done should one attempt to consider more than one complexity at a time. The purpose of this work is not to provide a complete description of drift-wave turbulence in tokamaks; rather, it is to provide an understanding of the balance between linear and nonlinear terms arising from a stochastic differential equation. Only when this is correctly understood does it make sense to consider further complications such as inhomogeneity, kinetic formulations, and realistic tokamak geometry. Although our study of the statistically homogeneous problem might receive criticism from parts of the plasma physics community as being too simplistic, the idea of breaking complicated problems up into smaller, more manageable problems is hardly new. Indeed, this concept of *modularity* seems to be a recurrent theme under which much historical advance in science has occurred.

Occasionally, we will also impose the restriction that the turbulence be statistically *stationary*, which means that ensemble-averaged quantities are invariant under temporal translation. However, unless otherwise stated it will be assumed that the turbulence is statistically homogeneous but not necessarily stationary or isotropic.

The assumption of homogeneity allows Eq. (I.14) to be written

$$\begin{aligned} \frac{\partial}{\partial t} \mathcal{L}\psi(\mathbf{x}_1, t) + \int_{-\infty}^{\infty} d\mathbf{x}_2 \nu(\mathbf{x}_1 - \mathbf{x}_2) \mathcal{L}\psi(\mathbf{x}_2, t) \\ = \int_{-\infty}^{\infty} \int_{-\infty}^{\infty} d\mathbf{x}_2 d\mathbf{x}_3 U(\mathbf{x}_1 - \mathbf{x}_2, \mathbf{x}_1 - \mathbf{x}_3) \psi(\mathbf{x}_2, t) \psi(\mathbf{x}_3, t). \end{aligned} \quad (\text{I.15})$$

The convolutions in this equation can be simplified by transforming into Fourier space, where they become products. We will suppose that the system is periodic in a box of size  $L^d$ , where  $d$  is the dimension of the space. If there is no such finite length  $L$ , one can use integral Fourier transforms to obtain continuum versions of the following transformed equations.

Define the *discrete* Fourier transform  $\psi_{\mathbf{k}}(t)$  of  $\psi(\mathbf{x}, t)$  by

$$\psi_{\mathbf{k}}(t) \doteq \frac{1}{L^d} \int d\mathbf{x} e^{-i\mathbf{k}\cdot\mathbf{x}} \psi(\mathbf{x}, t),$$

the *integral* Fourier transform  $\hat{\nu}(\mathbf{k})$  of  $\nu(\mathbf{x}_1 - \mathbf{x}_2)$  by

$$\hat{\nu}(\mathbf{k}) \doteq \int d\mathbf{r} e^{-i\mathbf{k}\cdot\mathbf{r}} \nu(\mathbf{r}),$$

and the *integral* Fourier transform  $\hat{U}(\mathbf{p}, \mathbf{q})$  of  $U(\mathbf{x}_1 - \mathbf{x}_2, \mathbf{x}_1 - \mathbf{x}_3)$  by

$$\hat{U}(\mathbf{p}, \mathbf{q}) \doteq \int d\mathbf{r} e^{-i\mathbf{p}\cdot\mathbf{r}} \int d\mathbf{s} e^{-i\mathbf{q}\cdot\mathbf{s}} U(\mathbf{r}, \mathbf{s}).$$

Also, assume that the operator  $\mathcal{L}$  is multiplicative in Fourier space, so that

$$\mathcal{L}_{\mathbf{k}}\psi_{\mathbf{k}}(t) = \frac{1}{L^d} \int d\mathbf{x} e^{-i\mathbf{k}\cdot\mathbf{x}} \mathcal{L}\psi(\mathbf{x}, t).$$

One can readily show (see Appendix B) that in Fourier space Eq. (I.15) appears as

$$\frac{\partial}{\partial t} \mathcal{L}_{\mathbf{k}}\psi_{\mathbf{k}}(t) + \hat{\nu}(\mathbf{k}) \mathcal{L}_{\mathbf{k}}\psi_{\mathbf{k}} = \sum_{\mathbf{p}, \mathbf{q}} \delta_{\mathbf{k}-\mathbf{p}-\mathbf{q}, 0} \hat{U}(\mathbf{p}, \mathbf{q}) \psi_{\mathbf{p}}(t) \psi_{\mathbf{q}}(t). \quad (\text{I.16})$$

It is noteworthy that *integral* Fourier components appear in Eq. (I.16), even though we seek a *discrete* representation appropriate to bounded or periodic geometries. The presence of integral transforms is a consequence of the integral  $x$  space convolutions in Eq. (I.15).

The reality conditions  $\psi_{-\mathbf{k}} = \psi_{\mathbf{k}}^*$  and  $\hat{U}(-\mathbf{p}, -\mathbf{q}) = \hat{U}^*(\mathbf{p}, \mathbf{q})$  allow us to write our stochastic equation in a more symmetric form, which facilitates proofs of conservation properties:

$$\boxed{\left( \frac{\partial}{\partial t} + \nu_{\mathbf{k}} \right) \psi_{\mathbf{k}}(t) = \frac{1}{2} \sum_{\mathbf{k}+\mathbf{p}+\mathbf{q}=0} M_{\mathbf{k}\mathbf{p}\mathbf{q}} \psi_{\mathbf{p}}^*(t) \psi_{\mathbf{q}}^*(t),} \quad (\text{I.17})$$

in terms of the mode-coupling coefficient  $M_{\mathbf{k}pq} \doteq 2\mathcal{L}_{\mathbf{k}}^{-1}\widehat{U}^*(\mathbf{p}, \mathbf{q})$  and the linear damping  $\nu_{\mathbf{k}} \doteq \widehat{\nu}(\mathbf{k})$ . In this work, we allow both of these coefficients to be complex. Equation (I.17) will frequently be referred to as the *fundamental equation*.

Let us now define some important statistical quantities associated with Eq. (I.17). The simplest statistical moment one may consider is the mean field. In this work we will assume that the mean fields are frozen in time. Therefore, it is possible to choose our variable  $\psi_{\mathbf{k}}(t)$  to represent a *perturbation* from the mean, so that  $\langle \psi_{\mathbf{k}}(t) \rangle = 0$ . This is not an essential requirement and is imposed here only for reasons of simplicity.

It is clear that without any loss of generality we may assume in Eq. (I.17) the symmetry

$$M_{\mathbf{k}pq} = M_{\mathbf{k}qp}. \quad (\text{I.18})$$

Another important symmetry possessed by many such systems is<sup>9</sup>

$$\sigma_{\mathbf{k}}M_{\mathbf{k}pq} + \sigma_{\mathbf{p}}M_{\mathbf{p}q\mathbf{k}} + \sigma_{\mathbf{q}}M_{\mathbf{q}\mathbf{k}\mathbf{p}} = 0, \quad (\text{I.19})$$

for some time-independent nonrandom *real* quantity  $\sigma_{\mathbf{k}}$ . Let us denote by  $\bar{\sigma}$  the operator in  $\mathbf{x}$  space such that the discrete Fourier transform of  $\bar{\sigma}^{1/2}\psi(\mathbf{x}, t)$  is just  $\sigma_{\mathbf{k}}^{1/2}\psi_{\mathbf{k}}$ . Equation (I.19) is then easily shown to imply that the nonlinear terms of Eq. (I.17) conserve the total generalized “energy,” defined as

$$E \doteq \frac{1}{2} \int d\mathbf{x} \bar{\sigma} \langle \psi^2(\mathbf{x}, t) \rangle = \frac{1}{2} \sum_{\mathbf{k}} \sigma_{\mathbf{k}} \langle |\psi_{\mathbf{k}}(t)|^2 \rangle, \quad (\text{I.20})$$

using Parseval’s Theorem. For some problems (e.g., two-dimensional turbulence), Eq. (I.19) may be satisfied by more than one choice of  $\sigma_{\mathbf{k}}$ ; this implies the existence of more than one nonlinear invariant.

We also define the two-time correlation function

$$C_{\mathbf{k}}(t, t') \doteq \langle \psi_{\mathbf{k}}(t) \psi_{\mathbf{k}}^*(t') \rangle$$

and the equal-time correlation function

$$C_{\mathbf{k}}(t) = C_{\mathbf{k}}(t, t),$$

so that  $E \doteq \frac{1}{2} \sum_{\mathbf{k}} \sigma_{\mathbf{k}} C_{\mathbf{k}}(t)$ . Another statistical quantity of which we will make extensive use later is the *infinitesimal response function* or *propagator* (nonlinear Green’s function)  $R_{\mathbf{k}}(t, t')$ . This is defined to be the ensemble-averaged infinitesimal response to a source function  $\bar{\eta}_{\mathbf{k}}(t)$  added to the right-hand side of Eq. (I.17):

$$R_{\mathbf{k}}(t, t') \doteq \left\langle \frac{\delta \psi_{\mathbf{k}}(t)}{\delta \bar{\eta}_{\mathbf{k}}(t')} \right\rangle_{\bar{\eta}_{\mathbf{k}}=0}.$$

---

<sup>9</sup>This symmetry is related to the Manley-Rowe relations for the wave actions [Armstrong *et al.* 1962, Sagdeev and Galeev 1969].

The functional derivative here is defined as the coefficient of the lowest-order term of the power series expansion in  $\delta\bar{\eta}_{\mathbf{k}}$  of the induced perturbation  $\delta\psi_{\mathbf{k}}$ . This definition is more complicated than the corresponding definition of the linear impulse response because the nonlinear response depends on the amplitude of the added source function in a nonlinear fashion; one cannot simply scale out a coefficient appearing in front of the impulse function  $\delta(t-t')$ .

As in the theory of linear Green's functions, it is convenient to define the Heaviside unit step function:

$$H(\tau) \doteq \int_{-\infty}^{\tau} d\bar{\tau} \delta(\bar{\tau}). \quad (\text{I.21})$$

If we construct the Dirac  $\delta$  function symmetrically about zero, this definition implies that  $H(0) = 1/2$ . Likewise, the equal-time response function  $R_{\mathbf{k}}(t, t)$  evaluates to  $1/2$  [although  $\lim_{t' \rightarrow t-} R_{\mathbf{k}}(t, t') = 1$ ].

In stationary turbulence, the two-time correlation and response functions will depend only on the difference of their time arguments:  $C_{\mathbf{k}}(t, t') \doteq \mathcal{C}_{\mathbf{k}}(t-t')$  and  $R_{\mathbf{k}}(t, t') \doteq R_{\mathbf{k}}(t-t')$ . Typically,  $\mathcal{C}_{\mathbf{k}} \rightarrow 0$  fast enough as  $\tau \doteq t-t' \rightarrow \infty$  so that  $\mathcal{C}_{\mathbf{k}}$  is integrable with respect to  $\tau$ . A useful measure of the time scale on which this happens is the autocorrelation time  $\tau_{\text{ac}}$ :

$$\tau_{\text{ac}} \doteq \frac{1}{\mathcal{C}_{\mathbf{k}}(0)} \int_0^{\infty} d\tau \mathcal{C}_{\mathbf{k}}(\tau).$$

### Closure problem:

Suppose we want to obtain an evolution equation for  $C_{\mathbf{k}}(t, t')$ . From Eq. (I.17), we have for  $t \neq t'$ :

$$\left( \frac{\partial}{\partial t} + \nu_{\mathbf{k}} \right) C_{\mathbf{k}}(t, t') = \frac{1}{2} \sum_{\mathbf{k}+\mathbf{p}+\mathbf{q}=\mathbf{0}} M_{\mathbf{k}\mathbf{p}\mathbf{q}} \langle \psi_{\mathbf{p}}^*(t) \psi_{\mathbf{q}}^*(t) \psi_{\mathbf{k}}^*(t') \rangle. \quad (\text{I.22})$$

For  $t = t'$ , one must take care to recognize that the  $\partial/\partial t$  operator by definition acts only on the first argument of  $C(t, t')$ , so that the chain rule must be used to compute an evolution equation for  $C(t, t)$ :

$$\begin{aligned} \frac{\partial}{\partial t} C_{\mathbf{k}}(t, t) &= \frac{\partial}{\partial t} C_{\mathbf{k}}(t, t') \Big|_{t'=t} + \frac{\partial}{\partial t'} C_{\mathbf{k}}(t, t') \Big|_{t'=t} \\ &= \frac{\partial}{\partial t} C_{\mathbf{k}}(t, t') \Big|_{t'=t} + \frac{\partial}{\partial t} C_{\mathbf{k}}(t', t) \Big|_{t'=t} \\ &= 2 \operatorname{Re} \frac{\partial}{\partial t} C_{\mathbf{k}}(t, t') \Big|_{t'=t}. \end{aligned} \quad (\text{I.23})$$

In the last line we have made use of the Hermiticity relation  $C_{\mathbf{k}}(t, t') = C_{\mathbf{k}}^*(t', t)$ .

We are presented with a major difficulty in Eq. (I.22) in that the unknown *triplet correlation function*  $\langle \psi_{\mathbf{p}}^*(t) \psi_{\mathbf{q}}^*(t) \psi_{\mathbf{k}}^*(t') \rangle$  appears on the right-hand side. We could, of course, form the equation (for  $t \neq t'$ ):

$$\left( \frac{\partial}{\partial t'} + \nu_{\mathbf{k}} \right) \langle \psi_{\mathbf{k}}^*(t') \psi_{\mathbf{p}}^*(t) \psi_{\mathbf{q}}^*(t) \rangle = \frac{1}{2} \sum_{\mathbf{k} + \bar{\mathbf{p}} + \bar{\mathbf{q}} = 0} M_{\mathbf{k}\bar{\mathbf{p}}\bar{\mathbf{q}}}^* \langle \psi_{\bar{\mathbf{p}}}(t') \psi_{\bar{\mathbf{q}}}(t') \psi_{\mathbf{p}}^*(t) \psi_{\mathbf{q}}^*(t) \rangle, \quad (\text{I.24})$$

but this clearly gets us nowhere because of the appearance of a new unknown, the fourth-order moment. We are witnessing the development of an infinite *moment hierarchy*. Any truncation of this hierarchy leads to an unclosed set of equations; this is known as the *closure* problem. This difficulty is the chief obstacle in developing a satisfactory theory of turbulence; to date, it still has not been fully circumvented.

It is worth pointing out that such closure problems occur whenever one takes averages of a nonlinear equation. The difficulty we are experiencing here is quite analogous to the closure problem that arises when one averages a nonlinear kinetic (phase-space) equation with respect to *velocity* to obtain an unclosed hierarchy of fluid equations. In our case, we begin with a nonlinear fluid equation and average it over all *realizations*. Bearing this analogy in mind, it would seem appropriate to consider the methods that have been used to close the kinetic hierarchy. The most elementary approach would neglect all moments above some order.

Moment truncation is a poor approach to the statistical closure problem. This has been demonstrated by Kraichnan [1961], who showed for a simple stochastic oscillator that the infinite series of moment values needed to compute the response function is not uniformly convergent. No matter at what stage one truncates, the resulting approximation diverges as  $t \rightarrow \infty$ , in total violation of the true statistics.

Another approach, borrowed from statistical field theory, is based on truncation of the *cumulant* hierarchy. For example, one might close the BBGKY equations at second order by neglecting the heat flux. Cumulants are defined as the residuals left when moments are expanded into lower-order moments by the relations appropriate for Gaussian statistics [Kubo 1962]. Neglecting the cumulants at some order is equivalent to assuming that the statistics *at that order* satisfy the same relations as do Gaussian variables. For instance, in the absence of mean fields the fourth-order cumulant of four statistical variables  $a, b, c,$  and  $d$  is defined by

$$\langle\langle abcd \rangle\rangle \doteq \langle abcd \rangle - \langle ab \rangle \langle cd \rangle - \langle ac \rangle \langle bd \rangle - \langle ad \rangle \langle bc \rangle.$$

For this case, the lowest nontrivial order at which the “cumulant-discard hypothesis” may be applied is fourth order. Neglecting the fourth-order cumulant is not the same as assuming that the statistics are Gaussian since this assumption is only made at fourth order. Hence, this is known as the *quasinormal* approximation [Millionschtchikov 1941, Proudman and Reid 1954, Tatsumi 1957]. Assuming that

the statistics are truly Gaussian is not very useful for turbulence theories since that would imply that odd moments like the triplet correlation in Eq. (I.22) vanish. This corresponds to an approximation in which the nonlinearity is totally neglected in the equation for the correlation function!

The cumulant-discard hypothesis has been shown to be superior to the moment-discard hypothesis, yet it still lacks uniform asymptotic validity as  $t \rightarrow \infty$  [Kraichnan 1961]. Numerical simulations of the quasinormal approximation to fluid turbulence have demonstrated serious unphysical behaviour such as negative energies [Ogura 1963]. The quasinormal closure has also been shown to violate the near-equilibrium statistics grossly by incorrectly predicting a time-reversible behaviour [Orszag 1970].

#### I.C.4 Concept of realizability

A general difficulty with statistical closures is that there is a great deal of arbitrariness in the choice of relations used to express high-order moments in terms of lower-order moments. Worse, a closure picked “at random” will likely lead to unphysical behaviour just as the moment- and cumulant-discard hypotheses do. We can, however, greatly reduce the arbitrariness and at the same time ensure physically acceptable behaviour by imposing the requirement of *realizability*.

A closure is said to be realizable if there exists an underlying probability density function for the statistics it predicts [Kraichnan 1985]. Realizability is equivalent to the existence of a stochastic problem for which the closure is an *exact* statistical solution, *even though it may only be an approximate solution to the original dynamical problem*.

Figure I.2 illustrates the concept of realizability for a simple closure developed in Chapter III. The graphs depict the evolution of the energy-like quantity  $C \doteq \langle |\psi|^2 \rangle$ , which, for the original stochastic problem, must obviously remain positive. However, since the exact equation for  $C$  involves an unknown triplet correlation function, one must be content with an approximation. We might obtain a closure by making certain intuitive hypotheses about the higher-order statistical moments. Unfortunately, the chances are very good that such an approximation will be badly behaved; for example, as in the closure shown at the top of the figure, this may even involve the prediction of negative energies! In contrast, the realizable statistical closure depicted at the bottom succeeds in reproducing the positivity of  $C$ , because its solutions are constrained by *some* underlying amplitude equation. Since no such constraint is placed on the nonrealizable closure, it can quite readily predict negative values for  $C$ .

Of course, the realizability of a closure does not necessarily imply that the predicted results will accurately represent the true dynamics. In fact, for each

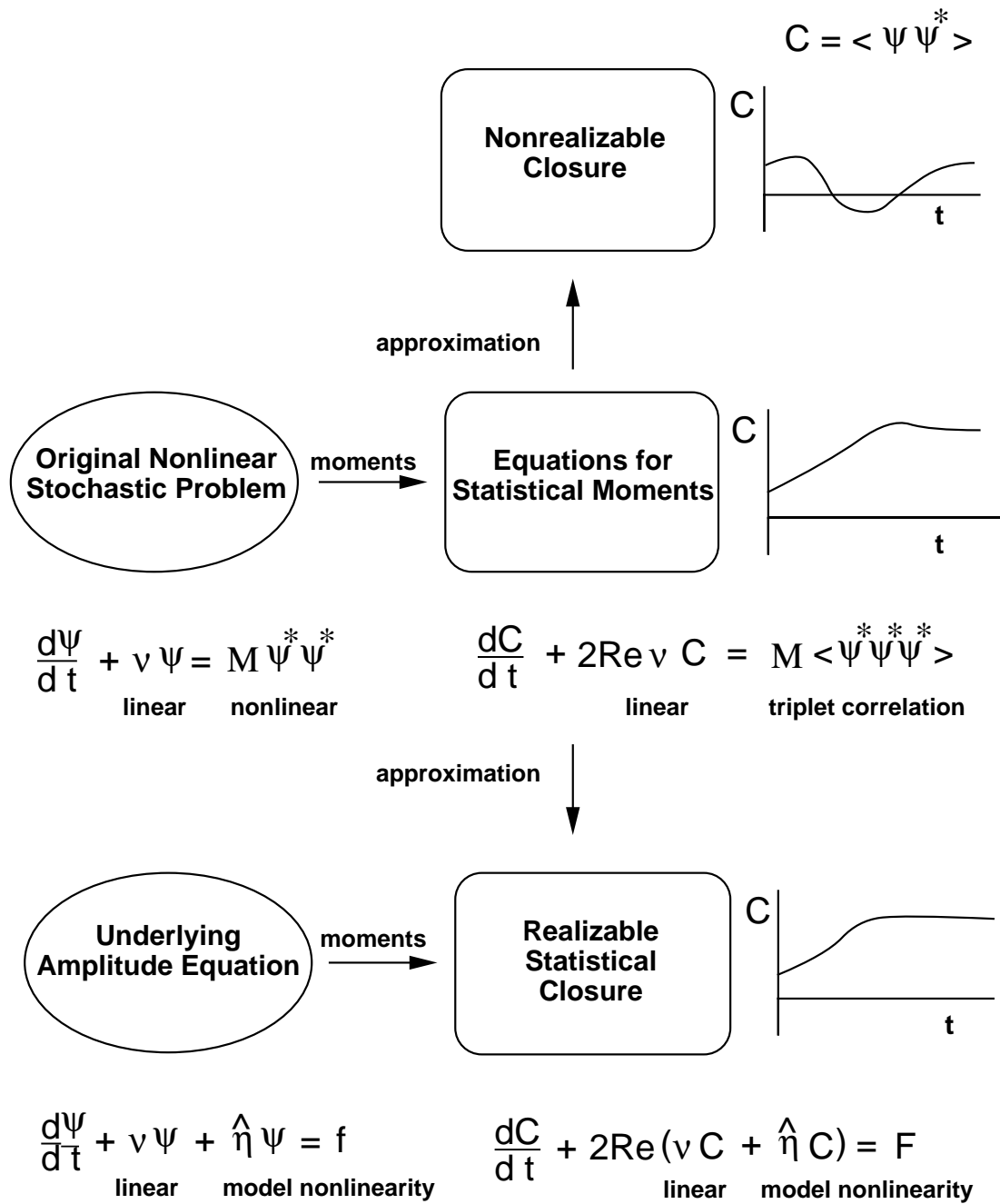


Figure I.2: Concept of realizability.

given dynamical problem, there exist an infinite number of realizable closures. One must therefore choose the underlying model equation judiciously so as to model the exact dynamics as closely as possible. It may seem to the reader that this is where the real difficulty lies and that the requirement of realizability is a very weak constraint. In a sense this is so and we will eventually impose several other criteria during our search for plausible statistical closures in order to reduce this arbitrariness. Realizability is, in essence, the very least that one should require of a statistical closure if the predicted results are to bear any relation to reality. For this reason, it is with some surprise that we will encounter in Chapter III the fact that two of the most popular statistical closures<sup>10</sup> in the contexts of plasma physics and geophysics are not even guaranteed to be realizable!

### I.C.5 Concept of Markovian

Suppose that at every time  $t$  all possible observables associated with a system can be related by a one-to-one mapping to the components of some vector  $\Psi(t)$ . This is known as a *state vector*, in that it completely describes the state of the system at any time. For the moment, it is convenient to imagine that the system evolves discretely in time, as depicted in Fig. I.3. A *Markovian* description of a system is one in which the evolution of  $\Psi$  depends explicitly on only the most recent time value, not on the previous time history. Equivalently, all of the dependence on past conditions must be passed to the future through the current value of the state variable.<sup>11</sup>

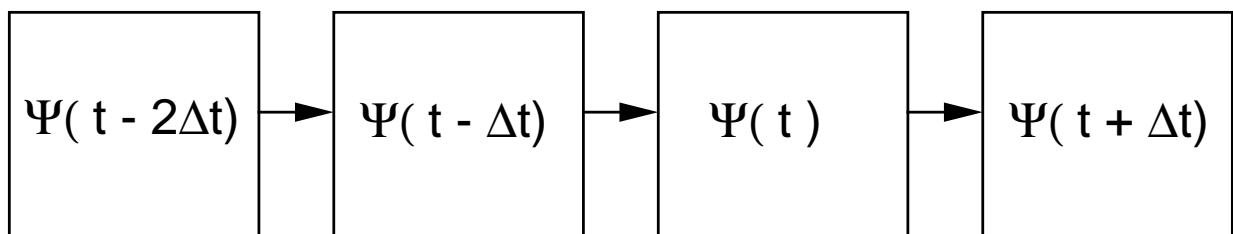
In this work, we will be most interested in Markovian descriptions because their solution typically entails much less computational effort than non-Markovian formulations. Sometimes one may refer to the actual physical system as being Markovian, but strictly speaking this term should be applied only to the *mathematical description* of the system. We emphasize this because it is often possible to convert a non-Markovian description into a Markovian one by the introduction of an auxiliary parameter as an extra component of the (now augmented) state vector [Wang and Uhlenbeck 1945]. The purpose of this parameter is essentially to carry the time-history information *explicitly* from the past to the future. Provided that this parameter itself can be computed in a Markovian manner, knowing only the current value of the state vector, this type of model will be called *almost-Markovian* [Kraichnan 1971b]. Even though the auxiliary parameter is not an observable of

---

<sup>10</sup>These closures are known by the initials TFM and EDQNM; they will be defined in the next two chapters.

<sup>11</sup>There is an analogy here to the representation of a differential equation (which, for the appropriate state vector, can be treated as Markovian) as a (non-Markovian) integral equation. Recall that a differential equation may always be written as an integral equation, but not *vice versa*.

## Markovian system



## Non-Markovian system

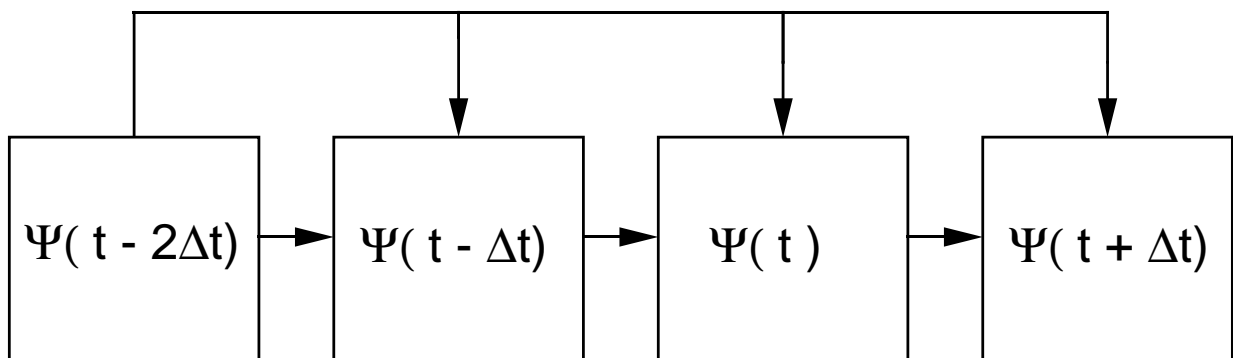


Figure I.3: Concept of Markovian.

the physical system, the augmented description may be evolved essentially as if it were in fact Markovian.

### I.C.6 Passive *vs.* self-consistent problems

The nonlinear stochastic equation Eq. (I.17) is self-consistent, in that the strength of the nonlinearity is determined by the fluctuation level. However, it is also possible to consider passive problems in which an external stochastic parameter enters into the nonlinearity. For example, consider the stochastic oscillator problem proposed by Kraichnan [1961] and Kubo [1963, and refs. therein],

$$\frac{\partial}{\partial t}\psi(t) + i\tilde{\omega}(t)\psi(t) = 0, \quad (\text{I.25})$$

where  $\tilde{\omega}(t)$  is a specified stationary Gaussian process, statistically independent of  $\psi$ , with zero mean. Although this problem is clearly linear in  $\psi$ , it is *nonlinear in stochastic variables*. For this reason, the closure problem is encountered even when this simple-looking equation is ensemble-averaged. In fact, in the case where  $\tilde{\omega}$  is time-independent, the stochastic oscillator poses an especially difficult test of closures, “displaying great sensitivity to inadequacies in approximation schemes” [Kraichnan 1961]. We will illustrate some of the closures considered in this work by applying them to the stochastic oscillator in Chapter II.

Fully self-consistent problems like turbulence are more difficult than passive problems. For this reason, turbulence composed of many interactions is sometimes approximated passively. One assumes that the dominant effect on any particular mode is provided by a background of interactions specified independently of the excitation level of that mode. However, it is often not clear how to specify the passive turbulent background. Moreover, even if a form for the passive field can be determined, one will likely end up violating important conservation laws by misrepresenting the self-consistent effects.

## I.D Analytical transport estimates

Our goal is to compute, for example, the particle flux  $\mathbf{F}$  in

$$\frac{\partial}{\partial t}\langle n \rangle = -\nabla \cdot \mathbf{F}. \quad (\text{I.26})$$

Here,  $\langle n \rangle$  is the ensemble average of the particle density. To begin, note that upon averaging the local continuity equation

$$\frac{\partial}{\partial t}n = -\nabla \cdot (\mathbf{v}n), \quad (\text{I.27})$$

one obtains Eq. (I.26) with

$$\mathbf{\Gamma} = \langle \mathbf{v} \rangle \langle n \rangle + \langle \tilde{\mathbf{v}} \tilde{n} \rangle,$$

where  $\tilde{\mathbf{v}}$  and  $\tilde{n}$  are the fluctuating velocity and density, respectively.

We see here that because Eq. (I.27) is nonlinear in the random variables  $\mathbf{v}$  and  $n$ , the ensemble-averaged equation contains a second-order moment. Note in particular that the flux depends on the *cross-correlation* between the density and potential in addition to the *fluctuation level*. Upon writing equations for the second- and then higher-order moments, we again encounter the unclosed hierarchy of moment equations. Let us now outline the different approaches that have been used to deal with the statistical closure problem and discuss their relative merits.

### I.D.1 Linear theory

The first approach normally considered when a nonlinear equation is encountered in physics is linearization. This is for the simple reason that many methods, including transform techniques, are available for solving a linear differential equation. Comparatively few techniques are known for solving nonlinear differential equations analytically. Of course, a nonstochastic nonlinear equation would normally present little resistance to numerical solution. The difficulty here is that the equations are stochastic and we want to know the statistics obtained by ensemble-averaging over many realizations. For many applications this is computationally infeasible (e.g., the solution of the Navier-Stokes equations at high Reynolds number). So the “obvious” solution is merely to ignore the nonlinearity and obtain the solution of the resulting linearized system.

Linearization is valid only when the nonlinear terms are sufficiently small compared to the linear terms. By definition, this is not the case for well-developed turbulence. For the incompressible Navier-Stokes equations, the linear theory is trivial, representing only the effects of viscous dissipation. For problems of plasma physics, one typically obtains a more complicated linear theory involving electromagnetic wave effects. When Fourier-transformed in time and space, the linear equation often leads to a dispersion relation, the roots of which determine the normal mode frequencies at which all of the energy must be concentrated. As mentioned previously, this discrete energy spectrum is completely at odds with observed spectra. In addition, linearization will often not conserve the total energy of the system because it neglects the back reaction of waves on the free energy sources driving the waves in the first place. Clearly, a nonlinear theory is needed to account for the energy drain exerted by growing waves on these sources.

## I.D.2 Dimensional analysis

Dimensional analysis is a useful procedure for analyzing the scaling relations to which an equation may give rise. It leads to relations for a transport coefficient  $D$  of the general form

$$D = CF(\epsilon_1, \epsilon_2, \dots)X^\alpha Y^\beta \dots,$$

where  $C$  is a numerical coefficient,  $\epsilon_1, \epsilon_2, \dots$  are dimensionless parameters, and  $X, Y, \dots$  are dimensional parameters. Dimensional analysis proceeds by determining all scale transformations that leave the equation invariant and imposing these same invariances on the transport coefficient [Connor 1988]. Note that this gives more information than would elementary considerations of the dimensional units of which  $D$  is composed [Buckingham 1914]. Such a procedure would correctly give the scaling of  $D$  with  $X$  and  $Y$ . One might even succeed in identifying possible dimensionless parameters, but there would be no way to discern from these the set of parameters upon which  $D$  actually depends. The invariances of the equation itself must be considered in order to identify the behaviour with respect to dimensionless quantities. An example of such a dimensionless constant for fluid turbulence is the Reynolds number  $R$ , from which we discover the concept of similarity among a whole class of flows with different parameters.

Dimensional analysis can be quite helpful when there are relatively few length or time scales, for example, compared to the number of equations. When many length or time scales exist, one obtains many dimensionless parameters and less information is available from the scaling law. Moreover, dimensional analysis cannot predict either  $C$  or the functional form of  $F$ . These require a more detailed analysis of the balance of linear and nonlinear effects than dimensional considerations alone can provide.

## I.D.3 Mixing-length estimates

Consider a flow characterized by a mean velocity shear in the  $x$  direction. Prandtl attempted to close the moment hierarchy associated with the Navier-Stokes equation with the following approximation for the turbulent momentum flux [Tennekes and Lumley 1972],

$$\rho\langle\tilde{u}_x\tilde{u}_y\rangle \approx \rho v\ell\frac{\partial\langle u_y\rangle}{\partial x}, \quad (\text{I.28})$$

where  $v$  is the rms level of the turbulent velocity  $\tilde{\mathbf{u}}$  and  $\ell$  is known as the *mixing length*. Note that  $v\ell$  plays the role of an *eddy viscosity*, which we think of as the effective viscosity introduced by turbulent fluctuations on the mean flow.

The physical reasoning behind Eq. (I.28) is similar to the calculation of thermal diffusivity in the kinetic theory of gases. Heat is transported by a diffusion of

particles exhibiting a random walk with step size equal to the mean free path between molecular collisions. According to Fick's law, the heat flux is proportional to the gradient of the temperature. Analogously, the mixing length plays the role of a mean free path and the momentum flux is assumed to be proportional to the gradient in the mean velocity profile. The reason  $\ell$  is known as the mixing length is that it represents the correlation length between the velocity and position of a moving fluid element. The turbulence mixes up the velocity, so that after the fluid has traveled a distance  $\ell$  the velocity is completely uncorrelated with position.

Prandtl proceeded to postulate that the rms fluctuating velocity is

$$v \approx \ell \left| \frac{\partial \langle u_y \rangle}{\partial x} \right|. \quad (\text{I.29})$$

This is deduced from the assumptions that the fluctuating velocities are approximately isotropic, so that  $\langle \tilde{u}_x \tilde{u}_y \rangle \approx v^2$ , and that they arise from the turbulent momentum transport just discussed.

Equations like Eq. (I.29) are widely used in both plasma physics and fluid dynamics to relate the gradient of the fluctuations of some quantity to the gradient of its mean. For example, it implies for drift waves that  $k_\perp n_e = n_0/L_n$ , where  $n_0$  is the mean number density. For adiabatic electrons this means

$$k_\perp \frac{e\varphi}{T_e} = \frac{1}{L_n},$$

or, in our dimensionless units,  $k_\perp \Phi = 1$ . Here,  $k_\perp$  is the wavenumber measured perpendicular to the magnetic field. The mixing-length estimate is therefore equivalent to the statement that in a saturated state the  $\mathbf{E} \times \mathbf{B}$  velocity should equal the diamagnetic velocity  $V_d$  [Kadomtsev 1965].

Mixing-length estimates may be a reasonable approximation on a local basis, but unfortunately they often are employed when only an externally imposed boundary condition on the profile is known. It is not necessarily correct to assume that the gradient of a local mean velocity is proportional to the *global* velocity gradient deduced from the assumption of a linear profile since most of the variation in the velocity profile could take place in a small region, or *boundary layer*, that could control the transport.

A practical difficulty with the mixing-length model is that the mixing length  $\ell$  is usually not known. The physical reasoning behind the mixing-length formula is based on an analogy with near-equilibrium statistical mechanics. The classical kinetic theory of gases is very different from the nonequilibrium statistical mechanics of turbulence, and it cannot be used to predict theoretical values for  $\ell$ . For simple geometries the dependence of  $\ell$  on the coordinates can sometimes be determined on the basis of similarity arguments and empirical data [Landau and Lifshitz 1987].

However, when there is more than one length or velocity scale, it is not clear how to choose  $\ell$ . Often it is argued that  $\ell$  should be chosen to be about the size of the largest eddies since they clearly dominate the momentum transport. This means that  $\ell$  should be about the same size as the width of the flow. However, the arguments underlying this *gradient-transport* model are based on a Taylor series expansion that breaks down for such large mixing lengths [Tennekes and Lumley 1972].

Why, then, does the mixing-length model have such widespread use in calculations of turbulent transport? Two reasons can be given. First, being a semi-empirical theory, it sometimes *can* give good agreement with experiment. However, Landau and Lifshitz [1987] point out that good agreement can actually be obtained with many different expressions for the turbulent viscosity, so these experimental tests are not adequate to discriminate between the underlying theories. Prandtl himself was aware of experimental situations where the mean velocity profile has a local maximum at which the Reynolds stress does not vanish [Stanišić 1988]. Clearly this contradicts Eq. (I.28). Second, heuristic though the derivation of the mixing-length formula may be, it essentially amounts to dimensional analysis. All of the difficulty is embedded in the determination of  $\ell$ ; the fallacy enters only when one tries to assume  $\ell$  is constant or has a particular form. In fact, Tennekes and Lumley argue that the mixing-length formula “is merely a dimensional necessity in a turbulent shear flow dominated by a single velocity scale  $v$  and a single length scale  $\ell$ .” If there are more scales, which is the case in most turbulence problems, they caution, “In other words, mixing-length theory is useless because it cannot predict anything substantial; it is confusing because no two versions of it can be made to agree with each other.”

#### I.D.4 Survey of statistical approaches

Undoubtedly, a more sophisticated theory of the energy balances and nonlinear dynamics is required to go beyond linear theory or the previous scaling arguments based on dimensional considerations. Historically many different approaches have been proposed, which we shall now discuss.

##### Systematic, perturbative:

Quasilinear theory [Sagdeev and Galeev 1969] and weak-turbulence theory [Sagdeev and Galeev 1969, Davidson 1972] are perturbative approaches that regard nonlinear terms as perturbations to linear theory. Quasilinear theory uses linear theory to compute the correlation between the fluctuating fields; mode-coupling effects on those fluctuations are completely neglected. The linear solutions for the fluctuations are then used to compute an evolution equation for the mean field. Conventional use of the term “quasilinear” in plasma turbulence often refers to the

situation where a flux, quadratic in fluctuating quantities, is computed from linear theory. Strictly speaking, however, the term *quasilinear* should be reserved for the case in which a nonlinear equation for the mean field, in terms of this flux, is actually used to calculate the fluctuation level.

Weak-turbulence theory goes to higher order than does quasilinear theory by accounting for mode-coupling effects such as the three-wave interaction and wave-particle interaction. Different versions of weak-turbulence theory accomplish this either by assuming that the fluctuations obey Gaussian statistics or that their phases are distributed randomly.

First, we will describe the classical application of the quasilinear procedure to an unmagnetized plasma, where one encounters linear and nonlinear interactions between individual particles and the electrostatic waves arising from collective effects of other particles. In this approximation we neglect the part of this interaction involving the modification of the particle trajectories by waves. In particular, we neglect the important effect of electrostatic trapping of the particles in the local potential wells created by the waves. We use only the *unperturbed* particle orbits to evaluate the  $\tilde{\mathbf{E}} \cdot \partial \tilde{f} / \partial \mathbf{v}$  nonlinearity of the Vlasov equation. This leads to the following velocity-space equation for the mean distribution function:

$$\boxed{\frac{\partial}{\partial t} \langle f \rangle = \frac{\partial}{\partial \mathbf{v}} \cdot \mathbf{D} \cdot \frac{\partial \langle f \rangle}{\partial \mathbf{v}}}, \quad (\text{I.30})$$

where  $\mathbf{D} \doteq D \hat{\mathbf{k}} \hat{\mathbf{k}}$  and

$$D = \lim_{\epsilon \rightarrow 0} \frac{e^2}{m^2} \int \frac{d\mathbf{k}}{(2\pi)^3} \int_{-\infty}^{\infty} \frac{d\omega}{2\pi} \frac{1}{-i(\omega - \mathbf{k} \cdot \mathbf{v} + i\epsilon)} \langle |\hat{E}(\mathbf{k}, \omega)|^2 \rangle \quad (\text{I.31})$$

is the quasilinear “diffusion” coefficient. Here,  $\hat{E}(\mathbf{k}, \omega)$  is the Fourier transform of the Eulerian electric field  $\tilde{E}(\mathbf{x}, \tau)$  in both space and time. The causality requirement of the Inverse Fourier Theorem dictates that the  $\omega$  integration contour be chosen to lie *above* all poles of the integrand. In this case the contour must be deformed above the pole at  $\mathbf{k} \cdot \mathbf{v}$ . This is expressed compactly by the Plemelj formula,

$$\lim_{\epsilon \rightarrow 0} \frac{1}{\omega - \mathbf{k} \cdot \mathbf{v} + i\epsilon} = \text{P} \frac{1}{\omega - \mathbf{k} \cdot \mathbf{v}} - \pi i \delta(\omega - \mathbf{k} \cdot \mathbf{v}), \quad (\text{I.32})$$

which separates the contributions of nonresonant and resonant particles, respectively. Kaufman [1972] pointed out that only the resonant portion of Eq. (I.32) is associated with diffusion. He thus resolved the paradox of the negative diffusion coefficient that seems to appear when Eq. (I.31) is evaluated for  $\gamma < 0$ .

In the one-dimensional case, this analysis has been used to explain the flattening of the distribution function observed during saturation of the so-called bump-on-the-tail instability [Sagdeev and Galeev 1969, Tsunoda *et al.* 1987]. One argues that

the instability is turned off by removing the driving source of free energy through a diffusion process. In this way, quasilinear theory goes beyond linear theory in attempting to account partially for the back-reaction of the waves on the mean distribution function.

Upon closing the quasilinearized Vlasov equation with the Poisson equation, one could then solve for the electrostatic fluctuations in terms of  $\partial\langle f \rangle / \partial \mathbf{v}$ . By evolving the mean distribution function with Eq. (I.30), it is thus possible to obtain the fluctuation level without further argument.

Important favourable features of classical quasilinear theory include the facts that it satisfies reasonable conservation laws for energy and momentum [Kaufman 1972] and that it is realizable [Orszag and Kraichnan 1967]. Unfortunately, quasilinear theory has been found to overestimate transport in both real experiments and in numerical simulations.<sup>12</sup> For example, this has been indicated by direct numerical simulations, both gyrokinetic and fluid, of simplified versions of the  $\eta_i$  mode [Lee and Tang 1988, Ottaviani *et al.* 1990]. These computer simulations provide particularly convincing demonstrations of the failure of quasilinear theory since the linear theory of the numerical system is known exactly, independent of the controversial issue of which instability is actually responsible for tokamak transport. Another inconsistency of quasilinear theory is that it does not explain the experimentally observed saturation in the presence of nonvanishing density gradients. Quasilinear theory would predict that the drift-wave instability would continue growing until the free energy source is removed by the flattening of the density profile.

Two assumptions are invoked in deriving quasilinear theory: first, one neglects mode-coupling effects in evaluating the cross-correlations; second, one assumes that the electrostatic trapping time  $\tau_{\text{tr}}$  of the particles is much longer than the linear autocorrelation time  $\tau_{\text{ac}}$  of the electric field. For the Vlasov problem one can estimate  $\tau_{\text{tr}} = (m/ekE)^{1/2}$  as the typical time for which particles are trapped by the waves. The second assumption also implies that the time scale on which the distribution function evolves is much longer than the autocorrelation time, which leads to the diffusive behaviour of the resonant contribution to Eq. (I.30).

In contrast to the application of quasilinear theory to the Vlasov case just considered, where an evolution equation for the mean field provides an estimate of the level of turbulence, this is not the usual practice in quasilinear flux estimates. Modern quasilinear calculations (see, e.g., Rewoldt *et al.* [1987]) do not normally take into account the evolution of the mean field, either for reasons of computational simplicity or because there are physical constraints, such as boundary conditions, that force the mean field to persist. These estimates only provide a diffusion coefficient in terms of the level of turbulence; they do not solve for the turbulent fluctuation

---

<sup>12</sup>However, quasilinear theory *is* appropriate for some situations, such as the problem of passive advection in the limit of short autocorrelation time [Krommes and Smith 1987].

level itself. In plasma turbulence, a mixing-length argument is often invoked to determine the fluctuation level, but as emphasized previously, such arguments are of limited validity.

Quasilinear theory can be used to compute velocity space diffusion coefficients by assuming that the fluctuations of electrostatic waves are chaotic enough to cause the particles to exhibit a random walk in velocity space. The velocity diffusion coefficient associated with a random walk with step size  $\delta v(t)$  is

$$D = \lim_{t \rightarrow \infty} \frac{\langle \delta v^2(t) \rangle}{2t}. \quad (\text{I.33})$$

Now consider the limit of an infinite number of steps, each having infinitesimal step size, such that the resulting motion is differentiable. We may then define the Lagrangian acceleration magnitude of a particle,  $\tilde{a}(\tilde{\mathbf{x}}(t), t) \doteq e\tilde{E}(\tilde{\mathbf{x}}(t), t)/m$ . Suppose that the two-time Lagrangian correlation of the electric field is stationary, so that  $\langle \tilde{E}(\tilde{\mathbf{x}}(t), t)\tilde{E}(\tilde{\mathbf{x}}(t'), t') \rangle = f(t - t')$  for some functional  $f$  of  $\tilde{\mathbf{x}}$  with finite area  $\int_{-\infty}^{\infty} d\tau f(\tau)$ . Then Eq. (I.33) is equivalent to [Krommes 1990]

$$D = \frac{e^2}{m^2} \int_0^{\infty} d\tau \langle \tilde{E}(\tilde{\mathbf{x}}(\tau), \tau)\tilde{E}(\tilde{\mathbf{x}}(0), 0) \rangle.$$

In terms of the spatially Fourier-transformed fluctuating electric field  $\hat{E}(\mathbf{k}, \tau)$ , this becomes

$$D = \frac{e^2}{m^2} \int_0^{\infty} d\tau \int \frac{d\mathbf{k}}{(2\pi)^3} \int \frac{d\mathbf{k}'}{(2\pi)^3} \langle e^{i\mathbf{k} \cdot \Delta\tilde{\mathbf{x}}(\tau)} e^{i(\mathbf{k}+\mathbf{k}') \cdot \tilde{\mathbf{x}}(0)} \hat{E}(\mathbf{k}, \tau)\hat{E}(\mathbf{k}', 0) \rangle,$$

where  $\Delta\tilde{\mathbf{x}}(\tau) \doteq \tilde{\mathbf{x}}(\tau) - \tilde{\mathbf{x}}(0)$ . If the statistics are homogeneous, this last result will not depend on the value of  $\tilde{\mathbf{x}}(0)$ . Upon averaging with respect to  $\tilde{\mathbf{x}}(0)$ , we deduce that  $\mathbf{k} + \mathbf{k}' = 0$ , so

$$D = \frac{e^2}{m^2} \int_0^{\infty} d\tau \int \frac{d\mathbf{k}}{(2\pi)^3} \langle e^{i\mathbf{k} \cdot \Delta\tilde{\mathbf{x}}(\tau)} \hat{E}(\mathbf{k}, \tau)\hat{E}^*(\mathbf{k}, 0) \rangle. \quad (\text{I.34})$$

Suppose we wish to calculate  $D$  for an unmagnetized plasma. The hypothesis of short autocorrelation time allows us to pretend that the particles move along unperturbed trajectories since under this assumption they do not receive a directed kick for any significant time. Hence,  $\Delta\tilde{\mathbf{x}}(\tau) \approx \mathbf{v}\tau$ , where  $\mathbf{v}$  is the mean velocity. Then

$$\begin{aligned} D &= \frac{1}{2} \frac{e^2}{m^2} \int_{-\infty}^{\infty} d\tau \int \frac{d\mathbf{k}}{(2\pi)^3} e^{i\mathbf{k} \cdot \mathbf{v}\tau} \langle \hat{E}(\mathbf{k}, \tau)\hat{E}^*(\mathbf{k}, 0) \rangle \\ &= \frac{1}{2} \frac{e^2}{m^2} \int \frac{d\mathbf{k}}{(2\pi)^3} \langle |\hat{E}(\mathbf{k}, \mathbf{k} \cdot \mathbf{v})|^2 \rangle. \end{aligned} \quad (\text{I.35})$$

The factor of  $1/2$  arose because we symmetrized the time integral to facilitate the Fourier transformation. It is clear that an independent calculation of the fluctuation level (the autocorrelation function) is required in order for this formula to be of use.

The diffusion coefficient Eq. (I.35) illustrates that quasilinear diffusion is a resonant phenomenon, in that all of the contribution comes from the frequency component that is zero in the frame of the moving particle. Upon comparing this result to Eq. (I.31), we see that our random walk result corresponds to the resonant term of Eq. (I.32). The nonresonant term is absent from Eq. (I.35) since only the resonant particles contribute to diffusion.

Let us now move on to illustrate the weak-turbulence approach for our generic self-consistent nonlinear stochastic equation, Eq. (I.17):

$$\left(\frac{\partial}{\partial t} + \nu_{\mathbf{k}}\right)\psi_{\mathbf{k}}(t) = \frac{1}{2} \sum_{\mathbf{k}+\mathbf{p}+\mathbf{q}=0} M_{\mathbf{k}\mathbf{p}\mathbf{q}}\psi_{\mathbf{p}}^*(t)\psi_{\mathbf{q}}^*(t).$$

Let  $\nu_{\mathbf{k}} = -\gamma_{\mathbf{k}} + i\omega_{\mathbf{k}}$ , where the linear growth rate  $\gamma_{\mathbf{k}}$  and frequency  $\omega_{\mathbf{k}}$  are both real. Also, let  $M_{\mathbf{k}\mathbf{p}\mathbf{q}} = \epsilon\bar{M}_{\mathbf{k}\mathbf{p}\mathbf{q}}$ , where  $\epsilon \ll 1$ . If  $\gamma_{\mathbf{k}} \ll \omega_{\mathbf{k}}$  and  $M_{\mathbf{k}\mathbf{p}\mathbf{q}} \ll 1$ , then to lowest order in  $\epsilon$  we have well-defined waves  $\psi_{\mathbf{k}}^{(0)}(t)$ , which we assume to obey Gaussian statistics. Expand  $\psi_{\mathbf{k}}$  in powers of  $\epsilon$ :

$$\psi_{\mathbf{k}} \doteq \psi_{\mathbf{k}}^{(0)} + \epsilon\psi_{\mathbf{k}}^{(1)} + \epsilon^2\psi_{\mathbf{k}}^{(2)} + \dots$$

Upon collecting like powers of  $\epsilon$  in our nonlinear equation, we determine relations leading to  $\psi_{\mathbf{k}}^{(n)} \propto [\psi_{\mathbf{k}}^{(0)}]^{(n+1)}$  for  $n \geq 0$ . Now for Gaussian statistics, odd moments of  $\psi_{\mathbf{k}}^{(0)}$  such as  $\langle \psi_{\mathbf{k}}^{(1)}(t)\psi_{\mathbf{k}}^{(0)}(t') \rangle$  vanish. The lowest-order expansion beyond linear theory for  $C_{\mathbf{k}}(t, t')$  is then given by

$$C_{\mathbf{k}}(t, t') = \langle \psi_{\mathbf{k}}^{(0)}(t)\psi_{\mathbf{k}}^{(0)}(t') \rangle + \langle \psi_{\mathbf{k}}^{(1)}(t)\psi_{\mathbf{k}}^{(1)}(t') \rangle + \langle \psi_{\mathbf{k}}^{(0)}(t)\psi_{\mathbf{k}}^{(2)}(t') \rangle + \langle \psi_{\mathbf{k}}^{(2)}(t)\psi_{\mathbf{k}}^{(0)}(t') \rangle.$$

We use our perturbation results to express each of the ensemble averages in terms of  $\psi_{\mathbf{k}}^{(0)}$  alone. Then, upon using the Gaussian hypothesis to express fourth-order moments in terms of second-order moments, we are led to a closed equation for the equal-time correlation function:

$$\boxed{\left(\frac{\partial}{\partial t} + \nu_{\mathbf{k}}\right)C_{\mathbf{k}}(t) + 2 \operatorname{Re} \hat{\eta}_{\mathbf{k}}(t)C_{\mathbf{k}}(t) = 2S_{\mathbf{k}}(t).} \quad (\text{I.36})$$

Here,

$$\hat{\eta}_{\mathbf{k}}(t) \doteq \pi \sum_{\mathbf{k}+\mathbf{p}+\mathbf{q}=0} \delta(\omega_{\mathbf{k}}+\omega_{\mathbf{p}}+\omega_{\mathbf{q}})M_{\mathbf{k}\mathbf{p}\mathbf{q}}M_{\mathbf{p}\mathbf{q}\mathbf{k}}^*C_{\mathbf{q}}(t)$$

represents (typically positive) nonlinear damping. The term

$$S_{\mathbf{k}}(t) \doteq \frac{\pi}{2} \sum_{\mathbf{k}+\mathbf{p}+\mathbf{q}=\mathbf{0}} \delta(\omega_{\mathbf{k}}+\omega_{\mathbf{p}}+\omega_{\mathbf{q}}) |M_{\mathbf{k}\mathbf{p}\mathbf{q}}|^2 C_{\mathbf{p}}(t)C_{\mathbf{q}}(t),$$

which is always positive, provides a source of fluctuation energy. It represents the nonlinear “beating” of waves  $\mathbf{p}$  and  $\mathbf{q}$  to generate a contribution to wave  $\mathbf{k}$ , whereas  $\eta_{\mathbf{k}}$  typically represents the inverse process. Equation (I.36) is known as the wave kinetic equation and expresses the energy “budget” between nonlinear and linear terms. Its validity is restricted to weakly turbulent systems. Nevertheless, we will eventually be led to a renormalized equation appropriate for strong turbulence that is quite reminiscent of Eq. (I.36).

Unfortunately, both quasilinear and weak-turbulence theory fail for the strong-turbulence problems of interest since the expansion parameter ( $\sim \Delta\omega/\omega$ , where  $\Delta\omega$  is the nonlinear frequency shift) is of order unity. The weak-turbulence perturbation series may diverge for such cases, leading to secularities in the predicted time behaviour. The solution to this problem will be to consider *renormalized* perturbation methods that provide closed-form expressions representing the strong-turbulence limit of these divergent series.

### **Heuristic, renormalized:**

The main weakness of both the quasilinear and weak turbulence theories is that they are not renormalized. For example, no information is contained in quasilinear theory about the *perturbed* particle trajectories. Let us now discuss the heuristic approaches to renormalization based on Dupree’s suggestion that the effect of the turbulent fluctuations on the particle trajectories can largely be described as a diffusive process [Dupree 1966]. Calculations based on this notion indicate that the effect of stochasticity is to broaden the  $\delta$  function resonances found in linear and quasilinear theory. This is the basis for the resonance-broadening theory (RBT). Unfortunately, this is not a complete theory of turbulence; although it describes (in a heuristic manner) the effects of waves on particles, it does not account for the back reaction of diffusing particles on the fields. Hence, the resonance-broadening theory does not conserve energy [Orszag and Kraichnan 1967, Dupree and Tetreault 1978]; it amounts to a passive calculation of turbulence. Finally, it does not predict the experimentally observed continuum of excited frequencies. Instead, the predicted spectrum consists of a sum of  $\delta$  functions located at the same normal mode frequencies as deduced from linear theory!<sup>13</sup>

<sup>13</sup>Shortly, we will see that RBT predicts an expression for the diffusion coefficient that does involve *broadened*  $\delta$  functions; however, the normal mode frequencies of the renormalized dielectric function remain unchanged. We encounter here the ironic result that absolutely no resonant broadening of the energy spectrum is predicted by RBT!

In light of the above arguments, let us reconsider our expression for the random-walk diffusion coefficient, Eq. (I.34). If we assume that the autocorrelation function of the electric field is statistically independent of the  $\exp(i\mathbf{k}\cdot\Delta\tilde{\mathbf{x}}(\tau))$  factor, then

$$D = \frac{e^2}{m^2} \int_0^\infty d\tau \int \frac{d\mathbf{k}}{(2\pi)^3} \langle e^{i\mathbf{k}\cdot\Delta\tilde{\mathbf{x}}(\tau)} \rangle \langle \hat{E}(\mathbf{k}, \tau) \hat{E}^*(\mathbf{k}, 0) \rangle.$$

Note that the assumption of statistical independence is implicit in the test-wave expansion carried out by Dupree [1966] but is not justifiable for strong turbulence, where the electric field is self-consistently coupled to the particle motion. Proceeding, let us assume that the turbulent fluctuations are Gaussian. Cumulant expansion then gives [Weinstock 1969]

$$\langle \exp(i\mathbf{k}\cdot\Delta\tilde{\mathbf{x}}) \rangle = \exp(i\mathbf{k}\cdot\mathbf{v}\tau - \frac{1}{2}k^2 \langle |\Delta\tilde{\mathbf{x}}|^2 \rangle),$$

where the first term in the exponential arises from free streaming and  $\langle |\Delta\tilde{\mathbf{x}}|^2 \rangle(\tau) = 2D\tau^3/3$  is the average spatial dispersion due to the random walk in velocity space. This brings us to the result obtained by Dupree for the strong-turbulence diffusion coefficient,

$$D = \frac{e^2}{m^2} \int_0^\infty d\tau \int \frac{d\mathbf{k}}{(2\pi)^3} \int_{-\infty}^\infty \frac{d\omega}{2\pi} e^{i(\mathbf{k}\cdot\mathbf{v}-\omega)\tau - \frac{1}{3}k^2 D\tau^3} \langle |\hat{E}(\mathbf{k}, \omega)|^2 \rangle.$$

In this formula we see the appearance of a nonlinear time  $\tau_{\text{nl}} = (k^2 D/3)^{-1/3}$ , which Dupree calls the “trapping” time. We shall not use this terminology since in regimes of strong stochasticity the conventional picture of electrostatic trapping of particles by waves is not valid due to the breakup of KAM surfaces. Instead, we picture a regime in which particles diffuse randomly through velocity space, resulting in chaotic motion in  $x$  space on the characteristic time scale of  $\tau_{\text{nl}}$ .

Since one important objective of plasma turbulence research is to understand stochasticity in the presence of strong magnetic fields, let us now consider the addition of a magnetic field  $B$  to the above discussion. We will analyze only the gyrocenter motion, which has a component perpendicular to the magnetic field driven by the  $\mathbf{E}\times\mathbf{B}$  drift and a parallel component subject to free streaming. This changes the character of the random walk from diffusion in velocity space to diffusion in  $x$  space since the perpendicular random motion is now governed by a fluctuating *velocity*, as opposed to an acceleration. The spatial separation is now given by  $\langle |\Delta\tilde{\mathbf{x}}(\tau)|^2 \rangle = 2D\tau$  and one obtains the diffusion coefficient [Dupree 1967]

$$D = \frac{e^2}{m^2} \int_0^\infty d\tau \int \frac{d\mathbf{k}}{(2\pi)^3} \int_{-\infty}^\infty \frac{d\omega}{2\pi} e^{i(\mathbf{k}\cdot\mathbf{v}_\parallel - \omega)\tau - k_\perp^2 D\tau} \langle |\hat{E}(\mathbf{k}, \omega)|^2 \rangle,$$

which becomes

$$D = \frac{e^2}{m^2} \int \frac{d\mathbf{k}}{(2\pi)^3} \int_{-\infty}^\infty \frac{d\omega}{2\pi} \frac{k_\perp^2 D}{(\omega - \mathbf{k}\cdot\mathbf{v}_\parallel)^2 + k_\perp^4 D^2} \langle |\hat{E}(\mathbf{k}, \omega)|^2 \rangle. \quad (\text{I.37})$$

Here we clearly see the resonance broadening brought about by the nonlinear terms. The  $\perp$  subscript on the wavenumber emphasizes that the diffusion in this strongly magnetized case is *across* the magnetic field lines.

Even though Dupree's account of the effect of stochasticity on particle trajectories is heuristically motivated and is only approximate, it does succeed in removing the singularity associated with linear theory. If we had neglected the nonlinearity by using the unperturbed spatial separation  $\Delta\tilde{\mathbf{x}}(\tau) = \mathbf{v}_{\parallel}\tau$ , we would have obtained the above result in the limit where  $D$  in the integrand is taken to zero:

$$\begin{aligned} D &= \frac{e^2}{m^2} \int \frac{d\mathbf{k}}{(2\pi)^3} \int_{-\infty}^{\infty} \frac{d\omega}{2\pi} \pi\delta(\omega - \mathbf{k}\cdot\mathbf{v}_{\parallel}) \langle |\hat{E}(\mathbf{k}, \omega)|^2 \rangle \\ &= \frac{1}{2} \frac{e^2}{m^2} \int \frac{d\mathbf{k}}{(2\pi)^3} \langle |\hat{E}(\mathbf{k}, \mathbf{k}\cdot\mathbf{v}_{\parallel})|^2 \rangle, \end{aligned}$$

which is the corresponding (unrenormalized) quasilinear result.

In linear theory, the normal modes of the plasma are given by the roots of the dielectric function (which expresses the ratio of the applied electric field to the actual field, taking account of the plasma polarization). The denominator  $-i(\omega - \mathbf{k}\cdot\mathbf{v}_{\parallel})$  that appears in the (quasi-) linear diffusion coefficient corresponding to Eq. (I.31) also appears in the expression for the linear dielectric. In Dupree's theory, the broadening factor  $\eta_{\mathbf{k}} \doteq k_{\perp}^2 D$  appears only in the combination  $\omega + i\eta_{\mathbf{k}}$ . [Since  $D$  is real, Eq. (I.37) only determines the combination  $\omega \pm i\eta_{\mathbf{k}}$ ; one must consider a complex quantity like the propagator or dielectric function to discern the correct sign.] It is therefore not surprising to learn that the renormalized dielectric function predicted by RBT is obtained simply by substituting  $\omega + i\eta_{\mathbf{k}}$  for  $\omega$  in the expression for the linear dielectric. This implies that the normal modes  $\omega_{\mathbf{k}} + i\gamma_{\mathbf{k}}$  of the turbulent plasma are related to those of the linear plasma,  $\omega_{\mathbf{k}}^{(\ell)} + i\gamma_{\mathbf{k}}^{(\ell)}$ , by

$$\omega_{\mathbf{k}} + i\eta_{\mathbf{k}} + i\gamma_{\mathbf{k}} = \omega_{\mathbf{k}}^{(\ell)} + i\gamma_{\mathbf{k}}^{(\ell)},$$

so that

$$\omega_{\mathbf{k}} = \omega_{\mathbf{k}}^{(\ell)}, \quad \gamma_{\mathbf{k}} = \gamma_{\mathbf{k}}^{(\ell)} - \eta_{\mathbf{k}}.$$

In a steady state,  $\gamma_{\mathbf{k}}$  vanishes and the second relation expresses a balance between linear drive and nonlinear dissipation. Thus, resonance broadening provides a saturation mechanism that prevents fluctuations from growing arbitrarily large. This is quite different than saturation by quasilinear flattening, which states instead that  $\gamma_{\mathbf{k}}^{(\ell)} = 0$ .

Dupree [1967] used this steady-state balance to predict that  $\gamma_{\mathbf{k}}^{(\ell)} = k_{\perp}^2 D$  for magnetized plasmas. Dupree interpreted the  $\gamma_{\mathbf{k}}^{(\ell)}$  in this formula as the growth rate of the fastest-growing mode. He argued that this is where the energy spectrum would ultimately peak. However, in the physical problem energy transfer between modes

can occur, so the steady-state energy peak need not correspond to the maximum of the linear growth rate. Moreover, the total  $\gamma_{\mathbf{k}}$  need not vanish for all  $\mathbf{k}$  but only in some average sense. Thus this expression for  $D$  should really be written

$$D = \frac{\bar{\gamma}_{\mathbf{k}}^{(\ell)}}{\bar{k}_{\perp}^2}.$$

Here, the bars indicate characteristic values obtained by some kind of spectrally weighted average.

Later, Dupree proposed that small-scale phase space structures called *clumps* should be treated on an equal footing with waves and particles. He added a friction term to the velocity-space diffusion equation predicted by quasilinear theory for the mean distribution function [Dupree 1970]. This was obtained by decomposing the fluctuating distribution function  $\tilde{f}$  into a coherent part driven directly by the fluctuating electric field  $\tilde{E}$ , a clump part, and finally a mode-coupling part. He then neglected the mode-coupling part and proposed the “clump algorithm” [Dupree 1972] as a procedure for calculating the incoherent response, analogous to the kinetic theory of discrete test particles. This *clump theory* has become popular in plasma turbulence. However, Krommes [1986] and Krommes and Kim [1988] have shown that it is only an accurate description for scales much shorter than those appropriate to transport calculations, particularly when the clump algorithm is applied to fluid equations [Dupree 1974]. Therefore we shall not consider clump theory further in this work.

### Systematically renormalized closures:

At last we come to the main subject of this work, namely the class of techniques that we will refer to as *systematically renormalized* closures. We are searching for an analytic theory of turbulence that is both renormalized, because we are interested in describing fully developed turbulence, and systematically derived, because we would like to obtain from it quantitative information such as transport coefficients. None of the methods described thus far meets both of these requirements. While we are willing to be content with an approximation, it must have a firm mathematical foundation and lead to physically reasonable solutions. Although insight can be obtained by studying and recognizing the desirable features of the previous theories, none of them is satisfactory for a complete understanding of turbulent transport.

Fortunately, examples of theories that have both of these properties *do* exist. There is a class of renormalized statistical approximations that are systematic closures of the full (divergent) perturbation series. These are obtained by neglecting, on the basis of certain statistical hypotheses, certain terms such that the remaining terms can be summed to a closed (renormalized) form that represents the exact

statistical solution of a related stochastic model. The modified perturbation series still contains terms of all orders in the expansion parameter in such a way that the renormalized form remains nonsecular even in the strong-turbulence regime, unlike any finite truncation of the moment or cumulant hierarchy. In this work we will be concerned with *second-order* closures, which evolve the two-time correlation function in terms of itself, the response function, and the mean field (if considered). These closures also provide similar evolution equations for the response function and mean field, so the entire system is *self-consistently* coupled.

The general form of a statistical closure in the absence of mean fields is

$$\left(\frac{\partial}{\partial t} + \nu_{\mathbf{k}}\right) C_{\mathbf{k}}(t, t') + \overbrace{\int_0^t d\bar{t} \Sigma_{\mathbf{k}}(t, \bar{t}) C_{\mathbf{k}}(\bar{t}, t')}^{\text{nonlinear damping}} = \overbrace{\int_0^{t'} d\bar{t} \mathcal{F}_{\mathbf{k}}(t, \bar{t}) R_{\mathbf{k}}^*(t', \bar{t})}^{\text{nonlinear noise}}, \quad (\text{I.38a})$$

$$\left(\frac{\partial}{\partial t} + \nu_{\mathbf{k}}\right) R_{\mathbf{k}}(t, t') + \int_{t'}^t d\bar{t} \Sigma_{\mathbf{k}}(t, \bar{t}) R_{\mathbf{k}}(\bar{t}, t') = \delta(t - t'). \quad (\text{I.38b})$$

These equations specify an initial-value problem for which  $t = 0$  is the initial time. The system can be written in an even more symmetrical manner by replacing the lower limit  $t'$  on the integral in Eq. (I.38b) with 0. Since  $R_{\mathbf{k}}(\bar{t}, t')$  vanishes for  $\bar{t} < t'$  this modification has no effect for all times  $t' \geq 0$ . We then note that identical operators act on  $C_{\mathbf{k}}$  and  $R_{\mathbf{k}}$  on the left-hand sides of Eqs. (I.38).

It is instructive to compare the form of Eq. (I.38a) with the wave kinetic equation, Eq. (I.36). In both cases, the original nonlinearity in Eq. (I.17) has become separated into two effects: one describing nonlinear damping and one modeling nonlinear noise. Note that this structure is reminiscent of a Langevin equation. However, the nonlinear damping and noise in Eqs. (I.38) are determined on the basis of fully nonlinear statistics. That is, the linear  $\delta$  function resonances appearing in Eq. (I.36) have been renormalized to include nonlinear broadening effects such as those described by Dupree. It is worth remarking that, given appropriate forms for  $\Sigma_{\mathbf{k}}$  and  $\mathcal{F}_{\mathbf{k}}$ , Eqs. (I.38) would be an exact description of the second-order statistics. Unfortunately, this merely shifts the difficulty to the determination of these new functions.

The most well-known example of a statistical closure is the direct-interaction approximation (DIA) [Kraichnan 1958a, 1959a, 1961]. This provides specific *ap-*

proximate forms for  $\Sigma_{\mathbf{k}}$  and  $\mathcal{F}_{\mathbf{k}}$ :

$$\Sigma_{\mathbf{k}}(t, \bar{t}) = - \sum_{\mathbf{k}+\mathbf{p}+\mathbf{q}=\mathbf{0}} M_{\mathbf{k}\mathbf{p}\mathbf{q}} M_{\mathbf{p}\mathbf{q}\mathbf{k}}^* R_{\mathbf{p}}^*(t, \bar{t}) C_{\mathbf{q}}^*(t, \bar{t}), \quad (\text{I.39a})$$

$$\mathcal{F}_{\mathbf{k}}(t, \bar{t}) = \frac{1}{2} \sum_{\mathbf{k}+\mathbf{p}+\mathbf{q}=\mathbf{0}} |M_{\mathbf{k}\mathbf{p}\mathbf{q}}|^2 C_{\mathbf{p}}^*(t, \bar{t}) C_{\mathbf{q}}^*(t, \bar{t}). \quad (\text{I.39b})$$

The resulting equations satisfy the same conservation laws (arising from symmetries in the mode-coupling coefficients) as those obeyed by the primitive dynamical equation. In the limit of weak turbulence, the DIA equations correctly reduce to perturbation theory [Kraichnan 1961]. Another pleasing property of the DIA is that the multiple-field formulation is covariant to general linear transformations on the stochastic variables [Ottaviani *et al.* 1991]. Also, the closure equations are the exact statistical moments of a certain underlying stochastic equation [Kraichnan 1970a]; hence the DIA is realizable.

There are infinitely many other ways of obtaining a renormalized expression from the weak turbulence perturbation series by neglecting select terms, but it has been shown that most of these schemes lead to physically unacceptable solutions [Kraichnan 1961]. For example, they might predict the impossible situation of a negative value for  $C_{\mathbf{k}}(t, t)$  (i.e., a negative energy)! In contrast, the DIA, because it is realizable, leads to physically reasonable solutions. We will focus closely on this important realizability property when we begin the development of other statistical closures.

Normally, Eqs. (I.38) are solved as an initial value problem, evolving the coupled set from specified initial conditions on the equal-time covariances. However, Eq. (I.38b) can be used to write Eq. (I.38a) instead as

$$C_{\mathbf{k}}(t, t') = \int_{-\infty}^{\infty} d\bar{t} \int_{-\infty}^{\infty} d\bar{t}' R_{\mathbf{k}}(t, \bar{t}) \mathcal{F}_{\mathbf{k}}(\bar{t}, \bar{t}') R_{\mathbf{k}}^*(t', \bar{t}'), \quad (\text{I.40})$$

or, formally,  $C_{\mathbf{k}} = R_{\mathbf{k}} \mathcal{F}_{\mathbf{k}} R_{\mathbf{k}}^\dagger$ . Here we regard the two-time indices as continuum matrix indices. One of the advantages of this representation is that it relates the desired positive-semidefinite nature of  $C_{\mathbf{k}}(t, t')$  to that of  $\mathcal{F}_{\mathbf{k}}(t, t')$ . This form will play a crucial role in our development of realizable Markovian closures. Note that Eq. (I.40) is not well suited to numerical work because the nonlinearity appears in two places: partly in  $R_{\mathbf{k}}$  and partly in  $\mathcal{F}_{\mathbf{k}}$ . Care must be taken when making further approximations (e.g., temporal discretization or outright neglect of terms) to treat all of the nonlinear terms consistently, lest conservation laws be violated. In addition, the initial conditions are intricately entangled within  $\mathcal{F}_{\mathbf{k}}$ , obscuring the causal nature of the equation. In any case, numerical solution of Eq. (I.40)

would typically require the introduction of a relaxation parameter, resulting in a scheme similar to the initial value representation. In this work, then, the numerical computations will be performed using Eq. (I.38); the symmetric form, Eq. (I.40), will be used only to investigate certain analytical properties.

## I.E Statistical closure *vs.* direct simulation

Let us now discuss the relative merits of statistical closure methods and direct simulation of the fundamental dynamics. Notice that when Eqs. (I.39) are inserted into Eqs. (I.38), the resulting set of equations is highly nonlinear in the unknowns  $C_{\mathbf{k}}$  and  $R_{\mathbf{k}}$ . In fact, closure equations are generally intractable to solve analytically without making drastic approximations. It is quite reasonable to ask, then, just what has been accomplished. After all, we began with a nonlinear equation Eq. (I.17), and, after making some so-far unjustified approximations on the resulting moment hierarchy, ended up with a coupled nonlinear *system* of equations. At first, it might appear that we have made no progress at all!

However, Eqs. (I.38) have a distinct advantage over Eq. (I.17) in that, although they are still nonlinear, they are not stochastic. The statistical variables appearing in Eqs. (I.38) *vary much more slowly* with respect to wavenumber and time than the original highly fluctuating variable  $\psi_{\mathbf{k}}(t)$ . This allows one to use wavenumber partitions (possibly nonuniformly spaced) to reduce the required number of modes [Leith and Kraichnan 1972, Bowman and Krommes 1988]. The difficulty with Eq. (I.17) is that it is both nonlinear *and* stochastic. Nonlinear equations can be solved numerically if the resolution requirements are not too great, and for this reason closure equations can sometimes be solved for cases where computation of the fundamental equation is not feasible. This is especially true in problems involving high degrees of symmetry and homogeneity; for example, closures have been used to study isotropic turbulence at Reynolds numbers far beyond the range accessible by spectral or pseudo-spectral codes applied to the primitive dynamics [Kraichnan 1964a].

In contrast, direct simulation of high-Reynolds number turbulence is limited by the range of scales involved. Since the dissipation scales are of order  $R^{3/4}$  times smaller than the energy-containing scales [Landau and Lifshitz 1987], in three dimensions this means that  $R^{9/4}$  spatial degrees of freedom must be retained. Furthermore, since the time scale of energy evolution is roughly the turnover time of the large-scale eddies, the Courant condition for numerical stability implies that at least  $R^{3/4}$  time steps are required for significant evolution of the flow. Thus, the total computation time is at least of order  $R^3$ . To circumvent this difficulty, hybrid techniques such as large-eddy simulations have been developed; these methods combine numerical simulation of the large scales with an analytical model for the

subgrid physics.

### I.E.1 Ensemble average *vs.* time average

Another reason for preferring closures over direct simulation is that closures are built directly from physically significant quantities like generalized diffusion coefficients and correlation functions. Primitive numerical data generally cannot be represented in such terms since this data corresponds to a single realization only. If one literally wants to compare the ensemble average for the two methods, many (often thousands) of realizations of the primitive dynamical system must be evolved and then averaged. This is greatly detrimental to the competitiveness of direct simulation.

However, the ensemble averaging just described is rarely done in practice. In fact, we know of only three cases where such a computation was actually reported in the literature: two of these were attempts to validate the DIA for systems of three interacting waves [Kraichnan 1963, Krommes 1982] and the third was a study of a system of test waves involving a moderate number (91) of interacting triads [Meiss *et al.* 1979]. The usual practice is to invoke an assumption of ergodicity so that an ensemble average becomes equivalent to a time average. To calculate a time average, only one realization is required, but now the evolution must be carried far out in time beyond the saturated steady state, if such a state even exists. Moreover, the time-averaging method cannot be used to study transient behaviour such as the viscous decay of excited turbulence. It is sometimes argued that the time-averaging method is the one more appropriate to any individual experiment. However, there are philosophical reasons, already given, as to why the ensemble average is actually preferable: we want to use an average that reflects the consensus of many simultaneous such experiments so that the numbers we quote are not sensitive to slight variations in the initial configuration [Balescu 1975].

### I.E.2 Identification of nonlinear interactions

Another argument that can be made in favor of closures is that people think analytically. Closures help provide an analytical understanding of the detailed nonlinear interactions that operate in a turbulent system. For example, statistical closures partition the effects of the nonlinear interactions into distinct classes of terms (e.g., “diffusion” *vs.* “polarization”; “coherent” *vs.* “incoherent”). These terms can be turned off one by one in order to study their relative importance. In contrast, the original dynamical equations usually have these different effects lumped together into one term (for example, the  $\mathbf{E} \times \mathbf{B}$  advection nonlinearity). If one turns this term off, the equation loses all of its nonlinear features [Krommes 1984a].

## I.F Overview of this work

To summarize the discussion presented thus far, Table I.1 presents a hierarchy of several popular approaches to plasma turbulence.<sup>14</sup> The previous discussion has emphasized severe inadequacies not only with linear theory but also with three important methods for extrapolating beyond linear theory: namely, the quasilinear, resonance broadening, and weak turbulence theories. In contrast, the Markovian closure and direct-interaction approximation, being systematically renormalized, appear to be much better candidates for a theory of strong turbulence. Ultimately, one might anticipate continuing up this hierarchy, constructing a sequence of progressively more complicated closures that converges to the exact solution.

More will be said regarding this objective in Chapter II, where the topic of systematically renormalized closures is considered in greater detail. This review will discuss a general scheme, namely the formalism of Martin, Siggia, and Rose [1973] (MSR), under which closures like the direct-interaction approximation can be derived. Other promising closure techniques that have become popular alternatives to the DIA for quantitative studies of turbulence will also be surveyed. These include Markovian closures, decimation, mapping closures, and the renormalization group method. Chapter II will focus primarily on the direct-interaction approximation. Several different derivations of the DIA will be given. This approximation will be illustrated by applying it to a number of pedagogical problems. Emphasis is placed on properties of the DIA that can be proven analytically. Both the advantages and disadvantages of this approximation are discussed; in particular, this work will address the reason that researchers have virtually abandoned the DIA in recent years as a tool for studying fluid turbulence. Arguments are given to suggest that the particular difficulties that led to this state of affairs in fluid turbulence may not be of such great concern for plasma transport calculations. Moreover, one of these difficulties, namely the incorrect modeling of the inertial range (which is largely irrelevant for transport calculations), can be circumvented by using a related Markovian formulation known as the test-field model (TFM) [Kraichnan 1971b, 1972].

Overall, the DIA has many of the properties desired of a closure. Unfortunately, as the discussion in Chapter II will emphasize, its application to multi-dimensional inhomogeneous turbulence remains a formidable challenge due to its restrictive computational scaling with time. Practical turbulence problems often require the use of many time steps to evolve to a steady state, and even on modern supercomputers the situation is quite discouraging. Stimulated by computational considerations, this work therefore proceeds in Chapter III to consider simpler Markovianized versions of the direct-interaction approximation that are faster to compute but nevertheless

---

<sup>14</sup>This list is not exhaustive; it serves only to illustrate the logical position of statistical closures relative to a sample of the many alternative theories of turbulence.

| Theory                           | Comments   |
|----------------------------------|--|
| Linear Theory                    | <ul style="list-style-type: none"> <li>— delta function energy spectrum [solution of <math>\mathcal{D}^{(\ell)}(\mathbf{k}, \omega) = 0</math>]</li> <li>— not valid in strong turbulence regime</li> <li>— does not conserve energy</li> </ul>  |
| Quasilinear Theory               | <ul style="list-style-type: none"> <li>— allows for back-reaction of waves on <math>\langle f_0 \rangle</math></li> <li>— conserves energy</li> <li>— assumes waves do not significantly affect particle orbits in a wave period (no electrostatic trapping)</li> <li>— does not explain experimentally observed saturation with <math>\nabla n \neq 0</math></li> </ul>   |
| Resonance Broadening             | <ul style="list-style-type: none"> <li>— accounts for nonlinear modification of particle orbits</li> <li>— predicts a broadening of linear resonances due to stochasticity</li> <li>— assumes particle perturbations by wave are diffusive</li> <li>— delta function energy spectrum [solution of <math>\mathcal{D}^{(nl)}(\mathbf{k}, \omega) = 0</math>]</li> <li>— does not treat electric field self-consistently</li> </ul> |
| Weak Turbulence Theory           | <ul style="list-style-type: none"> <li>— perturbative but goes to higher order than quasilinear theory</li> <li>— mode-coupling effects appear (three wave interactions)</li> <li>— self-consistent</li> <li>— expansion parameter <math>\Delta\omega/\omega \sim 1</math> for tokamaks</li> </ul>   |
| Markovian Closure                | <ul style="list-style-type: none"> <li>— realizable</li> <li>— nonlocal in space</li> <li>— local in time (has only equal-time correlation functions)</li> <li>— clearly identifies mode-coupling effects and nonlinear modifications to the growth rate</li> </ul>  |
| Direct-Interaction Approximation | <ul style="list-style-type: none"> <li>— nonlocal in space and time</li> <li>— more realistic than Markovian closure</li> <li>— two-time correlation functions yield <math>\tau_{ac}</math> (interaction time)</li> <li>— violates Random Galilean Invariance</li> </ul>   |
| Higher order DIA-like closures   | <ul style="list-style-type: none"> <li>— potentially more accurate than the DIA</li> <li>— potential difficulties with realizability</li> <li>— computationally infeasible</li> </ul>  |
| Exact Solution                   | <ul style="list-style-type: none"> <li>— requires direct numerical computation</li> <li>— ensemble average requires <i>many</i> realizations</li> <li>— time average assumes ergodic theorem; must run long after saturation</li> </ul>  |

Table I.1: Hierarchy of several important theories of turbulence.

do capture *some* of the desirable features of the DIA.

The most important contribution of this work begins with the observation that the conventional example of a DIA-based Markovian closure severely violates realizability in the presence of linear wave phenomena. Waves are absent from the linear term of the incompressible fluid equations for which this closure was originally designed. Furthermore, no general multiple-field formulation of this closure is given anywhere in the literature. We require that such a formulation be systematically obtained from the direct-interaction approximation and that it satisfy the properties of realizability, covariance, and conservation of all of the fundamental quadratic invariants. It turns out to be very difficult to meet all of these constraints. However, we take advantage of this fact: these constraints may be used to reduce the arbitrariness of the closure. We are eventually led to a new approximation, which we call the realizable Markovian closure (RMC), that satisfies all of these criteria. The main advance here is the recognition of a form for the Fluctuation-Dissipation ansatz more suitable than the equilibrium one as an approximation for nonequilibrium systems. We suggest that the RMC is more closely related to the DIA than any of the other proposed Markovian closures in the literature; we expect its performance to be superior, except for the inaccurate modeling of the inertial range. Fortunately, if the inertial range scaling is actually considered to be important, there is a way to construct a related closure along the lines of the TFM. Unlike the TFM, which is also not realizable in the presence of waves, this latter closure both is realizable *and* captures the correct inertial-range behaviour.

In Chapter IV, we discuss the numerical implementation of the previously discussed closures for two-dimensional anisotropic turbulence. We employ a technique of wavenumber reduction for which statistical closures are particularly suited. This involves partitioning the wavenumber space into bins over which the statistical variables are smoothly varying. The approach used here is an anisotropic generalization of the isotropic wavenumber bin-averaging method of Leith and Kraichnan [1972]. Next, we describe the numerical predictor-corrector algorithm employed in the code DIA [Krommes and Bowman 1988, Bowman and Krommes 1988], which was used to obtain numerical solutions of many of the closures to be discussed in this work. This is a *generic* code, in that it may be programmed to solve a wide variety of turbulence problems, including, in principle, those involving inhomogeneities, kinetic descriptions, or a third dimension. It includes several novel features, including a facility that implements a dynamically adjusted variable time step.

In Chapters V and VI we discuss the applications of this work to a pedagogical problem of three interacting waves and to the Terry-Horton equation for drift-wave turbulence, respectively. The results indicate that, particularly for systems with many interacting modes, the closure techniques work remarkably well in comparison with direct simulations of the primitive dynamical equations.

Finally, in Chapter VII we summarize the material we have presented and discuss possibilities for future applications. In discussing some of the limitations of statistical closures, we briefly mention a promising and largely unexplored alternative to the methods considered in this work. Known as the “optimum theory,” this approach uses functional analysis to determine rigorous bounds to the turbulent flux that a given nonlinear equation can sustain. However, this technique has its own difficulties. It is likely that a satisfactory understanding of turbulence will be achieved only with the combined use of many approaches, including statistical closures, the optimum theory, and direct numerical simulation. To limit our scope, therefore, the primary focus of this work will be on the method of statistical closures.

Several appendices are included at the end; these contain results such as proofs of theorems that are too involved to appear in the main body.

# Chapter II

## General Theory of Systematically Renormalized Closures

A seminal example of a systematic renormalization of classical perturbation theory is the direct-interaction approximation [Kraichnan 1958a, 1958b, 1958c, 1959a, 1961]. Before going into a detailed examination of this statistical closure, let us first describe the logical framework into which it naturally fits.

### II.A Overview of closure techniques

The general formalism of Martin, Siggia, and Rose [1973] (MSR) constructs a formal but exact closure (assuming Gaussian initial statistics; *cf.* 17) for which the DIA is, in a certain sense, the lowest-order iterative approximation. Their formalism thus provides one possible framework for the development of higher-order closures and logically helps set the stage for the discussion of the DIA itself. Alternative routes to the development of statistical closures are also examined, such as the mixed Eulerian/Lagrangian schemes and series reversion, along with more practical schemes that have generated recent interest, such as various Markovian closures, the renormalization group (RNG) approach, decimation, and mapping closures.

#### II.A.1 Renormalized perturbation theory and MSR

For quantum mechanical systems, renormalized field theories have been known for a long time. These include the diagrammatic scheme of Feynman [1949a, 1949b] and the equivalent functional equations of Schwinger [1951a, 1951b]. The equivalence was established by Dyson [1949a, 1949b], who summed up disconnected diagrams into a closed form by the introduction of a “mass operator”  $\Sigma$ . In view of these successes, it is perhaps surprising that an equivalent renormalized theory

of *classical* systems was not developed until some twenty years later. One could imagine the possibility of obtaining a classical renormalized theory from the quantum one in the limit  $\hbar \rightarrow 0$ . While attempts to derive such a theory for plasmas have been made [Wyld and Pines 1962, Dubois 1967], this approach is not generally effective. For example, classical dissipative systems clearly have no quantum analog since friction is a phenomenon that appears only in macroscopic descriptions.<sup>1</sup>

Fortunately, substantial progress has been made in the search for a purely classical renormalization. Most important is the work of Martin *et al.* [1973] and the related works of Rose [1974] and Phythian [1975, 1976]. They develop an elegant functional representation in which a renormalized matrix “mass” operator  $\mathbf{\Sigma}$  and a renormalized tensor “vertex” operator  $\mathbf{\Gamma}$  are introduced by analogy with the mass and charge renormalizations, respectively, of quantum mechanics. A closed system of four equations is thereby obtained for the four matrices  $\mathbf{\Sigma}$ ,  $\mathbf{\Gamma}$ , a generalized mean field, and a generalized covariance, thus providing an exact formal description of the statistics, given Gaussianly distributed initial conditions.

Let us adopt the fundamental equation introduced in the previous chapter, Eq. (I.17), for some fluctuating variable  $\psi_{\mathbf{k}}$ . An important aspect of the MSR formalism is that it treats the covariance and infinitesimal response functions on an equal footing through the introduction of an adjoint operator  $\hat{\psi}_{\mathbf{k}}$ . This operator satisfies the commutation relation [Rose 1974]

$$[\psi_{\mathbf{k}}(x, t), \hat{\psi}_{\mathbf{k}}(x', t)] = \delta(x - x'), \quad (\text{II.1})$$

where  $[A, B] \doteq AB - BA$ , and has Fourier components obeying

$$\left(\frac{\partial}{\partial t} - \nu_{\mathbf{k}}^*\right) \hat{\psi}_{\mathbf{k}}(t) = - \sum_{\mathbf{k}+\mathbf{p}+\mathbf{q}=\mathbf{0}} M_{\mathbf{p}\mathbf{q}\mathbf{k}} \hat{\psi}_{\mathbf{p}}^*(t) \psi_{\mathbf{q}}^*(t), \quad (\text{II.2})$$

such that  $\langle \hat{\psi}_{\mathbf{k}}(t) \psi_{\mathbf{k}}(t') \rangle = 0$ .<sup>2</sup> Next, Martin *et al.* [1973] constructed a time-ordering operation (denoted by a “+” subscript)

$$\langle A(t)B(t') \rangle_+ \doteq H(t - t') \langle A(t)B(t') \rangle + H(t' - t) \langle B(t')A(t) \rangle,$$

where H is the Heaviside function defined by Eq. (I.21).

---

<sup>1</sup>Of course, the molecular forces underlying friction could be incorporated explicitly into the system under consideration, so that the overall quantum mechanical Hamiltonian is conservative, but this would involve the enormous complexity of a microscopic theory. It is just this unnecessary detail one is trying to avoid by adopting a classical description in the first place. Certainly, reduction of a classical renormalized theory from the quantum analog is not what is sought.

<sup>2</sup>Note that there is no rule  $\langle \psi_{\mathbf{k}}(t) \hat{\psi}_{\mathbf{k}}(t') \rangle = 0$ . This asymmetry is connected with the causal nature of the initial value problem.

One can then show that the correlation function  $C_{\mathbf{k}}$  and response function  $R_{\mathbf{k}}$  (cf. pg. 21) satisfy the conjugate relations

$$\begin{aligned} C_{\mathbf{k}}(t, t') &= \langle \psi_{\mathbf{k}}(t) \psi_{\mathbf{k}}^*(t') \rangle_+; \\ R_{\mathbf{k}}(t, t') &= \langle \psi_{\mathbf{k}}(t) \widehat{\psi}_{\mathbf{k}}^*(t') \rangle_+. \end{aligned}$$

The time-ordering operation ensures that  $R_{\mathbf{k}}(t, t')$  vanishes for  $t \leq t'$ , as is required by causality.

In the higher-dimensional space consisting of the set of ordered pairs  $(\psi_{\mathbf{k}}, \widehat{\psi}_{\mathbf{k}})$ , there is thus a manifest symmetry between the statistical variables. In this new space the response and correlation functions appear as components of a generalized covariance matrix. The fundamental equation has a form similar to Eq. (I.17) but with new coefficients: in particular, the old mode-coupling coefficient  $M$  is replaced by a matrix we shall denote by  $\gamma$  (not to be confused with the linear growth rate). In diagrammatic terminology,  $\gamma$  is the *bare vertex* multiplier.

Martin *et al.* [1973] now introduce a generating functional for the mean response to perturbations of the fundamental equation. Derivatives of this functional, upon removal of the perturbation, reduce to the desired generalized statistical functions. Closed-form functional equations describing the evolution of the generator can now be obtained directly from the equations of motion, without the introduction of a moment hierarchy.

Unfortunately, these statistical equations are extremely complicated and *highly coupled*. In practice, their solution requires some sort of expansion in a small parameter. The choice used by MSR is the matrix extension  $\mathbf{\Gamma}$  of the skewness parameter  $\bar{\Gamma}$ . The skewness parameter is defined by

$$\bar{\Gamma} \doteq \frac{\langle \langle \psi^3 \rangle \rangle}{\langle \langle \psi^2 \rangle \rangle^{3/2}}$$

and is a statistical measure of the departure from Gaussianity. Equivalently, the closed equations are solved by expanding the unobservable (bare) vertex  $\gamma$  in powers of the observable (dressed) vertex  $\mathbf{\Gamma}$ . (This particular choice is not uniformly small for all scales.) By doing this, one is effectively led to an expansion of triple moments in an infinite power series in the covariance. Finite truncations of the MSR series are generally expected to be much better behaved than elementary perturbative expansions in powers of the Reynolds number [Kraichnan 1977], which give unphysical results even for moderate Reynolds number turbulence. The lowest-order truncation of the MSR expansion is actually the direct-interaction approximation derived by Kraichnan using more elementary “first principles” arguments (to be described later). In this truncation, the vertex function  $\mathbf{\Gamma}$  reduces simply to  $\gamma$  (the mode-coupling coefficient); only the renormalized mass operator  $\mathbf{\Sigma}$  appears explicitly at

this order. The power of the functional approach is evident here; compare the enormously more complicated derivation of the DIA from a diagrammatic procedure [Wyld and Pines 1962]. The advance brought about by the MSR formalism is that it allows one to consider (in an efficient way) successive refinements of the DIA, which if convergent<sup>3</sup> would lead systematically to closed equations representing the exact solution.

Another possible procedure is to expand  $\Gamma$  in powers of  $\gamma$ ; however, beyond lowest order this leads to certain ill-behaved higher-order closures first discussed by Kraichnan [1961]. He showed that the average response functions predicted by these closures for the Gaussian stochastic oscillator diverge in time. The lowest-order truncation (the DIA) is exceptional in that it is realizable, thus guaranteeing reasonable behaviour. Kraichnan did discover a partial summation at the next order that he believes *is* realizable; this corresponds to the second-lowest-order truncation of the original MSR scheme discussed in the previous paragraph. However, it is believed that at even higher orders this procedure also leads to secularities [Krommes 1984b]. The fact that higher-order closures are not necessarily realizable is a major deficiency of the MSR perturbation method.<sup>4</sup> Krommes [1984b] has suggested a possible generalization involving a continued fraction representation, based on the notion that resonant functions should be approximated by expanding their *reciprocal* to avoid the ill behaviour that results from “expanding out” a resonance. However, as Krommes admits, this generalization is almost certainly of only conceptual interest because of its extreme technical complexity.

The adjoint operator introduced above is equivalent to the operator  $\hat{\psi}_{\mathbf{k}} = -\delta/\delta\psi_{\mathbf{k}}$  [Rose 1974]. Thus, in light of the commutation relation Eq. (II.1), we observe that the relationship between  $\psi$  and  $\hat{\psi}$  is reminiscent of the role of the quantum mechanical variables for position and momentum. In fact, the functional representation given by MSR also has a path integral formulation just as in the case of quantum mechanics. Another route to the functional MSR formalism, which does not require the introduction of noncommuting operators, has been described by Phythian [1977] and Jensen [1981, and refs. therein]. This is achieved by representing the correlation and response functions in terms of functional integrals.

---

<sup>3</sup>Convergence is by no means guaranteed. For example, terms of the form  $\exp(-1/\epsilon)$  have asymptotic expansions in  $\epsilon$  that vanish identically; such exponential effects may not be captured in the functional Taylor series truncations of renormalized perturbation theory [Kraichnan 1966a]. However, the alternative approach of statistical decimation, to be discussed later, provides a framework that does suggest a convergent sequence of approximations.

<sup>4</sup>However, there is strong evidence that alternative expansions based on Padé approximants do lead to realizable closures [Kraichnan 1970b, Orszag 1991].

## II.A.2 Eulerian *vs.* Lagrangian formulations

Another serious difficulty with the MSR formalism is that it is based on Eulerian correlation functions. This implies that any finite perturbative truncation of the renormalized equations, unlike primitive truncations of the moment hierarchy, introduces a spurious coupling between the large and small spatial scales. This results from the violation of a statistical property known as random Galilean invariance (RGI) [Kraichnan 1964b]. The exact statistics dictate that the ensemble-averaged velocity of the small scales should be invariant to random Galilean transformations. In other words, the small scales should not be affected by (uniform) advection occurring on the large scales, even if the magnitude and direction of the large-scale velocity is different in each realization. For our purposes it is convenient to assume that the ensemble-averaged advection velocity has zero mean. The (exact) Eulerian *two-time* correlation function *is* affected by this uniform advection since, at displaced times, which particular fluid elements pass a fixed point will depend on the advecting velocity. However, the energy associated with a given scale depends only on the *equal-time* Eulerian covariance and will be invariant to these random Galilean transformations. In the full renormalized perturbation series, intricate cancellations among the two-time statistics of all orders allow the equal-time statistics to be random Galilean invariant. In contrast, any finite truncation of the renormalized perturbation series built out of two-time covariances will violate random Galilean invariance. That is, the energy spectrum will be contaminated since the renormalized closure will *inexactly* relate the evolution of equal-time statistics to two-time statistics. It is only when one sums to all orders that this spurious transfer of energy from the large to the small scales disappears [Kraichnan 1977].<sup>5</sup>

We shall see later that the most serious effect of the RGI violation for the DIA closure is that it results in an incorrect inertial range. For isotropic three-dimensional turbulence, instead of the Kolmogorov inertial-range scaling  $E(k) \sim k^{-5/3}$  one obtains a scaling of  $k^{-3/2}$ . That the DIA exponent is higher than the actual exponent is not surprising in light of the above arguments since the DIA *overestimates* the transfer of energy from the production to the dissipation ranges, which tends to reduce the slope.

One solution to this problem is to consider Lagrangian correlation functions, which are measured along the trajectory of a moving fluid element. By heuristically modifying the DIA equations into a Lagrangian representation, Kraichnan [1965] developed the Lagrangian-history DIA and the abridged Lagrangian-history DIA. This was done by introducing a generalized velocity  $u(x, t | s)$ , representing the velocity at the *measuring* time  $s$  of the fluid element that passed through the

---

<sup>5</sup>Kadomtsev [1965] independently recognized the difficulties of the DIA in representing the interactions between the large and small scales. His arguments were less mathematically precise than those of Kraichnan [1964b].

point  $x$  at the *labeling* time  $t$ . Hence  $u(x, t | t)$  is the ordinary Eulerian velocity and  $u(x, 0 | s)$  is the Lagrangian velocity of a fluid element that was at position  $x$  at the initial time  $s = 0$ . Not surprisingly, there is substantial arbitrariness in the details of this heuristic generalization. Worse, so far no underlying stochastic amplitude equation has been found for either of the Lagrangian closures [Kraichnan 1971b]. The unabridged Lagrangian closure is much more complicated than the DIA; while it is believed to predict the Kolmogorov inertial-range scaling correctly, according to Leslie [1973a] this has never been tested. However, the abridged Lagrangian-history DIA has been integrated numerically [Kraichnan 1966b, Herring and Kraichnan 1979] and found to reproduce the correct inertial range, with a Kolmogorov constant well within the scatter of experimental data [Leslie 1973a]. A related approximation is the strain-based Lagrangian-history closure, in which triple moments are expanded in powers of the Lagrangian covariance of the mean rate of strain, rather than of the velocity field [Kraichnan and Herring 1978]. A numerical comparison of the strain-based and velocity-based closures for two- and three-dimensional fluid turbulence has been presented by Herring and Kraichnan [1979].

Later, Kraichnan [1977] discovered a more systematic approach for deriving both Eulerian and Lagrangian renormalized closures based on the powerful method of functional series reversion. Series reversion is a method for inverting the functional equation  $f(x) = \mathcal{P}(g(x))$ , where  $\mathcal{P}$  represents a power series, to obtain  $g(x)$  as a function of  $f(x)$ . This is done by inserting successive approximations of  $g(x)$  into all but the lowest-order term of the power series, beginning with the zeroth-order approximation  $g(x) = f(x)$ , and then isolating the lowest-order term.

Renormalization by series reversion proceeds by formally expanding nonlinear statistical functions in terms of their linearized counterparts and then reverting the resulting series to express the linear statistics in terms of the nonlinear statistics. Next, one inserts the latter expressions back into the linearized quantities appearing in the unreverted series. Upon collecting like powers of  $M$  (the mode-coupling coefficient), at each order one obtains renormalized equations, beginning with the DIA. In the context of renormalization by series reversion, the arbitrariness in the heuristic derivations of the Lagrangian closures becomes clearer. It results from the nonuniqueness of the reversion method when one tries to express perturbed correlations having four time indices in terms of unperturbed correlations having only two time indices [Kraichnan 1977]. A noteworthy advantage of the method of series reversion is that closures may be obtained without the requirement that the initial conditions be Gaussianly distributed.

### II.A.3 Markovian closures

Even the lowest-order Eulerian renormalization, the DIA, is tremendously difficult to solve for many practical problems. The main difficulty is the number of computations required to calculate the time-history integrals appearing in Eqs. (I.38). For this reason, simpler Markovian closures that neglect much of the detailed time history have been developed in the literature. For example, we obtain a Markovian closure if we specify in Eqs. (I.38) the following forms for  $\Sigma_{\mathbf{k}}$  and  $\mathcal{F}_{\mathbf{k}}$ :

$$\Sigma_{\mathbf{k}}(t, \bar{t}) = \hat{\eta}_{\mathbf{k}}(t) \delta(t - \bar{t}), \quad (\text{II.3a})$$

$$\mathcal{F}_{\mathbf{k}}(t, \bar{t}) = F_{\mathbf{k}}(t) \delta(t - \bar{t}). \quad (\text{II.3b})$$

To have a complete set of equations, one must also provide forms for  $\hat{\eta}_{\mathbf{k}}(t)$  and  $F_{\mathbf{k}}(t)$  based on either physical insight or comparison to a more sophisticated closure like the DIA. The DIA seems to be an appropriate starting point for the development of Markovian closures since it is realizable and arises naturally as the lowest-order truncation of the MSR renormalization. In this work, our main focus will be on the development of such Markovian closures.

Another reason for considering Markovian closures has been given by Kraichnan. Recall that it is the *two-time* correlation functions that spuriously carry the interactions between large and small scales into the equal-time DIA equations. Since Markovian closures involve only equal-time correlation functions, it is not surprising that the additional freedom obtained by not specifying the intricacies of the two-time behaviour permits modifications that restore random Galilean invariance. An example of such a heuristically modified Markovian closure is the test-field model. In contrast, Kraichnan [1971b] sought in vain for a similar realizable modification of the DIA, but he was led to the conclusion that the two-time behaviour was too intertwined to allow an analogous remedy.

### II.A.4 Other schemes

We now discuss several more recent schemes that have all shown promise in characterizing aspects of turbulence.

#### Renormalization group approach:

Renormalization group analysis [Yakhot and Orszag 1986] is founded on the premise that hydrodynamic turbulence in the inertial range can be described on the basis of *similarity* arguments. The motivation for this concept arises from the apparent universality and self-similarity of the Kolmogorov inertial range.

The RNG approach begins by introducing the modified Navier-Stokes equation

$$\frac{\partial}{\partial t} \mathbf{u} + \mathbf{u} \cdot \nabla \mathbf{u} = \tilde{\mathbf{f}} - \frac{1}{\rho} \nabla P + \mu \nabla^2 \mathbf{u}, \quad (\text{II.4})$$

where  $\tilde{\mathbf{f}}$  is a random force chosen to model the small-scale velocities. The underlying postulate of the RNG method is that  $\tilde{\mathbf{f}}$  can be chosen so that Eq. (II.4) provides a correct description of turbulence on the larger scales. In support of this is the observation that Eqs. (I.1) and (II.4) agree in the mean, as is readily apparent by ensemble-averaging both equations and noting that  $\langle \tilde{\mathbf{f}} \rangle = 0$ .

Next, Yakhot and Orszag express the inertial-range velocity in terms of the respective contributions  $u_>$  and  $u_<$  from neighbouring larger and smaller wavenumber bands. The assumption that the effect of the small scales can be modeled as a random force in Eq. (II.4) leads to an expansion for  $u_>$  in terms of  $u_<$ , from which equations of motion for  $u_<$  can be derived. Self-similarity is then used to derive recursion relations that model the entire inertial range. The RNG theory has been used to predict the Kolmogorov constant as well as many other dimensionless parameters of fluid turbulence. Recently, Longcope and Sudan [1990] have applied the method to problems in MHD turbulence. Renormalization group theory has also been used to formulate subgrid models for large-eddy simulations [Yakhot and Orszag 1989].

Kraichnan [1987] has critically analyzed the RNG approach. To him, the most striking insight of the RNG theory is that the entire energy dynamics can, in some sense, be understood by considering only the interactions of widely separated wavenumbers. However, in Kraichnan's opinion the physical content of the RNG theory given by Yakhot and Orszag [1986] is equivalent to a simpler perturbative approximation (the "distant-interaction algorithm") that does not require the successive elimination of infinitesimal wavenumber shells.<sup>6</sup> Kraichnan also points out a deficiency of the RNG approach: the only explicit contact made with the Navier-Stokes equations is in the determination of the interaction coefficients of highly nonlocal wavenumber triads and in the conservation of energy by the nonlinear terms.

### **Decimation and realizability inequalities:**

Constrained decimation [Kraichnan 1985, Williams *et al.* 1987, Kraichnan and Chen 1989] is essentially a method of statistical interpolation. The objective is to develop a generalized Langevin equation for a set of sample modes that are evolved explicitly. The effect of the remaining modes is represented by a stochastic forcing

---

<sup>6</sup>However, Kraichnan's critique of the RNG is still controversial; [Orszag 1991] contends that the RNG theory is not equivalent to the distant-interaction algorithm.

term in the equations for the retained modes. However, statistical symmetries arising from the initial conditions and the equations of motion restrict the behaviour of the discarded modes. This leads to constraints, expressed in terms of moments of the sample modes alone, on the entire joint probability distribution of the two classes of modes. For example, there is a constraint that enforces energy conservation by the nonlinear terms. Other constraints serve to enforce certain *realizability inequalities* [Kraichnan 1980], such as the Schwarz inequality, that are necessary for the moments to be derivable from an underlying probability distribution.

As more constraints are added, it is expected that the scheme should, in principle, converge systematically to the exact solution. In the limit of very strong decimation, the closure may be analyzed perturbatively. The DIA equations are obtained for a particular choice of constraints [Kraichnan 1988]. A notable advantage of the decimation approach is that it is possible to constrain the dynamics so as to enforce random Galilean invariance. For the development of realizable closures, decimation provides a powerful alternative to the methods described in this work.

### Mapping Closures:

Statistical closures like the DIA appear to be incapable of predicting the apparently universal phenomenon of small-scale intermittency. For example, the DIA obtains the incorrect (Gaussian) value  $5/3$  for the *vorticity kurtosis*  $\langle |\omega|^4 \rangle / \langle |\omega|^2 \rangle^2$ , which is a measure of the spottiness of the vorticity and dissipation [Kraichnan and Chen 1989].

Kraichnan [1990a] and She and Orszag [1991] have advocated the use of *mapping closures* [Chen *et al.* 1989a, Chen and Kraichnan 1990] to develop models for intermittency. Mapping closures manipulate not moments but entire probability distributions. One constructs a nonlinear map that transforms a Gaussian reference probability density function to a dynamically evolving non-Gaussian PDF that represents the actual statistics. By expressing the non-Gaussian statistics in terms of the known statistical properties of the Gaussian reference field, systematic closures can be obtained in a completely non-perturbative manner. The Jacobian of the mapping transformation can effectively describe processes such as the vortex-stretching mechanism conventionally believed to play a role in the development of intermittency. Typically, the transformation is nonstochastic and is locally determined in terms of the field amplitude and gradient. It is self-consistently computed by matching the evolution of specified one-point PDF's to the actual evolution under the dynamical equations.

Kraichnan [1990b] has recently obtained with a mapping closure the encouraging prediction of  $35/3$  for the vorticity kurtosis. This is much closer to experimentally measured values than the Gaussian value of  $5/3$  [Kraichnan 1990b].

A particular advantage of mapping closures is that they can readily handle highly singular or extremely intermittent underlying PDF's. However, significant challenges face mapping closures: for the Navier-Stokes equations these include the handling of the pressure term and the problem of distinguishing between two- and three-dimensional turbulence.

## II.B Direct-interaction approximation

Let us now give a more detailed discussion of the direct-interaction approximation. First we will describe a number of derivations of this approximation to help clarify the underlying assumptions. We will illustrate applications to several pedagogical problems and then move on to discuss some of its important properties.

### II.B.1 Derivations

A qualitative description of a procedure for obtaining the DIA equations based on series reversion has already been given. Historically, several other derivations precede that one. Most significantly, it is from the following derivation that the DIA has taken on its name.

#### Direct vs. indirect interactions:

Kraichnan's original derivation of the DIA is based on two reasonable-sounding hypotheses [Kraichnan 1958a, 1959a]. First, he assumes that in a highly turbulent system consisting of the interactions of many modes (and in which any externally-excited modes are statistically independent) the statistical dependence between any small group of modes is weak. This is the *weak-dependence* hypothesis.

Kraichnan points out that weak dependence does not imply complete statistical independence such that cross-correlations between two distinct modes would vanish since the number of these *skew* moments is so large that their total contribution is significant. Thus, weak dependence does not contradict the observed non-normality of the two-point velocity distribution. However, it *is* assumed that the initial conditions are Gaussianly distributed, as are any external forces, so that the statistical dependences among the modes are induced wholly by the nonlinear terms of Eq. (I.17) [Kraichnan 1959a].

Second, he assumes that the dominant contribution to the triple moments appearing in the second-order evolution equation comes from the *direct interaction* of triads  $\mathbf{k}$ ,  $\mathbf{p}$ , and  $\mathbf{q}$ . Kraichnan supports this with the intuitive argument that "turbulence is a mixing process that degrades information so that the indirect in-

teraction of three modes through the turbulent motion as a whole should not convey phase information among them. . . .” This is the *direct-interaction* hypothesis.

By indirect interaction, Kraichnan means, for example, the influence of a fourth mode  $\mathbf{k}'$  on  $\mathbf{k}$  through its intermediate effect on  $\mathbf{p}$ , which then interacts with  $\mathbf{q}$ . It must be emphasized that the direct-interaction approximation will not totally disregard such processes; instead, it will model these effects only approximately by discarding the associated phase information.<sup>7</sup> There will be indirect exchanges of *energy* in the final equations due to the evolution and interaction of the energies of each mode; however, the associated phase information is lost after each direct triad interaction.

In our notation, Kraichnan sets up the functional equation

$$\left\langle \sum_{\mathbf{k}} L_{\mathbf{k}}(t) L_{\mathbf{k}}^*(t') \right\rangle = 0, \quad (\text{II.5})$$

where

$$L_{\mathbf{k}}(t) \doteq \left( \frac{\partial}{\partial t} + \nu_{\mathbf{k}} \right) \psi_{\mathbf{k}}(t) - \frac{1}{2} \sum_{\mathbf{k}+\mathbf{p}+\mathbf{q}=\mathbf{0}} M_{\mathbf{k}\mathbf{p}\mathbf{q}} \psi_{\mathbf{p}}^*(t) \psi_{\mathbf{q}}^*(t),$$

which provides both necessary and sufficient conditions so that, in all realizations (except possibly for a set of measure zero),  $\psi_{\mathbf{k}}$  satisfies our fundamental equation Eq. (I.17). Equation (II.5) places restrictions on the second-, third-, and fourth-order moments of  $\psi_{\mathbf{k}}$ , but it leaves the higher structure of the probability density function  $P$  largely *undetermined* (although it must satisfy certain realizability conditions in terms of the specified lower-order moments). Kraichnan argues that it is necessary to supplement Eq. (II.5) with further information. He advocates the variational criterion

$$\delta \int P \log P d\Gamma = 0,$$

subject to the constraints  $\int P d\Gamma = 1$ , Eq. (II.5), and appropriate integral constraints such as constant mean energy. Here  $\Gamma$  is a parameter uniquely identifying each distinct realization. The justification for this variational hypothesis is obtained from the expectation that, given the assumption of weak dependence, a turbulent system will tend to a state of *maximal randomness*, subject only to the restrictions imposed by the equations of motion. Of course, one could consider constraints on the distribution more severe than Eq. (II.5) and for this reason Kraichnan admits there is some arbitrariness in the formulation. However, given that higher-order moments are rarely known experimentally, he argues that this arbitrariness may not be significant.

---

<sup>7</sup>This is analogous to Boltzmann’s *Stosszahlansatz* (literally, collision number hypothesis), which is the assumption in statistical mechanics that the memory of previous phase correlations is lost after each collision.

If one accepts the variational principle just stated, one can then attempt to justify the plausibility of the direct-interaction hypothesis. Recognizing that the difficulties of perturbation theory arise from the assumption of weak turbulence, Kraichnan contemplates the opposite limit where the turbulence is *strong*. Beginning with the fully turbulent state, consider the effect of switching *off* just one direct triad interaction  $(\mathbf{k}, \mathbf{p}, \mathbf{q})$ . Let us use the notation  $\psi_{\mathbf{k}} \doteq \psi_{\mathbf{k}}(t)$  and  $\psi'_{\mathbf{k}} \doteq \psi_{\mathbf{k}}(t')$ . Now the triplet correlation  $\langle \psi'_{\mathbf{k}} \psi_{\mathbf{p}}^* \psi_{\mathbf{q}}^* \rangle$  appearing in Eq. (I.22) enters Eq. (II.5) only *via* the coefficients  $M_{\mathbf{k}\mathbf{p}\mathbf{q}}$ ,  $M_{\mathbf{p}\mathbf{q}\mathbf{k}}$ , and  $M_{\mathbf{q}\mathbf{k}\mathbf{p}}$  of the *direct* interaction. The indirect interaction does not enter into the constraints at all. It thus seems reasonable, given maximal randomness, that the distribution would adjust itself so that the remaining (indirect) interaction is negligible. After all, if the amplitudes entering the indirect interaction were completely randomized (obeying exact statistical independence), one would expect their contribution to the triplet moment to vanish. In a similar manner, Kraichnan argues that the indirect contribution to the fourth-order moment is also negligible.

We will now use a similar procedure, removing just one triad from the background of fully interacting fluctuations, to formulate *self-consistent* equations for the evolution of the background. The assumption of weak dependence states that the background will not depend significantly on the removal of this one interaction. Thus, we perturb about the *exact* state of the system, rather than about the uncoupled (linear) state. Decompose  $\psi_{\mathbf{k}} = \bar{\psi}_{\mathbf{k}} + \Delta\psi_{\mathbf{k}}$ , where  $\bar{\psi}_{\mathbf{k}}$  is the amplitude of mode  $\mathbf{k}$  after the removal of the direct triad interaction  $(\mathbf{k}, \mathbf{p}, \mathbf{q})$ . Then

$$\left(\frac{\partial}{\partial t} + \nu_{\mathbf{k}}\right)(\bar{\psi}_{\mathbf{k}} + \Delta\psi_{\mathbf{k}}) = M_{\mathbf{k}\mathbf{p}\mathbf{q}}\psi_{\mathbf{p}}^*\psi_{\mathbf{q}}^* + \frac{1}{2} \sum_{\substack{\mathbf{k}+\bar{\mathbf{p}}+\bar{\mathbf{q}}=0 \\ \bar{\mathbf{p}} \neq \mathbf{p}}} M_{\mathbf{k}\bar{\mathbf{p}}\bar{\mathbf{q}}}(\bar{\psi}_{\bar{\mathbf{p}}}^* + \Delta\psi_{\bar{\mathbf{p}}}^*)(\bar{\psi}_{\bar{\mathbf{q}}}^* + \Delta\psi_{\bar{\mathbf{q}}}^*).$$

To lowest order in  $\Delta\psi_{\mathbf{k}}$ ,

$$\left(\frac{\partial}{\partial t} + \nu_{\mathbf{k}}\right)\Delta\psi_{\mathbf{k}} - \sum_{\substack{\mathbf{k}+\bar{\mathbf{p}}+\bar{\mathbf{q}}=0 \\ \bar{\mathbf{p}} \neq \mathbf{p}}} M_{\mathbf{k}\bar{\mathbf{p}}\bar{\mathbf{q}}}\bar{\psi}_{\bar{\mathbf{p}}}^*\Delta\psi_{\bar{\mathbf{q}}}^* = M_{\mathbf{k}\mathbf{p}\mathbf{q}}\psi_{\mathbf{p}}^*\psi_{\mathbf{q}}^*.$$

The term on the right-hand side is, by definition, of order  $\Delta\psi_{\mathbf{k}}$ . At this order, we can now drop the bar on  $\psi_{\bar{\mathbf{p}}}$  and remove the restriction  $\bar{\mathbf{p}} \neq \mathbf{p}$  from the summation. By introducing the random response function  $\widetilde{R}_{\mathbf{k}}$  of Eq. (I.17), which obeys

$$\left(\frac{\partial}{\partial t} + \nu_{\mathbf{k}}\right)\widetilde{R}_{\mathbf{k}}(t, t') - \sum_{\mathbf{k}+\bar{\mathbf{p}}+\bar{\mathbf{q}}=0} M_{\mathbf{k}\bar{\mathbf{p}}\bar{\mathbf{q}}}\psi_{\bar{\mathbf{p}}}^*(t)\widetilde{R}_{\bar{\mathbf{q}}}(t, t') = \delta(t-t'), \quad (\text{II.6})$$

we may then write the direct contribution of the triad  $(\mathbf{k}, \mathbf{p}, \mathbf{q})$  to mode  $\mathbf{k}$  as

$$\Delta\psi_{\mathbf{k}}(t) = \int_0^t d\bar{t} \widetilde{R}_{\mathbf{k}}(t, \bar{t}) M_{\mathbf{k}\mathbf{p}\mathbf{q}}\psi_{\mathbf{p}}^*(\bar{t})\psi_{\mathbf{q}}^*(\bar{t}). \quad (\text{II.7})$$

Now, according to the direct-interaction hypothesis the triplet correlation of the three modes in our triad arises only from the direct contributions of that triad. Thus, to first order the triplet correlation is just the sum of three terms, each involving the direct contributions of the triad to one of the members of the correlation:

$$\langle \psi_{\mathbf{k}}'^* \psi_{\mathbf{p}}^* \psi_{\mathbf{q}}^* \rangle = \langle \Delta \psi_{\mathbf{k}}'^* \psi_{\mathbf{p}}^* \psi_{\mathbf{q}}^* \rangle + \langle \psi_{\mathbf{k}}'^* \Delta \psi_{\mathbf{p}}^* \psi_{\mathbf{q}}^* \rangle + \langle \psi_{\mathbf{k}}'^* \psi_{\mathbf{p}}^* \Delta \psi_{\mathbf{q}}^* \rangle.$$

This becomes, using Eq. (II.7),

$$\begin{aligned} \langle \psi_{\mathbf{k}}'^* \psi_{\mathbf{p}}^* \psi_{\mathbf{q}}^* \rangle &= \int_{-\infty}^{t'} d\bar{t} M_{\mathbf{k}\mathbf{p}\mathbf{q}}^* \langle \widetilde{R}_{\mathbf{k}}^*(t', \bar{t}) \psi_{\mathbf{p}}(\bar{t}) \psi_{\mathbf{q}}(\bar{t}) \psi_{\mathbf{p}}^* \psi_{\mathbf{q}}^* \rangle \\ &+ \int_0^t d\bar{t} M_{\mathbf{p}\mathbf{q}\mathbf{k}}^* \langle \psi_{\mathbf{k}}'^* \widetilde{R}_{\mathbf{p}}^*(t, \bar{t}) \psi_{\mathbf{q}}(\bar{t}) \psi_{\mathbf{k}}(\bar{t}) \psi_{\mathbf{q}}^* \rangle \\ &+ \int_0^t d\bar{t} M_{\mathbf{q}\mathbf{k}\mathbf{p}}^* \langle \psi_{\mathbf{k}}'^* \psi_{\mathbf{p}}^* \widetilde{R}_{\mathbf{q}}^*(t, \bar{t}) \psi_{\mathbf{k}}(\bar{t}) \psi_{\mathbf{p}}(\bar{t}) \rangle. \end{aligned}$$

Weak dependence implies that  $\widetilde{R}_{\mathbf{k}}$  can be treated as statistically independent of  $\psi_{\mathbf{p}}$  and  $\psi_{\mathbf{q}}$ , so

$$\begin{aligned} \langle \psi_{\mathbf{k}}^*(t') \psi_{\mathbf{p}}^*(t) \psi_{\mathbf{q}}^*(t) \rangle &= \int_{-\infty}^{t'} d\bar{t} M_{\mathbf{k}\mathbf{p}\mathbf{q}}^* R_{\mathbf{k}}^*(t', \bar{t}) C_{\mathbf{p}}^*(t, \bar{t}) C_{\mathbf{q}}^*(t, \bar{t}) \\ &+ \int_0^t d\bar{t} M_{\mathbf{p}\mathbf{q}\mathbf{k}}^* R_{\mathbf{p}}^*(t, \bar{t}) C_{\mathbf{k}}(\bar{t}, t') C_{\mathbf{q}}^*(t, \bar{t}) \\ &+ \int_0^t d\bar{t} M_{\mathbf{q}\mathbf{k}\mathbf{p}}^* R_{\mathbf{q}}^*(t, \bar{t}) C_{\mathbf{k}}(\bar{t}, t') C_{\mathbf{p}}^*(t, \bar{t}), \end{aligned}$$

where  $R_{\mathbf{k}} \doteq \langle \widetilde{R}_{\mathbf{k}} \rangle$ . Upon inserting the above result into the evolution equation for  $C_{\mathbf{k}}(t, t')$  in the case  $t \neq t'$  [Eq. (I.22)], we obtain the DIA covariance equation:

$$\left( \frac{\partial}{\partial t} + \nu_{\mathbf{k}} \right) C_{\mathbf{k}}(t, t') + \int_0^t d\bar{t} \Sigma_{\mathbf{k}}(t, \bar{t}) C_{\mathbf{k}}(\bar{t}, t') = \int_0^{t'} d\bar{t} \mathcal{F}_{\mathbf{k}}(t, \bar{t}) R_{\mathbf{k}}^*(t', \bar{t}), \quad (\text{I.38a})$$

where the symmetry  $M_{\mathbf{k}\mathbf{p}\mathbf{q}} = M_{\mathbf{k}\mathbf{q}\mathbf{p}}$  is used to write

$$\Sigma_{\mathbf{k}}(t, \bar{t}) = - \sum_{\mathbf{k}+\mathbf{p}+\mathbf{q}=\mathbf{0}} M_{\mathbf{k}\mathbf{p}\mathbf{q}} M_{\mathbf{p}\mathbf{q}\mathbf{k}}^* R_{\mathbf{p}}^*(t, \bar{t}) C_{\mathbf{q}}^*(t, \bar{t}), \quad (\text{I.39a})$$

$$\mathcal{F}_{\mathbf{k}}(t, \bar{t}) = \frac{1}{2} \sum_{\mathbf{k}+\mathbf{p}+\mathbf{q}=\mathbf{0}} |M_{\mathbf{k}\mathbf{p}\mathbf{q}}|^2 C_{\mathbf{p}}^*(t, \bar{t}) C_{\mathbf{q}}^*(t, \bar{t}). \quad (\text{I.39b})$$

We still need an equation for  $R_{\mathbf{k}}$ . The response  $\delta\psi_{\mathbf{k}}$  due to an infinitesimal perturbation  $\delta\bar{\eta}_{\mathbf{k}}(t')$  added to the right-hand side of the fundamental equation Eq. (I.17)

obeys, to first order in  $\delta\bar{\eta}_{\mathbf{k}}$ ,

$$\left(\frac{\partial}{\partial t} + \nu_{\mathbf{k}}\right)\delta\psi_{\mathbf{k}}(t) = \sum_{\mathbf{k}+\mathbf{p}+\mathbf{q}=\mathbf{0}} M_{\mathbf{k}\mathbf{p}\mathbf{q}}\psi_{\mathbf{q}}^*(t)\delta\psi_{\mathbf{p}}^*(t) + \delta\bar{\eta}_{\mathbf{k}}(t'). \quad (\text{II.8})$$

The perturbation is introduced only into mode  $\mathbf{k}$ ; the equation for  $\delta\psi_{\mathbf{p}}$  is just

$$\left(\frac{\partial}{\partial t} + \nu_{\mathbf{k}}\right)\delta\psi_{\mathbf{p}} - \sum_{\substack{\mathbf{p}+\bar{\mathbf{q}}+\bar{\mathbf{k}}=\mathbf{0} \\ \bar{\mathbf{k}}\neq\mathbf{k}}} M_{\mathbf{p}\bar{\mathbf{q}}\bar{\mathbf{k}}}\psi_{\bar{\mathbf{q}}}^*\delta\psi_{\bar{\mathbf{k}}}^* = M_{\mathbf{p}\mathbf{q}\mathbf{k}}\psi_{\mathbf{q}}^*\delta\psi_{\mathbf{k}}^*. \quad (\text{II.9})$$

We may then express

$$\delta\psi_{\mathbf{p}}(t) = \int_0^t d\bar{t} \bar{T}R_{\mathbf{p}}(t, \bar{t}) M_{\mathbf{p}\mathbf{q}\mathbf{k}}\psi_{\mathbf{q}}^*(\bar{t})\delta\psi_{\mathbf{k}}^*(\bar{t}), \quad (\text{II.10})$$

where the response function  $\bar{T}R_{\mathbf{p}}$  is obtained by replacing the right-hand side of Eq. (II.9) with an infinitesimal source  $\delta\bar{\eta}_{\mathbf{p}}(t')$ . Weak dependence states that  $\bar{T}R_{\mathbf{p}} \approx \widetilde{R}_{\mathbf{p}}$  since the neglected term of the sum in Eq. (II.9) contributes negligibly to perturbations in  $\psi_{\mathbf{p}}$  induced by  $\delta\bar{\eta}_{\mathbf{p}}$ . Substitution of Eq. (II.10) into Eq. (II.8) then yields

$$\left(\frac{\partial}{\partial t} + \nu_{\mathbf{k}}\right)\delta\psi_{\mathbf{k}}(t, t') = \sum_{\mathbf{k}+\mathbf{p}+\mathbf{q}=\mathbf{0}} M_{\mathbf{k}\mathbf{p}\mathbf{q}}M_{\mathbf{p}\mathbf{q}\mathbf{k}}^* \int_0^t d\bar{t} \psi_{\mathbf{q}}^*(\bar{t})\widetilde{R}_{\mathbf{p}}^*(t, \bar{t})\psi_{\mathbf{q}}(\bar{t})\delta\psi_{\mathbf{k}}(\bar{t}) + \delta\bar{\eta}_{\mathbf{k}}(t').$$

One can then compute  $R_{\mathbf{k}}(t, t') \doteq \langle \delta\psi_{\mathbf{k}}(t)/\delta\bar{\eta}_{\mathbf{k}}(t') \rangle$ , evaluated at  $\bar{\eta}_{\mathbf{k}}(t') = 0$ , to arrive at the DIA equation for the mean response function:

$$\boxed{\left(\frac{\partial}{\partial t} + \nu_{\mathbf{k}}\right)R_{\mathbf{k}}(t, t') + \int_{t'}^t d\bar{t} \Sigma_{\mathbf{k}}(t, \bar{t})R_{\mathbf{k}}(\bar{t}, t') = \delta(t-t').} \quad (\text{I.38b})$$

Weak dependence was invoked here to factor the response functions out of the ensemble average.

Equations (I.38) and (I.39) provide the complete coupled set of equations of the DIA. Despite the systematic derivation given here, the DIA is still only an approximation. The above closure equations are direct consequences of Kraichnan's two hypotheses; however, the direct-interaction hypothesis, in particular, is not always valid. Although admittedly the indirect interactions are individually weaker than the direct interactions, there are many more of them; when summed, their combined effect may be just as significant as the direct contribution. To make contact with the MSR formalism, we note that the skewness parameter  $\bar{\Gamma}$  is a measure of this indirect contribution; in the lowest-order truncation this contribution is totally neglected.

Fortunately, the plausibility of the DIA can be established on other grounds. Most importantly, we will now examine two underlying stochastic models that prove that the DIA is realizable. In turn, this guarantees that the statistics predicted by the DIA, although not generally exact, are at least constrained to satisfy the same realizability inequalities as obeyed by the exact statistics.

### Random coupling model:

Kraichnan [1958c] proposed the following modification of Eq. (I.17),

$$\left(\frac{\partial}{\partial t} + \nu_{\mathbf{k}}\right)\psi_{\mathbf{k}}(t) = \frac{1}{2} \sum_{\mathbf{k}+\mathbf{p}+\mathbf{q}=0} \phi_{\mathbf{k}\mathbf{p}\mathbf{q}} M_{\mathbf{k}\mathbf{p}\mathbf{q}} \psi_{\mathbf{p}}^*(t) \psi_{\mathbf{q}}^*(t), \quad (\text{II.11})$$

where  $\phi_{\mathbf{k}\mathbf{p}\mathbf{q}}$  has the *same* time-independent value in every realization. Subject to being fully symmetric in its indices and invariant to reflection of its wavenumber indices about the origin, we construct  $\phi_{\mathbf{k}\mathbf{p}\mathbf{q}}$  to have the values  $+1$  or  $-1$  *at random* for each distinct triad  $(\mathbf{k}, \mathbf{p}, \mathbf{q})$ .

Since  $|\phi_{\mathbf{k}\mathbf{p}\mathbf{q}}|^2 = \phi_{\mathbf{k}\mathbf{p}\mathbf{q}} \phi_{\mathbf{p}\mathbf{q}\mathbf{k}}^* = 1$ , Kraichnan argued that computation of the direct contribution to the triple moments and response function will result in the same equations, Eqs. (I.38) and Eqs. (I.39), as we obtained for the original problem. The indirect contributions involve several *distinct* elementary interactions; therefore, when one sums over all possible indirect combinations, random cancellations between the participating interactions will occur. In the limit of many modes, the indirect contribution to the second-order statistics vanishes. Thus, the DIA equations *exactly* describe the statistical evolution of this random coupling model.<sup>8</sup>

### Langevin representation:

The DIA is also the exact statistical solution to a generalized Langevin equation,

$$\boxed{\left(\frac{\partial}{\partial t} + \nu_{\mathbf{k}}\right)\psi_{\mathbf{k}}(t) + \int_0^t d\bar{t} \Sigma_{\mathbf{k}}(t, \bar{t}) \psi_{\mathbf{k}}(\bar{t}) = f_{\mathbf{k}}(t),} \quad (\text{II.12})$$

with  $\Sigma_{\mathbf{k}}$  prescribed by Eq. (I.39a) and  $f_{\mathbf{k}}(t)$  determined as follows [Kraichnan 1970a, Leith 1971]. Generate random fields  $\xi_{\mathbf{k}}(t)$  and  $\hat{\xi}_{\mathbf{k}}$  that are statistically independent of each other and the initial value of  $\psi_{\mathbf{k}}$  such that their covariances satisfy  $\langle \xi_{\mathbf{k}}(t) \xi_{\mathbf{k}}^*(t') \rangle = \langle \hat{\xi}_{\mathbf{k}}(t) \hat{\xi}_{\mathbf{k}}^*(t') \rangle = C_{\mathbf{k}}(t, t')$ . (This is possible since  $C_{\mathbf{k}}$  is positive-semidefinite, as can be established independently with the random coupling model.)

<sup>8</sup>Strictly speaking, Kraichnan [1961] employed the term *random coupling model* only for a case in which the random couplings represent interactions among an *infinite collection* of similar systems, instead of among wavenumber triads. He adopted the coupling coefficients  $\phi_{\mathbf{k}\mathbf{p}\mathbf{q}} = \exp(i\theta_{\mathbf{k}\mathbf{p}\mathbf{q}})$ , for which the phases  $\theta_{\mathbf{k}\mathbf{p}\mathbf{q}}$  are distributed uniformly in  $[0, 2\pi]$ .

Then construct

$$f_{\mathbf{k}}(t) \doteq \frac{1}{\sqrt{2}} \sum_{\mathbf{k}+\mathbf{p}+\mathbf{q}=\mathbf{0}} M_{\mathbf{k}\mathbf{p}\mathbf{q}} \xi_{\mathbf{p}}^*(t) \widehat{\xi}_{\mathbf{q}}^*(t).$$

Let us now verify the above claim. Clearly, the response function of Eq. (II.12) is just Eq. (I.38b). If we multiply Eq. (II.12) by  $\psi_{\mathbf{k}}^*(t')$  and ensemble average, we obtain

$$\left( \frac{\partial}{\partial t} + \nu_{\mathbf{k}} \right) C_{\mathbf{k}}(t, t') + \int_0^t d\bar{t} \Sigma_{\mathbf{k}}(t, \bar{t}) C_{\mathbf{k}}(\bar{t}, t') = \langle f_{\mathbf{k}}(t) \psi_{\mathbf{k}}^*(t') \rangle.$$

Upon using the relation

$$\psi_{\mathbf{k}}(t) = \int_0^t d\bar{t} R_{\mathbf{k}}(t, \bar{t}) f_{\mathbf{k}}(\bar{t}),$$

we obtain Eq. (I.38a) with

$$\mathcal{F}_{\mathbf{k}}(t, \bar{t}) = \langle f_{\mathbf{k}}(t) f_{\mathbf{k}}^*(\bar{t}) \rangle.$$

Hence the DIA is the exact solution to the second-order statistics of an underlying (generalized) Langevin equation.

### Recipe:

There is another way of obtaining the DIA equations that is more heuristic than the methods already described. This can be used to deduce the appropriate form of the DIA equations for a new physics problem. Let us outline the technique as it applies to the covariance equation; the response function can be obtained in a similar fashion.

We begin by formally expanding the fundamental equation in powers of the mode-coupling coefficient. The procedure then consists of two steps. First, using the unperturbed propagator, we express the triplet correlation function appearing in the covariance equation as a fourth-order correlation. To evaluate this fourth-order quantity, we apply the same cumulant discard hypothesis used in the quasinormal approximation.

Next, we heuristically replace the unperturbed propagator with the perturbed propagator, effectively renormalizing the closure made in the first step. This last step is the essence of the DIA and is responsible for its markedly superior behaviour compared to the quasinormal approximation.

### Alternative form of the DIA covariance equation:

It is interesting to remark that the DIA covariance equation may be equivalently written as

$$\frac{\partial}{\partial t} C_{\mathbf{k}}(t, t') + N_{\mathbf{k}}(t, t') = F_{\mathbf{k}}(t, t'),$$

where

$$N_{\mathbf{k}}(t, t') \doteq \nu_{\mathbf{k}} C_{\mathbf{k}}(t, t') - \sum_{\mathbf{k}+\mathbf{p}+\mathbf{q}=\mathbf{0}} M_{\mathbf{k}\mathbf{p}\mathbf{q}} M_{\mathbf{p}\mathbf{q}\mathbf{k}}^* \bar{\Theta}_{\mathbf{p}\mathbf{q}\mathbf{k}}^*(t, t, t'),$$

$$F_{\mathbf{k}}(t, t') \doteq \frac{1}{2} \sum_{\mathbf{k}+\mathbf{p}+\mathbf{q}=\mathbf{0}} |M_{\mathbf{k}\mathbf{p}\mathbf{q}}|^2 \bar{\Theta}_{\mathbf{k}\mathbf{p}\mathbf{q}}^*(t', t, t),$$

and

$$\bar{\Theta}_{\mathbf{k}\mathbf{p}\mathbf{q}}(t, s, t') \doteq \int_0^t d\bar{t} R_{\mathbf{k}}(t, \bar{t}) C_{\mathbf{p}}(s, \bar{t}) C_{\mathbf{q}}(t', \bar{t}).$$

The equal-time covariance equation can be expressed in an even simpler fashion:

$$\frac{\partial}{\partial t} C_{\mathbf{k}}(t) + 2 \operatorname{Re} N_{\mathbf{k}}(t) = 2 \operatorname{Re} F_{\mathbf{k}}(t), \quad (\text{II.13})$$

where  $N_{\mathbf{k}}(t) \doteq N_{\mathbf{k}}(t, t)$  and  $F_{\mathbf{k}}(t) \doteq F_{\mathbf{k}}(t, t)$  are defined in terms of  $\bar{\Theta}_{\mathbf{k}\mathbf{p}\mathbf{q}}(t) \doteq \bar{\Theta}_{\mathbf{k}\mathbf{p}\mathbf{q}}(t, t, t)$ . The symmetry

$$\bar{\Theta}_{\mathbf{k}\mathbf{p}\mathbf{q}}(t) \doteq \bar{\Theta}_{\mathbf{k}\mathbf{q}\mathbf{p}}(t) \quad (\text{II.14})$$

is reminiscent of the mode-coupling symmetry  $M_{\mathbf{k}\mathbf{p}\mathbf{q}} = M_{\mathbf{k}\mathbf{q}\mathbf{p}}$  and will be used in the proof of energy conservation below. We will make further contact with Eq. (II.13) when we Markovianize the DIA equations in Chapter III.

## II.B.2 Illustration of the DIA

Let us now discuss several nonlinear problems for which the DIA can be used to obtain approximate solutions. These examples serve to illustrate the nature of the approximations made by this closure.

### Stochastic Oscillator:

Consider the stochastic oscillator problem, introduced on pg. 28:

$$\frac{\partial}{\partial t} \psi(t) + i\tilde{\omega}(t) \psi(t) = 0, \quad (\text{I.25})$$

with  $\langle \tilde{\omega}(t) \rangle = 0$ . Suppose  $F(t, t') \doteq \langle \tilde{\omega}(t) \tilde{\omega}(t') \rangle \doteq F(t - t')$ , where

$$F(\tau) = \beta^2 e^{-\tau/\tau_{\text{ac}}}.$$

Here  $\beta^2$ , the equal-time variance of  $\tilde{\omega}$ , and  $\tau_{\text{ac}}$  are specified numbers. The dimensionless product  $K \doteq \beta^2 \tau_{\text{ac}}$  is known as the Kubo number.

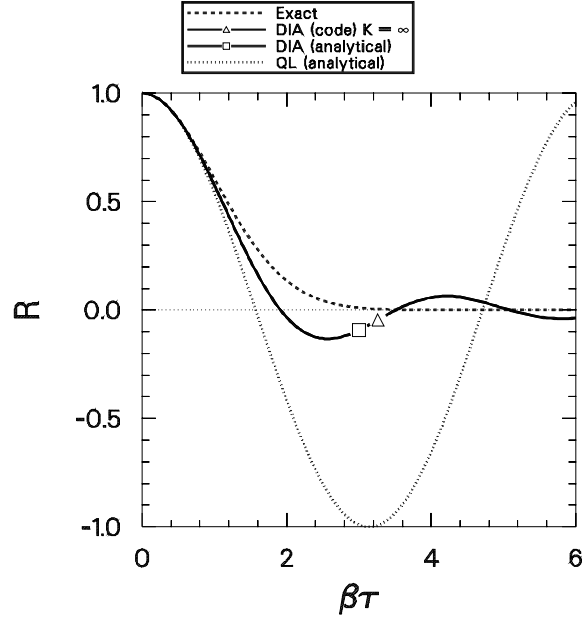


Figure II.1: Comparison of exact, DIA, and quasilinear (QL) results for the stochastic oscillator with  $K = \infty$ . The numerical prediction of the DIA code coincides with the analytical solution of the DIA, Eq. (II.17).

This particular stochastic problem is exceptional in that the exact solution for the response function is known [Kubo 1963],

$$R(\tau) = H(\tau) \exp(-K^2(\tau/\tau_{ac} - 1 + e^{-\tau/\tau_{ac}})).$$

Thus we are afforded with a rare opportunity to test the performance of the DIA against the exact analytical solution. Fig. II.1 illustrates this comparison for the Kubo value  $K = \infty$ , for which  $R(\tau) = H(\tau) \exp(-\beta^2\tau^2/2)$  (see also Frisch and Bourret [1970]).

Since the stochastic oscillator is a passive problem, it does not fit into the framework of our (self-consistent) fundamental equation, so we will need to determine independently the corresponding DIA equation. Let us now use the previously described recipe to obtain the response function in the direct-interaction approximation.

Add an infinitesimal perturbation to the right-hand side of Eq. (I.25). In terms of the linear response function  $R^{(0)}(\tau) = H(\tau)$ ,

$$\psi(t) = -i \int_0^t d\bar{t} R^{(0)}(t - \bar{t}) \tilde{\omega}(\bar{t}) \psi(\bar{t}), \quad (\text{II.15})$$

Iterate Eq. (I.25) by substituting Eq. (II.15) into the nonlinearity. Differentiation with respect to the perturbation then yields

$$\frac{\partial}{\partial \tau} R(\tau) + \int_0^\tau d\bar{\tau} \langle \tilde{\omega}(t) R^{(0)}(\tau - \bar{\tau}) \tilde{\omega}(\bar{t}) \tilde{R}(\bar{\tau}) \rangle = \delta(\tau).$$

Apply the quasinormal approximation to obtain

$$\frac{\partial}{\partial \tau} R(\tau) + \int_0^\tau d\bar{\tau} R^{(0)}(\tau - \bar{\tau}) F(\tau - \bar{\tau}) R(\bar{\tau}) = \delta(\tau).$$

Finally, we partially account for the effect of the cumulant just discarded by replacing the linear propagator  $R^{(0)}$  with the renormalized propagator  $R$ . (The linear propagator has no place in a strong turbulence theory.) The final DIA equation is

$$\frac{\partial}{\partial \tau} R(\tau) + \int_0^\tau d\bar{\tau} R(\bar{\tau}) F(\bar{\tau}) R(\tau - \bar{\tau}) = \delta(\tau). \quad (\text{II.16})$$

For the case  $K = \infty$ , the solution to Eq. (II.16) can be obtained by Fourier transformation [Kraichnan 1961]:

$$R(\tau) = \text{H}(\tau) \frac{J_1(2\beta\tau)}{\beta\tau} \quad (K = \infty). \quad (\text{II.17})$$

This analytical solution is graphed in Fig. II.1 and is in agreement with the numerical solution of Eq. (II.16). We also compare the DIA result to the quasilinear estimate to illustrate the degree of improvement that the DIA represents over simpler closures. The quasilinear result is severely deficient and does not exhibit the proper decay to zero. Although the DIA introduces a spurious oscillation and decays algebraically rather than exponentially, it largely captures the desired statistical information. For example, Krommes [1984b] points out that the areas under the DIA and exact curves agree to within about 20%. Since transport coefficients depend more on gross properties like the area than on detailed features, this gives us some confidence in our approach.

### Three interacting waves:

Kraichnan [1963] studied a simple conservative system of three interacting waves as a precursor to the computation of more realistic multimode problems. A slight generalization of this system to include linear effects is [Terry and Horton 1982, Krommes 1982]

$$\left( \frac{\partial}{\partial t} + \nu_k \right) \psi_k = M_k \psi_p^* \psi_q^*,$$

$$\begin{aligned}\left(\frac{\partial}{\partial t} + \nu_p\right)\psi_p &= M_p\psi_q^*\psi_k^*, \\ \left(\frac{\partial}{\partial t} + \nu_q\right)\psi_q &= M_q\psi_k^*\psi_p^*.\end{aligned}\tag{II.18}$$

In the truncated Navier-Stokes problem,  $k$ ,  $p$ , and  $q$  are the magnitudes of three fixed wavenumbers that satisfy the triangle relation  $\mathbf{k} + \mathbf{p} + \mathbf{q} = \mathbf{0}$  and  $M_k$ ,  $M_p$ , and  $M_q$  are the corresponding interaction coefficients, satisfying

$$M_k + M_p + M_q = 0.$$

We will not make further contact with this underlying motivation; instead, we will consider the system Eq. (II.18) as a mathematical problem in its own right. The objective is to compute the evolution of the covariance, both by direct numerical simulation and by solving the direct-interaction approximation. Although this model possesses only six degrees of freedom, in special cases it has been observed to exhibit bifurcation and stochasticity [Wersinger *et al.* 1980].

Equations (I.38) and (I.39) allow us to write down the DIA equations for this problem immediately. In our numerical work these same general equations are programmed into the code `DIA`; to solve different problems, we simply specify different subroutines for evaluating  $M_{\mathbf{k}\mathbf{p}\mathbf{q}}$ . We will consider this system in more detail in Chapter V.

### Oscillatory passive advection problem:

An important property of the DIA is that, unlike the quasinormal closure, it properly relaxes *irreversibly* to equilibrium [Orszag 1970]. However, the following previously unpublished example illustrates that the DIA possesses an *intrinsic irreversibility* that causes it to predict relaxation even in cases where the actual dynamics is oscillatory.

Consider a field  $\psi$  that is passively advected by a randomly phased oscillatory disturbance [Krommes 1991a]:

$$\frac{\partial}{\partial t}\psi + i\lambda\omega_0 \cos(\omega_0 t + \tilde{\varphi})\psi = 0.\tag{II.19}$$

Here  $\lambda$  is statistically sharp and the time-independent random variable  $\tilde{\varphi}$  is *uniformly* distributed between 0 and  $2\pi$ .

The corresponding response function  $\tilde{R}(\tau)$  is equal to the solution of Eq. (II.19) with initial condition  $\psi(0) = 1$ :

$$\begin{aligned}\tilde{R}(\tau) &= \exp(-i\lambda[\sin(\omega_0\tau + \tilde{\varphi}) - \sin \tilde{\varphi}]) \\ &= \sum_{n=-\infty}^{\infty} \sum_{n'=-\infty}^{\infty} J_n(\lambda)J_{n'}(\lambda)e^{-in(\omega_0\tau + \tilde{\varphi}) + in'\tilde{\varphi}}.\end{aligned}\tag{II.20}$$

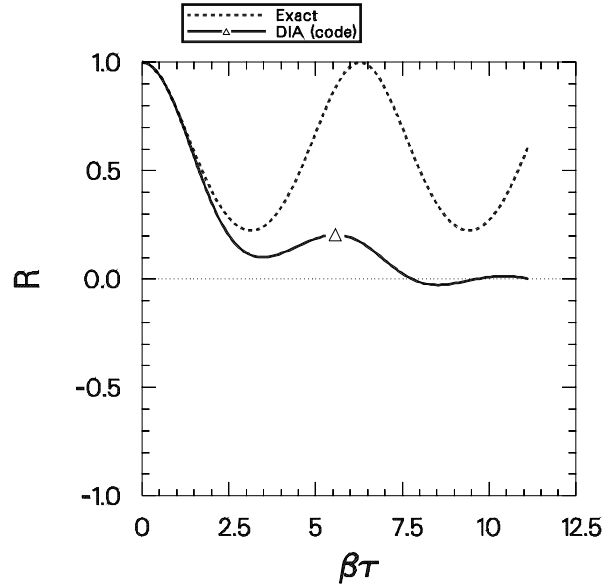


Figure II.2: Comparison of exact and DIA solutions of the oscillatory passive advection problem, Eq. (II.19), with  $\lambda = 1$  and  $\omega_0 \equiv \beta$ .

An ensemble average over the rectangular distribution of  $\tilde{\varphi}$  then yields

$$\langle \tilde{R}(\tau) \rangle = \sum_{n=-\infty}^{\infty} J_n^2(\lambda) e^{-in\omega_0\tau} \quad (\text{II.21})$$

$$= J_0(2\lambda \sin(\frac{1}{2}\omega_0\tau)). \quad (\text{II.22})$$

From this last line, we see that the exact solution oscillates forever, with period  $2\pi/\omega_0$  (note that  $J_0$  is an even function). Fig. II.2 depicts the exact behaviour in comparison to the numerical solution of the DIA for the case  $\lambda = 1$  and  $\omega_0 \equiv \beta$ . The DIA response function does not exhibit an asymptotic oscillation; rather, it relaxes irreversibly to zero. The underlying cause of this discrepancy is that the DIA does not properly handle coherence. In Eq. (II.20) we see that the exact solution involves an infinite number of random terms that sum coherently to produce the oscillatory behaviour described by Eq. (II.22). This situation is quite analogous to the behaviour of *solitons*, which are nonlinear solutions that maintain definite phase relations among their Fourier components. This allows them to retain a fixed shape as they propagate through an interacting medium.

By approximating the statistics, the DIA scrambles this coherency so that the resulting response function decays. The manner in which the DIA fails can be

illustrated by considering the related problem

$$\frac{\partial}{\partial t}\psi + i\lambda\tilde{\omega}\cos(\tilde{\omega}t + \tilde{\varphi})\psi = 0, \quad (\text{II.23})$$

where  $\tilde{\omega}$  is a Gaussian random variable, statistically independent of  $\psi$  and  $\varphi$ , with zero mean and variance  $\beta^2$ . The exact solution is now

$$\begin{aligned} \langle \tilde{R}(\tau) \rangle &= \sum_{n=-\infty}^{\infty} J_n^2(\lambda) \langle e^{-in\tilde{\omega}\tau} \rangle \\ &= \sum_{n=-\infty}^{\infty} J_n^2(\lambda) e^{-\frac{1}{2}n^2\beta^2\tau^2}. \end{aligned} \quad (\text{II.24})$$

The effect of replacing  $\omega_0$  by the random variable  $\tilde{\omega}$  is to destroy the coherency of the terms in Eq. (II.21) so that they interfere destructively when summed. The result is a solution that decays in time to the constant  $J_0^2(\lambda)$ . The statistical approximations of the DIA introduce a similar incoherency that also results in an asymptotic decay of the predicted response, although this decay is not as rapid as in Eq. (II.24).

In some respects, this situation may seem reminiscent of the analogous manner in which finite truncations of the (Eulerian) MSR perturbation series violate RGI, even though the full summation does not. In fact, it appears that there is a deep connection between random Galilean invariance and coherency. Random Galilean invariance is obeyed by the full summation because of an intricate relation between the two-time covariances that appear at each order in the evolution equation for the equal-time covariance. When the terms of the perturbation series are considered collectively, this coherency causes the sensitivity to random Galilean transformations exhibited by individual terms to disappear. To further strengthen the connection, we point out that the random-Galilean-invariant Lagrangian history closure is exact [Kraichnan 1977] for the Gaussian random oscillator, Eq. (I.25). This suggests that for the present problem the modifications used to enforce RGI might also fix the improper treatment of coherent effects.

### Hasegawa-Mima problem:

The DIA equations for the Hasegawa-Mima problem are readily obtained by substituting the expression for the corresponding mode-coupling coefficient,

$$M_{\mathbf{k}\mathbf{p}\mathbf{q}} \doteq \hat{\mathbf{z}} \cdot (\mathbf{p} \times \mathbf{q}) \left( \frac{q^2 - p^2}{1 + k^2} \right),$$

into Eqs. (I.39). This multimode problem will be studied extensively in Chapter VI.

### II.B.3 Properties

Let us now investigate some of the properties of the direct-interaction approximation.

#### Reduction to perturbation theory:

One of the important properties of the systematically renormalized DIA is that it reduces correctly to perturbation theory [Kraichnan 1961]. Thus, in the weak-turbulence limit, Eqs. (I.38) and (I.39) reduce to the wave kinetic equation Eq. (I.36).

#### Conservation laws and symmetries:

Given the symmetry Eq. (I.19), the generalized energy

$$E \doteq \frac{1}{2} \sum_{\mathbf{k}} \sigma_{\mathbf{k}} C_{\mathbf{k}}(t)$$

is conserved by Eq. (II.13) in the dissipationless case where  $\text{Re } \nu_{\mathbf{k}} = 0$ :

$$\begin{aligned} \frac{\partial}{\partial t} 2E &= \sum_{\mathbf{k}} \sigma_{\mathbf{k}} \frac{\partial}{\partial t} C_{\mathbf{k}}(t) \\ &= 2 \text{Re} \sum_{\mathbf{k}} \sigma_{\mathbf{k}} \sum_{\mathbf{k}+\mathbf{p}+\mathbf{q}=0} M_{\mathbf{k}\mathbf{p}\mathbf{q}} M_{\mathbf{p}\mathbf{q}\mathbf{k}}^* \bar{\Theta}_{\mathbf{p}\mathbf{q}\mathbf{k}}^*(t) + \text{Re} \sum_{\mathbf{k}} \sigma_{\mathbf{k}} \sum_{\mathbf{k}+\mathbf{p}+\mathbf{q}=0} M_{\mathbf{k}\mathbf{p}\mathbf{q}} M_{\mathbf{k}\mathbf{p}\mathbf{q}}^* \bar{\Theta}_{\mathbf{k}\mathbf{p}\mathbf{q}}^*(t) \\ &= \text{Re} \sum_{\mathbf{k}} \sigma_{\mathbf{k}} \sum_{\mathbf{k}+\mathbf{p}+\mathbf{q}=0} M_{\mathbf{k}\mathbf{p}\mathbf{q}} M_{\mathbf{p}\mathbf{q}\mathbf{k}}^* \bar{\Theta}_{\mathbf{p}\mathbf{q}\mathbf{k}}^*(t) \\ &\quad + \text{Re} \sum_{\mathbf{k}} \sigma_{\mathbf{q}} \sum_{\mathbf{k}+\mathbf{p}+\mathbf{q}=0} M_{\mathbf{q}\mathbf{p}\mathbf{k}} M_{\mathbf{p}\mathbf{k}\mathbf{q}}^* \bar{\Theta}_{\mathbf{p}\mathbf{k}\mathbf{q}}^*(t) \quad (\mathbf{k} \leftrightarrow \mathbf{q}) \\ &\quad + \text{Re} \sum_{\mathbf{k}} \sigma_{\mathbf{p}} \sum_{\mathbf{k}+\mathbf{p}+\mathbf{q}=0} M_{\mathbf{p}\mathbf{q}\mathbf{k}} M_{\mathbf{p}\mathbf{q}\mathbf{k}}^* \bar{\Theta}_{\mathbf{p}\mathbf{q}\mathbf{k}}^*(t) \quad (\mathbf{k} \rightarrow \mathbf{p} \rightarrow \mathbf{q} \rightarrow \mathbf{k}) \\ &= \text{Re} \sum_{\mathbf{k}} \sum_{\mathbf{k}+\mathbf{p}+\mathbf{q}=0} [\sigma_{\mathbf{k}} M_{\mathbf{k}\mathbf{p}\mathbf{q}} + \sigma_{\mathbf{q}} M_{\mathbf{q}\mathbf{k}\mathbf{p}} + \sigma_{\mathbf{p}} M_{\mathbf{p}\mathbf{q}\mathbf{k}}] M_{\mathbf{p}\mathbf{q}\mathbf{k}}^* \bar{\Theta}_{\mathbf{p}\mathbf{q}\mathbf{k}}^*(t) \\ &= 0. \end{aligned}$$

To obtain the last two lines, we invoked Eqs. (I.18), (I.19), and (II.14).

#### Self-consistency:

An important property of the DIA is self-consistency, in that the strength of the nonlinearity is determined directly from the statistics of  $\psi$ . Not all closures share this property. For example, if we applied Dupree's resonance-broadening theory to the Hasegawa-Mima equation, this would amount to a passive calculation, in

which the  $\mathbf{v}_E \cdot \nabla \nabla^2 \varphi$  nonlinearity is handled by assuming that  $\mathbf{v}_E$  can be specified independently of  $\nabla^2 \varphi$ . This neglects important nonlinear interactions. To illustrate, suppose we compute the DIA under the “passive assumption.” This would be equivalent to discarding the crossed-out terms in the full DIA expression for  $\Sigma_{\mathbf{k}}$  (along with a similar modification of  $\mathcal{F}_{\mathbf{k}}$ ) [Krommes *et al.* 1990]:

$$\Sigma_{\mathbf{k}}(t, \bar{t}) = - \sum_{\mathbf{k}+\mathbf{p}+\mathbf{q}=\mathbf{0}} (\hat{\mathbf{z}} \cdot \mathbf{p} \times \mathbf{q})^2 \left( \frac{q^2 - p^2}{1 + k^2} \right) \left( \frac{k^2 - q^2}{1 + p^2} \right) R_{\mathbf{p}}^*(t, \bar{t}) C_{\mathbf{q}}^*(t, \bar{t}).$$

Thus, the passive approximation amounts to retaining only *one* out of *four* possible nonlinear terms. Furthermore, since both parts of  $q^2 - p^2$  are involved in the important energy conservation symmetry

$$(1 + k^2)M_{\mathbf{k}\mathbf{p}\mathbf{q}} + (1 + p^2)M_{\mathbf{p}\mathbf{q}\mathbf{k}} + (1 + q^2)M_{\mathbf{q}\mathbf{k}\mathbf{p}} = 0,$$

such a drastic truncation of the nonlinear interactions does not conserve energy.

#### II.B.4 Covariant representation

The DIA has a *covariant* multiple-field formulation. This means that the *form* of the closure equations remains unaltered under general (nonunitary) linear transformations of the fundamental field variables. Physically, this is important for the unambiguous definition of the closure. One desires the same final predictions when the closure is applied to an original set of variables and to a transformed set [Ottaviani *et al.* 1991].

To illustrate a representation for the DIA that is explicitly covariant we employ the following notation. Consider the  $n$ -field system

$$\boxed{\frac{\partial}{\partial t} \psi^\alpha + \nu^\alpha_\delta \psi^\delta = \frac{1}{2} \sum_{\Delta} M^\alpha_{\beta\gamma} \psi^{\beta*} \psi^{\gamma*}.} \quad (\text{II.25})$$

Here, we introduce the compact notation  $\alpha \doteq (\hat{\alpha}, \mathbf{k})$ ,  $\beta \doteq (\hat{\beta}, \mathbf{p})$ , and  $\gamma \doteq (\hat{\gamma}, \mathbf{q})$ , where  $\hat{\alpha}$ ,  $\hat{\beta}$ , and  $\hat{\gamma}$  are (inhomogeneous) “species indices” that distinguish the multiple fields. Also,  $\Delta$  means obey the condition  $\mathbf{k} + \mathbf{p} + \mathbf{q} = \mathbf{0}$ , summing over  $\beta$  and  $\gamma$ .

The mode-coupling coefficients have the symmetry

$$M^\alpha_{\beta\gamma} = M^\alpha_{\gamma\beta}. \quad (\text{II.26})$$

Suppose

$$\sigma_{\alpha\bar{\alpha}} M^{\bar{\alpha}}_{\beta\gamma} + \sigma_{\beta\bar{\beta}} M^{\bar{\alpha}}_{\gamma\alpha} + \sigma_{\gamma\bar{\gamma}} M^{\bar{\alpha}}_{\alpha\beta} = 0 \quad (\text{II.27})$$

for some (not necessarily unique) Hermitian matrix  $\sigma$  so that the real quantity

$$E \doteq \frac{1}{2} \sigma_{\alpha'\alpha} \psi^\alpha \psi^{\alpha'*} \quad (\text{II.28})$$

is conserved. Here, we invoke the convention that, unless otherwise indicated, summation over repeated Greek indices is implied. We define the correlation function

$$C^{\alpha\alpha'}(t, t') \doteq \langle \psi^\alpha(t) \psi^{\alpha'*}(t') \rangle$$

and the response function

$$R^{\alpha}_{\alpha'}(t, t') \doteq \left\langle \frac{\delta \psi^\alpha(t)}{\delta \psi^{\alpha'}(t')} \right\rangle \Big|_{\bar{\eta}_{\mathbf{k}}=0}.$$

The covariant DIA equations are then found to be [Ottaviani *et al.* 1991]:

$$\frac{\partial}{\partial t} C^{\alpha\alpha'}(t, t') + \nu^\alpha_\delta C^{\delta\alpha'} + \int_0^t d\bar{t} \Sigma^\alpha_\delta(t, \bar{t}) C^{\delta\alpha'}(\bar{t}, t') = \int_0^{t'} d\bar{t} \mathcal{F}^{\alpha\delta}(t, \bar{t}) R^{\alpha'}_\delta(t', \bar{t}), \quad (\text{II.29a})$$

$$\frac{\partial}{\partial t} R^{\alpha}_{\alpha'}(t, t') + \nu^\alpha_\delta R^{\delta}_{\alpha'} + \int_0^t d\bar{t} \Sigma^\alpha_\delta(t, \bar{t}) R^{\delta}_{\alpha'}(\bar{t}, t') = \delta(t-t') \delta^{\alpha}_{\alpha'}, \quad (\text{II.29b})$$

where

$$\Sigma^\alpha_{\alpha'}(t, \bar{t}) = - \sum_{\Delta} M^\alpha_{\beta\gamma} M^{\bar{\beta}}_{\bar{\gamma}\alpha'} R^{\beta}_{\bar{\beta}}(t, \bar{t}) C^{\gamma\bar{\gamma}*}(t, \bar{t}), \quad (\text{II.30a})$$

$$\mathcal{F}^{\alpha\alpha'}(t, \bar{t}) = \frac{1}{2} \sum_{\Delta} M^\alpha_{\beta\gamma} M^{\alpha'}_{\bar{\beta}\bar{\gamma}} C^{\beta\bar{\beta}*}(t, \bar{t}) C^{\gamma\bar{\gamma}*}(t, \bar{t}). \quad (\text{II.30b})$$

In Appendix C, these multiple-field equations are shown to conserve any quadratically nonlinear invariant  $E$  defined by Eq. (II.28) and the mode-coupling symmetry Eq. (II.27). The structure of Eqs. (II.29) and (II.30) will play an important role in our development of multiple-field Markovian closures in Chapter III.

## II.B.5 Failures

We have already encountered the two principal weaknesses (aside from computational limitations) of the DIA: its violation of random Galilean invariance and its inability to describe the coherent effects associated with high-order statistics. Let us now address these issues.

**RGI violation:**

The direct-interaction approximation is not random Galilean invariant since this closure is constructed from Eulerian correlation functions. Kraichnan [1964b] and Kadomtsev [1965] pointed out that this failing is responsible for the incorrect inertial-range exponent predicted by the DIA. For three-dimensional turbulence, the correct exponent is  $-5/3$ , while the DIA predicts  $-3/2$ . The Kolmogorov exponent for the two-dimensional enstrophy cascade is  $-3$ , subject to logarithmic corrections [Kraichnan 1967, 1971a] that tend to lower it further; in contrast, the DIA predicts the value  $-5/2$ .

Since the Kolmogorov argument is based on dimensional considerations, at first it may appear surprising that the DIA, which is also dimensionally consistent, obtains the wrong exponent. Indeed, Eqs. (I.39) are *formally* compatible with the inertial-range power law  $E(k) \sim \epsilon^{2/3} k^{-5/3}$ : when this form is substituted into the covariances of Eqs. (I.38), the result is dimensionally consistent. The difficulty is that Eq. (I.38b) involves an integral (in the continuum representation) over  $p$  of a function that behaves like  $p^{-5/3}$  near the wavenumber origin [Leslie 1973a]. Because this integral is divergent, we must conclude that the DIA equations are incompatible with this *local* inertial-range form. Locality enters the above calculation in the assumption that the inertial-range dynamics are not affected by the long-wavelength behaviour of  $E(k)$ , which differs from the substituted inertial-range form. The divergence of the resulting integral indicates that this assumption was invalid and that there is significant nonlocal interaction between the inertial range and the energy-containing long wavelengths [Orszag 1977].

A heuristic argument can be given to underscore the discrepancy between the Kolmogorov argument and the DIA. The Kolmogorov argument on pg. 6 can be restated in terms of the eddy-turnover time  $\tau_{\text{eddy}} \doteq \ell/u$ . Since the eddy deformation that results from coupling to smaller scales is responsible for local energy transfer, the energy transfer rate  $\epsilon$  is just  $\tau_{\text{eddy}}^{-1} u^2 = u^3/\ell$ . The Kolmogorov exponents  $\alpha = 2/3$  and  $\beta = -5/3$  in  $E(k) \sim \epsilon^\alpha k^\beta$  then follow from the dimensional balance

$$\ell u^2 \sim \left( \frac{u^3}{\ell} \right)^\alpha \ell^{-\beta}.$$

In the DIA, the spurious coupling of the inertial range to longer scales results in an energy transfer rate  $\tau_{\text{DIA}}^{-1}$ ,

$$\tau_{\text{DIA}}^{-1} \doteq \tau_{\text{eddy}}^{-1} \left( \frac{\tau_s}{\tau_{\text{eddy}}} \right) = \frac{u^2}{\ell u_0},$$

where  $\tau_s \doteq \ell/u_0$  is the *sweeping*, or advection, time and  $u_0$  is a typical large-scale velocity. The peculiar form of this scaling arises from the reciprocal manner in

which the DIA determines the nonlinear damping rate. Specifically, the nonlinear damping that appears in Eq. (II.13),

$$\begin{aligned}\tau_{\text{DIA}}^{-1} &= 2 \operatorname{Re} \frac{1}{C_{\mathbf{k}}(t)} \sum_{\mathbf{k}+\mathbf{p}+\mathbf{q}=\mathbf{0}} M_{\mathbf{k}\mathbf{p}\mathbf{q}} M_{\mathbf{p}\mathbf{q}\mathbf{k}}^* \bar{\Theta}_{\mathbf{p}\mathbf{q}\mathbf{k}}^*(t) \\ &= -2 \operatorname{Re} \sum_{\mathbf{k}+\mathbf{p}+\mathbf{q}=\mathbf{0}} M_{\mathbf{k}\mathbf{p}\mathbf{q}} M_{\mathbf{p}\mathbf{q}\mathbf{k}}^* C_{\mathbf{q}}(t) \left( \frac{\bar{\Theta}_{\mathbf{p}\mathbf{q}\mathbf{k}}^*(t)}{C_{\mathbf{q}}(t)C_{\mathbf{k}}(t)} \right),\end{aligned}$$

is proportional both to the intensity of the turbulence [*via*  $C_{\mathbf{q}}(t)$ , which gives rise to the factor  $\tau_{\text{eddy}}^{-2} \propto u^2$ ] and to the characteristic triad interaction time,

$$\frac{\bar{\Theta}_{\mathbf{p}\mathbf{q}\mathbf{k}}^*(t)}{C_{\mathbf{q}}(t)C_{\mathbf{k}}(t)},$$

which is proportional to  $\tau_s$  since the two-time quantities in  $\bar{\Theta}_{\mathbf{p}\mathbf{q}\mathbf{k}}$  decay by phase mixing on the time scale  $\tau_s$ .

Let us use  $\tau_{\text{DIA}}^{-1}$  to compute the inertial-range exponent predicted by the DIA for three-dimensional turbulence. From the scaling

$$\ell u^2 \sim \left( \frac{u^4}{\ell u_0} \right)^\alpha \ell^{-\beta},$$

we determine  $\alpha = 1/2$  and  $\beta = -3/2$ . For the two-dimensional enstrophy cascade, this scaling is modified to

$$\ell u^2 \sim \left( \frac{u^4}{\ell^3 u_0} \right)^\alpha \ell^{-\beta},$$

so that  $\alpha = 1/2$  and  $\beta = -5/2$ .

In two dimensions, the relative error in the inertial-range modeling of the DIA appears to be worse than in three dimensions. Since the primary focus of this work is on two-dimensional turbulence, it is essential that we address this matter. First, in actual plasma turbulence there need not be a well-developed inertial range since energy is produced internally and dissipated on a wide range of scales. This is quite different than the canonical example of driven fluid turbulence, in which energy is injected only at the long wavelengths and dissipated only at the short wavelengths. If the concept of an inertial range is not relevant for plasma turbulence, then how can one even ask what the inertial-range exponent is? One might well argue that the fundamental property of random Galilean invariance should still play an important role in energy transfer; however, its violation should significantly affect the spectrum only in regions containing little energy. The magnitude of the spurious coupling is too small to affect substantially the wavenumbers where the energy is dominant. In calculations of turbulent transport, only this latter region contributes significantly

to the desired diffusion coefficients. Thus, for our purposes, the RGI violation may not be as serious a difficulty as it has been for fluid turbulence.

In addition to the Lagrangian-history closures, there exist several other methods for removing the unwanted advective dephasing effects contaminating the energy transfer. Kadomtsev [1965] suggests that the divergence of the response function integral can be removed by introducing a long-wavelength cutoff. Leslie [1973b] discusses other ways of removing the singularity. Edwards and McComb [1969] obtain an alternate response equation by maximizing the entropy of the turbulence. The most popular approach in the literature appears to be the heuristic test-field model [Kraichnan 1971b, 1972]. This is derived by writing the Navier-Stokes equations in terms of the compressive and solenoidal components of a “test” field that is advected by the fundamental velocity field  $\mathbf{u}$ . In the nonlinearity, the cross terms coupling the compressive and solenoidal parts of the test field are then neglected. By comparing the resulting equations with an underlying Langevin description for a Markovianized version of the DIA, Kraichnan obtains the TFM equations. We will consider this random-Galilean-invariant closure further in Chapter III.

### **Coherent structures:**

In the random coupling model representation, we catch a glimpse of the nature of the physical inaccuracy introduced by the DIA. Since the triad couplings of this underlying model are randomly phased, it appears that the DIA will not properly describe individual coherent structures, in which phase relations between the various triads are crucial. We have already presented an illustrative example of this failing for the oscillatory passive advection problem. Statistics of much (in fact, infinitely) higher order than the covariance are necessary to describe such soliton-like solutions completely. However, it is still possible that the nonlinear interaction of a homogenous bath of such coherent structures may result in a highly stochastic state that can adequately be described by low-order statistics [Krommes 1984b].

Recently, numerical simulations of the DIA have been used to predict statistics above second order by making use of an underlying stochastic representation [Kraichnan and Panda 1988, Chen *et al.* 1989b]. For decaying isotropic turbulence, the DIA correctly exhibits a depression of the total mean-square nonlinearity from the value appropriate to Gaussian statistics. This emphasizes that the DIA can capture *some* of the higher-order phenomena associated with non-Gaussian statistics.

## **II.B.6 Numerical considerations**

Let us briefly discuss the numerical implementation of the direct-interaction approximation in order to motivate our work in the following chapter. A more

complete discussion of this subject will be presented in Chapter IV.

Suppose we evolve the DIA numerically for a system with  $N_{\mathbf{k}}$  distinct modes by a total of  $N_t$  time steps each of size  $\Delta t$ . Upon taking account of the constraint  $\mathbf{k} + \mathbf{p} + \mathbf{q} = \mathbf{0}$  on the sum appearing in the wavenumber convolutions, we obtain the following scaling for the DIA operation count:

$$N_t^3 N_{\mathbf{k}} + N_t^2 N_{\mathbf{k}}^2. \quad (\text{II.31})$$

The first term represents the number of required operations to solve Eqs. (I.38); the second term represents the number of operations needed for Eqs. (I.39). An important point to emphasize here is that  $\Sigma_{\mathbf{k}}(t, \bar{t})$  and  $\mathcal{F}_{\mathbf{k}}(t, \bar{t})$  are both independent of  $t'$  [Dannevik 1990], so they need not be recomputed for different values of  $t'$ . In contrast, the computation of  $C_{\mathbf{k}}(t, t')$  requires, for each combination of  $t$  and  $t'$ , roughly  $N_t$  operations to perform the time convolutions. Since  $C_{\mathbf{k}}(t, t')$  is Hermitian, we need only compute the cases where  $t' \leq t$ ; there are  $\frac{1}{2}N_t^2$  such combinations. Therefore, the computation of all values of  $C_{\mathbf{k}}(t, t')$  having time indices between 0 and  $N_t\Delta t$  requires on the order of  $N_t^3$  operations.

For problems with a large number of modes it is clear that the second term of Eq. (II.31) will dominate for sufficiently small times. The number of time steps is determined by the ratio of the *saturation time* to the minimum of the linear and nonlinear time scales. The saturation time is the time needed for the system to evolve from specified initial conditions to a statistically stationary state intended to represent actual turbulence. For most practical problems, this can require hundreds or even thousands of time steps, depending on how close the initial state is to the final state. Which term of Eq. (II.31) ultimately dominates depends on the particular problem and the numerical technique used.

For example, when the mode-reduction technique described in Chapter IV is employed, one finds in practice that the  $N_t^3$  term is the restrictive one. For this case, however, Eq. (II.31) is not the correct result since the modes  $\mathbf{k}$  now represent *sample wavenumber bins* obtained by averaging over finite extents in wavenumber. The constraint  $\mathbf{k} + \mathbf{p} + \mathbf{q} = \mathbf{0}$  must now be relaxed to include neighbouring wavenumber bins. Depending on the details of the wavenumber geometry, the correct result lies somewhere between Eq. (II.31) and

$$N_t^3 N_{\mathbf{k}} + N_t^2 N_{\mathbf{k}}^3. \quad (\text{II.32})$$

It is important to bear in mind when comparing Eqs. (II.31) and (II.32) that the mode-reduction technique permits a much smaller  $N_{\mathbf{k}}$  in the latter case. In Chapter IV particular examples of the actual scaling will be considered.

## II.C DIA-based Markovian closures

For purposes of numerical computation, the above scaling of the DIA with  $N_t$  places severe restrictions on the time scales that can be simulated. Suppose the wavenumber bin-averaging technique is employed for two-dimensional turbulence computations. It is then possible to keep the number of modes  $N_{\mathbf{k}}$  sufficiently low to allow the numerical data to fit easily into the memory of a modern workstation or supercomputer.<sup>9</sup> Indeed, our experience has indicated that the main limitation in such computations is the *lack of sufficient CPU time*.

For many problems, one is interested not in the details of the *transient evolution* to the final state, but in the *saturated state* itself. Several possible resolutions therefore come to mind. First, we could solve the *steady-state* DIA equations [Ottaviani 1990a], which scale like  $N_t^2$  rather than  $N_t^3$ . However, this requires solving a highly nonlinear set of equations by some kind of iteration scheme. The usual practice in the solution of equations like this is to introduce a parameter that, when relaxed to zero, facilitates convergence of the system. One can imagine that perhaps there exist parameters more optimal than  $t$ , the time. If  $t$  were the optimal parameter, we would be back to a situation where the scaling is like  $N_t^3$ . It would be interesting to pursue this further by searching for parameters that yield scalings much closer to  $N_t^2$  than  $N_t^3$ .

Another way of improving the computational scaling of the DIA is to exploit the fact that in a turbulent system the response functions entering the time convolution integrals will eventually decay to zero. After a sufficient number of time steps, it is possible to cut off the time integrations so that the scaling tends toward  $\mathcal{O}(N_t^2)$ . However, in practice the  $\mathcal{O}(N_t^3)$  initial scaling of this scheme may prevent one from ever reaching the regime where the response functions have decayed. Moreover, even the optimistic scaling of  $\mathcal{O}(N_t^2)$  quickly becomes restrictive; we will therefore consider such possibilities no further.

The other approach that presents itself is some sort of Markovianization of the DIA so that all time-history effects are carried by an auxiliary parameter. This makes the situation much more manageable, reducing the computational scaling to  $\mathcal{O}(N_t)$  so that the closure effectively tracks the actual physical system linearly in time. To help illuminate the possibilities for Markovianization, consider the alternate form, Eq. (II.13), of the equal-time DIA covariance equation, expressed

---

<sup>9</sup>Of course, the total memory requirement is determined not only by the number of modes, but also by the number of time steps since at each stage one must store away the two-time information for later use in the evaluation of other time-history convolutions. The storage requirement thus scales as  $N_t^2 N_{\mathbf{k}}$ . This can eventually impose a limitation if all data is stored in volatile memory. However, much of this data can be stored temporarily in a magnetic disk file, holding only enough data in memory at any one time to evolve from one time step to the next. This scheme was suggested by Krommes [1984a] and has been implemented in the code DIA.

in terms of the auxiliary parameter  $\bar{\Theta}_{\mathbf{k}\mathbf{p}\mathbf{q}}(t)$ . Markovianization then amounts to developing an approximation for  $\bar{\Theta}_{\mathbf{k}\mathbf{p}\mathbf{q}}(t)$  that can be computed knowing only the previous values of  $C_{\mathbf{k}}(t)$  and  $\bar{\Theta}_{\mathbf{k}\mathbf{p}\mathbf{q}}(t)$ . No matter how crude the approximation is, the argument on pg. 71 ensures that all of the quadratically nonlinear invariants will be conserved.

It turns out that there is a great deal of arbitrariness in the formulation of Markovian closures, so to help us choose a physically reasonable one we will require that it be realizable and closely related to the DIA. In the next chapter we will consider DIA-based Markovian closures in great detail, concentrating particularly on the issue of realizability.

# Chapter III

## Theory of Markovian Closures

In the previous chapter we developed the direct-interaction approximation as a renormalized generalization of perturbation theory applicable to strong turbulence. Although this closure is only an approximation, it possesses several important properties such as self-consistency, energy conservation, and realizability. Unfortunately, the utility of the direct-interaction approximation as a tool for studying multi-dimensional inhomogeneous turbulence is limited by its discouraging computational scaling with time [ $\mathcal{O}(N_t^3)$ ]. For practical problems in turbulence, many time steps are often required to evolve the system to the desired steady state, and even on modern supercomputers the situation is quite disheartening. We are therefore interested in developing alternative closures that, while capturing some of the desirable features of the direct-interaction approximation, are faster to compute.

Two reasons can be given for the prohibitive computational scaling of the DIA. First, this approximation requires the calculation of an entire set of *two-time* statistical variables. Second, the evolution equations for these statistical quantities contain non-trivial time-history integrals. The physics questions of interest, however, primarily involve only *equal-time* quantities such as energies and cross-correlations; often, we would be satisfied with a closure involving only equal-time correlation functions. Moreover, one could gain even further computational improvement if the evolution equations did not involve time-history integrals, so that the evolution of the system could be computed solely on the basis of current variables. In Chapter I, we introduced the term *Markovian* to describe such dynamical systems, in which the future state is an explicit function of only the current state. Of course, this is not to say that the system has no dependence on past conditions. There is such a dependence, but the point is that it is an *implicit* dependence; the future is affected by the past only through the current values of the state variables.

In the next section we will identify various Markovian closures that have been used in the literature and discuss their nomenclature. We will then focus on a

particular Markovian closure that is derivable from the DIA. We emphasize serious difficulties in its application to systems involving wave phenomena (such as one finds ubiquitously in plasma physics and geophysics). In investigating this difficulty we will be led to propose a new but related closure that does not share this deficiency.

### III.A Overview of Markovian closures

One way of developing Markovian closures is to discard the detailed time-history information in the temporal convolutions of the DIA in favour of a triad interaction time  $\theta(t)$ . This auxiliary parameter is closely related to the quantity  $\bar{\Theta}(t)$  introduced in the alternate form for the DIA on pg. 64. Actually, such a closure is not Markovian because information from the previous state of the system enters into the equations not only through the current state variables but also through  $\theta$ . However, only the current value of  $\theta$  enters into the evolution equations; if  $\theta$  is considered to be one of the state variables, the closure can, in fact, be viewed as Markovian. It is in this sense that we will generally refer to closures of this type as “Markovian,” even though for such systems we should, strictly speaking, employ the term “almost Markovian” used by Kraichnan [1971b]. From the viewpoint of computational speed, the distinction is moot since the computational scalings of Markovian and almost-Markovian closures are both  $\mathcal{O}(N_t)$ , assuming that the auxiliary parameter can be evolved solely on the basis of its current value.

Historically, the first references to Markovian closures appear in the works of Kraichnan [1971b], Leith [1971], and Orszag [1977]. Kraichnan’s interest in Markovian closures was connected with his search for alterations to the generalized Langevin model underlying the DIA that would provide a model representation for the Lagrangian-history DIA. This search proved unsuccessful “because, in contrast to a covariance, in which just one of the factors averaged over can be changed from Eulerian to Lagrangian, an amplitude equation must be for either one field or the other.” However, the temporal behaviour of the DIA-based Markovian closure to be discussed shortly is sufficiently simple that modifications (leading to the test-field model) that restore random Galilean invariance are possible. The important feature of the unmodified Eulerian closure is that it has an underlying Langevin equation with a *white-noise* forcing  $f(t)$  and a nonlinear damping  $\eta(t)$ . No memory effects are present in this equation; instead, the time over which triad interactions occur enters into the model as the auxiliary parameter  $\theta$ . The steady-state form of this model reduces to an approximate stationary form of the DIA given by Kraichnan [1964c] in which the two-time statistical functions are modeled by characteristic damping factors. Kraichnan points out the close connection of this steady-state form to the random-phase theory of Edwards [1964]. In a Taylor expansion in powers of  $t$ , this Markovian closure agrees with both the DIA and the exact statistics up to and

including third order [Kraichnan 1971b].

Leith [1971] presents a related Markovian closure that is credited to Orszag. This eddy-damped quasinormal Markovian (EDQNM) closure is discussed extensively by Orszag [1977]. (Leith omits the qualifier “quasinormal,” but it is clearly implied.) According to Leith, the EDQNM is obtained by making the “best Markovian fit” to the DIA that is consistent with the underlying Langevin representation just discussed. From his presentation, it appears that the term “EDQNM” refers to an entire *family* of closures that depend on the choice of an *eddy-damping* parameter  $\mu_{\mathbf{k}}$  that “we still have freedom to adjust... to match the phenomenology of the inertial ranges.” The eddy damping models the combined effect of the viscosity introduced both by molecular forces and the turbulent eddies. In three dimensions, the scaling of the turbulent contribution to  $\mu_{\mathbf{k}}$  is often estimated as  $\epsilon^{1/3}k^{2/3}$ . A more general form that involves a spectral weighting of the energy is [Orszag 1977]

$$\mu_{\mathbf{k}} = \nu_{\mathbf{k}} + \left[ \int_0^k k^2 dk E(k) \right]^{1/2}. \quad (\text{III.1})$$

Eddy damping was introduced by Orszag [1970] as a remedy for the unphysical behaviour of the quasinormal approximation. Recall that the quasinormal approximation is obtained by neglecting fourth-order cumulants such as the one appearing in Eq. (I.24). When the result is appropriately integrated over time and substituted into Eq. (I.22), the equal-time quasinormal approximation becomes, for real  $\nu_{\mathbf{k}}$  and  $M_{\mathbf{k}\mathbf{p}\mathbf{q}}$ ,

$$\begin{aligned} \left( \frac{\partial}{\partial t} + 2\nu_{\mathbf{k}} \right) C_{\mathbf{k}}(t) &= \int_0^t d\bar{t} e^{-(\nu_{\mathbf{k}} + \nu_{\mathbf{p}} + \nu_{\mathbf{q}})(t-\bar{t})} \\ &\times \sum_{\mathbf{k}+\mathbf{p}+\mathbf{q}=\mathbf{0}} \left[ M_{\mathbf{k}\mathbf{p}\mathbf{q}}^2 C_{\mathbf{p}}(\bar{t}) C_{\mathbf{q}}(\bar{t}) + 2M_{\mathbf{k}\mathbf{p}\mathbf{q}} M_{\mathbf{p}\mathbf{q}\mathbf{k}} C_{\mathbf{q}}(\bar{t}) C_{\mathbf{k}}(\bar{t}) \right]. \end{aligned} \quad (\text{III.2})$$

Orszag traced the nonrealizability of the quasinormal closure (demonstrated numerically by Ogura [1963]) to the appearance of only linear viscous effects in the memory-cutoff integral in Eq. (III.2). He argued that memory of the past should be lost faster than this since phase correlations between modes are destroyed by “nonlinear scrambling.” Noting that the discarded fourth-order cumulants could no longer provide a damping mechanism to bound the third-order cumulants, he advocated replacing the viscous damping  $\nu_{\mathbf{k}}$  with the total (linear plus turbulent) eddy viscosity  $\mu_{\mathbf{k}}$ :

$$\begin{aligned} \left( \frac{\partial}{\partial t} + 2\mu_{\mathbf{k}} \right) C_{\mathbf{k}}(t) &= \int_0^t d\bar{t} e^{-(\mu_{\mathbf{k}} + \mu_{\mathbf{p}} + \mu_{\mathbf{q}})(t-\bar{t})} \\ &\times \sum_{\mathbf{k}+\mathbf{p}+\mathbf{q}=\mathbf{0}} \left[ M_{\mathbf{k}\mathbf{p}\mathbf{q}}^2 C_{\mathbf{p}}(\bar{t}) C_{\mathbf{q}}(\bar{t}) + 2M_{\mathbf{k}\mathbf{p}\mathbf{q}} M_{\mathbf{p}\mathbf{q}\mathbf{k}} C_{\mathbf{q}}(\bar{t}) C_{\mathbf{k}}(\bar{t}) \right]. \end{aligned} \quad (\text{III.3})$$

Leith [1971] called this closure the “eddy-damped quasnormal approximation.” Unfortunately, it is not realizable as it stands [Orszag 1977]. However, by making the Markovian assumption<sup>1</sup> that the time scale on which the memory integral decays is much faster than the time scale on which the covariances evolve, Orszag arrived at the eddy-damped quasnormal Markovian closure, in which the covariances on the right-hand side are now evaluated at the current time  $t$ :

$$\left(\frac{\partial}{\partial t} + 2\nu_{\mathbf{k}}\right)C_{\mathbf{k}}(t) = \int_0^t d\bar{t} e^{-(\mu_{\mathbf{k}}+\mu_{\mathbf{p}}+\mu_{\mathbf{q}})(t-\bar{t})} \times \sum_{\mathbf{k}+\mathbf{p}+\mathbf{q}=\mathbf{0}} \left[M_{\mathbf{k}\mathbf{p}\mathbf{q}}^2 C_{\mathbf{p}}(t)C_{\mathbf{q}}(t) + 2M_{\mathbf{k}\mathbf{p}\mathbf{q}}M_{\mathbf{p}\mathbf{q}\mathbf{k}}C_{\mathbf{q}}(t)C_{\mathbf{k}}(t)\right]. \quad (\text{III.4})$$

For real  $\mu_{\mathbf{k}}$ , an underlying Langevin equation [Leith 1971] establishes the realizability of this closure.

Let us say more about the determination of  $\mu_{\mathbf{k}}$ . Lesieur [1987, p. 107] acknowledges that “the choice of  $\mu_{\mathbf{k}}$  is more difficult in non isotropic situations, for instance for problems where waves (Rossby waves, inertial or gravity waves) interact with turbulence. . . , and this is still an open question.” Unfortunately, the terminology in the literature is confusing. In addition to the phenomenological form [Eq. (III.1)] for  $\mu_{\mathbf{k}}$  in Eq. (III.4), Orszag [1970] suggested a more fundamental treatment based on the direct-interaction approximation. This is how  $\mu_{\mathbf{k}}$  is obtained in Kraichnan’s Markovian closure. We will refer to this choice as the “DIA-based EDQNM,” or simply, the EDQNM.<sup>2</sup> The reasoning here is that we do not wish to abandon all of our previous arguments supporting the need for a systematic theory by suddenly introducing a phenomenological or dimensionally determined  $\mu_{\mathbf{k}}$  at this stage.

However, the DIA-based EDQNM does not solve the problem of random Galilean invariance. The other choice is the “phenomenological EDQNM” obtained by using Eq. (III.1) for  $\mu_{\mathbf{k}}$ . The reason the phenomenological EDQNM has been used extensively in the fluid dynamics literature is that it is invariant to random Galilean transformations [Orszag 1977]. Nevertheless, the use of a scaling relation like Eq. (III.1) to obtain the eddy damping has the disadvantage of possessing an unknown numerical coefficient. [This parameter was omitted but should actually appear multiplying the spectral integral in Eq. (III.1).] This adjustable parameter detracts from one’s confidence in the predictive power of the “phenomenological EDQNM.” Furthermore, if random Galilean invariance (RGI) is the desired objective, this can be achieved in a somewhat more systematic fashion by using the test-field model,

<sup>1</sup>This lacks fundamental justification (unless the system is sufficiently close to a steady state), but it does ensure that the rate of change of the energy spectrum depends only on current values of the spectrum. Orszag used this property to prove realizability.

<sup>2</sup>The DIA-based EDQNM has been referred to as the “rationalized eddy-damped Markovian approximation” by Herring [1975].

which can be obtained from the DIA-based EDQNM. Numerical comparison of the phenomenological EDQNM and the TFM has shown that the former “may be regarded as a rational approximation to, and simplification of the TFM, except at small wavenumbers, where an additional eddy-dissipative term is needed to produce satisfactory results. . .” [Herring *et al.* 1982]. It is precisely these kinds of difficulties we are trying to avoid by using a systematically derived closure.

In plasma physics, the term EDQNM is often used as here, to describe a Markovian closure obtained from the DIA. One of the reasons for this is that it is not clear how to include nonlinear wave effects in the phenomenological EDQNM since the eddy viscosity defined by Eq. (III.1) is inherently real. Proper renormalization of linear wave effects has also been an issue in geophysical applications. (This remark applies equally well to the related test-field model used by Holloway and Hendershott [1977], in which the frequency renormalization was simply neglected.) In fluid turbulence, the term EDQNM usually refers to the phenomenological closure, which has the advantage of predicting the correct Kolmogorov inertial range.

The confusion seems to originate with whether the modifier “eddy-damped” refers to the general mechanism of nonlinear scrambling described above or to the specific case of decorrelation on the eddy-turnover time scale. We have adopted the terminology that seems appropriate based on an examination of the earliest references to the EDQNM [Leith 1971, Orszag 1977]. It appears that the original motivation in these works was to fix the gross violations of the quasinormal closure by introducing some sort of eddy damping, phenomenological or otherwise, while Markovianizing to ensure realizability. Especially in plasma transport problems where RGI does not seem to be significant, it thus seems unreasonable to restrict the use of the term “EDQNM” to only the phenomenological member of this family.

### III.B DIA-based one-field EDQNM closure

Let us now restrict our attention to the DIA-based eddy-damped quasinormal Markovian closure. In this section we present a systematic derivation of this closure from the DIA. The presentation represents an amalgamation of the works of Orszag [1970, 1977] and Kraichnan [1971b], written in the general notation of our fundamental equation, Eq. (I.17). We allow for a linear frequency and complex mode coupling, but unlike the related work of Holloway and Hendershott [1977] we renormalize the frequency as well as the growth rate. A related complex version of the DIA-based EDQNM was previously presented by Koniges and Leith [1987], but no mention was made of its serious deficiencies, which we will soon encounter.<sup>3</sup>

---

<sup>3</sup>Koniges and Leith [1987] incorrectly claimed that their complex Markovian closure (always) has an underlying Langevin equation.

### III.B.1 Derivation of the EDQNM from the DIA

We begin by writing the DIA equation for the equal-time correlation function, using Eqs. (I.38a), (I.39), and (I.23):

$$\begin{aligned} \left(\frac{\partial}{\partial t} + 2 \operatorname{Re} \nu_{\mathbf{k}}\right) C_{\mathbf{k}}(t) - 2 \operatorname{Re} \int_0^t d\bar{t} \sum_{\mathbf{k}+\mathbf{p}+\mathbf{q}=\mathbf{0}} M_{\mathbf{k}\mathbf{p}\mathbf{q}} M_{\mathbf{p}\mathbf{q}\mathbf{k}}^* R_{\mathbf{p}}^*(t, \bar{t}) C_{\mathbf{q}}^*(t, \bar{t}) C_{\mathbf{k}}(\bar{t}, t) \\ = \operatorname{Re} \int_0^t d\bar{t} \sum_{\mathbf{k}+\mathbf{p}+\mathbf{q}=\mathbf{0}} |M_{\mathbf{k}\mathbf{p}\mathbf{q}}|^2 C_{\mathbf{p}}^*(t, \bar{t}) C_{\mathbf{q}}^*(t, \bar{t}) R_{\mathbf{k}}^*(t, \bar{t}). \end{aligned} \quad (\text{III.5})$$

Note that computation of even the equal-time DIA covariance requires knowledge of the two-time correlation functions, so that its solution requires about as much computational effort as solving for the entire set of two-time correlation functions.

Now, unlike the equal-time correlation function, the equal-time response function is not a useful quantity upon which to formulate a theory of turbulence. After all, the equal-time limit is trivial:

$$\begin{aligned} \lim_{t' \rightarrow t^-} R(t, t') &= 1, \\ \lim_{t' \rightarrow t^+} R(t, t') &= 0. \end{aligned}$$

The two-time information contained in the propagator is essential to any theory of turbulence. Discarding this information would prevent even linear theory from being correctly modeled. So the most we can hope to achieve in the way of simplification is to replace the  $R_{\mathbf{k}}$  equation,

$$\left(\frac{\partial}{\partial t} + \nu_{\mathbf{k}}\right) R_{\mathbf{k}}(t, t') - \int_{t'}^t d\bar{t} \sum_{\mathbf{k}+\mathbf{p}+\mathbf{q}=\mathbf{0}} M_{\mathbf{k}\mathbf{p}\mathbf{q}} M_{\mathbf{p}\mathbf{q}\mathbf{k}}^* R_{\mathbf{p}}^*(t, \bar{t}) C_{\mathbf{q}}^*(t, \bar{t}) R_{\mathbf{k}}(\bar{t}, t') = \delta(t-t'), \quad (\text{III.6})$$

with a Markovian form such as

$$\frac{\partial}{\partial t} R_{\mathbf{k}}(t, t') + \mu_{\mathbf{k}}(t, t') R_{\mathbf{k}}(t, t') = \delta(t-t'). \quad (\text{III.7})$$

Such a form is actually equivalent to Eq. (III.6) for<sup>4</sup>

$$\mu_{\mathbf{k}}(t, t') = \begin{cases} -\frac{\partial}{\partial t} \log R_{\mathbf{k}}(t, t') & \text{for } R_{\mathbf{k}}(t, t') \neq 0; \\ 0 & \text{otherwise.} \end{cases}$$

Thus there always exists a  $\mu_{\mathbf{k}}$  that reduces Eq. (III.6) to Eq. (III.7); therefore, there is no *inherent* loss of generality in considering Markovian forms like Eq. (III.7). Of course, in practice we do not know  $\mu_{\mathbf{k}}(t, t')$  or  $R_{\mathbf{k}}(t, t')$  and we will have to be content with an approximation. We will return to the choice of  $\mu_{\mathbf{k}}$  later.

<sup>4</sup>The logarithm that appears here is the complex logarithm, defined to within an additive imaginary constant that disappears upon differentiation.

### Fluctuation-Dissipation ansatz:

Let us address the difficulty mentioned above regarding the appearance of two-time correlation functions in the equal-time covariance equation, Eq. (III.5). Given that we have already established the need for a two-time  $R_{\mathbf{k}}$  equation, the question arises as to whether we can make use of the two-time response function to approximate the two-time correlation function. In fact, in thermal equilibrium there exists an exact relation, known as the Fluctuation-Dissipation Theorem [Kraichnan 1959b, Deker and Haake 1975, Leith 1975], between these two statistical quantities:

$$C_{\mathbf{k}}(t, t') = R_{\mathbf{k}}(t, t')C_{\mathbf{k}}(\infty) \quad (t > t'). \quad (\text{III.8})$$

[The case  $t < t'$  is obtained by using the Hermiticity relationship  $C_{\mathbf{k}}(t', t) = C_{\mathbf{k}}^*(t, t')$ .]

In thermal equilibrium, statistical quantities are stationary, so that  $C_{\mathbf{k}}(t, t') = \mathcal{C}_{\mathbf{k}}(t - t')$ . Hence  $C_{\mathbf{k}}(t) = \mathcal{C}_{\mathbf{k}}(0) = C_{\mathbf{k}}(t')$ , and Eq. (III.8) is equivalent to either

$$C_{\mathbf{k}}(t, t') = R_{\mathbf{k}}(t, t')C_{\mathbf{k}}(t) \quad (t > t') \quad (\text{III.9})$$

or

$$C_{\mathbf{k}}(t, t') = R_{\mathbf{k}}(t, t')C_{\mathbf{k}}(t') \quad (t > t'). \quad (\text{III.10})$$

The first assumption used to simplify the DIA is to adopt the former relationship even out of thermal equilibrium. Although not exact, this assumption is not entirely unreasonable, as one often finds empirically that the qualitative two-time behaviour of  $C_{\mathbf{k}}$  and  $R_{\mathbf{k}}$  are similar (e.g., see Figs. V.47 and V.48). The primary reason for choosing Eq. (III.9) over Eq. (III.10) is that in the *absence* of wave phenomena Eq. (III.9) always leads to a realizable closure, while Eq. (III.10) does not [Orszag 1977]. We will return to this issue later.

The FD ansatz, as we shall call Eq. (III.9), results in a remarkable simplification of Eq. (III.5). It is convenient to express the result in terms of the triad interaction time  $\theta_{\mathbf{k}\mathbf{p}\mathbf{q}}$ ,

$$\theta_{\mathbf{k}\mathbf{p}\mathbf{q}}(t) \doteq \int_0^t d\bar{t} R_{\mathbf{k}}(t, \bar{t}) R_{\mathbf{p}}(t, \bar{t}) R_{\mathbf{q}}(t, \bar{t}). \quad (\text{III.11})$$

Then we obtain

$$\begin{aligned} \left( \frac{\partial}{\partial t} + 2 \operatorname{Re} \nu_{\mathbf{k}} \right) C_{\mathbf{k}}(t) - 2 \operatorname{Re} \sum_{\mathbf{k}+\mathbf{p}+\mathbf{q}=\mathbf{0}} M_{\mathbf{k}\mathbf{p}\mathbf{q}} M_{\mathbf{p}\mathbf{q}\mathbf{k}}^* \theta_{\mathbf{k}\mathbf{p}\mathbf{q}}^*(t) C_{\mathbf{q}}(t) C_{\mathbf{k}}(t) \\ = \operatorname{Re} \sum_{\mathbf{k}+\mathbf{p}+\mathbf{q}=\mathbf{0}} |M_{\mathbf{k}\mathbf{p}\mathbf{q}}|^2 \theta_{\mathbf{k}\mathbf{p}\mathbf{q}}^*(t) C_{\mathbf{p}}(t) C_{\mathbf{q}}(t). \end{aligned} \quad (\text{III.12})$$

It is instructive to compare this covariance equation to the alternate form, Eq. (II.13), for the DIA.

Physically, at any time  $t$ , the new quantity  $\theta_{\mathbf{k}\mathbf{p}\mathbf{q}}$  represents the time for which the modes  $\mathbf{k}$ ,  $\mathbf{p}$ , and  $\mathbf{q}$  have been interacting. Note that Eq. (III.11) is consistent with the expectation that, at time  $t$ , the interaction should cease if any of these three modes, excited by disturbances in the interval  $[0, t)$ , have decayed. In other words,  $\theta_{\mathbf{k}\mathbf{p}\mathbf{q}}$  represents an effective time for which all three modes are active.

Note that Eq. (III.12) can be written in the compact form

$$\boxed{\left(\frac{\partial}{\partial t} + 2 \operatorname{Re} \nu_{\mathbf{k}}\right) C_{\mathbf{k}}(t) + 2 \operatorname{Re} \hat{\eta}_{\mathbf{k}}(t) C_{\mathbf{k}}(t) = 2 F_{\mathbf{k}}(t)} \quad (\text{III.13})$$

by defining a nonlinear damping rate,

$$\hat{\eta}_{\mathbf{k}}(t) \doteq - \sum_{\mathbf{k}+\mathbf{p}+\mathbf{q}=\mathbf{0}} M_{\mathbf{k}\mathbf{p}\mathbf{q}} M_{\mathbf{p}\mathbf{q}\mathbf{k}}^* \theta_{\mathbf{k}\mathbf{p}\mathbf{q}}^*(t) C_{\mathbf{q}}(t), \quad (\text{III.14})$$

and a nonlinear noise term,

$$F_{\mathbf{k}}(t) \doteq \frac{1}{2} \operatorname{Re} \sum_{\mathbf{k}+\mathbf{p}+\mathbf{q}=\mathbf{0}} |M_{\mathbf{k}\mathbf{p}\mathbf{q}}|^2 \theta_{\mathbf{k}\mathbf{p}\mathbf{q}}^*(t) C_{\mathbf{p}}(t) C_{\mathbf{q}}(t). \quad (\text{III.15})$$

As alluded to earlier, Eq. (III.13) can be considered a Markovian description of the system if  $\theta_{\mathbf{k}\mathbf{p}\mathbf{q}}$  is regarded as one of the state variables.

### Markovianization of the mass operator:

We still need to determine the interaction time, which can be computed from the response function, so we now return to the problem of finding an approximate equation for  $R_{\mathbf{k}}$ . First, note that Eq. (III.13) can be quickly recovered from the original DIA covariance equation,

$$\left(\frac{\partial}{\partial t} + 2 \operatorname{Re} \nu_{\mathbf{k}}\right) C_{\mathbf{k}}(t) + 2 \operatorname{Re} \int_0^t d\bar{t} \Sigma_{\mathbf{k}}(t, \bar{t}) C_{\mathbf{k}}(\bar{t}, t) = 2 \operatorname{Re} \int_0^t d\bar{t} \mathcal{F}_{\mathbf{k}}(t, \bar{t}) R_{\mathbf{k}}^*(t, \bar{t}),$$

by the crude approximations

$$\Sigma_{\mathbf{k}}(t, \bar{t}) = \hat{\eta}_{\mathbf{k}}(t) \delta(t - \bar{t}), \quad (\text{II.3a})$$

$$\mathcal{F}_{\mathbf{k}}(t, \bar{t}) = F_{\mathbf{k}}(t) \delta(t - \bar{t}). \quad (\text{II.3b})$$

Suppose we apply Eq. (II.3a) to the DIA equation for  $R_{\mathbf{k}}$ ,

$$\left(\frac{\partial}{\partial t} + \nu_{\mathbf{k}}\right) R_{\mathbf{k}}(t, t') + \int_0^t d\bar{t} \Sigma_{\mathbf{k}}(t, \bar{t}) R_{\mathbf{k}}(\bar{t}, t') = \delta(t - t').$$

Then we obtain

$$\left(\frac{\partial}{\partial t} + \nu_{\mathbf{k}}\right) R_{\mathbf{k}}(t, t') + \hat{\eta}_{\mathbf{k}}(t) R_{\mathbf{k}}(t, t') = \delta(t-t').$$

This, we note, is a special case of Eq. (III.7) with  $\mu_{\mathbf{k}}(t, t') = \nu_{\mathbf{k}} + \hat{\eta}_{\mathbf{k}}(t)$ . From here on, we will denote the total linear and nonlinear damping by

$$\eta_{\mathbf{k}} \doteq \nu_{\mathbf{k}} + \hat{\eta}_{\mathbf{k}},$$

so that

$$\frac{\partial}{\partial t} R_{\mathbf{k}}(t, t') + \eta_{\mathbf{k}}(t) R_{\mathbf{k}}(t, t') = \delta(t-t'). \quad (\text{III.16})$$

Finally, we attempt to use Eq. (III.16) to determine a differential equation for Eq. (III.11). One must be careful with the generalized functions that arise in this calculation. To avoid the difficulty of a  $\delta$  function appearing in a one-sided integral, evaluate Eq. (III.11) as

$$\theta_{\mathbf{k}\mathbf{p}\mathbf{q}}(t) = \int_0^{t^-} d\bar{t} R_{\mathbf{k}}(t, \bar{t}) R_{\mathbf{p}}(t, \bar{t}) R_{\mathbf{q}}(t, \bar{t}).$$

Since the integrand is bounded on the interval  $[0, t]$ , the function  $\theta_{\mathbf{k}\mathbf{p}\mathbf{q}}(t)$  is continuous and hence the above limit equals Eq. (III.11). Differentiating this form yields no  $\delta$  function contribution:

$$\begin{aligned} \frac{\partial}{\partial t} \theta_{\mathbf{k}\mathbf{p}\mathbf{q}}(t) &= R_{\mathbf{k}}(t, t^-) R_{\mathbf{p}}(t, t^-) R_{\mathbf{q}}(t, t^-) \\ &\quad - [\eta_{\mathbf{k}}(t) + \eta_{\mathbf{p}}(t) + \eta_{\mathbf{q}}(t)] \int_0^{t^-} d\bar{t} R_{\mathbf{k}}(t, \bar{t}) R_{\mathbf{p}}(t, \bar{t}) R_{\mathbf{q}}(t, \bar{t}). \end{aligned}$$

Thus  $\theta_{\mathbf{k}\mathbf{p}\mathbf{q}}$  is the solution to

$$\frac{\partial}{\partial t} \theta_{\mathbf{k}\mathbf{p}\mathbf{q}} + (\eta_{\mathbf{k}} + \eta_{\mathbf{p}} + \eta_{\mathbf{q}}) \theta_{\mathbf{k}\mathbf{p}\mathbf{q}} = 1, \quad (\text{III.17a})$$

with initial condition

$$\theta_{\mathbf{k}\mathbf{p}\mathbf{q}}(0) = 0. \quad (\text{III.17b})$$

In summary, the entire Markovianization proceeds as follows. We apply the FD ansatz, Eq. (III.9), to the equal-time DIA covariance equation and note that the resulting form is equivalent to assuming Eqs. (II.3). We then use one of these, Eq. (II.3a), to also Markovianize the response function equation. We are left with

the following closed system known as the EDQNM:

$$\frac{\partial}{\partial t} C_{\mathbf{k}}(t) + 2 \operatorname{Re} \eta_{\mathbf{k}}(t) C_{\mathbf{k}}(t) = 2F_{\mathbf{k}}(t), \quad (\text{III.18a})$$

$$\eta_{\mathbf{k}}(t) \doteq \nu_{\mathbf{k}} - \sum_{\mathbf{k}+\mathbf{p}+\mathbf{q}=\mathbf{0}} M_{\mathbf{k}\mathbf{p}\mathbf{q}} M_{\mathbf{p}\mathbf{q}\mathbf{k}}^* \theta_{\mathbf{k}\mathbf{p}\mathbf{q}}^*(t) C_{\mathbf{q}}(t), \quad (\text{III.18b})$$

$$F_{\mathbf{k}}(t) \doteq \frac{1}{2} \operatorname{Re} \sum_{\mathbf{k}+\mathbf{p}+\mathbf{q}=\mathbf{0}} |M_{\mathbf{k}\mathbf{p}\mathbf{q}}|^2 \theta_{\mathbf{k}\mathbf{p}\mathbf{q}}^*(t) C_{\mathbf{p}}(t) C_{\mathbf{q}}(t), \quad (\text{III.18c})$$

$$\frac{\partial}{\partial t} \theta_{\mathbf{k}\mathbf{p}\mathbf{q}} + (\eta_{\mathbf{k}} + \eta_{\mathbf{p}} + \eta_{\mathbf{q}}) \theta_{\mathbf{k}\mathbf{p}\mathbf{q}} = 1, \quad \theta_{\mathbf{k}\mathbf{p}\mathbf{q}}(0) = 0. \quad (\text{III.18d})$$

As desired, the computational scaling of this system is  $\mathcal{O}(N_t)$ , a vast improvement over the  $\mathcal{O}(N_t^3)$  scaling of the DIA.

### III.B.2 Properties of the EDQNM

#### Short-time behaviour:

For small  $t$ ,

$$\theta_{\mathbf{k}\mathbf{p}\mathbf{q}} \sim t.$$

This is consistent with the short-time result obtained by applying perturbation theory to the exact statistics when the nonlinearity is weak. We see that no effect of nonlinear scrambling enters  $\theta_{\mathbf{k}\mathbf{p}\mathbf{q}}$  initially because the phase decorrelations that lead to loss of memory have not yet developed: the nonlinear interactions are allowed to act for the full time  $t$  over which the system has evolved.

#### Steady state:

The steady-state solution for  $\theta_{\mathbf{k}\mathbf{p}\mathbf{q}}$  is

$$\theta_{\mathbf{k}\mathbf{p}\mathbf{q}}(\infty) = \frac{1}{\eta_{\mathbf{k}} + \eta_{\mathbf{p}} + \eta_{\mathbf{q}}}. \quad (\text{III.19})$$

In this situation, we see that the effects of nonlinear scrambling are so great as to dominate  $\theta_{\mathbf{k}\mathbf{p}\mathbf{q}}$  and cause it to achieve this limiting value.

Only the real part of Eq. (III.19) enters explicitly into the energy equation. Upon denoting  $\eta_{\mathbf{k}} \doteq \rho_{\mathbf{k}} + ia_{\mathbf{k}}$  we may write

$$\operatorname{Re} \theta_{\mathbf{k}\mathbf{p}\mathbf{q}}(\infty) = \frac{\rho_{\mathbf{k}} + \rho_{\mathbf{p}} + \rho_{\mathbf{q}}}{(\rho_{\mathbf{k}} + \rho_{\mathbf{p}} + \rho_{\mathbf{q}})^2 + (a_{\mathbf{k}} + a_{\mathbf{p}} + a_{\mathbf{q}})^2}. \quad (\text{III.20})$$

Now the equation for  $\theta_{\mathbf{k}\mathbf{p}\mathbf{q}}$  has the exact solution

$$\theta_{\mathbf{k}\mathbf{p}\mathbf{q}}(t) = \int_0^t dt' \exp\left(-\int_{t'}^t d\bar{t} [\eta_{\mathbf{k}}(\bar{t}) + \eta_{\mathbf{p}}(\bar{t}) + \eta_{\mathbf{q}}(\bar{t})]\right), \quad (\text{III.21})$$

from which it is clear that a steady state will be achieved only if

$$\lim_{t \rightarrow \infty} \text{Re}(\eta_{\mathbf{k}} + \eta_{\mathbf{p}} + \eta_{\mathbf{q}}) > 0. \quad (\text{III.22})$$

Therefore, if a steady state exists,  $\text{Re} \theta_{\mathbf{k}\mathbf{p}\mathbf{q}}(\infty)$  will be positive. We will make use of this important property in Section III.C.

### Energy conservation:

The EDQNM conserves the generalized energy defined by Eq. (I.20):

$$\frac{1}{2} \frac{\partial}{\partial t} \sum_{\mathbf{k}} \sigma_{\mathbf{k}} C_{\mathbf{k}}(t) = 0.$$

This is implied by the relation

$$\text{Re} \sum_{\mathbf{k}} \sigma_{\mathbf{k}} [F_{\mathbf{k}} - \hat{\eta}_{\mathbf{k}} C_{\mathbf{k}}] = 0,$$

which is a result of Eq. (I.18) and Eq. (I.19).

Alternatively, by defining

$$\bar{\Theta}_{\mathbf{k}\mathbf{p}\mathbf{q}} = \theta_{\mathbf{k}\mathbf{p}\mathbf{q}} C_{\mathbf{p}}(t) C_{\mathbf{q}}(t),$$

we may write the EDQNM equations in the form of Eq. (II.13). The argument on pg. 71 can then be applied to prove that any quadratic invariant of the fundamental equation is conserved by the nonlinear terms of the EDQNM.

### III.B.3 Realizability issues of the EDQNM

#### Wave-free dynamics:

In the absence of wave phenomena or complex mode-coupling coefficients, the EDQNM closure is the exact statistical solution of the Langevin equation [Leith 1971]

$$\left(\frac{\partial}{\partial t} + \nu_{\mathbf{k}}\right) \psi_{\mathbf{k}}(t) + \hat{\eta}_{\mathbf{k}}(t) \psi_{\mathbf{k}}(t) = f_{\mathbf{k}}(t). \quad (\text{III.23})$$

Here,  $\nu_{\mathbf{k}}$  is real; Eqs. (III.18b), (III.18d), and (III.16) then imply that  $\hat{\eta}_{\mathbf{k}}$ ,  $\theta_{\mathbf{k}\mathbf{p}\mathbf{q}}$ , and  $R_{\mathbf{k}}$  are also real. We specify that the driving term  $f_{\mathbf{k}}$  is a *white-noise* random process with autocorrelation function  $\langle f_{\mathbf{k}}(t) f_{\mathbf{k}}^*(t') \rangle \doteq 2F_{\mathbf{k}} \delta(t-t')$ . Note that this is possible if and only if  $F_{\mathbf{k}}(t) \geq 0$ . This is the *realizability condition*. From Eq. (III.18c) it is clear that this is equivalent to  $\theta_{\mathbf{k}\mathbf{p}\mathbf{q}} \geq 0$ . This condition is obeyed here because Eq. (III.21) is the integral of a real, non-negative function and hence  $\theta_{\mathbf{k}\mathbf{p}\mathbf{q}}(t) \geq 0$ . This result is reassuring since the interpretation of  $\theta_{\mathbf{k}\mathbf{p}\mathbf{q}}$  as an interaction *time* makes sense only if  $\theta_{\mathbf{k}\mathbf{p}\mathbf{q}}$  is real and non-negative.

The response function  $R_{\mathbf{k}}$  of  $\psi_{\mathbf{k}}$  clearly obeys Eq. (III.16). We now compute the evolution equation for the quadratic quantity  $C_{\mathbf{k}}(t) \doteq \langle \psi_{\mathbf{k}}(t) \psi_{\mathbf{k}}^*(t) \rangle$ . Upon using the relation

$$\psi_{\mathbf{k}}(t) = \int_0^t d\bar{t} R_{\mathbf{k}}(t, \bar{t}) f_{\mathbf{k}}(\bar{t}),$$

one finds the anticipated result,

$$\frac{\partial}{\partial t} C_{\mathbf{k}}(t) + 2 \operatorname{Re} \eta_{\mathbf{k}}(t) C_{\mathbf{k}}(t) = 2F_{\mathbf{k}}(t).$$

The EDQNM closure thus exactly predicts the energy evolution of the system described by Eq. (III.23) in the absence of wave phenomena or complex mode-coupling coefficients. In other words, there exists an underlying statistical amplitude equation for this closure. This implies that the EDQNM is realizable for wave-free dynamics such as the incompressible Navier-Stokes turbulence for which it was originally proposed [Leith 1971, Orszag 1977]. Again, we emphasize that the importance of the realizability constraint on a closure is that it guarantees that the predicted results are physically possible. In the next section we will discover that wave effects can lead to a violation of the above realizability condition. The numerical consequence of this may entail violently unstable behaviour, which can result in energies that approach  $\pm\infty$  (*cf.* Fig. III.1)!

### Wave dynamics:

Now let us consider the general case, where either linear waves are present, the mode coupling is complex, or both. Write

$$\eta \doteq \eta_{\mathbf{k}} + \eta_{\mathbf{p}} + \eta_{\mathbf{q}} \doteq \rho + ia$$

for real  $\rho$  and  $a$ .

For simplicity, let us first consider the case where  $\eta$  is constant in time. Then

$$\theta_{\mathbf{k}\mathbf{p}\mathbf{q}}(t) = \frac{1 - e^{-(\rho+ia)t}}{\rho + ia}. \quad (\text{III.24})$$

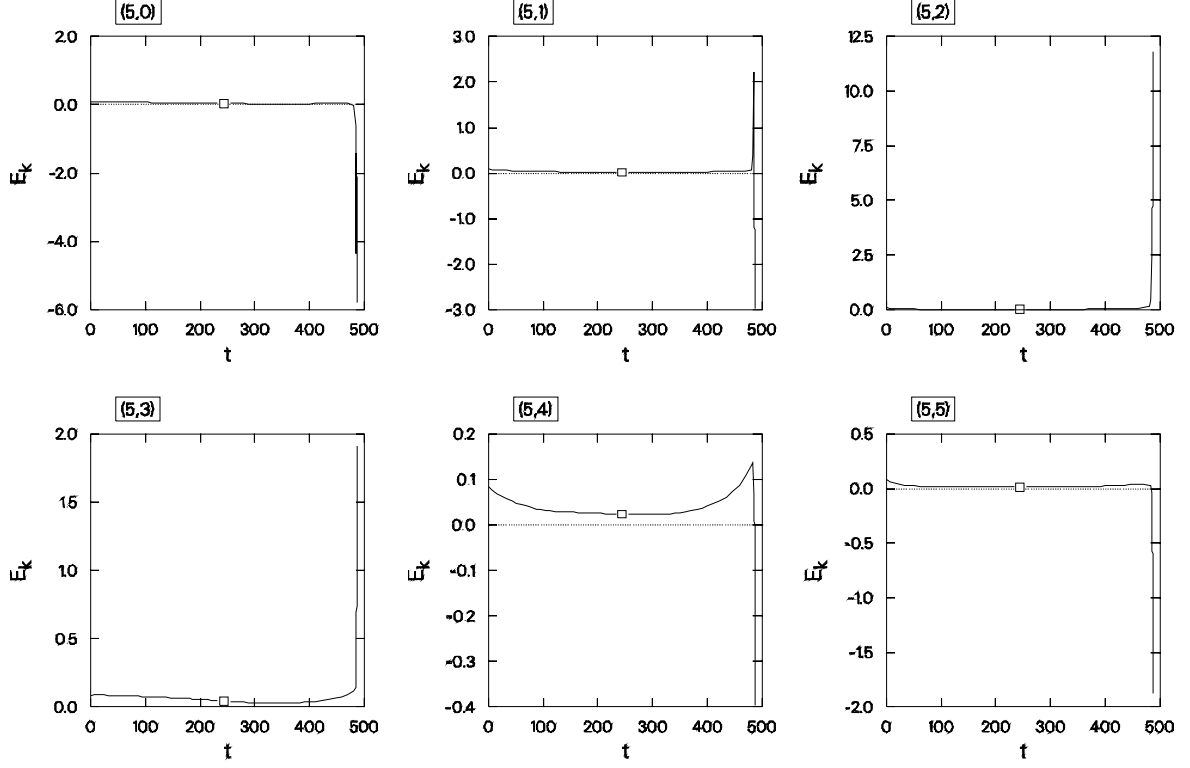


Figure III.1: Violently unstable behaviour that can arise in the application of the EDQNM closure to drift-wave turbulence. We observe that near  $t = 500$  the sample mode energies  $E_k$  diverge to  $\pm\infty$ .

Wave effects cause  $\theta_{\mathbf{k}\mathbf{p}\mathbf{q}}$  to be no longer real. What happens to the interpretation of  $\theta_{\mathbf{k}\mathbf{p}\mathbf{q}}$  as an interaction time?

Recall that the necessary and sufficient condition for the existence of Eq. (III.23) is that the real function  $F_{\mathbf{k}}(t)$  be non-negative. In turn, this is equivalent to

$$\text{Re } \theta_{\mathbf{k}\mathbf{p}\mathbf{q}}(t) \geq 0. \quad (\text{III.25})$$

Indeed, since only  $\text{Re } \theta_{\mathbf{k}\mathbf{p}\mathbf{q}}$  enters the energy equation, it seems natural that only the *real* part of  $\theta_{\mathbf{k}\mathbf{p}\mathbf{q}}$  should be thought of as the interaction time. The realizability constraint still dictates that this time be non-negative.

At this point it is worthwhile to check what happens to Eq. (III.24) when  $a = 0$ :

$$\theta_{\mathbf{k}\mathbf{p}\mathbf{q}}(t) = \frac{1 - e^{-\rho t}}{\rho}.$$

For both  $\rho > 0$  and  $\rho < 0$  we see that Eq. (III.25) holds. The case  $\rho = 0$  also is realizable since by this we mean the limiting solution

$$\theta_{\mathbf{k}\mathbf{p}\mathbf{q}} = t.$$

However, when  $a \neq 0$ ,

$$\text{Re } \theta_{\mathbf{k}\mathbf{p}\mathbf{q}}(t) = \frac{1}{\rho^2 + a^2} \left[ \rho - \rho e^{-\rho t} \cos(at) + a e^{-\rho t} \sin(at) \right].$$

It is easy to find values of  $\rho$ ,  $a$ , and  $t$  that violate the realizability condition. For example, in the special case  $\rho = 0$  one deduces

$$\text{Re } \theta_{\mathbf{k}\mathbf{p}\mathbf{q}}(t) = \frac{1}{a} \sin(at),$$

which oscillates about zero.

### Example of the nonrealizability of the EDQNM:

The above illustration is pedagogical and is inadequate as an actual example of the nonrealizability of the EDQNM closure. After all, we have only demonstrated that in a case where  $\eta$  happened to be constant in time (a case that we have not even shown to exist) the closure cannot be written as the exact statistical solution of a Langevin equation. Realizability requires only that there exist some underlying amplitude equation; it does not actually demand that the underlying equation be a Langevin equation.

We now demonstrate an actual stochastic problem for which the corresponding EDQNM closure cannot be written as the exact statistical solution to *any* underlying amplitude equation. Consider the following degenerate system of three interacting waves:

$$\begin{aligned} \left( \frac{\partial}{\partial t} + \frac{1}{2}i\omega - \frac{1}{2}\gamma \right) \psi_k(t) &= M \psi_p^* \psi_q^*, \\ \left( \frac{\partial}{\partial t} + \frac{1}{2}i\omega - \frac{1}{2}\gamma \right) \psi_p(t) &= -M \psi_q^* \psi_k^*, \\ \frac{\partial}{\partial t} \psi_q(t) &= 0. \end{aligned}$$

For this system, the EDQNM closure is:

$$\begin{aligned}\frac{\partial C_k}{\partial t} - \gamma C_k + 2M^2 \operatorname{Re} \theta C_q C_k &= 2M^2 \operatorname{Re} \theta C_p C_q, \\ \frac{\partial C_p}{\partial t} - \gamma C_p + 2M^2 \operatorname{Re} \theta C_q C_p &= 2M^2 \operatorname{Re} \theta C_k C_q, \\ \frac{\partial C_q}{\partial t} &= 0, \\ \frac{\partial \theta}{\partial t} + \eta \theta &= 1, \\ \eta &= -\gamma + i\omega + 2M^2 \theta^* C_q.\end{aligned}$$

Set  $C_q(0) = 1$ , so that  $C_q(t) = 1$  for all  $t$ . We can solve this system by noting that

$$\frac{\partial}{\partial t}(C_k + C_p) = \gamma(C_k + C_p),$$

so that  $E(t) \doteq \frac{1}{2}[C_k(t) + C_p(t)] = E_0 e^{\gamma t}$ , with  $E_0 \doteq \frac{1}{2}[C_k(0) + C_p(0)] > 0$ . The covariance equation for mode  $k$  is then

$$\frac{\partial C_k}{\partial t} - \gamma C_k + 4M^2 \operatorname{Re} \theta C_k = 4M^2 E_0 e^{\gamma t} \operatorname{Re} \theta.$$

By employing the integrating factor

$$P(t) \doteq e^{-\gamma t + 4M^2 \int dt \operatorname{Re} \theta},$$

the solution is found to be

$$C_k = e^{\gamma t} \left( E_0 + K e^{-4M^2 \int dt \operatorname{Re} \theta} \right), \quad (\text{III.26})$$

where  $K$  is a constant. To find  $\theta$  we specialize to the case where  $\omega = \gamma$  and take  $\epsilon \doteq M^2 |\theta|/\gamma \ll 1$ , so that

$$\eta = \gamma[-1 + i + \mathcal{O}(\epsilon)].$$

Then letting  $\nu = (-1 + i)\gamma$  we have

$$\begin{aligned}\int dt \theta &= \int dt \left( \frac{1 - e^{-\nu t}}{\nu} \right) + \mathcal{O}(\epsilon) \\ &= \frac{t}{\nu} + \frac{e^{-\nu t}}{\nu^2} + \mathcal{O}(\epsilon) \\ &= -\left( \frac{1 + i}{2\gamma} \right) t + \frac{i}{2\gamma^2} e^{(1-i)\gamma t} + \mathcal{O}(\epsilon),\end{aligned}$$

so that

$$\operatorname{Re} \int dt \theta = \frac{1}{2\gamma} \left[ -t + \gamma^{-1} e^{\gamma t} \sin \gamma t \right] + \mathcal{O}(\epsilon).$$

We substitute this into Eq. (III.26) to obtain

$$C_k(t) = e^{\gamma t} \left\{ E_0 + [C_k(0) - E_0] \exp(2M^2[\gamma^{-1}(t - \gamma^{-1} e^{\gamma t} \sin \gamma t) + \mathcal{O}(\epsilon)]) \right\},$$

where we have evaluated  $K = C_k(0) - E_0$ .

For the EDQNM to be realizable, this solution must be non-negative. However, this is not always so. Consider, for example, the case where  $C_k(0) = 0$  and evaluate  $C_k$  at  $t = \pi/\gamma$ :

$$\begin{aligned} C_k(\pi/\gamma) &= E_0 e^{\pi} \left( 1 - e^{2M^2[\pi + \mathcal{O}(\epsilon)]} \right) \\ &< 0 \quad (\epsilon \ll 1). \end{aligned}$$

Hence for this problem the EDQNM is not realizable. We verify this conclusion in Fig. III.2, where we illustrate both the nonrealizable EDQNM closure predictions and the (by definition, realizable) exact ensemble-averaged solution for the parameters  $\gamma = 0.02$ ,  $M = 0.003$ , and  $E_0 = 1$ . We emphasize that the difficulty is related to the negative interaction time depicted in Fig. III.3. In contrast, the DIA solution, graphed in Fig. III.5, is realizable and accurately tracks the exact dynamics. The numerical methods used to obtain these results will be discussed in Chapters IV and V.

This failure represents a serious deficiency of the EDQNM that to our knowledge has not been previously reported in the literature, although some researchers [Bartello 1990] appear to have been aware of the difficulties that can ensue if  $\theta_{\mathbf{k}\mathbf{p}\mathbf{q}}$  becomes negative. Therefore, let us now carefully assess the origin of this difficulty.

### Origin of the nonrealizability of the EDQNM:

The EDQNM can be derived from the DIA. For problems with a linear frequency, the EDQNM is not always realizable. However, the DIA is always realizable. The question naturally arises, ‘‘What is the origin of the nonrealizability?’’ The answer, we will find, is that nonrealizability arises from the Fluctuation-Dissipation ansatz.

Recall that the two-time DIA energy equation can be written:

$$C_{\mathbf{k}}(t, t') = \int_{-\infty}^{\infty} d\bar{t} \int_{-\infty}^{\infty} d\bar{t}' R_{\mathbf{k}}(t, \bar{t}) \mathcal{F}_{\mathbf{k}}(\bar{t}, \bar{t}') R_{\mathbf{k}}^*(t', \bar{t}'), \quad (\text{I.40})$$

or, formally,  $C_{\mathbf{k}} = R_{\mathbf{k}} \mathcal{F}_{\mathbf{k}} R_{\mathbf{k}}^\dagger$ . Realizability of a second-order closure essentially requires that  $C_{\mathbf{k}}$  be a positive-semidefinite matrix, where time plays the role of a

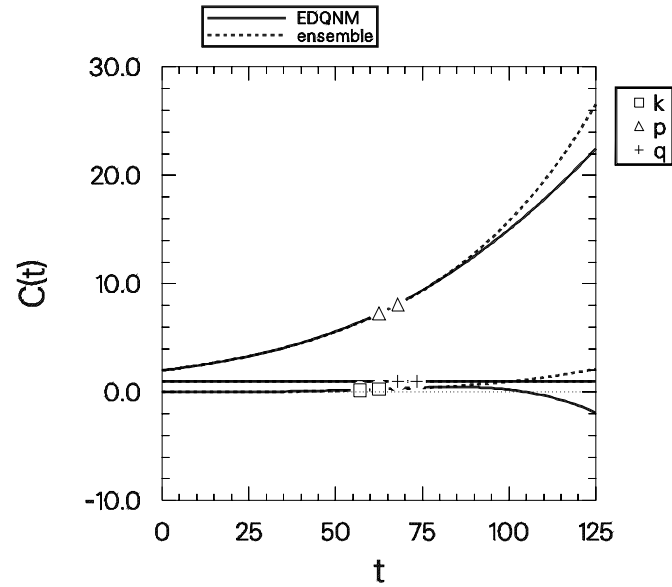


Figure III.2: Example of the nonrealizability of the EDQNM for wave phenomena.

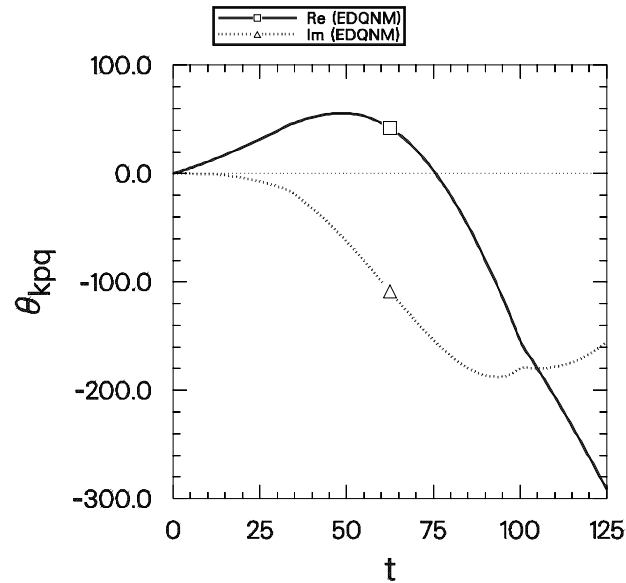


Figure III.3: Illustration of the negative interaction time underlying the nonrealizability encountered in Fig. III.2.

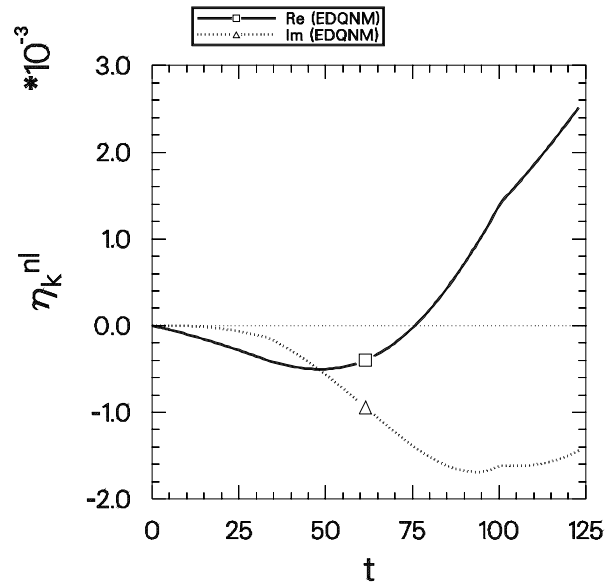


Figure III.4: Evolution of the eddy damping  $\hat{\eta}_k$  in the nonrealizable case of Fig. III.2.

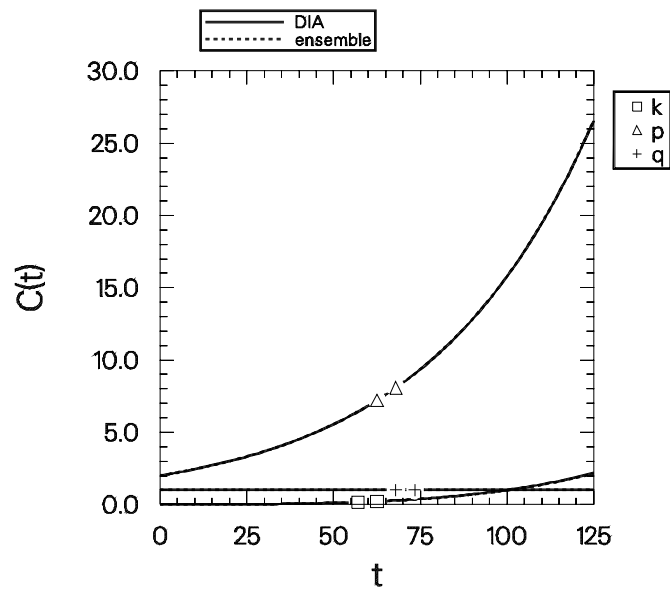


Figure III.5: DIA solution for the case considered in Fig. III.2. The ensemble and DIA solutions coincide (to within the numerical accuracy of the graph).

continuum matrix index:

$$\int_{-\infty}^{\infty} dt \int_{-\infty}^{\infty} dt' \phi^*(t) C_{\mathbf{k}}(t, t') \phi(t') \geq 0 \quad \forall \phi(t).$$

Now

$$\mathcal{F}_{\mathbf{k}}(t, \bar{t}) = \frac{1}{2} \sum_{\mathbf{k}+\mathbf{p}+\mathbf{q}=\mathbf{0}} |M_{\mathbf{k}\mathbf{p}\mathbf{q}}|^2 C_{\mathbf{p}}^*(t, \bar{t}) C_{\mathbf{q}}^*(t, \bar{t}) \quad (\text{III.27})$$

is positive-semidefinite if  $C_{\mathbf{p}}$  and  $C_{\mathbf{q}}$  are:

$$\begin{aligned} & \int_{-\infty}^{\infty} dt \int_{-\infty}^{\infty} dt' \phi^*(t) \mathcal{F}_{\mathbf{k}}(t, t') \phi(t') \\ &= \frac{1}{2} \sum_{\mathbf{k}+\mathbf{p}+\mathbf{q}=\mathbf{0}} |M_{\mathbf{k}\mathbf{p}\mathbf{q}}|^2 \int_{-\infty}^{\infty} dt \int_{-\infty}^{\infty} dt' \phi^*(t) C_{\mathbf{p}}^*(t, t') C_{\mathbf{q}}^*(t, t') \phi(t') \\ &\geq 0, \end{aligned}$$

where the last line follows from Theorem 1 proved in Appendix F. We then conclude that Eq. (I.40) *preserves* the positive-semidefinite nature of the covariances.

Thus the energy evolution equation in the form of Eq. (I.40) is *consistent* with the realizability of the DIA. However, the EDQNM applies the FD ansatz,

$$C_{\mathbf{k}}(t, t') = R_{\mathbf{k}}(t, t') C_{\mathbf{k}}(t) + R_{\mathbf{k}}^*(t', t) C_{\mathbf{k}}^*(t'),$$

to Eq. (III.27), yielding

$$\begin{aligned} \mathcal{F}_{\mathbf{k}}(t, \bar{t}) = \frac{1}{2} \sum_{\mathbf{k}+\mathbf{p}+\mathbf{q}=\mathbf{0}} |M_{\mathbf{k}\mathbf{p}\mathbf{q}}|^2 & [R_{\mathbf{p}}^*(t, \bar{t}) C_{\mathbf{p}}^*(t) R_{\mathbf{q}}^*(t, \bar{t}) C_{\mathbf{q}}^*(t) \\ & + R_{\mathbf{p}}(\bar{t}, t) C_{\mathbf{p}}(\bar{t}) R_{\mathbf{q}}(\bar{t}, t) C_{\mathbf{q}}(\bar{t})]. \end{aligned}$$

The motivation for doing this is to put all the two-time information into a single quantity  $\theta_{\mathbf{k}\mathbf{p}\mathbf{q}}$ . However, in the process, realizability has been lost, as this expression for  $\mathcal{F}_{\mathbf{k}}$  is no longer always positive-semidefinite.

For example, consider the case where  $\frac{1}{2} \sum_{\mathbf{k}+\mathbf{p}+\mathbf{q}=\mathbf{0}} |M_{\mathbf{k}\mathbf{p}\mathbf{q}}|^2 = 1$ ,  $C_{\mathbf{p}}(t) = C_{\mathbf{q}}(t) = |t|^{1/2}$ , and  $R_{\mathbf{p}}(t, \bar{t}) = R_{\mathbf{q}}(t, \bar{t}) = \text{H}(t - \bar{t})$ . Then given

$$\phi(t) = \begin{cases} t - 1 & \text{for } 0 < t < 2, \\ 0 & \text{otherwise,} \end{cases}$$

we find

$$\begin{aligned} & \int_{-\infty}^{\infty} dt \int_{-\infty}^{\infty} dt' \phi^*(t) \mathcal{F}_{\mathbf{k}}(t, t') \phi(t') \\ &= \int_0^2 dt \int_0^t dt' (t-1)t(t'-1) + \int_0^2 dt \int_t^2 dt' (t-1)t'(t'-1) \\ &= \int_0^2 dt (t-1) \left[ t(\frac{1}{2}t^2 - t) + \frac{1}{3}2^3 - \frac{1}{2}2^2 - (\frac{1}{3}t^3 - \frac{1}{2}t^2) \right] \\ &= \int_0^2 dt \left( \frac{1}{6}t^4 - \frac{2}{3}t^3 + \frac{1}{2}t^2 + \frac{2}{3}t - \frac{2}{3} \right) \\ &= -\frac{4}{15} < 0. \end{aligned}$$

This simple example establishes that  $\mathcal{F}_{\mathbf{k}}$  need not be positive-semidefinite even if  $C_{\mathbf{k}}(t)$  and  $R_{\mathbf{k}}(t, t')$  are non-negative numbers for all  $t$  and  $t'$ . We are not suggesting, however, that these simple expressions for  $C_{\mathbf{k}}$  and  $R_{\mathbf{k}}$  are consistent with the other EDQNM equations. We have already illustrated an example that proves that the entire coupled set of EDQNM equations can predict negative energies. Our purpose here is to illustrate that the above *form* of  $\mathcal{F}_{\mathbf{k}}$  is not *implicitly* guaranteed to be positive-semidefinite, in contrast to the inherently positive-semidefinite form of Eq. (III.27). If one desired, the equal-time version of Eq. (I.40) could be inverted to obtain  $\mathcal{F}_{\mathbf{k}}(\bar{t}, \bar{t})$  in terms of the nonrealizable solution for  $C_{\mathbf{k}}(t, t)$  found in the example on pg. 93. The result would be a *self-consistent*  $\mathcal{F}_{\mathbf{k}}$  that violates positive-semidefiniteness.

It is now clear that of the two assumptions, Eq. (III.9) and Eq. (II.3a), we used to transform the DIA into the EDQNM, it is only the former that is responsible for the loss of realizability. Although Markovianization of the  $R_{\mathbf{k}}$  equation does alter the value of  $R_{\mathbf{k}}$  appearing (symmetrically) in Eq. (I.40), the non-negative character of the energy spectrum is preserved by that Markovianization.

### Steady-state ansatz:

In section III.B.2, we found that if a steady state exists,  $\text{Re}\theta_{\mathbf{k}\mathbf{p}\mathbf{q}}(\infty) > 0$ . This implies that, at the very least, the steady-state  $F_{\mathbf{k}}$  will be positive. If one is interested in only the steady-state physics, in principle one can simply solve the EDQNM equations in the steady state. However, there may be computational and theoretical difficulties associated with extracting the correct root of the resulting nonlinear coupled system [Koniges and Krommes 1982, Krommes 1984a].

Normally, the practice is to evolve the energy equation coupled to the steady-state *form*, Eq. (III.19), of  $\theta_{\mathbf{k}\mathbf{p}\mathbf{q}}$  [Holloway and Hendershott 1977]. We call this the “quasistationary” form of  $\theta_{\mathbf{k}\mathbf{p}\mathbf{q}}$ . The acausal nature of this formulation is physically disturbing. Even worse, there is no guarantee that at each time step exactly one of the roots of the coupled system will correspond to a non-negative  $\text{Re}\eta$ . Hence, neither realizability nor uniqueness of the solution is guaranteed with this approach.

The principal goal of this work is the development of a DIA-based Markovian closure that is guaranteed to be realizable. The aim is to consider a modification of the EDQNM  $\theta_{\mathbf{k}\mathbf{p}\mathbf{q}}$  equation, Eq. (III.18d), that will ensure realizability for all times. The clue we learn from the quasistationary approach is that we need not tamper with the steady state in order to accomplish this. Thus, we seek an evolution equation for  $\theta_{\mathbf{k}\mathbf{p}\mathbf{q}}$  that guarantees realizability but still evolves to the steady-state form given by the unmodified EDQNM closure. This singles out a particular realizable time-asymptotic solution that is continuously connected, in some sense, to the initial root at  $t = 0$ . The steady state actually achieved may not be unique, but the condition of realizability does help to constrain the set of admissible solutions.

Ideally, one would like to keep the transient evolution closely tied to that of the actual physical system. Unfortunately, Markovianization inherently entails meddling with the evolution to the steady state. In Section III.C we will present our original attempt at constructing a generally realizable EDQNM that, while highly constrained, is unfortunately rather *ad hoc*. Worse, we discover in Section III.D that the multiple-field generalization of this closure is seriously flawed since it does not conserve all of the fundamental quadratic invariants of the nonlinear terms. We are eventually led to the conclusion that the realizable EDQNM must be entirely abandoned in favour of a superior closure, the realizable Markovian closure, to be developed in Sections III.E and III.F. Nevertheless, the next two sections help to motivate the need for the RMC. In addition, the following material will help elucidate the difficulties involved in the construction of a satisfactory realizable multiple-field closure.

### III.C Realizable one-field EDQNM closure

We wish to replace Eq. (III.18d) with an equation that possesses a solution satisfying the following requirements:

1.  $\theta_{\mathbf{k}\mathbf{p}\mathbf{q}} \sim t$  for small  $t$ .
2.  $\lim_{t \rightarrow \infty} \theta_{\mathbf{k}\mathbf{p}\mathbf{q}} = 1/(\eta_{\mathbf{k}} + \eta_{\mathbf{p}} + \eta_{\mathbf{q}})$ .
3.  $\text{Re } \theta_{\mathbf{k}\mathbf{p}\mathbf{q}} \geq 0 \quad \forall t \geq 0$ .
4.  $\theta_{\mathbf{k}\mathbf{p}\mathbf{q}}$  must reduce to Eq. (III.18d) for real  $\eta$ .

That is, we want to make a modification to the *transient* dynamics in order to achieve a *realizable* evolution to the steady state. The EDQNM is actually realizable for any  $\theta_{\mathbf{k}\mathbf{p}\mathbf{q}}$  satisfying criterion 3. The other criteria ensure that the resulting approximation corresponds as closely as possible to a DIA-based Markovian closure. Note that criterion 1, which follows from both the DIA and perturbation theory, implies that the initial condition  $\theta_{\mathbf{k}\mathbf{p}\mathbf{q}}(0) = 0$  must be respected. Also, criterion 4 is imposed to restrict our attention only to closures that are *generalizations* of the EDQNM for applications involving wave phenomena. In Section III.E we will drop this restriction for reasons explained there. At this point in the discussion, however, criterion 4 seems reasonable in light of the fact that the difficulties experienced with realizability are not present in the wave-free situation for which the EDQNM was originally developed.

### III.C.1 Motivation

In terms of the simplified notation

$$\eta \doteq \eta_{\mathbf{k}} + \eta_{\mathbf{p}} + \eta_{\mathbf{q}}$$

and  $\theta \doteq \theta_{\mathbf{k}\mathbf{p}\mathbf{q}}$ , Eq. (III.18d) may be written

$$\frac{\partial}{\partial t}\theta + \eta\theta = 1. \quad (\text{III.28})$$

One way to satisfy criterion 3 is to consider

$$\frac{\partial}{\partial t}\theta + (\text{Re } \eta)\theta = 1;$$

however, this equation clearly violates criterion 2. Nevertheless, the correct steady state can be recovered if we simultaneously modify the source term on the right-hand side:

$$\frac{\partial}{\partial t}\theta + (\text{Re } \eta)\theta = \frac{\text{Re } \eta}{\eta}. \quad (\text{III.29})$$

This form can easily be shown to satisfy all but criterion 1. The violation of this criterion is serious when Eq. (III.29) and the remaining EDQNM equations are applied to a system of three interacting waves, such as Eq. (II.18), in which the linear terms are purely *imaginary* and the mode coupling is real. One quickly discovers that this system does not evolve since  $\text{Re } \eta$  is initially zero and at later times is proportional to the instantaneous value of  $\text{Re } \theta$ . Thus Eq. (III.18b) coupled with Eq. (III.29) results in a static situation in which neither  $\theta$  nor  $C_{\mathbf{k}}$  changes in time.

One may attempt to enforce the correct initial scaling  $\theta \sim t$  by heuristically adding a function to the right-hand side of Eq. (III.29) that restores the desired small-time behaviour but vanishes in the steady state. For example, we could modify Eq. (III.29) to

$$\frac{\partial}{\partial t}\theta + \text{Re } \eta\theta = \frac{\text{Re } \eta + i \text{Im } \eta e^{-(\text{Re } \eta)t}}{\eta}. \quad (\text{III.30})$$

The exponential function added here might be justified by noting, for the case where  $\text{Re } \eta$  is constant, that this is just the Green's function for the left-hand side of Eq. (III.29). Note that if Eq. (III.29) reaches a steady state, then  $\text{Re } \eta(\infty)$  must be positive. This guarantees that the exponential function just added disappears in the steady state.

This last form satisfies all four of our criteria. However, the pragmatic presentation here is based mostly on intuition and quick remedies. Before proceeding, it would perhaps be best to give a *somewhat* more systematic derivation, in which the chain of modifications just introduced is collapsed into a single assumption.

### III.C.2 Derivation of the realizable EDQNM

Let us denote

$$\eta \doteq \rho + ia$$

for real  $\rho$  and  $a$ . Begin by rewriting Eq. (III.28) as

$$\frac{\partial}{\partial t}\theta + \rho\theta = \frac{\rho}{\eta}(\eta\theta) + (1 - \eta\theta). \quad (\text{III.31})$$

For the case where  $\eta$  is *constant*, the product  $\eta\theta$  appearing here evaluates to

$$\eta\theta = 1 - e^{-\eta t}. \quad (\text{III.32})$$

It is the oscillatory nature of the (generally complex) right-hand side, when substituted into Eq. (III.31), that is responsible for nonrealizability. Therefore we modify Eq. (III.32) to

$$\eta\theta = 1 - e^{-\rho t}.$$

By substituting this into Eq. (III.31) we obtain

$$\begin{aligned} \frac{\partial}{\partial t}\theta + \rho\theta &= \frac{\rho}{\eta}(1 - e^{-\rho t}) + e^{-\rho t} \\ &= \frac{\rho + ia e^{-\rho t}}{\rho + ia} \quad (\eta \text{ constant}), \end{aligned} \quad (\text{III.33})$$

which agrees with Eq. (III.30). For the case of constant  $\eta$ , our modified equation has the exact solution

$$\theta(t) = \frac{1}{\rho + ia}(1 - e^{-\rho t}) + te^{-\rho t},$$

for which the real part is clearly non-negative:

$$\text{Re } \theta(t) = \frac{\rho}{\rho^2 + a^2}(1 - e^{-\rho t}) + te^{-\rho t} > 0,$$

no matter what real value  $\rho$  takes on.

For  $\eta = \eta(t)$  we generalize Eq. (III.33) to

$$\boxed{\frac{\partial}{\partial t}\theta + \rho\theta = \frac{\rho + ia e^{-\int_0^t \rho(\bar{t}) d\bar{t}}}{\rho + ia}, \quad \theta(0) = 0.} \quad (\text{III.34})$$

Replacing Eq. (III.18d) with Eq. (III.34) transforms Eqs. (III.18) into what we will term the “realizable EDQNM.” We now investigate the effect of this modification on the properties of the closure.

### III.C.3 Properties of the realizable EDQNM

The realizable EDQNM and the original EDQNM are compared pictorially in Fig III.6, where we emphasize the important properties of our modified  $\theta$  equation.

#### Short-time behaviour:

For small  $t$ ,

$$\theta \sim t.$$

#### Steady state:

If  $\lim_{t \rightarrow \infty} \rho > 0$ , then  $\theta$  achieves the steady-state value

$$\theta(\infty) = \frac{1}{\rho + ia}.$$

#### Realizability:

The real part of Eq. (III.34) satisfies

$$\frac{\partial}{\partial t} \text{Re } \theta + \rho \text{Re } \theta = \frac{\rho^2 + a^2 e^{-\int_0^t \rho(\bar{t}) d\bar{t}}}{\rho^2 + a^2} \doteq h(t).$$

The solution,

$$\text{Re } \theta = e^{-\int_0^t \rho(\bar{t}) d\bar{t}} \int_0^t h(s) e^{\int_0^s \rho(\bar{t}) d\bar{t}} ds,$$

is certainly non-negative, being the integral of a non-negative function.<sup>5</sup> Hence this new closure is realizable even in the presence of waves.

#### Energy conservation:

Since Eqs. (III.18b) and (III.18c) remain unchanged, the realizable EDQNM also conserves the generalized energy Eq. (I.20).

#### Reduction to the original EDQNM:

When  $\eta$  is real, Eq. (III.34) reduces to Eq. (III.28). Hence, Eq. (III.34) is a generalization of the original EDQNM for problems involving a linear frequency.

---

<sup>5</sup>We assume that  $\rho$  does not develop singularities.

### Comparison of Triad Interaction Times

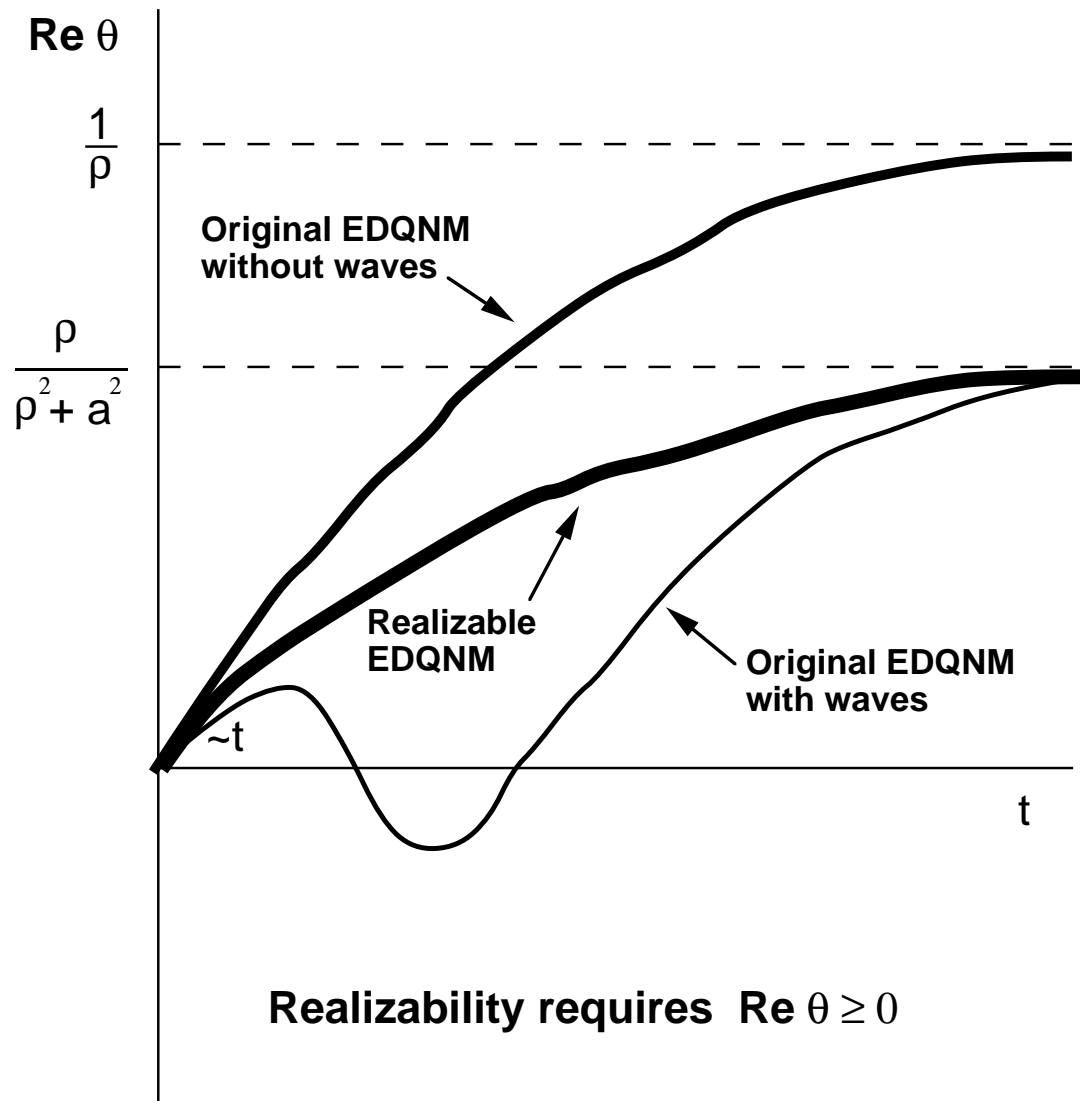


Figure III.6: Comparison of the realizable EDQNM and the original EDQNM.

## III.D Realizable multiple-field EDQNM closure

In the next section we construct a generalization of the one-field realizable EDQNM that is designed for systems involving multiple fields. Unfortunately, after much effort we will discover that this generalization does not conserve all of the fundamental quadratic invariants of Eq. (II.25); we will therefore be forced to discard it. The material in this section is included only to illustrate the kinds of difficulties that must be faced in the formulation of multiple-field closures and to help motivate the need for the superior approach adopted in Sections III.E and III.F.

### III.D.1 Motivation: inhomogeneous test-field model

Kraichnan's paper on the inhomogeneous test-field model [Kraichnan 1972] describes a procedure for extending the one-field TFM to multiple fields. The same procedure allows one to extend the EDQNM in the presence of only Hermitian effects. We generalize this procedure to handle non-Hermitian effects as well.

### III.D.2 Covariant formulation

Let us use the multiple-field notation of Section II.B.4. Our goal is to formulate a realizable closure that conserves the energy. Therefore, for the remainder of this section we will focus on a single invariant  $E$  and use the corresponding Hermitian matrix  $\sigma$  as a *metric tensor* to define covariant components such as

$$\psi_\alpha \doteq \sigma_{\alpha\alpha'} \psi^{\alpha'},$$

so that  $E = \psi^\alpha \psi_\alpha^* = \psi_\alpha \psi^{\alpha*}$ . Similarly, we define

$$\begin{aligned} M_{\alpha\beta\gamma} &= \sigma_{\alpha\alpha'} M^{\alpha'}_{\beta\gamma}, \\ \nu_\alpha^s &= \sigma_{\alpha\alpha'} \nu^{\alpha'}_r \sigma^{rs}, \\ \sigma^{\alpha\alpha'} &= \sigma_{\alpha\alpha'}^{-1}. \end{aligned}$$

From Eq. (II.26) we note that  $M_{\alpha\beta\gamma}$  sums cyclically to zero.

Guided by the one-field case, our objective is to develop a closure that is the exact solution to the Langevin equation

$$\frac{\partial}{\partial t} \psi^\alpha + \eta^\alpha_\delta \psi^\delta = f^\alpha.$$

The correlation function  $C^{\alpha\alpha'} \doteq \langle \psi^\alpha \psi^{\alpha'*} \rangle$  evolves as

$$\boxed{\frac{\partial}{\partial t} C^{\alpha\alpha'} + \eta^\alpha_\delta C^{\delta\alpha'} + C^{\alpha\delta} \eta^{\alpha'}_\delta^* = 2F^{\alpha\alpha'}}, \quad (\text{III.35})$$

where  $F^{\alpha\alpha'} \doteq \langle f^\alpha f^{\alpha'*} \rangle$ .

Note that  $C^{\alpha\alpha'} = \langle \psi^\alpha \psi^{\alpha'*} \rangle = C^{\alpha'\alpha*}$ . This is the general covariant definition of Hermiticity. For an arbitrary tensor  $\boldsymbol{\eta}$ , the Hermitian part is defined in a strictly contravariant representation. For example, let  $\eta^{\alpha\beta}$  represent the components of the matrix that operates on the covariant components of a vector  $\boldsymbol{\psi}$  to produce the contravariant components of the vector  $\boldsymbol{\eta}\boldsymbol{\psi}$ . The Hermitian part of  $\boldsymbol{\eta}$  then has the contravariant components

$$\frac{1}{2}(\eta^{\alpha\beta} + \eta^{\beta\alpha*}).$$

Now suppose that we are given the components of  $\boldsymbol{\eta}$  in a mixed representation such as  $\eta^\alpha{}_\beta$ . To compute the components of the Hermitian part of  $\boldsymbol{\eta}$ , we must first use the metric tensor to express  $\boldsymbol{\eta}$  in a strictly contravariant representation:

$$\eta^{\alpha\beta} = \eta^\alpha{}_{\bar{\beta}} \sigma^{\bar{\beta}\beta}.$$

Thus, in the mixed representation the Hermitian part  $\boldsymbol{\eta}^h$  and anti-Hermitian part  $\boldsymbol{\eta}^a$  of  $\boldsymbol{\eta}$  may be expressed respectively as

$$\begin{aligned} \eta^h{}^\alpha{}_\beta &= \frac{1}{2} \left( \eta^\alpha{}_\beta + \eta^{\beta'}{}_{\bar{\beta}}{}^* \sigma^{\bar{\beta}\alpha*} \sigma_{\beta'\beta} \right), \\ \eta^a{}^\alpha{}_\beta &= -\frac{1}{2}i \left( \eta^\alpha{}_\beta - \eta^{\beta'}{}_{\bar{\beta}}{}^* \sigma^{\bar{\beta}\alpha*} \sigma_{\beta'\beta} \right). \end{aligned}$$

Note that  $\boldsymbol{\eta}^h$  and  $\boldsymbol{\eta}^a$  are both Hermitian matrices. The term  $\eta^{\beta'}{}_{\bar{\beta}}{}^* \sigma^{\bar{\beta}\alpha*} \sigma_{\beta'\beta}$  defines the components of the adjoint tensor  $\boldsymbol{\eta}^\dagger$ . These definitions are covariant: if  $\boldsymbol{\psi}$  is transformed to  $\bar{\boldsymbol{\psi}} \doteq \mathbf{T}\boldsymbol{\psi}$  then  $\boldsymbol{\eta}$  transforms as  $\mathbf{T}\boldsymbol{\eta}\mathbf{T}^{-1}$ ,  $\boldsymbol{\sigma}^{-1}$  transforms as  $\mathbf{T}\boldsymbol{\sigma}^{-1}\mathbf{T}^\dagger$ , and  $\boldsymbol{\eta}\boldsymbol{\sigma}^{-1}$  transforms as  $\mathbf{T}\boldsymbol{\eta}\boldsymbol{\sigma}^{-1}\mathbf{T}^\dagger$ .

Let us now consider the matrix generalization of Eq. (III.11),

$$\theta^{\alpha\beta\gamma}{}_{\alpha'\beta'\gamma'}(t) = \int_0^t dt' R^\alpha{}_{\alpha'}(t, t') R^{\beta}{}_{\beta'}(t, t') R^\gamma{}_{\gamma'}(t, t'). \quad (\text{III.36})$$

We seek an evolution equation for  $\theta^{\alpha\beta\gamma}{}_{\alpha'\beta'\gamma'}$  that will lead to a realizable closure. First, let us simplify the notation by defining

$$\eta^{\alpha\beta\gamma}{}_{\alpha'\beta'\gamma'} \doteq \eta^\alpha{}_{\alpha'} \delta^{\beta}{}_{\beta'} \delta^{\gamma}{}_{\gamma'} + \delta^\alpha{}_{\alpha'} \eta^\beta{}_{\beta'} \delta^{\gamma}{}_{\gamma'} + \delta^\alpha{}_{\alpha'} \delta^{\beta}{}_{\beta'} \eta^\gamma{}_{\gamma'}. \quad (\text{III.37})$$

The generalization of Eq. (III.28) can then be written

$$\frac{\partial}{\partial t} \boldsymbol{\theta} + \boldsymbol{\eta} \boldsymbol{\theta} = \mathbf{1}, \quad (\text{III.38})$$

which we interpret as a matrix equation for  $\theta^{\alpha\beta\gamma}{}_{\alpha'\beta'\gamma'}$  in terms of  $\eta^{\alpha\beta\gamma}{}_{\alpha'\beta'\gamma'}$  and the unit matrix  $\mathbf{1}$ . [Equivalently, it is a set of  $n^3$  by  $n^3$  equations, one for each triad  $(\mathbf{k}, \mathbf{p}, \mathbf{q})$ .] For the following discussion, let us decompose  $\boldsymbol{\theta}$  into its Hermitian part  $\boldsymbol{\theta}^h$  and its anti-Hermitian part  $\boldsymbol{\theta}^a$ .

The presence of noncommuting matrices in the multiple-field case leads to additional complexity. Motivated by the derivation for the scalar case given on pg. 102, let us rewrite Eq. (III.38) as

$$\frac{\partial}{\partial t} \boldsymbol{\theta} + \frac{1}{2} (\boldsymbol{\eta}^h \boldsymbol{\theta} + \boldsymbol{\theta} \boldsymbol{\eta}^h) = 1 - \frac{1}{2} i (\boldsymbol{\eta}^a \boldsymbol{\theta} + \boldsymbol{\theta} \boldsymbol{\eta}^a) + \frac{1}{2} [\boldsymbol{\theta}, \boldsymbol{\eta}] \quad (\text{III.39})$$

in terms of the commutator defined by  $[A, B] \doteq AB - BA$ . The operator acting on  $\boldsymbol{\theta}$  in the left-hand side of this equation is the matrix analog of the operator appearing in the left-hand side of Eq. (III.31). We will soon see that this form is essential to the realizability requirement that  $\boldsymbol{\theta}^h$  must be positive-semidefinite, which is the matrix generalization of  $\text{Re } \theta_{\mathbf{k}\mathbf{p}\mathbf{q}} \geq 0$ .

The Hermitian and anti-Hermitian parts of Eq. (III.39) are respectively,

$$\frac{\partial}{\partial t} \boldsymbol{\theta}^h + \frac{1}{2} (\boldsymbol{\eta}^h \boldsymbol{\theta}^h + \boldsymbol{\theta}^h \boldsymbol{\eta}^h) = 1 + \frac{1}{2} (\boldsymbol{\eta}^a \boldsymbol{\theta}^a + \boldsymbol{\theta}^a \boldsymbol{\eta}^a) + \frac{1}{2} i [\boldsymbol{\theta}^h, \boldsymbol{\eta}^a] + \frac{1}{2} i [\boldsymbol{\theta}^a, \boldsymbol{\eta}^h], \quad (\text{III.39a})$$

$$\frac{\partial}{\partial t} \boldsymbol{\theta}^a + \frac{1}{2} (\boldsymbol{\eta}^h \boldsymbol{\theta}^a + \boldsymbol{\theta}^a \boldsymbol{\eta}^h) = -\frac{1}{2} (\boldsymbol{\eta}^a \boldsymbol{\theta}^h + \boldsymbol{\theta}^h \boldsymbol{\eta}^a) - \frac{1}{2} i [\boldsymbol{\theta}^h, \boldsymbol{\eta}^h] + \frac{1}{2} i [\boldsymbol{\theta}^a, \boldsymbol{\eta}^a]. \quad (\text{III.39b})$$

In the following analysis, we will make frequent use of two elementary results:

$$\begin{aligned} (\boldsymbol{\eta}^{-1})^h &= \boldsymbol{\eta}^{-1} \boldsymbol{\eta}^h \boldsymbol{\eta}^{-1\dagger}, \\ (\boldsymbol{\eta}^{-1})^a &= -\boldsymbol{\eta}^{-1} \boldsymbol{\eta}^a \boldsymbol{\eta}^{-1\dagger}. \end{aligned}$$

These results are analogous to the corresponding relations for the real and imaginary parts of reciprocals of complex numbers.

From Eq. (III.38) it is clear that the solution for the case where  $\boldsymbol{\eta}$  is *constant* is

$$\boldsymbol{\theta} = \boldsymbol{\eta}^{-1} (\mathbf{1} - e^{-\boldsymbol{\eta}t}).$$

As in the scalar case, we remove the oscillatory part of the exponential by modifying this equation to

$$\boldsymbol{\theta} = \boldsymbol{\eta}^{-1} (\mathbf{1} - e^{-\boldsymbol{\eta}^h t}).$$

First, let us examine the special case where  $\boldsymbol{\eta}$  is also *normal*, which means that  $\boldsymbol{\eta}$  and  $\boldsymbol{\eta}^\dagger$  commute. This will give us some insight into the nature of the general formulation. The assumption of normality greatly simplifies the matrix equations; for example, the expression for  $\boldsymbol{\theta}^a$  may then be written

$$\begin{aligned} \boldsymbol{\theta}^a &= (\boldsymbol{\eta}^{-1})^a (\mathbf{1} - e^{-\boldsymbol{\eta}^h t}) \\ &= -\boldsymbol{\eta}^{-1} \boldsymbol{\eta}^a \boldsymbol{\eta}^{-1\dagger} (\mathbf{1} - e^{-\boldsymbol{\eta}^h t}). \end{aligned}$$

Substitution of this solution into Eq. (III.39a) then yields

$$\begin{aligned}
\frac{\partial}{\partial t}\boldsymbol{\theta}^h + \frac{1}{2}(\boldsymbol{\eta}^h\boldsymbol{\theta}^h + \boldsymbol{\theta}^h\boldsymbol{\eta}^h) &= \mathbf{1} + \boldsymbol{\eta}^a\boldsymbol{\theta}^a \\
&= \boldsymbol{\eta}^{-1} \left[ \boldsymbol{\eta}\boldsymbol{\eta}^\dagger - (\boldsymbol{\eta}^a)^2 (\mathbf{1} - e^{-\boldsymbol{\eta}^h t}) \right] \boldsymbol{\eta}^{-1\dagger} \\
&= \boldsymbol{\eta}^{-1} \left[ (\boldsymbol{\eta}^h)^2 + (\boldsymbol{\eta}^a)^2 - (\boldsymbol{\eta}^a)^2 + (\boldsymbol{\eta}^a)^2 e^{-\boldsymbol{\eta}^h t} \right] \boldsymbol{\eta}^{-1\dagger} \\
&= \boldsymbol{\eta}^{-1} \left[ (\boldsymbol{\eta}^h + i\boldsymbol{\eta}^a e^{-\frac{1}{2}\boldsymbol{\eta}^h t}) (\boldsymbol{\eta}^h - i e^{-\frac{1}{2}\boldsymbol{\eta}^h t} \boldsymbol{\eta}^a) \right] \boldsymbol{\eta}^{-1\dagger}.
\end{aligned} \tag{III.40}$$

The final form portrays the positive-semidefinite nature of the right-hand side, which we will exploit in the proof of realizability.

Similarly, the exact equation for  $\boldsymbol{\theta}^a$ , Eq. (III.39b), becomes

$$\begin{aligned}
\frac{\partial}{\partial t}\boldsymbol{\theta}^a + \frac{1}{2}(\boldsymbol{\eta}^h\boldsymbol{\theta}^a + \boldsymbol{\theta}^a\boldsymbol{\eta}^h) &= -\boldsymbol{\eta}^a\boldsymbol{\theta}^h \\
&= \boldsymbol{\eta}^{-1} \left[ -\boldsymbol{\eta}^a\boldsymbol{\eta}^h (\mathbf{1} - e^{-\boldsymbol{\eta}^h t}) \right] \boldsymbol{\eta}^{-1\dagger}.
\end{aligned} \tag{III.41}$$

For  $\boldsymbol{\eta} = \boldsymbol{\eta}(t)$  (but still normal) we generalize Eqs. (III.40) and (III.41) to

$$\frac{\partial}{\partial t}\boldsymbol{\theta}^h + \frac{1}{2}(\boldsymbol{\eta}^h\boldsymbol{\theta}^h + \boldsymbol{\theta}^h\boldsymbol{\eta}^h) = \boldsymbol{\eta}^{-1}\boldsymbol{\Lambda}\boldsymbol{\Lambda}^\dagger\boldsymbol{\eta}^{-1\dagger}, \tag{III.42a}$$

$$\frac{\partial}{\partial t}\boldsymbol{\theta}^a + \frac{1}{2}(\boldsymbol{\eta}^h\boldsymbol{\theta}^a + \boldsymbol{\theta}^a\boldsymbol{\eta}^h) = \boldsymbol{\eta}^{-1} \left[ -\boldsymbol{\eta}^a\boldsymbol{\eta}^h (\mathbf{1} - \mathbf{G}\mathbf{G}^\dagger) \right] \boldsymbol{\eta}^{-1\dagger}, \tag{III.42b}$$

where  $\boldsymbol{\Lambda} \doteq \boldsymbol{\eta}^h + i\boldsymbol{\eta}^a\mathbf{G}$  and  $\mathbf{G}$  is the solution to

$$\frac{\partial}{\partial t}\mathbf{G} = -\frac{1}{2}\mathbf{G}\boldsymbol{\eta}^h, \quad \mathbf{G}(0) = \mathbf{1}.$$

For the general case where  $\boldsymbol{\eta}$  may not be normal, let us seek an equation for  $\boldsymbol{\theta}^h$  of the form

$$\begin{aligned}
\frac{\partial}{\partial t}\boldsymbol{\theta}^h + \boldsymbol{\chi}\boldsymbol{\theta}^h + \boldsymbol{\theta}^h\boldsymbol{\chi}^\dagger &= \boldsymbol{\chi}(\boldsymbol{\eta}^{-1})^h + (\boldsymbol{\eta}^{-1})^h\boldsymbol{\chi}^\dagger \\
&= \boldsymbol{\eta}^{-1} \left[ \boldsymbol{\eta}\boldsymbol{\chi}\boldsymbol{\eta}^{-1}\boldsymbol{\eta}^h + \boldsymbol{\eta}^h\boldsymbol{\eta}^{-1\dagger}\boldsymbol{\chi}^\dagger\boldsymbol{\eta}^\dagger \right] \boldsymbol{\eta}^{-1\dagger} \\
&= \boldsymbol{\eta}^{-1} \left[ \mathbf{Y}\boldsymbol{\eta}^h + \boldsymbol{\eta}^h\mathbf{Y}^\dagger \right] \boldsymbol{\eta}^{-1\dagger},
\end{aligned}$$

where  $\mathbf{Y} \doteq \boldsymbol{\eta}\boldsymbol{\chi}\boldsymbol{\eta}^{-1}$ . This form correctly reduces to the steady-state result  $\boldsymbol{\theta}^h = (\boldsymbol{\eta}^{-1})^h$ . To guarantee that  $\boldsymbol{\theta}^h$  is positive-semidefinite, it is easily seen (*cf.* pg. 111) that the matrix

$$\mathbf{Y}\boldsymbol{\eta}^h + \boldsymbol{\eta}^h\mathbf{Y}^\dagger$$

must also be positive-semidefinite. The only obvious choice (to within a positive scalar constant) that satisfies this requirement in general is  $\mathbf{Y} = \frac{1}{2}\boldsymbol{\eta}^h$ , which implies that  $\boldsymbol{\chi} = \frac{1}{2}\boldsymbol{\eta}^{-1}\boldsymbol{\eta}^h\boldsymbol{\eta}$ . To recover the correct small-time behaviour, we compare this to the above case of normal  $\boldsymbol{\eta}$ , where  $\boldsymbol{\chi} = \frac{1}{2}\boldsymbol{\eta}^h$ , and conclude that Eq. (III.42a) should generalize to

$$\frac{\partial}{\partial t}\boldsymbol{\theta}^h + \boldsymbol{\chi}\boldsymbol{\theta}^h + \boldsymbol{\theta}^h\boldsymbol{\chi}^\dagger = \boldsymbol{\eta}^{-1}\boldsymbol{\Lambda}\boldsymbol{\Lambda}^\dagger\boldsymbol{\eta}^{-1\dagger}. \quad (\text{III.43})$$

If we similarly look for an equation for  $\boldsymbol{\theta}^a$  of the form

$$\begin{aligned} \frac{\partial}{\partial t}\boldsymbol{\theta}^a + \boldsymbol{\chi}\boldsymbol{\theta}^a + \boldsymbol{\theta}^a\boldsymbol{\chi}^\dagger &= \boldsymbol{\chi}(\boldsymbol{\eta}^{-1})^a + (\boldsymbol{\eta}^{-1})^a\boldsymbol{\chi}^\dagger \\ &= -\frac{1}{2}\boldsymbol{\eta}^{-1}[\boldsymbol{\eta}^h\boldsymbol{\eta}^a + \boldsymbol{\eta}^a\boldsymbol{\eta}^h]\boldsymbol{\eta}^{-1\dagger}, \end{aligned}$$

we are led to the generalization

$$\frac{\partial}{\partial t}\boldsymbol{\theta}^a + \boldsymbol{\chi}\boldsymbol{\theta}^a + \boldsymbol{\theta}^a\boldsymbol{\chi}^\dagger = -\frac{1}{2}\boldsymbol{\eta}^{-1}[-\boldsymbol{\eta}^h(\mathbf{1} - \mathbf{G}\mathbf{G}^\dagger)\boldsymbol{\eta}^a + \boldsymbol{\eta}^a(\mathbf{1} - \mathbf{G}\mathbf{G}^\dagger)\boldsymbol{\eta}^h]\boldsymbol{\eta}^{-1\dagger}.$$

Upon combining these general results, we deduce the full equation for  $\boldsymbol{\theta}$ :

$$\boxed{\frac{\partial}{\partial t}\boldsymbol{\theta} + \boldsymbol{\chi}\boldsymbol{\theta} + \boldsymbol{\theta}\boldsymbol{\chi}^\dagger = \boldsymbol{\eta}^{-1}[\boldsymbol{\Lambda}\boldsymbol{\Lambda}^\dagger + i\boldsymbol{\Gamma}^h]\boldsymbol{\eta}^{-1\dagger},} \quad (\text{III.44})$$

where

$$\begin{aligned} \boldsymbol{\chi} &= \frac{1}{2}\boldsymbol{\eta}^{-1}\boldsymbol{\eta}^h\boldsymbol{\eta}, \\ \boldsymbol{\Lambda} &= \boldsymbol{\eta}^h + i\boldsymbol{\eta}^a\mathbf{G}, \\ \boldsymbol{\Gamma} &= -\boldsymbol{\eta}^h[\mathbf{1} - \mathbf{G}\mathbf{G}^\dagger]\boldsymbol{\eta}^a, \\ \frac{\partial}{\partial t}\mathbf{G} &= -\frac{1}{2}\mathbf{G}\boldsymbol{\eta}^h, \quad \mathbf{G}(0) = \mathbf{1}. \end{aligned}$$

We also need equations for  $F^{\alpha\alpha'}$  and  $\eta^{\alpha\alpha'}$ . We follow a procedure analogous to Kraichnan's generalization of the test-field model [Kraichnan 1972] except that we write the equations in a covariant form. Covariance requires that the equations remain invariant to general (nonunitary) transformations.

Consider the case where  $\mathbf{C}$ ,  $\mathbf{F}$ ,  $\boldsymbol{\sigma}$ , and  $\boldsymbol{\nu}$  are simultaneously diagonal. We then have  $n$  uncoupled one-field EDQNM closure equations, one for each field  $\alpha$ :

$$\begin{aligned} F^{\alpha\alpha} &= \frac{1}{2}\sum_{\Delta} |M^{\alpha}_{\beta\gamma}|^2 \text{Re} \theta^{\alpha\beta\gamma}_{\alpha\beta\gamma} C^{\beta\beta} C^{\gamma\gamma}, \\ \widehat{\eta}^{\alpha}_{\alpha} &= \sum_{\Delta} M^{\alpha}_{\beta\gamma} M^{\beta}_{\gamma\alpha} {}^* \theta^{\alpha\beta\gamma}_{\alpha\beta\gamma} {}^* C^{\gamma\gamma}, \\ \eta^{\alpha}_{\alpha} &= \nu^{\alpha}_{\alpha} + \widehat{\eta}^{\alpha}_{\alpha}. \end{aligned} \quad (\text{III.45})$$

Next we recast the diagonal equations in a form *invariant to transformation*. First, note that the underlying Langevin representation is based on the *square root* of  $\text{Re}\theta$ . In order to see this, we recall that for the one-field case  $F_{\mathbf{k}} \sim \text{Re}\theta_{\mathbf{k}\mathbf{p}\mathbf{q}}$ ; hence the corresponding Langevin noise process is

$$f_{\mathbf{k}} \sim (\text{Re}\theta_{\mathbf{k}\mathbf{p}\mathbf{q}})^{\frac{1}{2}}.$$

Recall that the eigenvalues of a Hermitian matrix are real. We will construct the square root of a Hermitian matrix using the principal square roots of its eigenvalues. This is an arbitrary choice that does not affect the predictions of the closure. If the negative roots of some of the eigenvalues are used, the extra minus signs are extraneous and will ultimately cancel out.

Thus we define  $\mathbf{h}$  and  $\mathbf{g}$  such that  $\boldsymbol{\theta}^{\text{h}} = \mathbf{h}\mathbf{h}$  and  $\boldsymbol{\theta}^{\text{a}} = \mathbf{g}\mathbf{g}$ . These matrix square roots are incorporated into new mode-coupling factors that, like  $M_{\alpha\beta\gamma}$  and  $M^{\alpha\beta\gamma}$ , sum cyclically to zero:

$$\begin{aligned} V^{\alpha\beta\gamma} &\doteq M^{\bar{\alpha}\bar{\beta}\bar{\gamma}} h_{\bar{\alpha}\bar{\beta}\bar{\gamma}}^{\alpha\beta\gamma}, \\ W^{\alpha\beta\gamma} &\doteq M^{\bar{\alpha}\bar{\beta}\bar{\gamma}} g_{\bar{\alpha}\bar{\beta}\bar{\gamma}}^{\alpha\beta\gamma}, \\ \bar{W}^{\alpha\beta\gamma} &\doteq g^{\alpha\beta\gamma} \bar{M}^{\bar{\alpha}\bar{\beta}\bar{\gamma}}. \end{aligned} \quad (\text{III.46})$$

The general form of Eq. (III.45) becomes

$$\begin{aligned} F^{\alpha\alpha'} &\doteq \frac{1}{2} \sum_{\Delta} V^{\alpha}_{\beta\gamma} V^{\alpha'}_{\beta'\gamma'}{}^* C^{\beta\beta'}{}^* C^{\gamma\gamma'}, \\ \hat{\eta}^{\alpha}_{\alpha'} &\doteq - \sum_{\Delta} (V^{\alpha}_{\beta\gamma} V^{\beta}_{\gamma'\alpha'}{}^* - \frac{i}{2} \bar{W}^{\alpha}_{\beta\gamma} W^{\beta}_{\gamma'\alpha'}{}^* - \frac{i}{2} W^{\alpha}_{\beta\gamma} \bar{W}^{\beta}_{\gamma'\alpha'}{}^*) C^{\gamma\gamma'}{}^*, \\ \eta^{\alpha}_{\alpha'} &= \nu^{\alpha}_{\alpha'} + \hat{\eta}^{\alpha}_{\alpha'}. \end{aligned} \quad (\text{III.47})$$

With the definitions given in this section, Eqs. (III.35), (III.44), and Eq. (III.47) then form a complete set of relations for the realizable multiple-field EDQNM. Let us now examine some of the properties of this proposed generalization of the one-field realizable EDQNM.

### III.D.3 Properties of the realizable multiple-field EDQNM

#### Short-time behaviour:

For small  $t$ , we obtain the desired result

$$\boldsymbol{\theta} \sim t\mathbf{1}.$$

**Steady state:**

The steady state, if it exists, is given by

$$\boldsymbol{\theta}(\infty) = \boldsymbol{\eta}^{-1},$$

in agreement with the steady-state form of the unmodified  $\boldsymbol{\theta}$  equation, Eq. (III.38).

**Realizability:**

Define the integrating factor  $\mathbf{P} \doteq \mathbf{P}(t)$  by

$$\frac{\partial}{\partial t} \mathbf{P} = \boldsymbol{\chi} \mathbf{P}, \quad \mathbf{P}(0) = \mathbf{1}.$$

Equation (III.43) can then be written as

$$\frac{\partial}{\partial t} \mathbf{P} \boldsymbol{\theta}^h \mathbf{P}^\dagger = \mathbf{P} \boldsymbol{\eta}^{-1} \boldsymbol{\Lambda} \boldsymbol{\Lambda}^\dagger \boldsymbol{\eta}^{-1} \mathbf{P}^\dagger.$$

Therefore,<sup>6</sup>

$$\boldsymbol{\theta}^h(s) = \mathbf{P}^{-1}(s) \left( \int_0^s dt \mathbf{P} \boldsymbol{\eta}^{-1} \boldsymbol{\Lambda} \boldsymbol{\Lambda}^\dagger \boldsymbol{\eta}^{-1} \mathbf{P}^\dagger \right) \mathbf{P}^{-1\dagger}(s). \quad (\text{III.48})$$

Hence  $\boldsymbol{\theta}^h$  is positive-semidefinite:

$$\mathbf{y}^\dagger \boldsymbol{\theta}^h(s) \mathbf{y} = \int_0^s dt \left[ \mathbf{y}^\dagger \mathbf{P}^{-1}(s) \mathbf{P} \boldsymbol{\eta}^{-1} \boldsymbol{\Lambda} \right] \left[ \mathbf{y}^\dagger \mathbf{P}^{-1}(s) \mathbf{P} \boldsymbol{\eta}^{-1} \boldsymbol{\Lambda} \right]^\dagger \geq 0.$$

Since  $\boldsymbol{\theta}^h$  is Hermitian, this result implies that it has positive eigenvalues. Thus  $\boldsymbol{\theta}^h$  can be factored into *Hermitian* square roots  $\mathbf{h}$ . Then Eqs. (III.47) hold and it is easy to show (*cf.* This is the generalization of the realizability condition  $F_{\mathbf{k}} \geq 0$ ).

**Energy conservation:**

In Appendix E, we show that the symmetries of the mode-coupling coefficients lead to the relation

$$\text{Re} \left( F^\alpha_\alpha - \widehat{\eta}^\alpha_\delta C^{\delta\alpha} \right) = 0.$$

In terms of the metric tensor  $\boldsymbol{\sigma}$ , this may be written

$$\text{Re} \left[ \left( F^{\alpha\alpha'} - \widehat{\eta}^\alpha_\delta C^{\delta\alpha'} \right) \sigma_{\alpha'\alpha} \right] = 0.$$

Note that the summation convention for repeated indices is invoked here.

One may then readily verify that the generalized energy

$$E \doteq \frac{1}{2} \sigma_{\alpha'\alpha} \psi^\alpha \psi^{\alpha'*} \quad (\text{II.28})$$

is conserved by the nonlinear terms of Eq. (III.35).

<sup>6</sup>In this work, we reserve the notation  $f^{-1}(x)$  as a shorthand for  $1/f(x)$ , instead of the more conventional denotation as the functional inverse of  $f$ .

### III.D.4 Failure to conserve quadratic invariants

In Chapter I we presented a simple fluid model, Eqs. (I.12), that describes the coupling of electrostatic potential  $\varphi$  and ion pressure  $P$  in the  $\eta_i$  mode. To solve for the statistical evolution of this system, one would like to employ a multifield Markovian closure such as the one just constructed. The nonlinear terms of the fundamental equations, Eqs. (I.12), lead to the conservation of *four* distinct quadratic invariants:

$$\begin{aligned} E_0 &\doteq \frac{1}{2} \sum_{\mathbf{k}} (1 + k^2) \langle |\varphi_{\mathbf{k}}|^2 \rangle, \\ E_1 &\doteq \frac{1}{2} \sum_{\mathbf{k}} \langle |P_{\mathbf{k}}|^2 \rangle, \\ U &\doteq \frac{1}{2} \sum_{\mathbf{k}} k^2 (1 + k^2) \langle |\varphi_{\mathbf{k}}|^2 \rangle, \\ I &\doteq \text{Re} \sum_{\mathbf{k}} (1 + k^2) \langle \varphi_{\mathbf{k}} P_{\mathbf{k}}^* \rangle, \end{aligned}$$

as may be readily verified in the absence of dissipation. Here  $E_0$  and  $U$  correspond to the energy and enstrophy invariants of the Hasegawa-Mima problem. The two new invariants present a significant difficulty. Namely, the realizable multiple-field EDQNM closure is only guaranteed to conserve the single quantity  $E$  given by Eq. (II.28). Each of the above invariants corresponds to a different choice of the metric tensor  $\sigma$  upon which the closure may be built. In other words, we may choose  $E$  to be any one of these four invariants. That invariant—and possibly only that invariant—will be conserved.

A numerical test of this multifield closure has been conducted for the case where  $E = E_0 + E_1$ , which corresponds to the choice

$$\sigma = \begin{pmatrix} 1 + k^2 & 0 \\ 0 & 1 \end{pmatrix}$$

for the metric tensor. Indeed, in Fig. III.7 we find that this quantity is conserved, while the remaining invariants are not. In contrast, Fig. III.8 illustrates that the DIA conserves all of the quadratic invariants.

Clearly, this failure, which appears only upon consideration of multiple fields, is a serious defect of our realizable EDQNM. Perhaps there are physics problems that are governed largely by just one nonlinear invariant, but this is certainly not the general case. In Chapter I we described the close connection between the nonlinear invariants and the resulting cascade phenomena in the inertial range. For example, in two-dimensional fluid turbulence the presence of two invariants leads to markedly different spectra than for the three-dimensional case, for which there is only one invariant. Since the steady-state Kolmogorov energy spectrum is intricately linked

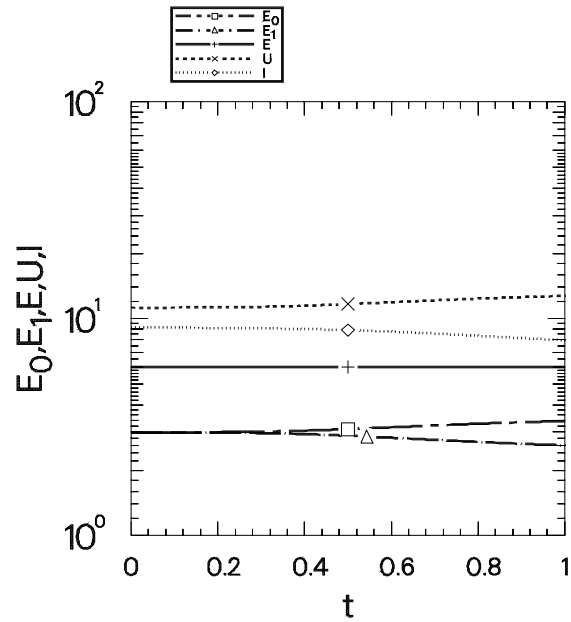


Figure III.7: Realizable EDQNM evolution of the quadratic invariants for the two-field  $\eta_i$  problem.

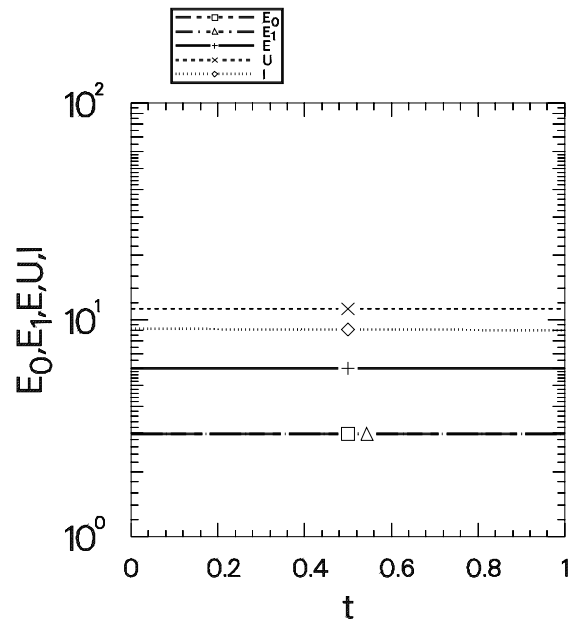


Figure III.8: DIA evolution of the quadratic invariants for the two-field  $\eta_i$  problem.

to both the number and type of conserved invariants, it seems essential that any admissible approximation should respect these properties. For example, in the above  $\eta_i$  mode problem it is important that  $E_0$  and  $E_1$  be *separately* conserved (not just their sum).

The difficulty has been traced back to the method we have borrowed from Kraichnan [1972] to enact the multiple-field generalization, particularly the procedure used to obtain the non-diagonal form of the equations by transforming away from a diagonal representation. In fact, his inhomogeneous test-field model suffers from the same deficiency. In both cases, conservation of multiple invariants is guaranteed only if the invariants commute with one another, so that they are *simultaneously* diagonalizable (in the field variables). This is a consequence of the construction of the multifield equations: in the diagonal frame of reference, the realizable multiple-field EDQNM will conserve the specified  $E$  and any other invariants that are also diagonal. For example, if one instead chose  $E = E_0$  one would find, just as in the Hasegawa-Mima case, that  $U$  is also conserved, but not  $E_1$  or  $I$ . The prospect of circumventing this difficulty within the present framework is remote [Kraichnan 1990c].

### III.E Realizable Markovian closure (RMC)

In the previous section we encountered a serious drawback with our multiple-field version of the realizable EDQNM. Much work (not described here) went into an examination of alternative approaches for finding the matrix equivalents of Eqs. (III.18), but the only covariant generalization that satisfied all of the criteria for  $\theta$  was the scheme just given. Unfortunately, the final difficulty—the lack of conservation of quadratic invariants—proved to be insurmountable. Not only could we find no analytic proof that non-commuting invariants are conserved, but we actually demonstrated a counterexample numerically. Moreover, the greater our scrutiny of this problem, the more it seemed that the root of our troubles lay at the very philosophy of the approach. That is, instead of eliminating the nonrealizability at the point it first set in, we made a heuristic modification of the  $\theta$  equation to correct it *a posteriori*. In a sense, what we did was to fix one mistake with a second mistake, hoping that all would work out well in the end.

It was with great reluctance that we finally abandoned our entire scheme for generalizing the EDQNM. Nevertheless, reconsideration of the problem turned out to be quite fruitful. We have already pointed out that realizability was first violated at the point where the FD ansatz, Eq. (III.9), was made. It is interesting to ask if there exist other ways of relating  $C_{\mathbf{k}}$  and  $R_{\mathbf{k}}$  that reduce to the FD ansatz in the steady state but result in a realizable closure. In other words, since the FD ansatz is an approximation anyway, can we conceive of a modified form that would

Markovianize the DIA covariance equation and fix the realizability problem in a single step, thereby reducing the number of approximations made?

Of course, fewer approximations alone do not guarantee a better theory. Ultimately the merits of any closure must be judged by comparison against direct simulation. But a closure more systematically linked to the DIA has a better hope of handling such problems as realizability, covariance, and conservation of invariants. It is important to remember that the DIA has all of these properties. With this motivation, we now begin the development of the realizable Markovian closure.

### III.E.1 Modified Fluctuation-Dissipation ansatz

We wish to replace the Fluctuation-Dissipation ansatz with a relation that reduces to the FD ansatz in the steady state, but leads to a realizable closure.

First, we note that the FD ansatz used to develop the EDQNM,

$$C_{\mathbf{k}}(t, t') = R_{\mathbf{k}}(t, t') C_{\mathbf{k}}(t) + C_{\mathbf{k}}(t') R_{\mathbf{k}}^*(t', t), \quad (\text{III.49})$$

differs from the appropriate result for the transient two-time covariance computed from a Langevin equation:

$$C_{\mathbf{k}}(t, t') = R_{\mathbf{k}}(t, t') C_{\mathbf{k}}(t') + C_{\mathbf{k}}(t) R_{\mathbf{k}}^*(t', t). \quad (\text{III.50})$$

The latter result is also in agreement with perturbation theory [Martin *et al.* 1973, pg. 432]. Of course, in the steady state these two equations agree. The question before us is: in general, which of these two relations is appropriate for constructing the transient evolution of a Markovian closure? It turns out that neither of the above forms guarantees realizability since the covariance is not evaluated symmetrically in the time indices. The example given on pg. 98 can be used to demonstrate this for both forms.

Realizability is guaranteed if  $C_{\mathbf{k}}(t, t')$  is a positive-semidefinite matrix in its time indices. We are therefore motivated to look at the following “compromise” between Eq. (III.49) and Eq. (III.50):

$$C_{\mathbf{k}}(t, t') = C_{\mathbf{k}}^{1/2}(t) r_{\mathbf{k}}(t, t') C_{\mathbf{k}}^{1/2*}(t'), \quad (\text{III.51})$$

where

$$r_{\mathbf{k}}(t, t') = R_{\mathbf{k}}(t, t') + R_{\mathbf{k}}^*(t', t)$$

and  $C_{\mathbf{k}}^{1/2}$  is the principal square root of the *real* part of  $C_{\mathbf{k}}$ . In the end we will show that the  $C_{\mathbf{k}}$  predicted by the RMC is in fact real, so that this distinction is moot. The choice of the principal root is arbitrary; the actual branch used has no effect

on the resulting closure.<sup>7</sup> It is interesting to note that the form of Eq. (III.51) has previously appeared in the literature [Kraichnan 1971b], although to our knowledge only in the context of steady-state turbulence, in which it cannot be distinguished from Eq. (III.49) or Eq. (III.50).

Under what conditions is this two-time  $C_{\mathbf{k}}$  positive-semidefinite, or, equivalently, is  $r_{\mathbf{k}}$  positive-semidefinite? The equation for  $R_{\mathbf{k}}$  is obtained as before by applying the Markovianization  $\Sigma_{\mathbf{k}}(t, \bar{t}) = \hat{\eta}_{\mathbf{k}}(t) \delta(t - \bar{t})$  to the DIA response function equation:

$$\frac{\partial}{\partial t} R_{\mathbf{k}}(t, t') + \eta_{\mathbf{k}}(t) R_{\mathbf{k}}(t, t') = \delta(t - t').$$

We now employ the following theorem, proved in Appendix F.

**Theorem 2:** *If  $\text{Re } \eta_{\mathbf{k}}(t) \geq 0 \quad \forall t$ , then the function  $r_{\mathbf{k}}$  defined by*

$$r_{\mathbf{k}}(t, t') \doteq \begin{cases} \exp(-\int_{t'}^t \eta_{\mathbf{k}}(\bar{t}) d\bar{t}) & \text{for } t \geq t', \\ \exp(-\int_t^{t'} \eta_{\mathbf{k}}^*(\bar{t}) d\bar{t}) & \text{for } t < t' \end{cases}$$

*is positive-semidefinite.*

In light of Theorem 1, this implies that the noise term

$$\mathcal{F}_{\mathbf{k}}(t, \bar{t}) = \frac{1}{2} \sum_{\mathbf{k}+\mathbf{p}+\mathbf{q}=\mathbf{0}} |M_{\mathbf{k}\mathbf{p}\mathbf{q}}|^2 C_{\mathbf{p}}^{1/2*}(t) r_{\mathbf{p}}^*(t, \bar{t}) C_{\mathbf{p}}^{1/2}(\bar{t}) C_{\mathbf{q}}^{1/2*}(t) r_{\mathbf{q}}^*(t, \bar{t}) C_{\mathbf{q}}^{1/2}(\bar{t}) \quad (\text{III.52})$$

is positive-semidefinite provided  $\text{Re } \eta_{\mathbf{p}}(t) \geq 0$  and  $\text{Re } \eta_{\mathbf{q}}(t) \geq 0$ .

If the initial condition is non-negative, it then follows that  $C_{\mathbf{k}}(t)$  is real and non-negative:

$$C_{\mathbf{k}}(t, t) = \int d\bar{t} d\bar{\bar{t}} R_{\mathbf{k}}(t, \bar{t}) \mathcal{F}_{\mathbf{k}}(\bar{t}, \bar{\bar{t}}) R_{\mathbf{k}}^*(t, \bar{\bar{t}}) \geq 0. \quad (\text{III.53})$$

This leads to the following modification of the EDQNM, which we call the realizable Markovian closure (RMC):

$$\frac{\partial}{\partial t} C_{\mathbf{k}}(t) + 2 \text{Re } \eta_{\mathbf{k}}(t) C_{\mathbf{k}}(t) = 2F_{\mathbf{k}}(t), \quad (\text{III.54a})$$

$$\eta_{\mathbf{k}}(t) \doteq \nu_{\mathbf{k}} - \sum_{\mathbf{k}+\mathbf{p}+\mathbf{q}=\mathbf{0}} M_{\mathbf{k}\mathbf{p}\mathbf{q}} M_{\mathbf{p}\mathbf{q}\mathbf{k}}^* \Theta_{\mathbf{p}\mathbf{q}\mathbf{k}}^*(t) C_{\mathbf{q}}^{1/2}(t) C_{\mathbf{k}}^{-1/2}(t), \quad (\text{III.54b})$$

$$F_{\mathbf{k}}(t) \doteq \frac{1}{2} \text{Re} \sum_{\mathbf{k}+\mathbf{p}+\mathbf{q}=\mathbf{0}} |M_{\mathbf{k}\mathbf{p}\mathbf{q}}|^2 \Theta_{\mathbf{k}\mathbf{p}\mathbf{q}}(t) C_{\mathbf{p}}^{1/2}(t) C_{\mathbf{q}}^{1/2}(t), \quad (\text{III.54c})$$

$$\frac{\partial}{\partial t} \Theta_{\mathbf{k}\mathbf{p}\mathbf{q}} + [\eta_{\mathbf{k}} + \mathcal{P}(\eta_{\mathbf{p}}) + \mathcal{P}(\eta_{\mathbf{q}})] \Theta_{\mathbf{k}\mathbf{p}\mathbf{q}} = C_{\mathbf{p}}^{1/2} C_{\mathbf{q}}^{1/2}, \quad \Theta_{\mathbf{k}\mathbf{p}\mathbf{q}}(0) = 0, \quad (\text{III.54d})$$

<sup>7</sup>This follows from the form of the final equations, Eqs. (III.54), in which the square roots of the covariance appear quadratically, resulting in the cancellation of any overall minus signs in the definition of the square root.

where  $\mathcal{P}(\eta) \doteq \text{Re } \eta \text{H}(\text{Re } \eta) + i \text{Im } \eta$  and  $\text{H}$  is the Heaviside unit step function. The effect of the  $\mathcal{P}$  operator is to force the real part of  $\eta$  to be non-negative. As desired, this modification has no effect in the steady state since  $\text{Re } \eta$  must already be non-negative in order for the  $R_{\mathbf{k}}$  equation to reach a steady state. Upon comparing Eq. (III.54c) to Eq. (III.18c), we see that the *effective* triad interaction time  $\theta_{\mathbf{k}\mathbf{p}\mathbf{q}}^{\text{eff}}$  entering the noise equation is

$$\theta_{\mathbf{k}\mathbf{p}\mathbf{q}}^{\text{eff}}(t) \doteq \Theta_{\mathbf{k}\mathbf{p}\mathbf{q}}(t) C_{\mathbf{p}}^{-1/2}(t) C_{\mathbf{q}}^{-1/2}(t).$$

Note that  $\theta_{\mathbf{k}\mathbf{p}\mathbf{q}}^{\text{eff}}(\infty)$  equals the interaction time  $\theta_{\mathbf{k}\mathbf{p}\mathbf{q}}(\infty)$  defined in Eq. (III.11).

The physical content of Eq. (III.51) may be expressed as follows. For  $t \geq t'$ , the FD equilibrium relation  $C_{\mathbf{k}}(t, t')/C_{\mathbf{k}}(\infty) = R_{\mathbf{k}}(t, t')$  should be restated out of equilibrium as a balance between the *correlation coefficient*

$$\frac{C_{\mathbf{k}}(t, t')}{C_{\mathbf{k}}^{1/2}(t) C_{\mathbf{k}}^{1/2}(t')}$$

and the response function  $R_{\mathbf{k}}(t, t')$ . This means that the time scale on which the response to infinitesimal fluctuations decays is equal to the time for which temporally displaced finite amplitudes are correlated with each other. Since amplitude decorrelation and decay of infinitesimal disturbances both occur by interaction with the turbulent background, it is intuitively reasonable that the time scales for these two processes should be equal.

Theorem 2 has established that  $C_{\mathbf{k}}(t, t')$  in Eq. (III.51) is positive-semidefinite whenever  $\text{Re } \eta_{\mathbf{k}}(t) \geq 0$ . This restriction on  $\eta_{\mathbf{k}}$  has a physical basis. For the case of constant  $\eta_{\mathbf{k}}$  the Markovianized response function is just

$$R_{\mathbf{k}}(t, t') = e^{-\eta_{\mathbf{k}}(t-t')} \text{H}(t - t').$$

For a turbulent system, the condition  $\text{Re } \eta_{\mathbf{k}} \geq 0$  is simply the consequence of the expectation that as  $t - t' \rightarrow \infty$  the response function should decay to zero, so that memory of initial perturbations is lost. In light of Eq. (III.51), this implies that  $C_{\mathbf{k}}(t, t') \rightarrow 0$  as  $|t - t'| \rightarrow \infty$ . In other words, the condition  $\text{Re } \eta_{\mathbf{k}} \geq 0$  is *physically* necessary to ensure that amplitudes evaluated at well-separated times are decorrelated with one another.

Let us briefly return to the degenerate case of three interacting waves that we used earlier to disprove the realizability of the original EDQNM closure. In Fig. III.9 we give the RMC solution corresponding to Fig. III.2. We note that, just as is the case with the DIA solution, the energies remain non-negative.

Since the quantity  $\Theta_{\mathbf{k}\mathbf{p}\mathbf{q}}$  is symmetric only in its last two indices (unlike  $\theta_{\mathbf{k}\mathbf{p}\mathbf{q}}$ , which is completely symmetric in all three indices), we obtain for the degenerate three-wave case two generalized interaction times,  $\Theta_{k\mathbf{p}\mathbf{q}}$  and  $\Theta_{\mathbf{p}\mathbf{q}k}$ . These quantities are graphed in Figs. III.10 and III.11, respectively.

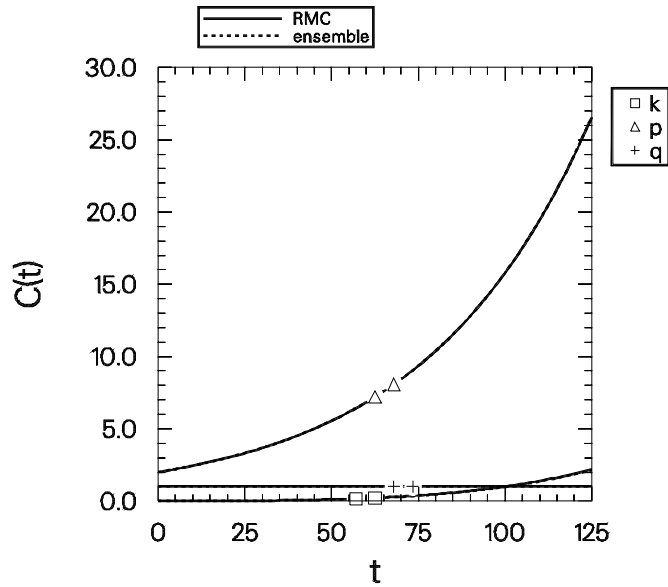


Figure III.9: RMC evolution of the mean covariances in the degenerate three-wave case of Fig. III.2. The ensemble and RMC solutions coincide (to within the numerical accuracy of the graph).

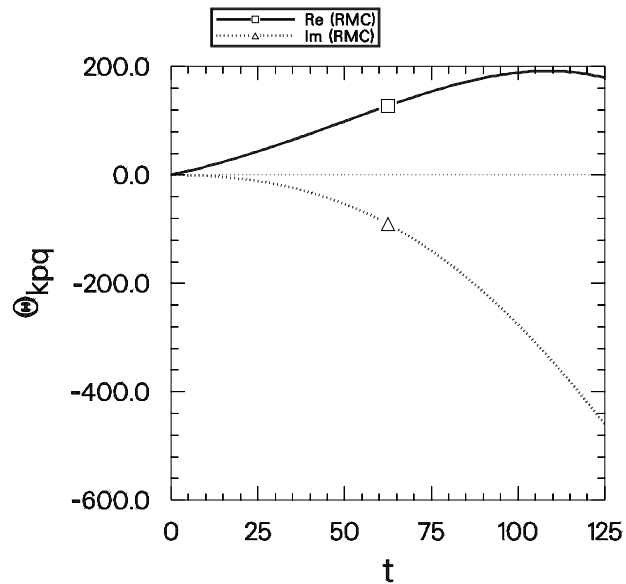


Figure III.10: Evolution of the quantity  $\Theta_{kpq}$  of the RMC closure for the degenerate three-wave case of Fig. III.2.

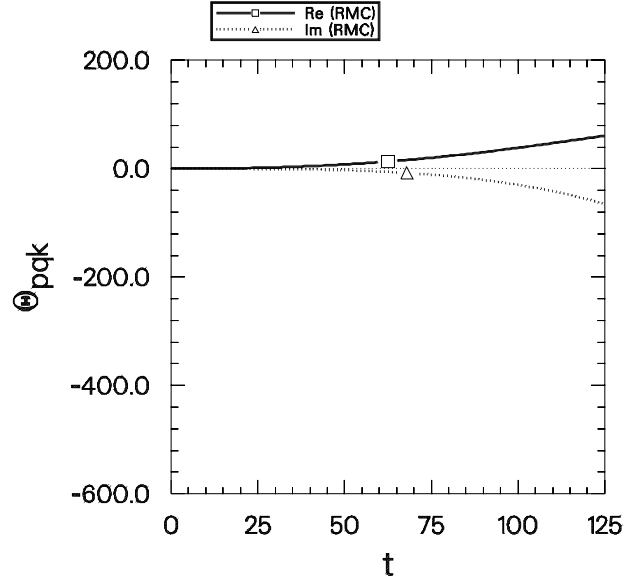


Figure III.11: Evolution of the quantity  $\Theta_{pqk}$  of the RMC closure for the degenerate three-wave case of Fig. III.2.

### III.E.2 Properties of the RMC

Let us now describe some of the properties of the RMC.

#### Short-time behaviour:

For small  $t$ , Eq. (III.54d) implies that

$$\Theta_{kpq} \sim t C_{\mathbf{p}}^{1/2}(0) C_{\mathbf{q}}^{1/2}(0).$$

Thus for nonzero initial conditions on the energies, the effective triad interaction time  $\theta_{kpq}^{\text{eff}}$  has the correct initial scaling:

$$\theta_{kpq}^{\text{eff}} \sim t.$$

#### Steady state:

If  $\lim_{t \rightarrow \infty} \text{Re} \eta_{\mathbf{k}} > 0$ ,  $\lim_{t \rightarrow \infty} \text{Re} \eta_{\mathbf{p}} > 0$ , and  $\lim_{t \rightarrow \infty} \text{Re} \eta_{\mathbf{q}} > 0$ , then  $\theta_{kpq}^{\text{eff}}$  achieves the desired steady-state value:

$$\theta_{kpq}^{\text{eff}}(\infty) = \frac{1}{\eta_{\mathbf{k}} + \eta_{\mathbf{p}} + \eta_{\mathbf{q}}}.$$

**Langevin representation:**

The RMC has the underlying Langevin equation

$$\boxed{\frac{\partial}{\partial t} \psi_{\mathbf{k}}(t) + \eta_{\mathbf{k}}(t) \psi_{\mathbf{k}}(t) = f_{\mathbf{k}}(t)}, \quad (\text{III.55})$$

which is constructed as follows.

Since the  $\mathcal{P}$  operator ensures that the  $\text{Re } \eta_{\mathbf{p}}(t)$  and  $\text{Re } \eta_{\mathbf{q}}(t)$  entering Eq. (III.52) are both non-negative, we conclude that  $\mathcal{F}_{\mathbf{k}}$  is indeed positive-semidefinite. Therefore, a source function  $f_{\mathbf{k}}(t)$  can be obtained by factoring  $\mathcal{F}_{\mathbf{k}}$ :

$$\mathcal{F}_{\mathbf{k}}(t, t') = \langle f_{\mathbf{k}}(t) f_{\mathbf{k}}^*(t') \rangle.$$

Unlike the corresponding quantities for the EDQNM, the functions  $f_{\mathbf{k}}$  are *not*  $\delta$  correlated. This gives the RMC more credibility than the EDQNM, especially for modeling oscillatory phenomena where the time scales may be crucial. It is intuitively plausible that much of the difficulty we have experienced in developing a realizable EDQNM may reside in a subtle connection between the white-noise approximation and the presence of wave phenomena [Krommes 1989].

By taking moments of Eq. (III.55), we find

$$\frac{\partial}{\partial t} C_{\mathbf{k}}(t) + 2 \text{Re } \eta_{\mathbf{k}}(t) C_{\mathbf{k}}(t) = 2 \text{Re} \langle f_{\mathbf{k}}(t) \psi_{\mathbf{k}}^*(t) \rangle.$$

Upon using the relation

$$\psi_{\mathbf{k}}(t) = \int_0^t d\bar{t} R_{\mathbf{k}}(t, \bar{t}) f_{\mathbf{k}}(\bar{t}),$$

we obtain

$$\begin{aligned} \frac{\partial}{\partial t} C_{\mathbf{k}}(t) + 2 \text{Re } \eta_{\mathbf{k}}(t) C_{\mathbf{k}}(t) &= 2 \text{Re} \int_0^t d\bar{t} \mathcal{F}_{\mathbf{k}}(t, \bar{t}) R_{\mathbf{k}}^*(t, \bar{t}) \\ &= \text{Re} \sum_{\mathbf{k}+\mathbf{p}+\mathbf{q}=\mathbf{0}} |M_{\mathbf{k}\mathbf{p}\mathbf{q}}|^2 \Theta_{\mathbf{k}\mathbf{p}\mathbf{q}}(t) C_{\mathbf{p}}^{1/2}(t) C_{\mathbf{q}}^{1/2}(t), \end{aligned} \quad (\text{III.56})$$

which agrees with Eq. (III.54a).

To further illuminate the physics contained in our modified FD ansatz, let us differentiate Eq. (III.51) with respect to  $t$  for the case  $t > t'$ . We find

$$\begin{aligned} \frac{\partial}{\partial t} C_{\mathbf{k}}(t, t') &= \frac{\partial}{\partial t} [C_{\mathbf{k}}^{1/2}(t) R_{\mathbf{k}}(t, t') C_{\mathbf{k}}^{1/2}(t')] \\ &= \frac{1}{2} C_{\mathbf{k}}^{-1/2}(t) \frac{\partial C_{\mathbf{k}}}{\partial t}(t) R_{\mathbf{k}}(t, t') C_{\mathbf{k}}^{1/2}(t') - C_{\mathbf{k}}^{1/2}(t) \eta_{\mathbf{k}}(t) R_{\mathbf{k}}(t, t') C_{\mathbf{k}}^{1/2}(t') \\ &= \frac{1}{2} \frac{\partial}{\partial t} [\log C_{\mathbf{k}}(t)] C_{\mathbf{k}}(t, t') - \eta_{\mathbf{k}}(t) C_{\mathbf{k}}(t, t') \\ &= -\check{\eta}_{\mathbf{k}}(t) C_{\mathbf{k}}(t, t'), \end{aligned} \quad (\text{III.57})$$

where

$$\check{\eta}_{\mathbf{k}}(t) \doteq \eta_{\mathbf{k}}(t) - \frac{1}{2} \frac{\partial}{\partial t} \log C_{\mathbf{k}}(t) \quad (\text{III.58})$$

represents the *total* effective damping rate. Still restricting our attention to the case  $t > t'$ , let us now compare Eq. (III.57) to the equation for  $C_{\mathbf{k}}(t, t')$  obtained by taking the appropriate moment of Eq. (III.55):

$$\frac{\partial}{\partial t} C_{\mathbf{k}}(t, t') + \eta_{\mathbf{k}}(t) C_{\mathbf{k}}(t, t') = \int_0^{t'} d\bar{t} \mathcal{F}_{\mathbf{k}}(t, \bar{t}) R_{\mathbf{k}}^*(t', \bar{t}). \quad (\text{III.59})$$

It then becomes clear that  $\check{\eta}_{\mathbf{k}}$  includes the effects of both damping (nonlinear and linear) in the term  $\eta_{\mathbf{k}}(t)$  and nonlinear noise in the term  $\frac{1}{2} \partial \log C_{\mathbf{k}}(t) / \partial t$ .

We can obtain corresponding definitions of  $\check{\eta}_{\mathbf{k}}$  for the closures obtained by applying the FD relations Eq. (III.49) and Eq. (III.50). These are, respectively,

$$\check{\eta}_{\mathbf{k} \text{ EDQNM}} \doteq \eta_{\mathbf{k}}(t) - \frac{\partial}{\partial t} \log C_{\mathbf{k}}(t), \quad (\text{III.60})$$

$$\check{\eta}_{\mathbf{k} \text{ Langevin}} \doteq \eta_{\mathbf{k}}(t). \quad (\text{III.61})$$

Although Eq. (III.60) contains a term modeling nonlinear noise that is similar to the one in Eq. (III.58), the form of Eq. (III.60) is *inconsistent* with the two-time covariance equation deduced from the wave-free EDQNM Langevin equation, which is (for  $t > t'$ ):

$$\begin{aligned} \frac{\partial}{\partial t} C_{\mathbf{k}}(t, t') + \eta_{\mathbf{k}}(t) C_{\mathbf{k}}(t, t') &= \int_0^{t'} d\bar{t} \delta(t - \bar{t}) R_{\mathbf{k}}^*(t', \bar{t}) \\ &= 0. \end{aligned} \quad (\text{III.62})$$

Thus, the assumption that  $f_{\mathbf{k}}$  is  $\delta$  correlated implies that the time-displaced covariance equation has no source term at all! Although an underlying Langevin representation exists for the wave-free EDQNM, we see that the statistics it predicts contradicts the FD ansatz, Eq. (III.9). It is clear that substantial physics has been sacrificed in the EDQNM. On the other hand, we see that Eq. (III.61) is consistent with Eq. (III.62) but is incomplete since it omits the important effect of nonlinear noise. In contrast, we see from Eq. (III.56) that the two-time statistics predicted by the modified FD ansatz are consistent with an underlying Langevin equation. Moreover, the entire temporal convolution structure of the DIA noise term is preserved by the RMC.

### Energy conservation:

In the absence of dissipation, the generalized energy Eq. (I.20) is conserved by the RMC. This is implied by the relation

$$\text{Re} \sum_{\mathbf{k}} \sigma_{\mathbf{k}} [F_{\mathbf{k}} - \hat{\eta}_{\mathbf{k}} C_{\mathbf{k}}] = 0,$$

which is a result of the fundamental mode-coupling symmetries.

Alternatively, by defining

$$\bar{\Theta}_{\mathbf{k}\mathbf{p}\mathbf{q}} = \Theta_{\mathbf{k}\mathbf{p}\mathbf{q}} C_{\mathbf{p}}^{1/2}(t) C_{\mathbf{q}}^{1/2}(t),$$

we may write the RMC equations in the form of Eq. (II.13). The argument on pg. 71 can then be applied to prove that any quadratic invariant of the fundamental equation is conserved by the nonlinear terms of the RMC.

### III.E.3 RGI modification

Kraichnan [1971b] constructed a random-Galilean-invariant closure, the test-field model, by applying Eq. (III.9) and Eq. (II.3a) to the modified Navier-Stokes system discussed on pg. 76. Unfortunately, the resulting closure is inappropriate for wave dynamics just as is the original EDQNM. For the test-field model, as well as the EDQNM, the proof of realizability was based on the fact that for Navier-Stokes turbulence the renormalized “damping” is real [Kraichnan 1971b]. When Holloway and Hendershott [1977] applied the test-field model to problems entailing wave effects, they did not renormalize the linear frequency.<sup>8</sup> Nevertheless, they did include the bare linear frequency in their expression for  $\theta$ . Consequently, the closure they used guarantees positivity of the energy spectrum only in a steady state. Their quasistationary formulation does not ensure that the transient energies are non-negative since  $\eta$  can achieve negative values during the evolution.

Fortunately, all of these difficulties can be overcome by using the modified Fluctuation-Dissipation ansatz, Eq. (III.51). The resulting realizable test-field model

---

<sup>8</sup>They argued that only the real part of the damping enters the energy equation. However, both the real and imaginary parts of the damping should enter the triad interaction time, as is apparent upon heuristic renormalization (as in resonance broadening theory) of the  $\delta$  function in the wave kinetic equation, Eq. (I.36), to a Lorentzian.

(RTFM) equations are

$$\frac{\partial}{\partial t} C_{\mathbf{k}}(t) + 2 \operatorname{Re} \eta_{\mathbf{k}}(t) C_{\mathbf{k}}(t) = 2F_{\mathbf{k}}(t), \quad (\text{III.63a})$$

$$\eta_{\mathbf{k}}(t) \doteq \nu_{\mathbf{k}} - \sum_{\mathbf{k}+\mathbf{p}+\mathbf{q}=\mathbf{0}} M_{\mathbf{k}\mathbf{p}\mathbf{q}} M_{\mathbf{p}\mathbf{q}\mathbf{k}}^* \Theta_{\mathbf{p}\mathbf{q}\mathbf{k}}^*(t) C_{\mathbf{q}}^{1/2}(t) C_{\mathbf{k}}^{-1/2}(t), \quad (\text{III.63b})$$

$$F_{\mathbf{k}}(t) \doteq \frac{1}{2} \operatorname{Re} \sum_{\mathbf{k}+\mathbf{p}+\mathbf{q}=\mathbf{0}} |M_{\mathbf{k}\mathbf{p}\mathbf{q}}|^2 \Theta_{\mathbf{k}\mathbf{p}\mathbf{q}}(t) C_{\mathbf{p}}^{1/2}(t) C_{\mathbf{q}}^{1/2}(t), \quad (\text{III.63c})$$

$$\frac{\partial}{\partial t} \Theta_{\mathbf{k}\mathbf{p}\mathbf{q}} + [\mathcal{P}(\eta_{\mathbf{k}}^{\text{S}} - \eta_{\mathbf{k}}) + \eta_{\mathbf{k}} + \mathcal{P}(\eta_{\mathbf{p}}^{\text{S}}) + \mathcal{P}(\eta_{\mathbf{q}}^{\text{S}})] \Theta_{\mathbf{k}\mathbf{p}\mathbf{q}} = C_{\mathbf{p}}^{1/2} C_{\mathbf{q}}^{1/2}, \quad \Theta_{\mathbf{k}\mathbf{p}\mathbf{q}}(0) = 0, \quad (\text{III.63d})$$

$$\eta_{\mathbf{k}}^{\text{S}}(t) \doteq \nu_{\mathbf{k}} + \sum_{\mathbf{k}+\mathbf{p}+\mathbf{q}=\mathbf{0}} M_{\mathbf{k}\mathbf{p}\mathbf{q}}^{\text{G}} M_{\mathbf{p}\mathbf{q}\mathbf{k}}^{\text{G}*} \Theta_{\mathbf{p}\mathbf{q}\mathbf{k}}^{\text{G}*}(t) C_{\mathbf{q}}^{1/2}(t) C_{\mathbf{k}}^{-1/2}(t), \quad (\text{III.63e})$$

$$\eta_{\mathbf{k}}^{\text{C}}(t) \doteq \nu_{\mathbf{k}} + g \sum_{\mathbf{k}+\mathbf{p}+\mathbf{q}=\mathbf{0}} M_{\mathbf{k}\mathbf{p}\mathbf{q}}^{\text{G}} M_{\mathbf{p}\mathbf{q}\mathbf{k}}^{\text{G}*} \Theta_{\mathbf{p}\mathbf{q}\mathbf{k}}^{\text{G}*}(t) C_{\mathbf{q}}^{1/2}(t) C_{\mathbf{k}}^{-1/2}(t), \quad (\text{III.63f})$$

$$\frac{\partial}{\partial t} \Theta_{\mathbf{k}\mathbf{p}\mathbf{q}}^{\text{G}} + [\eta_{\mathbf{k}}^{\text{C}} + \mathcal{P}(\eta_{\mathbf{p}}^{\text{S}}) + \mathcal{P}(\eta_{\mathbf{q}}^{\text{S}})] \Theta_{\mathbf{k}\mathbf{p}\mathbf{q}}^{\text{G}} = C_{\mathbf{p}}^{1/2} C_{\mathbf{q}}^{1/2}, \quad \Theta_{\mathbf{k}\mathbf{p}\mathbf{q}}^{\text{G}}(0) = 0. \quad (\text{III.63g})$$

Here, the superscripts S and C represent effects arising from the solenoidal and compressive parts,  $\psi^{\text{S}}$  and  $\psi^{\text{C}}$ , of the test field, respectively. The numerical factor  $g$  represents the number of solenoidal components associated with each compressive component. In three dimensions  $g = 2$ , while in two dimensions  $g = 1$ . Finally, the modified mode-coupling coefficients  $M_{\mathbf{k}\mathbf{p}\mathbf{q}}^{\text{G}}$  are obtained by neglecting the cross-coupling terms in the fundamental equations for  $\psi^{\text{S}}$  and  $\psi^{\text{C}}$ . This makes the small wavenumber contribution to  $\eta_{\mathbf{k}}^{\text{S}}$  and  $\eta_{\mathbf{k}}^{\text{C}}$  proportional to the mean-square shear, rather than the kinetic energy [Kraichnan 1971b]. What results is a closure invariant to random Galilean transformations. Note that in the absence of waves the steady-state forms of the RTFM and the original TFM agree.

### III.E.4 Comparison of the RMC with the realizable EDQNM

In a stationary state, the one-field equations of the original (non-realizable) EDQNM [Eqs. (III.18)], the realizable EDQNM [Eqs. (III.18a–c) and (III.34)], and the RMC [Eqs. (III.54)] are all identical. For this reason, the one-field realizable EDQNM and the RMC can both, at the very least, be justified as useful numerical schemes for obtaining a realizable steady state. There are, however, two particular advantages of the RMC relative to the realizable EDQNM.

First, the derivation of the RMC involves only two approximations. One of these, our modified FD ansatz, is applied at the point where non-realizability first enters (due to the invalidity of the FD assumption out of thermal equilibrium). The

modified FD ansatz, together with the Markovian assumption

$$\Sigma_{\mathbf{k}}(t, \bar{t}) = \hat{\eta}_{\mathbf{k}}(t) \delta(t - \bar{t}), \quad (\text{II.3a})$$

transforms the DIA equations *systematically* into the RMC equations. The realizable EDQNM, in contrast, was our first attempt at developing a realizable DIA-based Markovian closure and is rather *ad hoc*. After applying the FD ansatz and Markovianizing, we make an additional assumption to correct the effects of the non-realizability *a posteriori*. The result is a  $\theta$  equation that is much more difficult to justify and is also more complicated to compute.

Second, we will see in the next section that the RMC readily generalizes to multiple-field problems, conserving all the quadratic invariants of the primitive dynamical equation. In contrast, our multiple-field generalization of the EDQNM, inspired by Kraichnan's work on the inhomogeneous test-field model, can only be constructed to conserve a single invariant. We point out that no *general* multiple-field formulation of the EDQNM has been reported in the literature.<sup>9,10</sup>

Let us emphasize that the RMC is *not* merely a generalization of the EDQNM since even in the wave-free case the transient dynamics predicted by these closures differ. In fact, it should be clear from the nonrealizability of the EDQNM, the obstacles encountered in the multiple-field formulation, and the physically limiting assumption of  $\delta$ -correlated statistics for the underlying Langevin noise term that the EDQNM approach is not well-founded. By dropping criterion 4 of Section III.C we have been led to a closure that is more closely connected to the DIA. For example, the RMC and the DIA have a similar multiple-field structure and both have underlying (generalized) Langevin equations in which the random source function is not  $\delta$  correlated. We have already shown that criteria 1 and 2 of Section III.C are satisfied by the RMC, along with the appropriate realizability criterion, Eq. (III.53), which now replaces criterion 3.

---

<sup>9</sup>Carnevale *et al.* [1981] have discussed a multiple-field form for the EDQNM energy equation (involving an unspecified matrix  $\boldsymbol{\theta}$ ) that apparently *does* conserve all of the quadratic invariants. However, they place severe restrictions (that do not hold in general) on the interactions between elements of  $\boldsymbol{\theta}$  representing different fields. These authors also take for granted that one already has available a method for constructing a positive-semidefinite  $\boldsymbol{\theta}$ ; furthermore, they did not address the issue of realizability.

<sup>10</sup>Ottaviani *et al.* [1991] have suggested the use of a scalar  $\theta$  for the multiple-field EDQNM that is constructed from the trace of the full  $\eta$  matrix divided by the number of fields. Note that this choice does not account for the different interaction times associated with each of the field variables.

## III.F Multiple-field RMC

Unlike the construction of the multiple-field EDQNM closure, the multiple-field RMC equations will be developed without reference to any particular nonlinear invariant. In fact, the structure of the multiple-field RMC is much closer to the DIA than to the EDQNM, allowing it to conserve all of the quadratically nonlinear invariants. First, we need to develop a multiple-field generalization of our modified Fluctuation-Dissipation ansatz.

### III.F.1 Modified Fluctuation-Dissipation ansatz

Recalling the multiple-field notation of Section II.B.4, let us define the equal-time covariance  $\mathbf{C}_{\mathbf{k}}$  as the matrix with components

$$C^{\alpha\alpha'} \doteq \langle \psi^\alpha \psi^{\alpha'*} \rangle.$$

We need to define the analog of the square root factors  $C_{\mathbf{k}}^{1/2}(t)$  that appear in the one-field formulation. Begin by diagonalizing the Hermitian part  $\mathbf{C}_{\mathbf{k}}^h$  of  $\mathbf{C}_{\mathbf{k}}$  to obtain  $\widehat{\mathbf{C}}_{\mathbf{k}}^h$ . In the end, we will show that the  $\mathbf{C}_{\mathbf{k}}$  predicted by the RMC is in fact Hermitian, so that the Hermitian operator here is a redundancy. Now, there exists a matrix with components  $U^{\alpha_\delta}$  such that

$$C^{h\alpha\alpha'} \doteq U^{\alpha_\delta} \widehat{C}^{h\delta\delta} U^{\alpha'_\delta*}.$$

We then define

$$S^{\alpha\alpha'} \doteq U^{\alpha_\delta} (\widehat{C}^{h\delta\delta})^{1/2} U^{\alpha'_\delta*} = S^{\alpha'\alpha*},$$

where for each value of  $\delta$ ,  $(\widehat{C}^{h\delta\delta})^{1/2}$  is the principal square root of the real eigenvalue  $\widehat{C}^{h\delta\delta}$ . Although the choice of the principal root is arbitrary, the actual branch used has no effect on the resulting closure. Finally, let  $\mathbf{S}_{\mathbf{k}}$  be the matrix with components  $S^{\alpha_\delta}$  satisfying

$$C^{h\alpha\alpha'} \doteq S^{\alpha_\delta} S^{\delta\alpha'}.$$

Also, we will make use of the components  $S_{\delta\alpha'}$  defined from

$$S^{\alpha\delta} S_{\delta\alpha'} \doteq S^{\alpha_\delta} S^{\delta_{\alpha'}}.$$

To obtain the multiple-field RMC equations, we replace the covariances appearing in the noise term of the equal-time DIA with

$$C^{\alpha\alpha'}(t, t') = S^{\alpha_{\bar{\alpha}}}(t) \bar{r}^{\bar{\alpha}}_{\bar{\alpha}'}(t, t') S^{\bar{\alpha}'\alpha'}(t'), \quad (\text{III.64})$$

where

$$\bar{r}^{\alpha}_{\alpha'}(t, t') = \bar{R}^{\alpha}_{\alpha'}(t, t') + \bar{R}_{\alpha'}^{\alpha*}(t', t).$$

The elements  $\bar{R}^{\alpha}_{\alpha'}$  are components of the matrix  $\bar{\mathbf{R}}_{\mathbf{k}}(t, t')$ , which obeys  $\bar{\mathbf{R}}_{\mathbf{k}}(-\infty, t') = 0$  and

$$\frac{\partial}{\partial t} \bar{\mathbf{R}}_{\mathbf{k}}(t, t') + \bar{\boldsymbol{\eta}}_{\mathbf{k}}(t) \bar{\mathbf{R}}_{\mathbf{k}}(t, t') = \delta(t-t') \mathbf{1},$$

where  $\bar{\boldsymbol{\eta}}_{\mathbf{k}}(t) \doteq \mathbf{S}_{\mathbf{k}}^{-1}(t) \boldsymbol{\eta}_{\mathbf{k}}(t) \mathbf{S}_{\mathbf{k}}(t)$ . We define the components of transposed matrices like  $\bar{\mathbf{R}}_{\mathbf{k}}^{\text{T}} \equiv \bar{\mathbf{R}}_{\mathbf{k}}^{\dagger*}$  from

$$S^{\alpha}_{\delta} \bar{R}^{\delta}_{\bar{\delta}} S^{\bar{\delta}}_{\alpha'} = S^{\alpha\delta} \bar{R}^{\bar{\delta}}_{\delta} S_{\bar{\delta}\alpha'}.$$

The purpose of  $\mathbf{S}_{\mathbf{k}}(t)$  is to ensure that our FD ansatz reduces to the classical FD Theorem in the steady state. The  $\mathbf{S}_{\mathbf{k}}$  factors cancel in the one-field formulation, so they were not encountered previously. The classical FD Theorem is [Deker and Haake 1975]:

$$C^{\alpha\alpha'}(t, t') = R^{\alpha}_{\delta}(t, t') C^{\delta\alpha'}(\infty) + C^{\alpha\delta}(\infty) R^{\alpha'}_{\delta^*}(t', t). \quad (\text{III.65})$$

For a steady state, we have  $\bar{\mathbf{R}}_{\mathbf{k}} = \bar{\boldsymbol{\eta}}_{\mathbf{k}}^{-1} = \mathbf{S}_{\mathbf{k}}^{-1} \boldsymbol{\eta}_{\mathbf{k}}^{-1} \mathbf{S}_{\mathbf{k}} = \mathbf{S}_{\mathbf{k}}^{-1} \mathbf{R}_{\mathbf{k}} \mathbf{S}_{\mathbf{k}}$ . Equation (III.64) then becomes

$$\begin{aligned} C^{\alpha\alpha'}(t, t') &= R^{\alpha}_{\delta}(t, t') S^{\delta}_{\bar{\alpha}}(\infty) S^{\bar{\alpha}\alpha'}(\infty) + S^{\alpha}_{\bar{\alpha}}(\infty) S^{\delta\bar{\alpha}*}(\infty) R^{\alpha'}_{\delta^*}(t', t) \\ &= R^{\alpha}_{\delta}(t, t') C^{\text{h}\delta\alpha'}(\infty) + C^{\text{h}\alpha\delta}(\infty) R^{\alpha'}_{\delta^*}(t', t), \end{aligned}$$

which is the desired result, provided that we show  $\mathbf{C}_{\mathbf{k}}$  is Hermitian.

Realizability is guaranteed if  $\mathbf{C}_{\mathbf{k}}(t, t')$  is a positive-semidefinite matrix in *both* its species and time-indices:

$$\int dt dt' \boldsymbol{\phi}^{\dagger}(t) \mathbf{C}_{\mathbf{k}}(t, t') \boldsymbol{\phi}(t') \geq 0 \quad \forall \boldsymbol{\phi}(t).$$

This holds if and only if  $\bar{\mathbf{r}}_{\mathbf{k}}$  is also positive-semidefinite. We now employ the following theorem, proved in Appendix F.

**Theorem 4:** *Let  $\bar{\boldsymbol{\eta}}_{\mathbf{k}}(t)$  be a complex square matrix and  $\bar{\mathbf{R}}_{\mathbf{k}}(t, t')$  be the solution to*

$$\frac{\partial}{\partial t} \bar{\mathbf{R}}_{\mathbf{k}}(t, t') + \bar{\boldsymbol{\eta}}_{\mathbf{k}}(t) \bar{\mathbf{R}}_{\mathbf{k}}(t, t') = \delta(t-t') \mathbf{1},$$

*with  $\bar{\mathbf{R}}_{\mathbf{k}}(-\infty, t') = 0$ . If  $\bar{\boldsymbol{\eta}}_{\mathbf{k}}^{\text{h}}(t)$  is positive-semidefinite  $\forall t$ , then  $\bar{\mathbf{r}}_{\mathbf{k}}$  defined by*

$$\bar{\mathbf{r}}_{\mathbf{k}}(t, t') \doteq \bar{\mathbf{R}}_{\mathbf{k}}(t, t') + \bar{\mathbf{R}}_{\mathbf{k}}^{\dagger}(t', t)$$

*is positive-semidefinite.*

This implies that the noise term, with components

$$\mathcal{F}_{\mathbf{k}}^{\alpha\alpha'}(t, \bar{t}) = \frac{1}{2} \sum_{\Delta} M^{\alpha}_{\beta\gamma} M^{\alpha'}_{\bar{\beta}\bar{\gamma}} S^{\beta}_{\epsilon} S^{\beta'}_{\epsilon'}(t) \bar{r}^{\epsilon}_{\bar{\epsilon}}(t, \bar{t}) S^{\bar{\epsilon}\bar{\beta}}(\bar{t}) S^{\gamma}_{\lambda} S^{\gamma'}_{\lambda'}(t) \bar{r}^{\lambda}_{\bar{\lambda}}(t, \bar{t}) S^{\bar{\lambda}\bar{\gamma}}(\bar{t}),$$

is positive-semidefinite provided that for each  $t$  the matrices  $\bar{\eta}_{\mathbf{p}}^{\text{h}}(t)$  and  $\bar{\eta}_{\mathbf{q}}^{\text{h}}(t)$  are both positive-semidefinite.

If the initial condition is non-negative, it then follows that  $\mathbf{C}_{\mathbf{k}}(t)$  is Hermitian and positive-semidefinite:

$$\mathbf{C}_{\mathbf{k}}(t) \doteq \mathbf{C}_{\mathbf{k}}(t, t) = \int d\bar{t} d\bar{t}' \mathbf{R}_{\mathbf{k}}(t, \bar{t}) \mathcal{F}_{\mathbf{k}}(\bar{t}, \bar{t}') \mathbf{R}_{\mathbf{k}}^{\dagger}(t, \bar{t}').$$

We thus arrive at the multiple-field RMC equations, written here in a covariant representation:

$$\frac{\partial}{\partial t} C^{\alpha\alpha'} + \eta^{\alpha}_{\delta} C^{\delta\alpha'} + \eta^{\alpha'}_{\delta'} C^{\alpha\delta} = F^{\alpha\alpha'} + F^{\alpha'\alpha*}, \quad (\text{III.66a})$$

$$C^{\alpha\alpha'} = S^{\alpha}_{\delta} S^{\delta\alpha'},$$

$$\eta^{\alpha}_{\delta} C^{\delta\alpha'} \doteq \nu^{\alpha}_{\delta} C^{\delta\alpha'} - \sum_{\Delta} M^{\alpha}_{\beta\gamma} M^{\bar{\beta}}_{\bar{\gamma}\bar{\alpha}} S^{\gamma}_{\gamma'} S^{\alpha'}_{\beta'} \Theta^{\beta\gamma'\beta'} \bar{\gamma}\bar{\alpha}^*, \quad (\text{III.66b})$$

$$F^{\alpha\alpha'} \doteq \frac{1}{2} \sum_{\Delta} M^{\alpha}_{\beta\gamma} M^{\bar{\alpha}}_{\bar{\beta}\bar{\gamma}} S^{\beta}_{\beta'} S^{\gamma}_{\gamma'} \Theta^{\alpha'\beta'\gamma'} \bar{\beta}\bar{\gamma}^*, \quad (\text{III.66c})$$

$$\frac{\partial}{\partial t} \Theta^{\alpha'\beta'\gamma'} \bar{\alpha}\bar{\beta}\bar{\gamma} + \left[ \eta^{\alpha'}_{\mu} \delta^{\beta'}_{\epsilon} \delta^{\gamma'}_{\lambda} + \delta^{\alpha'}_{\mu} \mathcal{P}(\mathbf{S}_{\mathbf{p}}^{-1} \eta_{\mathbf{q}} \mathbf{S}_{\mathbf{p}})^{\beta'}_{\epsilon} \delta^{\gamma'}_{\lambda} \right. \\ \left. + \delta^{\alpha'}_{\mu} \delta^{\beta'}_{\epsilon} \mathcal{P}(\mathbf{S}_{\mathbf{q}}^{-1} \eta_{\mathbf{p}} \mathbf{S}_{\mathbf{q}})^{\gamma'}_{\lambda} \right] \Theta^{\mu\epsilon\lambda} \bar{\beta}\bar{\gamma} = \delta^{\alpha'}_{\bar{\alpha}} S^{\beta\bar{\beta}} S^{\gamma'\bar{\gamma}}. \quad (\text{III.66d})$$

Here,  $\mathcal{P}(\mathbf{H})$  for any Hermitian matrix  $\mathbf{H}$  is the obvious generalization of  $\mathcal{P}$  from the one-field case: in the diagonal frame of  $\mathbf{H}$ , let  $\mathcal{P}(\mathbf{H})$  be the matrix composed of the diagonal elements  $\text{Re } \lambda_i \mathbf{H}(\text{Re } \lambda_i)$ , where  $\lambda_i$  are the eigenvalues of  $\mathbf{H}$ . For any matrix  $\bar{\eta}$ , we then define  $\mathcal{P}(\bar{\eta}) \doteq \mathcal{P}(\bar{\eta}^{\text{h}}) + i\bar{\eta}^{\text{a}}$ . The effect of the  $\mathcal{P}$  operator is to force the Hermitian part of  $\bar{\eta}$  to be positive-semidefinite.

We now show that the introduction of the  $\mathcal{P}$  operator has no effect in a steady state, provided that the thermal-equilibrium FD relation is actually realizable in the steady state. In other words, we suppose that Eq. (III.65) holds exactly and that it predicts a positive-semidefinite two-time covariance:

$$C^{\alpha\alpha'}(t, t') = R^{\alpha}_{\delta}(t, t') C^{\delta\alpha'}(\infty) + C^{\alpha\delta}(\infty) R^{\alpha'}_{\delta'}(t', t).$$

Multiplying by  $\mathbf{S}^{-1}(\infty)$  on the left and  $\mathbf{S}(\infty)$  on the right, we conclude that the following quantities,

$$\begin{aligned} \bar{\mathbf{R}}_{\mathbf{k}} + \bar{\mathbf{R}}_{\mathbf{k}}^{\dagger} &= 2\bar{\mathbf{R}}_{\mathbf{k}}^{\text{h}} \\ &= 2(\bar{\eta}_{\mathbf{k}}^{-1})^{\text{h}} \\ &= \bar{\eta}_{\mathbf{k}}^{-1} (\bar{\eta}_{\mathbf{k}}^{\dagger} + \bar{\eta}_{\mathbf{k}}) \bar{\eta}_{\mathbf{k}}^{-1\dagger} \end{aligned}$$

are also positive-semidefinite. Thus,  $\bar{\eta}_{\mathbf{k}}^{\text{h}}$  is positive-semidefinite in a steady state if and only if the two-time covariance predicted by the FD relation is positive-semidefinite. If the latter condition does not hold, the RMC will still be realizable, because  $\mathcal{P}(\bar{\eta})$  is always positive-semidefinite. Of course, the closure cannot possibly satisfy the FD relation in that case, but this is of no concern since the FD relation would then be an unphysical approximation anyway. While we have not demonstrated the existence of such a case, the possibility has not been ruled out for a nonequilibrium system.

Finally, we emphasize that the resulting equations for the RMC are invariant under arbitrary linear transformations. The construction above was made without any explicit reference to a metric tensor and holds equally well in all frames of reference. Since the final RMC equations are independent of the particular reference frame, they may conveniently be evaluated in a frame where the components  $S^{\alpha}_{\alpha'}$  and  $S^{\alpha\alpha'}$  have identical values.

## III.F.2 Properties

### Short-time behaviour:

For small  $t$ ,

$$\Theta^{\alpha'\beta'\gamma'}_{\bar{\alpha}\bar{\beta}\bar{\gamma}} \sim t \delta^{\alpha'}_{\bar{\alpha}} S^{\beta'\bar{\beta}}(0) S^{\gamma'\bar{\gamma}}(0).$$

For nonzero initial conditions on the energies, the effective triad interaction time  $\theta^{\text{eff}}$  in the noise equation is then

$$\theta^{\text{eff}} \sim t\mathbf{1}.$$

This agrees with the short-time behaviour of Eq. (III.38).

### Steady state:

If  $\bar{\eta}_{\mathbf{p}}(\infty)$  and  $\bar{\eta}_{\mathbf{q}}(\infty)$  exist and have positive eigenvalues,  $\theta^{\text{eff}}$  approaches the solution

$$\begin{aligned} \theta^{\text{eff}}(\infty) &= (\boldsymbol{\eta}_{\mathbf{k}} \otimes \mathbf{1} \otimes \mathbf{1} + \mathbf{1} \otimes \boldsymbol{\eta}_{\mathbf{q}} \otimes \mathbf{1} + \mathbf{1} \otimes \mathbf{1} \otimes \boldsymbol{\eta}_{\mathbf{q}})^{-1} \\ &= \boldsymbol{\eta}^{-1}, \end{aligned}$$

where  $\mathbf{C} = \mathbf{A} \otimes \mathbf{B}$  is the outer product with components  $C^{ik}_{jl} = A^i_j B^k_l$  and use has been made of the definition Eq. (III.37). We therefore obtain the same steady-state form of  $\theta$  as predicted by the unmodified matrix equation, Eq. (III.38). This is consistent with the fact that in a steady state the modified FD ansatz Eq. (III.64) reduces to Eq. (III.65).

**Langevin representation:**

The multifield RMC equations have the corresponding underlying Langevin representation

$$\frac{\partial}{\partial t} \psi^\alpha(t) + \eta^\alpha_\delta(t) \psi^\delta(t) = f^\alpha(t),$$

where  $f^\alpha$  is determined from

$$F^{\alpha\alpha'}(t, t') = \langle f^\alpha(t) f^{\alpha'*}(t') \rangle.$$

**Conservation of quadratic invariants:**

Since the structure of the multiple-field DIA coupling has not been altered in the development of the multiple-field RMC, one finds that *all* quadratic invariants of the fundamental equation are conserved by the nonlinear terms of the RMC. Thus, by defining

$$\bar{\Theta}^{\alpha\beta\gamma} \bar{\alpha} \bar{\beta} \bar{\gamma} \doteq S^\beta_\epsilon S^\gamma_\lambda \Theta^{\alpha\epsilon\lambda} \bar{\alpha} \bar{\beta} \bar{\gamma},$$

we may write Eqs. (III.66) in the form of Eqs. (C.1). The proof of energy conservation in Appendix C can then be applied to prove that any quadratic invariant in the form of Eq. (II.28) is conserved by the nonlinear terms of the RMC.

This property is illustrated numerically in Fig. III.12 for the same  $\eta_i$  problem as considered in Fig. III.7 and Fig. III.8.

**III.F.3 RGI modification**

By analogy with the RGI modification introduced for the single-field RMC equations, one may also construct equations for the multiple-field realizable test-field model. This provides an alternative to the multiple-field closure given by Kraichnan [1972] that has the advantages of realizability in the presence of wave phenomena. Even in the absence of wave phenomena, this latter closure has the distinct advantage of conserving *all* quadratically nonlinear invariants. In contrast, Kraichnan's inhomogeneous test-field model conserves only a set of such invariants for which the corresponding  $\sigma$  matrices are simultaneously diagonalizable.

**III.G Summary**

In this chapter we have demonstrated an important and previously unrecognized result: in the presence of linear wave dynamics, the DIA-based EDQNM is not necessarily realizable since the triad interaction time can become negative. Note

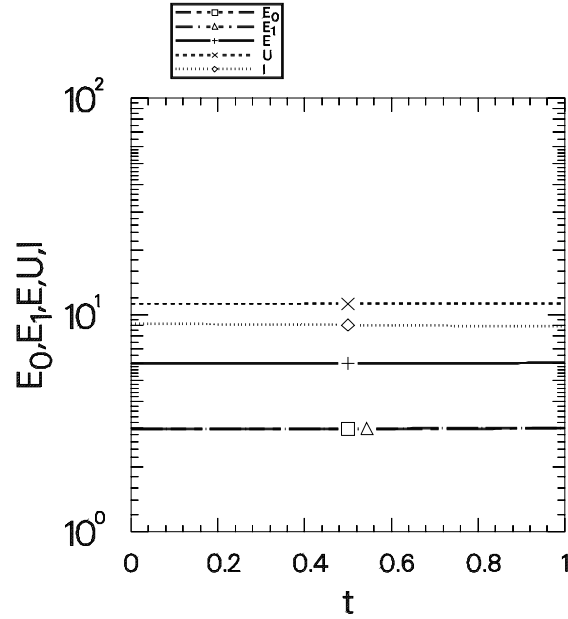


Figure III.12: RMC evolution of the quadratic invariants for the two-field  $\eta_i$  problem.

that the expression for the triad interaction time in this closure is derived from the DIA and *not* from a phenomenological model. This allows us to renormalize the frequency as well as the damping rate.

However, to investigate realistic drift-wave problems with statistical methods, we require a closure which is both Markovian and realizable, as was explained in Chapters I and II. In this chapter we have developed such a tool, the realizable Markovian closure (RMC), which unlike the EDQNM always meets both of these criteria. This closure is based on a form for the Fluctuation-Dissipation (FD) ansatz superior to the one normally used to derive the EDQNM from the DIA. We argue that this relation is more appropriate for nonstationary systems than the conventional form, although they both reduce to the FD Theorem in equilibrium. Upon applying this modified FD ansatz to the DIA and Markovianizing the response function equation, we obtained the equations for the realizable Markovian closure (RMC). Like the EDQNM, the RMC has an underlying Langevin representation; however, the underlying Langevin noise term of the RMC is not assumed to be  $\delta$  correlated. This is an important feature of the realizable Markovian closure that lends it more credibility than the EDQNM *even in the absence of wave effects*. In Appendix H, we will numerically demonstrate another significant difference: unlike the EDQNM, but like the DIA, the RMC does not predict a monotonic increase in entropy. That is, the RMC exhibits no Boltzmann-type  $H$  theorem; this is a conse-

quence of its close connection to the DIA. Our final accomplishment in this chapter was the demonstration that the RMC has a natural multiple-field generalization that is covariant to arbitrary linear transformations.

## Chapter IV

# Numerical Implementation of Statistical Closures

In this chapter we discuss techniques for the numerical implementation of two-dimensional anisotropic statistical closures. Most importantly, we develop a scheme of *mode reduction*, which is based on the property that the statistical quantities typically vary much more slowly in space than do the primitive dynamical variables. Since the number of modes required by direct numerical simulation of high Reynolds number turbulence is enormous (*cf.* 2), the possibility of dramatically reducing this number is one of the principal advantages of statistical closure methods. The procedure introduces certain time-independent geometrical weight factors that are calculated as an initial computational overhead for each new geometry or physics problem. The weight factors are used to evaluate new, effective mode-coupling coefficients that describe the interaction of certain statistically representative modes.

The usual practice in dealing with Navier-Stokes turbulence is to consider the equations for the truncated set of discrete Fourier amplitudes. The truncation wavenumber  $k_{\max}$  is chosen high enough so that in the wavenumber region characterized by  $k > k_{\max}$  dissipation is dominant and, consequently, turbulent activity is negligible. In numerical simulations of high-Reynolds number turbulence, this cut-off wavenumber is normally taken to be much lower than what is actually justified. This is necessary because of the lack of sufficient computer resolution to model the very short wavelengths. To compensate in part for this effect, an artificial dissipation known as the *hyperviscosity* is often introduced. This is intended to model the effective damping that the discarded wavenumbers (above the cutoff) would realistically exert on the truncated system through their coupling to the retained modes. One of the important advantages of statistical closures is that, due to their superior *scaling* with  $k_{\max}$ , they can sometimes be integrated much farther out in wavenumber space than can their spectral-code counterparts. Therefore, it is sometimes not necessary to adopt the artifice of hyperviscosity for closure computations.

For this reason, numerical solution of statistical closures may hold great promise for the understanding of fully-developed turbulence.

In this work, the numerical solution of closures is implemented in the time domain (as an initial value problem), although in principle it is also possible to formulate the problem in the frequency domain [Kadomtsev 1965, Horton 1986]. A predictor-corrector algorithm is used to *semi-implicitly* advance the time step, which implies that some attempt to enforce numerical stability is made by taking account of self-consistent effects at the next time step. The numerical results were obtained with the generic code DIA. This code is very flexible and may be programmed for a wide variety of physics problems, including all of those discussed in this work. We emphasize its modular design philosophy, which includes certain novel features that facilitate both interactive use and production runs. Currently, the code DIA implements the DIA, the original EDQNM closure, the realizable EDQNM closure, and the RMC for multiple-field, anisotropic, and homogenous turbulence in two dimensions. In addition, quasistationary forms of the Markovian closures may be computed. The code is documented with the modular FWEB system, which is a generalization of Knuth's original WEB system for PASCAL [Knuth 1984] that was developed by Krommes [1991b] to support a variety of programming languages, including C and FORTRAN.

Let us first describe the mode-reduction scheme that we shall employ. Such a procedure is essential to any practical application of closures to multi-dimensional turbulence.

## IV.A Bin-averaging technique

In this section we introduce an anisotropic version of a procedure originally used by Leith [1971] and Leith and Kraichnan [1972] for implementing the phenomenological EDQNM closure and the TFM for Navier-Stokes turbulence. It exploits the fact that statistical variables tend to vary slowly in wavenumber space compared to the rapid chaotic fluctuations of the (unaveraged) fundamental amplitudes. The variation of the statistical variables will be determined largely by nonstochastic quantities like the linear forcing. Thus, while only a relatively small number of modes is required to model the linear forcing and the statistical quantities adequately, many more will typically be required to model the mode-coupling and wavenumber convolution effects properly. We therefore *partition* the wavenumber space into coarse *bins* and evaluate the statistical variables only at a representative collection of modes.

If the mode-coupling coefficient also has a slow variation with respect to wavenumber, this reduction amounts to a counting of the contributions to the wavenumber convolution from wavenumbers lying within specified bins. For example, if a two-

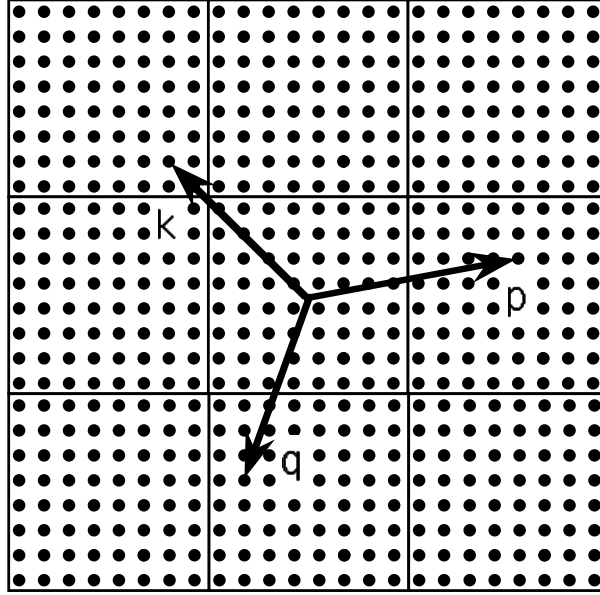


Figure IV.1: Coarse-graining of wavenumber space in a two-dimensional Cartesian bin geometry. The black dots represent individual modes.

dimensional Cartesian geometry is adopted, the corresponding  $\mathbf{k} + \mathbf{p} + \mathbf{q} = \mathbf{0}$  constraint separates into  $k_x + p_x + q_x = 0$  and  $k_y + p_y + q_y = 0$ . One may then readily compute the corresponding weight factor, which for this case is just the number of interacting modes lying within a specified triad of rectangular *bins*. The coarse-graining of wavenumber space “softens” the  $\mathbf{k} + \mathbf{p} + \mathbf{q} = \mathbf{0}$  constraint and allows wavenumbers from several neighbouring bins to interact with wavenumbers located in two other fixed bins. This is illustrated in Fig. IV.1. In contrast, the original  $\mathbf{k} + \mathbf{p} + \mathbf{q} = \mathbf{0}$  constraint uniquely specifies a wavenumber  $\mathbf{q}$  for each given combination of  $\mathbf{k}$  and  $\mathbf{p}$ .

However, the mode-coupling coefficient will often contain a factor that varies rapidly with wavenumber, such as the factor  $\hat{\mathbf{z}} \cdot \mathbf{p} \times \mathbf{q}$  in the Hasegawa-Mima problem. In this case, that factor should be averaged along with the  $\delta_{\mathbf{k}+\mathbf{p}+\mathbf{q},\mathbf{0}}$  convolution function. The result is in general a nontrivial problem, particularly in non-Cartesian geometries where the wavenumber bins are not made rectangular for reasons of symmetry.

#### IV.A.1 Continuum representation

The bin-averaging technique takes advantage of the property that the statistical quantities vary slowly relative to the rapidly varying convolution function  $\delta_{\mathbf{k}+\mathbf{p}+\mathbf{q},\mathbf{0}}$

by passing to the limit of a continuum of modes. This can be accomplished either by taking the limit  $L \rightarrow \infty$  of a discrete representation, in which  $L^{-d} \sum_{\mathbf{k}} \rightarrow (2\pi)^{-d} \int d\mathbf{k}$ , or equivalently by taking the Fourier integral transform of the original  $x$  space system. Here  $d$  represents the dimension of the space and  $L$  represents a periodicity length in each Cartesian direction. In this limit we define the continuum two-point correlation function by

$$C(\mathbf{k}) = \int_{-\infty}^{\infty} d\mathbf{r} e^{-i\mathbf{k}\cdot\mathbf{r}} \langle \psi(\mathbf{r})\psi(0) \rangle.$$

Suppose that this continuum space is divided into wavenumber bins by superimposing a coarse grid upon it. If the bins are sufficiently small, the variation of the statistical quantities over a bin will be negligible and we may replace them with their bin-averaged values. For instance, in a bin labeled by  $\mathbf{l}$  with measure<sup>1</sup>  $\Delta_{\mathbf{l}}$  we approximate  $C(\mathbf{k})$  by

$$C_{\mathbf{l}} \doteq \frac{1}{\Delta_{\mathbf{l}}} \int_{\Delta_{\mathbf{l}}} d\mathbf{k} C(\mathbf{k}).$$

This is a more reasonable definition for the value of  $C$  associated with bin  $\mathbf{l}$  than the central value  $C(\mathbf{k}_{\mathbf{l}})$ . In particular, this form leads to an evolution equation for  $C_{\mathbf{l}}$  that symmetrically involves an integration over  $\mathbf{k}$ ,  $\mathbf{p}$ , and  $\mathbf{q}$ . Such a form guarantees that the numerical approximation will conserve the generalized energy, Eq. (I.20).

The evolution equation for  $C_{\mathbf{l}}$  is obtained by averaging the continuum equation over the bin. For example, consider a typical term of a closure in the continuum representation:

$$\int \frac{d\mathbf{p}}{(2\pi)^d} \int d\mathbf{q} \delta(\mathbf{k}+\mathbf{p}+\mathbf{q}) f(\mathbf{k}, \mathbf{p}, \mathbf{q}) C^*(\mathbf{k}) C^*(\mathbf{p}) R^*(\mathbf{q}). \quad (\text{IV.1})$$

Here, we do not explicitly indicate any time dependences or integrals. The function  $f(\mathbf{k}, \mathbf{p}, \mathbf{q})$  is determined by the mode-coupling coefficient and is assumed to be time-independent.

Upon averaging Eq. (IV.1) over bin  $\mathbf{l}$  we obtain

$$\frac{1}{(2\pi)^d \Delta_{\mathbf{l}}} \int_{\Delta_{\mathbf{l}}} d\mathbf{k} \sum_{\mathbf{m}, \mathbf{n}} \int_{\Delta_{\mathbf{m}}} d\mathbf{p} \int_{\Delta_{\mathbf{n}}} d\mathbf{q} \delta(\mathbf{k}+\mathbf{p}+\mathbf{q}) f(\mathbf{k}, \mathbf{p}, \mathbf{q}) C^*(\mathbf{k}) C^*(\mathbf{p}) R^*(\mathbf{q}).$$

By assuming that  $C$  and  $R$  vary slowly over the bins, we can approximate this as

$$\frac{1}{(2\pi)^d \Delta_{\mathbf{l}}} \sum_{\mathbf{m}, \mathbf{n}} C_{\mathbf{l}}^* C_{\mathbf{m}}^* R_{\mathbf{n}}^* \int_{\Delta_{\mathbf{l}}} d\mathbf{k} \int_{\Delta_{\mathbf{m}}} d\mathbf{p} \int_{\Delta_{\mathbf{n}}} d\mathbf{q} \delta(\mathbf{k}+\mathbf{p}+\mathbf{q}) f(\mathbf{k}, \mathbf{p}, \mathbf{q}). \quad (\text{IV.2})$$

---

<sup>1</sup>In two dimensions, the measure of a bin is just its area.

If the integrand  $f(\mathbf{k}, \mathbf{p}, \mathbf{q})$  in Eq. (IV.2) is completely symmetric in  $\mathbf{k}$ ,  $\mathbf{p}$ , and  $\mathbf{q}$ , this approximation will preserve all the conservation properties arising from symmetries of the mode-coupling coefficients [Leith and Kraichnan 1972]. However, the mode-coupling coefficients are often not completely symmetric in all three indices. For example, the mode-coupling coefficients of the Hasegawa-Mima problem consist of a product of symmetric and asymmetric factors; these are respectively  $(\hat{\mathbf{z}} \cdot \mathbf{p} \times \mathbf{q})$  and  $(q^2 - p^2)/(1 + k^2)$ . The symmetry of the first factor is most readily seen by considering the triangle constructed from the vectors  $\mathbf{k}$ ,  $\mathbf{p}$ , and  $\mathbf{q}$  that must exist for any triad that enters the wavenumber convolution. By noting that  $(\hat{\mathbf{z}} \cdot \mathbf{p} \times \mathbf{q})$  is just twice the area of the enclosed triangle and upon recalling the formula  $[s(s-k)(s-p)(s-q)]^{1/2}$  for the area of a triangle in terms of its semiperimeter  $s \doteq \frac{1}{2}(k + p + q)$ , we may write this factor in the symmetric form

$$\hat{\mathbf{z}} \cdot \mathbf{p} \times \mathbf{q} = \frac{1}{2} \sqrt{(k + p + q)(p + q - k)(q + k - p)(k + p - q)}.$$

In general, let us decompose the mode-coupling coefficients into two factors. The first factor is assumed to be symmetric in all three indices and *isotropic*, as we have just shown for the  $(\hat{\mathbf{z}} \cdot \mathbf{p} \times \mathbf{q})$  factor of the Hasegawa-Mima problem. We also require that the symmetric factor can be written as a sum of terms with homogenous scaling, so that

$$f(a\mathbf{k}, a\mathbf{p}, a\mathbf{q}) = \sum_{n \in \mathcal{N}} a^n c_n f_n(k, p, q).$$

For the Hasegawa-Mima problem,  $\mathcal{N} = \{4\}$ ; that is, there is only one term and it is homogenous with degree 4. Note that the function  $f$  corresponding to the closure equations [cf. Eqs. (I.39)] always involves *two* mode-coupling factors.

In this work we will make the simplifying assumption that the remaining asymmetric factor varies *slowly* within each bin, as it typically does in the Hasegawa-Mima problem. In principle, this restriction is not actually necessary; however, we have found that it is computationally expedient to impose this assumption. We note that for continuous coupling coefficients, one may always achieve this property to arbitrary precision by reducing the size of the bins. If the asymmetric factor is slowly varying, we may evaluate it *outside* the integral along with the statistical variables.

The symmetries and scaling relations of the  $f_n$  functions greatly reduce the required number of weight factor computations. In addition, the complete symmetry of  $f$  with respect to its indices ensures that the above numerically-motivated approximation conserves all of the quadratically nonlinear invariants. In light of our theoretical efforts in Chapter III to develop closures that respect these invariants, at this stage we certainly do not want to violate important conservation laws by employing a poor numerical scheme.

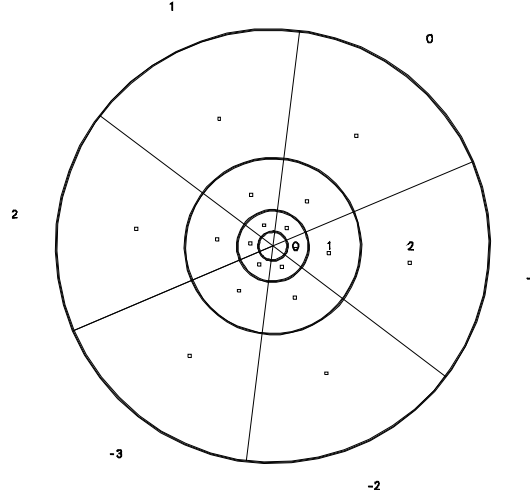


Figure IV.2: Logarithmic/linear polar bin geometry for  $3 \times 6$  bins. In the code DIA each bin is indexed by the coordinates indicated on the radial and azimuthal axes.

### IV.A.2 Wavenumber coordinate system

The mode-coupling coefficients in the Hasegawa-Mima problem are independent of angle; therefore, upon removal of the linear term the system will evolve toward an isotropic state. Anisotropy enters only through the linear term of the Hasegawa-Mima equation. When the nonlinearity is restored, a competition exists between this anisotropic drive and the tendency of the nonlinear terms to return the system to an isotropic state. For the two-dimensional problems of this work, we employ polar coordinates since we regard the anisotropy as a perturbation to an otherwise isotropic nonlinear equilibrium state.

It is often desirable on physical grounds (e.g., if the anticipated inertial-range energy spectrum has a power-law scaling) to use a logarithmically spaced grid in the radial direction (see Fig. IV.2). Actually, the integration technique described below will work for any grid spacing. Nevertheless, there are significant computational advantages in the use of a logarithmic grid. First, this dramatically reduces the size of the lookup table that is required to store the weight factors because we can then exploit the scaling properties of the integrand. Second, the use of a logarithmic grid minimizes the computational overhead required to calculate the weight factor table associated with each new geometrical configuration.

6.5in

### IV.A.3 Fourier harmonic expansion

An alternative scheme has been used by Herring [1975], who expanded the statistical variables in Fourier harmonics of the polar angle. If the turbulence is considered to be approximately isotropic, one can obtain an accurate representation by truncating the Fourier series at low order. In the bin procedure this would correspond to using only a few angular partitions. It would be useful to compare the advantages and disadvantages of Herring's approach with our anisotropic bin-averaging method. It is clear that one method will be more accurate than the other for certain specific angular distributions; in general, however, it has not yet been established which procedure most probably can achieve a given accuracy with the least computational effort. The Nyquist sampling theorem (of signal processing theory) might at first suggest that the sinusoidal basis functions used by Herring are more appropriate than the basis functions employed here, which in the angular direction essentially amount to square waves. However, since one can formulate a corresponding Nyquist theorem for square wave basis functions, there is actually no loss of efficiency in this choice [Krommes 1991a]. Indeed, there is a great advantage in the choice of square wave functions that stems from our ability to compute the geometric weight factors accurately and efficiently with the general algorithm presented in the next section.

## IV.B Geometric weight factors

The geometrical weight factors entering the summation in Eq. (IV.2) account for the numbers of discrete modes in bins  $\mathbf{m}$  and  $\mathbf{n}$  that interact together to affect modes in bin  $\mathbf{l}$ . Therefore, to implement the bin-averaging procedure we need to compute integrals of the following form over a polar bin:

$$\langle f \rangle_{\mathbf{k}\mathbf{p}\mathbf{q}} \doteq \int_{k_{<}}^{k_{>}} k dk \int_{\alpha_{<}}^{\alpha_{>}} d\alpha \int_{p_{<}}^{p_{>}} p dp \int_{\beta_{<}}^{\beta_{>}} d\beta \int_{q_{<}}^{q_{>}} q dq \int_{\gamma_{<}}^{\gamma_{>}} d\gamma \delta(\mathbf{k}+\mathbf{p}+\mathbf{q}) f(\mathbf{k}, \mathbf{p}, \mathbf{q}), \quad (\text{IV.3})$$

where  $\alpha$ ,  $\beta$ , and  $\gamma$  are the respective angles of  $\mathbf{k}$ ,  $\mathbf{p}$ , and  $\mathbf{q}$  with respect to some *fixed* reference. In making contact with the literature, note that these are related to, but *not* identical to, the interior angles of the triangle formed by  $\mathbf{k}$ ,  $\mathbf{p}$ , and  $\mathbf{q}$ . The relation between these two sets of angles is shown in Fig. IV.3. The subscript  $\mathbf{k}\mathbf{p}\mathbf{q}$  on the average in Eq. (IV.3) refers to the *central* wavenumbers of the bins. For the logarithmic/linear polar grid used here, it is natural to construct these central wavenumbers with a radial component equal to the geometric mean of the two radial boundary values and an angular component equal to the arithmetic mean of the

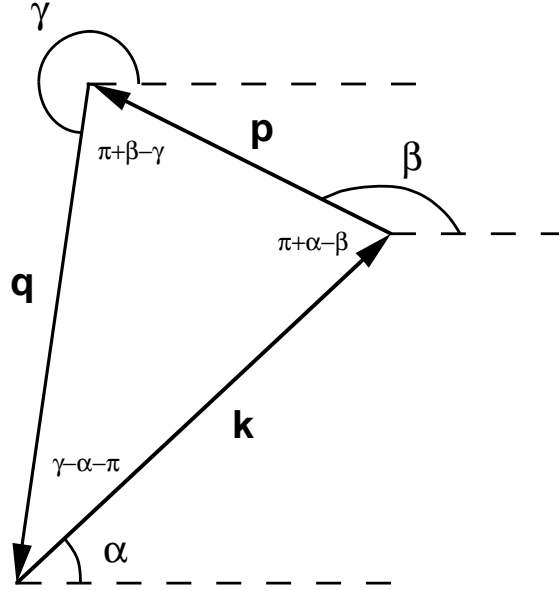


Figure IV.3: Relation between the angles associated with the convolution triangle.

two angular boundary values. A typical wavenumber bin geometry with 3 radial and 6 angular divisions is depicted in Fig. IV.2. To help illustrate the meaning of Eq. (IV.3) in terms of this picture, consider the case where  $f = 1$ . The bin average  $\langle 1 \rangle_{\mathbf{k}\mathbf{p}\mathbf{q}}$  represents the product of the areas of the  $\mathbf{p}$  and  $\mathbf{q}$  bins that interact to affect modes within the  $\mathbf{k}$  bin.

To compute the weight factor corresponding to the mass operator term for a given statistical closure [e.g., Eqs. (I.39)], we will set  $f(\mathbf{k}, \mathbf{p}, \mathbf{q})$  equal to the *symmetric* factors in  $-M_{\mathbf{k}\mathbf{p}\mathbf{q}}M_{\mathbf{p}\mathbf{q}\mathbf{k}}^*$ . We emphasize that the general algorithm discussed below will actually handle *any* function  $f(\mathbf{k}, \mathbf{p}, \mathbf{q})$ ; we will eventually invoke the restriction that  $f$  be symmetric and isotropic only to minimize the number of calls made to this algorithm. The corresponding weight factor for the noise term need not be integrated explicitly since it may be obtained from the conservation relation (I.19)

$$\sigma_{\mathbf{k}} |M_{\mathbf{k}\mathbf{p}\mathbf{q}}|^2 = -M_{\mathbf{k}\mathbf{p}\mathbf{q}}(\sigma_{\mathbf{p}}M_{\mathbf{p}\mathbf{q}\mathbf{k}}^* + \sigma_{\mathbf{q}}M_{\mathbf{q}\mathbf{k}\mathbf{p}}^*) = -\sigma_{\mathbf{p}}M_{\mathbf{k}\mathbf{p}\mathbf{q}}M_{\mathbf{p}\mathbf{q}\mathbf{k}}^* - \sigma_{\mathbf{q}}M_{\mathbf{k}\mathbf{q}\mathbf{p}}M_{\mathbf{q}\mathbf{p}\mathbf{k}}^*.$$

### IV.B.1 Isotropic case

It is instructive to first consider the isotropic problem previously studied by Kraichnan [1964a], Leith [1971], and Leith and Kraichnan [1972]. These authors numerically implemented closures for two-dimensional Navier-Stokes turbulence. We recall that the mode-coupling coefficients for the Hasegawa-Mima equation re-

duce, upon replacing the factors of  $(1 + k^2)$  with  $k^2$ , to those of the two-dimensional Navier-Stokes equation, Eq. (I.9).

For the special case studied by these authors we need to compute Eq. (IV.3) with the isotropic limits  $\alpha_{<} = \beta_{<} = \gamma_{<} = 0$  and  $\alpha_{>} = \beta_{>} = \gg = 2\pi$ . The above authors showed that the calculation can be greatly simplified by including only *one* factor of  $(\hat{\mathbf{z}} \cdot \mathbf{p} \times \mathbf{q})^2$ , namely  $pq |\sin(\beta - \gamma)|$ , in the bin average since this facilitates a natural change of variables from  $(p, \beta)$  to  $(p, q)$ , where  $q \doteq |\mathbf{k} + \mathbf{p}|$ . Specifically, they used the function  $f(\mathbf{k}, \mathbf{p}, \mathbf{q}) = |\sin(\beta - \gamma)|/2k$ .

Leith and Kraichnan approximately accounted for the contribution of the remaining factor by evaluating it at the central wavenumbers. This introduces significant error since  $|\sin(\beta - \gamma)|$  varies rapidly over the bin. They partially compensated for this effect by numerically evaluating (inexactly) subsidiary correction factors that approximate the effect of this quantity. We will not go into the details of these complexities here since the general procedure to be described shortly will circumvent all of these problems.<sup>2</sup> This special case serves only as an example to help motivate our solution of the full anisotropic problem with an arbitrary  $f$ .

From an examination of the one-dimensional result found in Appendix G, one is motivated to consider the decomposition

$$\int_{k_{<}}^{k_{>}} \int_{p_{<}}^{p_{>}} \int_{q_{<}}^{q_{>}} = \left( \int_0^{k_{>}} - \int_0^{k_{<}} \right) \left( \int_0^{p_{>}} - \int_0^{p_{<}} \right) \left( \int_0^{q_{>}} - \int_0^{q_{<}} \right),$$

which reduces Eq. (IV.3) to a sum of eight simpler integrals. The  $\mathbf{q}$  integration can be performed trivially. If we follow Leith and Kraichnan [1972] and choose  $f(\mathbf{k}, \mathbf{p}, \mathbf{q}) = |\sin(\beta - \gamma)|/2k$ , each resulting integral has the *form*

$$\frac{1}{2} \int_0^{\Delta k} dk \int_0^{2\pi} d\alpha \int_0^{\Delta p} p dp \int_0^{2\pi} d\beta H(\Delta q - |\mathbf{k} + \mathbf{p}|) |\sin(\beta - \gamma)|, \quad (\text{IV.4})$$

where now  $\gamma$  is the angle of  $\mathbf{q} \doteq -(\mathbf{k} + \mathbf{p})$ . Let us change variables from  $(p, \beta)$  to  $(p, q)$  so that, from the law of cosines,

$$2q dq = -2kp \sin(\beta - \alpha) d\beta,$$

or, upon using the law of sines,

$$|p d\beta| = \left| \frac{dq}{\sin(\beta - \gamma)} \right|.$$

---

<sup>2</sup>In fact, we will eventually underscore the generality of our procedure by evaluating Leith's correction factors (*cf.* In making this comparison, we will find significant differences. It should be mentioned that Leith and Kraichnan were aware of this discrepancy; they attempted to account for it by introducing yet another modification involving a phenomenological constant chosen to give the best fit for the inertial range.

We then find that

$$\begin{aligned} p \int_0^{2\pi} d\beta |\sin(\beta - \gamma)| &= p \int_{\alpha-\pi}^{\alpha} d\beta |\sin(\beta - \gamma)| + p \int_{\alpha}^{\alpha+\pi} d\beta |\sin(\beta - \gamma)| \\ &= 2 \int_{|k-p|}^{k+p} dq. \end{aligned}$$

Thus, Eq. (IV.4) simplifies to

$$2\pi \int_0^{\Delta k} dk \int_0^{\Delta p} dp \int_{|k-p|}^{\min(k+p, \Delta q)} dq = 2\pi \int_0^{\Delta k} dk \int_0^{\Delta p} dp [\min(k+p, \Delta q) - |k-p|], \quad (\text{IV.5})$$

which evaluates to the trilinear function of  $\Delta k$ ,  $\Delta p$  and  $\Delta q$ , Eq. (G.3), calculated in Appendix G.

We also include in Appendix G an interesting analytical solution to the one-dimensional problem in which the corresponding weight function is  $f(k, p, q) = 1$ . This formula could be used to compute the weight factor for a continuum two-dimensional Cartesian geometry by making use of the separability of the  $\delta(\mathbf{k}+\mathbf{p}+\mathbf{q})$  function. In addition, the one-dimensional problem is equivalent to the isotropic two-dimensional problem (in polar geometry) for the case  $f(\mathbf{k}, \mathbf{p}, \mathbf{q}) = 1/(4\pi^2 kp)$  since

$$\int_0^{2\pi} d\alpha \int_0^{2\pi} d\beta \int_0^{2\pi} d\gamma q \delta(\mathbf{k}+\mathbf{p}+\mathbf{q}) = \delta(k+p+q).$$

In fact, the method can easily be extended to any isotropic function separable in the wavenumber magnitudes. For example, one could obtain an isotropic formula for the two-dimensional polar case with  $f(\mathbf{k}, \mathbf{p}, \mathbf{q}) = 1$ . This could be used for an isotropic problem in which it is desired to evaluate consistently all of the mode-coupling coefficients at the central wavenumbers only.

We will pursue such possibilities no further since in this work the primary focus is on anisotropic turbulence. For anisotropic turbulence there is no completely analytic solution to the weight factor problem; instead, a combination of analytical and numerical techniques is required.

## IV.B.2 Anisotropic case

The isotropic calculation we just outlined, particularly the reduction to Eq. (IV.5), is an elegant algebraic alternative to the complicated geometric formulation of the problem given by Leith and Kraichnan [1972], who remark that the calculation “can be carried out as a straightforward but complex exercise in solid geometry and computer logic.” An important advantage of our algebraic formulation is that it leads to a useful anisotropic generalization that is relatively easy to compute. To our knowledge, this work is the first reported application of the bin-averaging approach to anisotropic turbulence.

**The problem:**

The integral to be computed is

$$\int_{k_{<}}^{k_{>}} k dk \int_{\alpha_{<}}^{\alpha_{>}} d\alpha \int_{p_{<}}^{p_{>}} p dp \int_{\beta_{<}}^{\beta_{>}} d\beta \int_{q_{<}}^{q_{>}} q dq \int_{\gamma_{<}}^{\gamma_{>}} d\gamma \delta(\mathbf{k}+\mathbf{p}+\mathbf{q}) f(\mathbf{k}, \mathbf{p}, \mathbf{q}), \quad (\text{IV.6})$$

where  $\alpha$ ,  $\beta$ , and  $\gamma$  are the angles of  $\mathbf{k}$ ,  $\mathbf{p}$ , and  $\mathbf{q}$  respectively.

**Analysis:**

Evaluation of the innermost two integrals of Eq. (IV.6) yields

$$\begin{aligned} & \int_{k_{<}}^{k_{>}} k dk \int_0^{\Delta\alpha} d\bar{\alpha} \int_{p_{<}}^{p_{>}} p dp \int_0^{\Delta\beta} d\bar{\beta} [\text{H}(q_{>} - |\mathbf{k} + \mathbf{p}|) - \text{H}(q_{<} - |\mathbf{k} + \mathbf{p}|)] \\ & \times [\text{H}(\gamma_{>} - \text{Arg}(-\mathbf{k} - \mathbf{p})) - \text{H}(\gamma_{<} - \text{Arg}(-\mathbf{k} - \mathbf{p}))] f(\mathbf{k}, \mathbf{p}, -\mathbf{k} - \mathbf{p}), \end{aligned}$$

where we have written  $\bar{\alpha} \doteq \alpha - \alpha_{<}$  and  $\bar{\beta} \doteq \beta - \beta_{<}$ , with  $\Delta\alpha \doteq \alpha_{>} - \alpha_{<}$  and  $\Delta\beta \doteq \beta_{>} - \beta_{<}$ . Here,  $\text{Arg}$  denotes the principal branch, taken in the interval  $[0, 2\pi)$ .

Without loss of generality, we order the variables so that  $\Delta\beta \geq \Delta\alpha$ . By changing these angular variables to  $\bar{r} \doteq \bar{\beta} - \bar{\alpha}$  and  $\bar{\alpha}$  and by denoting  $f(k, p, \bar{r}, \bar{\alpha}) \doteq f(\mathbf{k}, \mathbf{p}, -\mathbf{k} - \mathbf{p})$ , we may rewrite the integral as

$$\begin{aligned} & \int_{p_{<}}^{p_{>}} p dp \int_{k_{<}}^{k_{>}} k dk \int_{-\Delta\alpha}^{\Delta\beta} d\bar{r} [\text{H}(q_{>} - |\mathbf{k} + \mathbf{p}|) - \text{H}(q_{<} - |\mathbf{k} + \mathbf{p}|)] \\ & \times \int_{\bar{\alpha}_{<}(\bar{r})}^{\bar{\alpha}_{>}(\bar{r})} d\bar{\alpha} [\text{H}(\gamma_{>} - \text{Arg}(-\mathbf{k} - \mathbf{p})) - \text{H}(\gamma_{<} - \text{Arg}(-\mathbf{k} - \mathbf{p}))] f(k, p, \bar{r}, \bar{\alpha}). \quad (\text{IV.7}) \end{aligned}$$

Here,

$$\begin{aligned} \bar{\alpha}_{<}(\bar{r}) & \doteq \begin{cases} 0 & \text{if } \bar{r} \geq 0, \\ -\bar{r} & \text{if } \bar{r} < 0, \end{cases} \\ \bar{\alpha}_{>}(\bar{r}) & \doteq \begin{cases} \Delta\beta - \bar{r} & \text{if } \bar{r} \geq \Delta\beta - \Delta\alpha, \\ \Delta\alpha & \text{if } \bar{r} < \Delta\beta - \Delta\alpha. \end{cases} \end{aligned}$$

A particular branch of  $\text{Arg}(-\mathbf{k} - \mathbf{p})$  is given by

$$\arg(-\mathbf{k} - \mathbf{p}) = \alpha + \theta,$$

where, in terms of  $r \doteq \beta - \alpha = \bar{r} + \beta_{<} - \alpha_{<}$ ,

$$\theta \doteq \Theta(-k - p \cos r, -p \sin r) \pmod{2\pi}$$

and  $\Theta(x, y)$  is any given branch of the generalized arctangent function<sup>3</sup>:

$$\Theta(x, y) \doteq \begin{cases} \arctan \frac{y}{x} & \text{if } x > 0, \\ \pi + \arctan \frac{y}{x} & \text{if } x < 0, \\ 0 & \text{if } x = 0. \end{cases}$$

Thus one branch of the condition

$$\gamma_{<} \leq \arg(-\mathbf{k} - \mathbf{p}) \leq \gamma_{>}$$

can be written

$$\gamma_{<} - \alpha_{<} - \theta \leq \bar{\alpha} \leq \gamma_{>} - \alpha_{<} - \theta.$$

This enables us to do the  $\bar{\alpha}$  integration immediately:

$$\begin{aligned} h(k, p, \bar{r}) &\doteq \int_{\bar{\alpha}_{<}(\bar{r})}^{\bar{\alpha}_{>}(\bar{r})} d\bar{\alpha} [\mathrm{H}(\gamma_{>} - \mathrm{Arg}(-\mathbf{k} - \mathbf{p})) - \mathrm{H}(\gamma_{<} - \mathrm{Arg}(-\mathbf{k} - \mathbf{p}))] f(k, p, \bar{r}, \bar{\alpha}) \\ &= I[\min(\bar{\alpha}_{>}, \gamma_{>} - \alpha_{<} - \theta), \max(\bar{\alpha}_{<}, \gamma_{<} - \alpha_{<} - \theta)] \\ &\quad + I[\min(\bar{\alpha}_{>}, \gamma_{>} - \alpha_{<} - \theta + 2\pi), \max(\bar{\alpha}_{<}, \gamma_{<} - \alpha_{<} - \theta + 2\pi)] \\ &\quad + I[\min(\bar{\alpha}_{>}, \gamma_{>} - \alpha_{<} - \theta + 4\pi), \max(\bar{\alpha}_{<}, \gamma_{<} - \alpha_{<} - \theta + 4\pi)], \end{aligned} \quad (\text{IV.8})$$

where  $I[b, a] \doteq H(b - a) [g(k, p, \bar{r}, b) - g(k, p, \bar{r}, a)]$  and

$$g(k, p, \bar{r}, a) \doteq \int_0^a d\bar{\alpha} f(k, p, \bar{r}, \bar{\alpha}).$$

The latter integral is computed analytically and coded as a subroutine.<sup>4</sup> The  $2\pi$  and  $4\pi$  offsets<sup>5</sup> of the second and third terms of  $h(k, p, \bar{r})$  correctly give us the principal branch ( $\mathrm{Arg}$ ), assuming that all angular variables here are taken between 0 and  $2\pi$ . The problem has thus been reduced to a three-dimensional integration over  $p$ ,  $k$ , and  $\bar{r}$ .

Next, we change the Heaviside restrictions on  $|\mathbf{k} + \mathbf{p}|$  into restrictions on the limits of the  $\bar{r}$  integration. This eliminates unnecessary integration when the  $\bar{r}$  integrand is zero due to the magnitude restriction, which greatly speeds up the calculation. This is done as follows. For fixed  $p$  and  $k$ , solve the equations

$$\begin{aligned} q_{>}^2 &= k^2 + p^2 + 2kp \cos r_{2,3}, \\ q_{<}^2 &= k^2 + p^2 + 2kp \cos r_{1,4}, \end{aligned} \quad (\text{IV.9})$$

<sup>3</sup>The value of  $\Theta$  at the singular points  $(0, y)$  is arbitrary since this corresponds to points in the integration that precisely satisfy  $k = p \cos r$ , which may be removed since the integrand is bounded.

<sup>4</sup>For example, in the case where  $f$  is isotropic we obtain  $g(k, p, \bar{r}, a) = af(k, p, \bar{r}, 0)$ .

<sup>5</sup>These offsets arise from the observation that if  $\alpha \in [0, 2\pi]$  and  $\beta \in [0, 2\pi]$ , then  $\alpha - \beta \in [-2\pi, 2\pi]$ , etc.

for the  $r$ 's, taking them to lie in  $[0, 2\pi]$ . The magnitude restriction is then equivalent to the requirement that the principal angle of  $r \doteq \beta - \alpha$  lie in  $[r_1, r_2]$  or  $[r_3, r_4]$ . Next, compute  $\bar{r}_{1,2} = r_{1,2} - r_{\text{off}}$ , where  $r_{\text{off}}$  is the principal angle of  $\beta_{<} - \alpha_{<}$ . Adjust  $\bar{r}_1$  and  $\bar{r}_2$  to lie between  $[0, 2\pi]$  if possible. (Otherwise, if  $\bar{r}_1 < 0 < \bar{r}_2$ , split the interval  $[\bar{r}_1, \bar{r}_2]$  into  $[0, \bar{r}_2]$  and  $[2\pi + \bar{r}_1, 2\pi]$  and do the following procedure for each sub-interval.) The  $\bar{r}$  integral becomes

$$\left( \int_{\max(\Delta\beta - \Delta\alpha, \bar{r}_1)}^{\min(\Delta\beta, \bar{r}_2)} d\bar{r} + \int_{\max(0, \bar{r}_1)}^{\min(\Delta\beta - \Delta\alpha, \bar{r}_2)} d\bar{r} + \int_{\max(-\Delta\alpha, \bar{r}_1 - 2\pi)}^{\min(0, \bar{r}_2 - 2\pi)} d\bar{r} \right) h(k, p, \bar{r}). \quad (\text{IV.10})$$

Repeat this procedure for the  $[\bar{r}_3, \bar{r}_4]$  interval as well. To get the final answer to Eq. (IV.6), the sum of these two results is then multiplied by  $kp$  and integrated over  $k$  and  $p$ .

### Numerical Considerations:

Efficient numerical integration requires some analytical knowledge of the behaviour of the integrand to determine the appropriate sampling resolution. An adaptive Simpson method is used to achieve a specified relative accuracy. To work correctly, the integration routine needs a resolution parameter  $\Delta_{\text{max}}$ , which is set to the size of the smallest “structure” in the integrand.

There is a resolution requirement associated with the angular restriction in Eq. (IV.10). To circumvent this problem we make the stipulation, without loss of generality, that  $\Delta\gamma \doteq \gamma_{>} - \gamma_{<}$  is larger than  $\Delta\beta$  (and hence also  $\Delta\alpha$ ). Then if  $\text{Arg}(-\mathbf{k} - \mathbf{p})$  lies outside the interval  $[\gamma_{<}, \gamma_{>}]$  for both the endpoint evaluations of the  $\bar{r}$  integral, it will for every interior point as well, so the integral will vanish. Otherwise, the integrand will not vanish for at least one of the endpoints and there will be no problem with resolution, as the desired structure has been “captured”. With the above ordering, setting  $\Delta_{\text{max}}$  for the  $\bar{r}$  integral to  $\pi$  is sufficient to guarantee that the code samples the integrand with a fine enough resolution.

It is not hard to show that the size of the smallest structure for the  $p$  and  $k$  integrals is about  $q_{>} - q_{<}$ . To see this, consider the extreme cases of the magnitude restriction  $q_{<} \leq |\mathbf{k} + \mathbf{p}| \leq q_{>}$ :

$$\begin{aligned} p_{2,3} &= -k \cos r \pm \sqrt{q_{>}^2 - k^2 \sin^2 r}, \\ p_{1,4} &= -k \cos r \pm \sqrt{q_{<}^2 - k^2 \sin^2 r}. \end{aligned}$$

Note that  $p_3 \leq p_4 \leq p_1 \leq p_2$  and the integral is nonzero only on the intervals  $[p_3, p_4]$  and  $[p_1, p_2]$ . The resolution is determined by the minimum value, over  $k$  and  $r$ , of

$$\begin{aligned} \Delta p &\doteq p_4 - p_3 = p_2 - p_1 \\ &\geq q_{>} - q_{<}. \end{aligned}$$

The last inequality follows from the monotonicity of the function

$$f(x) \doteq \sqrt{x^2 - a^2} - x$$

for positive  $x$ . It is thus found that setting  $\Delta_{\max}$  to less than  $\frac{1}{2}(q_{>} - q_{<})$  eliminates any resolution problems.<sup>6</sup> In the code  $\Delta_{\max}$  is set to  $0.4(q_{>} - q_{<})$  for both the  $p$  and  $k$  integrals.

### Testing the algorithm:

The above algorithm was subjected to exhaustive tests that included comparison with known analytical solutions for certain anisotropic special cases. In addition, certain nontrivial consistency properties were checked. For example, the summation theorem for integrals was verified for thousands of random subdivisions of the partitions to ensure that no small structures in the integrand were being ignored.

We present in Table IV.1 our results for the two-dimensional isotropic problem that is discussed on pg. 139 and in Appendix G. Complete agreement was obtained with Table 1 of Leith and Kraichnan [1972]. In Table IV.2, we tabulate the exact values (accurate to the given number of digits) for the subsidiary correction factors that Leith and Kraichnan computed approximately and tabulated in their Table 2. Finally, we compare these correction factors to the true correction, tabulated in Table IV.3, that results from averaging both factors  $(\hat{\mathbf{z}} \cdot \mathbf{p} \times \mathbf{q})^2$  (as is done in the present work). The tabulated values are normalized in the same way as Leith's factors to facilitate comparison:

$$\bar{s}_{\text{actual}} \doteq \frac{\max(k_c, p_c, q_c)}{2k_c^2 p_c^2 q_c^2} \frac{\langle |pq \sin(\beta - \gamma)|^2 \rangle}{\langle |\sin(\beta - \gamma)| / 2k \rangle},$$

where  $k_c$ ,  $p_c$ , and  $q_c$  are the geometric means of the bin boundaries.

We see that there are substantial differences between Leith's correction factors and the true correction. All of these results were obtained merely by specifying different forms for the function  $f$  in the general anisotropic algorithm just described.

## IV.C Bin-coupling coefficients

Let us now discuss the computation of the bin-coupling coefficients that characterize the interaction of the sample wavenumber modes. As previously discussed,

---

<sup>6</sup>The factor of  $\frac{1}{2}$  is needed since the structure could be split equally among two adjacent intervals used in the numerical integration.

| j  | i = 0   | i = 1   | i = 2   | i = 3   | i = 4   |
|----|---------|---------|---------|---------|---------|
| 0  | 1.00000 | 1.00000 | 1.00000 | 1.00000 | 1.00000 |
| 1  | 1.00000 | 1.00000 | 1.00000 | 1.00000 | 1.00000 |
| 2  | 1.00000 | 1.00000 | 1.00000 | 1.00000 | 1.00000 |
| 3  | 1.00000 | 1.00000 | 1.00000 | 1.00000 | 0.92992 |
| 4  | 1.00000 | 1.00000 | 1.00000 | 0.92993 | 0.50000 |
| 5  | 1.00000 | 1.00000 | 0.98063 | 0.58651 | 0.09870 |
| 6  | 1.00000 | 1.00000 | 0.81399 | 0.21638 | 0.00047 |
| 7  | 1.00000 | 0.98693 | 0.52548 | 0.03106 | 0.00000 |
| 8  | 1.00000 | 0.90432 | 0.26284 | 0.00001 | 0.00000 |
| 9  | 1.00000 | 0.76577 | 0.10220 | 0.00000 | 0.00000 |
| 10 | 0.99946 | 0.60070 | 0.02521 | 0.00000 | 0.00000 |
| 11 | 0.97855 | 0.43976 | 0.00129 | 0.00000 | 0.00000 |
| 12 | 0.92205 | 0.31172 | 0.00000 | 0.00000 | 0.00000 |
| 13 | 0.84550 | 0.22042 | 0.00000 | 0.00000 | 0.00000 |
| 14 | 0.76057 | 0.15586 | 0.00000 | 0.00000 | 0.00000 |
| 15 | 0.67463 | 0.11021 | 0.00000 | 0.00000 | 0.00000 |

Table IV.1: Triangle volume fractions  $\bar{v}(i, j)$  for the isotropic problem of Leith and Kraichnan.

we assume, for computational efficiency, that the mode-coupling coefficients may be decomposed as

$$M_{\mathbf{k}\mathbf{p}\mathbf{q}} = S_{k\mathbf{p}\mathbf{q}} A_{\mathbf{k}\mathbf{p}\mathbf{q}},$$

where the antisymmetric factor  $A_{\mathbf{k}\mathbf{p}\mathbf{q}}$  is assumed to vary relatively *slowly* over each bin and the remaining factor  $S_{k\mathbf{p}\mathbf{q}}$  is a completely symmetric function of the wavenumber magnitudes only. For all of the problems in this work,  $S_{k\mathbf{p}\mathbf{q}}$  will have a homogenous scaling with degree (say)  $\lambda$ . This is the only part of the mode-coupling coefficients that is bin-averaged. The antisymmetric factor is evaluated outside the integral along with the statistical variables.

The properties of  $S_{k\mathbf{p}\mathbf{q}}$  greatly facilitate the computation of the effective mode-coupling coefficients. The general problem

$$\langle |S_{k\mathbf{p}\mathbf{q}}|^2 \rangle_{\mathbf{k}\mathbf{p}\mathbf{q}} \doteq \int_{k_{<}}^{k_{>}} k dk \int_{\alpha_{<}}^{\alpha_{>}} d\alpha \int_{p_{<}}^{p_{>}} p dp \int_{\beta_{<}}^{\beta_{>}} d\beta \int_{q_{<}}^{q_{>}} q dq \int_{\gamma_{<}}^{\gamma_{>}} d\gamma \delta(\mathbf{k} + \mathbf{p} + \mathbf{q}) |S_{k\mathbf{p}\mathbf{q}}|^2$$

then becomes

$$\begin{aligned} \langle |S_{k\mathbf{p}\mathbf{q}}|^2 \rangle_{\mathbf{k}\mathbf{p}\mathbf{q}} &= k_{<}^{4+2\text{Re}\lambda} \int_1^{k_{>}/k_{<}} \bar{k} d\bar{k} \int_0^{\alpha_{>}-\alpha_{<}} d\bar{\alpha} \int_{p_{<}/k_{<}}^{p_{>}/k_{<}} \bar{p} d\bar{p} \int_{\beta_{<}-\alpha_{<}}^{\beta_{>}-\alpha_{<}} d\bar{\beta} \\ &\quad \times \int_{q_{<}/k_{<}}^{q_{>}/k_{<}} \bar{q} d\bar{q} \int_{\gamma_{<}-\alpha_{<}}^{\gamma_{>}-\alpha_{<}} d\bar{\gamma} \delta(\bar{\mathbf{k}} + \bar{\mathbf{p}} + \bar{\mathbf{q}}) |S_{\bar{k}\bar{p}\bar{q}}|^2. \end{aligned} \quad (\text{IV.11})$$

| j  | i = 0   | i = 1   | i = 2   | i = 3   | i = 4   |
|----|---------|---------|---------|---------|---------|
| 0  | 0.90122 | 0.93055 | 0.95817 | 0.97605 | 0.98684 |
| 1  | 0.93055 | 0.95266 | 0.97966 | 0.99042 | 0.98662 |
| 2  | 0.95817 | 0.97966 | 0.99231 | 0.97190 | 0.91188 |
| 3  | 0.97605 | 0.99042 | 0.97190 | 0.88413 | 0.71825 |
| 4  | 0.98684 | 0.98662 | 0.91188 | 0.71826 | 0.54023 |
| 5  | 0.99208 | 0.96716 | 0.79870 | 0.57577 | 0.37584 |
| 6  | 0.99243 | 0.92707 | 0.68400 | 0.45424 | 0.15936 |
| 7  | 0.98787 | 0.86163 | 0.59663 | 0.32461 | 0.00000 |
| 8  | 0.97759 | 0.80176 | 0.52781 | 0.09375 | 0.00000 |
| 9  | 0.95960 | 0.75361 | 0.45663 | 0.00000 | 0.00000 |
| 10 | 0.92972 | 0.71766 | 0.35971 | 0.00000 | 0.00000 |
| 11 | 0.89513 | 0.69953 | 0.22445 | 0.00000 | 0.00000 |
| 12 | 0.87059 | 0.69337 | 0.00000 | 0.00000 | 0.00000 |
| 13 | 0.85292 | 0.68912 | 0.00000 | 0.00000 | 0.00000 |
| 14 | 0.83971 | 0.68561 | 0.00000 | 0.00000 | 0.00000 |
| 15 | 0.82952 | 0.68262 | 0.00000 | 0.00000 | 0.00000 |

Table IV.2: Exact values  $\bar{s}_{\text{exact}}(i, j)$  of the subsidiary correction factors used by Leith and Kraichnan.

| j  | i = 0   | i = 1   | i = 2   | i = 3   | i = 4   |
|----|---------|---------|---------|---------|---------|
| 0  | 0.88314 | 0.92489 | 0.95247 | 0.97037 | 0.98126 |
| 1  | 0.92489 | 0.97450 | 1.00253 | 1.01406 | 1.01089 |
| 2  | 0.95247 | 1.00253 | 1.01631 | 0.99663 | 0.93723 |
| 3  | 0.97037 | 1.01406 | 0.99663 | 0.90954 | 0.74714 |
| 4  | 0.98126 | 1.01089 | 0.93723 | 0.74712 | 0.57006 |
| 5  | 0.98666 | 0.99207 | 0.82633 | 0.60552 | 0.42501 |
| 6  | 0.98727 | 0.95284 | 0.71515 | 0.49469 | 0.20178 |
| 7  | 0.98312 | 0.88969 | 0.62893 | 0.37976 | 0.00000 |
| 8  | 0.97344 | 0.83371 | 0.56847 | 0.12056 | 0.00000 |
| 9  | 0.95639 | 0.78874 | 0.50548 | 0.00000 | 0.00000 |
| 10 | 0.92813 | 0.75482 | 0.41329 | 0.00000 | 0.00000 |
| 11 | 0.89641 | 0.74041 | 0.27676 | 0.00000 | 0.00000 |
| 12 | 0.87510 | 0.73981 | 0.00000 | 0.00000 | 0.00000 |
| 13 | 0.86052 | 0.74033 | 0.00000 | 0.00000 | 0.00000 |
| 14 | 0.85011 | 0.74069 | 0.00000 | 0.00000 | 0.00000 |
| 15 | 0.84238 | 0.74094 | 0.00000 | 0.00000 | 0.00000 |

Table IV.3: True corrections  $\bar{s}_{\text{actual}}(i, j)$  obtained by properly averaging both  $(\hat{\mathbf{z}} \cdot \mathbf{p} \times \mathbf{q})^2$  factors over each bin.

If we employ the logarithmic/linear polar partition already introduced, in which the ratio  $\delta \doteq k_{>}/k_{<}$  of successive radial bin boundaries and the difference  $\Delta\theta \doteq \alpha_{>} - \alpha_{<}$  of successive angular bin boundaries are constant, then Eq. (IV.3) depends on only 4 (not 12) parameters (e.g., the set  $\{p_{<}, \beta_{<}, q_{<}, \gamma_{<}\}$ ). Moreover, the cyclic symmetry of the integrand is used to further reduce the number of combinations that need to be explicitly computed. Many of the bin-coupling coefficients will vanish because no wavenumbers in the corresponding bins satisfy the triangle relation. Efficient tests are built into the algorithm used to compute Eq. (IV.6) to identify these cases with a minimum of computational effort.

### IV.C.1 Self-coupling effects

Recall that in the isotropic bin-averaging procedure used by Leith and Kraichnan [1972] only one of the symmetric mode-coupling factors,

$$f(\mathbf{k}, \mathbf{p}, \mathbf{q}) = \left(\frac{1}{2k}\right) |\sin(\beta - \gamma)|,$$

was actually averaged over the bins. However, as mentioned previously, the authors were concerned by the fact that the other rapidly varying  $|\sin(\beta - \gamma)|$  factor was not included in the integrand. Instead, it was evaluated at the central wavenumbers.

In this work we average both of these factors as one would desire. However, the mode-coupling coefficients also have slowly varying asymmetric factors, such as the  $(q^2 - p^2)/(1 + k^2)$  factors of the Hasegawa-Mima problem. As in the work of Leith and Kraichnan, these factors are evaluated only at the central wavenumbers. Since our weight factor algorithm can be used to integrate any function  $f$ , this approximation could, in principle, be avoided. However, our experience indicates that for realistic bin configurations the computational overhead for the entire set of weight factors can be unreasonable unless one can exploit homogeneous scaling properties and rotational invariance of  $f$ . Moreover, care must be taken that the conservation laws are not violated on a triad-by-triad basis if the asymmetric factors are bin-averaged. In contrast, since the symmetric factors remain symmetric after bin averaging, the associated conservation laws are preserved under the averaging operation.

For the long-wavelength Hasegawa-Mima problem, where  $M_{\mathbf{k}\mathbf{p}\mathbf{q}} \doteq (q^2 - p^2)(\hat{\mathbf{z}} \cdot \mathbf{p} \times \mathbf{q})$ , let us illustrate the difficulties that can occur if the  $(q^2 - p^2)$  factor is included in the average. To calculate the mass operator term we need to compute quantities like

$$\left\langle (q^2 - p^2)(k^2 - q^2) \right\rangle_S \doteq \left\langle (q^2 - p^2)(k^2 - q^2) |S_{k\mathbf{p}\mathbf{q}}|^2 \right\rangle_{\mathbf{k}\mathbf{p}\mathbf{q}}.$$

Suppose we want to calculate the average of the expression

$$(M_{\mathbf{k}\mathbf{p}\mathbf{q}} + M_{\mathbf{p}\mathbf{q}\mathbf{k}} + M_{\mathbf{q}\mathbf{k}\mathbf{p}})M_{\mathbf{p}\mathbf{q}\mathbf{k}}^*,$$

which must vanish if energy (for which  $\sigma_{\mathbf{k}} = 1$ ) is to be conserved. If the averaging operation is implemented accurately, so that it is linear, there is no difficulty with energy conservation:

$$\langle (q^2 - p^2)(k^2 - q^2) \rangle_S + \langle (k^2 - q^2)(k^2 - q^2) \rangle_S + \langle (p^2 - k^2)(k^2 - q^2) \rangle_S = \langle 0 \rangle_S = 0.$$

However, the enstrophy relation (for which  $\sigma_{\mathbf{k}} = k^2$ )

$$(k^2 M_{\mathbf{k}\mathbf{p}\mathbf{q}} + p^2 M_{\mathbf{p}\mathbf{q}\mathbf{k}} + q^2 M_{\mathbf{q}\mathbf{k}\mathbf{p}}) M_{\mathbf{p}\mathbf{q}\mathbf{k}}^* \quad (\text{IV.12})$$

is more difficult to implement conservatively. In terms of the central wavenumbers  $k_c$ ,  $p_c$ , and  $q_c$ , one discovers that

$$k_c^2 \langle (q^2 - p^2)(k^2 - q^2) \rangle_S + p_c^2 \langle (k^2 - q^2)(k^2 - q^2) \rangle_S + q_c^2 \langle (p^2 - k^2)(k^2 - q^2) \rangle_S \quad (\text{IV.13})$$

does not vanish in general. This should not be surprising since the coefficients  $k^2$  in Eq. (IV.12) have effectively been moved outside of the average in Eq. (IV.13). One could imagine replacing  $k_c$  with  $\langle k \rangle_S$  or  $\langle k^2 \rangle_S^{1/2}$  but these also do not lead to enstrophy conservation. The difficulty here cannot be circumvented even by redefining all of the central wavenumbers  $\{k_c\}$  to some yet unspecified but related non-negative numbers  $\{\xi_i\}$ .

For example, suppose we have a system with wavenumber bins labeled by the integers  $0, 1, 2, \dots$ . Let us define the following bin-averaged quantities in terms of integers  $l, m, n$ :

$$s_{lmn} \doteq \langle M_{\mathbf{k}\mathbf{p}\mathbf{q}} M_{\mathbf{p}\mathbf{q}\mathbf{k}}^* \rangle_{lmn} = \langle (q^2 - p^2)(k^2 - q^2) |S_{kpq}|^2 \rangle_{lmn},$$

$$n_{lmn} \doteq \langle |M_{\mathbf{k}\mathbf{p}\mathbf{q}}|^2 \rangle_{lmn} = \langle (q^2 - p^2)^2 |S_{kpq}|^2 \rangle_{lmn}.$$

On the right-hand side we indicate the values for the long-wavelength Hasegawa-Mima equation. By using Eqs. (I.18) and (I.19) (for  $\sigma_{\mathbf{k}} = 1$ ) we deduce the following relations:

$$s_{mln}^* = s_{lmn},$$

$$n_{lmn}^* = n_{lmn},$$

$$s_{lmn} + n_{mnl} + s_{nml} = 0,$$

$$s_{lmn} + n_{lmn} + s_{lnm} = 0.$$

The last result is just a combination of the first three and is particularly useful for numerical work. Both  $s_{lmn}$  and  $s_{lnm}$  are required to compute the mass operator in an optimized calculation that introduces the asymmetry  $m \leq n$ . Using this relation, we may then compute  $n_{lmn}$  without doing any further integration (*cf.* 139).

We would also like to satisfy the enstrophy conservation relation

$$\xi_l^2 s_{lmn} + \xi_m^2 n_{mnl} + \xi_n^2 s_{nml} = 0.$$

However, this is not possible in general. For  $l = n = 0$  and  $m = 1$  we obtain the simultaneous equations

$$s_{010} + n_{100} + s_{010} = 0, \quad (\text{IV.14a})$$

$$\xi_0^2 s_{010} + \xi_1^2 n_{100} + \xi_0^2 s_{010} = 0. \quad (\text{IV.14b})$$

These relations imply that

$$(\xi_1^2 - \xi_0^2)n_{100} = 0.$$

Now  $n_{100} = \langle (q^2 - p^2)^2 \rangle_{100}$  is clearly positive; it represents the noise effect introduced by the *self-coupling* of modes that originate in the same bin. Thus we are forced to conclude that the only possible solution to Eqs. (IV.14) occurs for  $\xi_1^2 = \xi_0^2$ . However, this corresponds to a degenerate solution for which the two invariants in Eqs. (IV.14) are no longer distinct. The  $\xi_l$  were introduced as *effective* “central” wavenumbers for each bin and it is essential that they be distinct. We thus see that it is impossible to satisfy both conservation relations Eqs. (IV.14) exactly. Since the bins represent collections of modes and are not physical quantities themselves, this finding is actually quite reasonable. There is no *a priori* reason why the same form of the enstrophy conservation law at the level of individual modes should hold at the level of wavenumber bins.

Provided that one recognizes that no bin-by-bin enstrophy conservation law can exist, it appears from the above discussion that it may still be possible to develop a conservative scheme that averages over the full mode-coupling coefficient. The practical motivation for doing this would be to improve the evaluation of weight factors such as  $n_{100}$ , in which the  $(p^2 - q^2)^2$  factor clearly varies rapidly over the bin labeled by 0. If the  $(p^2 - q^2)^2$  factor is evaluated outside of the average, one obtains the incorrect result of zero. In contrast, the neglected self-coupling effects contribute a small positive contribution to the exact coupling coefficient.

Since only a minority of the bin-coupling coefficients require such precise calculation, it seemed to us at first that a procedure that identified these cases and then performed the necessary computations would greatly increase the overall accuracy of our implementation. However, after much effort went into the development of such a procedure, it eventually became apparent that the extra computational cost far outweighed the benefits. Our experience has indicated that it is much better to model such self-coupling effects simply by increasing the number of bins, thereby reducing the relative error introduced by evaluating the asymmetric factors outside the integral. For this reason, in all of the following work self-coupling effects will be totally neglected and only the symmetric part of the mode-coupling coefficient will be averaged.

## IV.C.2 Multiple fields

The appropriate bin-coupling coefficients for multiple-field problems are

$$s^{\alpha}_{\beta\gamma\bar{\alpha}\bar{\gamma}} \doteq \left\langle M^{\alpha}_{\beta\gamma} M^{\bar{\beta}}_{\bar{\gamma}\bar{\alpha}} \right\rangle_{\mathbf{k}\mathbf{p}\mathbf{q}},$$

$$n^{\alpha}_{\beta\gamma\bar{\beta}\bar{\gamma}} \doteq \left\langle M^{\alpha}_{\beta\gamma} M^{\bar{\alpha}}_{\bar{\beta}\bar{\gamma}} \right\rangle_{\mathbf{k}\mathbf{p}\mathbf{q}},$$

where the wavenumber indices embedded in the augmented species indices of the left-hand side are interpreted as *central* wavenumbers.

These quantities satisfy the symmetries

$$s^{\beta}_{\alpha\gamma\bar{\alpha}\bar{\gamma}} = s^{\bar{\alpha}}_{\bar{\beta}\bar{\gamma}\alpha\gamma},$$

$$n^{\alpha}_{\beta\gamma\bar{\beta}\bar{\gamma}} = n^{\bar{\alpha}}_{\bar{\beta}\bar{\gamma}\alpha\beta\gamma},$$

$$s^{\alpha}_{\beta\gamma\bar{\alpha}\bar{\gamma}} + n^{\beta}_{\gamma\alpha\bar{\beta}\bar{\alpha}} + s^{\gamma}_{\beta\alpha\bar{\gamma}\bar{\alpha}} = 0,$$

$$s^{\alpha}_{\beta\gamma\bar{\alpha}\bar{\gamma}} + n^{\alpha}_{\beta\gamma\bar{\beta}\bar{\gamma}} + s^{\alpha}_{\gamma\beta\bar{\alpha}\bar{\beta}} = 0.$$

Again, the last result is the most useful one for numerical computation of the bin-coupling coefficients.

## IV.D Numerical code

The code DIA [Krommes and Bowman 1988, Bowman and Krommes 1988] is a multipurpose code developed for a wide class of physics problems. It is designed around a general kernel that implements the DIA and the DIA-based Markovian closures developed in Chapter III for the generic system described by Eq. (I.17). The code may be tailored to particular physics problems by the specification of routines that compute the coefficients appearing in our fundamental equation, Eq. (I.17) or (for multiple-field problems) Eq. (II.25). Let us now describe the particular time-stepping algorithm that is used for each closure.

### IV.D.1 Predictor-corrector algorithm

The basic time-stepping algorithm is a predictor-corrector scheme that is formally accurate to second order in the time step  $\Delta t$ . For the DIA, we employ the same scheme used by Kraichnan [1964a] in his original computations for isotropic turbulence. This semi-implicit method guarantees exact energy conservation and preserves the inviscid equilibrium solutions that are discussed in Chapter VI. In addition, if the nonlinearity is turned off, the algorithm solves linear theory exactly.

This property results from the use of the exact linear Green's function. This algorithm is used to evolve the energy in all three closures and also to compute the DIA response function. A related scheme is used to evolve the quantity  $\Theta_{\mathbf{k}\mathbf{p}\mathbf{q}}$  of the RMC.

For the realizable EDQNM, a superior algorithm is presented for the discrete time evolution of the triad interaction time  $\theta_{\mathbf{k}\mathbf{p}\mathbf{q}}$ . It exploits the Markovian form of the evolution equation in a manner that numerically guarantees the positivity of the energy spectrum. The use of an algorithm that does not corrupt realizability seems important since much effort went into the theoretical development of realizable Markovian closures; we have found that only a slight violation of realizability can result in highly unstable behaviour (*cf.* Fig. III.1). The difference between this algorithm and the one used for the energy equation appears only above second order. While the  $C_{\mathbf{k}}$  predictor and corrector can also be written in an explicitly positive-semidefinite form, the resulting time-stepping scheme no longer solves linear theory exactly.<sup>7</sup>

### DIA:

We now describe Kraichnan's predictor-corrector algorithm, which is the one used in the DIA to evolve both  $C_{\mathbf{k}}$  and  $R_{\mathbf{k}}$ . Both of Eqs. (I.38) are of the form

$$\frac{\partial C}{\partial t} + \nu C = \mathcal{S}(t) \equiv \mathcal{S}(t, \{C(t)\}),$$

where  $\mathcal{S}$  is a source term that is a functional of the statistical variables. Here,  $C$  represents  $C_{\mathbf{k}}$  and/or  $R_{\mathbf{k}}$ .

For the DIA, we use the following basic predictor-corrector scheme:

$$\begin{aligned} \widehat{C}(t+\Delta t) &= e^{-\nu\Delta t}C(t) + \Delta t\mathcal{S}(t), \\ C(t+\Delta t) &= e^{-\nu\Delta t}C(t) + \frac{1}{2}\Delta t \left[ e^{-\nu\Delta t}\mathcal{S}(t, \{C(t)\}) + \mathcal{S}(t+\Delta t, \{\widehat{C}(t+\Delta t)\}) \right]. \end{aligned}$$

This is derived as follows. The exact integral that steps forward one  $\Delta t$  is

$$C(t+\Delta t) = e^{-\nu\Delta t}C(t) + \int_t^{t+\Delta t} d\bar{t} e^{-\nu(t+\Delta t-\bar{t})}\mathcal{S}(\bar{t}).$$

Let us write

$$\bar{\tau} \doteq t - \bar{t}.$$

---

<sup>7</sup>We have also found an explicitly positive-semidefinite scheme that solves linear theory exactly, but unfortunately it no longer conserves the energy exactly.

Then

$$C(t+\Delta t) = e^{-\nu\Delta t}C(t) + e^{-\nu\Delta t} \int_{-\Delta t}^0 d\bar{\tau} e^{-\nu\bar{\tau}} \mathcal{S}(t-\bar{\tau}).$$

Now

$$\begin{aligned} \int_{-\Delta t}^0 d\bar{\tau} e^{-\nu\bar{\tau}} \mathcal{S}(t-\bar{\tau}) &\approx \int_{-\Delta t}^0 d\bar{\tau} (1 - \nu\bar{\tau}) [\mathcal{S}(t) - \bar{\tau}\mathcal{S}'(t)] \\ &= (\bar{\tau} - \frac{1}{2}\nu\bar{\tau}^2) \Big|_{-\Delta t}^0 \mathcal{S}(t) - \frac{1}{2} \bar{\tau}^2 \Big|_{-\Delta t}^0 \mathcal{S}' \\ &= (\Delta t + \frac{1}{2}\nu\Delta t^2)\mathcal{S}(t) + \frac{1}{2}\Delta t^2\mathcal{S}'. \end{aligned}$$

This whole expression remains correct through  $\mathcal{O}(\Delta t^2)$  if we approximate  $\mathcal{S}' \approx [\mathcal{S}(t+\Delta t) - \mathcal{S}(t)]/\Delta t$ . If we multiply by the required  $\exp(-\nu\Delta t) \approx 1 - \nu\Delta t$  and keep terms only through second order, the correction term becomes

$$\begin{aligned} (\Delta t - \frac{1}{2}\nu\Delta t^2)\mathcal{S}(t) + \frac{1}{2}\Delta t^2 \left[ \frac{\mathcal{S}(t+\Delta t) - \mathcal{S}(t)}{\Delta t} \right] &= \frac{1}{2}\Delta t [(1 - \nu\Delta t)\mathcal{S}(t) + \mathcal{S}(t+\Delta t)] \\ &\approx \frac{1}{2}\Delta t [e^{-\nu\Delta t}\mathcal{S}(t) + \mathcal{S}(t+\Delta t)]. \end{aligned}$$

Thus, we arrive at

$$C(t+\Delta t) \approx e^{-\nu\Delta t}C(t) + \frac{1}{2}\Delta t [e^{-\nu\Delta t}\mathcal{S}(t) + \mathcal{S}(t+\Delta t)]. \quad (\text{IV.15})$$

To get a first approximation to the  $C$  dependence of  $\mathcal{S}(t+\Delta t)$ , we use

$$\hat{C}(t+\Delta t) \approx [e^{-\nu\Delta t}C(t)] + \Delta t [\mathcal{S}(t)]. \quad (\text{IV.16})$$

This scheme is accurate through  $\mathcal{O}(\Delta t^2)$  [errors are  $\mathcal{O}(\Delta t^3)$ ] and handles linear theory exactly. By linear theory, we mean the situation where the linear coefficient is constant and appears wholly in  $\nu$  and no nonlinear terms are present, so that  $\mathcal{S}=0$ . With appropriate care, one can obtain the corresponding multiple-field formulation by replacing the factor  $e^{-\nu\Delta t}$  with the linear Green's matrix. Thus, for the unequal-time equations, the factor  $e^{-\nu\Delta t}$  in the above general discussion is replaced by the matrix  $e^{-\boldsymbol{\nu}\Delta t}$ ; for the equal-time equations, it is replaced by the premultiplier  $e^{-\boldsymbol{\nu}\Delta t}$  and the postmultiplier  $e^{\boldsymbol{\nu}^\dagger\Delta t}$  (*cf.*

Note that we do not need to advance the equal-time response function since

$$R_{\mathbf{k}}(t, t^-) = 1 \quad \forall t.$$

In the DIA code, it is convenient to change the time variables from  $(t, t')$  to  $(t | \tau)$ , where  $\tau \doteq t - t'$ . In this way, a statistically stationary state depends only on  $\tau$  and not  $t$ . We thus define new statistical functions like  $C(t | \tau) \doteq C(t, t')$ .

The code is designed to integrate the equations in the following schematic order:

$$\begin{array}{cccc}
 \uparrow & \bullet & \bullet & \bullet & \bullet \\
 t & 3 & 4 & 5 & \cdot \\
 & 1 & 2 & \cdot & \cdot \\
 & 0 & \cdot & \cdot & \cdot \\
 & & & & \tau \rightarrow
 \end{array}$$

That is, for each fixed  $t$ , we always evolve the equal-time ( $\tau = 0$ ) equations first; we then successively compute the remaining  $\tau$  values. The small dots represent values that are not computed or stored explicitly; values from this part of the  $(t | \tau)$  plane are computed using the Hermiticity of  $C_{\mathbf{k}}$ . (We never need to compute the response function at these points since it vanishes for  $\tau > t$ .)

### Realizable EDQNM:

In the realizable EDQNM, the above scheme is still used for evolving  $\mathbf{C}_{\mathbf{k}}(t)$  [cf. Eq. (III.35)].

For the  $\boldsymbol{\theta}$  equation, Eq. (III.44), we use a slightly different scheme in which a Green's function is used to write the equation in an explicitly positive-semidefinite form. One disadvantage of this scheme is that it does not handle the linear term  $\nu_{\mathbf{k}}$  exactly. However, since  $\theta_{\mathbf{k}\mathbf{p}\mathbf{q}}$  does not enter linear theory, this is of no real concern.

We wish to solve an equation of the form

$$\frac{\partial}{\partial t} \boldsymbol{\theta} + \boldsymbol{\chi} \boldsymbol{\theta} + \boldsymbol{\theta} \boldsymbol{\chi}^\dagger = \mathbf{Q}. \quad (\text{IV.17})$$

Suppose that we know  $\boldsymbol{\theta}(t_0)$  (for any *fixed*  $t_0$ ) and wish to compute an approximation for  $\boldsymbol{\theta}(t_0 + \Delta t)$ . Let us then define an integrating factor  $\mathbf{P} \doteq \mathbf{P}(t)$  by

$$\frac{\partial}{\partial t} \mathbf{P} = \boldsymbol{\chi} \mathbf{P}, \quad \mathbf{P}(t_0) = \mathbf{1}.$$

We obtain

$$\boldsymbol{\theta}(t) = \mathbf{P}^{-1} \left( \int_0^t d\bar{t} \bar{\mathbf{P}} \bar{\mathbf{Q}} \bar{\mathbf{P}}^\dagger \right) \mathbf{P}^{-1\dagger},$$

where the bars identify quantities that are evaluated at  $\bar{t}$ . Since  $\mathbf{P}(t_0) = \mathbf{1}$ , we may then write

$$\boldsymbol{\theta}(t_0 + \Delta t) = \mathbf{P}^{-1}(t_0 + \Delta t) \left[ \boldsymbol{\theta}(t_0) + \int_{t_0}^{t_0 + \Delta t} d\bar{t} \bar{\mathbf{P}} \bar{\mathbf{Q}} \bar{\mathbf{P}}^\dagger \right] \mathbf{P}^{-1\dagger}(t_0 + \Delta t).$$

Let us use the trapezoidal approximation

$$\int_{t_0}^{t_0 + \Delta t} f(\bar{t}) d\bar{t} = \left[ \frac{f(t_0 + \Delta t) + f(t_0)}{2} \right] \Delta t + \mathcal{O}(\Delta t^3).$$

Application of this approximation leads to

$$\boldsymbol{\theta}(t_0 + \Delta t) = \mathbf{P}^{-1}(t_0 + \Delta t) \left[ \boldsymbol{\theta}(t_0) + \mathbf{Q}(t_0) \frac{\Delta t}{2} + \mathbf{P}(t_0 + \Delta t) \mathbf{Q}(t_0 + \Delta t) \mathbf{P}^\dagger(t_0 + \Delta t) \frac{\Delta t}{2} \right] \mathbf{P}^{-1\dagger}(t_0 + \Delta t),$$

from which we obtain the following time-stepping algorithm, correct to second order in  $\Delta t$ :

$$\boldsymbol{\theta}(t_0 + \Delta t) = \mathbf{P}^{-1}(t_0 + \Delta t) \left[ \boldsymbol{\theta}(t_0) + \mathbf{Q}(t_0) \frac{\Delta t}{2} \right] \mathbf{P}^{-1\dagger}(t_0 + \Delta t) + \mathbf{Q}(t_0 + \Delta t) \frac{\Delta t}{2}.$$

(IV.18)

This algorithm should be compared to Eq. (IV.15), to which it reduces in the scalar limit  $\boldsymbol{\chi} \rightarrow \nu/2$ . The positive-semidefinite nature of  $\boldsymbol{\theta}$  is preserved by Eq. (IV.18), given that  $\mathbf{Q}$  is positive-semidefinite. This is proved by multiplying both sides of Eq. (IV.18) by  $\mathbf{y}^\dagger$  on the left and  $\mathbf{y}$  on the right and then noting that the result is a sum of non-negative numbers.

The predictor and corrector are then obtained upon substitution of approximations for  $\mathbf{P}^{-1}(t_0 + \Delta t)$  that are valid to first and second order, respectively. The latter are computed from the exact equation for the reciprocal of  $\mathbf{P}$ :

$$\frac{\partial \mathbf{P}^{-1}}{\partial t} = -\mathbf{P}^{-1} \frac{\partial \mathbf{P}}{\partial t} \mathbf{P}^{-1} = -\mathbf{P}^{-1} \boldsymbol{\chi},$$

A trapezoidal approximation of

$$\mathbf{P}^{-1}(t_0 + \Delta t) = \mathbf{1} - \int_{t_0}^{t_0 + \Delta t} \bar{\mathbf{P}}^{-1} \bar{\boldsymbol{\chi}} d\bar{t}$$

yields

$$\mathbf{P}^{-1}(t_0 + \Delta t) = \mathbf{1} - \boldsymbol{\chi}(t_0) \frac{\Delta t}{2} - \mathbf{P}^{-1}(t_0 + \Delta t) \boldsymbol{\chi}(t_0 + \Delta t) \frac{\Delta t}{2}.$$

This becomes

$$\mathbf{P}^{-1}(t_0 + \Delta t) \left[ \mathbf{1} + \boldsymbol{\chi}(t_0 + \Delta t) \frac{\Delta t}{2} \right] = \mathbf{1} - \boldsymbol{\chi}(t_0) \frac{\Delta t}{2}$$

or

$$\mathbf{P}^{-1}(t_0 + \Delta t) = \left[ \mathbf{1} - \boldsymbol{\chi}(t_0) \frac{\Delta t}{2} \right] \left[ \mathbf{1} + \boldsymbol{\chi}(t_0 + \Delta t) \frac{\Delta t}{2} \right]^{-1}. \quad (\text{IV.19})$$

The predicted value  $\mathbf{P}_1(t_0 + \Delta t)$  is obtained by substituting in the lowest-order approximation,  $\boldsymbol{\chi}(t_0 + \Delta t) \approx \boldsymbol{\chi}(t_0)$ :

$$\mathbf{P}_1^{-1}(t_0 + \Delta t) = \left[ \mathbf{1} - \boldsymbol{\chi}(t_0) \frac{\Delta t}{2} \right] \left[ \mathbf{1} + \boldsymbol{\chi}(t_0) \frac{\Delta t}{2} \right]^{-1}. \quad (\text{IV.20})$$

This allows one to compute the predicted value  $\chi_1(t_0 + \Delta t)$  to first order in  $\Delta t$ . The corrected value  $\mathbf{P}_2(t_0 + \Delta t)$  is then obtained by substitution of the approximation  $\chi(t_0 + \Delta t) \approx \chi_1(t_0 + \Delta t)$  into Eq. (IV.19):

$$\mathbf{P}_2^{-1}(t_0 + \Delta t) = \left[ \mathbf{1} - \chi(t_0) \frac{\Delta t}{2} \right] \left[ \mathbf{1} + \chi_1(t_0 + \Delta t) \frac{\Delta t}{2} \right]^{-1}. \quad (\text{IV.21})$$

Equations (IV.18), (IV.20), and (IV.21) constitute a complete time-stepping algorithm, accurate through second order in  $\Delta t$ , for any equation having the form of Eq. (IV.17). To determine  $\mathbf{Q}$ , we will also need a procedure for computing the Green's function  $\mathbf{G}$ . Since the evolution equation for  $\mathbf{G}$  is the same as the one obtained for  $\mathbf{P}^{-1}$  upon substitution of  $\frac{1}{2}\boldsymbol{\eta}^h$  for  $\chi$ , the algorithm is based on similarly modified versions of Eqs. (IV.20) and (IV.21).

### Nonrealizable EDQNM:

For comparison purposes, the nonrealizable EDQNM closure is also implemented in the DIA code. We write the  $\boldsymbol{\theta}$  equation for this closure in the form

$$\frac{\partial}{\partial t} \boldsymbol{\theta} + \boldsymbol{\eta}^h \boldsymbol{\theta} = \mathbf{1} - i\boldsymbol{\eta}^a \boldsymbol{\theta}.$$

Note that we evaluate  $\boldsymbol{\eta}^h \boldsymbol{\theta}$  on the left-hand side so that our numerical approximation will preserve the positive-semidefiniteness of  $\boldsymbol{\theta}^h$  *whenever this property holds exactly* (e.g., in the case where  $\boldsymbol{\eta}^a = 0$ ). (In contrast, Kraichnan's DIA predictor-corrector algorithm lumps the entire nonlinear term into the source term on the right-hand side.) We do not include  $\boldsymbol{\eta}^a$  along with  $\boldsymbol{\eta}^h$  on the left-hand side since this is unnecessary for the positive-semidefiniteness of  $\boldsymbol{\theta}^h$  and in fact a large value for  $\nu^a$  could then force the code to use an unreasonably small time step, since we do not use the exact Green's function to evaluate  $\mathbf{P}$ .

Given  $\boldsymbol{\theta}(t_0)$  (for any *fixed*  $t_0$ ), let us seek an approximation for  $\boldsymbol{\theta}(t_0 + \Delta t)$ . The integrating factor  $\mathbf{P} \doteq \mathbf{P}(t)$  is defined by

$$\frac{\partial}{\partial t} \mathbf{P} = \mathbf{P} \boldsymbol{\eta}^h, \quad \mathbf{P}(t_0) = \mathbf{1}.$$

Upon denoting  $\mathbf{Q} \doteq \mathbf{1} - i\boldsymbol{\eta}^a \boldsymbol{\theta}$ , we may write

$$\boldsymbol{\theta}(t) = \mathbf{P}^{-1} \left( \int_0^t d\bar{t} \bar{\mathbf{P}} \bar{\mathbf{Q}} \right).$$

Since  $\mathbf{P}(t_0) = \mathbf{1}$ , we find that

$$\boldsymbol{\theta}(t_0 + \Delta t) = \mathbf{P}^{-1}(t_0 + \Delta t) \left[ \boldsymbol{\theta}(t_0) + \int_{t_0}^{t_0 + \Delta t} d\bar{t} \bar{\mathbf{P}} \bar{\mathbf{Q}} \right].$$

Application of the trapezoidal approximation then leads to

$$\boldsymbol{\theta}(t_0 + \Delta t) = \mathbf{P}^{-1}(t_0 + \Delta t) \left[ \boldsymbol{\theta}(t_0) + \mathbf{Q}(t_0) \frac{\Delta t}{2} + \mathbf{P}(t_0 + \Delta t) \mathbf{Q}(t_0 + \Delta t) \frac{\Delta t}{2} \right],$$

from which we obtain the following time-stepping algorithm, correct to second order in  $\Delta t$ :

$$\boldsymbol{\theta}(t_0 + \Delta t) = \mathbf{P}^{-1}(t_0 + \Delta t) \left[ \boldsymbol{\theta}(t_0) + \mathbf{Q}(t_0) \frac{\Delta t}{2} \right] + \mathbf{Q}(t_0 + \Delta t) \frac{\Delta t}{2}.$$

Upon substitution of  $\boldsymbol{\eta}^h$  for  $\boldsymbol{\chi}$  in Eqs. (IV.20) and (IV.21), we then obtain a complete set of equations for the appropriate time-stepping algorithm, accurate through second order in  $\Delta t$ .

### **RMC:**

For the RMC, we wish to evolve an equation of the form [*cf.* Eq. (III.66d)]

$$\frac{\partial}{\partial t} \boldsymbol{\Theta} = \mathbf{Q},$$

where the entire damping term  $\boldsymbol{\eta} \boldsymbol{\Theta}$  is now incorporated into the source  $\mathbf{Q}$ , since the non-negativity of  $\boldsymbol{\Theta}$  is no longer an issue.

Given  $\boldsymbol{\Theta}(t_0)$  (for any *fixed*  $t_0$ ), we wish to approximate  $\boldsymbol{\Theta}(t_0 + \Delta t)$ . From

$$\boldsymbol{\Theta}(t) = \int_0^t d\bar{t} \bar{\mathbf{Q}}$$

we deduce

$$\boldsymbol{\Theta}(t_0 + \Delta t) = \boldsymbol{\Theta}(t_0) + \int_{t_0}^{t_0 + \Delta t} d\bar{t} \bar{\mathbf{Q}}.$$

Application of the trapezoidal approximation then leads to the following time-stepping algorithm, correct to second order in  $\Delta t$ :

$$\boldsymbol{\Theta}(t_0 + \Delta t) = \boldsymbol{\Theta}(t_0) + \frac{\Delta t}{2} [\mathbf{Q}(t_0) + \mathbf{Q}(t_0 + \Delta t)]. \quad (\text{IV.22})$$

Note that Eq. (IV.22) is just the matrix version of Kraichnan's original predictor-corrector algorithm with  $\boldsymbol{\nu}$  set to zero.

**Quasistationary EDQNM and RMC:**

In the DIA code, we also implement the quasistationary EDQNM and RMC closures [e.g., using Eq. (III.19)]. The one-field implementation amounts to solving equations that have an structure analogous to the coupled system

$$\theta = \frac{1}{\eta}, \quad (\text{IV.23a})$$

$$\eta = A\theta, \quad (\text{IV.23b})$$

where  $A$  is a constant that represents the effect of the mode-coupling coefficients in Eq. (III.18b). One immediately encounter difficulties with this formulation. Since it is equivalent to solving the equation

$$\eta = \frac{A}{\eta},$$

one discover that oscillations<sup>8</sup> prevent the numerical implementation from ever reaching the true solution,  $\sqrt{A}$ . A simple way of avoiding these oscillations is based on the application of the Newton-Raphson iteration method to the problem of computing a square root, which is what our calculation essentially amounts to. Let us find the value of  $\eta$  that makes

$$y = \eta^2 - A$$

vanish. Newton's extrapolation formula yields the recursion relation

$$\begin{aligned} \eta(t + \Delta t) &= \eta(t) - \frac{\eta^2(t) - A}{2\eta(t)} \\ &= \frac{1}{2} \left[ \eta(t) + \frac{A}{\eta(t)} \right], \end{aligned}$$

which, because of its quick convergence, is a popular way of numerically computing the square root of  $A$ . The second term on the right-hand side is readily evaluated using the original recurrence relation  $\eta(t) = A/\eta(t - \Delta t)$ . We may then substitute

$$\eta'(t + \Delta t) \doteq \frac{1}{2} [\eta(t) + \eta(t - \Delta t)]$$

for  $\eta(t + \Delta t)$  in Eq. (IV.23a) to obtain a recurrence relation for  $\theta(t + \Delta t)$  that quickly converges to the correct value,  $1/\sqrt{A}$ .

---

<sup>8</sup>If only the corrected values are examined, these oscillations can easily be missed since the period of this artificial oscillation coincides precisely with the natural period of the predictor-corrector scheme.

For the quasistationary formulation, one needs an initial value of  $\theta_{\mathbf{k}\mathbf{p}\mathbf{q}}$  that self-consistently determines values of  $\eta_{\mathbf{k}}$ ,  $\eta_{\mathbf{p}}$ , and  $\eta_{\mathbf{q}}$  satisfying the relation

$$\theta_{\mathbf{k}\mathbf{p}\mathbf{q}} = \frac{1}{\eta_{\mathbf{k}} + \eta_{\mathbf{p}} + \eta_{\mathbf{q}}}.$$

In general, the technique we use to determine this initial value is to run the code twice: on the first pass we fix the energies to their initial values and use the above algorithm to relax the coupled  $\theta$ - $\eta$  system to a solution; on the second pass we use this solution to initialize  $\theta$  and allow the energies to evolve simultaneously with this relaxation. Remember that only the *form* of  $\theta$  is fixed by the quasistationary closures; its *value* is *implicitly* evolved as a consequence of the evolution of the energies.

For the three-mode problem discussed in Chapter V an alternative procedure may be employed that directly solves the coupled  $\theta$ - $\eta$  system since for this case the system reduces to a quadratic equation in the single variable  $\theta_{\mathbf{k}\mathbf{p}\mathbf{q}}$ . However, in the complex three-wave problem one must actually solve a coupled set of two quadratic equations, because  $\theta_{\mathbf{k}\mathbf{p}\mathbf{q}}$  has both real and imaginary parts. The various cases that arise are presented in Appendix I. This specific three-wave method and the general procedure given in the previous paragraph have both been implemented in the DIA code.

## IV.D.2 Dynamic time stepping

The use of a variable time step is particularly important for problems involving growing amplitudes in which the nonlinear time becomes progressively smaller as the run proceeds. With a fixed time step, one is forced to use a time step equal to roughly the minimum nonlinear time encountered throughout the entire run. In a system that grows up from infinitesimal initial conditions, one would like to use the largest possible time step at the beginning of the run when the amplitudes are still small. Another reason for using an adjustable time step becomes apparent in Chapter V, where we study a system of three interacting waves that may exhibit nearly singular behaviour at periodic time intervals. The time increment that must be used to resolve this characteristic behaviour can be as small as  $10^{-14}$  times the overall time scale! Thus, the introduction of a variable time step not only can improve the efficiency of the calculation but also can greatly extend the time scale (by many orders of magnitude) over which we can evolve certain nearly singular systems.

There are two components to our dynamic time-stepping scheme: first, the code must handle variable time steps; second, we need a mechanism to adjust the time step dynamically based on stability considerations *without* user intervention. This

facilitates the efficient performance of large production runs in which the user may not be available to assess the need for a new time step. However, we do allow for this possibility as well.

### **Variable time step:**

For the Markovian closures, the use of a variable time step presents no difficulty since no time-history information is retained. However, the DIA contains time convolution integrals that must be evaluated using history data that is known only at nonuniform time intervals. Fortunately, the extension of the trapezoidal rule to handle nonuniform time steps turns out to be a trivial problem.

Suppose we wish to compute

$$\int_a^b dt f(t),$$

given only the values of  $f$  at the nonuniformly spaced points  $t_0, t_1, \dots, t_{n-1}, t_n$  indicated in Fig. IV.4, with  $t_0 \doteq a$  and  $t_n \doteq b$ . Denote the width of the intervals by  $\Delta t_i \doteq t_{i+1} - t_i$ . A trapezoidal approximation then yields

$$\begin{aligned} \int_a^b dt f(t) &\approx \sum_{i=0}^{n-1} \frac{f(t_i) + f(t_{i+1})}{2} \Delta t_i \\ &= \frac{1}{2} \sum_{i=0}^{n-1} f(t_i) \Delta t_i + \frac{1}{2} \sum_{i=1}^n f(t_i) \Delta t_{i-1} \\ &= f(t_0) \frac{\Delta t_0}{2} + \sum_{i=1}^{n-1} f(t_i) \left( \frac{\Delta t_i + \Delta t_{i-1}}{2} \right) + f(t_n) \frac{\Delta t_{n-1}}{2}. \end{aligned} \quad (\text{IV.24})$$

When all of the interval widths are equal, this formula reduces to the conventional trapezoidal rule. To implement the nonuniform trapezoidal rule, one need only store away the  $\Delta t_i$  associated with each time step as one computes each value  $f(t_i)$ . When  $f(t_i)$  is recalled in subsequent time-history operations, the associated  $\Delta t_i$  can then be used to evaluate Eq. (IV.24).

### **Dynamic adjustment of the time step:**

The two stages of the predictor-corrector algorithm provide a convenient means of dynamically estimating the numerical error. We define the error in any particular time step  $t$  to be

$$\epsilon(t) \doteq \max \left\{ \frac{|P(t) - C(t)|}{\max[|C(t)|, |C(t - \Delta t)|]} \right\},$$

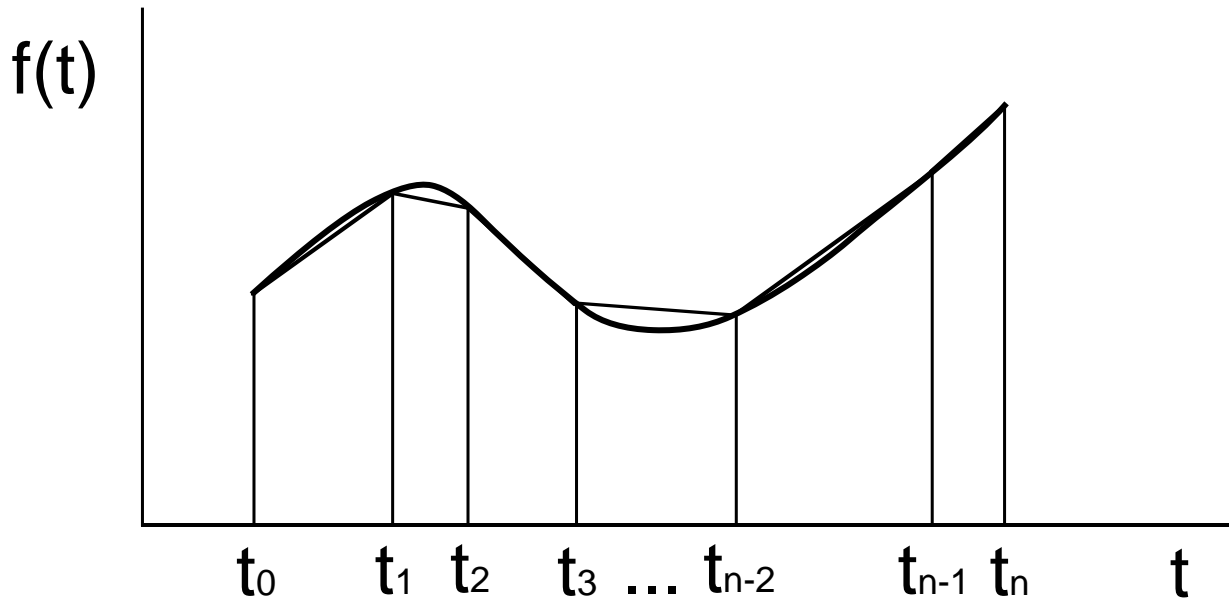


Figure IV.4: Approximation of the integral of  $f(t)$  using the nonuniform trapezoidal rule.

where  $P(t)$  is the predicted value of some quantity and  $C(t)$  is the corrected value. The outer maximum is taken over all explicitly evolved variables but not over derived variables such as  $\eta$ . The previous value  $C(t - \Delta t)$  is used to assist the time-stepping mechanism during a transition of a quantity through zero. If the error was computed solely by the ratio of the predictor-corrector difference to the current value of a corrected variable that happened to be passing through zero, this *relative* error could become arbitrarily large. For this reason the above measure of the error is taken with respect to both current and previous values; our formula removes the artifact just described by calculating a combination of relative and absolute errors. In the code, it is convenient to include the Green's function multiplier,  $e^{-\nu\Delta t}$ , in front of the expression for  $C(t - \Delta t)$ . Since linear theory is solved exactly, there is no need to restrict the time step to being smaller than the linear time.

We also implement a simple yet flexible option to adjust the time step whenever this error falls outside of a specified range. The user specifies two parameters that must bound the above error:

$$\text{tol}_{\min} \leq \epsilon \leq \text{tol}_{\max}.$$

If the inequality on the right is violated, the time step is considered to be too large for numerical stability and it is reduced by a factor of two. To avoid numerical instability and the propagation of the resulting error, the current time step is repeated

using the stored corrected data from the previous time step. If the inequality on the left is violated, the time step is considered to be too small for efficient numerical evolution and it is doubled. In this case there is no need to repeat the current time step.

By leaving the choice of the two tolerance parameters up to the user, the above scheme effectively avoids all of the complications associated with the estimation of numerical stability. Normally, these are chosen on the basis of practical experience to yield an efficient evolution that does not become unstable. Of course, even if the time stepping is stable, it may still be inaccurate; in this case the maximum error tolerance should be decreased. Through the use of convergence tests we have found that —when the numerical scheme is stable— the results are in practice sufficiently accurate, bearing in mind the inherent inaccuracies built into statistical closures. The dynamic time-stepping mechanism continually and automatically searches for the optimal time step and will even choose the best initial time step if the appropriate nonlinear time is not known. Note that by setting  $\text{tol}_{\min} = 0$  and  $\text{tol}_{\max} = \infty$  this mechanism can be disabled; the code is then forced to use the fixed time step that is initially specified.

### IV.D.3 Optimization of the DIA

On pg. 77, we referred to a particularly fruitful optimization of the DIA equations that has been discussed by Dannevik [1990]. This is based on the fact that the two-time quantities  $\Sigma_{\mathbf{k}}(t, \bar{t})$  and  $\mathcal{F}_{\mathbf{k}}(t, \bar{t})$  in Eqs. (I.38) do not depend on  $t'$ . Consequently, for sufficiently many modes and small times, solution of the resulting equations requires  $N_t^2$  rather than  $N_t^3$  operations. A similar observation applies to the species (and velocity) convolutions in the DIA closure. These optimizations have been successfully implemented in the code DIA and have led to a dramatic increase in performance.

### IV.D.4 Reality condition

For some problems (e.g., the Hasegawa-Mima problem but not the system of three interacting waves), we may obtain a further reduction in the number of retained modes by making use of the reality of  $\psi(\mathbf{x})$ . This leads to the *reality condition*

$$\psi_{-\mathbf{k}} = \psi_{\mathbf{k}}^*,$$

which in turn implies that

$$\begin{aligned} C_{-\mathbf{k}} &= C_{\mathbf{k}}^*, \\ R_{-\mathbf{k}} &= R_{\mathbf{k}}^*. \end{aligned}$$

For multiple-field problems, these relations still hold on an element by element basis. For each physical problem one may specify whether the reality condition should be invoked. With the reality condition invoked, we explicitly evolve only half of the modes, but we must then account for all four of the triad interactions  $(\mathbf{k}, \mathbf{p}, \mathbf{q})$ ,  $(\mathbf{k}, \mathbf{p}, -\mathbf{q})$ ,  $(\mathbf{k}, -\mathbf{p}, \mathbf{q})$ , and  $(\mathbf{k}, -\mathbf{p}, -\mathbf{q})$ .

### IV.D.5 Design features

The design philosophy of the code **DIA** originates with the need for a versatile tool that can be used both for developmental work, where the emphasis is on interactive capability, and for production runs, where the main consideration is efficiency. Care has been taken in the construction to allow the flexibility of running the code on either VAX (under the VMS operating system), SUN (under UNIX<sup>9</sup>), or CRAY computers. To enhance the portability of the code, the ANSI standard version of the C programming language was used, in addition to the widely available FORTRAN77 language. Let us now describe the particular features of the code that accomplish these goals.

#### **FWEB:**

The **DIA** code is organized and documented with the **FWEB** system<sup>10</sup> developed by Krommes [1991b], following the philosophy of the original **WEB** system for PASCAL [Knuth 1984]. **FWEB** is a modular system that allows the documentation to be included within the program itself. It uses the word processing environment **T<sub>E</sub>X** developed by Knuth [1986] to format the documentation side by side with the computer code in a printed document that thus conveniently presents both the algorithmical and numerical logic of the code. For example, a mathematical expression may be typeset in a form that is more readable than the programmed version. The final document also includes a table of contents, an index, and extensive cross-reference information. These features are extremely useful when one is dealing with a computer program of the size and complexity of the **DIA** code.

The modular structure of **FWEB** also provides a convenient way to organize a program into small logical units without the computational overhead of a subroutine call (which would inhibit vectorization). This is possible since the modular structure is untangled into a linear sequence of program statements just before the compilation phase. This has the disadvantage of introducing an extra preprocessing step in the development and debugging process. It is argued that this extra step is desirable

---

<sup>9</sup>UNIX is a trademark of Bell Laboratories.

<sup>10</sup>The **FWEB** user's manual, processors, and related files are currently available in the directory `/pub/fweb` of the Internet host `lyman.ppp1.gov` via anonymous ftp.

since the order in which a computer expects a sequence of statements to be declared may not coincide with the order in which the programmer may conceptualize the problem.

Another use we make of FWEB is that it allows one to write fragments of code, within the same program, in any or all of the languages C, RATFOR, and FORTRAN77. These fragments are integrated together at the link stage (when all external references are resolved). The RATFOR code is converted into efficient FORTRAN77 code so that a separate RATFOR processor is unnecessary. With the help of the FWEB system, we have found that the benefits of using *two* languages (C and RATFOR) for the DIA code outweigh the disadvantage of added complexity. It allows us to exploit the language that is best suited for the problem at hand. For example, C is the more economical of the two languages for the pointer operations that arise in the memory management scheme mentioned on pg. 78. It allows one to swap two memory buffers efficiently, an operation that arises frequently in our implementation of the time convolution integrals. On the other hand, C contains no built-in facility for handling complex numbers. Although possible, it is very inconvenient to carry out complex arithmetic in C. The RATFOR language is much more appropriate for this. In addition, since the vast majority of “number crunching” codes have been written in FORTRAN (or derivatives thereof like RATFOR), it has historically been the case that FORTRAN compilers were among the most efficient available. Indeed, over the years, intense effort has gone into their optimization and use of vector or parallel operations. In very recent times, this situation may be changing, particularly on supercomputers such as the CRAY, where the FORTRAN and C compilers are sometimes built on top of a language-independent kernel. Furthermore, a more recent version of the C language known as C<sup>++</sup> [Stroustrup 1987] allows one to define operators; with this facility, one could easily implement complex arithmetic. However, at the time of the initial design of the code (1984) such possibilities were not available; even today, we are not aware of any version of C<sup>++</sup> for the CRAY supercomputer (although presumably this will eventually be forthcoming).

In addition, FWEB provides a powerful macro facility that we use to keep the programming reasonably concise. This also improves the efficiency, reliability, and ease of program development since, if properly used, a macro facility enables common expressions to be changed globally with the redefinition of a single macro.

### **Modularity and specialization:**

The DIA code consists of two parts. First, there is a set of kernel routines that implement a general algorithm for solving the closure equations. This comprises by far the largest portion of the code. Second, in separate files there are problem-specific routines that can be compiled independently of the kernel. This *modularity*

is very convenient for developmental work. For example, if one wishes to switch physics problems, one need only relink the kernel with a different physics module.

Since DIA is a general-purpose tool, the statistical variables can depend on many arguments. In the most general formulation of the code, the (homogenous) two-point functions may depend on two velocity indices ( $v$  and  $v'$ ), two species indices ( $s$  and  $s'$ ), and three wavenumber labels ( $k_x$ ,  $k_y$ , and  $k_z$ ). The existence of both velocity and species indices is actually a mathematical redundancy since they are treated in an identical manner by the DIA equations. The only distinction is a conceptual one: in a kinetic formulation we use the velocity indices to represent a *continuum* of velocity values. In fact, one could develop a method of velocity bin averaging that would be analogous to our wavenumber bin-averaging scheme. In contrast, the species indices are considered to identify discrete physical fields. We point out that an inhomogeneity in the  $x$  direction (say) could be handled in the DIA code by using either the velocity or species indices to represent the corresponding two wavenumbers  $k_x$  and  $k'_x$  (or, equally well, the spatial variables  $x$  and  $x'$ ).

When numerical efficiency is a concern, the generality of this formulation can unfortunately become cumbersome. For example, in this work we will never directly examine kinetic effects; therefore, the velocity indices will always evaluate to zero and are extraneous. By clever use of macro expansions, it has been possible to write the DIA code in a manner that permits the elimination of any unwanted trivial dependencies of the statistical variables in the core numerical routines. In other words, one can produce from the generic master DIA file a more efficient version especially tailored to the problem at hand. For example, all of the velocity and/or species indices can be removed from the core routines of the code by changing a single flag. This *specialization* of the general DIA code can markedly increase its performance. The only disadvantage of specializing the code to a particular set of variables is that the kernel must then be recompiled. One thus loses some of the advantages gained by modularity, in that the specialized kernel by definition cannot be used as a general-purpose package. Fortunately, one always has the choice between having the greatest flexibility (modularity) and the greatest efficiency (specialization).

### **Initialization file:**

In Chapter VI we will find that one way of overcoming the restrictive computational scaling of the DIA is to use a Markovian closure to evolve the system to a saturated state. Upon initializing the DIA to this saturated state and evolving until transient effects die away, one can then economically fine tune this steady state to a solution of the DIA. We thus avoid the exertion of enormous computational effort just to evolve the DIA through the often uninteresting initial stage. For example, we often initialize the spectrum to infinitesimal values and use a Markovian closure to self-consistently determine the final amplitude. The resulting spectrum is

then fed into the DIA closure as an initial condition. To do this, a mechanism has been provided to allow one to specify the initial energy (or other) spectrum from generated computer data as well as from an analytical formula.

### **Restart capability:**

Often one does not initially know the number of time steps that will be required for a system to reach a saturated state. This is especially true when one uses a variable time step, as described below. Also, one may decide to extend a previous computer run. To avoid the wasteful practice of beginning a run all over again, starting from the initial conditions, one needs a *restart mechanism*. For the Markovian closure, this is conceptually simple to implement. For example, one could simply write out the final energy spectrum at the end of the first run and reinitialize the second run to this same spectrum using the initialization mechanism. However, since we desired to include the data from the first run in the final graphic output, slightly more work was required. The efficient but complicated memory management scheme in the DIA code made the implementation of a restart facility a nontrivial exercise even for the Markovian closure. For the DIA, the complications were even greater because all of the time-history buffers must be correctly reinitialized at the beginning of the second run. Nevertheless, restart facilities for all of the closures have been successfully implemented and thoroughly tested.

### **Vectorization and multi-tasking:**

Extensive work has gone into vectorizing DIA. Where advantageous, use has been made of vectorized library routines, and other highly specialized routines have been developed to obtain optimal performance on supercomputers like the CRAY. A computation-time histogram was used for each closure to identify the bottlenecks of the code; where possible, these were eliminated. Subroutine calls by the innermost routines are avoided since this inhibits vectorization. In some cases, this required restructuring the original design; for example, the bin-coupling coefficients are now stored in a large array during the initialization phase. The elements of this array are now accessible to the inner routines without the need for an intervening subroutine call.

The original design of DIA included some provisions for multitasking. The decision was made to multitask the  $k_z$  variable, so that calculations for different values of  $k_z$  would be performed *in parallel* on different processors to enhance computational speed. However, no adequate test of this sophisticated feature has been performed to date. In this work we only study two-dimensional turbulence and this feature is not used.

### Interactive message system:

A novel facility that makes use of system interrupts allows the user to poll the status of the code *while it is running*. One can thus examine or modify the values of certain quantities such as the time step, request that a graph (preview) of the current state be generated, temporarily halt the code and leave the user in the debugger, or even execute any preprogrammed function. To date, this facility is only operative when the code is run on the VAX and the CRAY.

### Previewing system:

Another useful facility is the preview system. This enables one to preview the state of the system before a run has completed. One can thus avoid costly mistakes by checking that the initial energy spectrum is correct. Subsequently, one can gauge how much progress has been made in the evolution toward a saturated state. One can produce a single graph either at a given time step or near a specified absolute time. Alternatively, one can generate a sequence of graphs at fixed intervals. In addition, when the run is complete, one can produce graphs for either the final state of the code or any intermediate state. The graphics facility for DIA is provided through a separate program. This division allows the graphics development to occur independently of the computational portion. A specialized collection of routines is used to communicate the data between the two parts of the code.

## IV.E Summary

In this chapter we have developed a general technique of wavenumber partitioning that can be used to implement statistical closures for *anisotropic* turbulence. This method exploits the smoothness of the statistical variables in wavenumber space; this is a property that is not afforded by the primitive dynamics. We have also discussed the time stepping scheme employed by the code DIA, in addition to several of its most distinctive features. In the following two chapters, we will harness the extensive capabilities of this code to solve statistical closures first for the case of three-interacting waves and then for the more complicated problem of drift wave turbulence in the presence of many interacting modes.

# Chapter V

## Application to Three Interacting Waves

Let us consider a slight generalization [Terry and Horton 1982, Krommes 1982] of the system of three interacting waves originally studied by Kraichnan [1963] in an early test of the direct-interaction approximation. We explicitly indicate the real and imaginary parts of the linearity, which model growth and oscillatory phenomena, respectively:

$$\begin{aligned}\left(\frac{\partial}{\partial t} - \gamma_k + i\omega_k\right)\psi_k &= M_k\psi_p^*\psi_q^*, \\ \left(\frac{\partial}{\partial t} - \gamma_p + i\omega_p\right)\psi_p &= M_p\psi_q^*\psi_k^*, \\ \left(\frac{\partial}{\partial t} - \gamma_q + i\omega_q\right)\psi_q &= M_q\psi_k^*\psi_p^*.\end{aligned}\tag{V.1}$$

It is instructive to study this problem as a precursor to the more difficult computation of turbulence involving many interacting modes. However, except for the severity of the truncation embodied in the above system, this model can be tailored to represent most of the other distinctive features of turbulence. For example, it provides for the mechanisms of both linear drive and nonlinear coupling. If the mode-coupling coefficients are chosen to satisfy Eq. (I.19) simultaneously for  $\sigma_k = 1$  and  $\sigma_k = k^2$ , then the corresponding invariants, energy and enstrophy, will be conserved. Furthermore, as we will discuss below, the system can exhibit true stochastic behaviour for particular choices of the parameters. The three-wave model thus presents us with a *paradigm* for the study of more realistic two-dimensional turbulence problems, such as we will undertake in the following chapter.<sup>1</sup>

---

<sup>1</sup>Of course, the three-wave problem does not exhibit the important characteristics of a cascade or an inertial range.

Let us begin with the case in which the mode-coupling coefficients are all real.<sup>2</sup> In the absence of dissipation, it is well known that Eqs. (V.1) are derivable from a conserved Hamiltonian and that there are two additional integrals of the motion; consequently, the resulting motion is *regular*, or nonstochastic. We will first consider Eqs. (V.1) in the absence of any linear terms to make contact with the results of Kraichnan [1963]. We are able to reproduce Kraichnan's figures completely and thereby partially validate our code.

Next, we will include the effects of finite *real* frequencies. This problem is amenable to treatment with the action-angle formalism (*cf.* Meiss [1979, 1982]). In the case where the frequencies satisfy a *resonance* condition<sup>3</sup>

$$\Delta\omega \doteq \omega_k + \omega_p + \omega_q = 0, \quad (\text{V.2})$$

one notes that the transformation  $\psi_k \rightarrow e^{-i\omega_k t}\psi_k$  reduces Eqs. (V.1) to the first case in which frequencies are absent. However, the nonresonant case, in which the frequency mismatch  $\Delta\omega$  is nonzero, cannot be reduced to the zero-frequency case and involves substantially different dynamics.<sup>4</sup> In particular, we will see that the Hamiltonian plays a nontrivial role in the nonresonant case and modifies the expected statistical equilibrium state. The Hamiltonian is cubic in the fundamental variable and is conserved by both the exact dynamics and the DIA but not by the (realizable) EDQNM or RMC. Consequently, the DIA leads to the expected final energies, but the Markovian closures do not. However, we speculate that the discrepancy encountered in such situations will diminish as the number of interacting modes (and hence the dimensionality of the system) is increased.

After examining Eqs. (V.1) in the absence of growth phenomena, we will proceed to the case of finite growth rates. We present analytical expressions for the steady-state solution (when it exists) to the exact dynamics and also to the closure equations. We compare these predictions to our numerical findings and obtain excellent agreement. Next, we focus on the special degenerate case studied extensively by Wersinger *et al.* [1980]. These authors categorized various parameter regimes including the cases of chaotic motion, stable cyclic motion, decay, and unbounded growth. In most of these cases, we find that the agreement between the closures and the ensemble is quite poor, except during the initial linear phase. We attribute this failure to a breakdown of the principle of maximal randomness in the three-mode truncation and to the mistreatment of phase correlation effects by the closures.

<sup>2</sup>Kraichnan [1963] considered the case where the coupling is purely imaginary; however, the transformation  $\psi_k \rightarrow i\psi_k$  reduces his case to our case of real mode coupling.

<sup>3</sup>This condition is called a resonance because the phase of  $\psi_k$  is then constant in the limit of no coupling [Meiss 1979].

<sup>4</sup>In the nonresonant case one can still apply the transformation  $\psi_k \rightarrow e^{-i\omega_k t}\psi_k$ . However, the new mode-coupling coefficients are now time-dependent. Since our closure equations do not take account of such effects, in this case we learn nothing new by transforming.

Finally, we consider the case of both complex mode-coupling coefficients and complex linearity, which is the one studied by Terry and Horton [1982], Krommes [1982], and Koniges and Leith [1987]. Again, we note significant discrepancies between the closure predictions and the ensemble results. This case amounts to a three-wave truncation of the full Terry-Horton model for drift waves that we will study in the next chapter. There, we will have an opportunity to determine whether the addition of more modes reduces the disagreement encountered in the three-wave problem.

## V.A Real mode coupling and zero growth

Suppose that the mode-coupling coefficients are real and satisfy Eq. (I.19) for both  $\sigma_k = 1$  and  $\sigma_k = k^2$ . If in addition the growth rates vanish, we find that the total energy and enstrophy,

$$E \doteq E_k + E_p + E_q$$

and

$$U \doteq U_k + U_p + U_q,$$

are conserved. Here,

$$E_k \doteq \frac{1}{2} \langle |\psi_k|^2 \rangle = \frac{1}{2} C_k$$

and

$$U_k \doteq \frac{1}{2} k^2 \langle |\psi_k|^2 \rangle = \frac{1}{2} k^2 C_k.$$

We assume that  $k^2$ ,  $p^2$  and  $q^2$  are not all equal, so that the invariants  $E$  and  $U$  are linearly independent.

There is also a third invariant, which we shall denote by  $\tilde{H}$ . This corresponds to the Hamiltonian for a description of the dynamics in which  $\psi_k$  and  $-i\psi_k^*/M_k$  are regarded as canonical variables [Hald 1976, Meiss 1979, Terry and Horton 1982]:

$$\tilde{H} \doteq -2 \operatorname{Im}(\psi_k \psi_p \psi_q) - \frac{\omega_k}{M_k} |\psi_k|^2 - \frac{\omega_p}{M_p} |\psi_p|^2 - \frac{\omega_q}{M_q} |\psi_q|^2. \quad (\text{V.3})$$

We will prove the invariance of  $\tilde{H}$  for dissipationless systems in Subsection V.A.2.

In general, the interest in the case of zero dissipation stems from the existence of analytical solutions for the statistics of dissipationless systems that are *mixing*, which assumes that “an arbitrary smooth initial ensemble confined to a constant-energy surface converges weakly to a uniform distribution over the energy surface” [Orszag 1970]. Weak convergence states that only finite-order statistical moments

converge, not the distribution itself. Convergence of the latter would contradict Liouville's Theorem, which establishes that the phase space density for a Hamiltonian system is conserved.

These analytical solutions correspond to the equipartition of energy found in statistical mechanics, which also assumes the mixing property. The equilibrium spectra are given in Appendix H, along with proofs that they represent solutions of the closure equations. For a system of many interacting modes, one might expect that the mixing assumption is well justified in a highly turbulent regime. The fact that the closure equations lead to the correct inviscid equilibria is a consequence of their conservation properties and gives one confidence in their appropriateness for modeling turbulence.

In this section, we illustrate statistical equilibria for the three-wave problem. Unfortunately, in the absence of dissipation Eqs. (V.1) are known to be integrable [Armstrong *et al.* 1962, Davidson and Kaufman 1969]; thus, this system is never mixing. We therefore expect to find discrepancies between the equipartition solutions of Appendix H and the exact dynamics. Consequently, we also anticipate differences between the predictions of the closures and the exact dynamics. Nevertheless, the various cases to be considered are useful as a preliminary test of the numerical implementation of the closures. Also, the following comparisons serve to illustrate the differences between several of the various closures we have discussed.

### V.A.1 Resonant case

In the resonant case we may (without loss of generality) restrict our attention to the case where the linear frequencies in Eqs. (V.1) are all zero. The ensemble-averaged Hamiltonian  $H \doteq \langle \tilde{H} \rangle$  then vanishes identically for initially Gaussian statistics. This means that  $H$  does not enter the statistical equilibrium Gibbs distribution function. Equations (V.1) then have only two nontrivial independent constants of the motion,  $E$  and  $U$ .

In Appendix H we show that these two invariants and the assumption that the dynamics is mixing lead to the following forms for the steady-state spectra [Kraichnan 1967]:

$$E_k = \frac{1}{2} \frac{1}{\alpha + \beta k^2} \quad (\text{V.4a})$$

and

$$U_k = \frac{1}{2} \frac{k^2}{\alpha + \beta k^2}. \quad (\text{V.4b})$$

The procedure used to determine these thermal equilibrium spectra from the initial conditions is illustrated schematically in Fig. V.1.

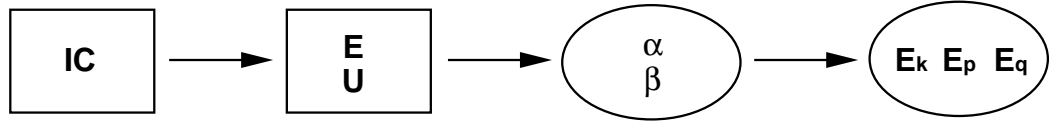


Figure V.1: Procedure used to determine the thermal equilibrium energies from the initial conditions for the inviscid case with exactly two quadratic invariants,  $E$  and  $U$ .

For example, consider the case where

$$\begin{aligned} k^2 = 3, & & p^2 = 9, & & q^2 = 6, \\ M_k = 1, & & M_p = 1, & & M_q = -2, \end{aligned} \quad (\text{V.5})$$

and

$$C_k(0) = 1.5, \quad C_p(0) = 0, \quad C_q(0) = 1.5. \quad (\text{V.6})$$

The statistical equilibrium may then be deduced from the following system of equations:

$$\begin{aligned} \frac{1}{\alpha + 3\beta} + \frac{1}{\alpha + 9\beta} + \frac{1}{\alpha + 6\beta} &= 3, \\ \frac{3}{\alpha + 3\beta} + \frac{9}{\alpha + 9\beta} + \frac{6}{\alpha + 6\beta} &= \frac{27}{2}. \end{aligned}$$

The solutions are given by

$$\alpha = \frac{4 \pm 2\sqrt{7}}{3}, \quad \beta = -\frac{2 \pm 4\sqrt{7}}{27}.$$

The root corresponding to the  $+$  sign implies that  $C_p = -0.9114$ . Since we do not allow negative energies, this solution is discarded. The other solution yields

$$C_k = 1.9114, \quad C_p = 0.4114, \quad C_q = 0.6771. \quad (\text{V.7})$$

In terms of the evolution of second-order statistics, this case is equivalent to the one studied by Kraichnan [1963, Fig. 3]. In Fig. V.2 we reproduce Kraichnan's results, which compare the evolution predicted by the DIA [Eqs. (I.38) and (I.39)] with the exact behaviour obtained by averaging the evolution of  $|\psi(t)|^2$  over a Gaussianly distributed ensemble. With the DIA closure we obtain final energies close to the expected statistical equilibrium values.<sup>5</sup> Upon extending the time integration further, we find that the steady-state covariances converge to those given in

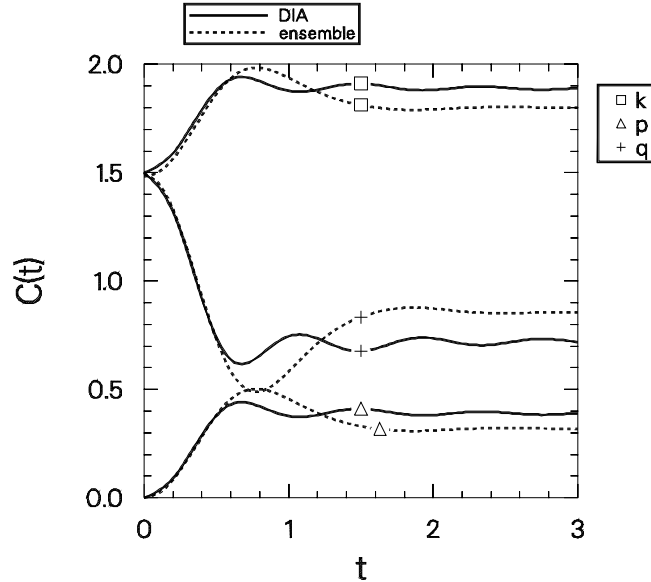


Figure V.2: DIA *vs.* exact evolution of the covariances of three waves with the asymmetric initial condition Eq. (V.6).

Eq. (V.7). However, there is a substantial discrepancy between the exact steady state and the statistical equilibrium since the three-wave system is not mixing.

As in Kraichnan's work, 5000 realizations were used to reduce the statistical error of the ensemble-averaged results to about 1.4%. This fluctuation error is clearly illustrated in Fig. V.3, which corresponds to the equipartition case:

$$C_k(0) = 1, \quad C_p(0) = 1, \quad C_q(0) = 1. \quad (\text{V.8})$$

The NAG routine D02BBF, based on a Runge-Kutta-Merson method, was employed to perform the numerical integrations of the fundamental equation. A tolerance of  $10^{-4}$  and double precision arithmetic were used to ensure overall numerical accuracy of the ensemble solution. The predictor-corrector scheme discussed in Chapter IV was used for the DIA computations.

Let us now compare the DIA results depicted in Fig. V.2 to those obtained with the DIA-based EDQNM closure, Eqs. (III.18). Note that for this real case the original [Eqs. (III.18)] and realizable EDQNM [Eqs. (III.18a-c) and (III.34)] are identical. The predicted mean energy evolution for the initial conditions of Eq. (V.6) is shown in Fig. V.4. Although the steady-state values obtained with the

---

<sup>5</sup>Kraichnan did not discuss the equipartition solutions in his original 1963 paper since Eqs. (V.4) had not yet been appreciated [Kraichnan 1967].

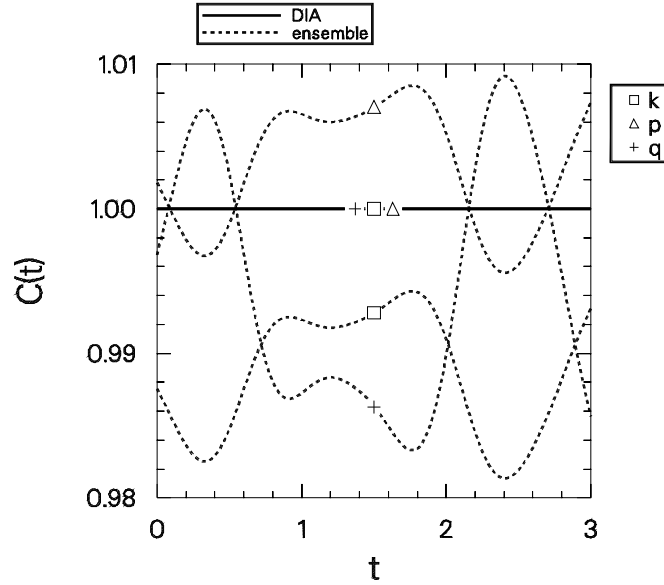


Figure V.3: Statistical fluctuation levels in an ensemble of 5000 realizations.

EDQNM are in complete agreement with Eq. (V.7), this closure predicts a much faster relaxation to the steady state than either the DIA or the exact solution. In other words, the EDQNM poorly represents the transient behaviour, as one might expect from the nature of its construction, which is based on the improper use of the Fluctuation-Dissipation Theorem and the Markovianization of the response function equation.

The corresponding result for the quasistationary EDQNM closure [Eqs. (III.18a–c) and (III.19)] is shown in Fig. V.5. Note that the transient modeling is much worse than in any of the previous results. This is a consequence of the acausal nature of this closure (*cf.* pg. 99). In particular, we see that the predicted small-time behaviour is totally wrong.

As mentioned in Chapter IV, the quasistationary closure may be implemented for a system of three waves either by directly solving the quadratic  $\theta$ – $\eta$  system, Eqs. (IV.23), or by using a two-pass scheme in which the initial value<sup>6</sup> of  $\theta$  is determined iteratively. Both procedures yield identical results to within the expected numerical accuracy. Let us illustrate the second method, which is the more general. The first step is depicted in Fig. V.6, in which  $\theta_{kpq}$  is evolved using Eq. (III.18d) without evolving the energies. The final value of  $\theta_{kpq}$  obtained in this manner is then used to initialize  $\theta_{kpq}(0)$  in a second run, as shown in Fig. V.7. In this step,

<sup>6</sup>The quasistationary form of the  $\theta$  equation implies that the initial value of  $\theta$  is nonzero and must be determined self-consistently with the  $\eta$  equation.

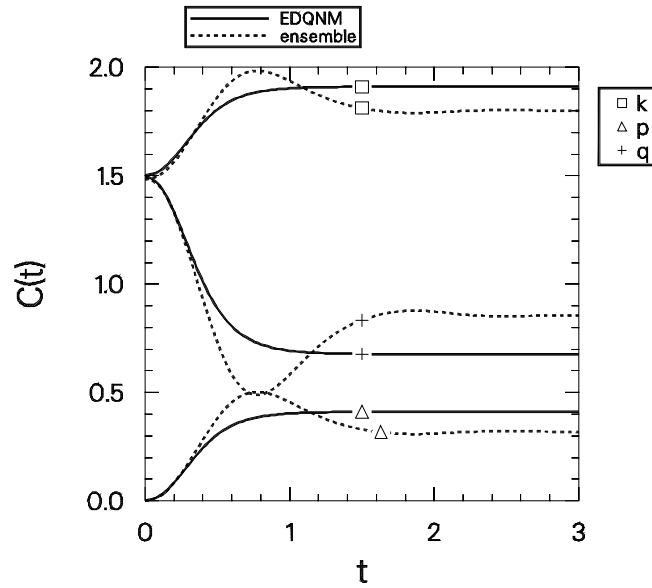


Figure V.4: EDQNM *vs.* exact evolution of the covariances of three waves with the asymmetric initial condition, Eq. (V.6).

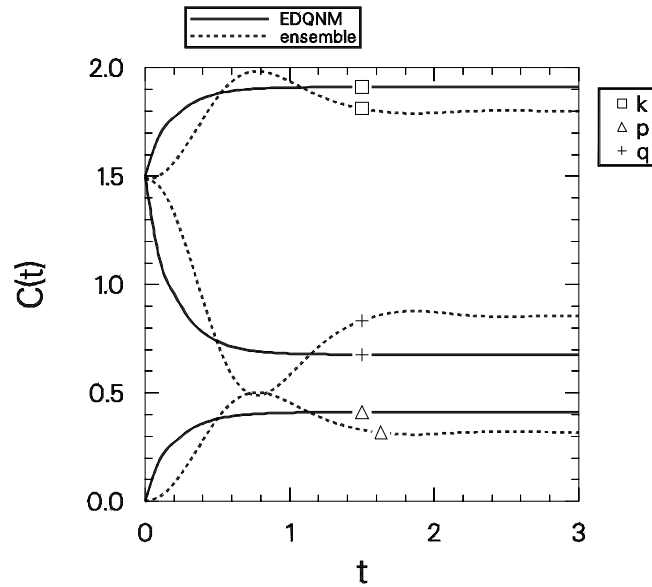


Figure V.5: Quasistationary EDQNM *vs.* exact evolution of the covariances of three waves with the asymmetric initial condition, Eq. (V.6).

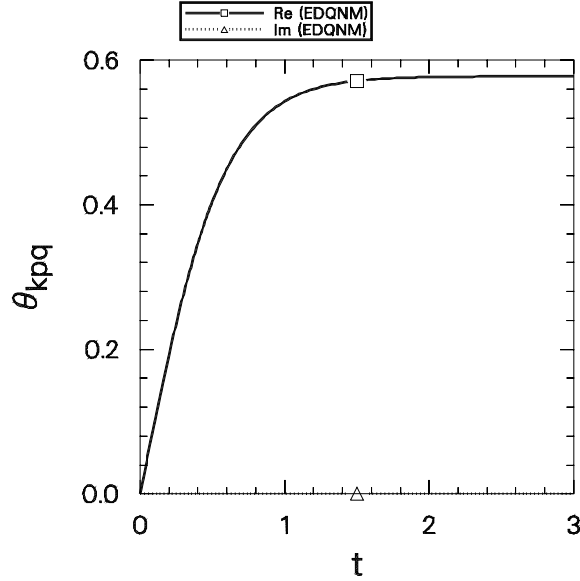


Figure V.6: Determination of the initial quasistationary EDQNM triad interaction time for the asymmetric initial condition, Eq. (V.6).

we use the quasistationary form of  $\theta_{kpq}$ , Eq. (III.19), and the energies are allowed to evolve, as illustrated in Fig. V.5. One thereby obtains a solution to the quasistationary closure. However, we do not suggest that there is any advantage to solving the quasistationary form; in fact, the above discussion serves to illustrate the difficulties embodied in its use. Computationally, there is little justification for not evolving both  $C_k$  and  $\theta_{kpq}$  simultaneously.

In Fig. V.8, we show the predictions of the RMC closure, Eqs. (III.54). Note that the RMC approaches the steady state less rapidly than the EDQNM closure but more rapidly than the DIA. In fact, it appears that the rate of approach is about the same rate as for the exact solution.

All of the Markovian closures just exhibited relax quickly to the expected statistical equilibrium values. For example, the final values obtained in Fig. V.8 are

$$C_k = 1.9115, \quad C_p = 0.4115, \quad C_q = 0.6770.$$

These agree to four decimal places with the exact values given in Eq. (V.7).

The DIA also predicts two-time spectral information, as shown in Figs. V.9 and V.10, which correspond to Kraichnan's Fig. 4 for the initial assignment given by Eq. (V.8). At the later time  $t = 20$  indicated in Fig. V.11, we see that the two-time covariance predicted by both the DIA and the ensemble decays to zero.

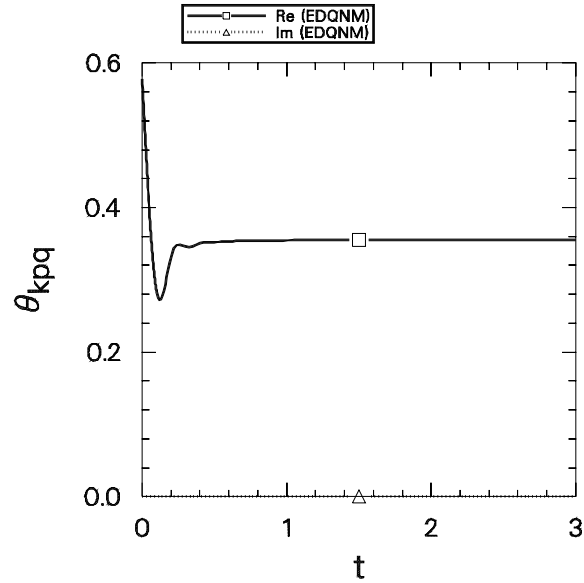


Figure V.7: Quasistationary EDQNM evolution of the triad interaction time, starting from the final value obtained in Fig. V.6.

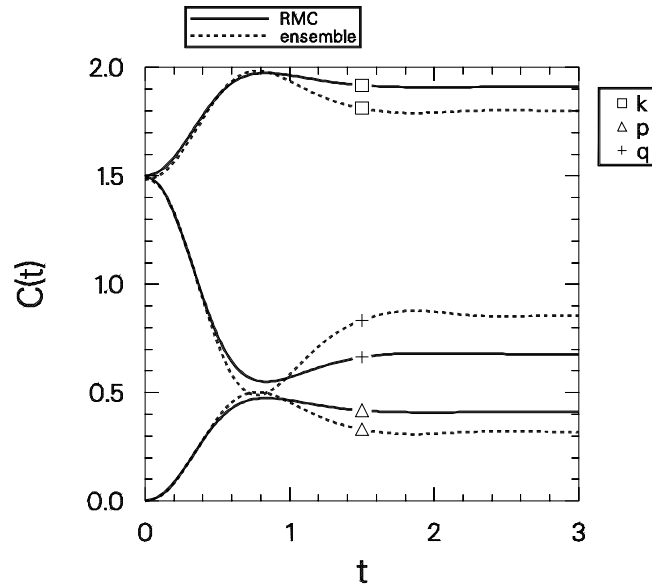


Figure V.8: RMC *vs.* exact evolution of the covariances of three waves with the asymmetric initial condition, Eq. (V.6).

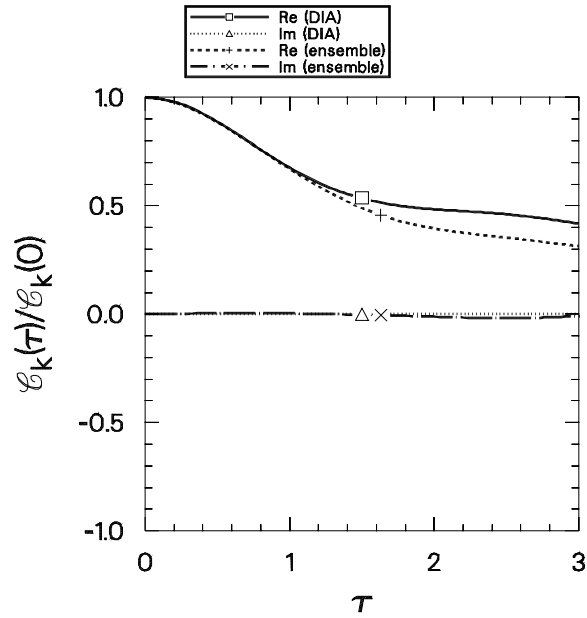


Figure V.9: Normalized two-time covariances  $\mathcal{C}_k(\tau)/\mathcal{C}_k(0)$  vs.  $\tau$  evaluated at  $t = 3$  for the equipartition case, Eq. (V.8).

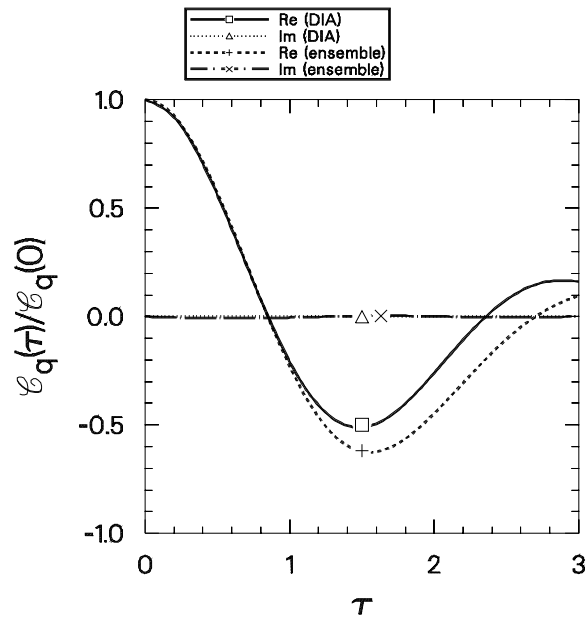


Figure V.10: Normalized two-time covariances  $\mathcal{C}_q(\tau)/\mathcal{C}_q(0)$  vs.  $\tau$  evaluated at  $t = 3$  for the equipartition case, Eq. (V.8).

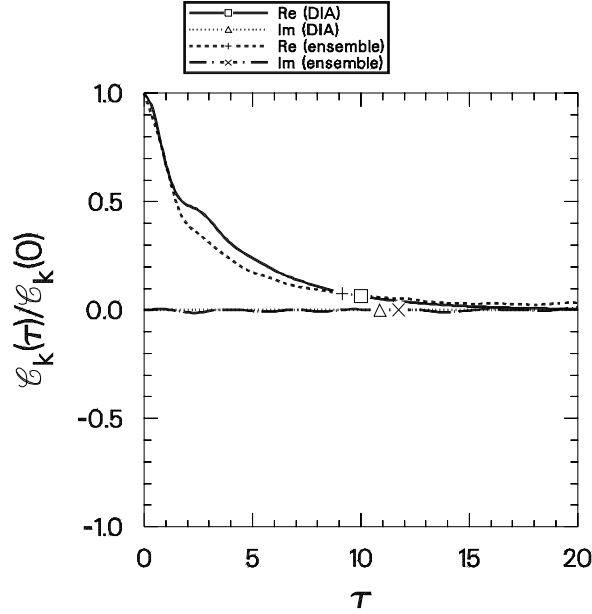


Figure V.11: Normalized two-time covariances  $\mathcal{C}_k(\tau)/\mathcal{C}_k(0)$  vs.  $\tau$  evaluated at  $t = 20$  for the equipartition case, Eq. (V.8).

To illustrate the Fluctuation-Dissipation Theorem, let us compare the two-time behaviour of  $R_q$  depicted in Fig. V.12 with that of  $C_q$  in Fig. V.10 at the final time  $t = 3$ . We see that the theorem, which requires that  $\mathcal{C}_q(\tau) = R_q(\tau)\mathcal{C}_q(0)$  in statistical equilibrium, is respected by the DIA solution; the closure has indeed reached the statistical equilibrium state discussed in Appendix H.

Kraichnan [1963] also considered the degenerate case in which the mode  $q$  does not evolve,

$$M_k = -1, \quad M_p = 1, \quad M_q = 0. \quad (\text{V.9})$$

He chose the average initial energies to be

$$C_k(0) = 2, \quad C_p(0) = 0, \quad C_q(0) = 1.$$

Note that the resulting coupled *linear* system is a special case of the one considered earlier on pg. 93. Calculations similar to the one given there may be used to obtain analytical expressions for the closure solutions. In addition, the exact solution may be obtained by averaging the analytical solution of the fundamental equation over the joint Gaussian distribution of the initial conditions.

The results can all be expressed in the form

$$C_k(t) = 1 + G(2t),$$

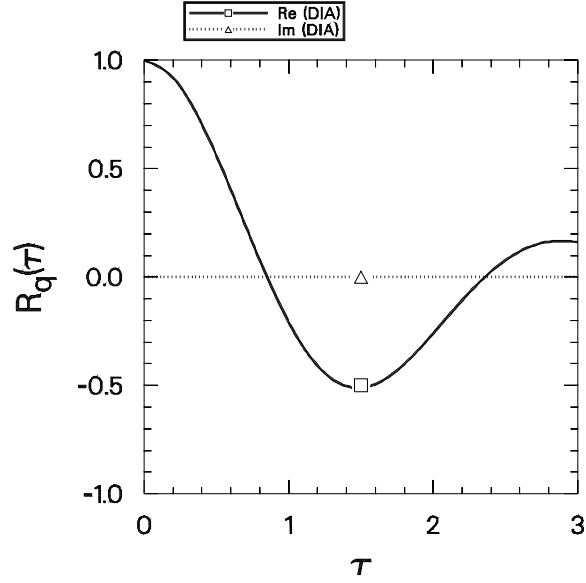


Figure V.12: DIA response function  $R_q(\tau)$  vs.  $\tau$  evaluated at  $t = 3$  for the equipartition case, Eq. (V.8).

$$\begin{aligned} C_p(t) &= 1 - G(2t), \\ C_q(t) &= 1, \end{aligned}$$

where the appropriate values of  $G(t)$  for various approximations are given by

|                        |   |
|------------------------|---|
| perturbation:          | $G(t) = 1 - \frac{1}{2}t^2,$                            |
| quasinormal:           | $G(t) = \cos t,$  |
| quasistationary EDQNM: | $G(t) = e^{-\sqrt{2}t},$                                |
| EDQNM:                 | $G(t) = \frac{1}{\cosh^2(t/\sqrt{2})},$                 |
| DIA:                   | $G(t) = \frac{J_1(2t)}{t},$                             |
| exact:                 | $G(t) = \int_0^\infty \cos(ts^{\frac{1}{2}})e^{-s} ds.$ |

With the exception of the two EDQNM results, these analytic solutions were previously reported by Kraichnan [1963]. An EDQNM result was given incorrectly by Koniges and Leith [1987].<sup>7</sup> Note that with the exception of the quasistationary EDQNM, all of these results agree through  $\mathcal{O}(t^2)$ :  $G(t) \approx 1 - t^2/2$ .

<sup>7</sup>Koniges and Leith [1987] reported the quasistationary result with the factor of  $\sqrt{2}$  omitted; this factor was also missed in their Eq. (19) and in the computations used to obtain their Fig. 7.

Graphs of the perturbation and quasinormal approximations may be found in Kraichnan [1963]. The divergence of the perturbation solution as  $t \rightarrow \infty$  is clearly evident. For the quasinormal approximation, Kraichnan pointed out that negative energies never arise in the presence of only three waves because the zero-fourth-cumulant assumption is satisfied exactly; indeed, we note that the inequality  $|G(t)| \leq 1$  in the above quasinormal solution supports this observation. (Kraichnan demonstrated that negative energies do occur for a case of five interacting waves.) However, the oscillatory nature of  $G(t)$  is at odds with the exact dynamics, in which  $G(t)$  decays to zero as  $t \rightarrow \infty$ .

Let us now discuss the formulae expected for the DIA-based EDQNM closure. The full EDQNM result given above is obtained upon substituting the solution to the  $\theta$  equation,

$$\theta = \frac{1}{\sqrt{2}} \tanh(\sqrt{2}t),$$

into Eq. (III.26) for the case where  $M^2 = 1$  and  $\gamma = 0$ . The quasistationary result is obtained by substituting the limiting value  $\theta(\infty) = 1/\sqrt{2}$  into Eq. (III.26). Note that since the initial conditions force  $G(0) = 1$ , the time-asymptotic form of  $G(t)$  for the full EDQNM disagrees with that of the quasistationary formulation by a factor of 4. For this reason, the temporal behaviour of a quasistationary closure should not be trusted.

Our formulae were checked numerically by computing the value of  $C_p$  at the time  $t = 1$ . The numerical result we obtained for the full EDQNM with 20 time steps, each of size 0.05, is 0.7888, in excellent agreement with the calculated value  $1 - 1/\cosh^2(\sqrt{2}) = 0.7892$ . For the quasistationary EDQNM, we obtain the corresponding result of 0.9403, in excellent agreement with the calculated value  $1 - \exp(-2\sqrt{2}) = 0.9409$ . These results are shown in Fig. V.13 and V.14.

We have not succeeded in deriving an analytical formula for the RMC prediction. The RMC equations for this problem are

$$\begin{aligned} \frac{\partial}{\partial t} C_k + 2\eta_k C_k &= 2\Theta_k C_p^{1/2}, \\ \frac{\partial}{\partial t} \Theta_k + (\eta_k + \eta_p)\Theta_k &= C_p^{1/2}, \\ \frac{\partial}{\partial t} \Theta_p + (\eta_k + \eta_p)\Theta_p &= C_k^{1/2}, \end{aligned}$$

where  $\eta_k = \Theta_p C_k^{-1/2}$ ,  $\eta_p = \Theta_k C_p^{-1/2}$ , and  $C_p = 2 - C_k$ . In this case  $\eta_k$  and  $\eta_p$  are equal to the effective interaction times. The above system may be written more conveniently in terms of only  $C_k$  and the interaction times. One finds

$$\frac{\partial C_k}{\partial t} + 2\eta_k C_k = 2\eta_p(2 - C_k),$$

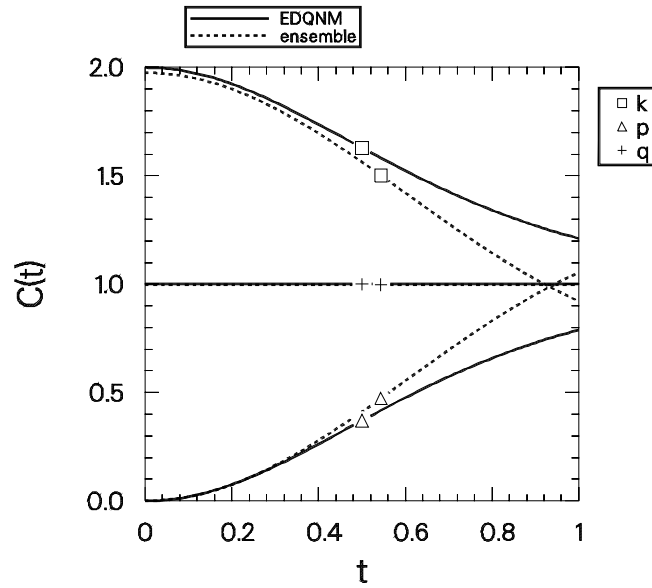


Figure V.13: Evolution of the EDQNM *vs.* exact covariances for the degenerate case, Eq. (V.9).

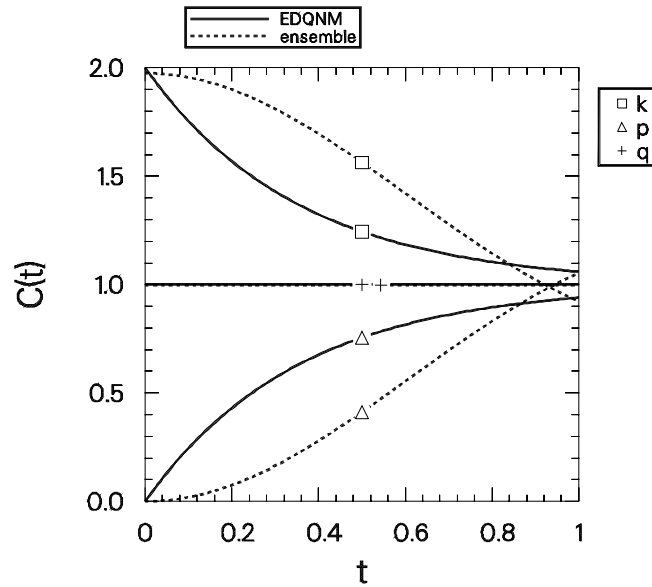


Figure V.14: Evolution of the quasistationary EDQNM *vs.* exact covariances for the degenerate case, Eq. (V.9)

$$\begin{aligned} \left(1 - \frac{\partial \eta_k}{\partial t}\right) C_k &= 2\eta_k \eta_p, \\ \left(1 - \frac{\partial \eta_p}{\partial t}\right) (2 - C_k) &= 2\eta_k \eta_p. \end{aligned}$$

Note that the initial conditions  $C_k(0) = 2$  and  $\eta_k(0) = \eta_p(0) = 0$  prevent one from assuming the form<sup>8</sup>

$$\left(1 - \frac{\partial \eta_p}{\partial t}\right) = C_k,$$

which would reduce this system to a second-order nonlinear differential equation.

We used a Runge-Kutta method with a step size of 0.0005 to integrate the above system of three equations numerically from  $t = 0$  to  $t = 1$ . We thereby obtained  $C_p(1) = 0.98$ , in agreement with the value of 0.9823 obtained from the DIA code with a time step of 0.05. This provides us with a consistency check that the RMC has been properly implemented. The RMC result is shown in Fig. V.15.

For comparison purposes, we also plot the DIA result in Fig. V.16. The expected DIA value for  $C_p(1)$  is  $1 - J_1(4)/2 = 1.033$  and the value obtained from the code with a time step of 0.05 is 1.032. The exact ensemble-averaged value is  $C_p(1) = 1.076$  in comparison to the value 1.054 obtained with 5000 realizations.

Note that relative to the EDQNM and the quasistationary EDQNM, the DIA and the RMC both give markedly superior agreement with the exact solution.

Thus far, we have witnessed two cases in which the RMC is superior to the EDQNM. This is reassuring, but let us remember that our original goal was to develop a Markovian closure that can handle linear frequencies. We will consider such effects in the next subsection.

## V.A.2 Nonresonant case

In order to thoroughly test the realizable Markovian closures developed in Chapter III, we need to examine a problem with nonzero frequencies. In this case one discovers that the Hamiltonian  $H$  of the three-wave problem no longer vanishes and significantly modifies the expected statistical equilibria. Unfortunately, this third invariant is not preserved by the Markovian closures. The predictions of the RMC and realizable EDQNM therefore differ substantially from the true solution. However, these closures do give the expected steady-state values for a system characterized by only the invariants of energy and enstrophy. Note that this failure is to be expected of any closure that conserves only quadratic invariants.

<sup>8</sup>Since the initial energy  $C_p(0) = 0$ , the value of  $\eta_p(0)$  appearing in these equations is actually indeterminate. In such situations we replace  $\eta_p(0)$  with  $\lim_{t \rightarrow 0^+} \eta_p(t) = 0$  since  $\Theta_k \sim t C_p^{1/2}(t)$  for small times.

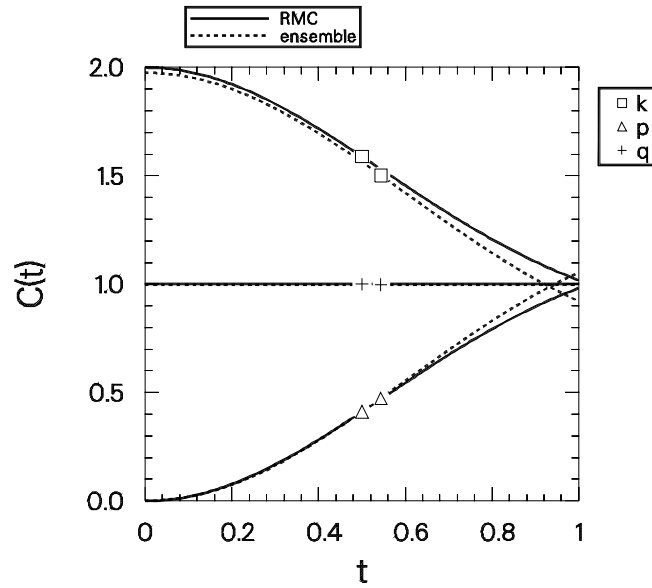


Figure V.15: Evolution of the RMC *vs.* exact covariances for the degenerate case, Eq. (V.9).

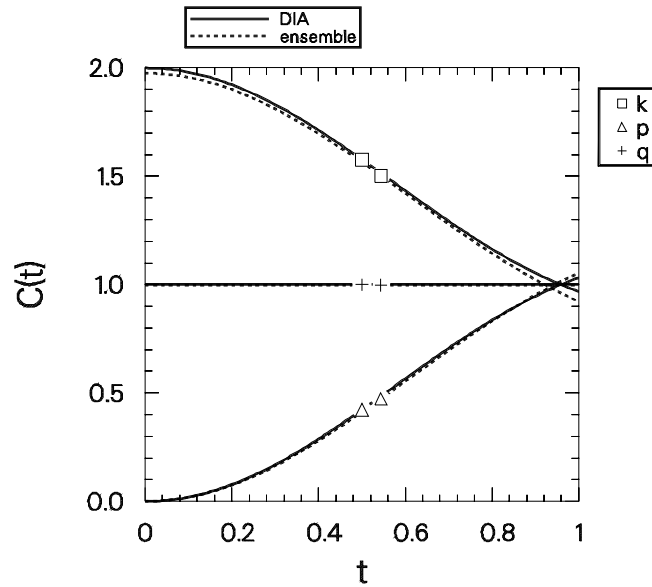


Figure V.16: Evolution of the DIA *vs.* exact covariances for the degenerate case, Eq. (V.9).

Before proceeding, let us note that the transformation  $\psi_k \rightarrow \exp((\Delta\omega/3 - \omega_k)t) \psi_k$  reduces Eqs. (V.1) (in the case of zero growth) to the form

$$\begin{aligned} \left(\frac{\partial}{\partial t} + i\frac{\Delta\omega}{3}\right)\psi_k &= M_k \psi_p^* \psi_q^*, \\ \left(\frac{\partial}{\partial t} + i\frac{\Delta\omega}{3}\right)\psi_p &= M_p \psi_q^* \psi_k^*, \\ \left(\frac{\partial}{\partial t} + i\frac{\Delta\omega}{3}\right)\psi_q &= M_q \psi_k^* \psi_p^*, \end{aligned} \quad (\text{V.10})$$

in which all three frequencies are equal.

As in the resonant case, the existence of three constants of the motion implies that the system is integrable; one may in principle solve for the time evolution in each realization [Terry and Horton 1982, Appendix B]. However, the quadrature involves the nontrivial task of inverting an elliptic integral. Moreover, we wish to know the mean evolution; the result of the quadrature must therefore be averaged over a Gaussian ensemble. In general, this appears to be an analytically intractable problem. It is possible that for certain choices of the mode-coupling coefficients the problem could be sufficiently simplified to allow an analytic solution; however, we will not pursue this here. Instead, we will be content with computing the exact solution numerically.

In principle, one might attempt to follow the statistical arguments of Appendix H, which assume that the system is mixing. The cubic form of the Hamiltonian, however, complicates the procedure. Fortunately, in the nonresonant case it is possible to obtain an exact analytical expression that relates the final amplitudes in each realization to the initial conditions through the values of the three invariants. This may be accomplished without invoking the (incorrect) assumption that the dynamics is mixing.

From Eqs. (V.10) we deduce three relations of the form

$$\frac{\partial\psi_k}{\partial t} \psi_p \psi_q + i\frac{\Delta\omega}{3} \psi_k \psi_p \psi_q = M_k |\psi_p|^2 |\psi_q|^2.$$

Upon summing these equations, we obtain

$$\frac{\partial}{\partial t}(\psi_k \psi_p \psi_q) + i\Delta\omega \psi_k \psi_p \psi_q = M_k |\psi_p|^2 |\psi_q|^2 + M_p |\psi_q|^2 |\psi_k|^2 + M_q |\psi_k|^2 |\psi_p|^2.$$

The real and imaginary parts of this relation are, respectively,

$$\begin{aligned} \frac{\partial}{\partial t}[\text{Re}(\psi_k \psi_p \psi_q)] - \Delta\omega \text{Im}(\psi_k \psi_p \psi_q) \\ = M_k |\psi_p|^2 |\psi_q|^2 + M_p |\psi_q|^2 |\psi_k|^2 + M_q |\psi_k|^2 |\psi_p|^2, \end{aligned} \quad (\text{V.11a})$$

$$\frac{\partial}{\partial t}[\text{Im}(\psi_k \psi_p \psi_q)] + \Delta\omega \text{Re}(\psi_k \psi_p \psi_q) = 0. \quad (\text{V.11b})$$

As an aside, we note that the invariance of  $\tilde{H}$  follows from the second relation:

$$\begin{aligned}\frac{\partial}{\partial t}\tilde{H} &= -2\frac{\partial}{\partial t}[\text{Im}(\psi_k\psi_p\psi_q)] - \frac{\Delta\omega}{3}\left[\frac{1}{M_k}\frac{\partial|\psi_k|^2}{\partial t} + \frac{1}{M_p}\frac{\partial|\psi_p|^2}{\partial t} + \frac{1}{M_q}\frac{\partial|\psi_q|^2}{\partial t}\right] \\ &= -2\frac{\partial}{\partial t}[\text{Im}(\psi_k\psi_p\psi_q)] - 2\Delta\omega \text{Re}(\psi_k\psi_p\psi_q) \\ &= 0.\end{aligned}$$

In a steady state, Eqs. (V.11a) and (V.3) yield the following result, from which the final amplitudes in each realization may be determined [Johnston 1989]:

$$\begin{aligned}\frac{\Delta\omega}{2}\left[\tilde{H} + \frac{\Delta\omega}{3}\left(\frac{|\psi_k|^2}{M_k} + \frac{|\psi_p|^2}{M_p} + \frac{|\psi_q|^2}{M_q}\right)\right] \\ = M_k|\psi_p|^2|\psi_q|^2 + M_p|\psi_q|^2|\psi_k|^2 + M_q|\psi_k|^2|\psi_p|^2.\end{aligned}\quad (\text{V.12})$$

Together with the energy and enstrophy conservation relations,

$$2\tilde{E} = |\psi_k|^2 + |\psi_p|^2 + |\psi_q|^2, \quad (\text{V.13a})$$

$$2\tilde{U} = k^2|\psi_k|^2 + p^2|\psi_p|^2 + q^2|\psi_q|^2, \quad (\text{V.13b})$$

this completes the system of equations needed to relate the final amplitudes to the values of the invariants.

### Geometrical interpretation of Eq. (V.12):

There is a geometrical interpretation of Eq. (V.12) due to Johnston [1989]. In the case where the frequencies vanish, we have noted that  $\tilde{H} = 0$ ; therefore

$$\begin{aligned}0 &= M_k|\psi_p|^2|\psi_q|^2 + M_p|\psi_q|^2|\psi_k|^2 + M_q|\psi_k|^2|\psi_p|^2 \\ &= |\psi_k|^2|\psi_p|^2|\psi_q|^2\left(\frac{M_k}{|\psi_k|^2} + \frac{M_p}{|\psi_p|^2} + \frac{M_q}{|\psi_q|^2}\right).\end{aligned}$$

In other words, in a steady state the vector

$$\mathbf{r} \doteq \left(\frac{1}{|\psi_k|^2}, \frac{1}{|\psi_p|^2}, \frac{1}{|\psi_q|^2}\right)$$

lies in the plane perpendicular to the vector  $(M_k, M_p, M_q)$ . Equations (V.13) state that the vectors  $(1, 1, 1)$  and  $(k^2, p^2, q^2)$  form a basis for this plane, so that

$$\mathbf{r} = \tilde{\alpha}(1, 1, 1) + \tilde{\beta}(k^2, p^2, q^2)$$

for some numbers  $\tilde{\alpha}$  and  $\tilde{\beta}$ . One then obtains relations reminiscent of the statistical equilibria:

$$|\psi_k|^2 = \frac{1}{\tilde{\alpha} + \tilde{\beta}k^2}.$$

The parameters  $\tilde{\alpha}$  and  $\tilde{\beta}$  may be determined in each realization from the values of  $\tilde{E}$  and  $\tilde{U}$ , respectively. However, upon ensemble averaging this result, one does not obtain Eqs. (V.4) because  $\langle 1/\tilde{x} \rangle \neq 1/\langle \tilde{x} \rangle$ . Nevertheless, this calculation does establish that the motion in each realization is confined to a particular plane.

If we include frequency effects in the above analysis, we find that the vector  $\mathbf{r}$  now has a component parallel to  $(M_k, M_p, M_q)$  and we obtain relations of the form

$$|\psi_k|^2 = \frac{1}{\tilde{\alpha} + \tilde{\beta}k^2 + \tilde{\epsilon}M_k}.$$

Since the conservation of energy and enstrophy guarantee that  $(1, 1, 1)$ ,  $(k^2, p^2, q^2)$ , and  $(M_k, M_p, M_q)$  form a basis for this three-dimensional space, the above relation does not restrict  $\psi_k$  to a smaller subset of this space. To determine  $\mathbf{r}$  in this case, one must solve the full set of three equations.

### Comparison to ensemble average and closure results:

Unfortunately, the closure problem is encountered if one attempts to take moments of Eq. (V.12) since  $\psi_p$  and  $\psi_q$  are (in general) statistically independent only at  $t = 0$ . We note that the value of  $H \doteq \langle \tilde{H} \rangle$  may be readily determined from the initial conditions:

$$H(0) = -\frac{\Delta\omega}{3} \left[ \frac{C_k(0)}{M_k} + \frac{C_p(0)}{M_p} + \frac{C_q(0)}{M_q} \right]$$

since  $\langle \text{Im}(\psi_k \psi_p \psi_q) \rangle$  vanishes for the initial Gaussian ensemble. However, the relation between  $H$  and the final energies involves an unknown triplet correlation function.

Nevertheless, one may still attempt to solve Eqs. (V.12) and (V.13) in each realization. Let us consider the case with  $\omega_k = \omega_p = \omega_q = 1$  and use the mode-coupling coefficients given in Eq. (V.5), along with the asymmetric initial condition

$$|\psi_k|^2(0) = 1.5, \quad |\psi_p|^2(0) = 0, \quad |\psi_q|^2(0) = 1.5.$$

The three constants of the motion evaluate to

$$\tilde{E} = \frac{3}{2}, \quad \tilde{U} = \frac{27}{4}, \quad \tilde{H} = -\frac{3}{4},$$

which we may then substitute into Eqs. (V.12) and (V.13) to determine the final amplitudes. The only admissible solution is given by

$$|\psi_k|^2 = 1.75, \quad |\psi_p|^2 = 0.25, \quad |\psi_q|^2 = 1.$$

Since the motion is integrable, one does not expect exponential sensitivity to the initial conditions. Therefore, it is plausible that upon ensemble averaging one should obtain covariances in the vicinity of these values.

Let us compare these approximate findings to the exact and DIA results shown in Fig. V.17, which differ from the case studied in Fig. V.2 by the inclusion of the linear frequencies  $\omega_k = \omega_p = \omega_q = 1$ . For the exact solution we obtain the steady-state values

$$C_k = 1.69, \quad C_p = 0.21, \quad C_q = 1.10,$$

whereas for the DIA we obtain

$$C_k = 1.72, \quad C_p = 0.22, \quad C_q = 1.10.$$

These results are in excellent agreement with each other and are reasonably close to the values calculated for a single realization above, thus confirming that this system does not exhibit exponential sensitivity to the initial conditions.

The realizable EDQNM and RMC results are shown in Fig. V.18 and V.19. As mentioned earlier, these Markovian closures predict the wrong stationary state since they respect only two of the three invariants. It is interesting to note that the RMC, which is structurally more similar to the DIA than to the EDQNM, exhibits an oscillation with the same period as the first half-oscillation of the exact solution and only gradually relaxes to the incorrect equilibrium. It appears that in some sense this closure attempts to track the DIA solution, but due to its Markovian nature it must ultimately relax to the same steady state as found with the realizable EDQNM. The gradual approach to this steady state is evident in the extended run of the RMC presented in Fig. V.20. Upon comparing to Figs. V.4 and V.8, we see that the final energies predicted by the Markovian closures are identical with those of the resonant case. Incidentally, the steady-state Markovian solution is also a stationary solution of the DIA equations, corresponding to the choice  $H = 0$ . However, since  $H \neq 0$  in the nonresonant case, this solution is not continuously connected to the initial conditions.

We speculate that the discrepancy between the predictions of the Markovian closures and the exact solution for the nonresonant case will be less significant for nonintegrable systems with many interacting modes. In Chapter VI, we will have a chance to test this conjecture.

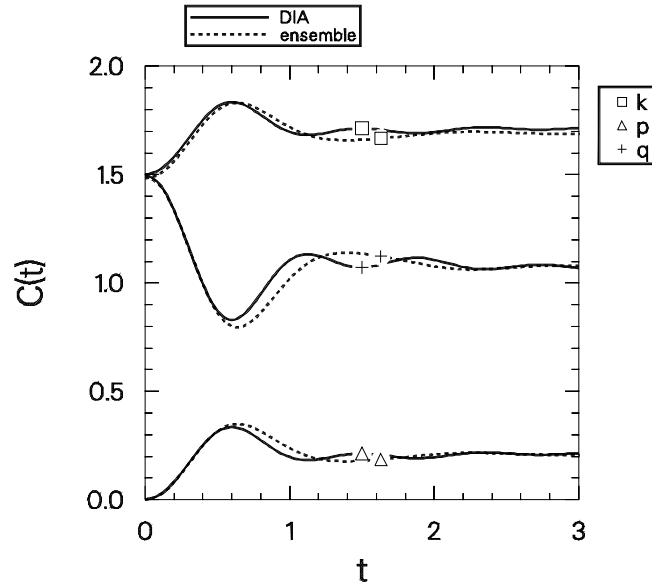


Figure V.17: DIA *vs.* exact evolution of the covariances of three waves with the mode coupling of Eq. (V.5) and the frequencies  $\omega_k = \omega_p = \omega_q = 1$ .

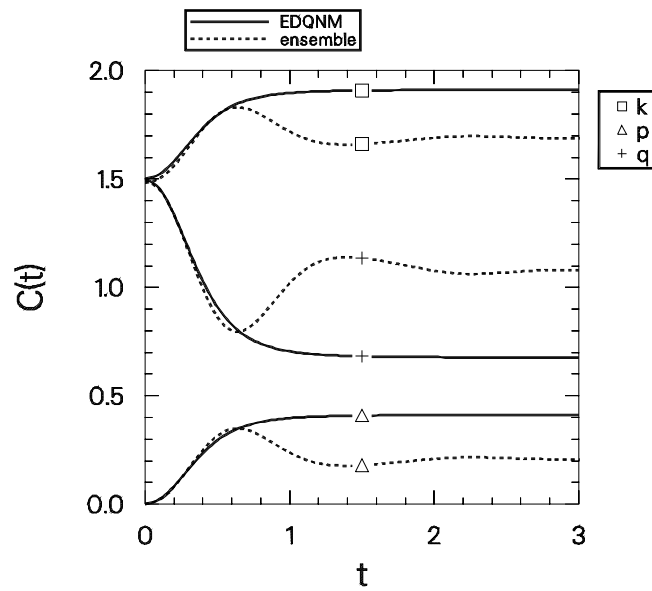
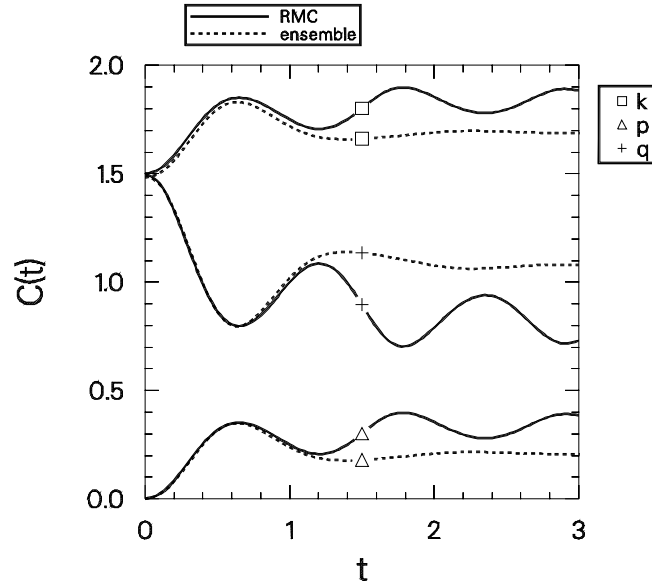
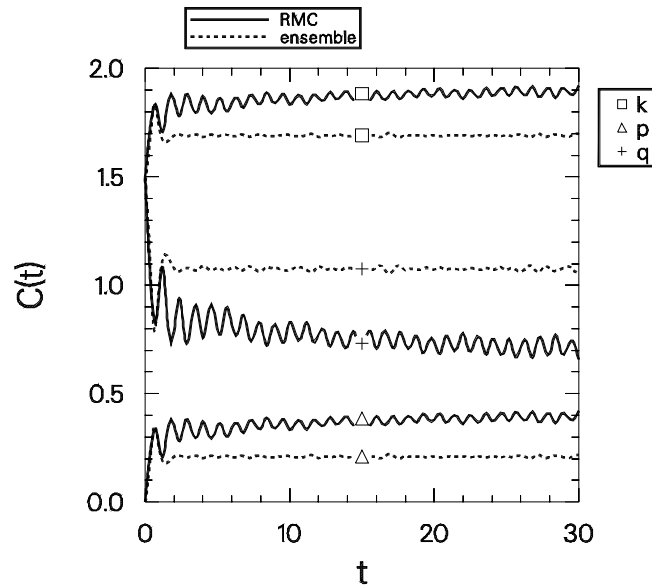


Figure V.18: Realizable EDQNM *vs.* exact evolution for the case in Fig. V.17.

Figure V.19: RMC *vs.* exact evolution for the case considered in Fig. V.17.Figure V.20: Extension of Fig. V.19 to the time  $t = 30$ .

## V.B Real mode-coupling and finite growth

When growth rates are included in the three-wave problem, the quantities  $\tilde{E}$ ,  $\tilde{U}$ , and  $\tilde{H}$  are no longer conserved. However, one can still obtain exact solutions for the steady-state energies, if these exist. (The existence of steady-state solutions depends on a variety of factors, as discussed on pg. 192.) Furthermore, in this case there exist closed expressions for the ensemble-averaged solution.

From Eq. (V.1) follow three equations of the form

$$\frac{\partial}{\partial t} |\psi_k|^2 = 2\gamma_k |\psi_k|^2 + 2M_k \operatorname{Re}(\psi_k \psi_p \psi_q),$$

from which we may deduce a steady-state balance equation [Johnston 1989]:

$$\frac{\gamma_k |\psi_k|^2}{M_k} = \frac{\gamma_p |\psi_p|^2}{M_p} = \frac{\gamma_q |\psi_q|^2}{M_q} = -\operatorname{Re}(\psi_k \psi_p \psi_q). \quad (\text{V.14})$$

If we account for growth effects in Eqs. (V.11), we now find

$$\begin{aligned} \frac{\partial}{\partial t} [\operatorname{Re}(\psi_k \psi_p \psi_q)] - \Delta\gamma \operatorname{Re}(\psi_k \psi_p \psi_q) - \Delta\omega \operatorname{Im}(\psi_k \psi_p \psi_q) \\ = M_k |\psi_p|^2 |\psi_q|^2 + M_p |\psi_q|^2 |\psi_k|^2 + M_q |\psi_k|^2 |\psi_p|^2, \end{aligned} \quad (\text{V.15a})$$

$$\frac{\partial}{\partial t} [\operatorname{Im}(\psi_k \psi_p \psi_q)] - \Delta\gamma \operatorname{Im}(\psi_k \psi_p \psi_q) + \Delta\omega \operatorname{Re}(\psi_k \psi_p \psi_q) = 0, \quad (\text{V.15b})$$

where  $\Delta\gamma \doteq \gamma_k + \gamma_p + \gamma_q$ . In a nontrivial steady state we must then satisfy

$$-[(\Delta\gamma)^2 + (\Delta\omega)^2] \operatorname{Re}(\psi_k \psi_p \psi_q) = \Delta\gamma (M_k |\psi_p|^2 |\psi_q|^2 + M_p |\psi_q|^2 |\psi_k|^2 + M_q |\psi_k|^2 |\psi_p|^2).$$

It is instructive to compare the form of the resulting equation for  $\operatorname{Re}(\psi_k \psi_p \psi_q)$  to the nonlinear terms of the steady-state EDQNM.

We may use Eq. (V.14) to express this result solely in terms of  $|\psi_k|^2$ :

$$\begin{aligned} [(\Delta\gamma)^2 + (\Delta\omega)^2] \frac{\gamma_k}{M_k} = \Delta\gamma |\psi_k|^2 \left( M_k \frac{\gamma_k M_p}{M_k \gamma_p} \frac{\gamma_k M_q}{M_k \gamma_q} + M_p \frac{\gamma_k M_q}{M_k \gamma_q} + M_q \frac{\gamma_k M_p}{M_k \gamma_p} \right) \\ = \Delta\gamma |\psi_k|^2 \frac{\gamma_k M_p M_q}{M_k \gamma_p \gamma_q} (\gamma_k + \gamma_p + \gamma_q), \end{aligned}$$

from which we obtain the steady-state formula [Johnston 1989]

$$|\psi_k|^2 = \frac{\gamma_p \gamma_q}{M_p M_q} \left[ 1 + \left( \frac{\Delta\omega}{\Delta\gamma} \right)^2 \right]. \quad (\text{V.16})$$

The corresponding results for  $|\psi_p|^2$  and  $|\psi_q|^2$  are obtained by cyclic permutation of the indices. Since all of the quantities in Eq. (V.16) are independent of the initial conditions, any nontrivial steady-state solution (the trivial solution  $C_k = C_p = C_q = 0$  is also possible) of the ensemble-averaged equations will be given by

$$C_k = \frac{\gamma_p \gamma_q}{M_p M_q} \left[ 1 + \left( \frac{\Delta\omega}{\Delta\gamma} \right)^2 \right]. \quad (\text{V.17})$$

From the form of Eq. (V.16) or from Eq. (V.14) we see that a nontrivial steady state is possible only if  $\gamma_k/M_k$ ,  $\gamma_p/M_p$ , and  $\gamma_q/M_q$  all have the same sign. Even if this criterion is satisfied, the *existence* of a nontrivial steady-state solution depends on other factors such as the initial conditions. Let us now illustrate a case where a nontrivial steady state is achieved for both a single realization and for an ensemble of realizations initialized in the neighbourhood of the values in Eq. (V.6).

Let us add the growth rates

$$\gamma_k = -1, \quad \gamma_p = -3, \quad \gamma_q = 1 \quad (\text{V.18})$$

to the nonresonant case studied in Fig. V.17, for which

$$M_k = 1, \quad M_p = 1, \quad M_q = -2. \quad (\text{V.5})$$

Equation (V.17) predicts the exact final energies

$$C_k = 3, \quad C_p = 1, \quad C_q = 6. \quad (\text{V.19})$$

Indeed, we see in Fig. V.21 that this is in agreement with the results for the ensemble. The DIA achieves essentially the same values at  $t = 10$ :

$$C_k = 3.00, \quad C_p = 1.01, \quad C_q = 5.99.$$

However, we note that the transient behaviour of the exact solution is poorly modeled by the DIA. This may be due to the mistreatment of phase coherence by the DIA. It can readily be demonstrated that to within a factor symmetric in  $k$ ,  $p$ , and  $q$ , Eq. (V.17) satisfies the steady-state DIA covariance equation. From the above numerical result, it appears that the factor is actually unity, but this has not yet been established analytically. (One needs to solve the integral equation for the response function in terms of  $\Delta\gamma$  and  $\Delta\omega$ .)

The results of the realizable EDQNM and RMC closures are depicted in Figs. V.22 and V.23. Note that the transient behaviour predicted by the RMC is similar to

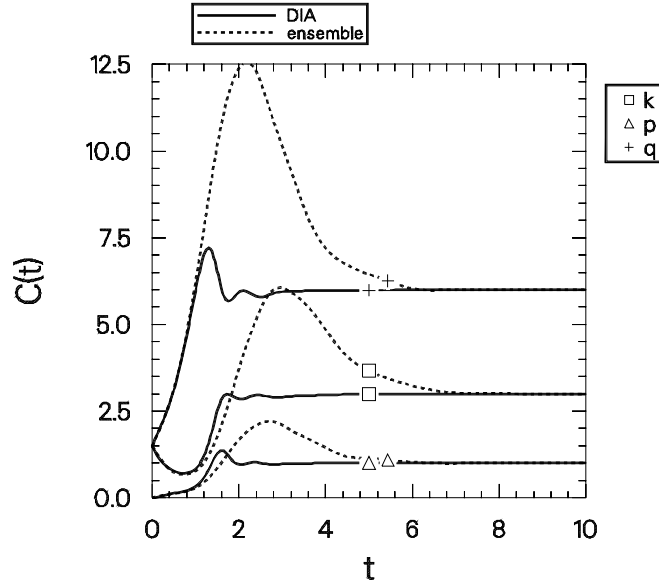


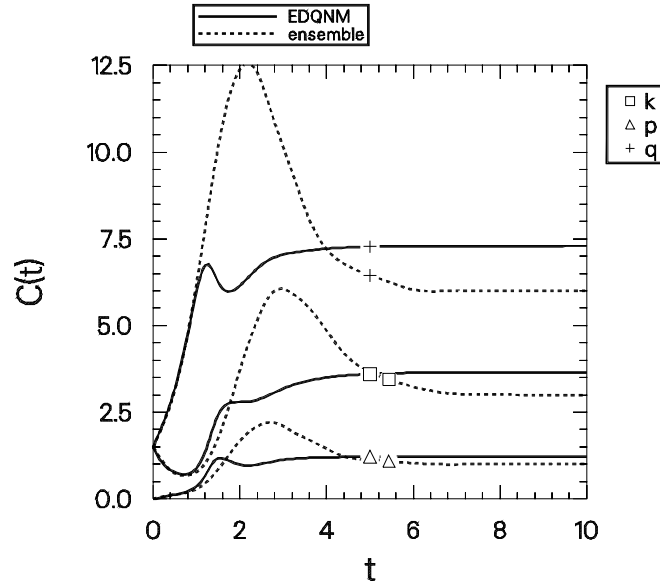
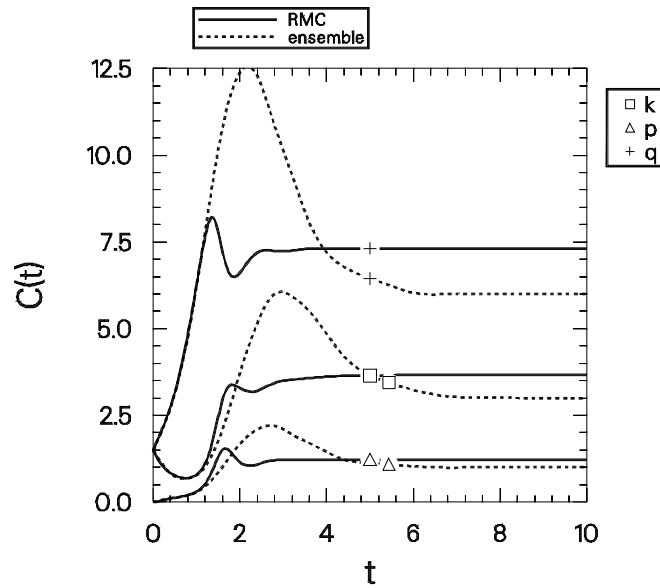
Figure V.21: Evolution of the DIA *vs.* exact covariances for the case considered in Fig. V.17 but with the assignments  $\gamma_k = -1$ ,  $\gamma_p = -3$ , and  $\gamma_q = 1$ .

that of the DIA. However, both of these Markovian closures achieve the incorrect steady-state values

$$C_k = 3.66, \quad C_p = 1.23, \quad C_q = 7.31. \quad (\text{V.20})$$

We note that each of these values is about 23% higher than the exact levels. This may seem like a large error, but it should be remembered that these values are obtained irrespective of the initial conditions. If one did not know the steady-state level, one could use the Markovian closures as tools to evolve the system to this approximate level and then “fine tune” the results with the DIA closure. This is accomplished by initializing the DIA to the final values obtained with the Markovian closures and allowing it to evolve until the transients have died away. This is illustrated in Fig. V.24. We obtain the same final results as in Fig. V.21 with a tremendous savings (a factor of 10) in computation time.

Even the DIA fails to represent some aspects of the nonlinear dynamics properly. In Fig. V.25, we compare the DIA solution for the two-time covariance  $\mathcal{C}_k(\tau)/\mathcal{C}_k(0)$  with the very different behaviour of the exact solution. The pronounced disagreement here is probably a result of the fact that this three-wave system is not sufficiently turbulent for the principle of maximal randomness, upon which the DIA is founded, to hold.

Figure V.22: Realizable EDQNM *vs.* exact evolution for the case in Fig. V.21.Figure V.23: RMC *vs.* exact evolution for the case considered in Fig. V.21.

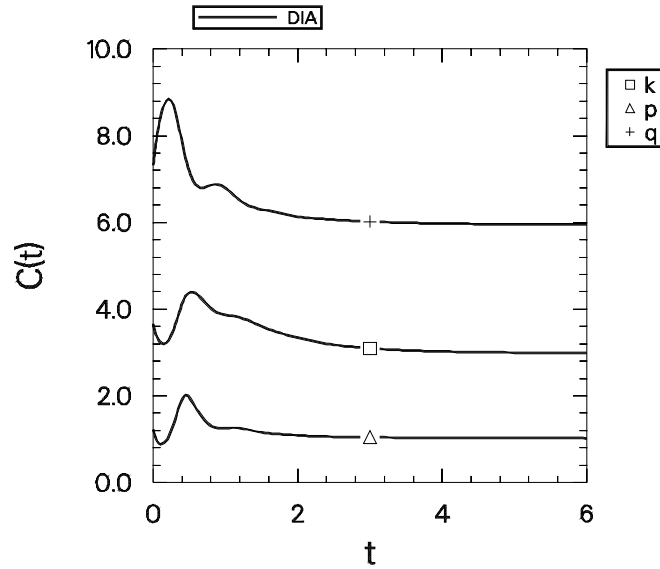


Figure V.24: DIA evolution from the Markovian steady state given by Eq. (V.20) to the correct state given by Eq. (V.19).

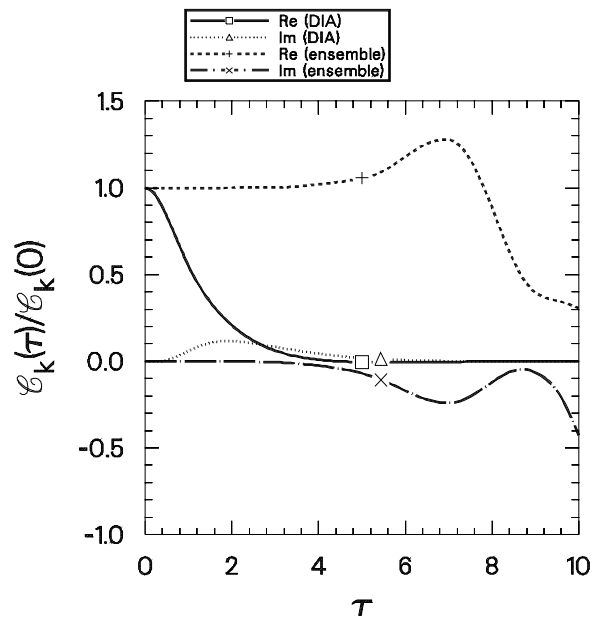


Figure V.25: Normalized two-time covariances  $\mathcal{C}_k(\tau)/\mathcal{C}_k(0)$  vs.  $\tau$  for the case considered in Fig. V.21.

In this case of three waves with real mode coupling, a simple analytical solution can be given for the steady-state EDQNM (or RMC) equations [Ottaviani 1990b]. Let us denote  $\theta \doteq X + iY$ . The steady-state balance appears as

$$-\gamma_k C_k = M_k X (M_k C_p C_q + M_p C_q C_k + M_q C_k C_p), \quad (\text{V.21a})$$

$$-\gamma_p C_p = M_p X (M_k C_p C_q + M_p C_q C_k + M_q C_k C_p), \quad (\text{V.21b})$$

$$-\gamma_q C_q = M_q X (M_k C_p C_q + M_p C_q C_k + M_q C_k C_p), \quad (\text{V.21c})$$

from which we deduce

$$-\frac{\gamma_k C_k}{M_k X} = -\frac{\gamma_p C_p}{M_p X} = -\frac{\gamma_q C_q}{M_q X} = \xi, \quad (\text{V.22})$$

where

$$\xi \doteq M_k C_p C_q + M_p C_q C_k + M_q C_k C_p.$$

The equation for  $C_k$  may be expressed solely in terms of  $\xi$  upon multiplying both sides of Eq. (V.21a) by  $\gamma_k \gamma_p \gamma_q$  and using Eq. (V.22):

$$\gamma_k \gamma_p \gamma_q M_k X \xi = M_k X^3 \xi^2 (\gamma_k M_k M_p M_q + \gamma_p M_p M_q M_k + \gamma_q M_q M_k M_p),$$

from which follows an equation for  $\xi$ :

$$\xi = \frac{M_k M_p M_q}{\gamma_k \gamma_p \gamma_q} \Delta \gamma X^2 \xi^2.$$

It may be readily verified that the solution  $\xi = 0$  corresponds to the equipartition case considered earlier. For a driven system, this solution is generally unstable and it is the other root,

$$\xi = \frac{\gamma_k \gamma_p \gamma_q}{M_k M_p M_q} \frac{1}{\Delta \gamma X^2}, \quad (\text{V.23})$$

in which we are interested.

The stationary solution for  $\theta$  is just  $1/\eta$ , where

$$\begin{aligned} \eta &\doteq \eta_k + \eta_p + \eta_q \\ &= -\Delta \gamma + i\Delta \omega - 2(X + iY)(M_k M_p C_q + M_p M_q C_k + M_q M_k C_p). \end{aligned}$$

With the help of Eq. (V.22) and Eq. (V.23), the real part of  $\eta$  may be written

$$\begin{aligned} \frac{X}{X^2 + Y^2} &= -\Delta \gamma + 2X^2 \xi M_k M_p M_q \left( \frac{1}{\gamma_k} + \frac{1}{\gamma_p} + \frac{1}{\gamma_q} \right) \\ &= -\Delta \gamma + 2 \frac{1}{\Delta \gamma} \gamma_k \gamma_p \gamma_q \left( \frac{1}{\gamma_k} + \frac{1}{\gamma_p} + \frac{1}{\gamma_q} \right) \\ &= -\frac{\gamma_k^2 + \gamma_p^2 + \gamma_q^2}{\Delta \gamma}. \end{aligned}$$

The imaginary part of  $\eta$  may be written in terms of the real part:

$$\begin{aligned}\frac{-Y}{X^2 + Y^2} &= \Delta\omega - \frac{Y}{X} \left( \frac{X}{X^2 + Y^2} + \Delta\gamma \right) \\ &= \Delta\omega - \frac{Y}{X^2 + Y^2} - \frac{Y}{X} \Delta\gamma,\end{aligned}$$

from which we conclude

$$Y = \frac{\Delta\omega}{\Delta\gamma} X.$$

Let us solve for  $X$  and  $Y$  in terms of the dimensionless parameter

$$P \doteq \frac{(\Delta\gamma)^2}{\gamma_k^2 + \gamma_p^2 + \gamma_q^2}.$$

We obtain

$$\begin{aligned}X &= -P \frac{\Delta\gamma}{(\Delta\gamma)^2 + (\Delta\omega)^2}, \\ Y &= -P \frac{\Delta\omega}{(\Delta\gamma)^2 + (\Delta\omega)^2}.\end{aligned}$$

The solution for  $C_k$  is then found to be

$$C_k = -\frac{M_k}{\gamma_k} X \frac{\gamma_k \gamma_p \gamma_q}{M_k M_p M_q} \frac{1}{\Delta\gamma X^2},$$

or,

$$C_k = \frac{\gamma_p \gamma_q}{M_p M_q} \frac{1}{P} \left[ 1 + \frac{(\Delta\omega)^2}{(\Delta\gamma)^2} \right].$$

This differs from Eq. (V.17) by the factor  $1/P$ . For the growth rates given in Eq. (V.18) the value of  $1/P$  is  $11/9 \approx 1.22$ , which is consistent with our finding that the Markovian levels are about 23% higher than the exact ones. We recall that the derivation of the Markovian closures involved the application of a Fluctuation-Dissipation ansatz [Eq. (III.9) or Eq. (III.51)] and a Markovianization procedure [Eq. (II.3a)]. It seems probable that the discrepancy just demonstrated arises from the Markovianization process itself and not from the use of the FD ansatz since the steady-state DIA solution we have found roughly satisfies the FD relation (compare Figs. V.25 and V.26) and is in agreement with Eq. (V.19).

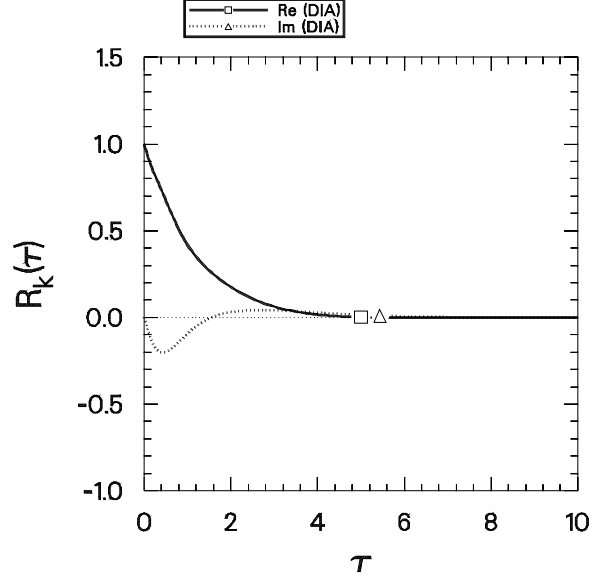


Figure V.26: DIA response function  $R_k(\tau)$  vs.  $\tau$  for the case considered in Fig. V.21.

### V.B.1 Classification of Wersinger *et al.* [1980]

Wersinger *et al.* [1980] considered the following special case of Eq. (V.1):

$$\begin{aligned}
 \frac{\partial \psi_k}{\partial t} + (-1 + i\Delta)\psi_k &= \psi_p^* \psi_q^*, \\
 \frac{\partial \psi_p}{\partial t} + \Gamma \psi_p &= -\psi_q^* \psi_k^*, \\
 \frac{\partial \psi_q}{\partial t} + \Gamma \psi_q &= -\psi_k^* \psi_p^*.
 \end{aligned} \tag{V.24}$$

Here the initial conditions  $\psi_p(0)$  and  $\psi_q(0)$  are taken to be identical, so that  $\psi_p(t) = \psi_q(t)$  for all  $t \geq 0$ .

For analytical work, it is often convenient to represent the fundamental variables by their amplitude and phase:

$$\begin{aligned}
 \psi_k &= a_1 e^{i\phi_1}, \\
 \psi_p &= a_2 e^{i\phi_2}, \\
 \psi_q &= a_3 e^{i\phi_3}.
 \end{aligned}$$

Equations (V.24) may then be equivalently expressed in terms of  $a_1$ ,  $a_2$ , and  $\phi \doteq$

$\phi_1 + \phi_2 + \phi_3$ :

$$\begin{aligned}\frac{\partial a_1}{\partial t} &= a_1 + a_2^2 \cos \phi, \\ \frac{\partial a_2}{\partial t} &= -a_2(\Gamma + a_1 \cos \phi), \\ \frac{\partial \phi}{\partial t} &= -\Delta + \left(2a_1 - \frac{a_2^2}{a_1}\right) \sin \phi.\end{aligned}$$

These are the equations studied by Wersinger *et al.* [1980, Eqs. 5]. Let us now examine some of the cases considered in their Table 1, for the case  $\Delta = 2$ . We use the initial conditions

$$C_k(0) = 4.0, \quad C_p(0) = 4.0, \quad C_q(0) = 4.0,$$

which agrees with the initial conditions  $a_1(0) = a_2(0) = 2.0$  used by Wersinger *et al.*

For  $1 < \Gamma < 3$ , Wersinger *et al.* [1980] claimed that the dynamical variables oscillated with an exponentially increasing envelope. However, they actually acknowledged that the case  $\Gamma = 3$  is “near marginally stable, with eigenvalue. . . slightly less than unity.” There must, therefore, exist a critical value  $\Gamma_c < 3$  at which stability sets in. For these initial conditions we verified numerically that this critical value lies between 2.85 and 2.86. In Fig. V.27, we graph the DIA and the ensemble-averaged solution (for 5000 realizations) for the unstable case  $\Gamma = 2$ . The DIA incorrectly predicts stable behaviour; this is not surprising, however, since this regime is not stochastic and is characterized by phase coherence. We recall that the DIA mistreats coherent effects. Noting the rapid growth exhibited by the exact solution, we attribute the observed large discrepancy to exponential compounding of the errors incurred by the mistreatment of phase coherence.

As  $\Gamma$  is increased above 2.86 one obtains stable cyclic motion: first about a single fixed point (Fig. V.28), then about two fixed points (Fig. V.29), about four fixed points (Fig. V.30), and so on, until the critical value  $\Gamma = 13.16$  is reached. At this point a transition from a stable thirty-two point periodic cycle to a chaotic regime occurs. The latter case is represented in Fig. V.31. We note that even in this supposedly stochastic state the DIA solution is an order of magnitude too small. For comparison, we also graph the realizable EDQNM prediction (Fig. V.32) and the RMC result (Fig. V.33).

In the realizable EDQNM solution, we note particularly bizarre behaviour in the covariance function, beginning with an essentially vertical drop near  $t = 2$ . In addition, we find in Fig. V.34 the presence of a sharp upward spike in the function  $\theta_{kpq}$  at this same time. A similar feature is observed in  $\eta_k$ , as illustrated in Fig. V.35. These findings have been carefully checked to ensure that they are not a result of a numerical instability or other computational artifact. To handle such nearly singular behaviour, it was essential to invoke the dynamic time-stepping mechanism: the

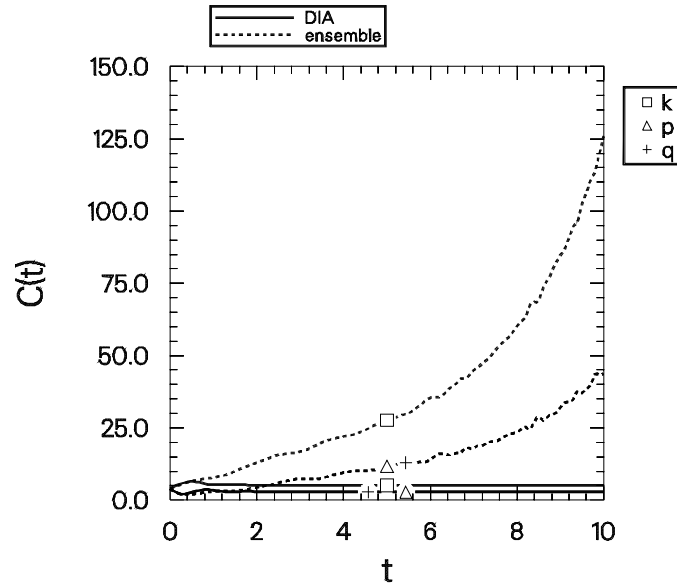


Figure V.27: DIA *vs.* ensemble evolution for the case of Wersinger *et al.* with  $\Delta = 2$  and  $\Gamma = 2$ .

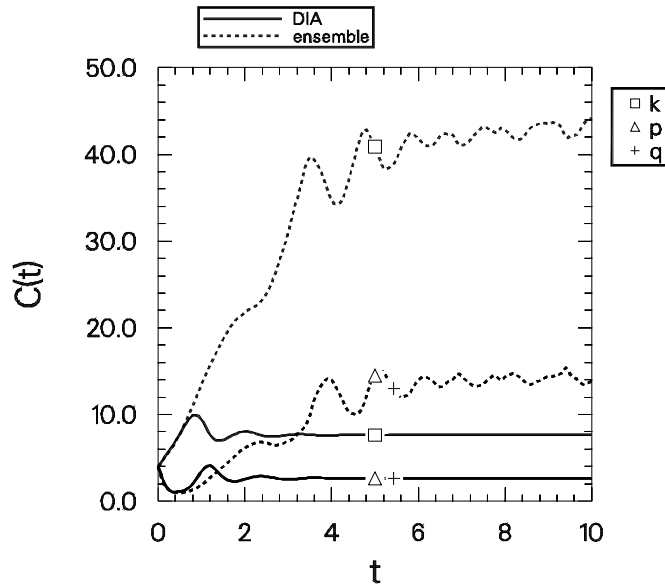


Figure V.28: DIA *vs.* ensemble evolution for the case of Wersinger *et al.* with  $\Delta = 2$  and  $\Gamma = 3$ .

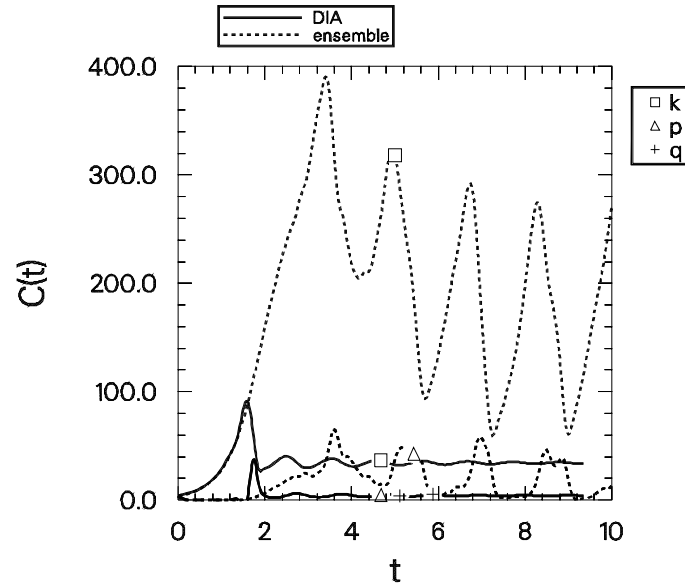


Figure V.29: DIA *vs.* ensemble evolution for the case of Wersinger *et al.* with  $\Delta = 2$  and  $\Gamma = 9$ .

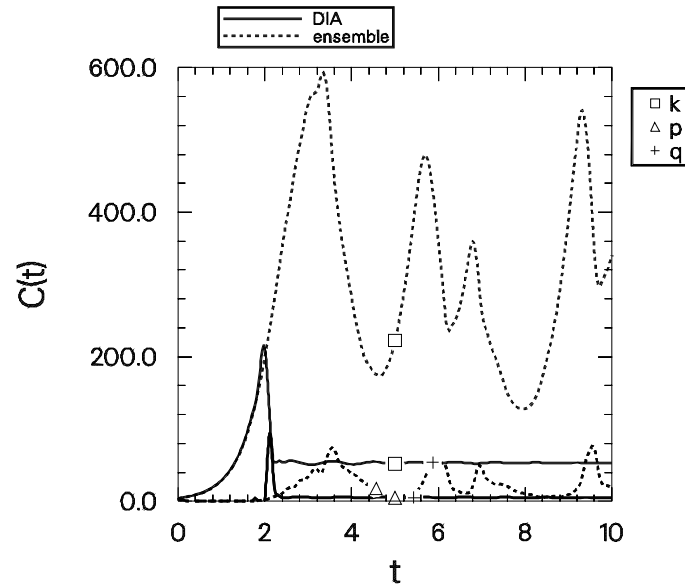


Figure V.30: DIA *vs.* ensemble evolution for the case of Wersinger *et al.* with  $\Delta = 2$  and  $\Gamma = 12$ .

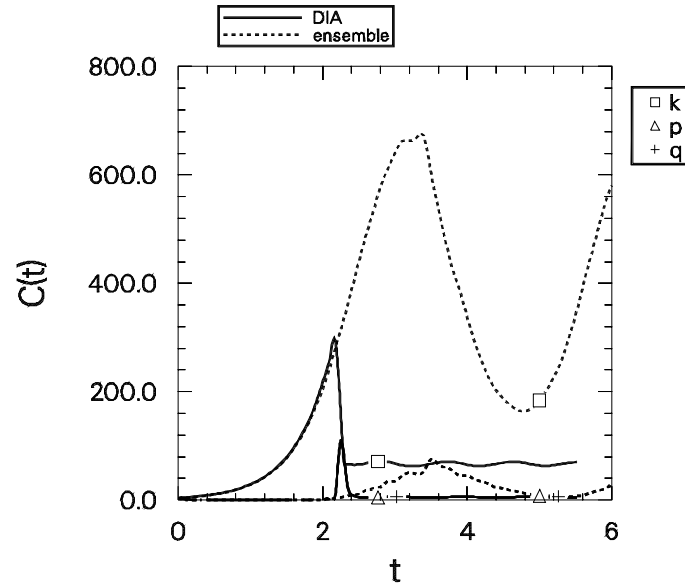


Figure V.31: DIA *vs.* ensemble evolution for the case of Wersinger *et al.* with  $\Delta = 2$  and  $\Gamma = 13.18$ .

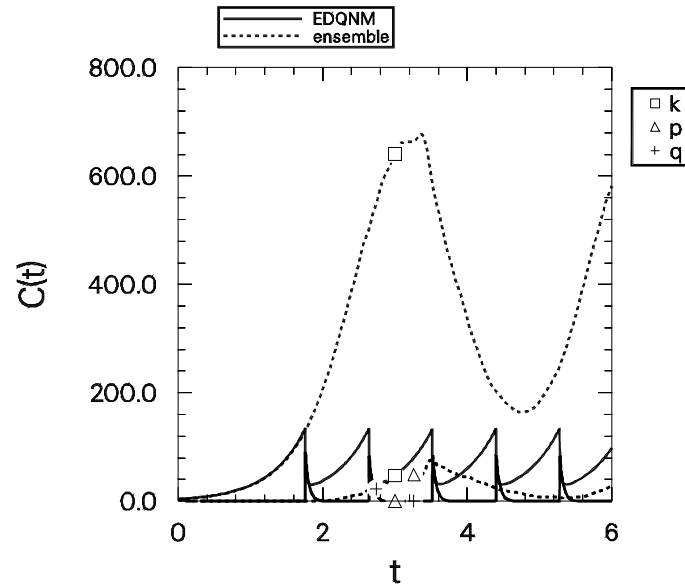


Figure V.32: Realizable EDQNM *vs.* ensemble evolution for the case of Wersinger *et al.* with  $\Delta = 2$  and  $\Gamma = 13.18$ .

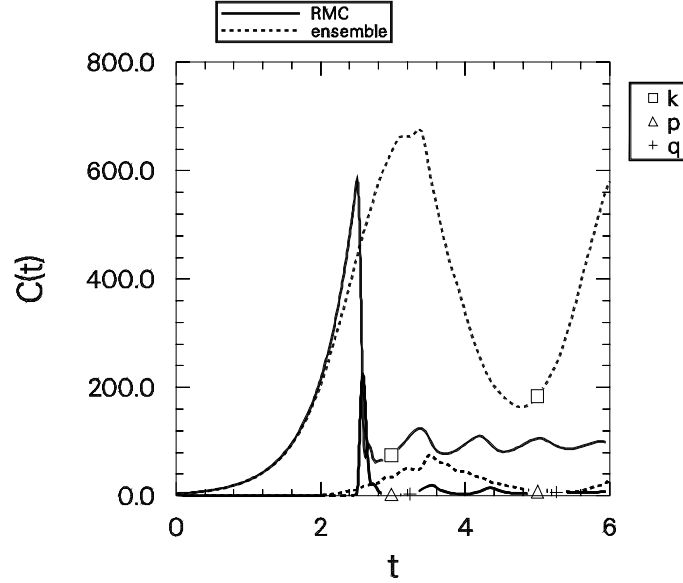


Figure V.33: RMC *vs.* ensemble evolution for the case of Wersinger *et al.* with  $\Delta = 2$  and  $\Gamma = 13.18$ .

ratio of the maximum to the minimum time step needed for this run was  $10^8$ ! To be sure that this behaviour is not the result of a numerical instability or an effect introduced by the dynamic time-stepping, we considered the realizable EDQNM solution for the case where  $\Gamma = 6$ . One obtains qualitatively similar behaviour for this reduced value of  $\Gamma$ , except that the ratio of the maximum and minimum time steps is now only 128. We were therefore able to turn off the dynamic time-stepping facility and use 60 000 fixed time steps of size 0.0001 (a factor of 8 smaller than the minimum time step actually required) to produce the graph shown in Fig. V.36, which is qualitatively similar to the result obtained for  $\Gamma = 13.18$  in Fig. V.32. We note that the  $\delta$  function behaviour of  $\theta$  in Fig. V.34 is also evident in the corresponding graph for  $\Gamma = 6$ , shown in Fig. V.37. We verified that the dynamic time-stepping scheme produces results identical to those of Figs. V.36 and V.37 (but requires only 430 time steps).

We note that the RMC solution does not exhibit this singular behaviour: although Figs. V.32 and V.33 are qualitatively similar, the transitions in the RMC case are much more gradual. For purposes of comparison, we also depict the solution of  $\Theta_{kpq}$  for the RMC in Fig. V.38. In addition, we note that for this case the transient behaviour predicted by the RMC is actually superior to that of the DIA (although it would be a misleading to draw any general conclusion from this observation).

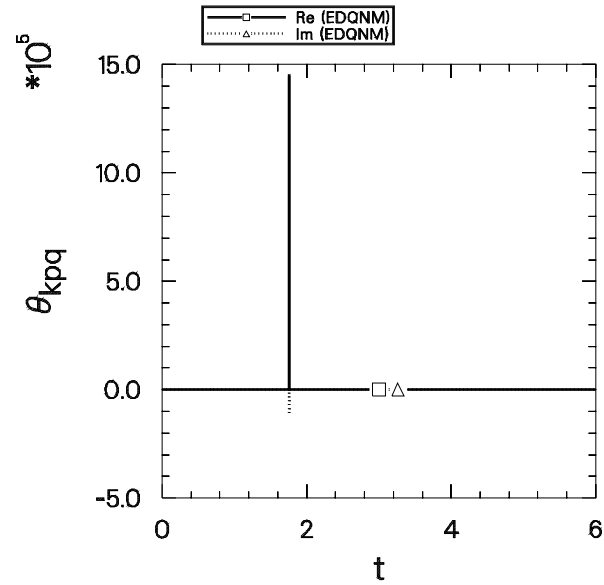


Figure V.34: Realizable EDQNM evolution of  $\theta_{kpq}$  for the case of Wersinger *et al.* with  $\Delta = 2$  and  $\Gamma = 13.18$ .

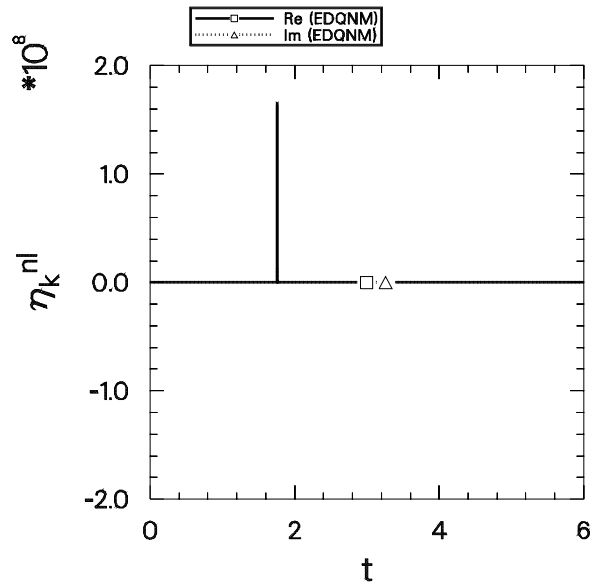


Figure V.35: Realizable EDQNM evolution of  $\eta_k$  for the case of Wersinger *et al.* with  $\Delta = 2$  and  $\Gamma = 13.18$ .

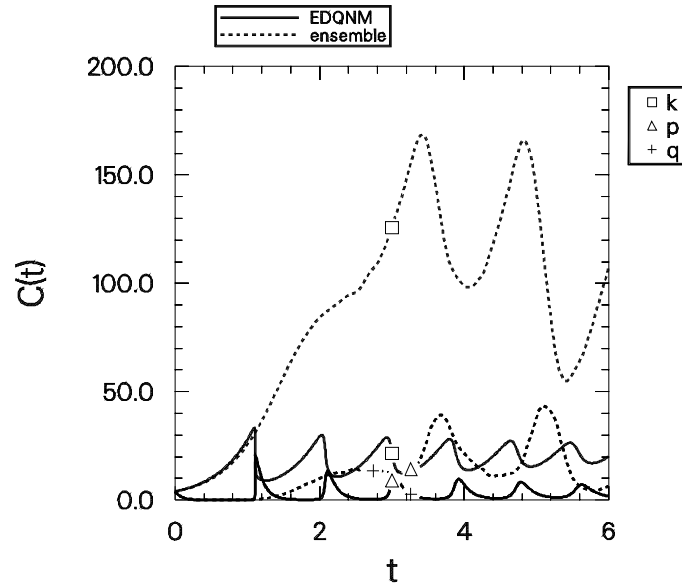


Figure V.36: Realizable EDQNM *vs.* ensemble evolution for the case of Wersinger *et al.* with  $\Delta = 2$  and  $\Gamma = 6$ .

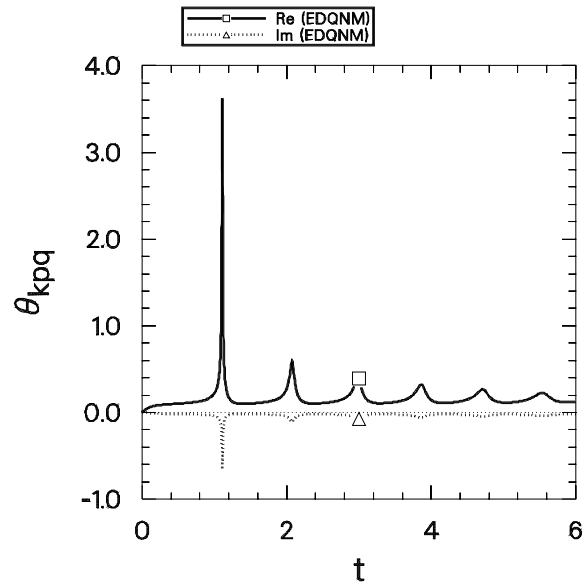


Figure V.37: Realizable EDQNM evolution of  $\theta_{kpq}$  for the case of Wersinger *et al.* with  $\Delta = 2$  and  $\Gamma = 6$ .

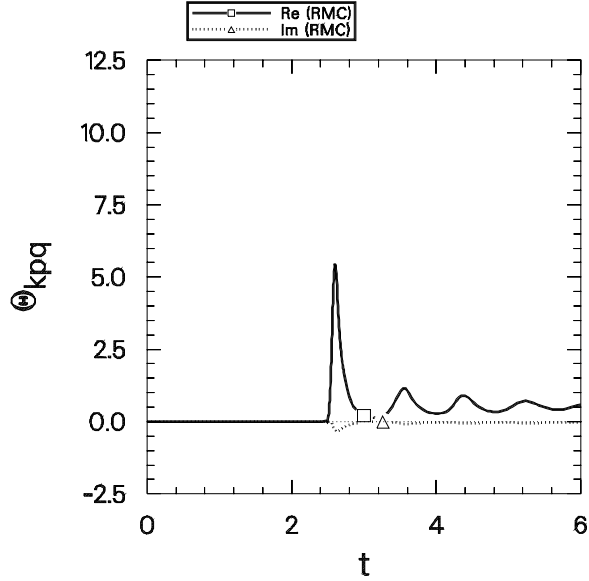


Figure V.38: RMC evolution of  $\Theta_{kpq}$  for the case of Wersinger *et al.* with  $\Delta = 2$  and  $\Gamma = 13.18$ .

While these results may seem to cast doubt on the utility of closures, we emphasize again that this problem represents a severe test of these approximations in that only three interacting modes are retained. For example, one does not expect the principle of maximal randomness to hold. Furthermore, coherent effects, which are mistreated by statistical closures, probably play a much more important role in the three-wave problem than in multimode turbulence. Indeed, we will see in the next chapter that the discrepancies encountered in applications to multimode turbulence are substantially smaller.

## V.C Complex mode-coupling and finite growth

Our ultimate interest in statistical closures derives from the problem of drift-wave turbulence. When a nonadiabatic correction is included in the Hasegawa-Mima equation, one obtains the Terry-Horton equation, as was discussed on pg. 10. Nonadiabaticity introduces complex mode-coupling coefficients into our three-wave truncation, Eq. (V.1). This case was first considered by Hald [1976] in the absence of linear effects. As in the case of real mode-coupling, he noted that the motion is integrable: it exhibits “sometimes periodic, in general ergodic, but never mixing” behaviour.

Here, we include both growth and oscillatory effects in the linearity, so that this problem constitutes the most general case of Eq. (V.1). Let us illustrate the solution of this system for the parameters given by Terry and Horton [1982]. This problem, which is expected to exhibit intrinsic stochasticity, has also been considered by Krommes [1982] and Koniges and Leith [1987].

First, let us clear up some misprints in the literature regarding the numerical values of the drift-wave parameters. The caption of Fig. 6 in Terry and Horton [1982] states that  $\mathbf{G} = (-0.035, 0.2297, -0.2012)$ . This should read  $\mathbf{G} = (-0.035, 0.2297, -0.1947)$  so that the sum  $G_1 + G_2 + G_3$  equals zero, as required by their Eq. 12. There is also a typographical error in Koniges and Leith [1987, pg. 3066]. The values of the mode-coupling coefficients should read

$$M_k = -0.1888 + i0.0588, \quad M_p = 0.1448 - i0.1562, \quad M_q = 0.05390 + i0.1537.$$

Note that the coefficient  $\hat{\mathbf{z}} \cdot \mathbf{p} \times \mathbf{q}$  is arbitrarily set to 1 for this case. With these corrections, the parameters of these works are in agreement with the values used by Krommes [1982]. The growth rates and frequencies are given by

$$\begin{aligned} \gamma_k &= 0.1600, & \gamma_p &= -0.2500, & \gamma_q &= -0.0191, \\ \omega_k &= 0.8349, & \omega_p &= -1.2305, & \omega_q &= 0.4989. \end{aligned}$$

We point out that the invariant given by Krommes [1982] is incorrect for the case of complex mode-coupling. The correct result is

$$W \doteq \frac{1}{2} \sum_{\mathbf{k}} |1 + \chi_{\mathbf{k}}|^2 |\Phi_{\mathbf{k}}|^2.$$

In Fig. V.39 we compare the solution of the DIA to the ensemble average. We see that the DIA results are higher than the exact ones by as much as 36%. However, it is plausible that as more interacting modes are included in the system the agreement will become better since the weak dependence assumption will likely be of greater validity. In comparing this result to the graph of Krommes [1982, Fig. 2], note that the DIA solution obtained in that work had not yet achieved a steady state. Unfortunately we were unable to reproduce the transient behaviour he found since the initial condition for mode  $k$  is not given in his paper. To obtain an accurate and numerically stable evolution to the steady state, during most of the run we used a time step of about 0.25. Our run required 450 time steps. The dynamic time-stepping mechanism effectively saved us from using 30 additional time steps since in the early stages of the run a time step of 0.5 was tolerable. In view of the  $\mathcal{O}(N_t^3)$  scaling of the DIA, this represents a substantial savings in computer time.

In Fig. V.40 we plot the two-time covariance for this case. We note significant disagreement between the DIA and the ensemble predictions as far as the *phases* are concerned, although the *amplitude* levels are similar.

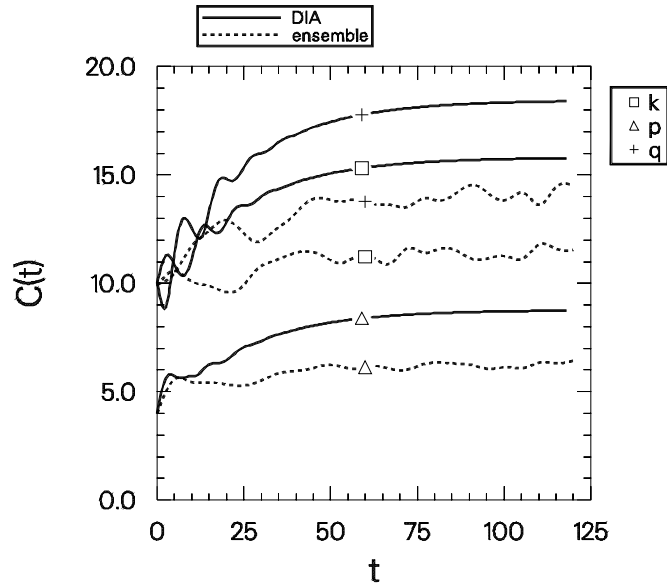


Figure V.39: DIA *vs.* exact evolution of the covariances of three turbulent drift waves.

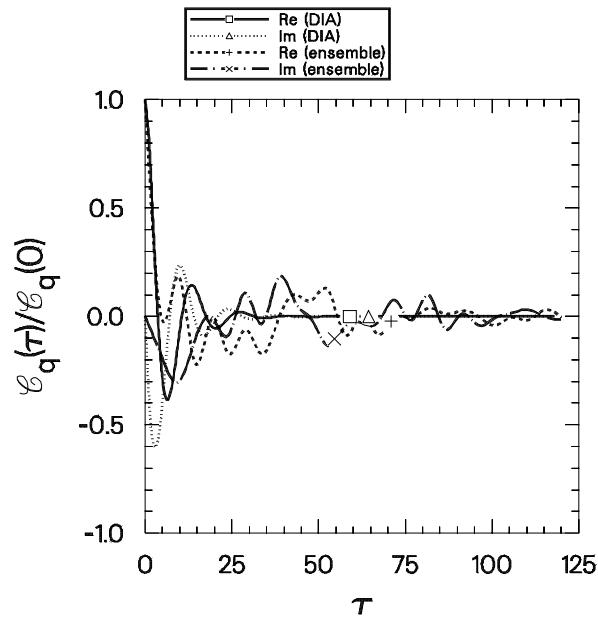


Figure V.40: Normalized two-time covariances  $\mathcal{C}_q(\tau)/\mathcal{C}_q(0)$  *vs.*  $\tau$  evaluated at  $t = 120$  for the turbulent drift-wave case.

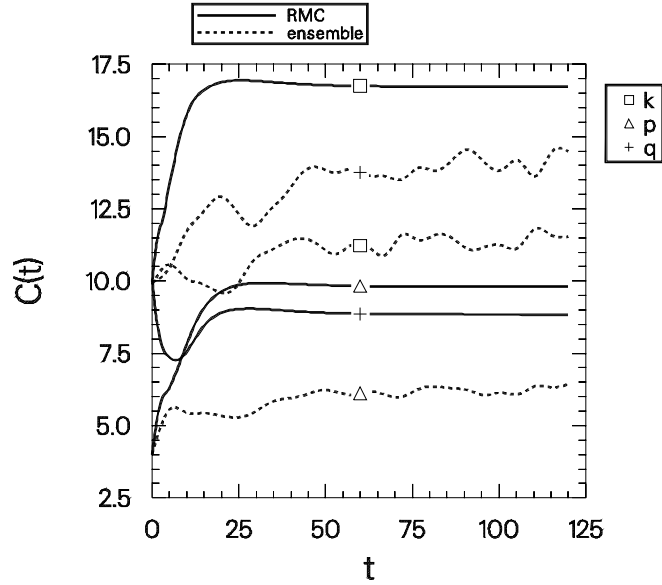


Figure V.41: RMC *vs.* exact evolution of the covariances of three turbulent drift waves.

Figure V.41 presents the RMC solution. In this case we see that the RMC is a poorer model of the true dynamics than the DIA. In particular, the RMC predicts that mode  $q$  should be the most weakly excited of the three modes, whereas in the true dynamics it is the most strongly excited. A similar result is obtained for the realizable EDQNM (which we do not illustrate). Nevertheless, as we have previously illustrated, one may use these Markovian closures to determine the steady-state fluctuation level approximately and thereby reduce the amount of computation required to obtain a saturated DIA solution.

Finally, let us refer to the results of Koniges and Leith [1987, Figs. 8]. They used the initial conditions

$$C_k(0) = C_p(0) = C_q(0) = 1.0.$$

The complex version of the quasistationary EDQNM employed by Koniges adopted the unusual definition

$$\theta_{kpq}(t) = \frac{1}{\eta_k^*(t) + \eta_p^*(t) + \eta_q^*(t)}, \quad (\text{V.25})$$

instead of the correct quasistationary form, Eq. (III.19) [Koniges 1989]. Note that this added conjugate operator was entirely omitted from their Eq. 17 since it was also missed in their Eq. 10, which they state is the complex conjugate of their

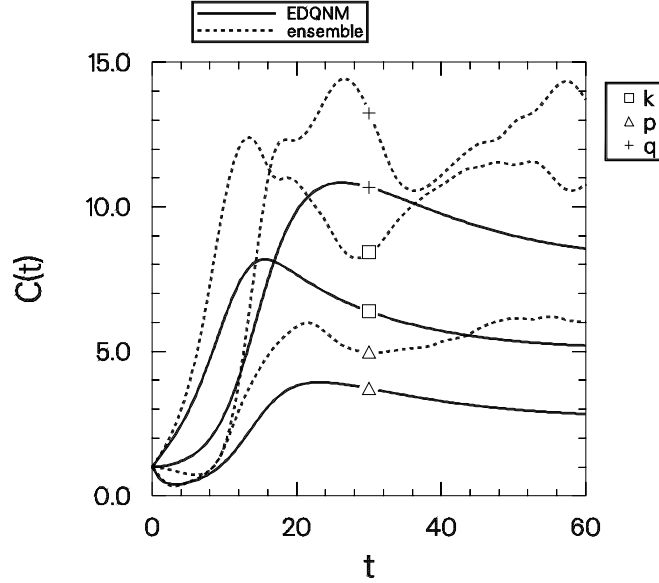


Figure V.42: Correctly scaled results, obtained using Eq. (V.25), that correspond to Fig. 8 of Koniges and Leith [1987].

Eq. 17. Another error appears in the labeling of their Fig. 8b, which describes the ensemble-averaged evolution of the quantity  $\frac{1}{2}\langle\Phi_k\Phi_{-k}\rangle$  (which equals the covariance divided by two). This extra factor of one-half invalidates the comparison they make of the closure results to the exact solution. The correctly scaled graph is shown in Fig V.42; here, our closure solution uses the above conjugate definition for the quasistationary  $\theta$ .

The use of the correct quasistationary form of  $\theta_{kpq}$  leads to the evolution shown in Fig. V.43. The only motivation for the conjugate operator in Eq. (V.25) was that it was believed to yield better agreement with the exact solution [Koniges 1989]; however, upon comparison with the correctly scaled results, we see that this is not the case. Incidentally, in these figures the appropriate quadratic equation for  $\theta$  was used, following the original work of Koniges and Leith [1987].

For comparison purposes, we illustrate the results obtained with the realizable EDQNM, the RMC, and the DIA for this case in Figs. V.44, V.45, and V.46. We note that only the DIA predicts even approximate agreement with the ensemble solution.

We have already illustrated (see Figs. V.10 and V.12) steady-state solutions of the DIA that exactly satisfy the Fluctuation-Dissipation Theorem. One may appreciate the qualitative validity of this relation even for nonstationary systems by comparing Figs. V.47 and V.48, which depict the DIA behaviours of  $\mathcal{C}_k(\tau)/\mathcal{C}_k(0)$

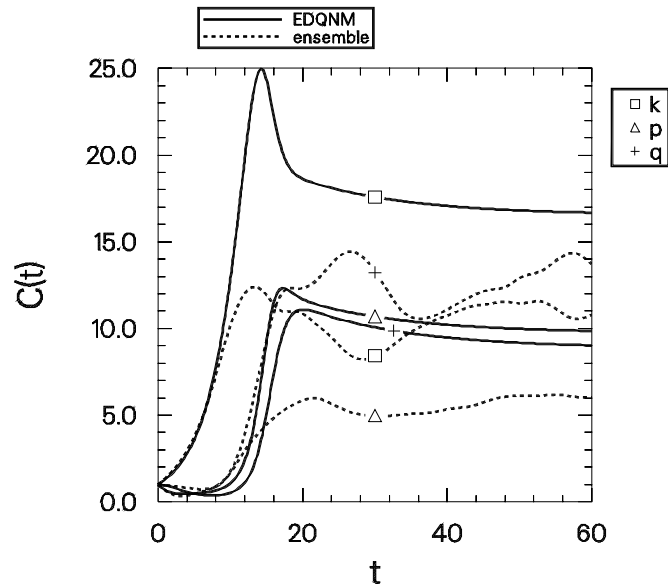


Figure V.43: Quasistationary EDQNM *vs.* exact solution obtained using Eq. (III.19) and corresponding to the case of Fig. V.42.

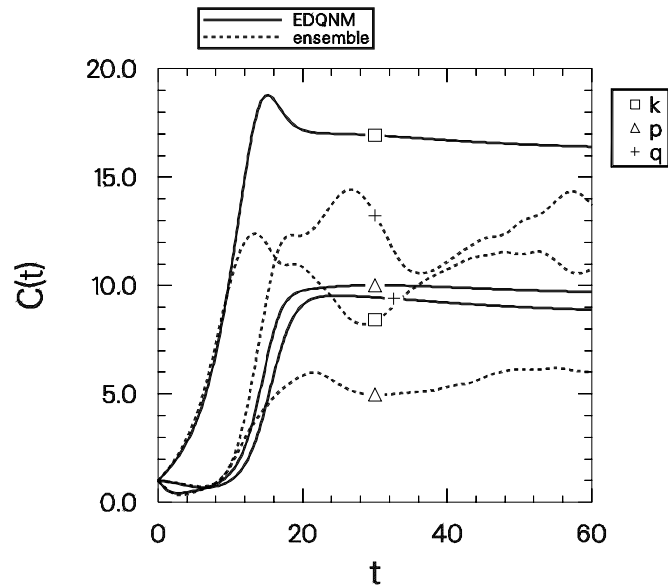


Figure V.44: Realizable EDQNM *vs.* exact solution corresponding to the case of Fig. V.42.

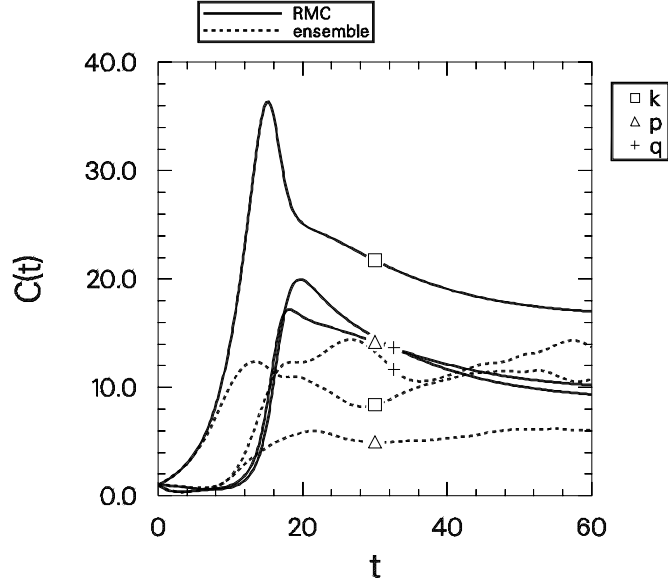


Figure V.45: RMC *vs.* exact solution corresponding to the case of Fig. V.42.

and  $R_k(\tau)$  at the transient time  $t = 15$  for the turbulent drift-wave case of Fig. V.46.

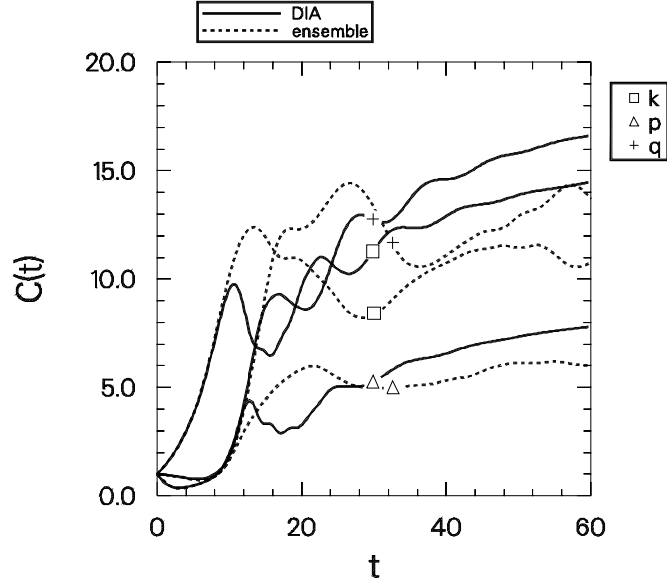
## V.D Multiple-field formulation

A partial test of the multiple-field closures in this work may be constructed by rewriting the one-field complex system, Eqs. (V.1), as a two-field system of real equations. For example, the first of Eqs. (V.1) may be written

$$\begin{aligned} \left( \frac{\partial}{\partial t} - \gamma_k \right) \psi_k^r - \omega_k \psi_k^i &= M_k^r (\psi_p^r \psi_q^r - \psi_p^i \psi_q^i) + M_k^i (\psi_p^r \psi_q^i + \psi_p^i \psi_q^r), \\ \left( \frac{\partial}{\partial t} - \gamma_k \right) \psi_k^i + \omega_k \psi_k^r &= M_k^i (\psi_p^r \psi_q^r - \psi_p^i \psi_q^i) - M_k^r (\psi_p^r \psi_q^i + \psi_p^i \psi_q^r). \end{aligned}$$

Upon defining

$$\begin{aligned} \gamma_k &= \begin{pmatrix} \psi_k^r \\ \psi_k^i \end{pmatrix}, \\ \nu_k &= \begin{pmatrix} -\gamma_k & -\omega_k \\ \omega_k & -\gamma_k \end{pmatrix}, \\ \mathbf{M}_k &= \begin{pmatrix} \mathbf{M}_k^r \\ \mathbf{M}_k^i \end{pmatrix}, \end{aligned}$$

Figure V.46: DIA *vs.* exact solution corresponding to the case of Fig. V.42.

$$\mathbf{M}_k^r = \begin{pmatrix} M_k^r & M_k^i \\ M_k^i & -M_k^r \end{pmatrix},$$

$$\mathbf{M}_k^i = \begin{pmatrix} M_k^i & -M_k^r \\ -M_k^r & -M_k^i \end{pmatrix},$$

we may then write Eqs. (V.1) as three real matrix equations of the form

$$\boxed{\frac{\partial \bar{c}_k(t)}{\partial t} + \nu_k \bar{c}_k(t) = \mathbf{M}_k \bar{c}_p(t) \bar{c}_q(t).}$$

In component form this appears as Eq. (II.25).

This system was implemented numerically for the multiple-field DIA, the realizable EDQNM, and the RMC. The numerical results of the two-field formulation agreed exactly with the one-field formulation for all of the cases discussed in this chapter, including the resonant and nonresonant cases. The connection between the predictions of these two equivalent formulations is expressed by the following formulae:

$$\begin{aligned} \operatorname{Re} C &= (C^{rr} + C^{ii}), & \operatorname{Im} C &= (C^{ir} - C^{ri}), \\ \operatorname{Re} R &= (R^{rr} + R^{ii}), & \operatorname{Im} R &= (R^{ir} - R^{ri}), \\ \operatorname{Re} \eta &= \frac{1}{2}(\eta^{rr} + \eta^{ii}), & \operatorname{Im} \eta &= \frac{1}{2}(\eta^{ir} - \eta^{ri}), \end{aligned}$$

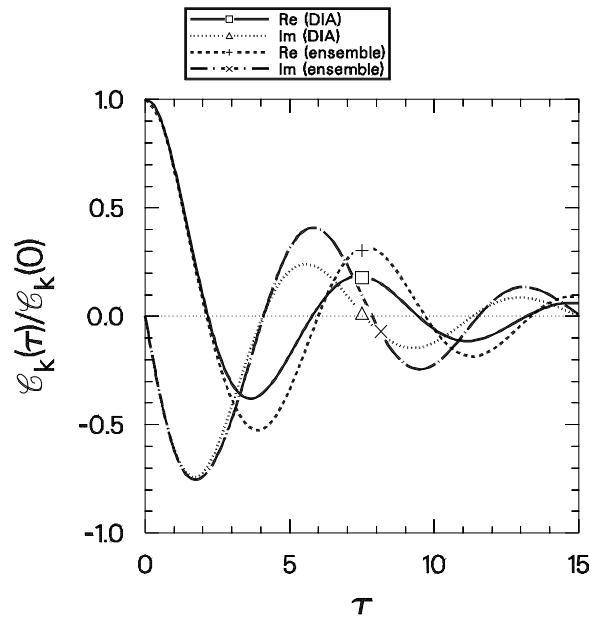


Figure V.47: Normalized two-time covariances  $\mathcal{C}_k(\tau)/\mathcal{C}_k(0)$  vs.  $\tau$  evaluated at  $t = 15$  for the turbulent drift-wave case.

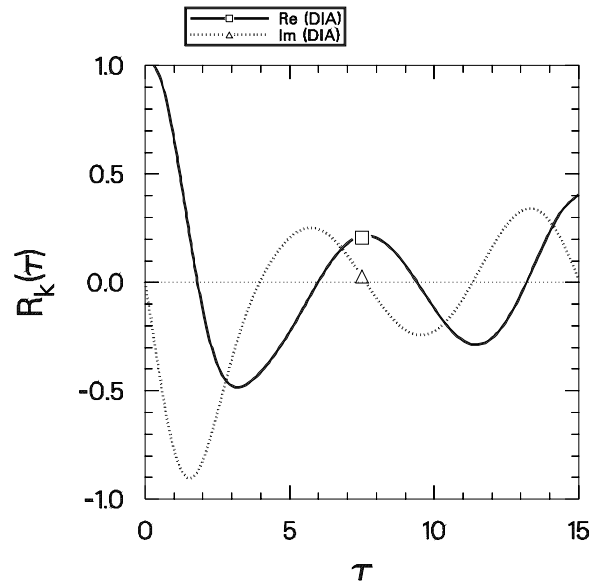


Figure V.48: DIA response function  $R_k(\tau)$  vs.  $\tau$  evaluated at  $t = 15$  for the turbulent drift-wave case.

Note that the Hermiticity of  $\mathbf{C}(t)$  implies that  $\text{Im } C(t) = 0$ .

This test is not sophisticated enough to identify the failure of the multiple-field realizable EDQNM discussed in Chapter III. The only quadratic invariants of this system are  $E$  and  $U$ . These correspond to the metric tensors

$$\sigma = \begin{pmatrix} 1 & 0 \\ 0 & 1 \end{pmatrix}$$

and

$$\sigma = \begin{pmatrix} k^2 & 0 \\ 0 & k^2 \end{pmatrix},$$

which are simultaneously diagonalizable. Hence, as expected, both of these invariants are conserved by the multiple-field realizable EDQNM. In addition, we point out that  $\nu_k$  is normal for this case and one finds numerically that the predicted  $\boldsymbol{\eta}_k$  is also normal.<sup>9</sup> Thus only the normal form for  $\boldsymbol{\theta}$ , Eq. (III.42), is actually being tested here. A more sophisticated test has been implemented for the  $\eta_i$  problem, the results of which appear in Figs. III.7, III.8, and III.12.

## V.E Summary

In this chapter we have tested the predictions of several statistical closures (including the DIA, the realizable EDQNM, and the RMC) against the exact statistical evolution for the problem of three interacting waves. In the resonant, dissipationless case we generally obtained good agreement; the closures all relaxed to the expected equilibrium form. However, in the nonresonant, dissipationless case the predictions of the Markovian closures differed substantially from both the expected equilibrium form and the exact statistics. We pointed out that this discrepancy results from the failure of the Markovian closures to conserve the Hamiltonian for this problem. In contrast, the DIA, which conserves this invariant, relaxes to the correct equilibrium form.

When dissipation was introduced into the three-wave problem, we generally found that the closures poorly modeled the transient dynamics. However, in a case where each realization of the exact solution achieves a steady state the DIA did obtain the correct final energies. In the stochastic cases studied by Wersinger *et al.* [1980] the disagreement was more pronounced; the closures appear to be incapable of modeling such highly truncated dynamical systems. Similar conclusions were reached in the case of complex mode-coupling.

---

<sup>9</sup>It has not yet been proven that the  $\boldsymbol{\eta}_k$  predicted by the multiple-field realizable EDQNM is normal whenever  $\nu_k$  is normal. In any event, such a result would be of little practical interest since we have already rejected this closure.

In the following chapter we will have an opportunity to test our assertion that the inability of closures to describe the three-wave problem with dissipation is primarily a consequence of the limited number of modes in this example. We expect that statistical closures will be more suitable candidates for the study of multimode turbulence.

# Chapter VI

## Application to Drift-Wave Turbulence

In this chapter we present numerical solutions of statistical closures for simple fluid models of two-dimensional drift-wave turbulence. Considering the limit of adiabatic electrons, we begin our study with the Hasegawa-Mima equation to emphasize several important features of the nonlinear drift-wave problem. To illustrate the dual cascade it is useful to consider the isotropic forced Hasegawa-Mima problem, for which the diamagnetic velocity vanishes, since in the short-wavelength limit this reduces to conventional two-dimensional turbulence. For pedagogical reasons we will inject energy and enstrophy into the system only through a narrow wavenumber band (unlike the typical situation in plasma turbulence, where energy and enstrophy enter the system at many scales). This will lead to the development of two inertial ranges: one characterized by an inverse energy cascade and the other by a direct enstrophy cascade. Upon inclusion of the diamagnetic velocity in the linear term, we then solve the anisotropic forced Hasegawa-Mima equation in the short-wavelength limit. The closure predictions are compared with results obtained by conventional numerical simulations using a pseudo-spectral code written by Ottaviani *et al.* [1990, 1991]. A hyperviscosity is introduced in this latter case to allow the use of a reduced inertial range, which facilitates the numerical computation of the simulation results. Good agreement is obtained between the two results, especially in the modeling of the slope of the inertial-range energy spectrum.

Next, we will proceed to the case of nonadiabatic electrons, using the more general Terry-Horton equation. Here, the nonadiabatic effects enter both in the linear term and in complex mode-coupling coefficients. One of our objectives is to compute a diffusion coefficient for the particle flux, which we will find is much higher than a simple mixing-length estimate. We also emphasize the role of the complex, anisotropic mode-coupling in altering the properties of the steady-state spectrum: for example, we find that the nonadiabatic case does not exhibit a dual

cascade and is highly anisotropic even at small scales. However, since the case of complex mode-coupling is conceptually more difficult, it is sensible to consider the simpler Hasegawa-Mima equation first.

## VI.A Continuum *vs.* discrete representations

Most of the formulae in this work have been expressed in the discrete wavenumber representation. However, in Chapter IV we emphasized the utility of a continuum representation for modeling a large number of interacting modes. Therefore, at this point let us present several expressions that connect the continuum and discrete representations. If we use the Fourier transform conventions given on pg. 20, the total energy may be expressed as [*cf.* Eq. (I.20)]

$$\begin{aligned} E &\doteq \frac{1}{2} \int_{-\infty}^{\infty} d\mathbf{x} \bar{\sigma} \langle \psi^2(\mathbf{x}, t) \rangle \\ &= \frac{1}{2} \sum_{\mathbf{k}} \sigma_{\mathbf{k}} C_{\mathbf{k}} \\ &= \frac{1}{2} \frac{1}{(2\pi)^d} \int_{-\infty}^{\infty} d\mathbf{k} \sigma_{\mathbf{k}} C(\mathbf{k}). \end{aligned}$$

When the wavenumber space is partitioned into bins of measure  $\Delta_{\mathbf{l}}$ , as described in Chapter IV, we may approximate  $E$  as<sup>1</sup>

$$E = \sum_{\mathbf{l}} E_{\mathbf{l}},$$

where

$$E_{\mathbf{l}} \doteq \frac{1}{2} \frac{1}{(2\pi)^d} \Delta_{\mathbf{l}} \sigma_{\mathbf{l}} C_{\mathbf{l}}$$

is the energy associated with bin  $\mathbf{l}$ .

We may also express  $E$  in terms of the spectral function  $E(k)$  such that  $E = \int_0^{\infty} E(k) dk$ , where in a polar representation

$$\begin{aligned} E(k) &\doteq \frac{1}{2} \frac{1}{(2\pi)^d} \sum_i k \Delta\theta_i \sigma_{\mathbf{l}_i} C_{\mathbf{l}_i} \\ &= \sum_i \frac{\Delta\theta_i}{\Delta_{\mathbf{l}_i}} k E_{\mathbf{l}_i}. \end{aligned}$$

The sum here is over all bins  $\mathbf{l}_i$  of angular width  $\Delta\theta_i$  containing the wavenumber  $k$ . In our geometry, these bins all have the same angular width:  $\Delta\theta_i \equiv \Delta\theta$ . The contribution to  $E(k)$  from each bin  $\mathbf{l}_i \doteq (l_i, \theta_i)$  containing the wavenumber  $k$  is:

$$[E(k)]_{\theta_i} \doteq \frac{1}{2} \frac{1}{(2\pi)^d} k \Delta\theta \sigma_{\mathbf{l}_i} C_{\mathbf{l}_i}.$$

---

<sup>1</sup>For  $\sigma_{\mathbf{k}} = 1$ , this result is exact.

## VI.B Inviscid Hasegawa-Mima problem

Drift-wave turbulence arises from a competition between a (generally anisotropic) linear drive and the isotropizing effects and saturation of the nonlinearity. Before considering the full problem of driven turbulence, it is advantageous to study these two effects in isolation of each other. For example, one may study the relatively trivial linear evolution in the absence of the nonlinear terms. A more interesting study results from the removal of the linear growth and damping effects, so that one can focus solely on the interactions of the nonlinear terms. As in two-dimensional turbulence, dissipation enters the Hasegawa-Mima problem only through the linear term. In the absence of forcing and dissipation, one finds that the nonlinear terms relax the system to the isotropic thermal equilibrium state that is described next.

### VI.B.1 Inviscid equilibrium

Kraichnan [1967] used the equipartition arguments of statistical mechanics to propose the discrete form

$$E_k = \frac{1}{2} \frac{1}{\alpha + \beta k^2} \quad (\text{VI.1}).$$

for the steady-state spectrum of *inviscid* two-dimensional isotropic turbulence (truncated to a finite  $k_{\min}$  and  $k_{\max}$ ). This equilibrium form assumes that the dynamics is mixing, which is a plausible conjecture for systems with many interacting modes. In the continuum representation, we need to include the volume element factor  $k$ :

$$E(k) = \frac{1}{2} \left( \frac{1}{2\pi} \right) \frac{k}{\alpha + \beta k^2} \quad (\text{VI.2}).$$

Equation (VI.2) is also the appropriate equilibrium form for the Hasegawa-Mima problem, as one may readily show by applying the calculation in Appendix H to the case where  $\sigma_{\mathbf{k}} = 1 + k^2$  and  $\sigma_{\mathbf{k}} = k^2(1 + k^2)$  form a complete set of invariants. In Appendix H we also establish that Eq. (VI.1) is a steady-state solution to the statistical closures considered in this work. Figure VI.1 illustrates the initial relaxation by the RMC closure [Eqs. (III.54)] of the inviscid Hasegawa-Mima problem from an initially anisotropic state toward the isotropic equilibrium state given by Eq. (VI.2). Here, we indicate the temporal evolution of 5 radial  $\times$  6 angular representative modes with markers that grow larger as time proceeds. The different marker shapes identify successive angular bins, which are labeled by 0, 1, and 2. Note that the reality condition allows us to evolve only 3 angular bins explicitly. The equilibrium solution is depicted by the solid curve. The final state depicted in Fig. VI.2 illustrates that equilibrium is eventually achieved quite precisely. This represents an important and nontrivial test of the nonlinear routines of our numerical code.

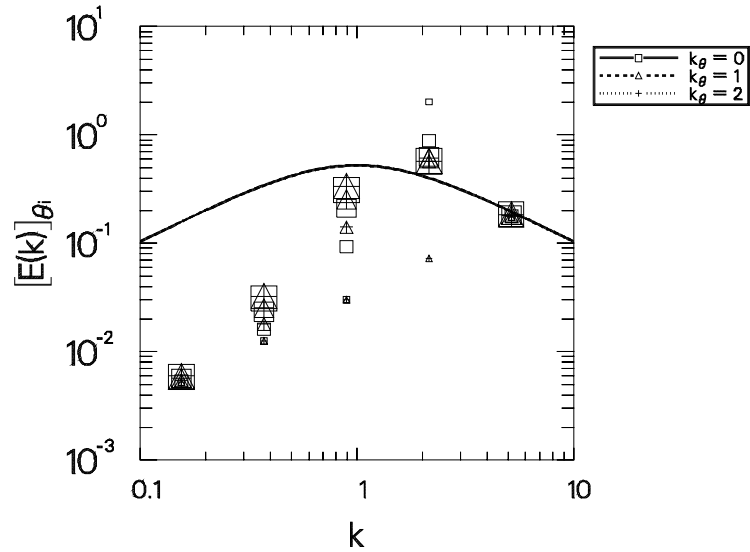


Figure VI.1: Initial relaxation of the inviscid Hasegawa-Mima problem to the equilibrium solution Eq. (VI.2). Since this problem is isotropic, the equilibrium curves for the three wavenumber angles coincide.

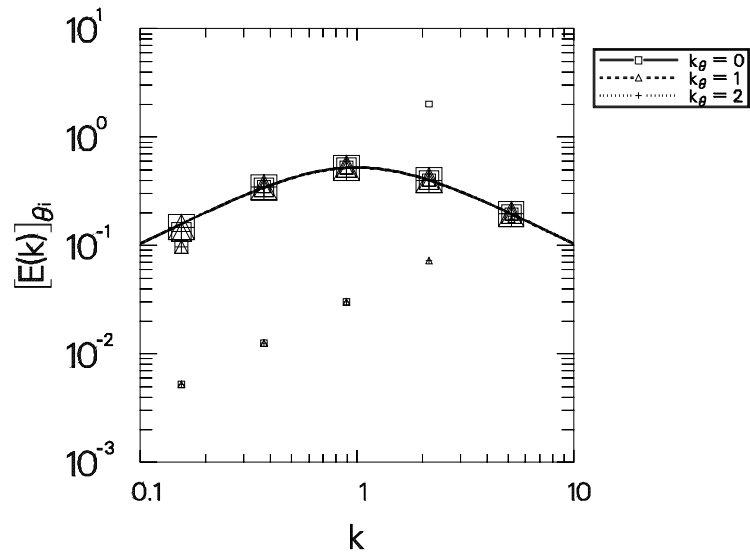


Figure VI.2: Final relaxation of the inviscid Hasegawa-Mima problem to the equilibrium solution Eq. (VI.2).

## VI.B.2 Driven two-dimensional fluid turbulence

Having considered the inviscid equilibrium problem, we would now like to combine the effects of linear forcing and viscous damping. We begin by considering the isotropic problem corresponding to two-dimensional fluid turbulence, for which one can demonstrate inertial-range power-law scalings [Orszag 1977] of the steady-state energy spectrum for both the DIA and Markovian closures.

Recall that upon substitution of  $k^2$  for the  $(1 + k^2)$  factors of the Hasegawa-Mima equation and the removal of the diamagnetic velocity  $V_d$ , the Hasegawa-Mima problem reduces to the conventional equation for two-dimensional turbulence,

$$k^2 \frac{\partial}{\partial t} \Phi_{\mathbf{k}} = \hat{\gamma}_k \Phi_{\mathbf{k}} + \frac{1}{2} \sum_{\mathbf{k}+\mathbf{p}+\mathbf{q}=0} \hat{\mathbf{z}} \cdot (\mathbf{p} \times \mathbf{q}) (q^2 - p^2) \Phi_{\mathbf{p}}^* \Phi_{\mathbf{q}}^*. \quad (\text{VI.3})$$

Note that the mode-coupling coefficients,  $\hat{\mathbf{z}} \cdot (\mathbf{p} \times \mathbf{q}) (q^2 - p^2) / k^2$ , now have a homogeneous scaling with wavenumber; in a steady state this property may be used to determine an analytical scaling for the inertial-range energy spectrum.

We model the effects of short- and long-wavelength damping and of non-adiabatic forcing by introducing the isotropic growth rate  $\hat{\gamma}_k$ , defined by

$$\hat{\gamma}_{\mathbf{k}} \doteq -\gamma_0 \exp\left(-\frac{k^2}{k_0^2}\right) - \nu_0 k^n + \frac{\gamma_f k^2}{\Delta_f} \begin{cases} 1 & \text{if } k_f - \frac{1}{2}\Delta_f < k < k_f + \frac{1}{2}\Delta_f, \\ 0 & \text{otherwise.} \end{cases} \quad (\text{VI.4})$$

The form of the first term, which models damping at the long wavelengths, was motivated by Horton [1986]. Usually, the added phenomenological growth rate is chosen to model kinetic effects that are omitted in a fluid description, as explained on pg. 12. Here, however, we choose a growth function that is positive in only a very narrow region of wavenumber space (unlike the situation encountered in actual plasma physics problems) in order to elucidate the dual cascade properties of two-dimensional turbulence. By restricting the injection of energy and enstrophy to a limited wavenumber band, we are readily able to follow the transfer of these quantities to the other wavenumbers.

Let us adopt the parameters

$$\gamma_0 = 2.0, \quad k_0 = 0.1, \quad \nu_0 = 4 \times 10^{-8}, \quad n = 4,$$

$$k_f = 1.543, \quad \Delta_f = 1.671, \quad \gamma_f = 0.25.$$

These parameters have been chosen to restrict the injection of energy and enstrophy to exactly eight consecutive radial bins for a  $64 \times 1$  bin configuration spanning the

region between  $k = 1/16$  and  $k = 1024$ . The  $k^2$  factor in Eq. (VI.4) ensures that the function  $k^{-2}\hat{\gamma}_{\mathbf{k}}$  is constant over these bins, thereby ensuring that the linear term is treated exactly by the bin-averaging scheme. The choice  $n = 4$  corresponds to the true viscosity. Later, we will consider the choice  $n = 10$ , which corresponds to a hyperviscosity. We will establish that the artifice of a hyperviscosity does not significantly alter the inertial-range dynamics and is therefore a valid technique for limiting the wavenumber domain.

Note that the mechanism we use to inject energy into the system differs from the usual situation in fluid turbulence studies, where the energy injection arises from an external random stirring force rather than through a linear growth rate. The physical mechanism underlying the energy injection is not crucial to the concepts we wish to illustrate; we choose the latter scheme since it is the appropriate one for modeling nonlinear plasma instabilities.

### Steady-state spectrum:

For the case of  $64 \times 1$  bins, the evolution of the quadratic quantities

$$E = \frac{1}{2} \sum_{\mathbf{k}} k^2 \langle |\Phi_{\mathbf{k}}|^2 \rangle, \quad (\text{VI.5a})$$

$$U = \frac{1}{2} \sum_{\mathbf{k}} k^4 \langle |\Phi_{\mathbf{k}}|^2 \rangle, \quad (\text{VI.5b})$$

$$P = \frac{1}{2} \sum_{\mathbf{k}} k^6 \langle |\Phi_{\mathbf{k}}|^2 \rangle, \quad (\text{VI.5c})$$

as predicted by the RMC closure is shown in Fig. VI.3. The quantity  $P$ , known as the palinstrophy, is proportional to the rate of enstrophy dissipation and provides a global measure of turbulent activity [Santangelo *et al.* 1989]. Note that unlike the energy and enstrophy, the palinstrophy is *not* conserved by the nonlinear terms of Eq. (VI.3).

The saturated energy spectrum is presented in Fig. VI.4. The dotted line indicates the initial energy spectrum, whereas the solid line indicates the final energy spectrum. The chain-dashed line indicates the linear growth rate and is plotted against the right-hand axis. The two inertial ranges, characterized by power-law decays, are clearly visible to the left and right of the energy injection range located in the vicinity of  $k = 1.5$ . The slope of the energy spectrum (obtained by finite differencing) is plotted in Fig VI.5.<sup>2</sup> In the energy inertial range, between  $k = 0.4$  and  $k = 0.7$ , we see that the slope achieves the nearly constant value of about  $-2$ .

<sup>2</sup>The dissipation range is poorly modeled in Fig. VI.5, as is evident from the small upward curvature of the spectrum for  $k > 100$ . This results from too small a choice for the upper wavenumber boundary; the curvature reflects the tendency for the system to evolve toward absolute thermal equilibrium. One could obtain the proper exponential decay in this region by extending the upper

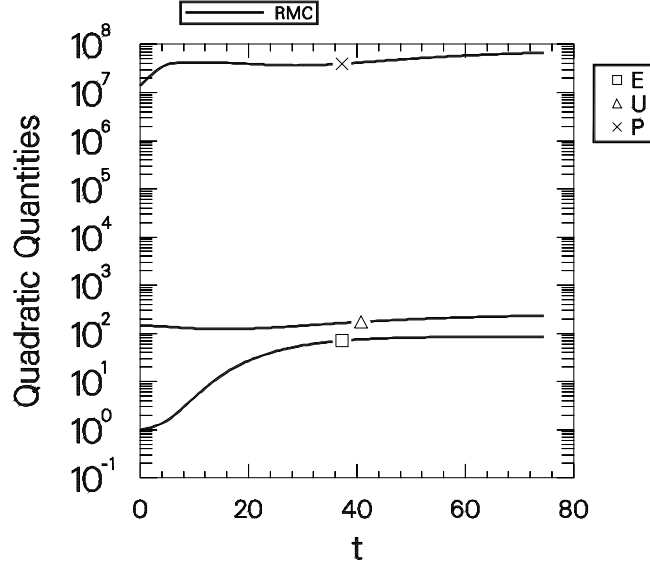


Figure VI.3: Evolution of the quadratic quantities  $E$ ,  $U$ , and  $P$  [Eqs. (VI.5)] for two-dimensional fluid turbulence.

This is substantially lower than the Kolmogorov value of  $-5/3$ ; we attribute this to the very limited extent of the energy inertial range. One could readily extend this range by replacing the exponential factor in Eq. (VI.4) with a long-wavelength damping that varies as a high inverse power of the wavenumber.

Our primary interest in this case is in the enstrophy inertial range. We see in Fig. VI.5 that the slope is not quite constant in this region. However, we recall that the corrected Kolmogorov law is

$$E(k) = C'_K \zeta^{2/3} k^{-3} \left[ \log \left( \frac{k}{k_f} \right) \right]^{-1/3}. \quad (\text{I.8})$$

Therefore, we graph in Fig. VI.6 the “corrected slope,” defined by

$$\frac{d \log \left[ E(k) \log (k/k_f)^{1/3} \right]}{d \log k}. \quad (\text{VI.6})$$

---

wavenumber boundary; our experience with similar computations at lower resolution indicates that an additional decade of (logarithmically-spaced) wavenumbers would be sufficient. The slope of the inertial range is not affected by the small amount of energy that is “piling up” at the very short wavelengths. This will become evident when we illustrate the effect of adding a hyperviscosity in Figs. VI.7 and VI.9.

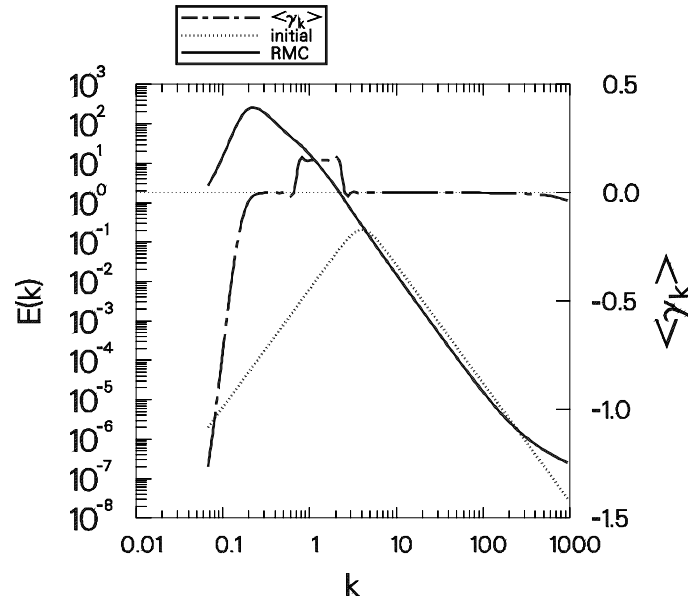


Figure VI.4: Saturated energy spectrum of two-dimensional fluid turbulence.

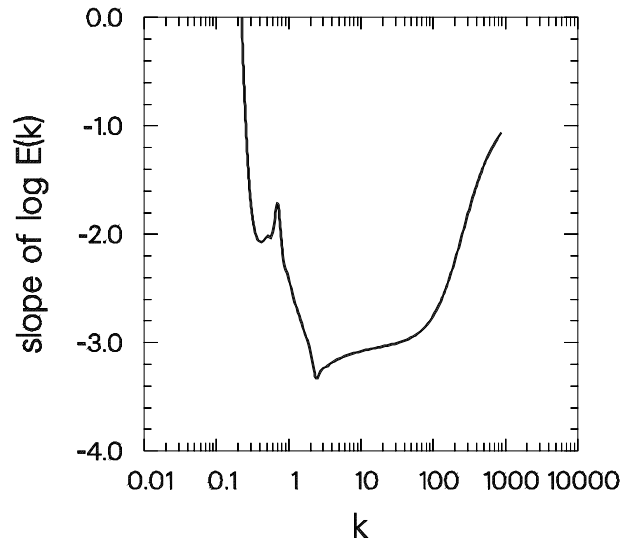


Figure VI.5: Logarithmic slope of the energy spectrum in Fig. VI.4.

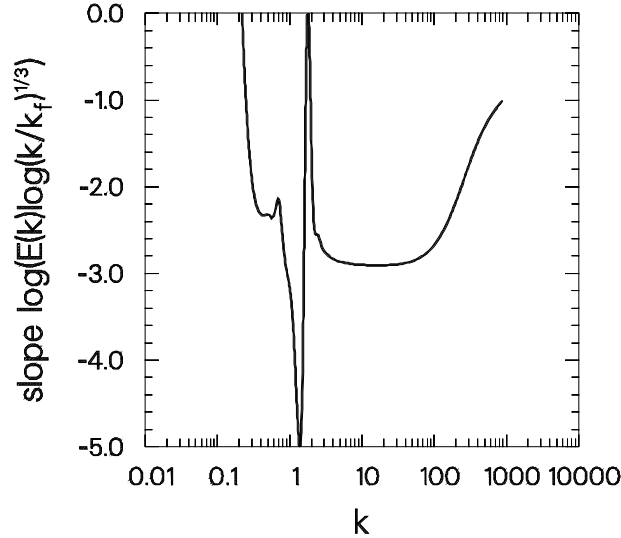


Figure VI.6: Corrected logarithmic slope of the energy spectrum in Fig. VI.4.

In this manner, we obtain a constant corrected slope of about  $-2.9$  between  $k = 6$  and  $k = 40$ . This value is slightly higher than the Kolmogorov value  $-3$ , but lower than the value  $-2.5$ , which is the theoretically expected slope for the inertial-range prediction of the RMC, since this closure is *not* random Galilean invariant.<sup>3</sup>

One may estimate the dissipation wavenumber  $k_d$  by equating the approximate strength of the nonlinear and linear terms:

$$\nu_0 k_d^4 \Phi(k_d) = k_d^4 \Phi(k_d) \Phi(k_d).$$

To determine  $\Phi(k_d)$  we need to evaluate the excitation level  $\Phi(k_f)$  by balancing the injection term with the nonlinear term:

$$\gamma_f k_f^2 \Phi(k_f) = k_f^4 \Phi(k_f) \Phi(k_f),$$

from which we obtain  $\Phi(k_f) = \gamma_f / k_f^2$ . Upon using the inertial range scaling law

<sup>3</sup>We are not yet certain of the reason for the discrepancy between the numerical slope and the theoretically predicted slope. However, since the Kolmogorov law is an asymptotic result valid for  $k_d/k_f \rightarrow \infty$ , we speculate that the discrepancy may disappear as the inertial range is extended. We have considered the possibility that perhaps the bin-averaging procedure somehow has removed the divergence that is responsible for the theoretical slope of  $-2.5$  instead of the Kolmogorov value  $-3$ . However, we believe that this is not the case since the numerical value  $-2.9$  does not seem to be sensitive to the number of bins used; in the limit where this number is large, the bin-averaging procedure reduces to a conventional discretization.

$\Phi(k) \sim [k^{-3}E(k)]^{1/2} \sim k^{-3}$ , we arrive at the dissipation-range balance

$$\nu_0 = \Phi(k_d) = \frac{\gamma_f}{k_f^2} \left( \frac{k_d}{k_f} \right)^{-3}.$$

From this last result, we deduce that  $k_d = [\nu_0/(\gamma_f k_f)]^{-1/3}$ . For  $\nu_0 = 4 \times 10^{-8}$ , we obtain  $k_d = 213$ . The reason that the dissipation range is poorly modeled in Fig. VI.4 is that the upper wavenumber boundary ( $k = 1024$ ) has been chosen too close to  $k_d$ . For this case, we estimate the Reynolds number  $UL/\nu$  to be about  $10^{10}$ , using the length scale  $L = 2\pi/0.2 \approx 30$  and energy  $\frac{1}{2}U^2 = 86$  determined by the code.

Often, a hyperviscosity is introduced to reduce the number of required modes. In Fig. VI.7 we illustrate the steady-state energy spectrum obtained by modifying the viscosity exponent  $n$  from 4 to 10 and setting the coefficient  $\nu_0$  to  $10^{-22}$ . Physically, one argues that since in the inertial range enstrophy transfer occurs only to the higher wavenumbers and the inverse energy transfer is negligible, this modification to the dissipation dynamics cannot affect the slope of the inertial-range energy spectrum. Upon comparing Fig. VI.7 with Fig. VI.4, we see that this is indeed the case. When the hyperviscosity is used, the corrected slope appears as in Fig. VI.9. In the inertial range we obtain the same value for the corrected slope,  $-2.9$ , as in the case where  $n = 4$ .

For this case, the dissipation wavenumber  $k_d$  is given by  $[\nu_0/(\gamma_f k_f)]^{-1/9} = 250$ . This is in good agreement with the wavenumber at which the dissipation range is seen to begin in Fig. VI.9.

### Energy transfer:

Although the inertial-range spectrum may suggest the direction of energy transfer, a more explicit representation of the flow of energy through wavenumber space may be obtained with the nonlinear energy transfer function  $\Pi_E(k)$  [Kraichnan 1959a],

$$\Pi_E(k) \doteq 2 \operatorname{Re} \int_k^\infty d\bar{k} T(\bar{k}),$$

where  $T(\bar{k})$  embodies the nonlinear terms of the energy equation:

$$\frac{\partial}{\partial t} E(\bar{k}) + 2 \operatorname{Re} \nu_{\bar{k}} E(\bar{k}) = 2 \operatorname{Re} T(\bar{k}).$$

Here  $\nu_k$  is the appropriate energy-weighted angular average of  $\nu_{\mathbf{k}}$ . The physical interpretation of  $\Pi_E(\bar{k})$  will be discussed shortly. The precise definition of  $T(\bar{k})$  is dependent on the expression used for the triplet correlation function appearing in

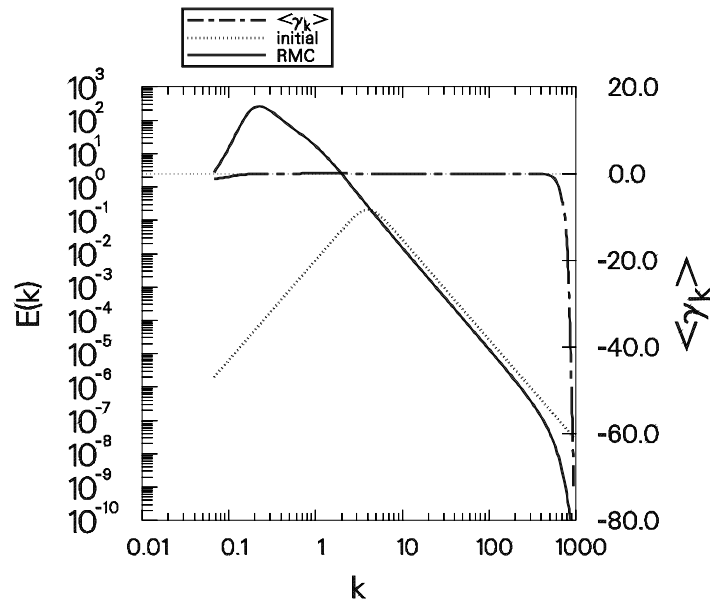


Figure VI.7: Saturated energy spectrum for two-dimensional fluid turbulence with hyperviscosity.

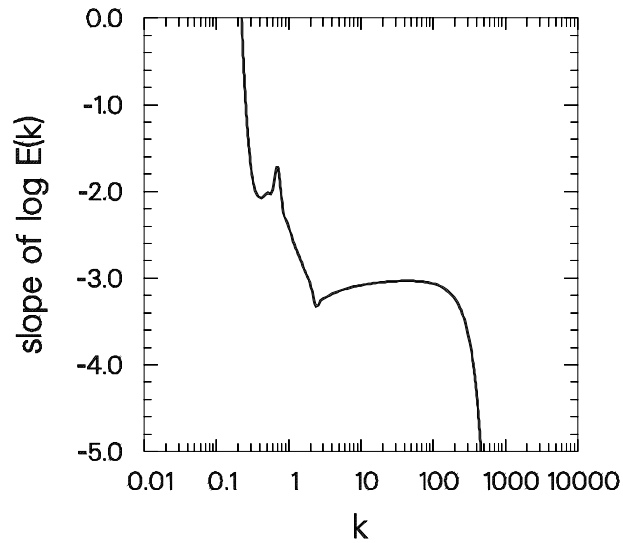


Figure VI.8: Logarithmic slope of the energy spectrum in Fig. VI.7.

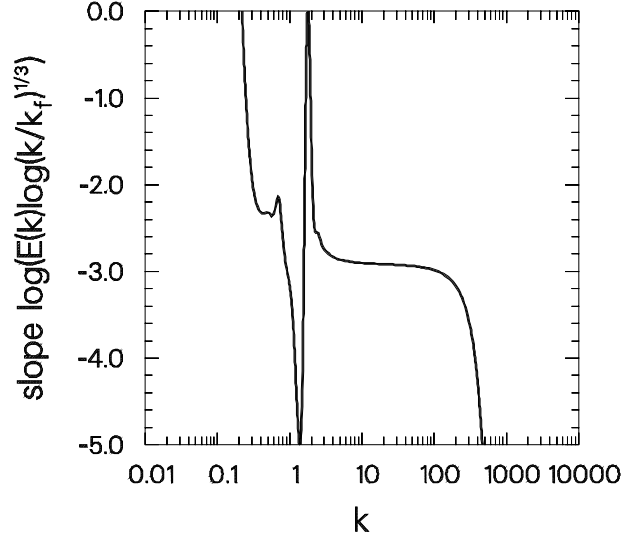


Figure VI.9: Corrected logarithmic slope of the energy spectrum in Fig. VI.7.

Eq. (I.22). In the bin approximation, suppose that a given closure appears as

$$\frac{\partial}{\partial t} C_{\mathbf{l}} + 2 \operatorname{Re} N_{\mathbf{l}} = 2 \operatorname{Re} F_{\mathbf{l}},$$

where  $N_{\mathbf{l}}$  and  $F_{\mathbf{l}}$  represent the nonlinear damping and source terms, respectively. Then  $T(l_r)$  is defined as

$$T(l_r) \doteq \frac{1}{2} \frac{1}{(2\pi)^2} \sum_{l_\theta} l_r \Delta\theta \sigma_{\mathbf{l}} (F_{\mathbf{l}} - N_{\mathbf{l}}),$$

so that

$$\Pi_E(k) \doteq \frac{1}{(2\pi)^2} \sum_{l_r=k}^{\infty} \sum_{l_\theta} \Delta_{\mathbf{l}} \sigma_{\mathbf{l}} \operatorname{Re}(F_{\mathbf{l}} - N_{\mathbf{l}}).$$

Here,  $l_r$  and  $l_\theta$  are the radial and angular components of the central wavenumber associated with bin  $\mathbf{l}$ .

If the nonlinear terms are conservative, then

$$\int_0^\infty d\bar{k} T(\bar{k}) = 0, \quad (\text{VI.7})$$

so that  $\Pi_E$  may be equivalently written as

$$\Pi_E(k) = -2 \operatorname{Re} \int_0^k d\bar{k} T(\bar{k}).$$

Additionally, we note that Eq. (VI.7) implies that

$$\Pi_E(0) = \Pi_E(\infty) = 0. \quad (\text{VI.8})$$

Let us also define the total linear forcing into all wavenumbers higher than  $k$  by  $\epsilon_E(k) \doteq 2 \operatorname{Re} \int_k^\infty d\bar{k} \nu_{\bar{k}} E(\bar{k})$ . The flow of energy to the high wavenumbers across a surface of constant wavenumber  $k$  may then be written in terms of its nonlinear and linear contributions:

$$\frac{\partial}{\partial t} \int_k^\infty d\bar{k} E(\bar{k}) = \Pi_E(k) - \epsilon_E(k).$$

A positive (negative) value for  $\Pi_E(k)$  represents a flow of energy to wavenumbers higher (lower) than  $k$ . Thus, for a two-dimensional inverse energy cascade one would expect  $\Pi_E(k)$  to be *negative* to the *left* of the energy injection range. Similarly, the enstrophy transfer function,  $\Pi_U(k)$ , should be *positive* to the *right* of the range of enstrophy injection. These properties of forced isotropic two-dimensional turbulence are clearly evident in Figs. VI.10 and Figs. VI.11, which were produced using the RMC closure approximation. The solid and dashed lines respectively depict the linear ( $\epsilon$ ) and nonlinear ( $\Pi$ ) contributions to the energy and enstrophy transfer underlying the energy spectrum of Fig. VI.4, represented here by the chain-dashed curve. Since the linear and nonlinear contributions nearly balance, we deduce that the system is close to a steady state. We also note that Eq. (VI.8) is obeyed by both  $\Pi_E(k)$  and  $\Pi_U(k)$  since both energy and enstrophy are conserved in this two-dimensional problem. At earlier times, one finds that although Eq. (VI.8) is still satisfied, the linear contribution differs substantially from the nonlinear contribution; this indicates that the spectrum is still evolving.

### Computation statistics:

Let us now briefly present some computation statistics for the two-dimensional turbulence case just studied. The number of distinct wavenumber triads associated with our isotropic  $64 \times 1$  bin configuration is 11 759. The computation of the corresponding bin-coupling coefficients took 1 minute of CPU time on a SparcStation 1+.

The two aspects of the computation were performed on the machine best suited to the task at hand. The bin-averaging procedure involves many nested subroutine calls and is not readily vectorizable; in contrast, the closure computation, with its long loops over the wavenumber triads, is highly vectorizable. The actual statistical evolution was therefore performed on the CRAY-2/8 machine located at the National Energy Research Supercomputer Center. Vectorization resulted in a remarkable increase in speed: solving the closure on the CRAY-2 (in 64 bit arithmetic) can typically be faster than on the SparcStation (in 32 bit arithmetic) by a

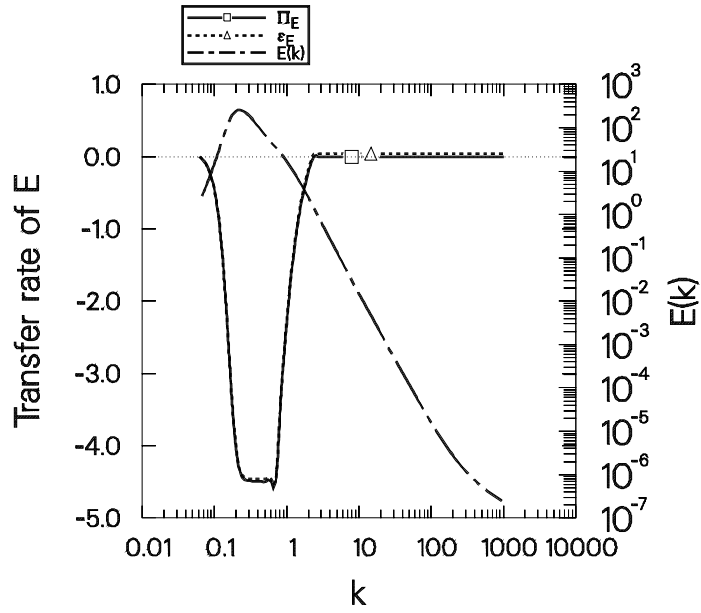


Figure VI.10: Energy transfer for the spectrum given in Fig. VI.4.

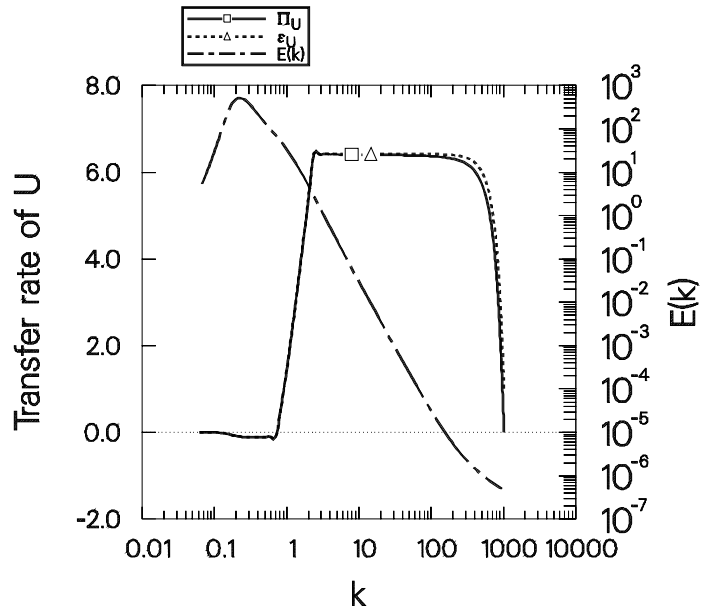


Figure VI.11: Enstrophy transfer for the spectrum given in Fig. VI.4.

factor of 50 or more, depending on the total number of triads. Nevertheless, the evolution depicted in Fig. VI.3, which required 700 000 variable-length time steps, took 631 CPU minutes on the CRAY-2.

### **Inertial range scaling of closures:**

One of the principal advantages of Markovian statistical closures is that the scaling of computation time with Reynolds number is superior to that of conventional numerical simulations. For example, it follows from the Kolmogorov argument that the ratio of the wavelengths of enstrophy injection to those of enstrophy dissipation in two-dimensional turbulence is proportional to  $R^{1/2}$ . A uniform rate of enstrophy transfer in the inertial range then implies that the ratio of the largest to smallest time scales must also be proportional to  $R^{1/2}$ . Thus, conventional simulations of two-dimensional turbulence require computation times proportional to  $R^{3/2}$ . In contrast, the number of modes required in a statistical closure computation with logarithmically spaced bins scales as  $\log R^{1/2}$  (assuming that the degree of anisotropy does not depend on the Reynolds number). Now if  $R$  is sufficiently large, the number of wavenumber pairs that must be evolved scales more like the square than the cube of the number of modes (*cf.* pg. 77) since the convolution constraint for the bin-averaging procedure reduces in this limit to the continuum form  $\mathbf{k} + \mathbf{p} + \mathbf{q} = \mathbf{0}$ . Thus the total computation time scales as  $R^{1/2}(\log R^{1/2})^2$ , or simply as  $R^{1/2} \log^2 R$ . Therefore, for sufficiently high Reynolds number turbulence, one concludes that closure computations will require less effort than conventional simulations. We emphasize that the gain we achieve here arises from the relative smoothness of the statistical variables in wavenumber space. Although we have assumed that the anisotropy is independent of  $R$ , it is clear that even if substantial dependence on  $R$  were introduced, our conclusion would not change.

## **VI.C Short-wavelength Hasegawa-Mima equation**

To employ the full power of the anisotropic bin-averaging technique developed in Chapter IV, we now wish to study the effect of setting the normalized diamagnetic velocity  $V_d$  to unity. This will introduce an anisotropic oscillation into the system. Although this oscillation will not *directly* affect the energy evolution, it will introduce a frequency mismatch (and anisotropy) into the expression for the triad interaction time, which can in turn affect the energy spectrum.

Let us consider a case for which numerical simulation data has been computed by Ottaviani *et al.* [1991] using a conventional pseudo-spectral code. To facilitate the latter computation, a hyperviscosity is introduced to reduce the extent of the active dissipation range. To minimize the computational effort, only the regime

between  $k = 1$  and  $k = 64$  is modeled. We again use the scale-invariant mode coupling considered on pg. 221. This choice considerably simplifies the analysis of the inertial range dynamics and allows one to make contact with the Rossby wave problem.

The effects of short- and long-wavelength damping and of non-adiabatic forcing will be modeled by the isotropic growth rate  $\hat{\gamma}_k$ , which we redefine here as

$$\hat{\gamma}_{\mathbf{k}} \doteq -D_1 k^{10} - D_2 k^{-2} + \frac{\gamma_f k^2}{\Delta_f} \begin{cases} 1 & \text{if } k_f - \frac{1}{2}\Delta_f < k < k_f + \frac{1}{2}\Delta_f, \\ 0 & \text{otherwise.} \end{cases} \quad (\text{VI.9})$$

The case we study has

$$\begin{aligned} D_1 &= 10^{-13}, & D_2 &= 0.05, \\ k_f &= 4.212, & \Delta_f &= 1.088, & \gamma_f &= 0.0625. \end{aligned}$$

These parameters were chosen so that the injection range occupies exactly two bins when 32 radial bins are used. The  $k^2$  factor in Eq. (VI.9) ensures that the function  $k^{-2}\hat{\gamma}_{\mathbf{k}}$  is constant over a bin, so that the linear term is treated exactly by the bin-averaging scheme.

For the closure computation discussed in the following subsection, we employed a bin geometry of  $32 \times 6$  bins. Because the reality condition (which takes into account of the symmetry  $\mathbf{k} \rightarrow -\mathbf{k}$ ) was invoked, only 3 angular bins were evolved explicitly. To reduce any redundancy in the mode assignments arising from the additional symmetry  $k_x \rightarrow -k_x$  (for fixed  $k_y$ ), we aligned the bin boundaries at  $\theta = -\pi/2$ , where  $\theta$  represents the angular component of  $\mathbf{k}$ . The bin centers are then located at  $\theta = -2\pi/3$ ,  $\theta = 0$ , and  $\theta = 2\pi/3$ . The linear growth rate and frequency is plotted in Figs. VI.12 and Figs. VI.13. The symbols indicate the bin-averaged values of the growth rate and frequency; any displacement of these values from the continuous curves is due to variations of these quantities over a bin.

### VI.C.1 Comparison of closure *vs.* numerical simulation

In Fig. VI.14 we compare the evolution of the quadratic quantities  $E$ ,  $U$ , and  $P$ , as predicted by the RMC ( $32 \times 6$  polar modes) and a single realization of Ottaviani's pseudo-spectral code ( $128 \times 128$  Cartesian modes).<sup>4</sup>

We see that the total energy is modeled reasonably well by the closure, while the enstrophy and palinstrophy predictions differ substantially. We emphasize that

---

<sup>4</sup>The closure computation evolved 96 575 distinct triads a total of 20 000 time steps; this required 171 minutes on the CRAY-2. The wavenumber bin averaging took 49 CPU minutes on the SparcStation. In comparison, the numerical simulation required roughly 60 minutes on the CRAY-2.

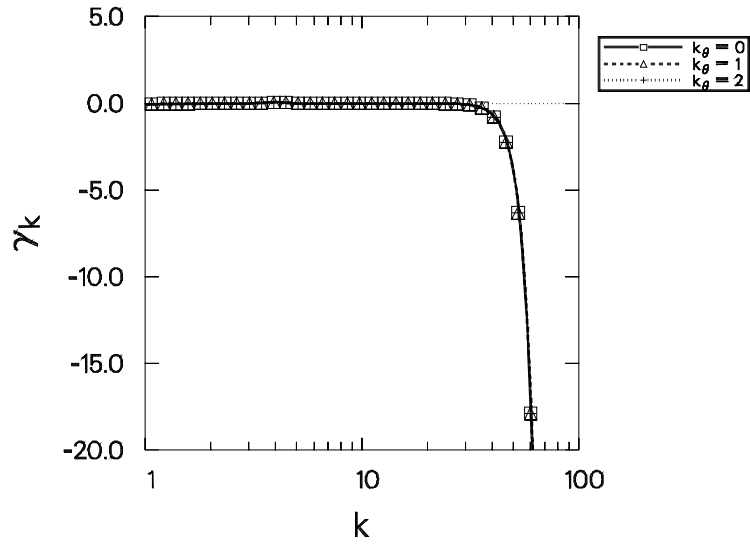
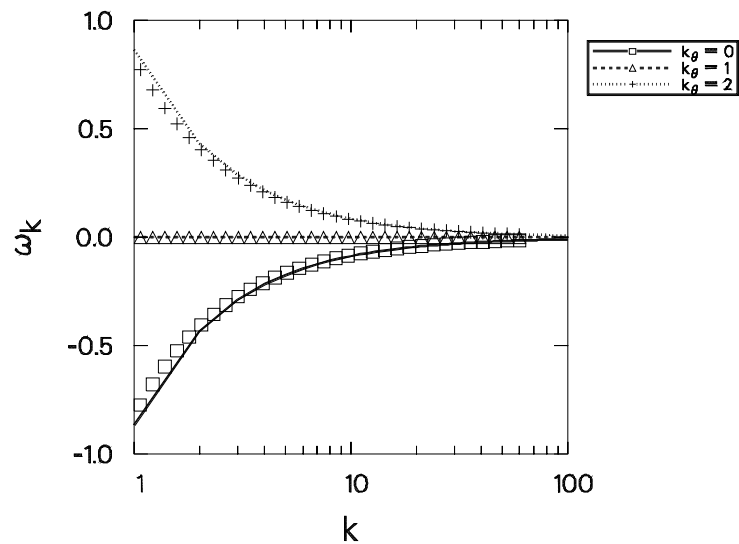


Figure VI.12: Linear growth rate defined in Eq. (VI.9).

Figure VI.13: Frequency  $k_y V_d / k^2$  used in the short-wavelength Hasegawa-Mima problem.

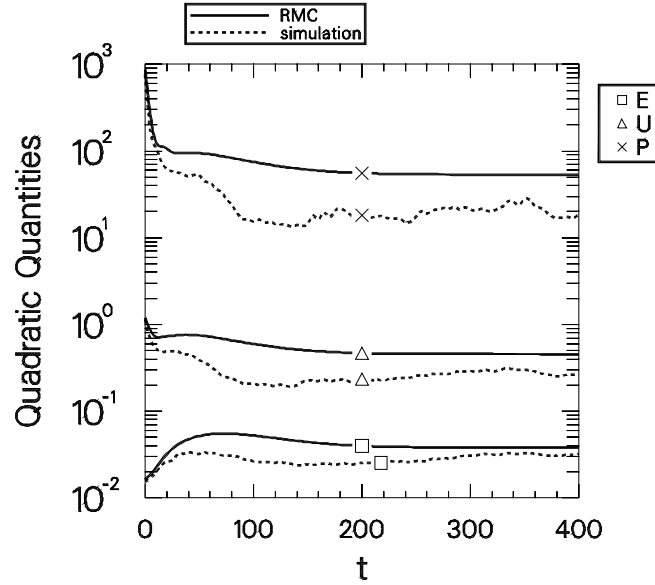


Figure VI.14: Comparison of the time evolution of quadratic quantities predicted by the RMC and conventional numerical simulation.

the simulation data presented here represents only a single realization. Although no time average has been performed on the simulation data, the average over wavenumber helps to reduce the fluctuations in the plotted quantities. An appreciation for the size of these fluctuations may be gained upon considering a second realization of this system, depicted in Fig. VI.15. We stress that the simulation data here is limited by the relatively small number of retained fundamental modes and represents only a numerical approximation, not an exact solution, to Eq. (VI.3).

In Fig. VI.16 we graph the energy spectrum determined from the two computations. A second realization of the simulation data is depicted in Fig. VI.17. The initial energy spectrum,

$$E(k) \propto k^3/[1 + (k/4)^6],$$

is indicated by the dotted line, while the solid and dashed lines depict the closure and simulation results, respectively. The fluctuations mentioned above are particularly evident at the long wavelengths, where relatively few angular modes exist for each fixed radial wavenumber. The angle-averaged growth rate, which is dominated by the hyperviscosity, is also indicated in terms of the units on the right axis.

We see that the respective slopes of the spectrum in the enstrophy inertial range between  $k = 7$  and  $k = 11$  are in rough agreement, although the absolute energy levels predicted by the simulation in this region are lower than those of the closure. The slope of the energy spectrum determined by the closure is evaluated numerically

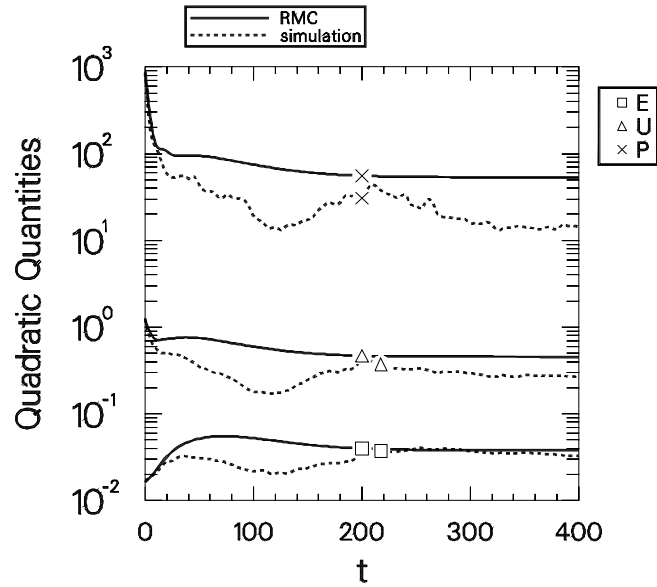


Figure VI.15: Comparison of the time evolution of quadratic quantities predicted by the RMC and a second realization of the simulation.

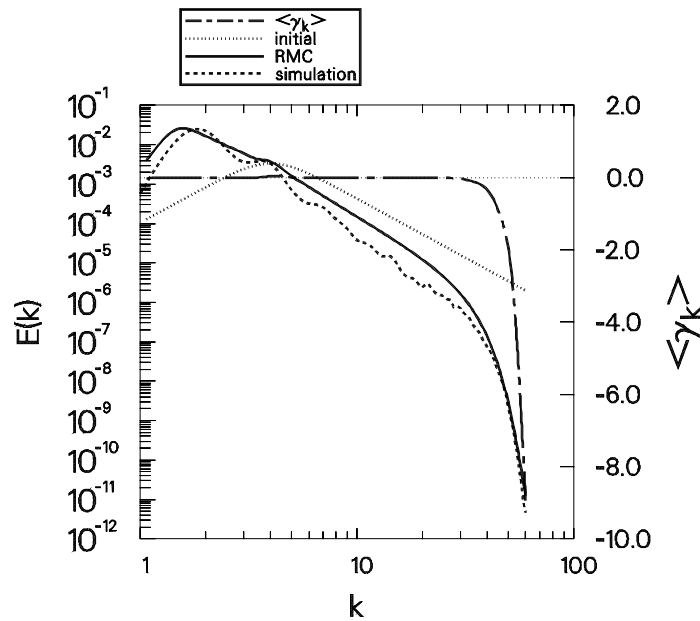


Figure VI.16: Comparison of the steady-state energy spectra predicted by the RMC and conventional numerical simulation.

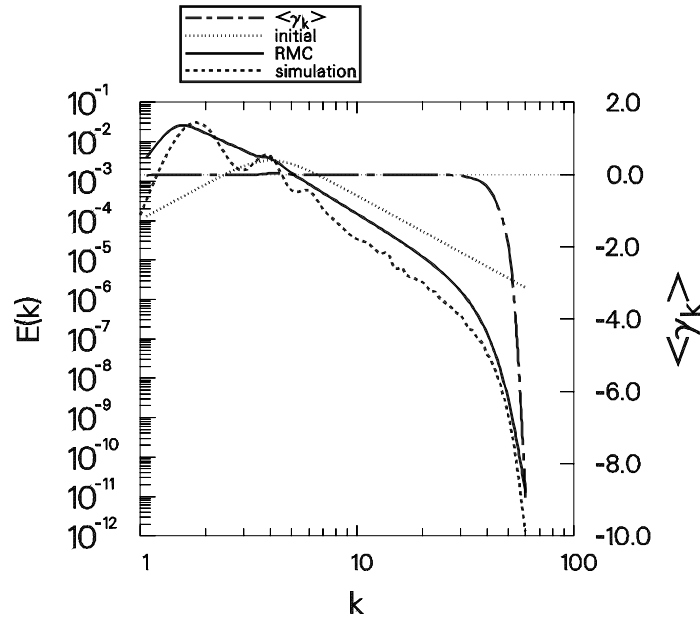


Figure VI.17: Energy spectra predicted by the RMC and second realization of the simulation.

in Figure VI.18. In the enstrophy range, the slope takes on the value of about  $-3.4$ . The corrected slope defined by Eq. (VI.6) and depicted in Fig. VI.19 does not appear to be constant in the inertial range. This is likely due to the fact that the enstrophy range is not well developed in this case since the dissipation wavenumber  $k_d = 24$  is only a factor of six larger than the wavenumbers of enstrophy injection.

One expects the role of the diamagnetic velocity  $V_d$  to be relatively small for this case since the wavenumbers are all larger than unity. One encounters anisotropy only at the longest wavelengths, as is readily apparent in Fig. VI.20, where we graph the angular standard deviation of the spectrum normalized to the mean energy in each wavenumber shell. The three-dimensional plot in Fig. VI.21 displays the short-wavelength isotropy pictorially. In this illustration, the spectrum is arbitrarily truncated after the outermost central wavenumber; one is thus viewing the intersection of the spectrum with this truncating plane.

The dual cascade is clearly evident in the graphs of the energy and enstrophy transfer, Figs. VI.22 and Figs. VI.23. However, a new feature is observed in Fig. VI.23 that we did not see in Fig. VI.11: there is significant enstrophy transfer to the long wavelengths, although the dominant transfer is still to the small scales. This is likely related to the fact that the long-wavelength region is highly anisotropic; the conventional picture of the enstrophy transfer in isotropic turbulence does not apply.

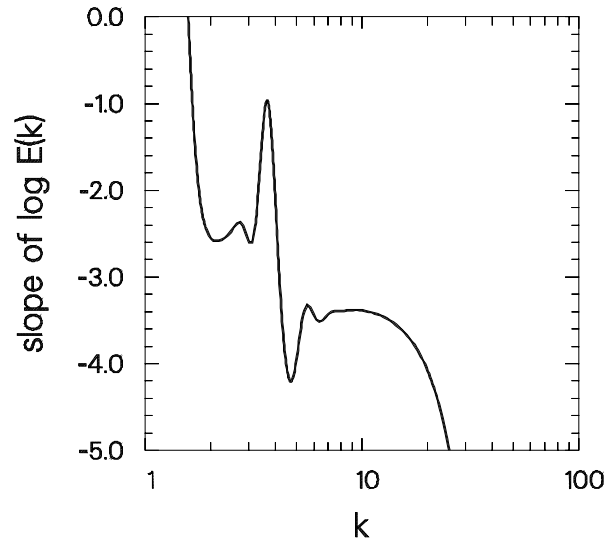


Figure VI.18: Logarithmic slope of the RMC energy spectrum in Fig. VI.16.

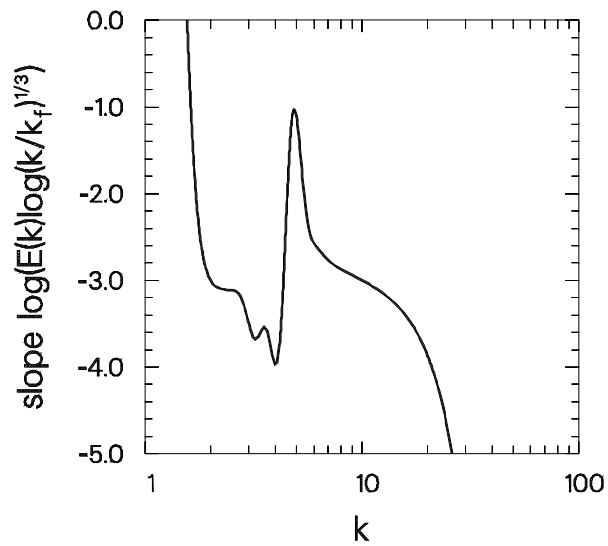


Figure VI.19: Corrected logarithmic slope of the RMC energy spectrum in Fig. VI.16.

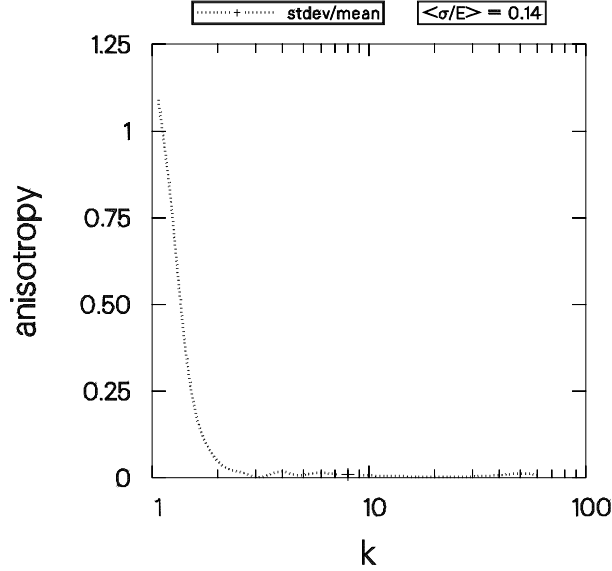


Figure VI.20: Anisotropy of the energy spectrum of Fig. VI.16.

### VI.C.2 Two-time statistics

By initializing the DIA closure [Eqs. (I.38) and (I.39)] with the steady-state spectrum just found using the RMC closure, we were able to evolve the DIA 134 time steps, or a time interval of 1.4, and found no significant differences except at the very high wavenumbers, where the energy spectrum increased slightly. Some of the modes, particularly those at the longest wavelengths, appear to be still evolving at this stage. This DIA run took about 2.6 hours on the CRAY-2; we lack the computational power to evolve the DIA much further with this many modes. Nevertheless, in this nearly stationary state it is still interesting to examine the two-time correlation and response function data, as depicted in Figs. VI.24 and VI.25. In each set, the top three graphs correspond to the modes located at  $k = 14$ ; the bottom three correspond to modes at  $k = 16$ . Note that the Fluctuation-Dissipation relation is quite well satisfied.

## VI.D Hasegawa-Mima equation

Let us now return to the full Hasegawa-Mima equation,

$$(1 + k^2) \frac{\partial}{\partial t} \Phi_{\mathbf{k}} = -ik_y V_d \Phi_{\mathbf{k}} + \hat{\gamma}_k \Phi_{\mathbf{k}} + \frac{1}{2} \sum_{\mathbf{k}+\mathbf{p}+\mathbf{q}=0} \hat{\mathbf{z}} \cdot (\mathbf{p} \times \mathbf{q}) (q^2 - p^2) \Phi_{\mathbf{p}}^* \Phi_{\mathbf{q}}^*, \quad (\text{VI.10})$$

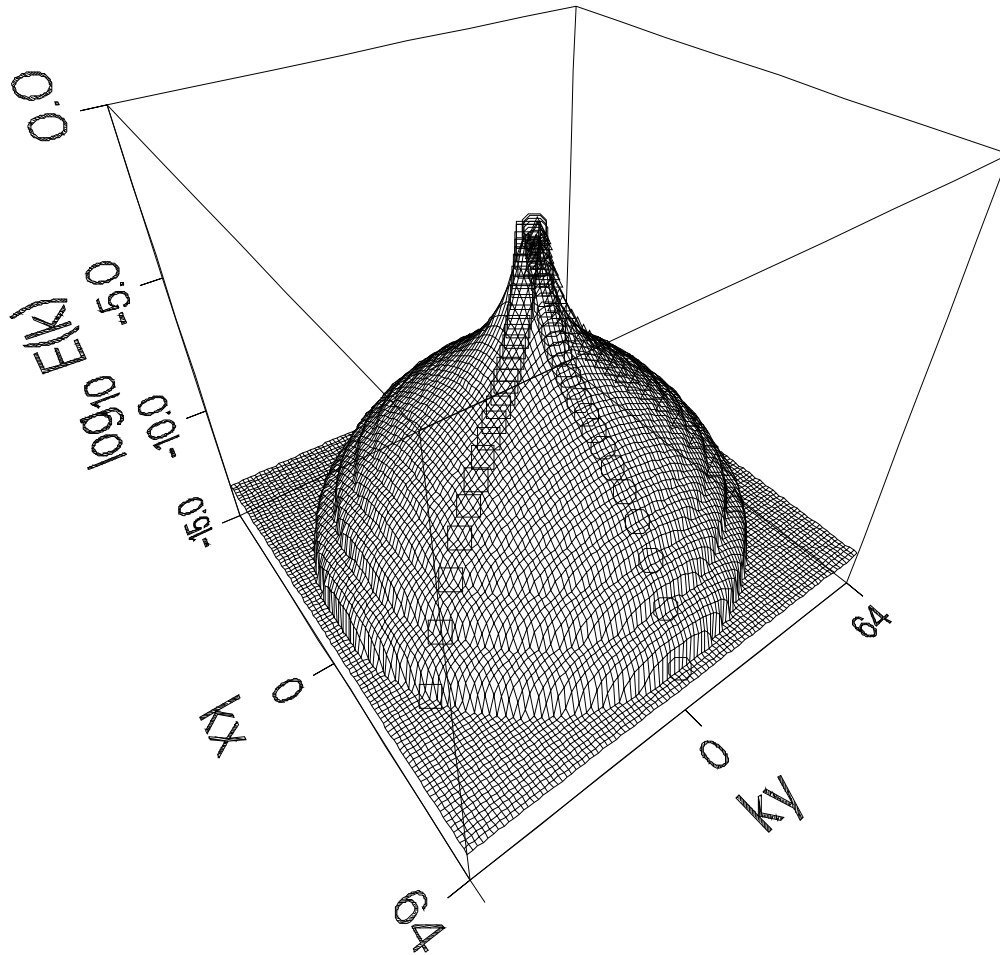


Figure VI.21: Three-dimensional view of the energy spectrum of Fig. VI.16.

and consider the growth rate function  $\hat{\gamma}_k = (1 + k^2)\gamma_k$  used by Waltz [1983], where

$$\gamma_k = 0.06 \left[ 1 - 0.5 \left( \frac{|k_x| - 0.5}{0.5} \right)^2 - 0.5 \left( \frac{|k_y| - 0.5}{0.5} \right)^2 \right] - 0.05.$$

This function is illustrated in Fig. VI.26. It reaches its maximum value of 0.01 at  $(k_x, k_y) = (0.5, 0.5)$  and is damped at both high and low  $k$ . The frequency function  $ik_y V_d / (1 + k^2)$  is shown in Fig. VI.27. The symbols on these plots indicate

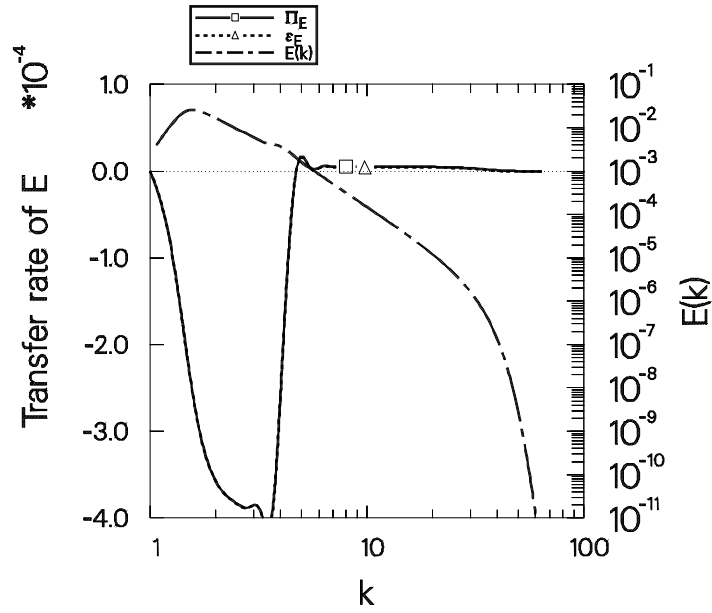


Figure VI.22: Energy transfer for the RMC prediction in Fig. VI.16.

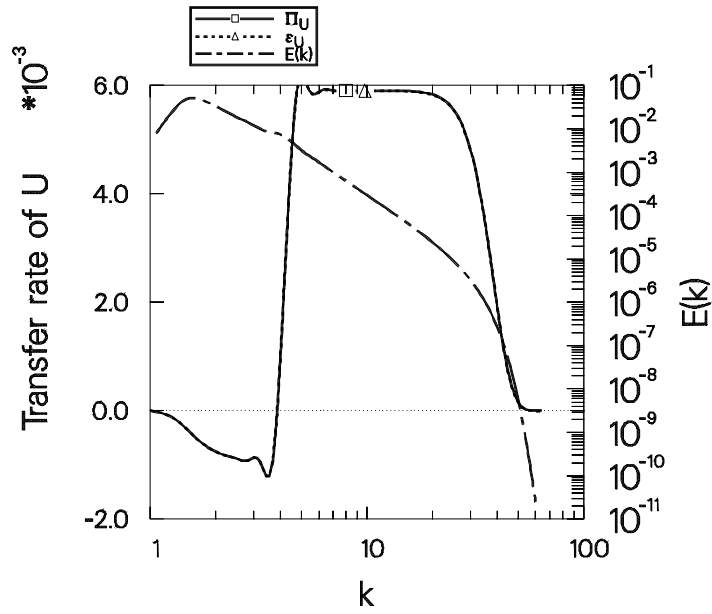


Figure VI.23: Enstrophy transfer for the RMC prediction in Fig. VI.16.

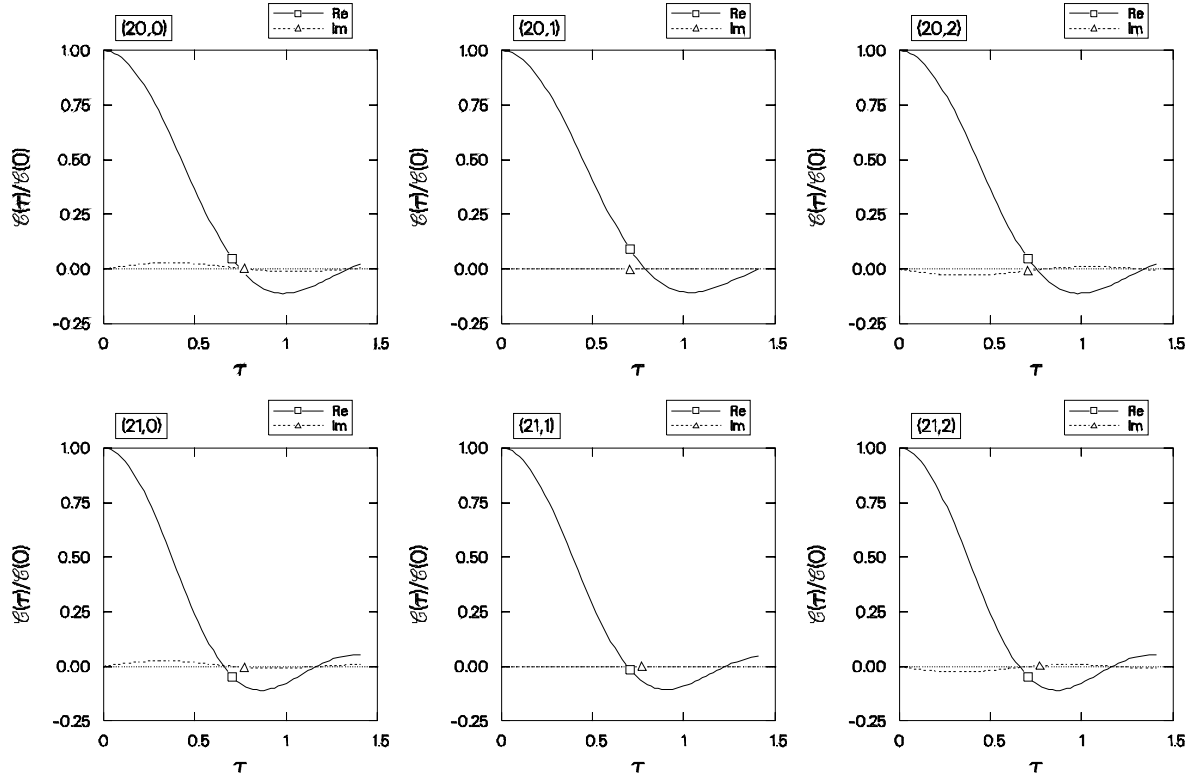


Figure VI.24: Typical correlation function data obtained by initializing the DIA with the spectrum of Fig. VI.16.

the value of the functions at the bin centers, using the geometry discussed below. Note that although the symmetry  $\mathbf{k} \rightarrow -\mathbf{k}$  is exploited to reduce the number of modes, we do not make explicit use of the additional symmetry  $k_x \rightarrow -k_x$  (for fixed  $k_y$ ).

Waltz used  $11 \times 11$  Cartesian modes uniformly spaced between  $-1$  and  $1$  in each direction. To emulate Waltz's layout as closely as possible in polar geometry, we use a  $6 \times 20$  bin geometry. With the RMC closure, we evolved the code from an equilibrium distribution to the steady state depicted in Fig. VI.28.<sup>5</sup>

<sup>5</sup>This anisotropic closure computation required 5 CPU minutes on the CRAY-2, much less than the 50 CRAY minutes quoted by Waltz for his conventional simulation. The bin-averaging for the 19 708 distinct triads required 10 CPU minutes on the SparcStation. This comparison demonstrates that the computational advantages of statistical closures are not limited to the case of

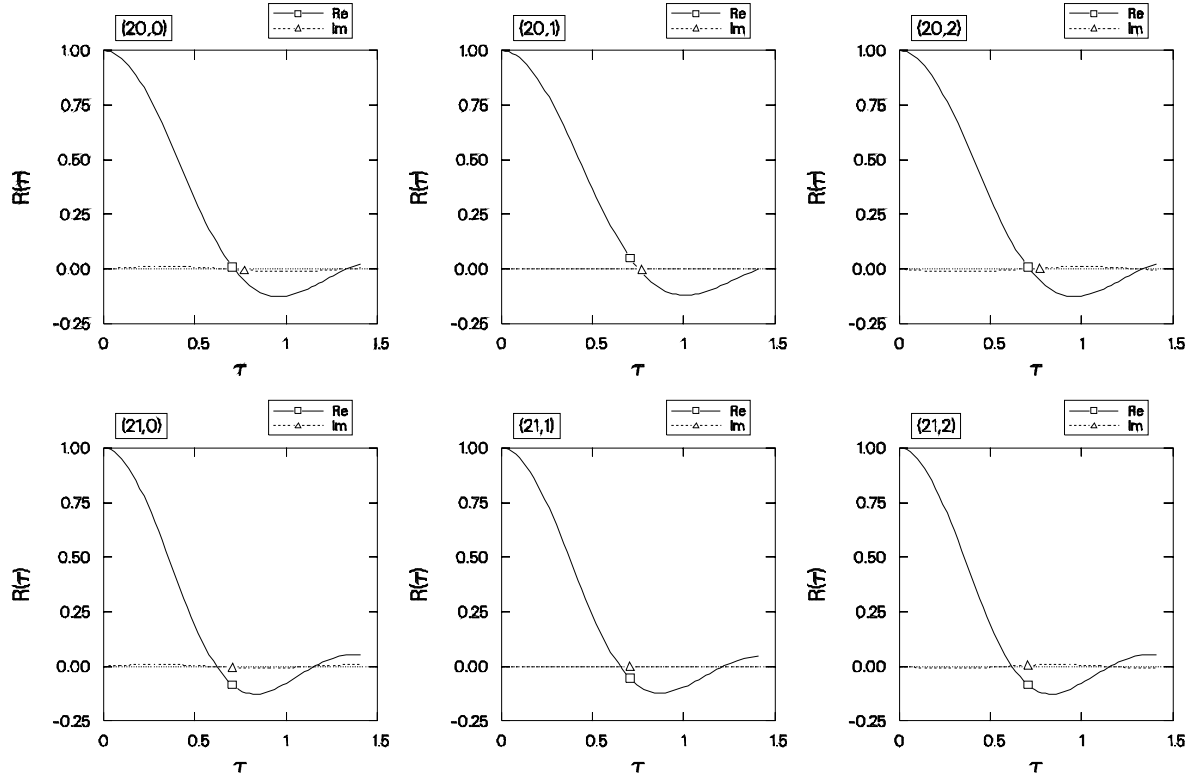


Figure VI.25: Typical response function data obtained by initializing the DIA with the spectrum of Fig. VI.16.

Waltz solved the quasistationary EDQNM equations; in a steady state, these agree with the RMC equations.<sup>6</sup> He obtained the final energy  $E = 2.18$  and enstrophy  $U = 0.58$  with his closure, whereas we obtained the values  $E = 1.05$  and  $U = 0.30$ . We attribute the discrepancies to differences in the resolution, which for both runs is limited, especially in the radial direction. His numerical simulation (with a simple Fourier space convolution code HYDR), produced the final values  $E = 1.4 \pm 0.7$  and  $U = 0.38 \pm 0.22$ . We note that both Waltz's and our

---

isotropic turbulence.

<sup>6</sup>Waltz [1983, pg. 171] describes his equations as the result of applying a “resonance approximation” to “the DIA weak coupling theory”; in addition, he often refers to his approximation as the DIA itself. However, his equations actually correspond to the strong turbulence approximation we know as the quasistationary EDQNM.

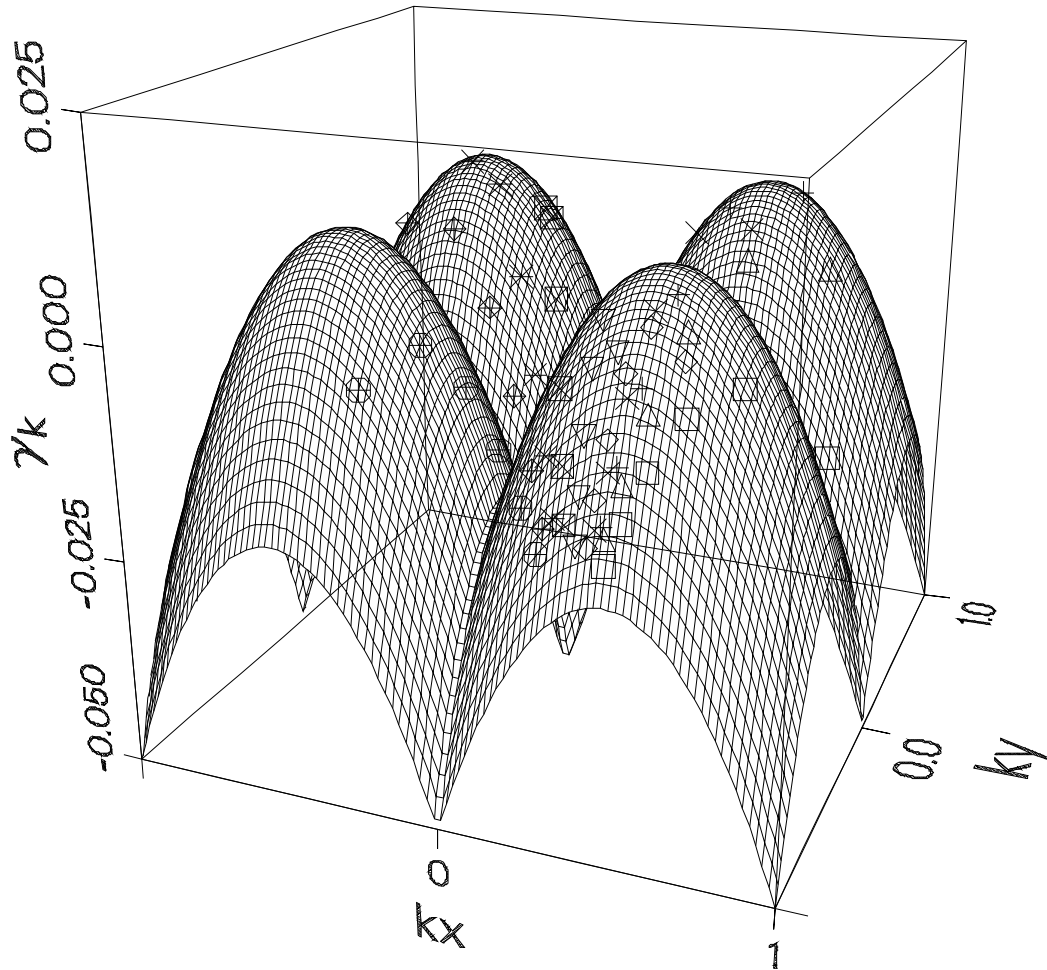


Figure VI.26: Three-dimensional view of the growth rate used by Waltz.

RMC results fall well within the range of these simulation values, although ours are substantially closer.

### VI.D.1 Two-time statistics

We have also obtained a stationary DIA solution for this case. This was obtained by initializing the DIA with the solution obtained with the RMC closure. We first

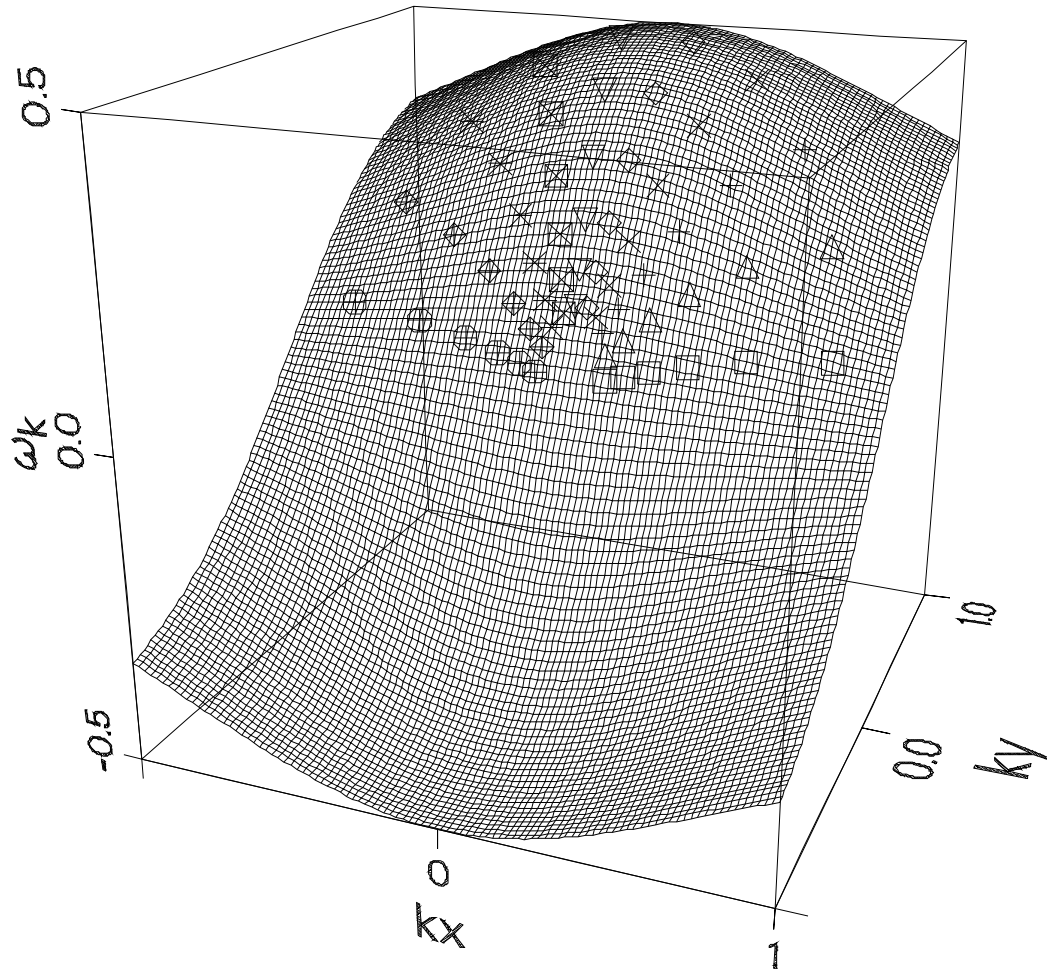


Figure VI.27: Three-dimensional view of the frequency function  $ik_y V_d / (1 + k^2)$ .

ran the DIA 180 time steps, or 214 time units. This took a total of 158 CPU minutes on the CRAY-2 machine. The final time step required 2.3 CPU minutes and the total computation time appeared to be increasing as the square of the number of time steps, as one expects for a system with many modes [*cf.* Eq. (II.31)]. At this time it was clear that the system had not yet reached a steady state; however, the energies had significantly evolved beyond their initial values. We therefore began

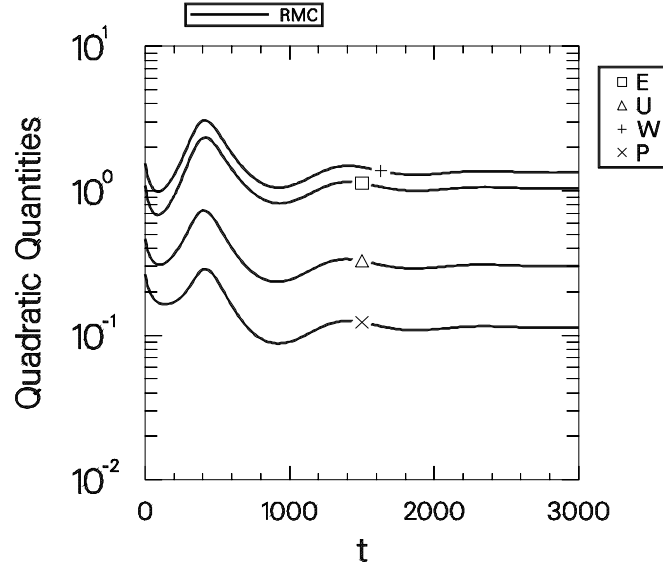


Figure VI.28: RMC evolution of the quadratic invariants for Waltz's problem.

a second DIA run initialized with the final energies from the previous DIA run.<sup>7</sup> After 120 iterations, the stationary state shown in Fig. VI.29 was obtained. This latter phase required an additional 49 CPU minutes. The total energy obtained with the DIA was about 20% higher than the level predicted by the RMC. Sample correlation and response function data are illustrated in Figs. VI.30 and VI.31. Again, we note that these results satisfy the Fluctuation-Dissipation relation.

## VI.E Terry-Horton problem

Drift waves described by the Hasegawa-Mima equation are purely oscillatory in linear theory unless one phenomenologically introduces a growth rate. This was done in the previous sections to account partially for destabilizing kinetic effects omitted from this simple fluid description. However, we discussed in Chapter I that growth effects can also enter the problem through the mode-coupling coefficients, which become complex in the presence of nonadiabatic electrons. Thus, the Terry-Horton equation, Eq. (I.11), heuristically accounts for nonadiabatic effects with the introduction of the so-called  $i\delta$  model. In our notation,  $\delta \equiv \chi''$ , the imaginary part

<sup>7</sup>A more sophisticated technique for extending the computational power of the DIA, which partially accounts for the non-Gaussian statistics predicted during a previous evolution, has been developed by Rose [1985].

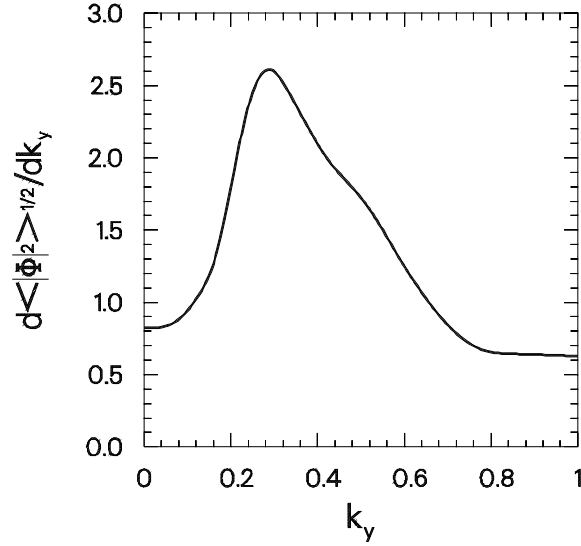


Figure VI.29: Root-mean-square DIA amplitude level averaged over  $k_x$  for Waltz's problem.

of the electron susceptibility.

There are important limitations to the Terry-Horton equation, namely that writing

$$n_e = (1 + i\chi'')\Phi$$

does not properly model the nonlinear dynamics of the electrons. That is, this relation is only linear in  $\Phi$ ; one actually expects  $n_e$  to also vary nonlinearly with  $\Phi$ . To account more correctly for the nonlinear nonadiabatic effects one should extend this model to a two-field system, where the nonadiabatic part of the electron density is evolved separately from the potential [Wakatani and Hasegawa 1984, Bowman and Krommes 1987, Gang *et al.* 1991]. Here, however, we are primarily interested in illustrating the computational procedure; we will therefore be content with evolving only the  $\Phi$  equation.

Let us recall the Terry-Horton equation:

$$\left( \frac{\partial}{\partial t} + \nu_{\mathbf{k}} \right) \Phi_{\mathbf{k}} = \frac{1}{2} \sum_{\mathbf{k}+\mathbf{p}+\mathbf{q}=0} \hat{\mathbf{z}} \cdot (\mathbf{p} \times \mathbf{q}) \frac{(\chi_{\mathbf{q}} - \chi_{\mathbf{p}})^*}{(1 + \chi_{\mathbf{k}})} \Phi_{\mathbf{p}}^* \Phi_{\mathbf{q}}^*. \quad (\text{I.11})$$

Following Horton [1986], we set  $\nu_{\mathbf{k}} = ik_y V_d / (1 + \chi_{\mathbf{k}}) - i\nu_0 k^4 / (1 + k^2)$  and  $\chi_{\mathbf{k}} = k^2 + i\delta_0 k_y (c_0 - k^2)$ . We point out that the function given for  $\nu_{\mathbf{k}}$  by Horton in

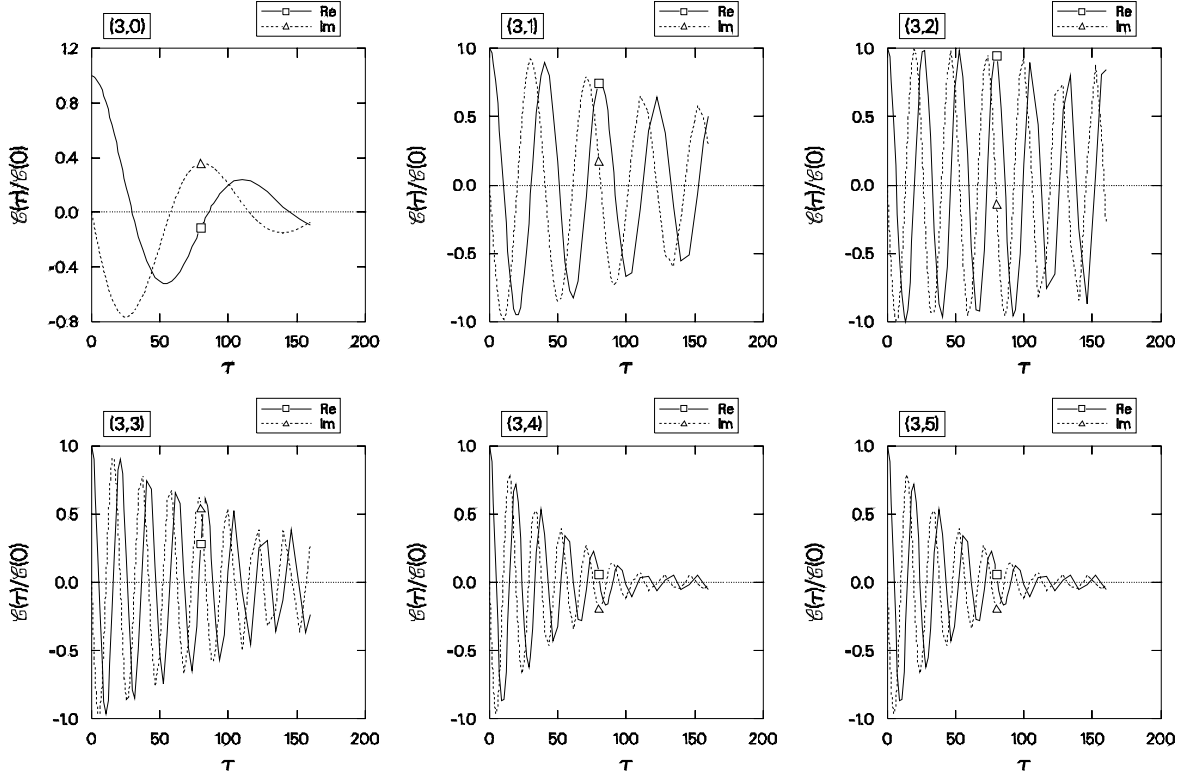


Figure VI.30: Typical correlation function data obtained by applying the DIA to Waltz's case.

his Eq. 7 is not what he actually used [Horton 1989]; instead, he neglected the nonadiabatic effects in the long- and short-wavelength damping. For his parameters this is actually a poor approximation; it markedly changes the character of the linear growth and frequency. Nevertheless, to facilitate comparison with Horton's work we adopt the same linear form that he used. Thus, we set  $\delta_0 = 1$ ,  $c_0 = -0.25$ , and  $\nu_0 = 0.15$ ; this corresponds to Horton's model for the trapped electron mode. Essentially, these instabilities are drift waves that have been destabilized by the effects of electrons trapped in the nonuniform magnetic field of a tokamak.

Note that no hyperviscosity is used for this study since we will solve only the closure equations; we will not attempt to simulate the evolution with a pseudo-spectral method.

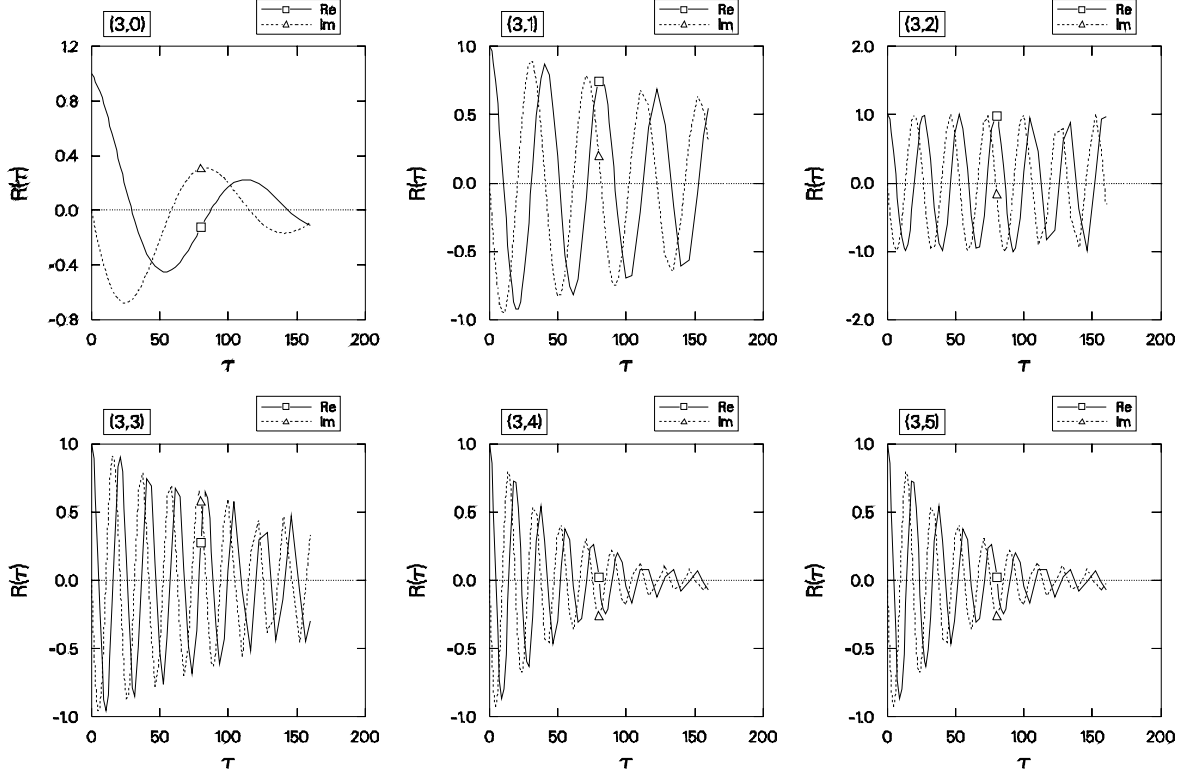


Figure VI.31: Typical response function data obtained by applying the DIA to Waltz's case.

### VI.E.1 Inviscid equilibrium

When the viscosity and diamagnetic velocity are both set to zero ( $\nu_0 = V_d = 0$ ), the Terry-Horton equation conserves the single invariant

$$W \doteq \frac{1}{2} \sum_{\mathbf{k}} |1 + \chi_{\mathbf{k}}|^2 \langle |\Phi_{\mathbf{k}}|^2 \rangle.$$

Therefore, a thermal equilibrium spectrum may still be deduced for this system, even though energy is no longer conserved. The equilibrium form

$$E_k = \frac{1 + k^2}{2\epsilon |1 + \chi_{\mathbf{k}}|^2} \quad (\text{VI.11})$$

follows from the results of Appendix H. Note that since there is only one invariant, this spectrum depends on a single parameter,  $\epsilon$ , instead of the two parameters  $\alpha$

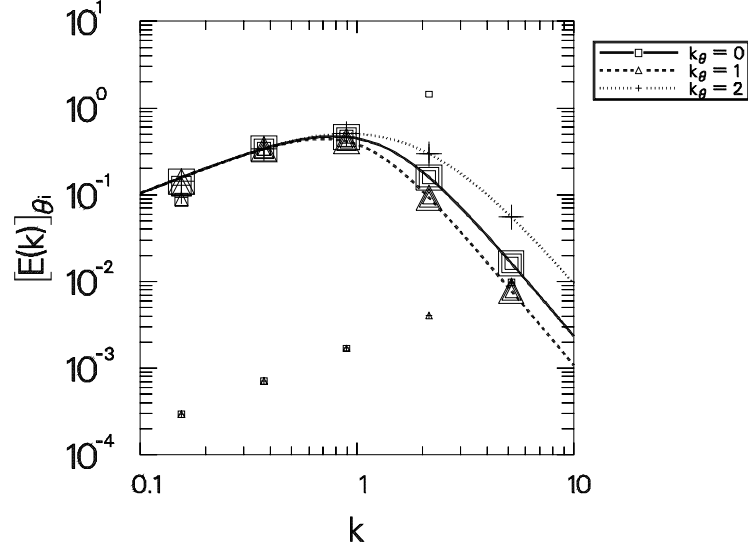


Figure VI.32: Relaxation of the inviscid Terry-Horton problem to the equilibrium solution Eq. (VI.11). The anisotropic mode-coupling leads to different equilibrium curves for each angle.

and  $\beta$ .

In Fig. VI.32 we illustrate the evolution of the energy spectrum to Eq. (VI.11). Since  $\chi_{\mathbf{k}}$  enters Eq. (VI.11), the equilibrium state is anisotropic, particularly at the short scales. This example serves as a partial check on the correct operation of the complex mode-coupling routines.

## VI.E.2 Saturated turbulent state

Let us now account for the effect of viscous damping with the parameter  $\nu_0 = 0.15$  and proceed to the study of saturated drift-wave turbulence with the aid of the RMC and DIA closures. Although a Markovian closure for this problem has previously been considered by Horton [1986] (in the frequency domain), he did not solve it. Instead he made some simplifying analytical approximations to avoid the difficult task of solving the closure numerically. At the long wavelengths Horton used an assumption of isotropy and locality in wavenumber space to obtain approximate spectra. He then asymptotically matched the long-wavelength results to expressions he derived for the short-wavelength region by using the eddy turnover time to estimate the rate of nonlinear transfer to the higher wavenumbers. Upon joining these approximate spectra continuously at both high and low wavenumbers,

Horton thereby obtained a scaling relation for the particle diffusion coefficient that is reminiscent of the empirical estimate  $\langle \gamma'_{\mathbf{k}} \rangle / \langle k_{\perp}^2 \rangle$  [Dupree 1967]. However, as he points out, his final expression neglects the contribution to the diffusion coefficient from the energy inertial range. In addition, the numerous rough approximations he invokes make it impossible to extract a reliable numerical value for the diffusion coefficient.

In this work, we wish to evaluate this diffusion coefficient more systematically, with the help of the numerical techniques we have developed. Therefore, in addition to determining the fluctuation level, we will be particularly interested in the issues of nonlinear transfer, anisotropy, the scaling of the nonlinear damping with wavenumber magnitude, and the prediction of a diffusion coefficient from our numerical data.

### **Wavenumber partition:**

To determine the required number of bins in the radial and angular directions, it is important to do a sensitivity analysis as the number of bins is varied. In the above studies of forced isotropic turbulence, we were unable to establish a systematic convergence to a fixed total energy level with the available computational resources. Apparently an extraordinarily large number (more than  $10^4$ ) of distinct wavenumber pairs is required in order to model these problems properly. Although one might attribute this to the relatively fast variation of the linear growth rate and the energy spectrum with wavenumber, this is probably not the most important source of error. One can argue that the self-coupling effects discussed in Chapter IV will be most significant for isotropic turbulence since the amount of wavenumber spaced spanned by bins of fixed radial extent will be largest for an isotropic configuration. In an anisotropic configuration, there will be several bins in each wavenumber shell; these will be properly coupled to one another. If the neglect of self-coupling effects is significant, it is typically only the noise term, not the nonlinear damping term, that is mistreated; one therefore expects the total energy to rise as the number of bins is increased. For isotropic turbulence, this is exactly the effect that was noted. Therefore, in order to obtain convergence of the total energy with a reasonable number of bins, it may be necessary to include the self-coupling effects, at least for isotropic problems. Although for anisotropic turbulence a general implementation of self-coupling effects seems impractical, the algorithm developed in Chapter IV could be readily used to include isotropic self-coupling effects since the total number of isotropic bin triads is relatively small.

For Horton's anisotropic problem, Table VI.1 shows that the total energy and other quadratic quantities have converged with respect to the number of radial bins (the convergence is best at the short scales, which dominate the wavenumber contributions to  $P$ ). Since the turbulence in this problem is highly anisotropic, in a

| Bins          | E  | U  | W  | P  |
|---------------|----|----|----|----|
| $8 \times 8$  | 43 | 13 | 59 | 11 |
| $16 \times 8$ | 50 | 17 | 72 | 17 |
| $32 \times 8$ | 41 | 16 | 63 | 17 |

Table VI.1: Variation of the steady-state spectrum of forced anisotropic turbulence as the number of radial bins is increased.

| Bins          | pairs   | triads  | CPU minutes                      |                       |
|---------------|---------|---------|----------------------------------|-----------------------|
|               |         |         | bin-averaging<br>SparcStation 1+ | evolution<br>CRAY-2/8 |
| $8 \times 8$  | 5 790   | 6 445   | 20                               | 6.5                   |
| $16 \times 8$ | 26 285  | 29 077  | 142                              | 37                    |
| $32 \times 8$ | 126 836 | 139 058 | 471                              | 197                   |

Table VI.2: Computation statistics for the three geometries in Table VI.1.

future study it would be desirable to also perform a convergence study with respect to the number of angular bins.

### Computation statistics:

In Table VI.2 we present typical computation statistics for the three anisotropic bin configurations used in the previous convergence demonstration. We tabulate the total number of contributing wavenumber pairs as determined by the bin-averaging routines, along with the number of distinct triads. The latter number differs from the number of wavenumber pairs since the contribution to mode  $\mathbf{k}$  from modes  $\mathbf{p}$  and  $\mathbf{q}$  requires evaluating  $\Theta$  for all *three* triads  $(\mathbf{k}, \mathbf{p}, \mathbf{q})$ ,  $(\mathbf{p}, \mathbf{q}, \mathbf{k})$ , and  $(\mathbf{q}, \mathbf{k}, \mathbf{p})$ , which may not necessarily be present in the full list of wavenumber pairs.<sup>8</sup> However, the total number of triads is not simply three times the number of pairs since permutations of a basic  $(\mathbf{k}, \mathbf{p}, \mathbf{q})$  triad may have already been accounted for. The symmetries arising from the reality condition further complicate the situation; considerable effort was made to avoid any redundancies in the triad assignments.

Computation times are given in Table VI.2 both for the bin-averaging calculation (which is required only once for each new wavenumber geometry) and for the evolution to a steady state. The computation times given for the bin-averaging procedure are expressed as CPU minutes on a SparcStation 1+, whereas those for

---

<sup>8</sup>This discussion applies to the RMC closure; our implementation also exploits the additional symmetries of  $\theta$  available under the EDQNM closure.

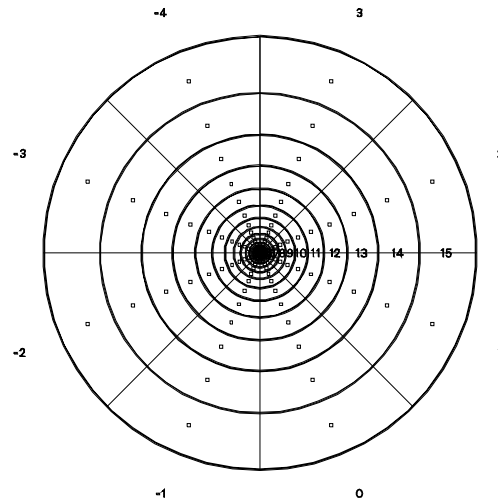


Figure VI.33: Wavenumber bin geometry used for Horton's problem.

the evolution to saturation are expressed as CPU minutes on a CRAY-2.

### Numerical results:

Let us adopt the  $16 \times 8$  bin geometry shown in Fig. VI.33. The linear growth and frequency appear as in Figs. VI.34 and VI.35, where the frequency and growth rate used for each bin are illustrated in the two-dimensional cross sections of Figs. VI.36 and Figs. VI.37, in which the different markers correspond to successive angular slices.

### Steady-state:

With this arrangement, we evolved the Terry-Horton equation with the RMC closure (Fig. VI.38) and obtained the saturated turbulent state indicated in Fig. VI.39. Note that no clear inertial range has developed. This is evident upon examining the slope of the spectrum, plotted in Fig. VI.40. Furthermore, we note in Figs. VI.41 and VI.42 that now *both* energy and enstrophy are transferred to the short wavelengths.<sup>9</sup> Thus, in the Terry-Horton model the removal of one of the non-

<sup>9</sup>Having anticipated this result, we did not include any damping at the long wavelengths. Indeed, we found that long-wavelength damping was not required in order for the system to reach a steady state.

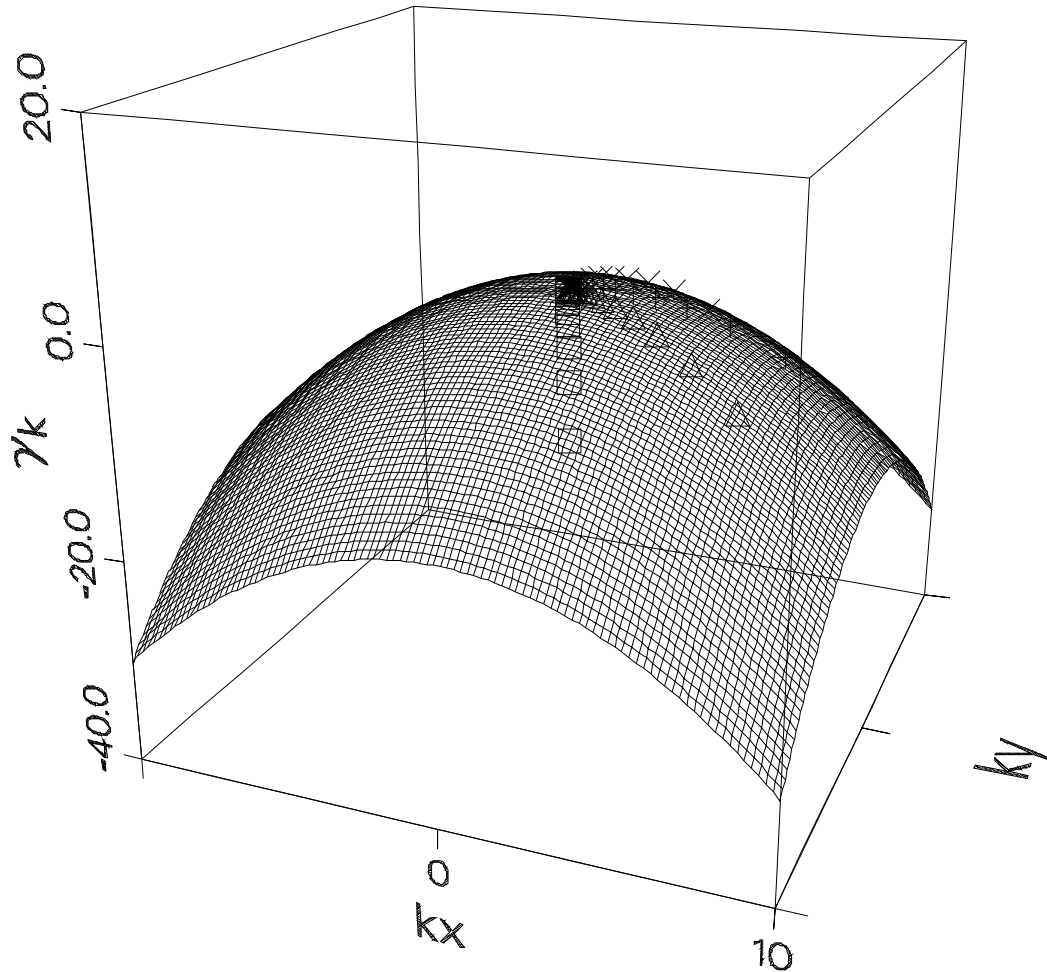


Figure VI.34: Three-dimensional view of the growth rate used by Horton.

linear invariants of the Hasegawa-Mima equation has led to the destruction of the dual cascade. This argument has often been made in distinguishing the drift-wave problem from two-dimensional turbulence; it is reassuring to see this phenomenon displayed so vividly in our numerical results. We further note, in view of Fig. VI.43, that the invariant  $W$  is also transferred to the short wavelengths. Moreover, we see that while  $\Pi_W$  satisfies Eq. (VI.8),  $\Pi_E$  and  $\Pi_U$  do not since only  $W$  is an invariant of the nonlinear terms.

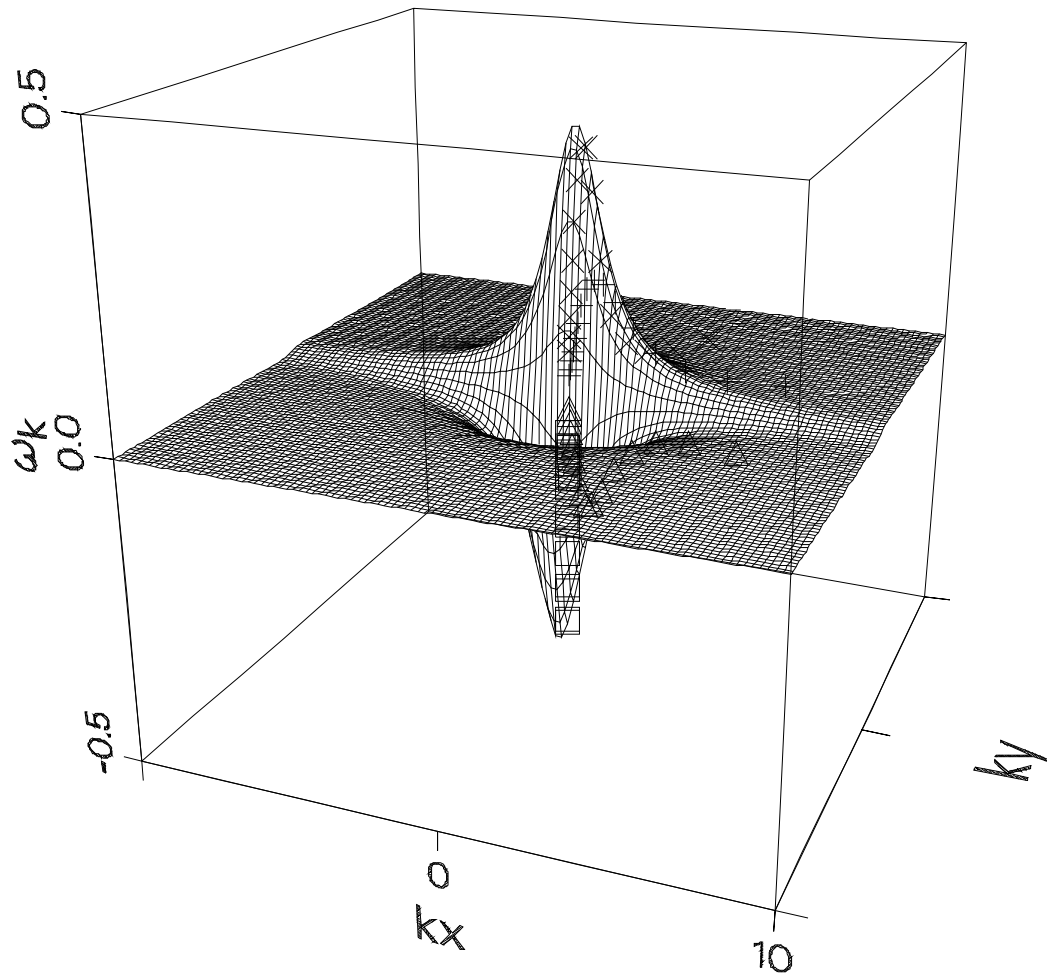


Figure VI.35: Three-dimensional view of the frequency used by Horton.

### Anisotropy:

In Fig. VI.44, we graph the degree of anisotropy in the saturated state as a function of wavenumber magnitude. We note significant anisotropy at the middle and short wavelengths. The anisotropy of the Terry-Horton system is also apparent in the three-dimensional view of the energy spectrum plotted in Fig. VI.45. These findings should not be surprising in view of the observation that even the unforced equilibrium state described by Eq. (VI.11) exhibits significant anisotropy

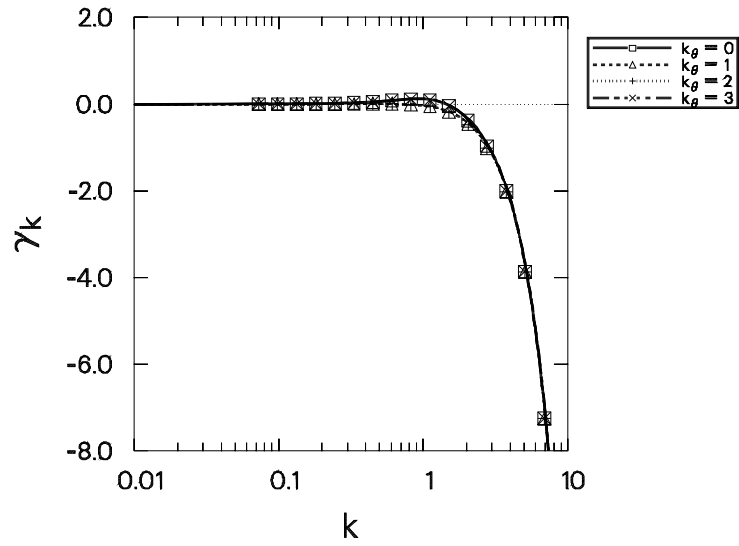


Figure VI.36: Two-dimensional cross sections of the growth rate used by Horton.

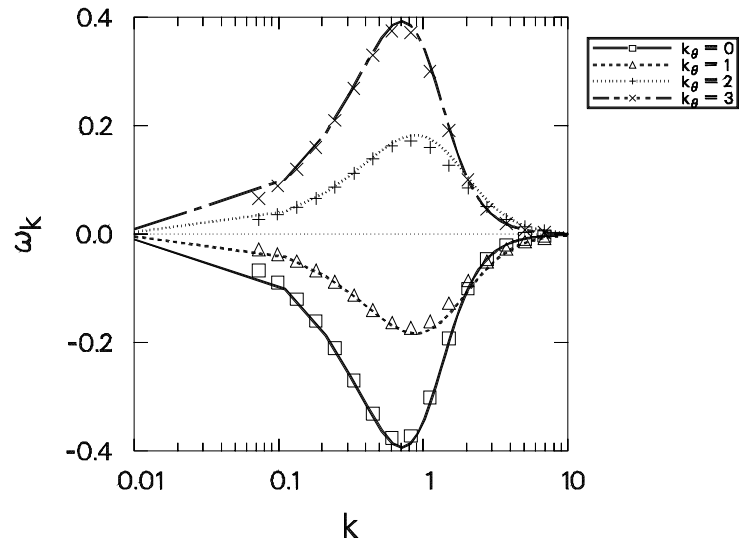


Figure VI.37: Two-dimensional cross sections of the frequency used by Horton.

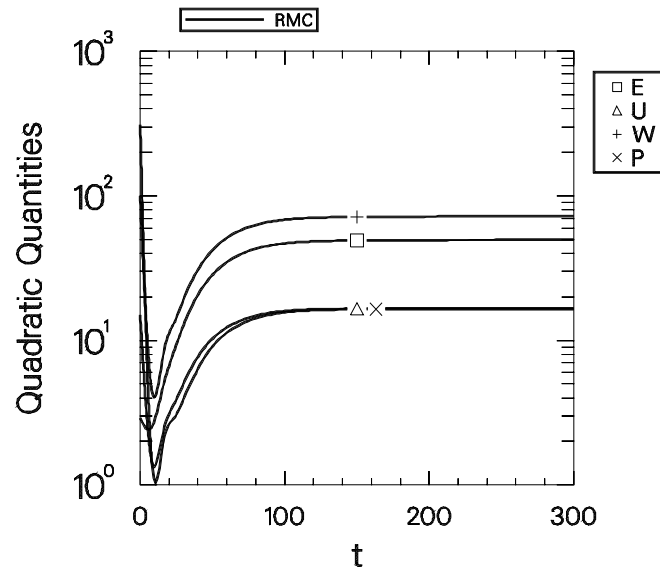


Figure VI.38: Evolution of the quadratic quantities for Horton's problem.

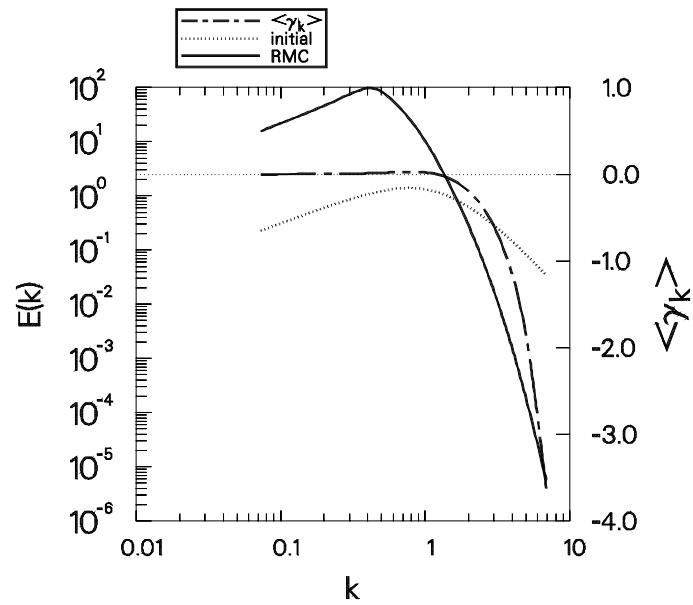


Figure VI.39: Saturated RMC energy spectrum for Horton's problem.

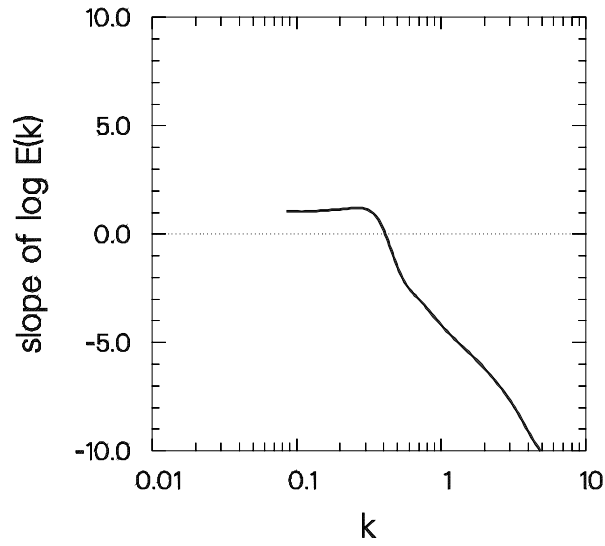


Figure VI.40: Logarithmic slope of the energy spectrum in Fig. VI.39.

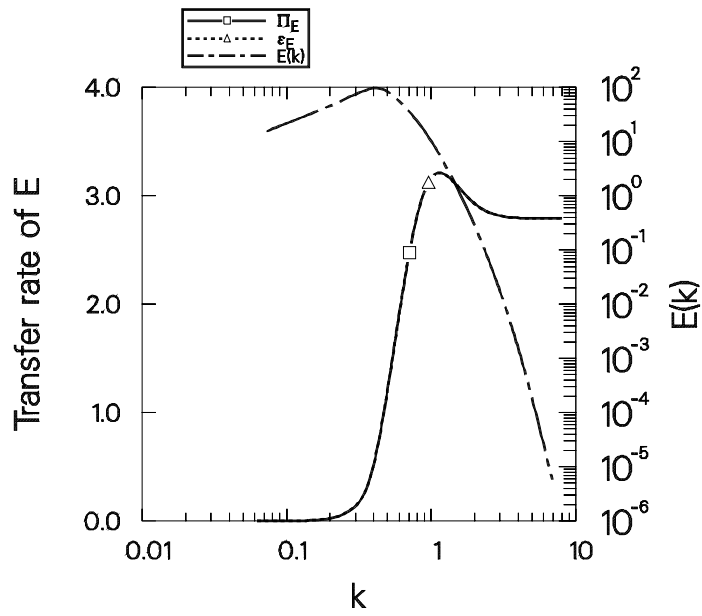


Figure VI.41: Energy transfer underlying the spectrum given in Fig. VI.39.

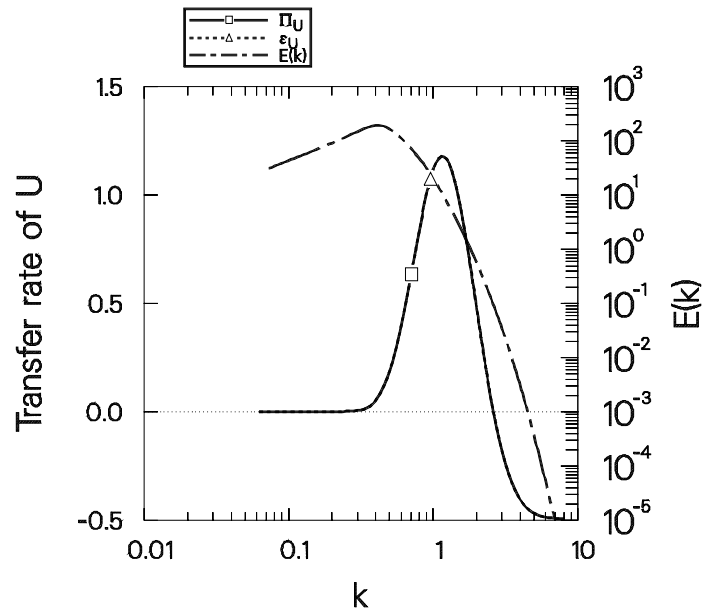


Figure VI.42: Enstrophy transfer underlying the spectrum given in Fig. VI.39.

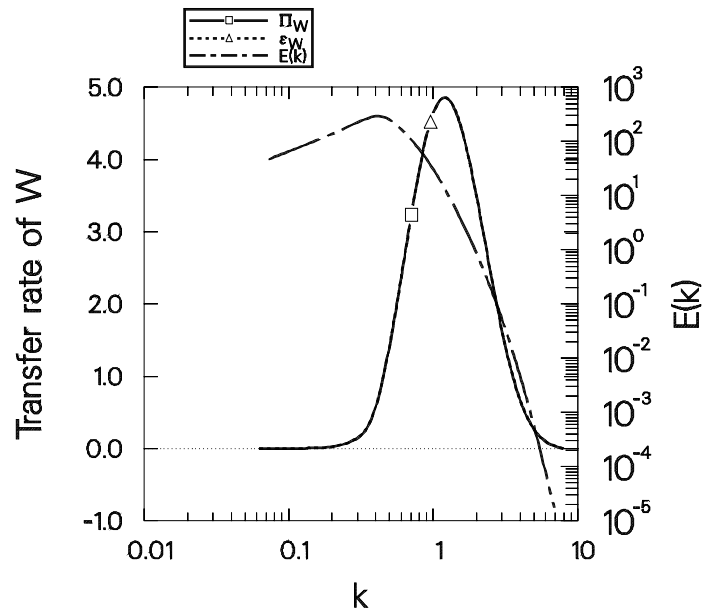


Figure VI.43: Transfer of the nonlinear invariant  $W$  for the spectrum of Fig. VI.39.

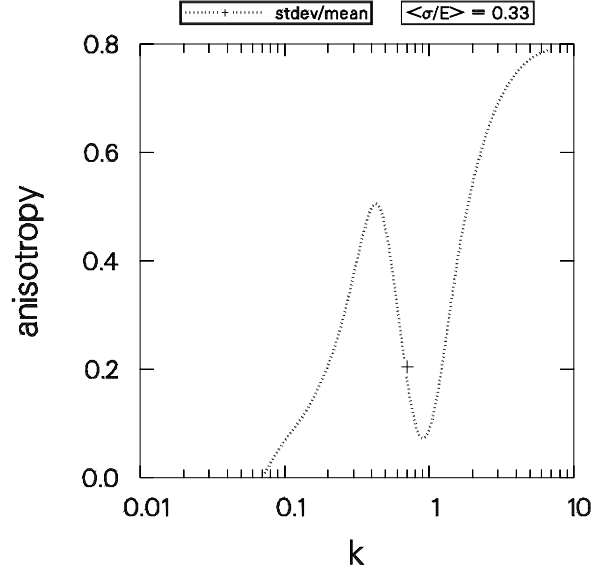


Figure VI.44: Anisotropy of the energy spectrum of Fig. VI.39.

originating from the imaginary part of the electron susceptibility. It appears that the procedure we have developed in this work for handling anisotropic turbulence has been well worth the effort. An isotropic approximation could not have captured the large variation of the drift-wave frequency and the electron susceptibility with wavenumber angle.

### VI.E.3 Two-time statistics

A nearly stationary DIA solution has been obtained for the Terry-Horton problem, yielding the energy spectrum depicted in Fig. VI.46. The correlation and response functions for the final state are graphed in Figs. VI.47 and VI.48. In this case we note significant violations of the imaginary part of the Fluctuation-Dissipation relation, although the real part is well satisfied. Presumably this can be traced to the presence of complex mode-coupling in Eq. (I.11); however, the explanation of this phenomenon remains a subject for future research.

### VI.E.4 Wavenumber scaling of the nonlinear damping

In Fig. VI.49 we present sample graphs of the scaling of  $\hat{\eta}_{\mathbf{k}}$  vs.  $k$ . At the long wavelengths, the arguments of Dupree [1967] might lead one to the (incorrect)

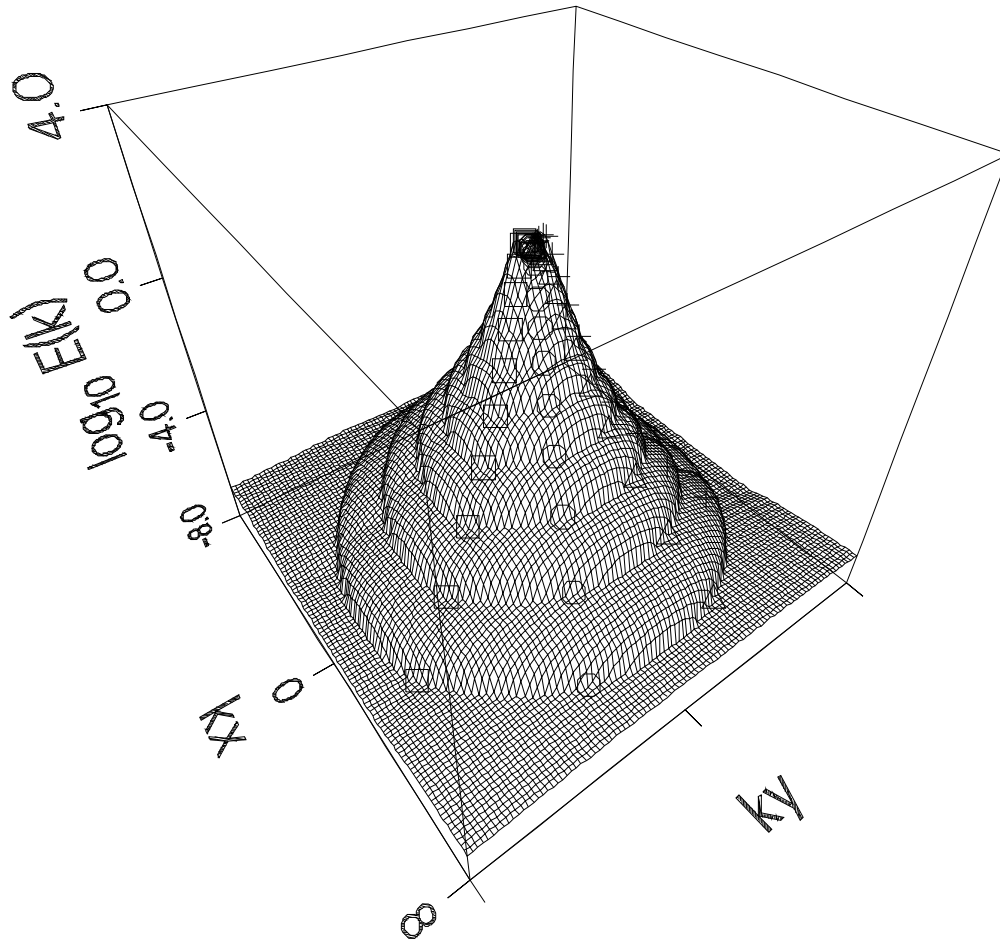


Figure VI.45: Three-dimensional view of the energy spectrum of Fig. VI.39.

scaling<sup>10</sup>

$$\hat{\eta}_{\mathbf{k}} \sim k^4 D. \quad (\text{VI.12})$$

Krommes *et al.* [1990] have shown that Eq. (VI.12) results from retaining only the terms that correspond to a passive approximation (*cf.* pg. 72). In contrast, a fully

---

<sup>10</sup>This corresponds to the conventional  $k^2 D$  scaling for the nonlinear damping rate as suggested by Dupree; here, an extra factor of  $k^2$  appears because the fundamental nonlinear interaction arises from the polarization drift.

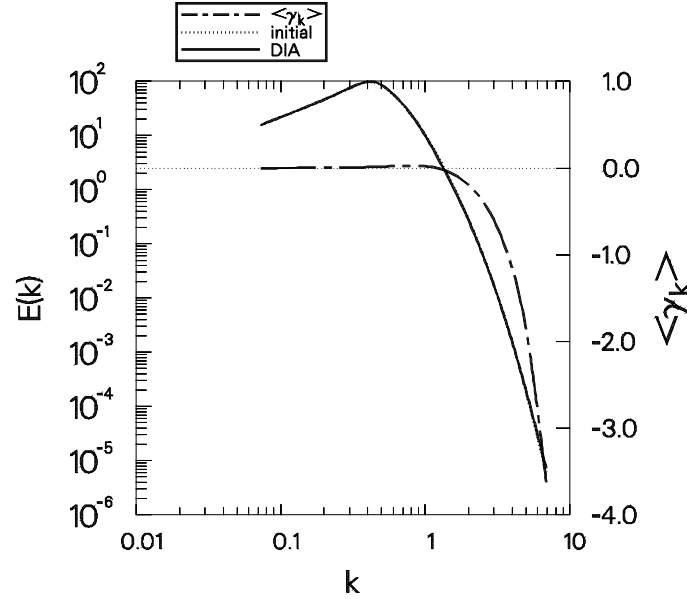


Figure VI.46: DIA energy spectrum for Horton's problem.

self-consistent analysis based on a Markovian closure may be used to deduce the approximate scaling relation [Krommes *et al.* 1990]

$$\hat{\eta}_{\mathbf{k}} \sim \begin{cases} -k^3 k_0 D & \text{for } k \ll k_0, \\ k V_E & \text{for } k \gg 1. \end{cases} \quad (\text{VI.13})$$

Here,  $k_0$  represents a characteristic energy-containing wavenumber less than 1. We see from Fig. VI.39 that  $k_0 = 0.4$  for our case.

The negative value of the predicted  $\hat{\eta}_{\mathbf{k}}$  at small wavenumbers represents nonlinear *forcing*. In Fig. VI.49, we see that at an angle corresponding to positive  $k_y$ ,  $\hat{\eta}_{\mathbf{k}}$  is in fact negative and appears to increase for a while in absolute value as  $k$  is increased. When  $k$  is large, however, the scaling of  $\hat{\eta}_{\mathbf{k}}$  appears to be approximately like  $k$ , as expected from Krommes' estimate and contrary to Eq. (VI.12). However, the coefficient  $V_E$  entering Eq. (VI.13), which is about 4.5 for this problem, somewhat overestimates the level of the nonlinear damping. This may be partly a consequence of nonadiabatic effects, which were not accounted for in the derivation of Eq. (VI.13).

Note that the scaling  $\hat{\eta}_{\mathbf{k}} \sim k$  in the inertial range differs from the scaling for the turnover time  $\tau_{\text{eddy}} \doteq \ell/u$ : the relation  $u^2 \sim kE(k) \sim k^{-2}$  indicates that  $\tau_{\text{eddy}}$  is in fact independent of wavenumber. The distinction between the turnover time and the predicted nonlinear damping rate is related to the failure of the RMC to exhibit random Galilean invariance.

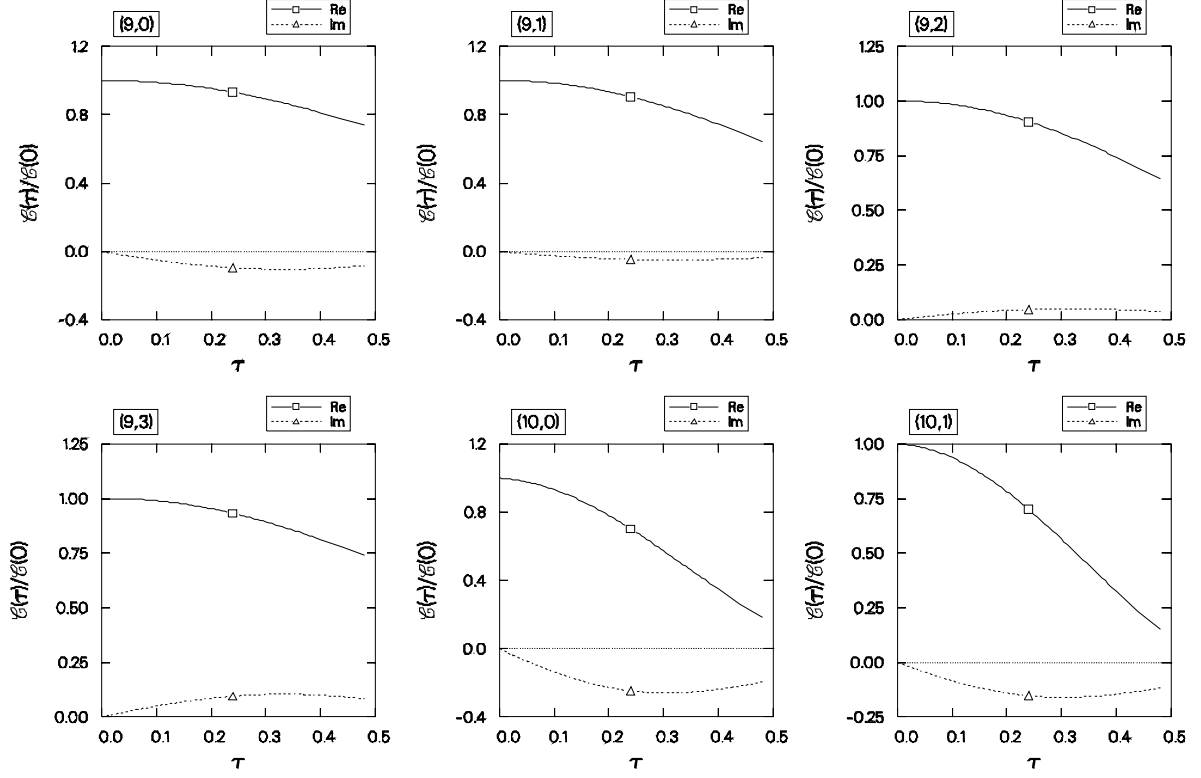


Figure VI.47: Typical correlation function data obtained by applying the DIA to Horton's case.

### VI.E.5 Diffusion coefficient

A primary objective of plasma turbulence research is the computation of transport coefficients such as the particle diffusion coefficient  $D$ . In this section we illustrate such a procedure and compare the result to an appropriate mixing-length formula.

The flux of electrons in the  $x$  direction is given by

$$\Gamma \doteq -D \frac{dn_0}{dx} = \langle V_{Ex} n_e \rangle.$$

where  $V_{Ex} = i\partial\Phi/\partial y$ ,  $n_e = (1 + i\chi'')\Phi$ , and  $n_0$  is the mean density. Because the Terry-Horton equation predicts an ambipolar flux [Krommes and Kim 1988],  $\Gamma$  is also equal to the ion flux.

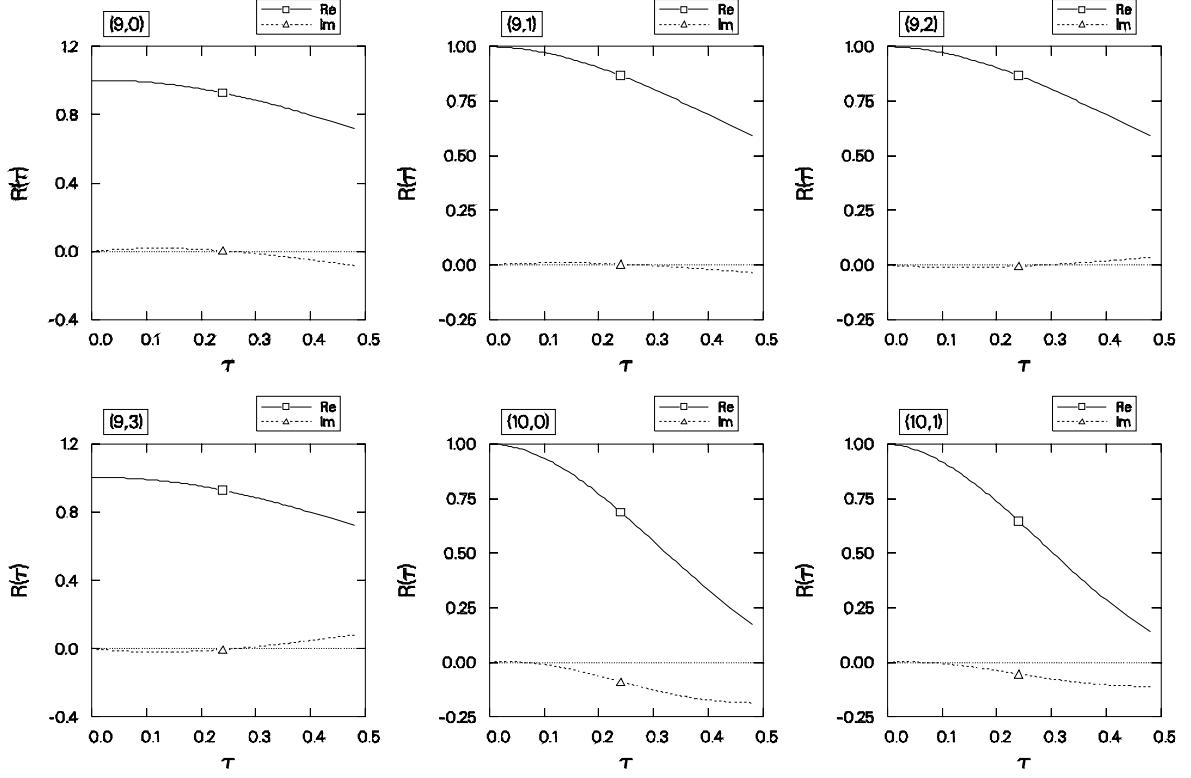


Figure VI.48: Typical response function data obtained by applying the DIA to Horton's case.

Since  $dn_0/dx = -1$  in our dimensionless units, we may write

$$D = \langle V_{Ex} n_e \rangle = \sum_{\mathbf{k}} (1 + i\chi_{\mathbf{k}}'') \Phi_{\mathbf{k}} (-ik_y \Phi_{\mathbf{k}})^*.$$

This simplifies to

$$D = - \sum_{\mathbf{k}} k_y \chi_{\mathbf{k}}'' I_{\mathbf{k}},$$

where  $I_{\mathbf{k}} = |\Phi_{\mathbf{k}}|^2$ . Upon denoting the imaginary part of the linear term in the absence of viscosity ( $\nu_0 = 0$ ) by  $\gamma_{\mathbf{k}}' \doteq -k_y \chi_{\mathbf{k}}'' / |1 + \chi_{\mathbf{k}}|^2$ , one obtains  $D = \sum_{\mathbf{k}} D_{\mathbf{k}}$ , with

$$D_{\mathbf{k}} = \frac{\gamma_{\mathbf{k}}'}{k_{\perp}^2} |1 + \chi_{\mathbf{k}}|^2 k_{\perp}^2 I_{\mathbf{k}}.$$

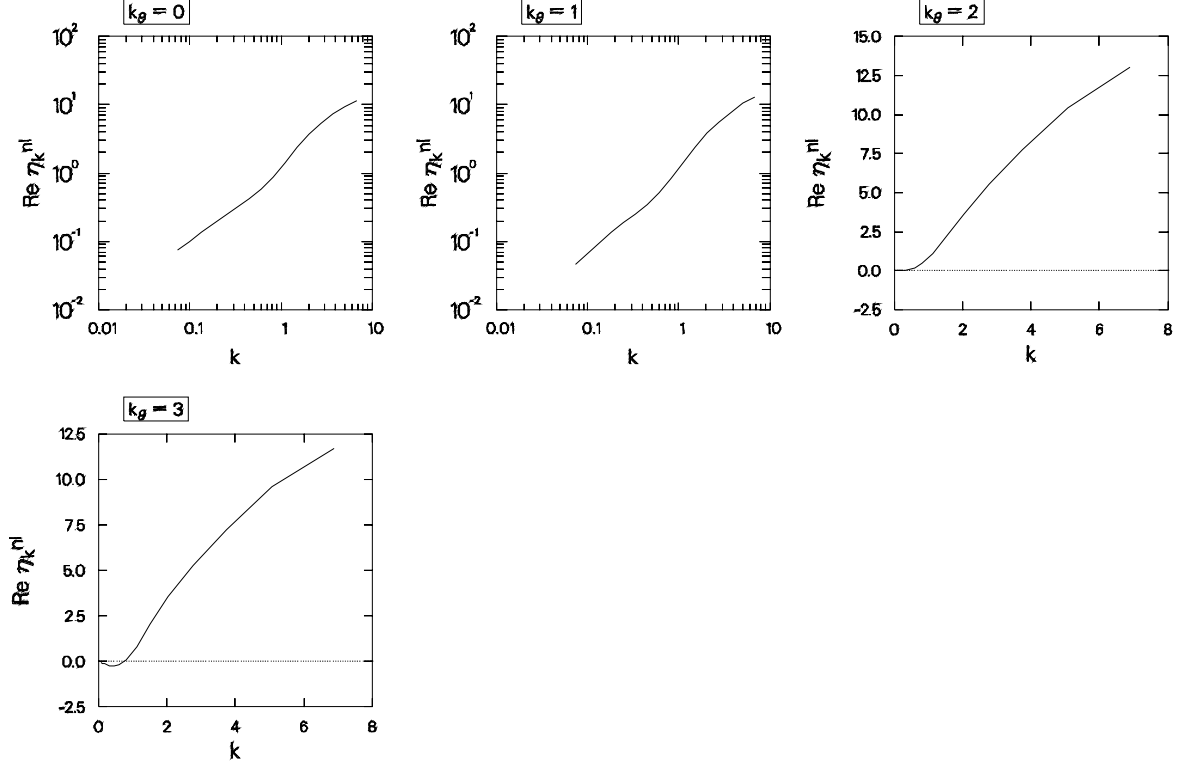


Figure VI.49: Scaling of  $\hat{\eta}_{\mathbf{k}}$  vs.  $k$  for Horton's problem. Logarithmic axes are used whenever  $\text{Re } \hat{\eta}_{\mathbf{k}}$  is strictly positive.

Here the notation  $k_{\perp} \doteq k$  is used to emphasize that  $\mathbf{k}$  represents a two-dimensional vector perpendicular to the magnetic field. If we define

$$\langle f \rangle_I \doteq \frac{\sum_{\mathbf{k}} f k_{\perp}^2 I_{\mathbf{k}}}{\sum_{\mathbf{k}} k_{\perp}^2 I_{\mathbf{k}}},$$

we may then write

$$D = \left\langle \frac{\gamma'_{\mathbf{k}}}{k_{\perp}^2} |1 + \chi_{\mathbf{k}}|^2 \right\rangle_I \sum_{\mathbf{k}} k_{\perp}^2 I_{\mathbf{k}}. \quad (\text{VI.14})$$

In Fig. VI.50, we compute the diffusion coefficient  $D$  and the square of the  $\mathbf{E} \times \mathbf{B}$  velocity,  $V_E^2 \doteq \sum_{\mathbf{k}} k_{\perp}^2 I_{\mathbf{k}}$ . These results were all obtained with the RMC closure.

We also calculate the spectrally averaged quantities  $\langle \gamma'_{\mathbf{k}} \rangle_I = 0.07$ ,  $\langle k_{\perp}^2 \rangle_I = 0.62$ , and  $\langle |1 + \chi_{\mathbf{k}}|^2 \rangle_I = 4.75$  so that we can compare our value  $D = 9.1$  to the approximate formula

$$D \approx \frac{\langle \gamma'_{\mathbf{k}} \rangle_I}{\langle k_{\perp}^2 \rangle_I} \langle |1 + \chi_{\mathbf{k}}|^2 \rangle_I \sum_{\mathbf{k}} k_{\perp}^2 I_{\mathbf{k}}. \quad (\text{VI.15})$$

Using this approximation, we obtain the value  $D = 11.7$ . We see that for this case the error introduced above in factoring an average is tolerable.<sup>11</sup>

The mixing-length assumption (*cf.* pg. 31), which asserts that  $V_E = V_d \doteq 1$  [Kadomtsev 1965], can be used to rewrite Eq. (VI.15) in the form

$$D_{\text{mixing}} \approx \frac{\langle \gamma'_{\mathbf{k}} \rangle_I}{\langle k_{\perp}^2 \rangle_I} \langle |1 + \chi_{\mathbf{k}}|^2 \rangle_I. \quad (\text{VI.16})$$

This is a more appropriate mixing-length estimate than the familiar form  $D = \langle \gamma'_{\mathbf{k}} \rangle_I / \langle k_{\perp}^2 \rangle_I$  (*à la* Dupree).

However, we find that the saturated level of  $V_E$  is  $\sqrt{20.5} = 4.5$ . This enhancement of the fluctuation level over the mixing-length level  $V_E = 1$  leads to a diffusion coefficient  $D = 9.1$  that is a factor of 16 higher than the value  $D_{\text{mixing}} = 0.57$  predicted by Eq. (VI.16). The difficulty here is that the mixing-length argument only implies a scaling relation ( $V_E \sim V_d$ ) and does not determine an actual fluctuation *level*. Note that if  $V_E \sim \alpha V_d$ , then  $D \sim \alpha^2$ .

Moreover, the simple mixing-length expression  $\langle \gamma'_{\mathbf{k}} \rangle_I / \langle k_{\perp}^2 \rangle_I = 0.12$  (as might be suggested by the arguments of Kadomtsev [1965, p. 107] and Dupree [1967]) underestimates  $D$  by a factor of 76. These results cast serious doubt on the validity of mixing-length estimates of transport; we suggest that extreme discretion be exercised when using simple estimates like  $\langle \gamma'_{\mathbf{k}} \rangle / \langle k_{\perp}^2 \rangle$  to predict the absolute *level*, rather than just the *scaling*, of the turbulent diffusion.

The contributions to  $D$  and  $V_E^2$  from each (continuum) wavenumber are presented graphically in Fig. VI.50, such that the integrals under the two curves equal  $D$  and  $V_E^2$ , respectively. As expected, we see that the dominant contributions come from the most excited wavenumbers; however, due to the additional powers of  $k$  in the expression for  $D$ , we see that the peak of the  $D(k)$  curve is shifted slightly to the higher wavenumbers.

Finally, it is worth remarking that the particle diffusion coefficient in the Terry-Horton problem is an entirely derived quantity: once the wavenumber fluctuation spectrum  $\langle \Phi_{\mathbf{k}} \rangle$  is known,  $D$  can be computed without further approximation. In

<sup>11</sup>The success of this factorization must be viewed as something of an accident. In other situations much larger errors may ensue. Consider, for example, the case of a Gaussianly distributed random variable  $x$  with zero mean and unit variance. Then  $\langle x^4/x^2 \rangle = \langle x^2 \rangle = 1$ , whereas  $\langle x^4 \rangle / \langle x^2 \rangle = 3$ , differing by 300% from the correct result.

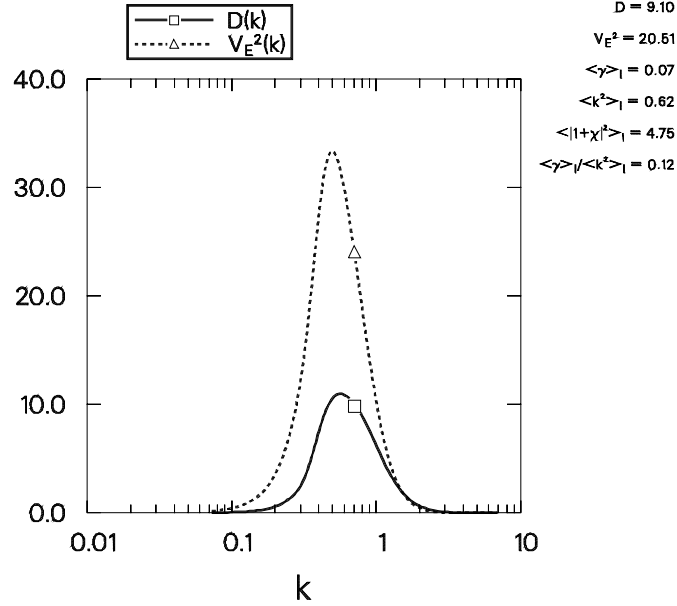


Figure VI.50: Diffusion coefficient and square of the  $\mathbf{E} \times \mathbf{B}$  velocity per unit wavenumber.

particular, the phase angle between  $n_e$  and  $\Phi$  is known *exactly* in this  $i\delta$  model (in terms of the specified linear growth rate). In more general situations this phase factor is nonlinear and random; its statistical effects must be determined by computing the cross-correlation function explicitly. Fortunately, an example of such a calculation is already contained implicitly in the Terry-Horton problem: the evaluation of the nonlinear damping and noise functions accounts for the wavenumber-dependent contributions to the cross-correlation  $\langle \mathbf{V}_E \omega_z \rangle$  (which physically represents the flux of the  $z$  component  $\omega_z \doteq -\nabla_{\perp}^2 \Phi$  of the vorticity). To the extent that the closure results can be inferred to be reasonable, we conclude that  $\langle \mathbf{V}_E \omega_z \rangle$  has been computed successfully, including not only the absolute fluctuation level, but also the nonlinear cross-correlation coefficient.

## VI.F Summary

In this chapter, we have successfully used statistical closures to obtain saturated states for both fluid and drift-wave turbulence in two-dimensions. We have presented graphs of both the evolution to this state and the final energy spectra. The dual cascade scenario has been demonstrated by examining the energy transfer function. However, we pointed out that this phenomenon is not present in the nonadiabatic drift-wave turbulence described by the Terry-Horton model. In comparison

of our closure results to conventional numerical simulation data (for a variant of the Hasegawa-Mima problem), quite reasonable agreement has been obtained. With the closure solutions, we also examined the degree of anisotropy in these problems: in the Hasegawa-Mima case anisotropy enters only at the long wavelengths, whereas in the Terry-Horton case anisotropy is present for both  $k < 1$  and  $k > 1$ .

In addition, we obtained DIA solutions for which we found correlation and response functions in good correspondence with the Fluctuation-Dissipation relation except for the Terry-Horton case, where agreement was obtained only for the real part of these functions. With the RMC closure, we obtained a scaling for the nonlinear damping coefficients  $\hat{\eta}_{\mathbf{k}}$  that contradicts simple passive estimates but is in reasonable qualitative agreement with analytical estimates of the self-consistent closure predictions. Our computation of a diffusion coefficient for the Terry-Horton problem is of particular relevance to the plasma physics community: the numerical results indicate that the mixing length formula  $D \sim \langle |1 + \chi_{\mathbf{k}}|^2 \rangle_I \langle \gamma'_{\mathbf{k}} \rangle_I / \langle k_{\perp}^2 \rangle_I$  is *not* a good approximation for the actual level of diffusion, although it may lead to insight about its scaling with characteristic wavenumber magnitude  $\langle k_{\perp} \rangle_I$  and linear growth rate  $\langle \gamma'_{\mathbf{k}} \rangle_I$ .

# Chapter VII

## Conclusions

In this final chapter, let us summarize the contributions of this work to the field of turbulence and outline possibilities for further research. In addition to addressing issues beyond the scope of this work, future research efforts could profitably apply our newly proposed statistical closure, the realizable Markovian closure (RMC), to a variety of nonlinear physics problems involving linear wave phenomena. The RMC has an important property: although the steady-state form of the RMC equations agrees with that of the widely used eddy-damped quasinormal Markovian (EDQNM) closure, the temporal evolution of the RMC to a stationary state is always realizable. This property is crucial; yet we have established both analytically and numerically that in the presence of linear wave dynamics the EDQNM equations can violate the important constraint of realizability and develop negative energies. This deficiency of the EDQNM is of more than just academic concern: numerically, we have witnessed (*cf.* Fig. III.1) that once negative energies develop the amplitudes may even diverge to infinity, terminating the numerical computation prematurely. Furthermore, even in the case of wave-free dynamics, we have demonstrated on both theoretical and numerical grounds that the RMC is superior to the EDQNM closure as an approximation of the transient behaviour.

In addition, we have presented general techniques for solving statistical closures in the context of anisotropic turbulence. Historically, the advantage of statistical closures over conventional numerical simulation methods has generally been recognized only for isotropic turbulence; for this reason anisotropic turbulence remains largely unexplored with closure techniques. We have developed a scheme of mode reduction based on an elegant anisotropic generalization of the isotropic bin-averaging technique pioneered by Leith and Kraichnan [1972]. The successful implementation and application of this method to the problem of drift-wave turbulence suggests that there is great potential for further research in this area. In light of this encouraging forecast, let us now review the contributions of this work.

## VII.A Summary; suggestions for further research

In Chapter I we reviewed the basic concepts and terminology of fluid dynamics; this is the historical context in which much of turbulence research has been conducted. For example, we introduced the concept of a dual cascade, along with the corresponding Kolmogorov laws, in conventional two-dimensional turbulence. The close connection between the Hasegawa-Mima equation for the drift wave and the two-dimensional Navier-Stokes equation was elucidated. We discussed our motivation for the study of drift-wave turbulence in the context of fusion research. Of particular importance is the computation of the turbulent enhancement of transport coefficients. This objective represents an essential component of a vigorous research program aimed at developing an understanding of the anomalous particle and thermal losses that are observed in current tokamak experiments.

With this goal in mind, the pedagogical concepts of a stochastic process, ensemble average, statistical functions, and a statistical closure were introduced. The importance of the realizability constraint in the construction of a statistical closure was stressed, as this ensures the existence of an underlying probability distribution for the predicted statistics. We then remarked on the computational advantages of Markovian statistical closures, which constitute the primary focus of this work.

To set the stage for our discussion of statistical closures, we reviewed several alternative theories of plasma turbulence, including linear theory, dimensional analysis, mixing-length estimates, quasilinear theory and the resonance-broadening theory. We argued that none of these theories adequately describe the strongly turbulent plasmas in which we are interested either because they are not renormalized or because they are not derived systematically. An example of an approximation for strong turbulence that we do consider to be systematically derived from plausible axioms is the statistical closure known as the direct-interaction approximation (DIA). Statistical closures have certain advantages over conventional numerical simulations: for example, they can provide an analytical insight into the nature of nonlinear interactions. Since our ultimate goal in plasma turbulence theory is not just the prediction of a numerical value for a transport coefficient but an actual *understanding* of the underlying physics, it seems likely that analytical techniques like statistical closures could play an important role in future research. Nevertheless, for most practical problems the solution of the highly coupled and nonlinear equations that define a statistical closure requires intensive numerical computation. Fortunately, the closure equations have a notable advantage over the primitive dynamical equations in that they are nonstochastic: statistical equations often possess smoothness and symmetries in both space and time that are not supported by the primitive dynamical equations. This distinction is crucial to the competitiveness of statistical closures. In Chapter IV, we exploited these statistical properties in the development of our anisotropic mode-reduction scheme.

We began our survey of statistical closures by introducing the classical renormalized perturbation theory developed by Martin *et al.* [1973], which provides a logical framework for the development of closures like the DIA. Alternative schemes such as decimation, mapping closures, and the renormalization group method were also briefly discussed. The distinction between Eulerian and Lagrangian formulations and their relation to the property of random Galilean invariance was stressed. We then focused on the Eulerian DIA equations and emphasized that the violation of this statistical property may not represent so serious a difficulty in plasma transport calculations as it has for fluid dynamics, especially since plasma problems typically do not exhibit a well-defined inertial range. After exhibiting several derivations of the DIA, we discussed certain analytical properties such as energy conservation, the reduction to perturbation theory, covariance, and most importantly, realizability, which follows from the existence of an underlying Langevin equation. In the future, we suggest that it might be fruitful to conduct an investigation of an optimal iteration scheme for obtaining a steady-state solution to the DIA.

Unfortunately, the solution of the DIA equations for a typical turbulence problem remains a formidable task, due to the presence of both two-time information and nontrivial time-history integrals in the evolution equations for the correlation and infinitesimal response function. Therefore, upon recalling our discussion of Markovian closures in Chapter I, we considered a simpler alternative to the DIA known as the EDQNM. In keeping with our desire for a systematically derived theory of turbulence, we focused on a particular version of the EDQNM that is derivable from the DIA. This derivation rests on two assumptions: the application of a Fluctuation-Dissipation (FD) ansatz and a Markovianization of the evolution equation associated with the response function. However, in this work we demonstrated that the invalidity of the first assumption out of thermal equilibrium can lead to severe violations of realizability when the EDQNM is applied to systems that exhibit linear wave phenomena. Let us emphasize that these difficulties do not occur when the EDQNM is applied to the fluid turbulence problems for which it was originally designed.

The task of developing a realizable Markovian closure in the context of linear wave dynamics thus presented itself. We eventually discarded our first attempt at constructing such a closure since it involved several arbitrary modifications with little physical justification; furthermore, it did not readily lend itself to a multiple-field generalization that conserved all of the fundamental quadratic invariants. Our second attempt was more systematic: by introducing a modified form of the FD relation, we corrected the nonrealizability at the step where it first entered the derivation of the EDQNM from the DIA. This modified FD ansatz guarantees the positive-semidefiniteness of the approximation used for the two-time covariances appearing in the DIA convolution integrals. Physically, the modified FD ansatz expresses a balance between the correlation coefficient of the fluctuations and the

infinitesimal response function. We substituted this relation into the DIA covariance equation and Markovianized the response function equation as before. The result was a new set of equations, which we proved are realizable. We named this approximation the realizable Markovian closure (RMC) after its most important characteristics.

Besides being realizable, the RMC has another important advantage over the EDQNM: its underlying Langevin equation preserves the entire temporal convolution structure of the noise term found in the corresponding DIA Langevin equation. That is, the underlying statistical noise term in the RMC is not assumed to be  $\delta$  correlated. In addition, we suggested that a similar modification to the test-field model will restore the realizability of this random-Galilean-invariant closure when it used to study wave phenomena. Our remaining effort in Chapter III was devoted to the construction of a covariant multiple-field formulation of the RMC equations with the aid of a multiple-field version of the modified FD ansatz. In a steady state this modified FD ansatz reduces to the appropriate equilibrium relation.

We consider the construction of the realizable Markovian closure to be the most important achievement of this work. Having accomplished this theoretical success, we proceeded in Chapter IV to discuss the numerical implementation of anisotropic statistical closures. Following Leith and Kraichnan [1972], we adopted a continuum wavenumber geometry that represents the limit of a large number of modes. Since the statistical variables tend to vary smoothly, one may profitably partition the wavenumber space and evaluate them only at a single point in each wavenumber bin. In contrast, the convolution function  $\delta(\mathbf{k}+\mathbf{p}+\mathbf{q})$  and the rapidly varying portion of the mode-coupling coefficients must be integrated over the entire area of the bins. Fortunately, since the mode-coupling coefficients are assumed to be time-independent, this complicated calculation needs to be performed only once for each new wavenumber geometry (or whenever the expression for the rapidly varying part of the mode-coupling coefficient is modified). The result of this computation is a set of bin-coupling coefficients that approximately describes the interactions between entire *bins* of modes rather than the fundamental modes themselves. The main contribution we have made in this area is the development of a general algorithm for bin averaging in a polar representation, which allows us to handle anisotropic turbulence. We described the difficulties that can arise in ensuring that conservation laws are not violated; in particular, one must consider the role of self-coupling effects arising from the interaction of two fundamental modes that lie within the same bin.

We also discussed the details of the predictor–corrector scheme used in the code DIA to evolve the statistical variables for each of the three closures — the DIA, the EDQNM, and the RMC — it is capable of solving. The implementation of a quasistationary algorithm for the EDQNM and RMC was also described; however, for both theoretical and numerical reasons we do not recommend the use of quasis-

tationary closures. For example, in Chapter V, we showed that the quasistationary EDQNM is a very poor model of the transient dynamics of the three-wave problem; moreover, there is little computational advantage in considering this acausal formulation. Chapter IV concluded with an overview of the design philosophy and novel features of the DIA code. Over the course of this research, many dramatic improvements in the capabilities, diagnostics, and efficiency were made to an early version of the DIA code, which was originally developed by Krommes. This included the introduction of the bin-averaging method, the implementation of multiple-field closures, a dynamically adjustable time step, a restart mechanism, vectorization, and many forms of optimization. Since some of the production runs that were discussed in Chapter VI required over 10 hours of CPU time on a CRAY-2 supercomputer, the efficiency gains turned out to be particularly important.

We suggest that the realizable test-field model (RTFM) described in Chapter III should eventually be implemented in the DIA code in order to test our assertion that a violation of random Galilean invariance will not affect the computation of plasma transport coefficients. We would also like to assess more carefully the relative merits of the Fourier harmonic expansion used by Herring [1975] and our anisotropic bin-averaging scheme. It would be worthwhile to investigate the accuracy of the bin-averaging scheme. The basic approximation amounts to a rectangular integration of the statistical functions, which are evaluated outside the wavenumber integrals. One might conclude that the error scales as the square of the bin size. However, the use of nonuniform bins (logarithmically spaced in the radial direction) complicates the situation, so that it is not clear how to draw any useful conclusions from this argument. It would be desirable to obtain a scaling relation that could be used to fit numerical data obtained in convergence studies of the bin-averaging scheme. Finally, we propose a re-examination of the possible ways to account for self-coupling effects in the bin-averaging calculation, especially for isotropic turbulence, where only one bin is available at each radial distance. In this work, considerable effort was expended to achieve this goal for the general anisotropic case. It was concluded that it was impractical to include these effects, as they greatly increase the number of bin-coupling coefficients that must be integrated directly. However, for the case of isotropic turbulence, or even for systems with limited anisotropy, the implementation of such a scheme may still be feasible.

In this work the DIA code was first applied to a problem of three interacting waves. This study also afforded a comparison of the relative merits of the DIA, EDQNM, and RMC approximations with the exact statistics obtained by taking moments of the direct numerical solution over many realizations. In the inviscid case, we noted that these closures all relaxed to the expected equilibrium form for the resonant problem, but only the DIA closure predicted the correct equilibrium result in the nonresonant case. We identified the origin of this discrepancy: the Markovian closures do not conserve the Hamiltonian, which constitutes a nontrivial

third invariant in the nonresonant case. This additional constraint on the dynamics modifies the expected equilibrium state. It would also be useful to determine whether the failure of the Markovian closures to conserve the three-wave Hamiltonian also has significant consequences for problems with many interacting modes.

We also examined a degenerate case where an exact analytical solution exists for most of the closures under study. This served as a convenient test of our numerical algorithm and provided a demonstration of the differences between each of the closures. Unfortunately, for the RMC closure we could only obtain a numerical solution in this degenerate case; perhaps for some other special case the RMC might have a simple analytical solution.

Upon the inclusion of growth rates in the three-wave problem, we developed exact expressions for the steady-state energies that are valid when each realization in the ensemble possesses a steady-state solution. In this case we found that although the DIA grossly misrepresented the transient evolution, it correctly predicted the energies in the final (nonstochastic) state; it would be interesting to determine under what conditions this latter results holds. On the other hand, the EDQNM and RMC both predicted final energies that differ from the true results by a dimensionless parameter  $P$  that depends on the distribution of the growth rates among the three modes.

Next, in the stochastic case considered by Wersinger *et al.* [1980], we generally found poor agreement between the statistical closures and the ensemble solutions. We attribute this disagreement to the absence of many interacting modes: one cannot expect the principle of maximal randomness, upon which these closures are founded, to apply to a system of only three modes. Again, one would like to achieve a better understanding of this failure. In the case we studied, particularly curious behaviour of the realizable EDQNM closure was observed, in which nearly singular behaviour developed as the parameter  $\Gamma$  was increased. The RMC did not exhibit this pathological behaviour; indeed, in virtually all cases we found that the RMC is a better representation of the true dynamics than the EDQNM.

Next, we included the effects of complex mode-coupling to make contact with previous studies of the three-wave Terry-Horton system performed by Terry and Horton [1982], Krommes [1982], and Koniges and Leith [1987]. Again, we found that in this highly truncated system the closures could not properly model the dynamics. It would be wise to conduct further comparisons of the closure predictions and the ensemble solutions for the stochastic cases. Perhaps by considering a related system with five or more modes, one could determine whether the failure of the closures is due solely to the limited number of modes. In addition, it would also be worthwhile to consider the issue of stability with respect to small perturbations, for both the closure solutions and the ensemble.

We completed Chapter V with a partial test of the multiple-field closures. This

test was constructed by taking the real and imaginary parts of the three-wave problem. Since the multiple-field DIA and RMC have both been successfully implemented in the code DIA, a tool now exists for the study of a two-field model of the  $\eta_i$  mode. As another example, it is well known that there are serious deficiencies in the  $i\delta$  model of drift waves; for example, the parameter  $\delta$  actually depends on the frequency [Mattor and Terry 1992]. Therefore, one might consider replacing the Terry-Horton equation with a two-field system [Bowman and Krommes 1987]. Another refinement with which one might hope to contend someday is the role of the magnetic shear, which tends to stabilize many of the modes found in a tokamak. Unfortunately, the inclusion of shear introduces an inhomogeneity that requires one to replace one wavenumber index with a pair of indices that act much like the species indices  $s$  and  $s'$ . Since the scaling of both the DIA and the RMC with respect to the number of species  $N_s$  is like  $N_s^6$ , both inhomogeneities and multiple species (or velocities) introduce formidable problems in general. Perhaps some further simplification of the multiple-field closures will be necessary in order to handle these complications.

Finally, in Chapter VI we applied the knowledge gained from previous chapters to the problem of drift-wave turbulence. We began our discussion with a clear demonstration of the relaxation of the Hasegawa-Mima problem to the expected equilibrium solution. Because of the close analogy between the Hasegawa-Mima equation and the two-dimensional Navier-Stokes equation, we proceeded with a pedagogical demonstration of isotropic two-dimensional turbulence, illustrating important concepts such as the dual cascade, the inertial range, and the nonlinear energy transfer. We obtained a corrected logarithmic slope of  $-2.9$ , which lies between the expected closure value of  $-2.5$  (for a closure that violates random Galilean invariance) and the Kolmogorov value of  $-3$ . In other words, we found that in practice the error in the modeling of the inertial range by the closure was less severe than expected. We do not yet know for certain the cause of the discrepancy between the numerical value  $-2.9$  and the theoretical closure value  $-2.5$ , but we suggest that this is a result of an insufficiently developed inertial range. It would be worthwhile to extend the inertial range by several decades to help settle this question. To obtain a better value for the slope of the inertial range energy spectrum, one might wish to model only the enstrophy inertial range. We recall that closures are capable of modeling inertial ranges spanning many decades because of their superior scaling with Reynolds number in comparison to direct simulations. (The ratio of the largest to smallest time scales will be the limiting factor.) In addition, it would be useful to determine the slope predicted numerically by the RMC (as well as the DIA) for three-dimensional turbulence.

The next case considered was the anisotropic short-wavelength Hasegawa-Mima equation. Here, we found good agreement between the closure predictions and two different realizations obtained by direct numerical simulation, especially in the

modeling of the total energy and the slope of the inertial range. This test helped to confirm our hopes that closures would fare substantially better in the presence of many interacting modes. However, we emphasize that this represents only a preliminary test and a more thorough and systematic comparison between closure computations and direct numerical simulation should be carried out as part of a future research program. In particular, the convergence of the bin-averaging scheme for this problem and the role of self-coupling effects should be examined further. The resolution of the direct simulation should also be improved. In addition, although we already perform an average over angle when computing the energy spectrum from the direct simulation data, it would be preferable to perform a time average, especially at the long wavelengths where there are very few modes at each fixed radial distance. We suggest a time average since the possibility of obtaining an ensemble average for such problems seems computationally prohibitive. Finally, one would like to evaluate the role of coherent structures by comparing the accuracy of statistical closures for cases in which coherent structures are present to cases in which they are absent.

This research effort culminated in a study of two models for drift-wave turbulence. In the adiabatic case the Hasegawa-Mima equation was evolved with the RMC to produce an amplitude shape and energy level similar to that found by Waltz [1983] with the quasistationary EDQNM. We also obtained a stationary DIA solution, complete with two-time functions. Both of our closure results compare well to the direct numerical solution obtained by Waltz [1983]; this provides a further confirmation of the applicability of statistical closures to systems with many modes. In the future, it would be worthwhile to solve the Hasegawa-Mima equation with an extended wavenumber domain to allow comparison of the scaling of the nonlinear damping coefficient  $\hat{\eta}_{\mathbf{k}}$  with wavenumber to the approximate scalings deduced by Krommes *et al.* [1990] for the adiabatic case. Unfortunately, in this work we determined the numerical scaling of  $\hat{\eta}_{\mathbf{k}}$  only in the nonadiabatic case; even there, however, the main features of the analytical estimate are observed.

In the nonadiabatic limit, we solved the Terry-Horton problem and (for a particular set of parameters) noted significant differences relative to our studies of Hasegawa-Mima turbulence. For example, we observed that the dual cascade was replaced by a single direct cascade of energy and enstrophy to the short wavelengths. We noted that anisotropy now appears at many wavenumbers, not just at the long wavelengths as it does in the adiabatic case. In fact, this anisotropy is present even in the inviscid equilibrium case with zero diamagnetic velocity: the origin of the short-wavelength anisotropy is in the electron susceptibility. We noted that while the Fluctuation-Dissipation relation was satisfied quite well by the Hasegawa-Mima solutions, only the real part of this relation appeared to be obeyed in the nonadiabatic case. It would be worthwhile to identify the role of the imaginary part of the electron susceptibility in the observed violation of the FD relation. As suggested

by Mattor and Terry [1992], our results should also be interpreted in terms of a *frequency* spectrum to facilitate comparison with observational data. These authors point out that limited spatial resolution typically makes it difficult to obtain experimental *wavenumber* spectra.

For the Terry-Horton problem, we have successfully demonstrated the convergence of our bin-averaging scheme in the radial direction. In future work, a convergence study in the angular dimension should also be performed.

Finally, we illustrated a procedure for obtaining a diffusion coefficient directly from the numerical data. Our diffusion coefficient was more than an order of magnitude higher than an appropriate mixing-length estimate. Also, the saturated  $\mathbf{E} \times \mathbf{B}$  velocity was more than a factor of four times larger than the diamagnetic velocity; the mixing-length analysis would suggest that in a saturated state these two velocities should be equal. We emphasize that empirical formulae based on mixing-length arguments may at best be useful only for extracting insight about the scaling of the particle diffusion with wavenumber and the linear growth rate. Even then, one must be careful to account for the scaling with linear growth rate of the *fluctuation level*, which also enters the expression for the diffusion coefficient. We propose that a future study of this latter relationship, based on the tools developed in this work, could have important implications for transport theories.

## VII.B Error estimates and the optimum theory

A principal difficulty with all of the previous methods, including statistical closures, is that in general no estimate is known for the error introduced by the underlying approximations. Unless the exact solution is available for comparison, there is no reliable way of establishing how closely these methods approximate the true dynamics.

However, there does exist a promising approach to the problem of turbulence that has the potential to provide such error estimates. This is the so-called optimum theory, which was pioneered by Howard [1963], Busse [1978], Krommes and Smith [1987], and Krommes and Kim [1990]. The most striking feature of this theory is that it poses a completely different question than do the other methods we have discussed. Rather than attempting to *approximate* the true transport level, it provides a *mathematically rigorous upper bound* for this level. The optimum theory employs functional calculus to determine the absolute maximum flux that a given nonlinear equation can sustain, subject to certain physical constraints such as energy conservation. Of course, this bound may not be very good; however, in practice one finds that as one adds more constraints the bound becomes closer to the exact solution (it will not become worse). Unfortunately, no complete procedure has yet been developed to determine a nontrivial lower bound for the flux. Clearly,

such a calculation is essential to our goal of obtaining an error estimate. It would then be clear when one had employed enough constraints to pinpoint the flux to within a specified resolution.

The optimum theory is often illustrated with simple pedagogical problems for which reasonable bounds can be obtained analytically. However, as the dynamics becomes more complicated, the system of Euler-Lagrange equations that results from the maximization becomes increasingly involved and typically requires much numerical computation. The complexity also increases as one seeks a more accurate bound with the introduction of additional constraints.<sup>1</sup> Also, there are difficulties in the generalization of the optimum theory to problems in which the fluctuations do not vanish at the boundaries.

Despite these difficulties, the optimum theory remains an intriguing alternative to the other methods discussed in this work. Some practical calculations, including the determination of a rigorous upper bound for the critical current in the reversed-field pinch, have already been successfully performed [Kim and Krommes 1990]. However, one must be careful in interpreting the results of a bounding calculation: for example, there is no guarantee that the scaling of a mathematical bound for the flux will bear any relation to the actual scaling in the physical system.

## VII.C Final remarks

Ultimately, it appears to the author that a complete mathematical and physical understanding of turbulence will require the interaction of many approaches. For example, one could conceivably use the optimum theory to provide an accuracy estimate for the predictions of a statistical closure, which could then be used to provide more detailed information than is available from the bound for some average quantity like the total energy.

To realize the ambitious goal of understanding turbulent transport, we expect that, along with the alternative theories discussed in Chapters I and II, the optimum theory, direct numerical simulation, and statistical closures will all play important roles. In particular, since closures deal naturally with the statistical variables that describe transport phenomena, they represent a compelling choice as tools for the study of turbulence.

---

<sup>1</sup>For an example of such a calculation, see Kim and Krommes [1988].

# Appendix A

## Elementary Derivation of the Terry-Horton Equation

For completeness, we record here an alternative derivation of the Terry-Horton equation directly from the MHD equations written in the laboratory frame. We follow closely the original discussion by Terry and Horton [1982]. Drift waves occur for  $v_{ti} \ll \omega/k_{\parallel} \ll v_{te}$  (cold ions, hot electrons). We therefore treat the ions as a fluid and the electrons as nearly adiabatic.

The equations for the perturbed quantities driven by a background density gradient are

$$\begin{aligned} \frac{\partial}{\partial t} n_i + \nabla \cdot (\mathbf{v}_i n_i) &= -\mathbf{v}_i \cdot \nabla n_0, \\ m_i \frac{d\mathbf{v}_i}{dt} &= e \left( \mathbf{E} + \frac{\mathbf{v}_i \times \mathbf{B}}{c} \right), \\ \frac{n_e}{n_0} &= \frac{e\varphi}{T_e} (1 + i\chi''), \\ n_e &= n_i. \end{aligned}$$

From the ion momentum equation,

$$\begin{aligned} \mathbf{v}_i &\approx \mathbf{v}_E + \mathbf{v}_p, \\ \mathbf{v}_E &\doteq c \frac{\mathbf{E} \times \mathbf{B}}{B^2}, \\ \mathbf{v}_p &\doteq -\frac{c}{\Omega_i B} \frac{d\mathbf{E}_{\perp}}{dt}, \end{aligned}$$

where  $\Omega_i \doteq eB/(m_i c)$ . Insert these relations into the ion continuity equation to obtain

$$\frac{\partial}{\partial t} n_i + \mathbf{v}_E \cdot \nabla n_i - n_i \nabla \cdot \left( \frac{c}{\Omega_i B} \frac{d\mathbf{E}_{\perp}}{dt} \right) = -\mathbf{v}_E \cdot \nabla n_0.$$

Here, we neglected  $\mathbf{v}_p \cdot \nabla n_i$  and  $\mathbf{v}_p \cdot \nabla n_0$  since  $\omega \ll \Omega_i$ . The low frequency of drift waves allows us to invoke the quasineutrality condition  $n_i = n_e$ . In terms of  $\varphi$ , we obtain

$$(1 + i\chi'') \frac{\partial}{\partial t} \varphi + \mathbf{v}_E \cdot \nabla (1 + i\chi'') \varphi - \rho_s^2 \frac{d}{dt} \nabla_{\perp}^2 \varphi = -V_d \frac{\partial \varphi}{\partial y},$$

where  $\rho_s^2 \doteq T_e / (m_i \Omega_i^2)$ . The adiabatic part of the second term vanishes because of the cross product in  $\mathbf{v}_E$ , so that

$$(1 + \chi) \frac{\partial}{\partial t} \varphi - \mathbf{v}_E \cdot \nabla \chi \varphi = -V_d \frac{\partial \varphi}{\partial y},$$

where  $\chi = -\rho_s^2 \nabla_{\perp}^2 + i\chi''$ .

Normalize the variables as on pg. 10. Upon taking Fourier transforms and symmetrizing, we obtain the Terry-Horton equation [Terry and Horton 1982, 1983]:

$$\left( \frac{\partial}{\partial t} + \nu_{\mathbf{k}} \right) \Phi_{\mathbf{k}} = \frac{1}{2} \sum_{\mathbf{k}+\mathbf{p}+\mathbf{q}=\mathbf{0}} \hat{\mathbf{z}} \cdot (\mathbf{p} \times \mathbf{q}) \frac{(\chi_{\mathbf{q}} - \chi_{\mathbf{p}})^*}{(1 + \chi_{\mathbf{k}})} \Phi_{\mathbf{p}}^* \Phi_{\mathbf{q}}^*, \quad (\text{I.11})$$

where  $\nu_{\mathbf{k}} = ik_y V_d / (1 + \chi_{\mathbf{k}})$ . The adiabatic limit ( $\chi_{\mathbf{k}} = k^2$ ) is the Hasegawa-Mima equation [Hasegawa and Mima 1977, 1978].

## Appendix B

# Fourier Transformation of Fundamental Equation

Apply the operator  $L^{-d} \int d\mathbf{x}_1 e^{-i\mathbf{k}\cdot\mathbf{x}_1}$  to Eq. (I.15):

$$\begin{aligned} & \frac{\partial}{\partial t} \mathcal{L}_{\mathbf{k}} \psi_{\mathbf{k}}(t) + \frac{1}{L^d} \int d\mathbf{x}_1 e^{-i\mathbf{k}\cdot\mathbf{x}_1} \int d\mathbf{x}_2 \frac{1}{(2\pi)^d} \int d\bar{\mathbf{p}} \hat{v}(\bar{\mathbf{p}}) e^{i\bar{\mathbf{p}}\cdot(\mathbf{x}_1-\mathbf{x}_2)} \sum_{\mathbf{p}} \mathcal{L}_{\mathbf{p}} \psi_{\mathbf{p}}(t) e^{i\mathbf{p}\cdot\mathbf{x}_2} \\ &= \frac{1}{L^d} \int d\mathbf{x}_1 e^{-i\mathbf{k}\cdot\mathbf{x}_1} \int d\mathbf{x}_2 \int d\mathbf{x}_3 \\ & \quad \times \frac{1}{(2\pi)^{2d}} \int d\bar{\mathbf{p}} \int d\bar{\mathbf{q}} \hat{U}(\bar{\mathbf{p}}, \bar{\mathbf{q}}) e^{i\bar{\mathbf{p}}\cdot(\mathbf{x}_1-\mathbf{x}_2)} e^{i\bar{\mathbf{q}}\cdot(\mathbf{x}_1-\mathbf{x}_3)} \sum_{\mathbf{p}} \psi_{\mathbf{p}}(t) e^{i\mathbf{p}\cdot\mathbf{x}_2} \sum_{\mathbf{q}} \psi_{\mathbf{q}}(t) e^{i\mathbf{q}\cdot\mathbf{x}_3}. \end{aligned}$$

Upon invoking the appropriate Inverse Fourier Theorems, we obtain

$$\begin{aligned} & \frac{\partial}{\partial t} \mathcal{L}_{\mathbf{k}} \psi_{\mathbf{k}}(t) + \frac{1}{L^d} \int d\mathbf{x}_1 e^{-i\mathbf{k}\cdot\mathbf{x}_1} \sum_{\mathbf{p}} \hat{v}(\mathbf{p}) e^{i\mathbf{p}\cdot\mathbf{x}_1} \mathcal{L}_{\mathbf{p}} \psi_{\mathbf{p}}(t) \\ &= \frac{1}{L^d} \int d\mathbf{x}_1 e^{-i\mathbf{k}\cdot\mathbf{x}_1} \sum_{\mathbf{p}, \mathbf{q}} \hat{U}(\mathbf{p}, \mathbf{q}) e^{i\mathbf{p}\cdot\mathbf{x}_1} e^{i\mathbf{q}\cdot\mathbf{x}_1} \psi_{\mathbf{p}}(t) \psi_{\mathbf{q}}(t), \end{aligned}$$

or simply

$$\frac{\partial}{\partial t} \mathcal{L}_{\mathbf{k}} \psi_{\mathbf{k}}(t) + \hat{v}(\mathbf{k}) \mathcal{L}_{\mathbf{k}} \psi_{\mathbf{k}} = \sum_{\mathbf{p}, \mathbf{q}} \delta_{\mathbf{k}-\mathbf{p}-\mathbf{q}, 0} \hat{U}(\mathbf{p}, \mathbf{q}) \psi_{\mathbf{p}}(t) \psi_{\mathbf{q}}(t). \quad (\text{I.16})$$

The reality conditions and definitions given on pg. 20 allow us to write this more symmetrically as

$$\boxed{\left( \frac{\partial}{\partial t} + \nu_{\mathbf{k}} \right) \psi_{\mathbf{k}}(t) = \frac{1}{2} \sum_{\mathbf{k}=\mathbf{p}+\mathbf{q}=0} M_{\mathbf{k}\mathbf{p}\mathbf{q}} \psi_{\mathbf{p}}^*(t) \psi_{\mathbf{q}}^*(t).} \quad (\text{I.17})$$

# Appendix C

## Conservation Properties of the Multiple-Field DIA

Let us now show that the multiple-field DIA, conserves the generalized energy, Eq. (II.28). The equal-time covariance equation of the multiple-field DIA, Eq. (II.29a), may be written

$$\frac{\partial}{\partial t} C^{\alpha\alpha'}(t) + N^{\alpha\alpha'}(t) + N^{\alpha'\alpha^*}(t) = F^{\alpha\alpha'}(t) + F^{\alpha'\alpha^*}(t), \quad (\text{C.1a})$$

where

$$N^{\alpha\alpha'}(t) \doteq \nu^{\alpha}_{\alpha'} - \sum_{\Delta} M^{\alpha}_{\beta\gamma} M^{\bar{\beta}}_{\bar{\gamma}\bar{\alpha}}{}^* \bar{\Theta}^{\beta\gamma\alpha'}_{\bar{\beta}} \bar{\gamma}\bar{\alpha}{}^*, \quad (\text{C.1b})$$

$$F^{\alpha\alpha'}(t) \doteq \frac{1}{2} \sum_{\Delta} M^{\alpha}_{\beta\gamma} M^{\bar{\alpha}}_{\bar{\beta}\bar{\gamma}}{}^* \bar{\Theta}^{\alpha'\beta\gamma}_{\bar{\alpha}} \bar{\beta}\bar{\gamma}{}^*, \quad (\text{C.1c})$$

$$\bar{\Theta}^{\alpha\beta\gamma}_{\bar{\alpha}} \bar{\beta}\bar{\gamma}(t) \doteq \int_0^t d\bar{t} R^{\alpha}_{\bar{\alpha}}(t, \bar{t}) C^{\beta\bar{\beta}}(t, \bar{t}) C^{\gamma\bar{\gamma}}(t, \bar{t}). \quad (\text{C.1d})$$

Note that Eq. (II.26) leads to the symmetry

$$\bar{\Theta}^{\alpha\beta\gamma}_{\bar{\alpha}} \bar{\beta}\bar{\gamma} = \bar{\Theta}^{\alpha\gamma\beta}_{\bar{\alpha}} \bar{\gamma}\bar{\beta}. \quad (\text{C.2})$$

We now show that Eq. (II.27) implies that a generalized energy of the form

$$E \doteq \frac{1}{2} \sigma_{\alpha'\alpha} \psi^{\alpha} \psi^{\alpha'*} \quad (\text{II.28})$$

is conserved by Eq. (C.1a) in the dissipationless case where  $\nu^{\alpha}_{\alpha'} + \nu^{\alpha'}_{\alpha^*} = 0$ . Upon recalling that  $\sigma$  is Hermitian, we may write

$$\begin{aligned} 2 \frac{\partial}{\partial t} E &= \sigma_{\alpha'\alpha} \frac{\partial}{\partial t} C^{\alpha\alpha'} \\ &= \sigma_{\alpha'\alpha} (F^{\alpha\alpha'} - N^{\alpha\alpha'}) + \sigma_{\alpha\alpha'}{}^* (F^{\alpha'\alpha^*} - N^{\alpha'\alpha^*}) \\ &= 2 \operatorname{Re} \sigma_{\alpha\alpha'} (F^{\alpha'\alpha} - N^{\alpha'\alpha}). \end{aligned}$$

Thus

$$\begin{aligned}
& 2 \frac{\partial}{\partial t} E \\
&= 2 \operatorname{Re} \sigma_{\alpha\alpha'} \sum_{\Delta} M^{\alpha'}_{\beta\gamma} M^{\bar{\beta}}_{\bar{\gamma}\bar{\alpha}} * \bar{\Theta}^{\beta\gamma\alpha}_{\bar{\beta}} \bar{\gamma}\bar{\alpha} * + \operatorname{Re} \sigma_{\alpha\alpha'} \sum_{\Delta} M^{\alpha'}_{\beta\gamma} M^{\bar{\alpha}}_{\bar{\beta}\bar{\gamma}} * \bar{\Theta}^{\alpha\beta\gamma}_{\bar{\alpha}} \bar{\beta}\bar{\gamma} * \\
&= \operatorname{Re} \sigma_{\alpha\alpha'} \sum_{\Delta} M^{\alpha'}_{\beta\gamma} M^{\bar{\beta}}_{\bar{\gamma}\bar{\alpha}} * \bar{\Theta}^{\beta\gamma\alpha}_{\bar{\beta}} \bar{\gamma}\bar{\alpha} * \\
&\quad + \operatorname{Re} \sigma_{\gamma\alpha'} \sum_{\Delta} M^{\alpha'}_{\beta\alpha} M^{\bar{\beta}}_{\bar{\alpha}\bar{\gamma}} * \bar{\Theta}^{\beta\alpha\gamma}_{\bar{\beta}} \bar{\alpha}\bar{\gamma} * \quad (\alpha \leftrightarrow \gamma, \quad \bar{\alpha} \leftrightarrow \bar{\gamma}) \\
&\quad + \operatorname{Re} \sigma_{\beta\alpha'} \sum_{\Delta} M^{\alpha'}_{\gamma\alpha} M^{\bar{\beta}}_{\bar{\gamma}\bar{\alpha}} * \bar{\Theta}^{\beta\gamma\alpha}_{\bar{\beta}} \bar{\gamma}\bar{\alpha} * \quad (\alpha \rightarrow \beta \rightarrow \gamma \rightarrow \alpha, \quad \bar{\alpha} \rightarrow \bar{\beta} \rightarrow \bar{\gamma} \rightarrow \bar{\alpha}) \\
&= \operatorname{Re} \sum_{\Delta} \left[ \sigma_{\alpha\alpha'} M^{\alpha'}_{\beta\gamma} + \sigma_{\gamma\alpha'} M^{\alpha'}_{\alpha\beta} + \sigma_{\beta\alpha'} M^{\alpha'}_{\gamma\alpha} \right] M^{\bar{\beta}}_{\bar{\gamma}\bar{\alpha}} * \bar{\Theta}^{\beta\gamma\alpha}_{\bar{\beta}} \bar{\gamma}\bar{\alpha} * \\
&= 0.
\end{aligned}$$

To obtain the last two lines, we invoked Eqs. (II.26), (II.27), and (C.2).

## Appendix D

# Positive Definiteness in the Realizable EDQNM

Here we show that the matrix  $\mathbf{F}$  encountered in the realizable EDQNM is positive-semidefinite. Begin by diagonalizing the covariance,

$$C^{\alpha\alpha'} = U^\alpha_\epsilon \widehat{C}^{\epsilon\epsilon} U^{\alpha'}_\epsilon^*,$$

where the eigenvalues  $\widehat{C}^{\epsilon\epsilon}$  are real and non-negative. From the definition of  $F^{\alpha\alpha'}$ , we find

$$\begin{aligned} F^{\alpha\alpha'} &\doteq \frac{1}{2} \sum_{\Delta} V^\alpha_{\beta\gamma} V^{\alpha'}_{\beta'\gamma'}{}^* C^{\beta\beta'}{}^* C^{\gamma'\gamma}, \\ &= \frac{1}{2} \sum_{\Delta} V^\alpha_{\beta\gamma} V^{\alpha'}_{\beta'\gamma'}{}^* U^\beta_\epsilon{}^* \widehat{C}^{\epsilon\epsilon} U^{\beta'}_\epsilon U^{\gamma'}_\lambda \widehat{C}^{\lambda\lambda} U^\gamma_\lambda{}^* \\ &= \frac{1}{2} \sum_{\Delta} \bar{V}^\alpha_{\epsilon\lambda} \bar{V}^{\alpha'}_{\epsilon\lambda}{}^* \widehat{C}^{\epsilon\epsilon} \widehat{C}^{\lambda\lambda}, \end{aligned}$$

where  $\bar{V}^\alpha_{\epsilon\lambda} \doteq V^\alpha_{\beta\gamma} U^\beta_\epsilon{}^* U^\gamma_\lambda{}^* \delta_{\mathbf{k}+\mathbf{p}+\mathbf{q},0}$ . In terms of  $X_{\epsilon\lambda} \doteq y_\alpha^* \bar{V}^\alpha_{\epsilon\lambda}$  we then find that

$$\begin{aligned} y_\alpha^* F^{\alpha\alpha'} y_{\alpha'} &= \frac{1}{2} X_{\epsilon\lambda} X_{\epsilon\lambda}^* \widehat{C}^{\epsilon\epsilon} \widehat{C}^{\lambda\lambda} \\ &= \frac{1}{2} |X_{\epsilon\lambda}|^2 \widehat{C}^{\epsilon\epsilon} \widehat{C}^{\lambda\lambda} \\ &\geq 0, \end{aligned}$$

reducing to a sum of non-negative numbers.

## Appendix E

# Energy Conservation of the Realizable EDQNM

We now show that the nonlinear terms of the realizable EDQNM conserve the fundamental invariant  $E$  upon which the closure was constructed. Referring to Eqs. (III.46) and (III.47), let

$$\begin{aligned}
S &\doteq (F^{\alpha\alpha'} - \hat{\eta}^\alpha_\delta C^{\delta\alpha'}) \sigma_{\alpha'\alpha} \\
&= F^\alpha_\alpha - \hat{\eta}^\alpha_\delta C^\delta_\alpha \\
&= F^\alpha_\alpha - \hat{\eta}_{\alpha\alpha'} C^{\alpha'\alpha} \\
&= \frac{1}{2} V^\alpha_{\beta\gamma} V_{\alpha\beta'\gamma'}^* C^{\beta\beta'} C^{\gamma'\gamma} \\
&\quad + V_{\alpha\beta\gamma} V^\beta_{\gamma'\alpha'} C^{\gamma\gamma'} C^{\alpha'\alpha} \\
&\quad - \frac{1}{2} i \bar{W}_{\alpha\beta\gamma} W^\beta_{\gamma'\alpha'} C^{\gamma\gamma'} C^{\alpha'\alpha} \\
&\quad - \frac{1}{2} i W_{\alpha\beta\gamma} \bar{W}^\beta_{\gamma'\alpha'} C^{\gamma\gamma'} C^{\alpha'\alpha} \\
&= \frac{1}{2} V_{\alpha\beta\gamma} V^\alpha_{\beta'\gamma'} C^{\beta\beta'} C^{\gamma'\gamma} \\
&\quad + \frac{1}{2} V_{\gamma\alpha\beta} V^\alpha_{\beta'\gamma'} C^{\beta\beta'} C^{\gamma'\gamma} \quad (\alpha \rightarrow \gamma \rightarrow \beta \rightarrow \alpha, \quad \alpha' \rightarrow \gamma' \rightarrow \beta' \rightarrow \alpha') \\
&\quad + \frac{1}{2} V_{\beta\alpha\gamma} V^\alpha_{\gamma'\beta'} C^{\gamma\gamma'} C^{\beta'\beta} \quad (\alpha \leftrightarrow \beta, \quad \alpha' \leftrightarrow \beta') \\
&\quad - \frac{1}{2} i \bar{W}_{\gamma\alpha\beta} W^\alpha_{\beta'\gamma'} C^{\beta\beta'} C^{\gamma'\gamma} \quad (\alpha \rightarrow \gamma \rightarrow \beta \rightarrow \alpha, \quad \alpha' \rightarrow \gamma' \rightarrow \beta' \rightarrow \alpha') \\
&\quad - \frac{1}{2} i \bar{W}_{\beta\alpha\gamma} W^\alpha_{\gamma'\beta'} C^{\gamma\gamma'} C^{\beta'\beta} \quad (\alpha \leftrightarrow \beta, \quad \alpha' \leftrightarrow \beta') \\
&\quad - \frac{1}{2} i W_{\gamma\alpha\beta} \bar{W}^\alpha_{\beta'\gamma'} C^{\beta\beta'} C^{\gamma'\gamma} \quad (\alpha \rightarrow \gamma \rightarrow \beta \rightarrow \alpha, \quad \alpha' \rightarrow \gamma' \rightarrow \beta' \rightarrow \alpha') \\
&\quad - \frac{1}{2} i W_{\beta\alpha\gamma} \bar{W}^\alpha_{\gamma'\beta'} C^{\gamma\gamma'} C^{\beta'\beta} \quad (\alpha \leftrightarrow \beta, \quad \alpha' \leftrightarrow \beta').
\end{aligned}$$

Since

$$\begin{aligned} V_{\alpha\beta\gamma} + V_{\beta\gamma\alpha} + V_{\gamma\alpha\beta} &= 0, \\ W_{\alpha\beta\gamma} + W_{\beta\gamma\alpha} + W_{\gamma\alpha\beta} &= 0, \\ \bar{W}_{\alpha\beta\gamma} + \bar{W}_{\beta\gamma\alpha} + \bar{W}_{\gamma\alpha\beta} &= 0, \end{aligned}$$

this reduces to

$$\begin{aligned} S = & \frac{1}{2}i\bar{W}_{\alpha\beta\gamma}W^{\alpha}_{\beta'\gamma'}*C^{\beta\beta'}*C^{\gamma'\gamma}, \\ & + \frac{1}{2}iW_{\alpha\beta\gamma}\bar{W}^{\alpha}_{\beta'\gamma'}*C^{\beta\beta'}*C^{\gamma'\gamma}. \end{aligned}$$

Then

$$\begin{aligned} 4 \operatorname{Re} S = & i\bar{W}_{\alpha\beta\gamma}W^{\alpha}_{\beta'\gamma'}*C^{\beta\beta'}*C^{\gamma'\gamma} \\ & - i\bar{W}_{\alpha\gamma'\beta'}*W^{\alpha}_{\gamma\beta}C^{\gamma'\gamma}C^{\beta\beta'}* \quad (\beta \leftrightarrow \gamma', \quad \beta' \leftrightarrow \gamma) \\ & + iW_{\alpha\beta\gamma}\bar{W}^{\alpha}_{\beta'\gamma'}*C^{\beta\beta'}*C^{\gamma'\gamma} \\ & - iW_{\alpha\gamma'\beta'}*\bar{W}^{\alpha}_{\gamma\beta}C^{\gamma'\gamma}C^{\beta\beta'}* \quad (\beta \leftrightarrow \gamma', \quad \beta' \leftrightarrow \gamma) \\ = & 0. \end{aligned}$$

Since the diagonal elements  $F^{\alpha}_{\alpha}$  are real, we conclude that

$$F^{\alpha}_{\alpha} - \hat{\eta}^{\alpha}_{\delta}C^{\delta}_{\alpha} - C^{\alpha}_{\delta}\hat{\eta}^{\delta*}_{\alpha} = 0.$$

Thus the nonlinear terms of Eq. (III.35) conserve  $E$ .

# Appendix F

## Proofs of Theorems

**Lemma 1:** *Consider a stochastic function space with inner product  $\rho(a, b) = \langle ab^* \rangle$  and for which the white-noise process  $u(t)$  provides an orthonormal basis:  $\langle u(t)u^*(t') \rangle = \delta(t - t')$ . A two-time nonstochastic function  $C$  can then be factorized as  $C(t, t') = \langle \psi(t)\psi^*(t') \rangle$  for some stochastic function  $\psi$  if and only if  $C$  is Hermitian and positive-semidefinite.*

Proof. Since the inner product is bilinear and  $\rho(a, a) \geq 0$ , the function  $\langle \psi(t)\psi^*(t') \rangle$  is clearly Hermitian and positive-semidefinite.

Conversely, suppose that a Hermitian matrix  $C$  is positive-semidefinite. Then there exists a diagonalizing unitary transformation  $U$  such that

$$C(t, t') = U(t, \bar{t}) \Lambda(\bar{t}) \delta(\bar{t} - \bar{t}') U^*(t', \bar{t}'),$$

with  $\Lambda(\bar{t}) \geq 0$  for all  $\bar{t}$ . Construct  $\psi(t) = U(t, \bar{t}) \Lambda^{1/2}(\bar{t}) u(\bar{t})$ . Then

$$\langle \psi(t)\psi^*(t') \rangle = U(t, \bar{t}) \Lambda^{1/2}(\bar{t}) \langle u(\bar{t})u^*(\bar{t}') \rangle \Lambda^{1/2}(\bar{t}') U^*(t', \bar{t}') = C(t, t').$$

*Q.E.D.*

**Theorem 1:** *If the two-time Hermitian functions  $F$  and  $G$  are positive-semidefinite, then so is the matrix with elements  $F(t, t') G(t, t')$ .*

Proof. By Lemma 1, one may factorize  $F(t, t') = \langle f(t)f^*(t') \rangle$  and  $G(t, t') = \langle g(t)g^*(t') \rangle$  in terms of the ensemble average  $\langle x \rangle \doteq \int d\mathcal{P} x_{\mathcal{P}}$  where  $x_{\mathcal{P}}$  are the realization-dependent values of the stochastic variable  $x$  and  $\mathcal{P}$  is the probability distribution for each realization. We assume that the integration over  $\mathcal{P}$  converges uniformly.

For any function  $\phi(t)$  consider

$$\begin{aligned} P_T &\doteq \int_{-T}^T dt \int_{-T}^T dt' \phi^*(t) F(t, t') G(t, t') \phi(t') \\ &= \int d\mathcal{P} \int d\mathcal{Q} \int_{-T}^T dt \int_{-T}^T dt' \\ &\quad \times \phi^*(t) f_{\mathcal{P}}(t) g_{\mathcal{Q}}(t) f_{\mathcal{P}}^*(t') g_{\mathcal{Q}}^*(t') \phi(t') \\ &= \int d\mathcal{P} \int d\mathcal{Q} |A_{\mathcal{P}\mathcal{Q}}|^2, \end{aligned}$$

where  $A_{\mathcal{P}\mathcal{Q}} = \int_{-T}^T dt \phi^*(t) f_{\mathcal{P}}(t) g_{\mathcal{Q}}(t)$ . From this last expression one sees that  $P_T \geq 0$  for all  $T$ ; thus,  $\lim_{T \rightarrow \infty} P_T \geq 0$ . Hence the element-by-element product of  $F$  and  $G$  is positive-semidefinite.

*Q.E.D.*

**Theorem 2:** *If  $\operatorname{Re} \eta(t) \geq 0 \quad \forall t$ , then the function  $r$  defined by*

$$r(t, t') \doteq \begin{cases} \exp(-\int_{t'}^t \eta(\bar{t}) d\bar{t}) & \text{for } t \geq t', \\ \exp(-\int_t^{t'} \eta^*(\bar{t}) d\bar{t}) & \text{for } t < t' \end{cases}$$

*is positive-semidefinite.*

Proof. Define  $u(t) = \int_0^t \operatorname{Re} \eta(\bar{t}) d\bar{t}$  and  $v(t) = \int_0^t \operatorname{Im} \eta(\bar{t}) d\bar{t}$ . Then

$$r(t, t') = \begin{cases} \exp(-[u(t)-u(t')] - i[v(t)-v(t')]) & \text{for } t \geq t', \\ \exp(-[u(t')-u(t)] - i[v(t)-v(t')]) & \text{for } t < t'. \end{cases}$$

Since  $\operatorname{Re} \eta(\bar{t}) \geq 0$ ,

$$\begin{aligned} t \geq t' &\Rightarrow u(t) \geq u(t'); \\ t < t' &\Rightarrow u(t) \leq u(t'). \end{aligned}$$

Thus

$$r(t, t') = \exp(-|u(t)-u(t')| - i[v(t)-v(t')]).$$

Consider

$$\begin{aligned} P &\doteq \int_{-\infty}^{\infty} \int_{-\infty}^{\infty} dt dt' \psi^*(t) r(t, t') \psi(t') \\ &= \int_{-\infty}^{\infty} \int_{-\infty}^{\infty} dt dt' \Psi^*(t) e^{-|u(t)-u(t')|} \Psi(t'), \end{aligned}$$

where  $\Psi(t) \doteq \psi(t) e^{iv(t)}$ . We want to prove that  $P \geq 0$ .

For real  $x$ , we have the identity,

$$e^{-|x|} = \frac{1}{\pi} \int_{-\infty}^{\infty} d\omega \frac{1}{1 + \omega^2} e^{-i\omega x},$$

proved by Fourier transformation. Hence

$$\begin{aligned} P &= \int_{-\infty}^{\infty} \int_{-\infty}^{\infty} dt dt' \Psi^*(t) \left[ \frac{1}{\pi} \int_{-\infty}^{\infty} d\omega \frac{1}{1 + \omega^2} e^{-i\omega[u(t)-u(t')]} \right] \Psi(t') \\ &= \frac{1}{\pi} \int_{-\infty}^{\infty} d\omega \frac{1}{1 + \omega^2} \int_{-\infty}^{\infty} dt \Psi^*(t) e^{-i\omega u(t)} \int_{-\infty}^{\infty} dt' \Psi(t') e^{i\omega u(t')} \\ &= \frac{1}{\pi} \int_{-\infty}^{\infty} d\omega \frac{1}{1 + \omega^2} |A(\omega)|^2, \end{aligned}$$

where  $A(\omega) \doteq \int_{-\infty}^{\infty} dt \Psi(t) e^{i\omega u(t)}$ . From this last expression we see that  $P \geq 0$ .

*Q.E.D.*

**Theorem 3:** *Every complex square matrix  $\mathbf{A}$  has a polar decomposition of the form*

$$\mathbf{A} = \mathbf{H}\mathbf{U}$$

where  $\mathbf{H} = \mathbf{H}^\dagger$  is positive-semidefinite and  $\mathbf{U}^\dagger \mathbf{U} = \mathbf{U}\mathbf{U}^\dagger = \mathbf{1}$ .

Proof [Gantmacher 1959]. Consider the positive-semidefinite matrix  $\mathbf{A}^\dagger \mathbf{A}$ . It has real, nonnegative eigenvalues that we denote by  $\rho_n^2$ , with  $\rho_n \geq 0$ . Also, there exists an orthonormal system of eigenvectors  $\mathbf{x}_n$  for which

$$\mathbf{A}^\dagger \mathbf{A} \mathbf{x}_n = \rho_n^2 \mathbf{x}_n.$$

The vectors  $\mathbf{A} \mathbf{x}_n$  are orthogonal:

$$(\mathbf{A} \mathbf{x}_n)^\dagger (\mathbf{A} \mathbf{x}_m) = \rho_n^2 \delta_{nm}.$$

Therefore, there exists an orthonormal system of vectors  $\mathbf{z}_n$  satisfying

$$\rho_n \mathbf{z}_n = \mathbf{A} \mathbf{x}_n.$$

Now define  $\mathbf{U}$  as the matrix that transforms  $\mathbf{x}_n$  to  $\mathbf{z}_n$  and  $\mathbf{H}$  as the matrix that transforms  $\mathbf{z}_n$  to  $\rho_n \mathbf{z}_n$ :

$$\mathbf{U} \mathbf{x}_n = \mathbf{z}_n,$$

$$\mathbf{H} \mathbf{z}_n = \rho_n \mathbf{z}_n.$$

Then  $\mathbf{H}\mathbf{U} \mathbf{x}_n = \mathbf{H} \mathbf{z}_n = \rho_n \mathbf{z}_n = \mathbf{A} \mathbf{x}_n$  for each eigenvector  $\mathbf{x}_n$ . Thus  $\mathbf{H}\mathbf{U} = \mathbf{A}$ . Since  $\mathbf{U}$  transforms from one orthogonal basis to another, it is unitary. Further,  $\mathbf{H}$  is diagonalizable by the unitary matrix composed of its eigenvectors  $\mathbf{z}_n$ ; its eigenvalues  $\rho_n$  are real and non-negative. Therefore  $\mathbf{H}$  is Hermitian and positive-semidefinite as claimed.

*Q.E.D.*

**Theorem 4:** Let  $\boldsymbol{\eta}(t)$  be a complex square matrix and  $\mathbf{R}(t, t')$  be the solution to

$$\frac{\partial}{\partial t} \mathbf{R}(t, t') + \boldsymbol{\eta}(t) \mathbf{R}(t, t') = \delta(t-t') \mathbf{1},$$

with  $\mathbf{R}(-\infty, t') = 0$ . If  $\boldsymbol{\eta}^h(t)$  is positive-semidefinite  $\forall t$ , then  $\mathbf{r}$  defined by

$$\mathbf{r}(t, t') \doteq \mathbf{R}(t, t') + \mathbf{R}^\dagger(t', t)$$

is positive-semidefinite.

Proof. Let  $\mathbf{P}$  be the solution to

$$\frac{\partial}{\partial t} \mathbf{P}(t) = \mathbf{P}(t) \boldsymbol{\eta}(t), \quad \mathbf{P}(0) = \mathbf{1}.$$

Write  $\mathbf{r}$  in terms of this integrating factor:

$$\mathbf{r}(t, t') \doteq \begin{cases} \mathbf{P}^{-1}(t) \mathbf{P}(t') & \text{for } t \geq t', \\ \mathbf{P}^\dagger(t) \mathbf{P}^{-\dagger}(t') & \text{for } t < t'. \end{cases}$$

Theorem 3 establishes the existence of a polar decomposition  $\mathbf{P} = \mathbf{H}\mathbf{U}$  for some positive-semidefinite Hermitian matrix  $\mathbf{H}$  and unitary matrix  $\mathbf{U}$ . We then find

$$\mathbf{r}(t, t') = \mathbf{U}^\dagger(t) \begin{cases} \mathbf{H}^{-1}(t) \mathbf{H}(t'), & \text{for } t \geq t' \\ \mathbf{H}(t) \mathbf{H}^{-1}(t'), & \text{for } t < t' \end{cases} \mathbf{U}(t').$$

Consider

$$\begin{aligned} P &\doteq \int_{-\infty}^{\infty} \int_{-\infty}^{\infty} dt dt' \boldsymbol{\psi}^\dagger(t) \mathbf{r}(t, t') \boldsymbol{\psi}(t') \\ &= \int_{-\infty}^{\infty} \int_{-\infty}^{\infty} dt dt' \boldsymbol{\Psi}^\dagger(t) \begin{cases} \mathbf{H}^{-1}(t) \mathbf{H}(t'), & \text{for } t \geq t' \\ \mathbf{H}(t) \mathbf{H}^{-1}(t'), & \text{for } t < t' \end{cases} \boldsymbol{\Psi}(t'), \end{aligned}$$

where  $\boldsymbol{\Psi}(t) \doteq \mathbf{U}(t) \boldsymbol{\psi}(t)$ . We want to prove that  $P \geq 0$ .

Denote the eigenvalues and orthonormal eigenvectors of  $\mathbf{H}(t)$  by  $\lambda_n(t)$  and  $\boldsymbol{\Psi}_n(t)$ , respectively. Since  $\mathbf{H}$  is positive-semidefinite, we know that  $\lambda_n \geq 0$ . Further,  $\mathbf{P}^{-1}$  always exists, being the solution to

$$\frac{\partial \mathbf{P}^{-1}}{\partial t} = -\mathbf{P}^{-1} \frac{\partial \mathbf{P}}{\partial t} \mathbf{P}^{-1} = -\boldsymbol{\eta} \mathbf{P}^{-1},$$

so that

$$0 \neq \det \mathbf{P} = \det \mathbf{H} \det \mathbf{U} = \det \mathbf{H}.$$

Therefore we conclude  $\lambda_n > 0$  and we have the following relations:

$$\begin{aligned}\mathbf{H}\Psi_n &= \lambda_n\Psi_n, \\ \mathbf{H}^{-1}\Psi_n &= \lambda_n^{-1}\Psi_n, \\ \Psi_n^\dagger\Psi_m &= \delta_{nm}.\end{aligned}$$

Since the eigenvectors form a complete basis in this space, we may, at each time  $t$ , expand  $\Psi$  in terms of them:

$$\Psi(t) = \sum_n a_n(t)\Psi_n(t).$$

We then obtain

$$P = \int_{-\infty}^{\infty} \int_{-\infty}^{\infty} dt dt' \sum_{n,m} a_n^*(t) \Psi_n^\dagger(t) \left\{ \begin{array}{l} \lambda_n^{-1}(t)\lambda_m(t'), \quad \text{for } t \geq t' \\ \lambda_n(t)\lambda_m^{-1}(t'), \quad \text{for } t < t' \end{array} \right\} a_m(t') \Psi_m(t'). \quad (\text{F.1})$$

We now demonstrate that  $\lambda_n(t)$  is a monotonic nondecreasing function of  $t$ . Differentiate

$$\mathbf{H}^2\Psi_n = \lambda_n^2\Psi_n$$

and multiply by  $\Psi_n^\dagger$  on the left to obtain

$$\Psi_n^\dagger \frac{\partial \mathbf{H}^2}{\partial t} \Psi_n + \Psi_n^\dagger \mathbf{H}^2 \frac{\partial \Psi_n}{\partial t} = \Psi_n^\dagger \frac{\partial \lambda_n^2}{\partial t} \Psi_n + \Psi_n^\dagger \lambda_n^2 \frac{\partial \Psi_n}{\partial t}. \quad (\text{F.2})$$

Upon expanding

$$\frac{\partial \Psi_n}{\partial t} = \sum_m b_{nm} \Psi_m,$$

we see that

$$\Psi_n^\dagger \mathbf{H}^2 \frac{\partial \Psi_n}{\partial t} = b_{nn} \lambda_n^2 = \Psi_n^\dagger \lambda_n^2 \frac{\partial \Psi_n}{\partial t}.$$

This reduces Eq. (F.2) to

$$\Psi_n^\dagger \frac{\partial \mathbf{H}^2}{\partial t} \Psi_n = \frac{\partial \lambda_n^2}{\partial t}.$$

Since  $\mathbf{P}\mathbf{P}^\dagger = \mathbf{H}\mathbf{U}\mathbf{U}^\dagger\mathbf{H} = \mathbf{H}^2$ , we can compute

$$\begin{aligned}\frac{\partial \mathbf{H}^2}{\partial t} &= \frac{\partial \mathbf{P}\mathbf{P}^\dagger}{\partial t} = \frac{\partial \mathbf{P}}{\partial t} \mathbf{P}^\dagger + \mathbf{P} \frac{\partial \mathbf{P}^\dagger}{\partial t} \\ &= \mathbf{P}\eta\mathbf{P}^\dagger + \mathbf{P}\eta^\dagger\mathbf{P}^\dagger \\ &= 2\mathbf{P}\eta^h\mathbf{P}^\dagger.\end{aligned}$$

Thus

$$\begin{aligned}
2\lambda_n \frac{\partial \lambda_n}{\partial t} &= \frac{\partial \lambda_n^2}{\partial t} \\
&= 2\boldsymbol{\Psi}_n^\dagger \mathbf{P} \boldsymbol{\eta}^h \mathbf{P}^\dagger \boldsymbol{\Psi}_n \\
&= 2(\mathbf{P}^\dagger \boldsymbol{\Psi}_n)^\dagger \boldsymbol{\eta}^h (\mathbf{P}^\dagger \boldsymbol{\Psi}_n) \\
&\geq 0,
\end{aligned}$$

where we have used the condition that  $\boldsymbol{\eta}^h$  is positive-semidefinite. Since  $\lambda_n > 0$ , we conclude

$$\frac{\partial \lambda_n}{\partial t} \geq 0.$$

If we define  $u_n(t) \doteq \log \lambda_n(t)$ , we then have the relations

$$\begin{aligned}
t \geq t' &\Rightarrow u_n(t) \geq u_n(t'), \\
t < t' &\Rightarrow u_n(t) \leq u_n(t'),
\end{aligned}$$

which allow us to rewrite Eq. (F.1) in the form

$$\begin{aligned}
P &= \int_{-\infty}^{\infty} \int_{-\infty}^{\infty} dt dt' \sum_{n,m} a_n^*(t) \boldsymbol{\Psi}_n^\dagger(t) e^{-|u_n(t)-u_m(t')|} a_m(t') \boldsymbol{\Psi}_m(t') \\
&= \int_{-\infty}^{\infty} \int_{-\infty}^{\infty} dt dt' \sum_{n,m} a_n^*(t) \boldsymbol{\Psi}_n^\dagger(t) \left[ \frac{1}{\pi} \int_{-\infty}^{\infty} d\omega \frac{1}{1+\omega^2} e^{-i\omega[u_n(t)-u_m(t')]} \right] a_m(t') \boldsymbol{\Psi}_m(t') \\
&= \frac{1}{\pi} \int_{-\infty}^{\infty} d\omega \frac{1}{1+\omega^2} \int_{-\infty}^{\infty} dt \sum_n a_n^*(t) \boldsymbol{\Psi}_n^\dagger(t) e^{-i\omega u_n(t)} \int_{-\infty}^{\infty} dt' \sum_m a_m(t') \boldsymbol{\Psi}_m(t') e^{i\omega u_m(t')} \\
&= \frac{1}{\pi} \int_{-\infty}^{\infty} d\omega \frac{1}{1+\omega^2} \mathbf{A}^\dagger(\omega) \mathbf{A}(\omega),
\end{aligned}$$

where  $\mathbf{A}(\omega) \doteq \int_{-\infty}^{\infty} dt \sum_n a_n(t) \boldsymbol{\Psi}_n(t) e^{i\omega u_n(t)}$ . From this last expression we see that  $P \geq 0$ .

*Q.E.D.*

# Appendix G

## Isotropic Weight Factors

### One-dimensional case:

For the one-dimensional case where  $f(k, p, q) = 1$ , there is an interesting analytical solution to the weight factor problem. The form of the answer serves to motivate our attack on the general problem, Eq. (IV.3).

Consider

$$\begin{aligned} I &\doteq \int_{k_<}^{k_>} dk \int_{p_<}^{p_>} dp \int_{q_<}^{q_>} dq \delta(k+p+q) \\ &= \int_0^{\Delta k} dk \int_0^{\Delta p} dp \int_0^{\Delta q} dq \delta(k+p+q+S), \end{aligned}$$

with  $\Delta k \doteq k_> - k_<$ ,  $\Delta p \doteq p_> - p_<$ ,  $\Delta q \doteq q_> - q_<$ , and  $S \doteq k_< + p_< + q_<$ . Upon invoking the Inverse Fourier Theorem, we find

$$\begin{aligned} I &= \int_0^{\Delta k} dk \int_0^{\Delta p} dp \int_0^{\Delta q} dq \int_{-\infty}^{\infty} \frac{d\alpha}{2\pi} e^{i\alpha(k+p+q+S)} \\ &= \frac{-1}{2\pi i} \int_{-\infty}^{\infty} d\alpha \frac{e^{i\alpha S}}{\alpha^3} (e^{i\alpha \Delta k} - 1)(e^{i\alpha \Delta p} - 1)(e^{i\alpha \Delta q} - 1) \tag{G.1} \\ &= \frac{-1}{2\pi i} \int_{-\infty}^{\infty} d\alpha \frac{e^{i\alpha S}}{\alpha^3} \left[ e^{i\alpha(\Delta k + \Delta p + \Delta q)} - e^{i\alpha(\Delta p + \Delta q)} - e^{i\alpha(\Delta k + \Delta q)} - e^{i\alpha(\Delta k + \Delta p)} \right. \\ &\quad \left. + e^{i\alpha \Delta k} + e^{i\alpha \Delta p} + e^{i\alpha \Delta q} - 1 \right]. \end{aligned}$$

In the complex plane, consider the integral

$$\int_C d\alpha \frac{1}{\alpha^3} e^{i\alpha \lambda},$$

where  $C$  is a contour lying on the real axis deformed in a small semicircle above the pole at  $\alpha = 0$ . (This choice is arbitrary since it is clear from Eq. (G.1) that the

final expression must be nonsingular.) We close this contour with a semicircle of radius  $R$  about the origin. For  $\lambda > 0$ , it is convenient to take the semicircle entirely in the upper-half plane since we may then make use of the well-known result that the contribution along the semicircular arc vanishes as  $R \rightarrow \infty$ . Since there are no poles within the enclosed contour, the integral along  $C$  must vanish. Similarly, for  $\lambda < 0$  we choose the semicircular arc in the lower-half plane since now the contribution from this arc vanishes. In the latter case, we pick up a contribution to the integral along  $C$  from the residue at  $\alpha = 0$ :

$$\frac{1}{2} \frac{d^2}{d\alpha^2} e^{i\alpha\lambda} \Big|_{\alpha=0} = -\frac{1}{2} \lambda^2.$$

Thus

$$\frac{1}{2\pi i} \int_C d\alpha \frac{1}{\alpha^3} e^{i\alpha\lambda} = \frac{1}{2} \lambda^2 \text{H}(-\lambda).$$

The final result is then

$$\begin{aligned} I &= -\frac{1}{2} [(S + \Delta k + \Delta p + \Delta q)^2 \text{H}(-S - \Delta k - \Delta p - \Delta q) \\ &\quad - (S + \Delta p + \Delta q)^2 \text{H}(-S - \Delta p - \Delta q) - (S + \Delta k + \Delta q)^2 \text{H}(-S - \Delta k - \Delta q) \\ &\quad - (S + \Delta k + \Delta p)^2 \text{H}(-S - \Delta k - \Delta p) + (S + \Delta k)^2 \text{H}(-S - \Delta k) \\ &\quad + (S + \Delta p)^2 \text{H}(-S - \Delta p) + (S + \Delta q)^2 \text{H}(-S - \Delta q) - S^2 \text{H}(-S)] \\ &= -\frac{1}{2} [(k_{>} + p_{>} + q_{>})^2 \text{H}(-k_{>} - p_{>} - q_{>}) - (k_{<} + p_{>} + q_{>})^2 \text{H}(-k_{<} - p_{>} - q_{>}) \\ &\quad - (k_{>} + p_{<} + q_{>})^2 \text{H}(-k_{>} - p_{<} - q_{>}) - (k_{>} + p_{>} + q_{<})^2 \text{H}(-k_{>} - p_{>} - q_{<}) \\ &\quad + (k_{>} + p_{<} + q_{<})^2 \text{H}(-k_{>} - p_{<} - q_{<}) + (k_{<} + p_{>} + q_{<})^2 \text{H}(-k_{<} - p_{>} - q_{<}) \\ &\quad + (k_{<} + p_{<} + q_{>})^2 \text{H}(-k_{<} - p_{<} - q_{>}) - (k_{<} + p_{<} + q_{<})^2 \text{H}(-k_{<} - p_{<} - q_{<})]. \end{aligned}$$

### Leith's isotropic case:

In section IV.B.1 we noted that the isotropic version of Eq. (IV.3),

$$\begin{aligned} J(k_{<}, k_{>}, p_{<}, p_{>}, q_{<}, q_{>}) &\doteq \langle f \rangle_{\mathbf{k}\mathbf{p}\mathbf{q}} \\ &= \int_{k_{<}}^{k_{>}} k dk \int_0^{2\pi} d\alpha \int_{p_{<}}^{p_{>}} p dp \int_0^{2\pi} d\beta \int_{q_{<}}^{q_{>}} q dq \int_0^{2\pi} d\gamma \delta(\mathbf{k} + \mathbf{p} + \mathbf{q}) f(\mathbf{k}, \mathbf{p}, \mathbf{q}), \end{aligned}$$

with  $f(\mathbf{k}, \mathbf{p}, \mathbf{q}) = |\sin(\beta - \gamma)|/2k$ , reduces to the sum of eight integrals:

$$\begin{aligned} &J(k_{<}, k_{>}, p_{<}, p_{>}, q_{<}, q_{>}) \\ &= I(k_{>}, p_{>}, q_{>}) - I(k_{>}, p_{>}, q_{<}) - I(k_{>}, p_{<}, q_{>}) + I(k_{>}, p_{<}, q_{<}) \\ &\quad - I(k_{<}, p_{>}, q_{>}) + I(k_{<}, p_{>}, q_{<}) + I(k_{<}, p_{<}, q_{>}) - I(k_{<}, p_{<}, q_{<}), \quad (\text{G.2}) \end{aligned}$$

where

$$I(\Delta k, \Delta p, \Delta q) \doteq 2\pi \int_0^{\Delta k} dk \int_0^{\Delta p} dp [\min(k + p, \Delta q) - |k - p|].$$

We will now compute an explicit form for  $I$ .

Without loss of generality, order the wavenumbers so that  $\Delta k \leq \Delta p \leq \Delta q$ . By normalizing the wavenumber magnitudes to  $\Delta q$ , we may write  $I = 2\pi\Delta q^3(I_1 - I_2)$ , where

$$\begin{aligned} I_1 &\doteq \int_0^{k_0} dk \int_0^{p_0} dp \min(k + p, 1), \\ I_2 &\doteq \int_0^{k_0} dk \int_0^{p_0} dp |k - p|, \end{aligned}$$

with normalized limits  $k_0 \doteq \Delta k/\Delta q$  and  $p_0 \doteq \Delta p/\Delta q$ .

The first integral is

$$\begin{aligned} I_1 &= \int_0^{k_0} dk \left[ \int_0^{\min(p_0, 1-k)} dp (k + p) + \text{H}(p_0 - 1 + k) \int_{1-k}^{p_0} dp \right] \\ &= \int_0^{k_0} dk \left[ k \min(p_0, 1 - k) + \frac{1}{2} \min^2(p_0, 1 - k) + \text{H}(p_0 - 1 + k)(p_0 - 1 + k) \right] \\ &= \int_0^{\min(1-p_0, k_0)} dk \left( kp_0 + \frac{1}{2}p_0^2 \right) \\ &\quad + \text{H}(k_0 + p_0 - 1) \int_{1-p_0}^{k_0} dk \left[ k(1 - k) + \frac{1}{2}(1 - k)^2 + (p_0 - 1 + k) \right] \\ &= \text{H}(k_0 + p_0 - 1) \left[ \frac{1}{2}(1 - p_0)^2 p_0 + \frac{1}{2}p_0^2(1 - p_0) \right. \\ &\quad \left. + \frac{1}{4}(1 - k_0)^3 - \frac{1}{4}p_0^3 + k_0 p_0 - (1 - p_0)p_0 \right] \\ &\quad + \text{H}(1 - k_0 - p_0) \left[ \frac{1}{2}k_0^2 p_0 + \frac{1}{2}p_0^2 k_0 \right] \\ &= \text{H}(k_0 + p_0 - 1) \left[ -\frac{1}{4}k_0^3 + \frac{1}{2}k_0^2 - \frac{1}{2}k_0 - \frac{1}{4}p_0^3 + \frac{1}{2}p_0^2 - \frac{1}{2}p_0 + k_0 p_0 + \frac{1}{4} \right] \\ &\quad + \text{H}(1 - k_0 - p_0) \left[ \frac{1}{2}k_0 p_0 (k_0 + p_0) \right]. \end{aligned}$$

The second integral is

$$\begin{aligned} I_2 &= \int_0^{k_0} dk \left[ \int_0^k dp (k - p) + \int_k^{p_0} dp (p - k) \right] \\ &= \int_0^{k_0} dk \left( k^2 - kp_0 + \frac{1}{2}p_0^2 \right) \\ &= \frac{1}{3}k_0^3 - \frac{1}{2}k_0^2 p_0 + \frac{1}{2}p_0^2 k_0. \end{aligned}$$

Upon combining these results, we obtain for the case  $\Delta k \leq \Delta p \leq \Delta q$

$$\begin{aligned}
\frac{1}{2\pi} I(\Delta k, \Delta p, \Delta q) &= -\frac{1}{4} \text{H}(\Delta k + \Delta p - \Delta q) \\
&\times \left[ \Delta k(\Delta k^2 - 3\Delta k\Delta q + 3\Delta q^2) + \Delta p(\Delta p^2 - 3\Delta p\Delta q + 3\Delta q^2) - \Delta q^3 - 6\Delta k\Delta p\Delta q \right] \\
&+ \frac{1}{2} \text{H}(\Delta q - \Delta k - \Delta p) [\Delta k\Delta p(\Delta k + \Delta p)] + \frac{1}{2} \Delta k\Delta p(\Delta k - \Delta p) - \frac{1}{3} \Delta k^3. \quad (\text{G.3})
\end{aligned}$$

By using this expression, we may then compute  $\langle f \rangle_{\mathbf{k}\mathbf{p}\mathbf{q}}$  using Eq. (G.2).

We have verified that the results so obtained are in complete agreement with the data given in Table 1 of Leith and Kraichnan [1972] and with the identical Table IV.1 of this work, which was obtained with our general anisotropic algorithm. (Table 1 of Leith's earlier paper [Leith 1971] is incorrect.) To demonstrate this, let us label the  $k$ ,  $p$ , and  $q$  bins by integers  $l$ ,  $m$ , and  $n$ , respectively. The boundaries of the logarithmically spaced bins used by Leith and Kraichnan are given by

$$\begin{aligned}
k_{<} &= 2^{l/F} \delta^{-1}, & k_{>} &= 2^{l/F} \delta, \\
p_{<} &= 2^{m/F} \delta^{-1}, & p_{>} &= 2^{m/F} \delta, \\
q_{<} &= 2^{n/F} \delta^{-1}, & q_{>} &= 2^{n/F} \delta,
\end{aligned}$$

where  $\delta \doteq 2^{1/(2F)}$ . For the case  $F = 4$ , they tabulate the ‘‘triangle volume fraction’’

$$\bar{v}(n - m, n - l) = \frac{1}{2\pi} \frac{J(k_{<}, k_{>}, p_{<}, p_{>}, q_{<}, q_{>})}{(k_{>} - k_{<})(p_{>} - p_{<})(q_{>} - q_{<})}.$$

Note that the volume fraction depends on only two parameters due to the homogeneous scaling of  $I(\Delta k, \Delta p, \Delta q)$ .

For example, consider the case  $l = 0$ ,  $m = 6$ , and  $n = 8$ , for which  $\delta = 2^{1/8}$ ,  $k_{<} = \delta^{-1}$ ,  $p_{<} = 2\sqrt{2}\delta^{-1}$ , and  $q_{<} = 4\delta^{-1}$ . Using Eqs. (G.2) and (G.3) we calculate

$$\begin{aligned}
J(k_{<}, k_{>}, p_{<}, p_{>}, q_{<}, q_{>}) &= - \sum_{h,i,j=0}^1 (-1)^{h+i+j} I(\delta^{2h} k_{<}, \delta^{2i} p_{<}, \delta^{2j} q_{<}) \\
&= 0.097589,
\end{aligned}$$

which gives  $\bar{v}(2, 8) = 0.26284$ , in agreement with the value quoted by Leith and Kraichnan [1972] and tabulated in Table IV.1.

# Appendix H

## Inviscid Equilibria

In the absence of dissipative effects we now show, assuming that the dynamics is mixing, that Eq. (I.17) evolves to the equipartition solutions found in statistical mechanics [Lee 1952, Kraichnan 1967, Fox and Orszag 1973]. The expectation that our fundamental equation will *tend* (at least to some degree) to exhibit such a relaxation to equilibrium is based on the existence of a Gibbs-type  $H$  theorem, which states that the information content in the distribution function is *minimal* for a Gaussian state [Carnevale *et al.* 1981]. For Gaussian initial conditions, one may then conclude that as the system evolves, the information content of a smooth distribution of Gaussian form cannot exceed its initial value. Equivalently, the entropy of the system, defined as

$$S(t) = \frac{1}{2} \sum_{\mathbf{k}} \log \langle |\psi_{\mathbf{k}}|^2(t) \rangle + \text{const},$$

must always be at least as large as its initial value  $S(0)$ . It achieves a maximum for moments corresponding to a Gibbs ensemble based on the initial energy. However, the entropy need not increase monotonically, as is illustrated by the result for the ensemble-averaged (exact) dynamics in Fig. H.1. In contrast, we will soon see that the EDQNM predicts a *monotonic* increase in the entropy. Note that since the exact dynamics does not exhibit a monotonically increasing entropy, there is no guarantee that the statistical equilibrium solutions we are about to derive will actually be achieved (and in fact substantial discrepancies exist between these solutions and the true dynamics in systems of only a few modes; *cf.* Chapter V.)

The statistical equilibrium solutions may be derived analytically. If  $\{\sum_{\mathbf{k}} \sigma_{\mathbf{k}}^{(i)} |\psi_{\mathbf{k}}|^2\}$  represents a *complete* set of the constants of the motion, one may obtain the most probable distribution function by maximizing the entropy functional subject to the constraints implied by the conserved invariants. This procedure yields the Gibbs

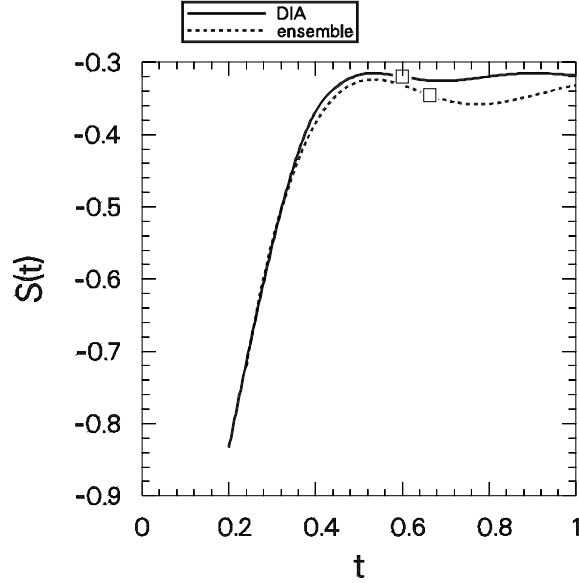


Figure H.1: DIA *vs.* exact evolution of the entropy of the three-wave system considered in Fig. V.2.

distribution for the ensemble:

$$\mathcal{N} \exp\left(-\frac{1}{2} \sum_i \alpha^{(i)} \sum_{\mathbf{k}} \sigma_{\mathbf{k}}^{(i)} |\psi_{\mathbf{k}}|^2\right),$$

where  $\mathcal{N}$  is a normalization constant and  $\alpha^{(i)}$  are real constants determined by the initial conditions.

Let us define

$$I_{\mathbf{k}} \doteq \left\langle \frac{1}{2} \sum_i \alpha^{(i)} \sigma_{\mathbf{k}}^{(i)} |\psi_{\mathbf{k}}|^2 \right\rangle.$$

We now exhibit the equipartition of the quantity  $I_{\mathbf{k}}$ . Upon denoting the real and imaginary parts of  $\psi_{\mathbf{k}}$  respectively by  $\psi_{\mathbf{k}}^r$  and  $\psi_{\mathbf{k}}^i$ , one finds for a system of  $N$  *independent* modes<sup>1</sup>

$$d\Gamma = d\psi_1^r d\psi_1^i d\psi_2^r d\psi_2^i \dots d\psi_N^r d\psi_N^i.$$

In terms of  $\lambda_{\mathbf{k}} \doteq \sum_i \alpha^{(i)} \sigma_{\mathbf{k}}^{(i)}$ , we calculate

$$\langle (\psi_{\mathbf{k}}^i)^2 \rangle = \langle (\psi_{\mathbf{k}}^r)^2 \rangle = \frac{\int d\Gamma (\psi_{\mathbf{k}}^r)^2 \exp\left(-\frac{1}{2} \sum_l \lambda_l [(\psi_l^r)^2 + (\psi_l^i)^2]\right)}{\int d\Gamma \exp\left(-\frac{1}{2} \sum_l \lambda_l [(\psi_l^r)^2 + (\psi_l^i)^2]\right)}$$

<sup>1</sup>If the reality condition  $\psi_{-\mathbf{k}} = \psi_{\mathbf{k}}^*$  is invoked, then in a system of  $2N$  modes only  $N$  of the modes are actually independent.

$$\begin{aligned}
&= \frac{\int d\psi_{\mathbf{k}}^r (\psi_{\mathbf{k}}^r)^2 \exp(-\frac{1}{2}\lambda_{\mathbf{k}} [(\psi_{\mathbf{k}}^r)^2 + (\psi_{-\mathbf{k}}^r)^2])}{\int d\psi_{\mathbf{k}}^r \exp(-\frac{1}{2}\lambda_{\mathbf{k}} [(\psi_{\mathbf{k}}^r)^2 + (\psi_{-\mathbf{k}}^r)^2])} \\
&= \frac{1}{2\lambda_{\mathbf{k}}}.
\end{aligned}$$

Since  $C_{\mathbf{k}} = \langle (\psi_{\mathbf{k}}^r)^2 \rangle + \langle (\psi_{-\mathbf{k}}^r)^2 \rangle$ , we then obtain the following equivalent expressions of equipartition,

$$\begin{aligned}
C_{\mathbf{k}} &= \frac{1}{\lambda_{\mathbf{k}}}, \\
I_{\mathbf{k}} &= \frac{1}{2}.
\end{aligned} \tag{H.1}$$

For example, if the only independent constants of the motion are the quadratic invariants corresponding to  $\sigma_{\mathbf{k}} = 1$  and  $\sigma_{\mathbf{k}} = k^2$ , we find that

$$C_{\mathbf{k}} = \frac{1}{\alpha + \beta k^2}$$

for two constants  $\alpha$  and  $\beta$ . These constants may be determined from the initial energy  $E_0$  and enstrophy  $U_0$ :

$$E_0 = \frac{1}{2} \sum_{\mathbf{k}} \frac{1}{\alpha + \beta k^2}, \tag{H.2}$$

$$U_0 = \frac{1}{2} \sum_{\mathbf{k}} \frac{k^2}{\alpha + \beta k^2}. \tag{H.3}$$

This requires inversion of the above equations. This may be done conveniently by expressing the ratio  $r \doteq U_0/E_0$  in terms of  $\rho \doteq \alpha/\beta$ , using the relation

$$\begin{aligned}
U_0 &= \frac{1}{2\beta} \sum_{\mathbf{k}} \left( 1 - \frac{\alpha}{\alpha + \beta k^2} \right) \\
&= \frac{1}{\beta} (N - \alpha E_0).
\end{aligned}$$

Here we assume that the reality condition is invoked, so that the total number of modes is  $2N$ . We find that

$$r = \frac{N}{\beta E_0} - \frac{1}{\rho},$$

or

$$r = 2N \left[ \sum_{\mathbf{k}} \frac{1}{\rho + k^2} \right]^{-1} - \rho.$$

Upon inverting the last equation for  $\rho(r)$  with a numerical root solver, we may determine  $\alpha$  and  $\beta$  from the relations

$$\beta = \frac{N\rho}{E_0(r\rho + 1)},$$

$$\alpha = \rho\beta.$$

### Closure solutions:

Let us now show that Eq. (H.1) is a steady-state solution of the EDQNM, the realizable EDQNM, and the RMC. The steady-state covariance equation for all of these closures has the form

$$-2 \sum_{\mathbf{k}+\mathbf{p}+\mathbf{q}=\mathbf{0}} \operatorname{Re} M_{\mathbf{k}\mathbf{p}\mathbf{q}} M_{\mathbf{p}\mathbf{q}\mathbf{k}}^* \theta_{\mathbf{k}\mathbf{p}\mathbf{q}}^* C_{\mathbf{q}} C_{\mathbf{k}} = \sum_{\mathbf{k}+\mathbf{p}+\mathbf{q}=\mathbf{0}} \operatorname{Re} |M_{\mathbf{k}\mathbf{p}\mathbf{q}}|^2 \theta_{\mathbf{k}\mathbf{p}\mathbf{q}} C_{\mathbf{p}} C_{\mathbf{q}}, \quad (\text{H.4})$$

which may be rewritten

$$\sum_{\mathbf{k}+\mathbf{p}+\mathbf{q}=\mathbf{0}} \left( \operatorname{Re} M_{\mathbf{k}\mathbf{p}\mathbf{q}} M_{\mathbf{p}\mathbf{q}\mathbf{k}}^* \theta_{\mathbf{k}\mathbf{p}\mathbf{q}}^* C_{\mathbf{q}} C_{\mathbf{k}} + \operatorname{Re} M_{\mathbf{k}\mathbf{p}\mathbf{q}} M_{\mathbf{q}\mathbf{p}\mathbf{k}}^* \theta_{\mathbf{k}\mathbf{p}\mathbf{q}}^* C_{\mathbf{p}} C_{\mathbf{k}} + \operatorname{Re} |M_{\mathbf{k}\mathbf{p}\mathbf{q}}|^2 \theta_{\mathbf{k}\mathbf{p}\mathbf{q}}^* C_{\mathbf{p}} C_{\mathbf{q}} \right) = 0.$$

Upon multiplying this balance equation by the real quantity  $\lambda_{\mathbf{k}}$ , we can show that the form Eq. (H.1) for the steady-state covariances is a solution. Let

$$\begin{aligned} Z_{\mathbf{k}} &\doteq \sum_{\mathbf{k}+\mathbf{p}+\mathbf{q}=\mathbf{0}} \left( \operatorname{Re} M_{\mathbf{k}\mathbf{p}\mathbf{q}} M_{\mathbf{p}\mathbf{q}\mathbf{k}}^* \theta_{\mathbf{k}\mathbf{p}\mathbf{q}}^* \frac{1}{\lambda_{\mathbf{q}}} + \operatorname{Re} M_{\mathbf{k}\mathbf{p}\mathbf{q}} M_{\mathbf{q}\mathbf{p}\mathbf{k}}^* \theta_{\mathbf{k}\mathbf{p}\mathbf{q}}^* \frac{1}{\lambda_{\mathbf{p}}} \right. \\ &\quad \left. + \operatorname{Re} M_{\mathbf{k}\mathbf{p}\mathbf{q}} \lambda_{\mathbf{k}} M_{\mathbf{k}\mathbf{p}\mathbf{q}}^* \theta_{\mathbf{k}\mathbf{p}\mathbf{q}}^* \frac{1}{\lambda_{\mathbf{p}}} \frac{1}{\lambda_{\mathbf{q}}} \right) \\ &= \sum_{\mathbf{k}+\mathbf{p}+\mathbf{q}=\mathbf{0}} \left[ \operatorname{Re} M_{\mathbf{k}\mathbf{p}\mathbf{q}} \left( \lambda_{\mathbf{k}} M_{\mathbf{k}\mathbf{p}\mathbf{q}}^* + \lambda_{\mathbf{p}} M_{\mathbf{p}\mathbf{q}\mathbf{k}}^* + \lambda_{\mathbf{q}} M_{\mathbf{q}\mathbf{p}\mathbf{k}}^* \right) \theta_{\mathbf{k}\mathbf{p}\mathbf{q}}^* \frac{1}{\lambda_{\mathbf{p}}} \frac{1}{\lambda_{\mathbf{q}}} \right]. \end{aligned}$$

Equation (I.19) then implies that  $Z_{\mathbf{k}} = 0$ ; therefore, Eq. (H.1) is indeed a steady-state solution to the closure equations.

Moreover, Eq. (H.1) is also consistent with the steady-state DIA equations. Consider the particular solution

$$C_{\mathbf{k}}(t, t') = R_{\mathbf{k}}(t, t') \frac{1}{\lambda_{\mathbf{k}}} \quad (\text{H.5})$$

where  $R_{\mathbf{k}}(t, t')$  is determined self-consistently from Eq. (I.38b). Provided that the latter equation has a solution, we see upon defining  $\theta_{\mathbf{k}\mathbf{p}\mathbf{q}}$  with Eq. (III.11) that Eq. (H.5) reduces the steady-state DIA to the form of Eq. (H.4). Hence, subject

to the above caveat, we see that the DIA also is consistent with the equipartition solutions. Since Eq. (H.5) is just the Fluctuation-Dissipation Theorem, we find that the DIA provides a plausible description of *both* the two-time and equal-time statistics in this dissipationless steady state.

In the context of wave-free turbulence, Carnevale *et al.* [1981] proved a Boltzmann-type  $H$  theorem for the EDQNM, which states that the entropy  $S$  increases *monotonically* from its initial value, as is depicted in Fig. H.2. This guarantees that the unforced, inviscid EDQNM actually evolves to the Gibbs distribution in the long-time limit. One may prove a similar theorem for the realizable EDQNM in the context of our general fundamental equation, Eq. (I.17). Consider

$$\begin{aligned} \frac{\partial S}{\partial t} &= \frac{1}{2} \sum_{\mathbf{k}} \frac{1}{C_{\mathbf{k}}} \frac{\partial C_{\mathbf{k}}}{\partial t} \\ &= \frac{1}{2} \sum_{\mathbf{k}} \frac{1}{C_{\mathbf{k}}} \sum_{\mathbf{k}+\mathbf{p}+\mathbf{q}=0} \left( 2 \operatorname{Re} M_{\mathbf{k}\mathbf{p}\mathbf{q}} M_{\mathbf{p}\mathbf{q}\mathbf{k}}^* \theta_{\mathbf{k}\mathbf{p}\mathbf{q}}^* C_{\mathbf{q}} C_{\mathbf{k}} + \operatorname{Re} |M_{\mathbf{k}\mathbf{p}\mathbf{q}}|^2 \theta_{\mathbf{k}\mathbf{p}\mathbf{q}}^* C_{\mathbf{p}} C_{\mathbf{q}} \right) \\ &= \frac{1}{2} \sum_{\mathbf{k}} \sum_{\mathbf{k}+\mathbf{p}+\mathbf{q}=0} C_{\mathbf{k}} C_{\mathbf{p}} C_{\mathbf{q}} \left[ \operatorname{Re} \theta_{\mathbf{k}\mathbf{p}\mathbf{q}} \left( \frac{2 \operatorname{Re} M_{\mathbf{k}\mathbf{p}\mathbf{q}} M_{\mathbf{p}\mathbf{q}\mathbf{k}}^*}{C_{\mathbf{k}} C_{\mathbf{p}}} + \frac{|M_{\mathbf{k}\mathbf{p}\mathbf{q}}|^2}{C_{\mathbf{k}}^2} \right) \right. \\ &\quad \left. + \operatorname{Im} \theta_{\mathbf{k}\mathbf{p}\mathbf{q}} \left( \frac{\operatorname{Im} M_{\mathbf{k}\mathbf{p}\mathbf{q}} \operatorname{Re} M_{\mathbf{p}\mathbf{q}\mathbf{k}} - \operatorname{Re} M_{\mathbf{k}\mathbf{p}\mathbf{q}} \operatorname{Im} M_{\mathbf{p}\mathbf{q}\mathbf{k}}}{C_{\mathbf{k}} C_{\mathbf{p}}} \right) \right]. \end{aligned}$$

The term in  $\operatorname{Im} \theta_{\mathbf{k}\mathbf{p}\mathbf{q}}$  disappears upon considering the symmetry  $\mathbf{k} \leftrightarrow \mathbf{p}$ . We may use the cyclic symmetry of  $\theta_{\mathbf{k}\mathbf{p}\mathbf{q}}$  to write the remaining terms in the form

$$\begin{aligned} \frac{\partial S}{\partial t} &= \frac{1}{4} \sum_{\mathbf{k}} \\ &\times \sum_{\mathbf{k}+\mathbf{p}+\mathbf{q}=0} C_{\mathbf{k}} C_{\mathbf{p}} C_{\mathbf{q}} \operatorname{Re} \theta_{\mathbf{k}\mathbf{p}\mathbf{q}} \left( \frac{M_{\mathbf{k}\mathbf{p}\mathbf{q}}}{C_{\mathbf{k}}} + \frac{M_{\mathbf{p}\mathbf{q}\mathbf{k}}}{C_{\mathbf{p}}} + \frac{M_{\mathbf{q}\mathbf{k}\mathbf{p}}}{C_{\mathbf{q}}} \right) \left( \frac{M_{\mathbf{k}\mathbf{p}\mathbf{q}}^*}{C_{\mathbf{k}}} + \frac{M_{\mathbf{p}\mathbf{q}\mathbf{k}}^*}{C_{\mathbf{p}}} + \frac{M_{\mathbf{q}\mathbf{k}\mathbf{p}}^*}{C_{\mathbf{q}}} \right) \\ &\geq 0. \end{aligned}$$

In the last line, use has been made of the realizability condition  $\operatorname{Re} \theta_{\mathbf{k}\mathbf{p}\mathbf{q}} \geq 0$ . Thus, entropy increases monotonically for the realizable EDQNM even in the presence of waves and complex mode-coupling.

We do not attempt to prove that our realizable multiple-field EDQNM satisfies an  $H$  theorem since it does not even conserve all of the fundamental quadratic invariants. We note that Carnevale *et al.* [1981] proved an  $H$  theorem for a multiple-field version of the EDQNM only in a highly restrictive case for which  $\boldsymbol{\theta}$  is assumed to be diagonal *in the field variables* and positive definite.

In Fig. H.1, we see that the DIA does *not* exhibit a Boltzmann-type  $H$  theorem; rather, it attempts to follow (to some degree) the nonmonotonic entropy evolution predicted by the exact dynamics. Similarly, we observe in Fig. H.3 that the closely

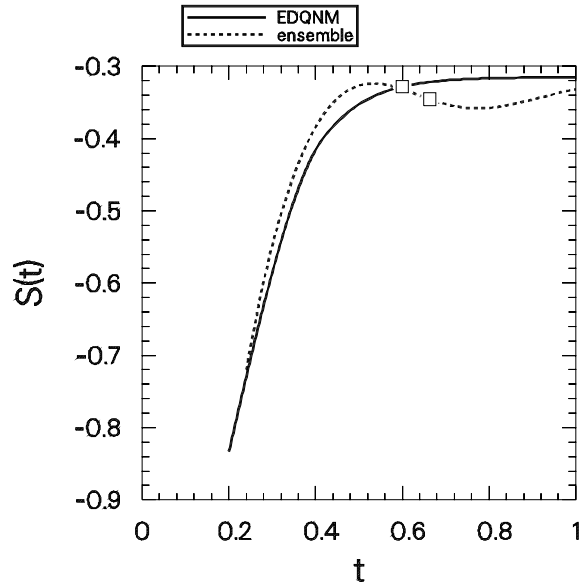


Figure H.2: EDQNM *vs.* exact evolution of the entropy of the three-wave system considered in Fig. V.2.

related RMC closure also predicts a nonmonotonic entropy evolution. Thus, we can be certain only in the case of the (realizable) EDQNM closure (on the basis of the entropy evolution alone) that the statistical equilibrium solutions will actually be achieved. Carnevale *et al.* [1981] explain that it is reasonable for the EDQNM to predict a monotonically increasing entropy since this closure involves only the instantaneous values of the second-order correlations and “the information given by just the second-order correlations degrades with time.” In contrast, the DIA and RMC both involve correlation data from not only the current time but from previous times as well.

In the preceding discussion, we have not ruled out the possibility of other steady-state solutions to the closure equations, nor have we discussed the form of the equilibrium solutions in the case of nonquadratic invariants. With similar techniques, one can handle invariants of higher order (in the field), although the calculations are more difficult. Inviscid equilibrium solutions also exist for multiple-field systems [Koniges *et al.* 1991].

It must be emphasized that these equilibria do not correspond at all to the actual saturated turbulent state obtained when the system is driven. What we discover from these considerations is that the nonlinear terms act continually toward restoring equilibrium; however, this state is never actually reached due to the disruptive effects of the linear drive and dissipation. Although we learn little about the re-

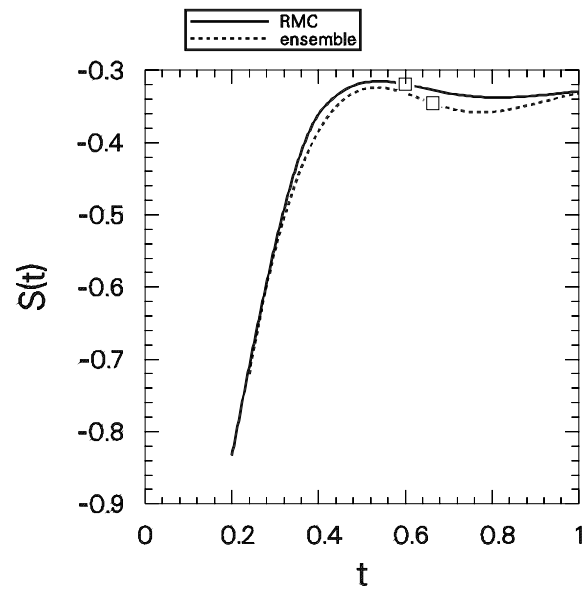


Figure H.3: RMC *vs.* exact evolution of the entropy of the three-wave system considered in Fig. V.2.

sulting fluctuation level, we do discover much about the spectral transfer properties (e.g., the cascade phenomena) embodied in the nonlinearity.

# Appendix I

## Three-Wave Quasistationary EDQNM Formulae

In the quasistationary EDQNM closure one must solve at each time step a coupled set of equations for  $\eta$  and  $\theta$  [Eqs. (III.18b) and (III.19)]. In the presence of only three interacting modes, this system has an analytical solution that has been used by previous researchers (e.g., Koniges and Leith [1987]) to implement a quasistationary closure. Let us now document this solution.

The equations are

$$\theta_{kpq} = \frac{1}{\eta_k + \eta_p + \eta_q},$$
$$\eta_k = i\omega_k - \gamma_k - \theta_{kpq}^* M_{kpq}^* (M_{pqk} C_q + M_{qkp} C_p).$$

These expressions may be combined into

$$\frac{1}{\theta_{kpq}} = i\Delta\omega - \Delta\gamma - \theta_{kpq}^* K,$$

where

$$\Delta\omega = \omega_k + \omega_p + \omega_q,$$
$$\Delta\gamma = \gamma_k + \gamma_p + \gamma_q,$$

and

$$K = M_{kpq}^* (M_{pqk} C_q + M_{qkp} C_p) \\ + M_{pqk}^* (M_{qkp} C_k + M_{kqp} C_q) \\ + M_{qkp}^* (M_{kqp} C_p + M_{pqk} C_k).$$

We want to solve the equation

$$|\theta|^2 K + (\Delta\gamma - i\Delta\omega)\theta + 1 = 0.$$

The real and imaginary parts of this equation are

$$\begin{aligned} (\theta_r^2 + \theta_i^2)K_r + \Delta\omega\theta_i + \Delta\gamma\theta_r + 1 &= 0, \\ (\theta_r^2 + \theta_i^2)K_i - \Delta\omega\theta_r + \Delta\gamma\theta_i &= 0, \end{aligned}$$

where  $\theta_r \doteq \text{Re } \theta$ ,  $\theta_i \doteq \text{Im } \theta$ ,  $K_r = \text{Re } K$ , and  $K_i = \text{Im } K$ .

In the case where  $K_i \neq 0$  let us define  $\lambda = K_r/K_i$ . When  $\Delta\omega - \lambda\Delta\gamma \neq 0$  the solution for  $\theta_r$  is obtained from the quadratic equation

$$\begin{aligned} K_r \left[ 1 + \left( \frac{\lambda\Delta\omega + \Delta\gamma}{\Delta\omega - \lambda\Delta\gamma} \right)^2 \right] \theta_r^2 + \left[ \Delta\gamma - \Delta\omega \frac{(\lambda\Delta\omega + \Delta\gamma)}{(\Delta\omega - \lambda\Delta\gamma)} + 2K_r \frac{(\lambda\Delta\omega + \Delta\gamma)}{(\Delta\omega - \lambda\Delta\gamma)^2} \right] \theta_r \\ + \frac{K_r}{(\Delta\omega - \lambda\Delta\gamma)^2} - \frac{\Delta\omega}{\Delta\omega - \lambda\Delta\gamma} + 1 = 0. \end{aligned}$$

The largest root<sup>1</sup> corresponds to the + (−) sign in the quadratic formula

$$\frac{-b \pm \sqrt{b^2 - 4ac}}{2a}$$

when  $K_r > 0$  ( $K_r < 0$ ). (The case  $K_r = 0$  must be treated separately.) The solution for  $\theta_i$  is obtained from

$$\theta_i = \frac{-1 - \theta_r(\lambda\Delta\omega + \Delta\gamma)}{\Delta\omega - \lambda\Delta\gamma}.$$

When  $K_i \neq 0$  and  $\Delta\omega - \lambda\Delta\gamma = 0$  we obtain  $\theta_r = -1/(\lambda\Delta\omega + \Delta\gamma)$ . The solution for  $\theta_i$  is found from

$$K_i\theta_i^2 + \Delta\gamma\theta_i + \frac{K_i}{(\lambda\Delta\omega + \Delta\gamma)^2} + \frac{\Delta\omega}{\lambda\Delta\omega + \Delta\gamma} = 0.$$

In the case where  $K_i = 0$  and  $\Delta\gamma \neq 0$  we find that

$$\left[ 1 + \frac{\Delta\omega^2}{\Delta\gamma} \right] K_r\theta_r^2 + \left( \frac{\Delta\omega^2}{\Delta\gamma} + \Delta\gamma \right) \theta_r + 1 = 0$$

and  $\theta_i = \Delta\omega\theta_r/\Delta\gamma$ . Again, we choose the + (−) sign in the quadratic formula when  $K_r > 0$  ( $K_r < 0$ ). The case  $K_r = 0$  yields  $\theta_r = -\Delta\gamma/(\Delta\omega^2 + \Delta\gamma^2)$ .

In the case where  $K_i = \Delta\gamma = 0$  but  $\Delta\omega \neq 0$  we obtain  $\theta_r = 0$  and

$$K_r\theta_i^2 + \Delta\omega\theta_i + 1 = 0.$$

Finally, in the case where  $K_i = \Delta\gamma = \Delta\omega = 0$  we arbitrarily take  $\theta_i = 0$  and  $\theta_r^2 = -1/K_r$ .

---

<sup>1</sup>The largest root for  $\text{Re } \theta$  is chosen to maximize the likelihood that the resulting quasistationary closure will be realizable.

# Bibliography

- [Armstrong *et al.* 1962] J. A. Armstrong, N. Bloembergen, J. Ducuing, and P. S. Pershan, *Phys. Rev.*, **127**:1918, 1962.
- [Balescu 1975] R. Balescu, *Equilibrium and Nonequilibrium Statistical Mechanics*, Wiley, New York, 1975.
- [Bartello 1990] P. Bartello, private communication, 1990.
- [Batchelor 1953] G. K. Batchelor, *The Theory of Homogenous Turbulence*, Cambridge Univ. Press, Cambridge, 1953.
- [Benzi *et al.* 1990] R. Benzi, G. Paladin, and A. Vulpiani, *Phys. Rev. A*, **42**:3654, 1990.
- [Bowman and Krommes 1987] J. C. Bowman and J. A. Krommes, *Bull. Am. Phys. Soc.*, **32**:1892, 1987.
- [Bowman and Krommes 1988] J. C. Bowman and J. A. Krommes, *Bull. Am. Phys. Soc.*, **33**:2022, 1988.
- [Buckingham 1914] E. Buckingham, *Phys. Rev.*, **4**:345, 1914.
- [Busse 1978] F. H. Busse, *Adv. Appl. Mech.*, **18**:77, 1978.
- [Carnevale *et al.* 1981] G. F. Carnevale, U. Frisch, and R. Salmon, *J. Phys. A: Math. Gen.*, **14**:1701, 1981.
- [Chandrasekhar 1960] S. Chandrasekhar, *Plasma Physics*, University of Chicago Press, Chicago, 1960.
- [Chen and Kraichnan 1990] S. Chen and R. H. Kraichnan, *Phys. Fluids A*, **2**, 1990.
- [Chen *et al.* 1984] L. Chen, R. B. White, and M. N. Rosenbluth, *Phys. Rev. Lett.*, **52**:1122, 1984.

- [Chen *et al.* 1989a] H.-D. Chen, S. Chen, and R. H. Kraichnan, *Phys. Rev. Lett.*, **63**:2657, 1989.
- [Chen *et al.* 1989b] H.-D. Chen, J. R. Herring, R. M. Kerr, and R. H. Kraichnan, *Phys. Fluids A*, **1**:1844, 1989.
- [Connor 1988] J. W. Connor, *Plasma Phys. and Controlled Fusion*, **30**:619, 1988.
- [Dannevik 1990] W. P. Dannevik, "Numerical model of multifield plasma turbulence based on DIA closure," in *Sherwood Theory Conference*, 1990, Williamsburg, Virginia.
- [Davidson and Kaufman 1969] R. C. Davidson and A. N. Kaufman, *J. Plasma Phys.*, **3**:97, 1969.
- [Davidson 1972] R. C. Davidson, *Methods in Nonlinear Plasma Theory*, Academic, New York, 1972.
- [Deker and Haake 1975] U. Deker and F. Haake, *Phys. Rev. A*, **11**:2043, 1975.
- [Doob 1953] J. L. Doob, *Stochastic Processes*, Wiley, New York, 1990 edition, 1953.
- [Drake *et al.* 1980] J. F. Drake, N. T. Gladd, C. S. Liu, and C. L. Chang, *Phys. Rev. Lett.*, **44**:994, 1980.
- [Dubin *et al.* 1983] D. H. E. Dubin, J. A. Krommes, C. Oberman, and W. W. Lee, *Phys. Fluids*, **26**:3524, 1983.
- [Dubois 1967] D. F. Dubois, in *Lectures in Theoretical Physics*, edited by W. E. Brittin and A. O. Barut, volume 9C, p. 469, Gordon and Breach, New York, 1967.
- [Dupree and Tetreault 1978] T. H. Dupree and D. J. Tetreault, *Phys. Fluids*, **21**:425, 1978.
- [Dupree 1966] T. H. Dupree, *Phys. Fluids*, **9**:1773, 1966.
- [Dupree 1967] T. H. Dupree, *Phys. Fluids*, **10**:1049, 1967.
- [Dupree 1970] T. H. Dupree, *Phys. Rev. Lett.*, **25**:789, 1970.

- [Dupree 1972] T. H. Dupree, *Phys. Fluids*, **15**:334, 1972.
- [Dupree 1974] T. H. Dupree, *Phys. Fluids*, **17**:100, 1974.
- [Dyson 1949a] F. J. Dyson, *Phys. Rev.*, **75**:486, 1949.
- [Dyson 1949b] F. J. Dyson, *Phys. Rev.*, **75**:1736, 1949.
- [Edwards and McComb 1969] S. F. Edwards and W. D. McComb, *J. Phys. A: Gen. Phys.*, **2**:157, 1969.
- [Edwards 1964] S. F. Edwards, *J. Fluid Mech.*, **18**:239, 1964.
- [Feynman 1949a] R. P. Feynman, *Phys. Rev.*, **76**:749, 1949.
- [Feynman 1949b] R. P. Feynman, *Phys. Rev.*, **76**:769, 1949.
- [Fox and Orszag 1973] D. G. Fox and S. A. Orszag, *Phys. Fluids*, **16**:169, 1973.
- [Frisch and Bourret 1970] U. Frisch and R. Bourret, *J. Math Phys.*, **11**:364, 1970.
- [Gang *et al.* 1991] F. Y. Gang, P. H. Diamond, J. A. Crotinger, and A. E. Koniges, *Phys. Fluids B*, **3**:955, 1991.
- [Gantmacher 1959] F. Gantmacher, *The Theory of Matrices*, Chelsea, New York, 1959.
- [Garcia *et al.* 1985] L. Garcia, P. H. Diamond, B. A. Carreras, and J. D. Callen, *Phys. Fluids*, **28**:2147, 1985.
- [Hald 1976] O. H. Hald, *Phys. Fluids*, **19**:914, 1976.
- [Hansen and Nicholson 1981] P. J. Hansen and D. R. Nicholson, *Phys. Fluids*, **24**:615, 1981.
- [Hasegawa and Mima 1977] A. Hasegawa and K. Mima, *Phys. Rev. Lett.*, **39**:205, 1977.
- [Hasegawa and Mima 1978] A. Hasegawa and K. Mima, *Phys. Fluids*, **21**:87, 1978.
- [Herring and Kraichnan 1979] J. R. Herring and R. H. Kraichnan, *J. Fluid Mech.*, **91**:581, 1979.

- [Herring *et al.* 1982] J. R. Herring, D. Schertzer, M. Lesieur, G. R. Newman, J. P. Chollet, and M. Larcheveque, *J. Fluid Mech.*, **124**:411, 1982.
- [Herring 1975] J. R. Herring, *J. Atmos. Sci.*, **32**:2254, 1975.
- [Holloway and Hendershott 1977] G. Holloway and M. C. Hendershott, *J. Fluid Mech.*, **82**:747, 1977.
- [Horton 1984] W. Horton, "Drift wave turbulence and anomalous transport," in *Handbook of Plasma Physics*, edited by M. N. Rosenbluth and R. Z. Sagdeev, volume 2: *Basic Plasma Physics II*, edited by A. A. Galeev and R. N. Sudan, chapter 6.4, p. 383, North-Holland, Amsterdam, 1984.
- [Horton 1986] W. Horton, *Phys. Fluids*, **29**:1491, 1986.
- [Horton 1989] W. Horton, private communication, 1989.
- [Howard 1963] L. N. Howard, *J. Fluid Mech.*, **17**:405, 1963.
- [Jensen 1981] R. J. Jensen, *J. Stat. Phys.*, **25**:183, 1981.
- [Johnston 1989] S. Johnston, private communication, 1989.
- [Kadomtsev 1965] B. B. Kadomtsev, *Plasma Turbulence*, Academic, Reading, MA, 1965, translated by L. C. Ronson.
- [Kaufman 1972] A. N. Kaufman, *J. Plasma Phys.*, **8**:1, 1972.
- [Kim and Krommes 1988] C.-B. Kim and J. A. Krommes, *J. Stat. Phys.*, **53**:1103, 1988.
- [Kim and Krommes 1990] C.-B. Kim and J. A. Krommes, *Phys. Rev. A*, **42**:7487, 1990.
- [Knuth 1984] D. E. Knuth, *The Computer Journal*, **27**:97, 1984.
- [Knuth 1986] D. E. Knuth, *The T<sub>E</sub>Xbook*, Addison Wesley, Reading, MA, 1986.
- [Kolmogorov 1941] A. Kolmogorov, *Dokl. Akad. Nauk SSSR*, **30**:301, 1941, Reprinted in *Proc. R. Soc. Lond.* A434, 9–13, 1991.

- [Kolmogorov 1962] A. N. Kolmogorov, *J. Fluid Mech.*, **13**:82, 1962, translation of lecture given at Marseilles, 1961.
- [Koniges and Krommes 1982] A. E. Koniges and J. A. Krommes, *Bull. Am. Phys. Soc.*, **27**:946, 1982.
- [Koniges and Leith 1987] A. E. Koniges and C. E. Leith, *Phys. Fluids*, **30**:3065, 1987.
- [Koniges *et al.* 1991] A. E. Koniges, J. A. Crotinger, W. P. Dannevik, G. F. Carnevale, P. H. Diamond, and F. Y. Gang, *Phys. Fluids B*, **3**:1297, 1991.
- [Koniges 1989] A. E. Koniges, private communication, 1989.
- [Kraichnan and Chen 1989] R. H. Kraichnan and S. Chen, *Physica D*, **37**:160, 1989.
- [Kraichnan and Herring 1978] R. H. Kraichnan and J. R. Herring, *J. Fluid Mech.*, **88**:355, 1978.
- [Kraichnan and Panda 1988] R. H. Kraichnan and R. Panda, *Phys. Fluids*, **31**:2395, 1988.
- [Kraichnan 1958a] R. H. Kraichnan, *Phys. Rev.*, **109**:1407, 1958.
- [Kraichnan 1958b] R. H. Kraichnan, *Phys. Fluids*, **1**:358, 1958.
- [Kraichnan 1958c] R. H. Kraichnan, "A theory of turbulence dynamics," in *Second Symposium on Naval Hydrodynamics*, pp. 29–44, Office of Naval Research Report ACR–38, 1958.
- [Kraichnan 1959a] R. H. Kraichnan, *J. Fluid Mech.*, **5**:497, 1959.
- [Kraichnan 1959b] R. H. Kraichnan, *Phys. Rev.*, **113**:1181, 1959.
- [Kraichnan 1961] R. H. Kraichnan, *J. Math. Phys.*, **2**:124, 1961.
- [Kraichnan 1963] R. H. Kraichnan, *Phys. Fluids*, **6**:1603, 1963.
- [Kraichnan 1964a] R. H. Kraichnan, *Phys. Fluids*, **7**:1030, 1964.
- [Kraichnan 1964b] R. H. Kraichnan, *Phys. Fluids*, **7**:1723, 1964.
- [Kraichnan 1964c] R. H. Kraichnan, *Phys. Fluids*, **7**:1163, 1964.

- [Kraichnan 1965] R. H. Kraichnan, *Phys. Fluids*, **8**:575, 1965.
- [Kraichnan 1966a] R. H. Kraichnan, “Invariance principles and approximation in turbulence dynamics,” in *Dynamics of Fluids and Plasmas*, edited by S. I. Pai, pp. 239–255, Academic, New York, 1966.
- [Kraichnan 1966b] R. H. Kraichnan, *Phys. Fluids*, **9**:1728, 1966.
- [Kraichnan 1967] R. H. Kraichnan, *Phys. Fluids*, **10**:1417, 1967.
- [Kraichnan 1970a] R. H. Kraichnan, *J. Fluid Mech.*, **41**:189, 1970.
- [Kraichnan 1970b] R. H. Kraichnan, “Turbulent diffusion: evaluation of primitive and renormalized perturbation series by Padé approximants and by expansion of stieltjes transforms into contributions from continuous orthogonal functions,” in *The Padé Approximant in Theoretical Physics*, edited by G. A. Baker and J. L. Gammel, pp. 129–170, Academic, London, 1970.
- [Kraichnan 1971a] R. H. Kraichnan, *J. Fluid Mech.*, **47**:525, 1971.
- [Kraichnan 1971b] R. H. Kraichnan, *J. Fluid Mech.*, **47**:513, 1971.
- [Kraichnan 1972] R. H. Kraichnan, *J. Fluid Mech.*, **56**:287, 1972.
- [Kraichnan 1974] R. H. Kraichnan, *J. Fluid Mech.*, **62**:305, 1974.
- [Kraichnan 1977] R. H. Kraichnan, *J. Fluid Mech.*, **83**:349, 1977.
- [Kraichnan 1980] R. H. Kraichnan, *Annals New York Academy of Sciences*, pp. 37–46, NYAS, New York, 1980.
- [Kraichnan 1985] R. H. Kraichnan, *Theoretical Approaches to Turbulence*, volume 58 of *Applied Mathematical Sciences Series*, chapter V, p. 91, Springer, New York, 1985.
- [Kraichnan 1987] R. H. Kraichnan, *Phys. Fluids*, **30**:2400, 1987.
- [Kraichnan 1988] R. H. Kraichnan, *J. Stat. Phys.*, **51**:949, 1988.
- [Kraichnan 1990a] R. H. Kraichnan, “Intermittent turbulence from closures,” in *Proceedings of the Sixth Beer-Sheva Seminar*, Jerusalem, 1990.

- [Kraichnan 1990b] R. H. Kraichnan, *Phys. Rev. Lett.*, **65**:575, 1990.
- [Kraichnan 1990c] R. H. Kraichnan, private communication, 1990.
- [Krall 1968] N. A. Krall, in *Advances in Plasma Physics*, edited by A. Simon and W. B. Thompson, volume 1, p. 153, Wiley, New York, 1968.
- [Krommes and Bowman 1988] J. A. Krommes and J. C. Bowman, *Bull. Am. Phys. Soc.*, **33**:2022, 1988.
- [Krommes and Kim 1988] J. A. Krommes and C.-B. Kim, *Phys. Fluids*, **31**:869, 1988.
- [Krommes and Kim 1990] J. A. Krommes and C.-B. Kim, *Phys. Fluids B*, **2**:1331, 1990.
- [Krommes and Smith 1987] J. A. Krommes and R. A. Smith, *Ann. Phys.*, **177**:246, 1987.
- [Krommes *et al.* 1983] J. A. Krommes, C. Oberman, and R. G. Kleva, *J. Plasma Phys.*, **30**:11, 1983.
- [Krommes *et al.* 1990] J. A. Krommes, J. C. Bowman, and M. Ottaviani, *Bull. Am. Phys. Soc.*, **35**:1957, 1990.
- [Krommes 1982] J. A. Krommes, *Phys. Fluids*, **25**:1393, 1982.
- [Krommes 1984a] J. A. Krommes, "Topics in the theory of statistical closure approximations for plasma physics," in *Statistical Physics and Chaos in Fusion Plasmas*, edited by C. W. Horton and L. E. Reichl, pp. 241–252, Wiley, New York, 1984.
- [Krommes 1984b] J. A. Krommes, "Statistical descriptions and plasma physics," in *Handbook of Plasma Physics*, edited by M. N. Rosenbluth and R. Z. Sagdeev, volume 2: *Basic Plasma Physics II*, edited by A. A. Galeev and R. N. Sudan, chapter 5.5, pp. 183–268, North-Holland, Amsterdam, 1984.
- [Krommes 1986] J. A. Krommes, *Phys. Fluids*, **29**:2756, 1986.
- [Krommes 1989] J. A. Krommes, private communication, 1989.

- [Krommes 1990] J. A. Krommes, Lecture notes on plasma turbulence, unpublished, 1990.
- [Krommes 1991a] J. A. Krommes, private communication, 1991.
- [Krommes 1991b] J. A. Krommes, *FWEB: A WEB system of structured documentation for multiple languages*, unpublished. Available online from <http://w3.pppl.gov/~kromm>. The complete FWEB release can be obtained via anonymous ftp from the directory /pub/fweb of the Internet host ftp.pppl.gov. FWEB is based on S. Levy's CWEB., 1991.
- [Kubo 1962] R. Kubo, J. Phys. Soc. Japan, **17**:1100, 1962.
- [Kubo 1963] R. Kubo, J. Math. Phys., **4**:174, 1963.
- [Landau and Lifshitz 1987] L. D. Landau and E. M. Lifshitz, *Fluid Mechanics*, volume 6 of *Course of Theoretical Physics*, Pergamon Press, Oxford, second edition, 1987.
- [Lee and Tang 1988] W. W. Lee and W. M. Tang, Phys. Fluids, **31**:612, 1988.
- [Lee 1952] T. D. Lee, Quart. J. Appl. Math., **10**:69, 1952.
- [Leith and Kraichnan 1972] C. E. Leith and R. H. Kraichnan, J. Atmos. Sci., **29**:1041, 1972.
- [Leith 1971] C. E. Leith, J. Atmos. Sci., **28**:145, 1971.
- [Leith 1975] C. E. Leith, J. Atmos. Sci., **32**:2022, 1975.
- [Lesieur 1987] M. Lesieur, *Turbulence in Fluids*, Martinus Nijhoff, Dordrecht, The Netherlands, 1987.
- [Leslie 1973a] D. C. Leslie, Rep. Prog. Phys., **36**:1365, 1973.
- [Leslie 1973b] D. C. Leslie, *Developments in the Theory of Turbulence*, Clarendon Press, Oxford, 1973.
- [Lichtenberg and Lieberman 1983] A. J. Lichtenberg and M. A. Lieberman, *Regular and Stochastic Motion*, volume 38 of *Applied Mathematical Sciences*, Springer, New York, 1983.

- [Longcope and Sudan 1990] D. W. Longcope and R. N. Sudan, “Renormalization group analysis of Alfvén turbulence in reduced MHD,” Technical Report LPS 90–10, Laboratory of Plasma Studies, Cornell University, Ithaca, NY, 1990.
- [Lorenz 1963] E. N. Lorenz, *J. Atmos. Sci.*, **20**:130, 1963.
- [Martin *et al.* 1973] P. C. Martin, E. D. Siggia, and H. A. Rose, *Phys. Rev. A*, **8**:423, 1973.
- [Mattor and Terry 1992] N. Mattor and P. W. Terry, *Phys. Fluids B*, **4**:1126, 1992.
- [Meiss *et al.* 1979] J. D. Meiss, N. Pomphrey, and K. M. Watson, *Proc. Natl. Acad. Sci. USA*, **76**:2109, 1979.
- [Meiss 1979] J. D. Meiss, *Phys. Rev. A*, **19**:1780, 1979.
- [Meiss 1982] J. D. Meiss, “Integrals of the test wave Hamiltonian: A special case,” in *Mathematical Methods in Hydrodynamics and Integrability in Dynamical Systems*, edited by M. Tabor and Y. Treve, pp. 293–300, New York, 1982, La Jolla Institute 1981, American Institute of Physics.
- [Millionschtchikov 1941] M. D. Millionschtchikov, *C. R. Acad. Sci. U.S.S.R.*, **32**:615, 1941.
- [Monin and Yaglom 1965] A. S. Monin and A. M. Yaglom, *Statistical Fluid Mechanics; Mechanics of Turbulence*, MIT Press, Cambridge, MA, 1965, English translation published in 1971, edited by John L. Lumley.
- [Mynick and Duvall 1989] H. E. Mynick and R. E. Duvall, *Phys. Fluids B*, **1**:750, 1989.
- [Ogura 1963] Y. Ogura, *J. Fluid Mech.*, **16**:33, 1963.
- [Orszag and Kraichnan 1967] S. A. Orszag and R. H. Kraichnan, *Phys. Fluids*, **10**:1720, 1967.
- [Orszag 1970] S. A. Orszag, *J. Fluid Mech.*, **41**:363, 1970.

- [Orszag 1977] S. A. Orszag, “Lectures on the statistical theory of turbulence,” in *Fluid Dynamics*, edited by R. Balian and J.-L. Peube, pp. 235–373, Gordon and Breach, London, 1977, (summer school lectures given at Grenoble University, 1973).
- [Orszag 1991] S. A. Orszag, private communication, 1991.
- [Ottaviani *et al.* 1990] M. Ottaviani, F. Romanelli, R. Benzi, M. Briscolini, P. Santangelo, and S. Succi, *Phys. Fluids B*, **2**:67, 1990.
- [Ottaviani *et al.* 1991] M. Ottaviani, J. C. Bowman, and J. A. Krommes, *Phys. Fluids B*, **3**:2186, 1991.
- [Ottaviani 1990a] M. Ottaviani, *Phys. Lett. A*, **143**:325, 1990.
- [Ottaviani 1990b] M. Ottaviani, private communication, 1990.
- [Pedlosky 1979] J. Pedlosky, *Geophysical Fluid Dynamics*, Springer, New York, 1979.
- [Phythian 1975] R. Phythian, *J. Phys. A*, **8**:1423, 1975.
- [Phythian 1976] R. Phythian, *J. Phys. A*, **9**:269, 1976.
- [Phythian 1977] R. Phythian, *J. Phys. A*, **10**:777, 1977.
- [Proudman and Reid 1954] I. Proudman and W. H. Reid, *Phil. Trans. R. Soc. Lond. Ser. A*, **247**:163, 1954.
- [Rewoldt *et al.* 1987] G. Rewoldt, W. M. Tang, and R. J. Hastie, *Phys. Fluids*, **30**:807, 1987.
- [Ritz *et al.* 1987] C. P. Ritz, D. L. Brower, T. L. Rhodes, R. D. Bengtson, S. Levinson, N. C. Luhmann, Jr., W. A. Peebles, and E. J. Powers, *Nucl. Fusion*, **27**:1125, 1987.
- [Rose and Sulem 1978] H. A. Rose and P. L. Sulem, *Le Journal de Physique*, **3**:441, 1978.
- [Rose 1974] H. A. Rose, *Aspects of the Statistical Dynamics of Classical Systems*, Ph.D. thesis, Harvard University, Cambridge, MA, 1974.

- [Rose 1985] H. A. Rose, *Physica D*, **14**:216, 1985.
- [Saffman 1970] P. Saffman, *Phys. Fluids*, **13**:2193, 1970.
- [Sagdeev and Galeev 1969] R. Z. Sagdeev and A. A. Galeev, *Nonlinear Plasma Theory*, Benjamin, New York, 1969.
- [Santangelo *et al.* 1989] P. Santangelo, R. Benzi, and B. Legras, *Phys. Fluids A*, **1**:1027, 1989.
- [Schwinger 1951a] J. Schwinger, *Proc. Natl. Acad. Sci.*, **37**:452, 1951.
- [Schwinger 1951b] J. Schwinger, *Proc. Natl. Acad. Sci.*, **37**:455, 1951.
- [Scott *et al.* 1991] B. D. Scott, H. Biglari, P. W. Terry, and P. H. Diamond, *Phys. Fluids B*, **3**:51, 1991.
- [She and Orszag 1991] Z.-S. She and S. A. Orszag, *Phys. Rev. Lett.*, **66**:1701, 1991.
- [She *et al.* 1991] Z.-S. She, E. Jackson, and S. A. Orszag, *Proc. R. Soc. Lond. Ser. A*, **434**:101, 1991.
- [Similon 1981] P. L. Similon, *A renormalized theory of drift wave turbulence in sheared magnetic fields*, Ph.D. thesis, Princeton University, Princeton, NJ, 1981.
- [Stanišić 1988] M. M. Stanišić, *The Mathematical Theory of Turbulence*, Springer, New York, second edition, 1988.
- [Stix 1973] T. H. Stix, *Phys. Rev. Lett.*, **30**:833, 1973.
- [Stroustrup 1987] B. Stroustrup, *The C++ Programming Language*, Addison-Wesley, Reading, MA, 1987.
- [Sun *et al.* 1985a] G.-Z. Sun, D. R. Nicholson, and H. A. Rose, *Phys. Rev. Lett.*, **54**:1664, 1985.
- [Sun *et al.* 1985b] G.-Z. Sun, D. R. Nicholson, and H. A. Rose, *Phys. Fluids*, **28**:2395, 1985.
- [Sun *et al.* 1986] G.-Z. Sun, D. R. Nicholson, and H. A. Rose, *Phys. Fluids*, **29**:1011, 1986.

- [Tatsumi 1957] T. Tatsumi, Proc. R. Soc. Lond. Ser. A, **239**:16, 1957.
- [Tennekes and Lumley 1972] H. Tennekes and J. L. Lumley, *A First Course in Turbulence*, MIT Press, Cambridge, MA, 1972.
- [Terry and Horton 1982] P. W. Terry and W. Horton, Phys. Fluids, **25**:491, 1982.
- [Terry and Horton 1983] P. W. Terry and W. Horton, Phys. Fluids, **26**:106, 1983.
- [Tibone *et al.* 1990] F. Tibone, G. Corrigan, and T. E. Stringer, “A quantitative assessment of  $\nabla T_i$ -driven turb. theory based on JET exp. data,” in *Proceedings of the 17-th European Conference on Controlled Fusion and Plasma Heating*, edited by G. Briffod, A. Nijssen-Vis, and F. C. Schüller, Amsterdam, 1990, European Physical Society, Geneva, 1990, Vol. 14B, Part II, p. 805.
- [Tsunoda *et al.* 1987] S. I. Tsunoda, F. Doveil, and J. Malmberg, Phys. Rev. Lett., **59**:2752, 1987.
- [Uhlenbeck and Ornstein 1930] G. E. Uhlenbeck and L. S. Ornstein, Phys. Rev., **36**:823, 1930, reprinted in *Selected Papers on Noise and Stochastic Processes*, edited by Nelson Wax, Dover Publications, New York, 1954.
- [Van Kampen 1976] N. G. Van Kampen, Phys. Rep., **24**:171, 1976.
- [Wakatani and Hasegawa 1984] M. Wakatani and A. Hasegawa, Phys. Fluids, **27**:611, 1984.
- [Waltz 1983] R. E. Waltz, Phys. Fluids, **26**:169, 1983.
- [Wang and Uhlenbeck 1945] M. C. Wang and G. E. Uhlenbeck, Rev. Mod. Phys., **17**, 1945, reprinted in *Selected Papers on Noise and Stochastic Processes*, edited by Nelson Wax, Dover Publications, New York, 1954.
- [Weinstock 1969] J. Weinstock, Phys. Fluids, **12**:1045, 1969.
- [Wersinger *et al.* 1980] J.-M. Wersinger, J. M. Finn, and E. Ott, Phys. Fluids, **23**:1142, 1980.

- [Williams *et al.* 1987] T. Williams, E. R. Tracy, and G. Vahala, Phys. Rev. Lett., **59**:1922, 1987.
- [Wyld and Pines 1962] H. W. Wyld, Jr. and D. Pines, Phys. Rev., **127**:1851, 1962.
- [Yakhot and Orszag 1986] V. Yakhot and S. A. Orszag, J. Sci. Comput., **1**:3, 1986.
- [Yakhot and Orszag 1989] V. Yakhot and S. A. Orszag, J. Sci. Comput., **4**:139, 1989.
- [Zarnstorff *et al.* 1990] M. C. Zarnstorff, N. L. Bretz, P. C. Efthimion, B. Grek, K. Hill, D. Johnson, D. Mansfield, D. McCune, D. K. Owens, H. Park, A. Ramsey, G. I. Schmidt, B. Stratton, E. Synakowski, and G. Taylor, in *Proceedings of the 17-th European Conference on Controlled Fusion and Plasma Heating*, edited by G. Briffod, A. Nijssen-Vis, and F. C. Schüller, Amsterdam, 1990, European Physical Society, Geneva, 1990, Vol. 14B, Part I, p. 42.